



Kent Academic Repository

Borys, Andryj M. (2018) *Synthesis and Properties of Main-Group Heterocyclic Radicals*. Doctor of Philosophy (PhD) thesis, University of Kent,.

Downloaded from

<https://kar.kent.ac.uk/69884/> The University of Kent's Academic Repository KAR

The version of record is available from

This document version

UNSPECIFIED

DOI for this version

Licence for this version

UNSPECIFIED

Additional information

Versions of research works

Versions of Record

If this version is the version of record, it is the same as the published version available on the publisher's web site. Cite as the published version.

Author Accepted Manuscripts

If this document is identified as the Author Accepted Manuscript it is the version after peer review but before type setting, copy editing or publisher branding. Cite as Surname, Initial. (Year) 'Title of article'. To be published in *Title of Journal*, Volume and issue numbers [peer-reviewed accepted version]. Available at: DOI or URL (Accessed: date).

Enquiries

If you have questions about this document contact ResearchSupport@kent.ac.uk. Please include the URL of the record in KAR. If you believe that your, or a third party's rights have been compromised through this document please see our [Take Down policy](https://www.kent.ac.uk/guides/kar-the-kent-academic-repository#policies) (available from <https://www.kent.ac.uk/guides/kar-the-kent-academic-repository#policies>).

Synthesis and Properties of Main-Group Heterocyclic Radicals

Andryj M. Borys

School of Physical Sciences

Canterbury

University of Kent

A thesis submitted for the degree of Doctor of Philosophy

August 2018

Declaration

The research presented in this thesis was carried out by the author at the University of Kent between September 2015 and August 2018. I declare that the work presented in this thesis is entirely that of the author unless specified in the text. This work has not been previously submitted, in whole or in part, for any other academic degree. The copyright of this thesis rests with the author.

Andryj M. Borys

August 2018

Publications

Work from this thesis, and carried out in the duration of this Ph.D. have been included in the following publications:

Donor-substituted phosphanes – surprisingly weak Lewis donors for phosphonium cation stabilisation

Ewan R. Clark, Andryj M. Borys and Kyle G. Pearce. *Dalton Trans.* 2016, **45**, 16125-16129.

Adducts of Donor-Functionalized Ar_3P with the Soft Lewis Acid I_2 : Probing Simultaneous Lewis Acidity and Basicity at Internally Solvated P(III) Centers

Andryj M. Borys and Ewan R. Clark. *Inorg. Chem.* 2017, **56** (8), 4622-4634.

Exploring the reactivity of donor-stabilised phosphonium cations: Lewis acid catalysed reduction of chlorophosphanes by silanes

Kyle G. Pearce, Andryj M. Borys, Ewan R. Clark and Helena J. Shepherd. *Inorg. Chem.* 2018, **57** (18), 11530-11536.

Synthesis and Electronic Properties of Persistent 1,2,4-Benzothiadiazinyl Radicals

Andryj M. Borys, Antonio Alberola, Dana J. Eisler, Jeremy M. Rawson, Ewan R. Clark. 2018, *In preparation.*

Exploring Structural Diversity in Phosphorus-Amidine Heterocycles

Andryj M. Borys and Ewan R. Clark. 2018, *In preparation.*

Crystal Structures of Asymmetric Mono-Substituted Amidines

Andryj M. Borys and Ewan R. Clark. 2018, *In preparation.*

Acknowledgements

My first and foremost thanks go to my supervisor Ewan for accepting me for this Ph.D. and introducing me to the wonderful world of main-group chemistry. I have learnt a lot from him over the past three years and aspire to be as enthusiastic and passionate about chemistry as he is. I look forward to seeing the Clark group grow, and the crazy research ideas become a reality. I would also like to thank the various members of the Clark group, particularly Kyle and Asad. It was a pleasure to see their synthetic skills and passion for chemistry develop, and I am happy to see them pursue further research in the field. Special thanks must go to Ollie for being the lab DJ – slow cannula filtrations are much more bearable with Thy Art is Murder playing at full blast!

I have made many great friends within the department during my time in Canterbury and I will truly miss everyone in office 208 and labs 212/308/310, who have made this journey so much fun. Thanks are also due to all of the other postgraduate and undergraduate students who have come and gone over the years, and have made demonstrating such a blast. This also includes the technicians, Jackie, Dave and JJ in particular, who were the true heroes and comedians of the teaching labs.

Research would've been severely hampered if it weren't for Ian, who was always on hand to refill liquid nitrogen dewars and replace argon cylinders. I would also like to thank the many other staff in the department, especially Helena and Paul, for their patience and technical support. This also extends to Greg Wildgoose and his group at UEA for cyclic voltammetry training. I greatly appreciate the time that Emma and Aniello have taken to stop for a chat, offer advice and take interest in my research and future plans. That just leaves Jen, my unofficial mentor, who drove/kept me (in)sane over the past three years. I sure I did the same though, so we'll call it even!

Special thanks go to all of the #RealTimeChem Twitter community for sharing great science and for sharing mine too. It has been wonderful to make so many friends across the world, and I am excited to meet them in the near future.

Finally, I would like to thank all of my family and friends for their continued support. I could not have done this without them.

Abbreviations

AFM	Antiferromagnetic
BBDTA	Benzo- <i>bis</i> -dithiazolyl
BDTA	Benzodithiazolyl
BSS	Broken Symmetry State
BTDA	Benzothiadiazinyl
CV	Cyclic Voltammetry
CW	Continuous Wave
DABCO	1,4-Diazabicyclo[2.2.2]octane
DCM	Dichloromethane
DDQ	2,3-Dichloro-5,6-dicyano- <i>p</i> -benzoquinone
DFT	Density Functional Theory
DMA	<i>N,N</i> -Dimethylaniline
DMAP	4- <i>N,N</i> -Dimethylaminopyridine
DMF	<i>N,N</i> -Dimethylformamide
DTA	Dithiazolyl
DTDA	Dithiadiazolyl
ECP	Effective Core Potential
EDG	Electron-Donating Group
EF	Edge-to-Face
EM	Electromagnetic
ENDOR	Electron Nuclear Double Resonance
EPR	Electron Paramagnetic Resonance
EWG	Electron-Withdrawing Group
FC	Field Cooled
FM	Ferromagnetic
HBA	Hydrogen Bond Acceptor
HBD	Hydrogen Bond Donor
HOMO	Highest Occupied Molecular Orbital
LUMO	Lowest Occupied Molecular Orbital
NBS	<i>N</i> -Bromo Succinimide
NHC	<i>N</i> -Heterocyclic Carbene
NMR	Nuclear Magnetic Resonance
OFF	Offset Face-to-Face
SCO	Spin Crossover

SCXRD	Single-Crystal X-Ray Diffraction
SOMO	Singly Occupied Molecular Orbital
SQUID	Superconducting Quantum Interference Device
TEMPO	2,2,6,6-Tetramethylpiperidin-1-yl-oxyl
THF	Tetrahydrofuran
TMEDA	<i>N,N,N',N'</i> -Tetramethylethylenediamine
TMS	Trimethylsilyl
TS	Triplet State
UV	Ultraviolet
WCA	Weakly Coordinating Anion
ZFC	Zero Field Cooled

Definition of Units

a	hyperfine coupling constant
A	Ampere
Å	Angstrom
\mathbf{B}	applied external magnetic field vector
C	Coulomb
C	Curie constant
e	electron charge = $1.6021766208(98) \times 10^{-19}$ C
E	energy or potential
$E_{1/2}$	half cell potential
emu	electromagnetic unit
F	Faraday's constant = $96485.33289(59)$ C mol ⁻¹
g	grams
g_e	free-electron g -factor
g_N	effective nuclear g -factor
h	Planck's constant = $6.626070040(81) \times 10^{-34}$ J s ⁻¹
\hbar	reduced Planck's constant = $1.054571800(13) \times 10^{-34}$ J s ⁻¹
H_{ex}	Heisenberg Hamiltonian
Hz	Hertz
I	magnetic spin
I	spin quantum number
J	magnetic exchange energy
J	Joules
K	Kelvin
m	metre
m_e	electron mass = $9.10938356(11) \times 10^{-31}$ kg
m_l	magnetic quantum number
mol	mole
m_s	electron spin angular momentum quantum number
Oe	Oersted
ppm	parts per million
R	universal gas constant = $8.3144598(48)$ J K ⁻¹ mol ⁻¹
\mathbf{S}	spin angular momentum
S	electron spin quantum number
s	seconds

T	temperature (K)
T	Tesla
T_C	Curie temperature (K)
T_N	Néel temperature (K)
U	Coulombic repulsion
ν	Frequency (Hz)
V	volts
δ	chemical shift (ppm)
θ	Weiss constant
μ_B	Bohr magneton = $9.274009994(57) \times 10^{-24} \text{ J T}^{-1}$
μ_N	nuclear magneton = $5.050783699(31) \times 10^{-27} \text{ J T}^{-1}$
μ_S	magnetic dipole moment
χ_m	magnetic susceptibility
χ_p	paramagnetic susceptibility
°C	Celsius

Definition of Chemical Terms

Ar	aryl
Dipp	2,6-diisopropylphenyl
Et	ethyl
ⁱ Pr	isopropyl
<i>m</i>	<i>meta</i>
Me	methyl
Mes	2,4,6-trimethylphenyl
Mes*	2,4,6-tri- <i>tert</i> -butylphenyl
NaBAR ^{Cl}	sodium <i>tetrakis</i> -(3,5-dichlorophenyl)-borate
NaBAR ^F	sodium <i>tetrakis</i> -(3,5- <i>bis</i> -trifluoromethylphenyl)-borate
ⁿ Bu	<i>n</i> -butyl
<i>o</i>	<i>ortho</i>
OTf	trifluoromethanesulfonate <i>aka</i> triflate
<i>p</i>	<i>para</i>
Ph	phenyl
Pr	propyl
R	variable group
^t Bu	<i>tert</i> -butyl
tolyl	methyl-phenyl
Tripp	2,4,6-triisopropylphenyl
xylyl	dimethyl-phenyl

Abstract

A family of substituted 1,2,4-benzothiadiazine 1-chlorides have been prepared by the treatment of *N*-arylamidines with neat SOCl_2 . This route resulted in partial chlorination of the benzo-fused ring. In a number of cases, species with mixed degrees of chlorination at susceptible positions were characterised by NMR spectroscopy or single-crystal X-ray diffraction. The S^{IV} chlorides show considerable variation in their solid-state structures, primarily in the degree of planarity, twisting of the pendant aryl-ring and orientation of fused-ring substituents. The 1,2,4-benzothiadiazines 1-chlorides undergo facile anion metathesis with GaCl_3 , whilst treatment with NaBAR^{Cl} afforded the neutral S^{III} radical.

Cyclic voltammetry studies on the 1,2,4-benzothiadiazines 1-chlorides reveal the presence of a radical monomer-dimer equilibria in solution. These equilibria were qualitatively assessed *via* variable concentration studies, whilst the reversibility of the 1-/0 and 0/1+ redox couples was probed *via* variable scan rate studies. The $E_{1/2}$ values for the two redox couples gave poor correlation with both the calculated SOMO energies of the radical and the LUMO energies of the S^{IV} chloride from DFT (UB3LYP/6-31g) calculations. The range of $E_{1/2}$ values however was small indicating that the substituents about the benzo-fused and pendant aryl-ring have minimal influence on the electronic structure of the radicals. This was supported by EPR spectroscopy measurements, which showed only minor variation in the *g*-values and hyperfine coupling constants within the radicals. The neutral S^{III} radicals can be prepared by one electron reduction of the S^{IV} chlorides with Ph_3P under mild conditions. The three 1,2,4-benzothiadiazinyl radicals characterised by SCXRD were shown to dimerise in the solid-state, but all showed different modes of association between the heterocyclic rings. Broken-symmetry calculations (UB3LYP/6-311g(d,p)) confirmed that this dimerisation leads to spin-pairing and diamagnetism within the radicals.

The synthetic routes optimised for the 1,2,4-benzothiadiazine 1-chlorides do not directly transfer to the isoelectronic fused-ring phosphorus-nitrogen heterocycles. Slow and careful development of the reaction conditions allowed the 1,2,4-benzophosphadiazines to be prepared under mild and simple conditions, through the introduction of an electron-donating and *para*-directing dimethylamido group. Attempts to transform these species into suitable radical precursors were met with limited success.

The reactions of *N*-arylamidines with halophosphines was found to be highly sensitive to both the reaction conditions and the substituents. A library of novel compounds has been exposed and explored, and where possible have been characterised by

multinuclear NMR spectroscopy and SCXRD. The structural complexity within these systems was supported by DFT calculations. Research was extended to the *N,N'*-diarylureas which highlighted that a number of factors influenced whether fused-ring or non-fused ring heterocycles were formed. In the case of electron-rich *N,N'*-diarylureas, isomerism between the two systems was observed.

A series of *ortho*-functionalised Ar_3PI_2 adducts have been prepared to investigate the effects of internal solvation on the donor strength of triaryl-phosphanes. The enhancement of donor strength for oxygen substituents was shown to occur by conjugation of the lone pairs through the aromatic system, and *via* internal solvation for the pendant nitrogen donors. This afforded the first neutral six-coordinate P^{III} species acting as a simultaneous Lewis acid and Lewis base. Nevertheless, the increased steric congestion about the phosphorus centre was shown to significantly oppose the increase in donor strength for these phosphanes. Crystallographic interrogation of the corresponding iodophosponium salts shows that the cationic complexes experience a greater influence of the steric bulk than their neutral precursors. The steric and electronic contributions to bonding have been analysed through computational studies to determine the factors governing the basicity of donor-functionalised phosphanes.

Table of Contents

Chapter 1 – Introduction	1
1.1 – Introduction to Radicals	2
1.2 – Introduction to Organic Materials	3
1.2.1 – Crystal Engineering	3
1.2.2 – Organic Magnets	3
1.3 – Introduction to Magnetism	4
1.3.1 – Molecular Bistability	7
1.4 – Introduction to Conductivity	7
1.4.1 – Conductivity in Organic Radicals	8
1.5 – Main-Group Radicals	9
1.5.1 – Nitrogen Radicals	9
1.5.2 – Nitrogen-Oxygen Radicals	10
1.5.3 – Sulfur-Nitrogen Radicals	11
1.5.4 – Selenium-Nitrogen Radicals	13
1.5.5 – Phosphorus-Centred Radicals	14
1.5.6 – Targeted Radicals	16
1.6 – Characterisation of Radicals	16
1.6.1 – Electron Paramagnetic Resonance Spectroscopy	17
1.6.1.1 – Background Theory	17
1.6.1.2 – The EPR Spectrum	20
1.6.2 – Electrochemical Studies	22
1.6.2.1 – Cyclic Voltammetry	22
1.7 – Conclusions	24
1.8 – References	26
Chapter 2 – 1,2,4-Benzothiadiazine 1-Chlorides	33
2.1 – Introduction to 1,2,4-Benzothiadiazines	34
2.2 – Introduction to 1,2,4-Benzothiadiazine 1-Chlorides	35
2.2.1 – Prior Synthesis of 1,2,4-Benzothiadiazines 1-Chlorides	36
2.2.1.1 – Route 1 – SCl ₂	36
2.2.1.2 – Route 2 – S ₂ Cl ₂	37
2.2.1.3 – Route 3 – SOCl ₂	37
2.3 – Synthesis of New Compounds	38
2.3.1 – Synthesis of Substituted <i>N</i> -Arylamidines	38

2.3.2 – Synthesis of Substituted 1,2,4-Benzothiadiazines 1-Chlorides	39
2.4 – Structural Studies of 1,2,4-Benzothiadiazine 1-Chlorides	43
2.4.1 – Crystal Structure of 2a	45
2.4.2 – Crystal Structure of 2b	45
2.4.3 – Crystal Structure of 2c	46
2.4.4 – Crystal Structure of 2d-α	46
2.4.5 – Crystal Structure of 2f	47
2.4.6 – Crystal Structure of 2g	48
2.4.7 – Crystal Structure of 2h	49
2.4.8 – Crystal Structure of [2j.H][HCl₂]	49
2.4.9 – Crystal Structure of 2k	50
2.4.10 – Crystal Structure of 2l	51
2.4.11 – Crystal Structure of 2s	51
2.4.12 – Crystal Structure of 2t	52
2.4.13 – Conformational Polymorphism	52
2.5 – Transformations of 1,2,4-Benzothiadiazine 1-Chlorides	53
2.5.1 – Anion Metathesis	53
2.5.2 – Hydrolysis	55
2.6 – <i>S</i> -Aryl 1,2,4-Benzothiadiazines	56
2.6.1 – Structural Studies of <i>S</i> -Aryl 1,2,4-Benzothiadiazines	57
2.6.1.1 – Crystal Structure of 6m	57
2.6.1.2 – Crystal Structural of 6n	58
2.6.2 – <i>N</i> -Methylation	58
2.7 – Conclusions	59
2.8 – Experimental	61
2.8.1 – Synthesis of Amidines	61
2.8.2 – Synthesis of 1,2,4-Benzothiadiazine 1-Chlorides	65
2.8.3 – Synthesis of S ^{IV} Cations	68
2.8.4 – Synthesis of 1,2,4-Benzothiadiazine 1-Oxides	68
2.8.5 – Synthesis of <i>S</i> -Aryl 1,2,4-Benzothiadiazines	68
2.9 – References	70
Chapter 3 – 1,2,4-Benzothiadiazinyl Radicals	73
3.1 – Introduction	74
3.2 – 1,2,4-Benzothiadiazinyl Radicals	74
3.2.1 – Radical Generation <i>via</i> Oxidation	75

3.2.2 – Radical Generation <i>via</i> Reduction	75
3.2.3 – Radical Generation <i>via</i> Comproportionation	76
3.3 – Electrochemical Studies	76
3.3.1 – Cyclic Voltammetry Results	77
3.3.2 – Computational Studies of the Redox Process	82
3.4 – Synthesis and Isolation of 1,2,4-Benzothiadiazinyl Radicals	83
3.5 – Structural Studies of 1,2,4-Benzothiadiazinyl Radicals	84
3.5.1 – Crystal Structure of 3a	85
3.5.2 – Crystal Structure of 3c	86
3.5.3 – Crystal Structure of 3e	88
3.5.4 – Comparison of Solid-State Structures	89
3.6 – Electron Paramagnetic Resonance	91
3.6.1 – EPR Results	92
3.6.2 – Computational Studies	98
3.7 – Magnetic Studies	99
3.7.1 – SQUID Results	99
3.7.2 – Magnetic Exchange Interactions	104
3.8 – Conclusions	108
3.9 – Future Work	109
3.10 – Experimental	110
3.10.1 – Synthesis of 1,2,4-Benzothiadiazinyl Radicals	110
3.10.2 – Computational Methods	111
3.11 – References	112
Chapter 4 – 1,2,4-Benzophosphadiazines	115
4.1 – Introduction to Fused-Ring Phosphorus-Nitrogen Heterocycles	116
4.1.1 – An Overview of 1,2,4-Benzophosphadiazines	116
4.2 – Attempted Syntheses of 1,2,4-Benzophosphadiazines	118
4.2.1 – Initial Studies with P ^V Sources	118
4.2.2 – Initial Studies with P ^{III} Sources	120
4.3 – <i>N,N</i> -Substituted Amidines	121
4.3.1 – Synthesis of <i>N,N</i> -Substituted Amidines	121
4.3.2 – Reactions with PhPCl ₂	121
4.4 – Electron-Rich Aromatics	123
4.4.1 – Initial Studies with Electron-Rich <i>N,N'</i> -Diarylureas	124
4.4.2 – Electron-Rich <i>N</i> -Arylamidines	126

4.4.2.1 – Synthesis of Electron-Rich <i>N</i> -Arylamidines	126
4.4.2.2 – Synthesis of 1,2,4-Benzophosphadiazines	126
4.4.2.3 – Crystal Structure of 19r.HCl	128
4.5 – Electron-Neutral Aromatics	130
4.6 – Functionalisation of 1,2,4-Benzophosphadiazines	132
4.6.1 – Deprotonation	132
4.6.2 – Oxidation	134
4.6.3 – <i>N</i> -Functionalisation	136
4.6.3.1 – <i>N</i> -Methylation	136
4.6.3.2 – <i>N</i> -Phosphination	138
4.6.4 – One Electron Oxidation	139
4.7 – Conclusions	140
4.8 – Future Work	140
4.9 – Experimental	142
4.9.1 – Synthesis of <i>N</i> -Arylamidines	142
4.9.2 - Synthesis of <i>N,N'</i> - and <i>N,N'</i> -Substituted Arylamidines	142
4.9.3 - Synthesis of <i>N'</i> -Phosphanyl- <i>N</i> -Arylamidines	144
4.9.4 – Synthesis of <i>N,N'</i> -Diarylureas	145
4.9.5 – Synthesis of 1,2,4-Benzophosphadiazines	146
4.10 – References	149
Chapter 5 – Structural Complexity in Phosphorus-Nitrogen Heterocycles	151
5.1 – A Brief Introduction to Phosphorus-Nitrogen Heterocycles	152
5.1.1 – Cyclophosph(III)azines	152
5.1.2 – Cyclophosph(V)azanes	154
5.1.3 – Urea-Ligated Phosphorus Heterocycles	154
5.1.4 – Phosphorus-Amidinate Chemistry	156
5.2 – Reactions of <i>N</i> -Arylamidines with PhPCl ₂	158
5.2.1 – <i>N</i> -Phenylbenzamidine	158
5.2.2 – <i>N</i> -3-Dimethylaminophenyl-benzamidine	160
5.2.3 – <i>N</i> -3-Methoxyphenyl-benzamidine	164
5.2.4 – <i>N</i> -4-Chlorophenyl-benzamidine	167
5.2.5 – <i>N</i> -2,6-Diisopropylphenyl-benzamidine	168
5.2.6 – <i>N</i> - <i>tert</i> -Butyl-benzamidine	168
5.2.7 – The Influence of Base	169
5.3 – Reactions of <i>N</i> -Arylamidines with NiPr ₂ PCl ₂	173

5.4 – Reactions of <i>N</i> -Arylamidines with Phosphorus Trihalides	174
5.4.1 – Phosphorus Trichloride	174
5.4.2 – Phosphorus Tribromide	175
5.4.3 – Phosphorus Triiodide	183
5.5 – Transformations of Phosphorus-Amidine Heterocycles	184
5.5.1 – Thermal Rearrangement	184
5.5.2 – Methylation	187
5.5.3 – One Electron Oxidation	189
5.6 – Reactions of <i>N,N'</i> -Diarylureas with Chlorophosphines	190
5.6.1 – Electron-Poor <i>N,N'</i> -Diarylureas	190
5.6.2 – Poorly Electrophilic Chlorophosphines	192
5.6.3 – Base Strength	193
5.6.4 – Phosphorus Trichloride	195
5.7 – Conclusions	197
5.8 – Future Work	198
5.9 – Experimental	199
5.9.1 – Synthesis of <i>N</i> -Arylamidines	199
5.9.2 – Synthesis of Phosphorus-Amidine Heterocycles	200
5.9.3 – Synthesis of <i>N,N'</i> -Diarylureas	202
5.9.4 – Synthesis of Phosphorus-Urea Heterocycles	202
5.10 – References	205
Chapter 6 – Donor-Functionalised Diiodophosphoranes	208
6.1 – Introduction	209
6.1.1 – A Brief Introduction to Main-Group Lewis Acids	209
6.1.2 – Introduction to Diiodophosphoranes	209
6.2 – Target Molecules	211
6.3 – Structural Studies of Donor-Functionalised Diiodophosphoranes	212
6.3.1 – Crystal Structure of 34a	213
6.3.2 – Crystal Structure of 34b	215
6.3.3 – Crystal Structure of 34c	216
6.3.4 – Crystal Structure of 34d	218
6.3.5 – Crystal Structure of 34e	219
6.4 – Synthesis and Structural Studies of Iodophosponium Salts	221
6.4.1 – Initial Synthesis	221
6.4.2 – Structural Studies	223

6.4.2.1 – Crystal Structure of [35a]BAr ^F	224
6.4.2.2 – Crystal Structure of [35b]BAr ^F	224
6.4.2.3 – Crystal Structure of [35d]BAr ^F	225
6.4.2.4 – Crystal Structure of [35g]BAr ^F	226
6.4.2.5 – Crystal Structure of [35d]I ₃	227
6.4.2.6 – Crystal Structure of [35e]I ₃	227
6.4.2.7 – Polymorphism in Ar ₃ PI ₄ Systems	228
6.5 – Computational Studies	229
6.5.1 – Bonding and Lewis Basicity of Functionalised Phosphanes	229
6.5.2 – Diiodophosphanes	232
6.5.3 – Iodophosponium Salts	233
6.5.4 – Summary of Computational Results	234
6.6 – Conclusions	235
6.7 – Experimental	236
6.7.1 – Synthesis of Aryl-Lithiums	236
6.7.2 – Synthesis of Donor-Functionalised Phosphanes	236
6.7.3 – Synthesis of Diiodophosphanes	238
6.7.4 – Synthesis of Iodophosponium Salts	239
6.8 – References	243
Supplementary Chapter 1 – Crystal Structures of <i>N</i>-Arylamidines	247
S1.1 – A Very Brief Introduction to Amidines	248
S1.2 – Monosubstituted Amidines	248
S1.3 – Structural Studies of Monosubstituted <i>N</i> -Arylamidines	249
S1.3.1 – Crystal Structure of 1a	252
S1.3.2 – Crystal Structure of 1b	253
S1.3.3 – Crystal Structure of 1c	254
S1.3.4 – Crystal Structure of 1d	255
S1.3.5 – Crystal Structure of 1e	256
S1.3.6 – Crystal Structure of 1f	257
S1.3.7 – Crystal Structure of 1g	258
S1.3.8 – Crystal Structure of 1h	259
S1.3.9 – Crystal Structure of 1i	260
S1.3.10 – Crystal Structure of 1j	261
S1.3.11 – Crystal Structure of 1k	262
S1.3.12 – Crystal Structure of 1l	263

S1.3.13 – Crystal Structure of 1m	265
S1.3.14 – Crystal Structure of 1n	266
S1.3.15 – Crystal Structure of 1o	267
S1.3.16 – Crystal Structure of 1p	268
S1.3.17 – Crystal Structure of 1r	269
S1.3.18 – Crystal Structure of 1t	270
S1.3.19 – Crystal Structure of 1u	271
S1.3.20 – Crystal Structure of 1'a	272
S1.4 – <i>N,N'</i> - and <i>N,N</i> -Substituted Amidines	273
S1.4.1 – Structural Studies	273
S1.4.2 – Crystal Structure of 11a	274
S1.4.3 – Crystal Structure of 12a	275
S1.4.4 – Crystal Structure of 13a	277
S1.5 – Conclusions	278
S1.6 – References	280
Appendix 1 – General Experimental	281
A1.1 – Starting Materials	282
A1.2 – Drying of Solvents	282
A1.3 – Air and Moisture Sensitive Techniques	282
A1.4 – NMR Spectroscopy	282
A1.5 – Single-Crystal X-Ray Diffraction	283
A1.6 – Cyclic Voltammetry	283
A1.7 – EPR Spectroscopy	283
A1.8 – SQUID Magnetometry	283
A1.9 – Elemental Analysis	284
A1.10 - References	284
Appendix 2 – Computational Details	285
A2.1 – 1,2,4-Benzothiadiazinyl Radicals	286
A2.1.1 – Electronic and EPR Studies	286
A2.1.1.1 – Example Input Files	286
A2.1.2 – Magnetic Exchange Interactions	287
A2.1.2.1 – Method and Example Input Files	287
A2.2 – Phosphorus-Nitrogen Heterocycles	290
A2.2.1 – Geometry Optimisations	290

A2.2.1.1 – Example Input Files	291
A2.2.2 – NICS Calculations	292
A2.2.2.1 – Example Input Files	293
A2.3 – Donor-Functionalised Diiodophosphoranes	294
A2.3.1 – Geometry Optimisations	294
A2.3.1.1 – Example Input Files	294
A2.4 – Cartesian Coordinates for Optimised Geometries	295
A2.5 – References	364
Appendix 3 – Crystallographic Data Tables	365
Appendix 4 – Miscellaneous Supplementary Data	392
A4.1 – Cyclic Voltammograms	393
A4.2 – Buried Volume Maps	394

Chapter 1

Introduction

“Put that cookie down! NOW!”

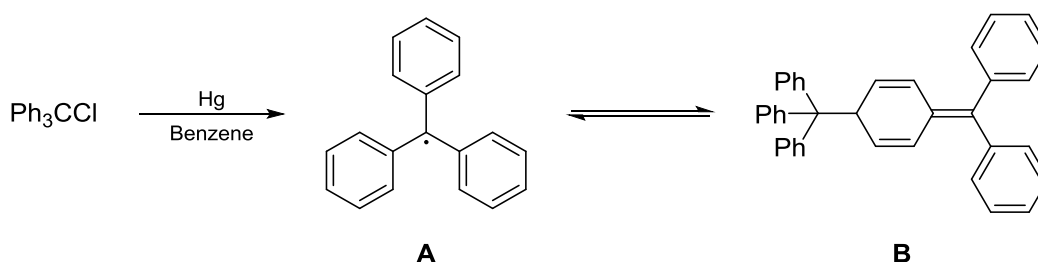
Jingle All The Way (1996)

1.1 – Introduction to Radicals

A radical is defined as a molecular entity possessing an unpaired electron.¹ Compounds with open-shell configurations are readily found for the metallic elements, where the core-like nature of the *d* or *f* orbitals stabilises them and hinders reaction. In contrast, open-shell organic compounds are typically highly reactive and unstable species. The notion that radicals can therefore be stable or persistent is still news to much of the chemical community, despite the fact that some species were synthesised over 150 years ago.² It is now well established however that certain kinds of molecular architectures can provide a versatile template to support stability in open-shell organic compounds.³

A stable radical is pragmatically defined as one that can be isolated and handled as a pure compound, whilst persistent radicals are only sufficiently long-lived to be observed by spectroscopic methods.⁴ Kinetic stability may be achieved by steric protection through incorporation of bulky substituents around the radical centre,⁵ whilst thermodynamic stability is achieved by electronic means, by lowering the energy of the singly occupied molecular orbital (SOMO), and inducing delocalisation of the unpaired electron. Many stable radicals employ a combination of these factors, and are typically heteroatom based since these are effective carriers of spin density.³

Earlier interest in stable radicals arose from their status as “novelty acts”, and explored the fundamental structure and bonding within these open-shell compounds. Gomberg’s landmark discovery of the triphenylmethyl radical **A** in 1900⁶ marked the discovery of organic free radical chemistry (Scheme 1.1.1). These radicals are best described as persistent since they exist in equilibrium with the dimeric species **B** and are not isolable. The tendency to dimerise however can be attenuated through substituent effects; *para*-nitro substitution on all three aryl rings renders these species monomeric in the solid-state,⁷ whilst the perchlorinated analogues are essentially chemically inert.⁸



Scheme 1.1.1: Synthesis and dimerisation of the triphenylmethyl radical.

Although significant research is still focused on the synthesis of novel stable radicals,⁹ many areas of chemistry take advantage of the properties afforded by the combination of an open-shell configuration and stability. Radicals have been employed as spin labels¹⁰ and spin traps^{11,12} to obtain structural, dynamic, and reactivity information on short-lived radical species using electron paramagnetic resonance (EPR) spectroscopy. There have also been widespread efforts into the development of new materials exhibiting properties such as magnetism and conductivity, for which stable radicals are promising candidates by virtue of containing unpaired electrons.¹³ Interest in organic materials stems from their versatility and ease of modification, as well as their unique properties which are not obtainable in conventional metal-based materials.

1.2 – Introduction to Organic Materials

Organic materials, such as synthetic polymers and fibres, play an important role in everyday life. More recently, interest has focused on organic materials which possess unusual properties including magnetism¹⁴ and conductivity.¹⁵ These properties are more commonly associated with metals and their oxides, and originate from the solid-state structure of the materials. Tailored organic syntheses should therefore provide an opportunity to control the solid-state structure, and hence the properties of organic materials.¹⁶

1.2.1 – Crystal Engineering

Crystal engineering is defined as “the understanding of intermolecular interactions in the context of crystal packing and the utilisation of such understanding in the design of new solids with desired physical and chemical properties.”¹⁷ The spatial arrangement of molecules in the solid-state is a result of many delicate non-covalent interactions of varying strength and directionality.¹⁸ Although many of these intermolecular interactions, termed *supramolecular synthons*,¹⁹ are well understood and established, the subtle balance between them is often difficult to control which means that the prediction of the crystal structure and design of tailored materials remains challenging.

1.2.2 – Organic Magnets

Magnetic materials have extraordinary technological importance with ubiquitous uses and applications in daily life. The majority of these materials however are based on metals ions and their oxides, and are often fabricated *via* energy intensive metallurgical methods as well as utilising elements in limited supply.²⁰ A great deal of research has therefore focused on the development of organic materials exhibiting magnetic properties.

Organic magnets may offer several advantages over typical metal-based materials, including solubility and flexibility, which may allow for alternative processing strategies.²¹ In addition, unique properties may be coupled to develop multifunctional “smart materials” in which the magnetism is modified by the action of external stimuli such as heat, light, or pressure.²² The opportunity to tailor these compounds at the molecular level through standard synthetic techniques ultimately offers the potential to design custom magnets for any given application.

Control of the solid-state structure of stable radicals should, in principle, give rise to paramagnetic materials in which magnetic communication between localised radical centres may lead to magnetic ordering at some finite temperature. Many radicals however have a tendency to dimerise in the solid-state, rendering the system diamagnetic. Significant efforts have therefore been directed at attempting to overcome this dimerisation, either by structural modification or co-crystallisation.²³

One major disadvantage of organic magnets, however, is that they have inherently larger molecular weights per magnetic moment compared to a metal-based material; most organic radicals are constructed with a single unpaired electron ($S = \frac{1}{2}$) with additional organic structural support to stabilise the radical. This typically results in significant separation of the spins and weaker exchange energies, ultimately leading to lower magnetic ordering temperatures. The major challenge in the field of organic magnetism is therefore to construct materials with higher magnetic ordering temperatures.

1.3 – Introduction to Magnetism

The phenomenon of magnetism arises from the presence of unpaired electrons and is therefore associated with d and f block metals and radicals (*i.e.* $S \neq 0$). Electrons possess a property called spin characterised by an intrinsic angular momentum which, from a classical perspective, generates a magnetic dipole moment. The net magnetic moment of a sample is therefore comprised of all the spins within the sample. Paired electrons give rise to a small magnetic moment opposing the direction of an applied magnetic field. This behaviour, known as diamagnetism, leads to a repulsive interaction and is exhibited by all substances.²⁴ This is a minor effect however and is often negligible compared to the other forms of magnetism associated with open-shell compounds.²⁵

Paramagnetism is the simplest form of magnetic behaviour and is observed in compounds with unpaired electrons. In the absence of an external magnetic field, the

non-interacting spins are randomly orientated due to thermal motion (Figure 1.3.1). In the presence of an applied magnetic field, the spins align in the direction of the applied field, resulting in an attractive interaction and increase in magnetisation. For *Curie*-type paramagnetism, which is observed in systems with localised unpaired electrons, the magnetisation has inverse temperature dependence. In contrast, *Pauli* paramagnetism, which is attributable to the itinerant electrons that promote metallic conductivity, is independent of temperature. Both *Pauli* and *Curie*-type paramagnetism are independent of the applied magnetic field strength.

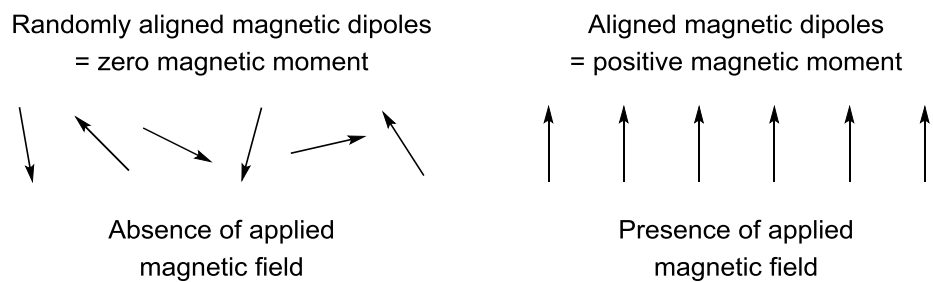


Figure 1.3.1: A simple model for paramagnetism.

Short-range interactions between the magnetic dipole moments of the unpaired spins can lead to magnetic ordering that is dependent on the strength of the applied magnetic field. Interactions which favour a parallel alignment of spins are described as ferromagnetic, whilst interactions favouring an anti-parallel alignment of spins are referred to as antiferromagnetic (Figure 1.3.2). If these interactions propagate throughout the solid-state structure then bulk (*i.e.* long-range) magnetic order can arise. The interactions are associated with an energy-gain resulting from occupying a lower energy state, and vary significantly in strength from system to system, and ultimately dictates the temperature at which magnetic ordering is observed.

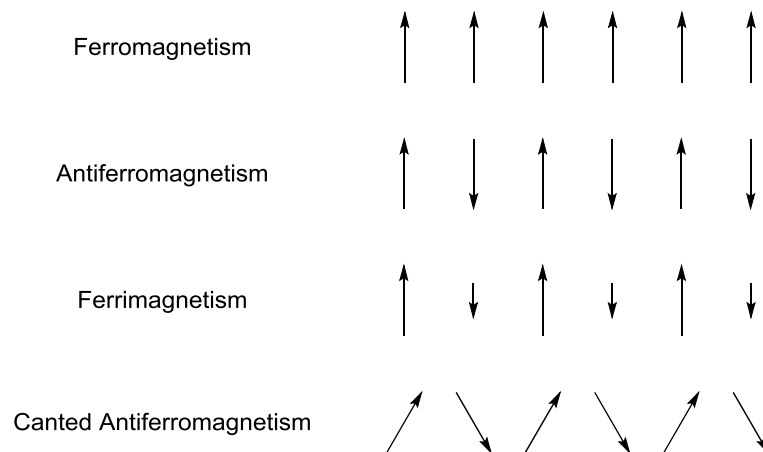


Figure 1.3.2: Types of magnetic ordering.

Ferromagnetism is a form of cooperative magnetism arising from concerted long-range order resulting from the parallel alignment of spins. The temperature at which the bulk magnetism of a solid switches from paramagnetic to ferromagnetic is known as the *Curie* temperature, T_c . The spontaneous ordering of the magnetic dipoles below T_c leads to a sudden and large increase in the magnetic susceptibility. In *soft* ferromagnetic materials, the magnetisation becomes zero when the applied magnetic field is removed. In contrast, *hard* ferromagnets display *hysteresis* and retain their magnetisation when the applied magnetic field is removed. This *remanent* magnetism is a familiar property associated with permanent magnets. Ferromagnetic materials may be demagnetised by heating above its *Curie* temperature (*e.g.* 1043 K for Fe).²⁶

Antiferromagnetism occurs when long-range magnetic order results from the antiparallel alignment of spins. The temperature at which the bulk magnetism of a solid switches from paramagnetic to antiferromagnetic is known as the *Néel* temperature, T_N . The spontaneous ordering of the magnetic dipoles leads to a net zero magnetic moment and sudden decrease in the magnetic susceptibility below T_N . At temperatures above T_N , the antiparallel alignment of adjacent magnetic dipoles is disrupted by thermal fluctuations.

Ferrimagnetism is observed in systems containing non-equivalent sub-lattices where the antiparallel alignment of spins between sub-lattices is of a different magnitude – *i.e.* the antiferromagnetic coupling is the dominant interaction. This gives rise to a net magnetic moment that is smaller in magnitude than the potential moment caused by the parallel alignment of all spins in the two sub-lattices. Canted antiferromagnetism is observed for systems with non-perfect co-parallel alignment of adjacent spins, and leads to a non-zero magnetic moment at absolute zero. This is commonly associated with low symmetry materials and arises through a competitive combination of isotropic and antisymmetric exchange interactions.²⁷

The nature of the interactions between spins is largely dominated by the solid-state structure of the compound. For molecular systems, the magnetic communication between spins on neighbouring molecules can arise either by direct overlap of the singly occupied molecular orbitals (SOMO), known as *direct exchange*, or through magnetically innocent atoms or functional groups, known as *superexchange*. The magnitude of the exchange interaction is therefore dependant on the distance between adjacent spins and the degree of orbital overlap. In both mechanisms, the orientation of the SOMOs will determine whether the interactions are ferro- or antiferromagnetic.

1.3.1 – Molecular Bistability

Molecular materials whose physical properties can be altered by external stimuli such as heat, light, or pressure, may find applications in the development of electronic switching and memory storage devices.^{16,28} Molecular bistability, defined as “the ability of a molecular system to be observed in two different electronic states in a certain range of external perturbation”,²⁹ is most commonly associated with transition metal-based spin-crossover materials.³⁰ The spin-crossover (SCO) phenomenon, first reported in 1931,^{31,32} is observed in octahedral $3d^n$ metal centres ($n = 4-7$) which can exist in either a high-spin or low-spin state depending on the relative ligand field strength and pairing energies. The low-spin state is enthalpically favoured whilst the high-spin state is entropically favoured, and SCO occurs when a perturbation causes a switch in the two spin-states.³⁰

The properties of organic radicals have also been shown to be perturbed by the influence of external stimuli²² and therefore show promise for the construction of molecular materials. Several sulfur-nitrogen radicals have been shown to exist as π -dimers ($S = 0$) at low temperatures and undergo a phase transition to monomeric π -stacked radicals ($S = \frac{1}{2}$) on heating.³³⁻³⁷ In some cases, the temperature of the dimer-to-monomer and monomer-to-dimer transitions differ leading to hysteresis³⁶⁻³⁹ and a well-defined region of magnetic bistability wherein the two states can exist.⁴²

1.4 – Introduction to Conductivity

Electronic conductivity arises due to the flow of electrons through a solid. The central aspect that determines the electrical properties is therefore the distribution and mobility of electrons. Electrons are assumed to occupy bands formed through the overlap of crystal orbitals that are delocalised throughout the solid. The lowest energy orbital is therefore fully bonding whilst the highest energy orbital is fully antibonding.⁴³ The band arising from the occupied orbitals is known as the valence band whilst the conduction band is populated by empty orbitals. The energy distribution of the orbitals is known as the *density of states*, and the highest available electron energy level at absolute zero is known as the *Fermi level*.⁴⁴

In a metallic conductor (**i** – Figure 1.4.1), the crystal orbitals form a continuous band with a non-zero density of states at the *Fermi level* (*i.e.* the highest occupied molecular orbital). In contrast, an insulator has a full valence band and empty conduction band (**v**), with a large band gap such that there are no thermally accessible states to allow for the conduction. Semiconductors are materials with a small band gap (**ii**), allowing

electrons to be promoted into the conduction band when the temperature is raised. This promotion of electrons results in positively charged *holes* in the valence band. The conductivity of semiconductors can be modulated through the introduction of charge carriers, known as *dopants*, moving the *Fermi* level to a position with a higher density of states. The introduction of dopants carrying excess electrons is known as *n*-type doping; these additional electrons occupy otherwise empty states in the conduction band (**iii**). The introduction of dopants that withdraw electrons from the filled valence band is known as *p*-type doping; this generates *holes* which allow the remaining electrons to move (**iv**).

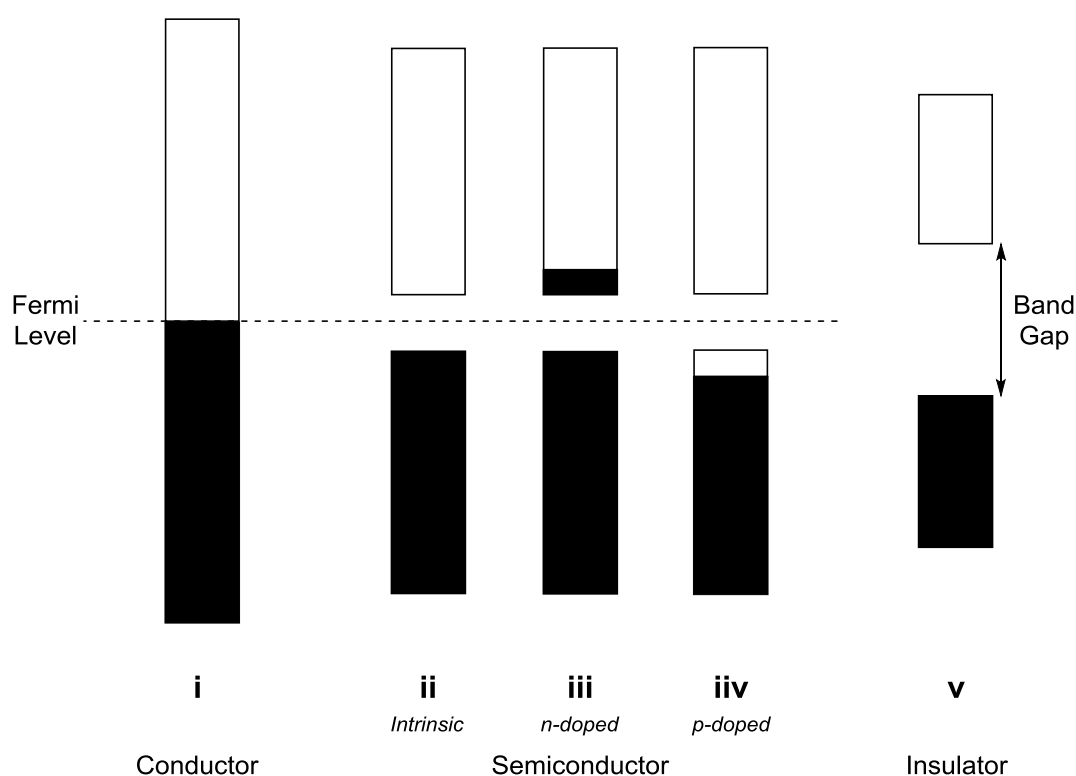


Figure 1.4.1: Band structures in conductors, semiconductors and insulators.

1.4.1 - Conductivity in Organic Radicals

The idea that neutral radicals could serve as building blocks in the construction of organic conductors was first proposed in 1975.⁴⁵ One of the consequences of having a regular band formed from half-filled orbitals (*i.e.* the SOMOs) is that the band must be half filled, resulting in a non-zero density of states at the *Fermi* level, akin to a metallic conductor, with the unpaired electron acting as a carrier of charge.

Despite the simplistic model, isolation of crystalline radicals which exhibit metallic conductivity has proven to be challenging, and a number of factors must be addressed.^{16,46} The primary issue faced with organic radicals is their tendency to form *S*

= 0 dimers in the solid-state.^{3,13} For many planar radicals, this dimerisation leads to arrays of distorted 1D π -stacks of alternating short and long contacts between molecules, known as *Peierls* distorted stacks.⁴⁴ This leads to an opening of the band gap at the *Fermi* level as the valence band becomes full, leading to an insulating state. When the dimerisation is overcome however, typically by steric protection, there is an intrinsically large *Coulombic* barrier to intermolecular charge transfer, U (*i.e.* the energy required for the transfer of an electron from one molecule to another). Additionally, suppression of the dimerisation inherently leads to a weakening of intermolecular interactions, resulting in poor SOMO overlap and a low electronic bandwidth, W . If the bandwidth is greater than the *Coulomb* repulsion ($W > U$) then a metallic state prevails, whilst an insulating state exists for systems where the unpaired electron is localised such that $W < U$.⁴⁷ Delocalisation of the unpaired electron and incorporation of heavy heteroatoms with more diffuse valence orbitals, has been shown to dramatically increase the bandwidth and lower the *Coulombic* barrier, resulting in improved conductivity in neutral radicals.^{48,49}

1.5 – Main-Group Radicals

The chemistry of stable radicals is dominated by heterocyclic open-shell compounds, and these are primarily synthesised for the development of organic materials exhibiting magnetic or conducting properties. The magnetic properties of carbon-centred radicals has received considerably less attention; phenalenyl and related radicals typically form diamagnetic π -dimers,⁵⁰ whilst the incorporation of bulky substituents to provide steric protection in triarylmethyl-type radicals prevents SOMO overlap and magnetic communication between radical centres. The latter factor can however be overcome by synthesising polyradicals in which the intramolecular magnetic ordering of the unpaired electrons occur through conjugated π -bonds.⁵¹ The following sections will highlight a few major classes of main-group (*i.e.* non-carbon centred) radicals, and focus on heterocyclic systems whose magnetic properties have been studied.

1.5.1 – Nitrogen Radicals

Many simple aminyl radicals [$R_2N\cdot$] are short-lived species, and rapidly dimerise to form hydrazines or undergo other radical degradation pathways.⁵² The incorporation of aminyl radicals into cyclic, π -conjugated frameworks to give phenazinyls such as **C** and **D** leads to significantly enhanced stability (Figure 1.5.1.1).^{53,54} Most stable phenazinyls are monomeric in solution at room temperature but form π -stacked dimers in the solid state.

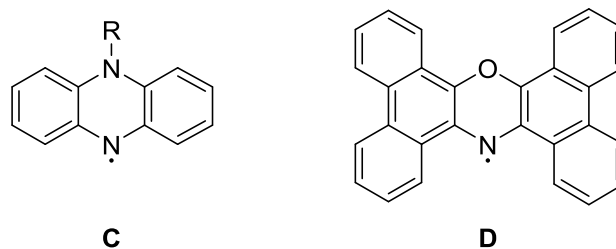


Figure 1.5.1.1: Phenazinyl radicals.

Hydrazyl radicals [R_2NNR'] are generally persistent and short-lived species, although the DPPH radical **E** (Figure 1.5.1.2) is well established as a stable radical and a common EPR reference compound.⁵⁵ Constraining the hydrazyl moiety into cyclic structures optimises the π orbital overlap between the heteroatoms, leading to stable radicals such as the 1,2,4-benzotriazinyl radicals **F**. Many derivatives of this family of radical, also known as Blatter radicals,⁵⁶ have exhibited relatively strong antiferromagnetic or ferromagnetic interactions in the solid state depending on the choice of substituents.⁵⁷⁻⁶² Verdadyl radicals **G** are another class of resonance-delocalised hydrazyls that are incredibly stable to both air and water without the need for sterically bulk substituents.^{63,64} This versatile class of radicals have been used as chelating radical ligands in the *metal-radical*⁶⁵ approach to form complexes and extended chains with interesting magnetic behaviour.⁶⁶⁻⁶⁸

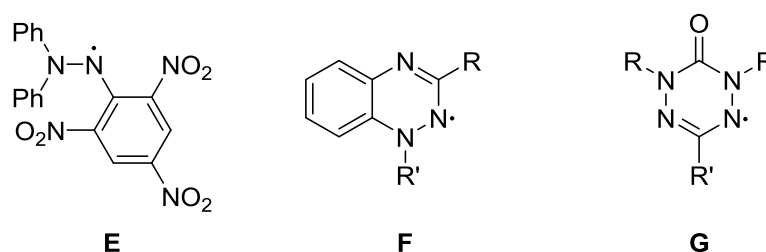


Figure 1.5.1.2: Hydrazyl, 1,2,4-benzotriazinyl and verdazyl radicals.

1.5.2 – Nitrogen-Oxygen Radicals

Nitroxides [$R_2NO\cdot$] are perhaps the most well-known family of stable radicals, and are the subject of many books and reviews.^{55,69,70} The stability of nitroxide radicals is attributed to a dipolar resonance contribution, with the unpaired electron occupying the N-O π^* orbital. Due to this remarkable stability, nitroxides such as the TEMPO⁷¹ radical **H** (Figure 1.5.2.1) have found use as mild, catalytic oxidising agents,⁷² and in applications such as spin-labelling.⁷³ The α -nitronyl nitroxide radical **I**, discovered in 1991, was the first organic compound to exhibit bulk ferromagnetism ($T_c = 0.65$ K).⁷⁴ The extremely low magnetic ordering temperatures of nitroxides are a consequence of

the long intermolecular contacts between radical centres stemming from the addition of bulky substituents, which disfavour the N-O...O-N interaction.

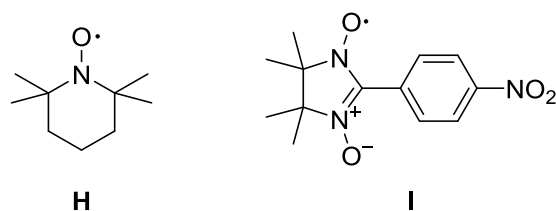


Figure 1.5.2.1: Nitroxide radicals.

1.5.3 – Sulfur-Nitrogen Radicals

Demarçay reported the first sulfur-nitrogen radical **J** (Figure 1.5.3.1) in 1880,² some 20 years prior to Gomberg's triphenylmethyl radical.⁶ Substitution about the heterocyclic ring with isoelectronic C-R groups reveals many potential isomers of which the 1,2,3,5-dithiadiazolyl (DTDA) **K** and 1,3,2-dithiazolyl (DTA) **L** radicals have been extensively studied due to their facile synthesis and stability.¹³

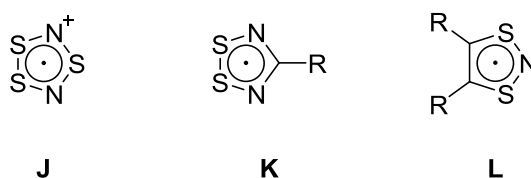


Figure 1.5.3.1: Five-membered sulfur-nitrogen radicals.

DTDA radicals were amongst the first major class of heterocyclic sulfur-nitrogen radicals to be investigated.⁷⁵ The radicals typically exist in a monomer-dimer equilibrium in solution, and many early derivatives adopt π -dimeric structures in the solid state. The choice of substituent heavily influences the dimer configuration but has little effect on the electronic properties of the radical, since the SOMO has a nodal plane at the heterocyclic carbon. Several monomeric DTDA radicals have been prepared by the introduction of fluorinated phenyl substituents.⁷⁶⁻⁷⁹ Subtle molecular modifications can have a significant consequence on the solid-state structure, and hence the magnetic properties. For example, the β -phase of **M1** (Figure 1.5.3.2) exhibits bulk magnetic ordering as a spin-canted antiferromagnet below 36 K,⁷⁷ whilst **M2** orders as a bulk ferromagnet below 1.3 K.⁷⁹ The application of pressure has been found to dramatically increase the magnetic ordering temperatures for both compounds.⁸⁰

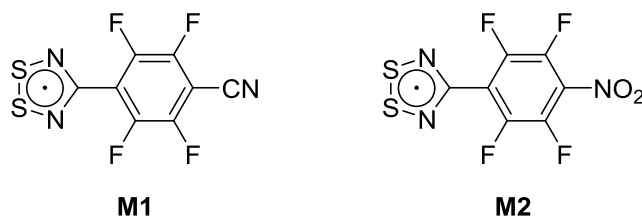


Figure 1.5.3.2: Fluorinated DTDA radicals.

Many DTA radicals are monomeric in the solid-state, with several examples co-existing in both the monomeric and dimeric form.³ Only one neutral derivative, the benzo-fused 1,3,2-dithiazolyl (BDTA)⁸¹ **N** (Figure 1.5.3.3), has been found to undergo bulk magnetic ordering and exhibits a phase transition to an antiferromagnetic state below 11 K. The benzo-*bis*-1,3,2-dithiazolyl diradicals (BBDTA) are also known but form spin-paired dimers in the solid-state.⁸² Radical-cation salts of BBDTA have been investigated in some detail.^{3,13} The tetrachlorogallate salt **O1** orders as a ferromagnet at 6.7 K,⁸³ whilst other non-solvated crystalline phases have been reported as diamagnetic π^* - π^* dimers.⁸⁴ Replacement of the anion with the paramagnetic tetrachloroferrate results in anion \cdots cation magnetic exchange interactions, and leads to a ferrimagnetic phase below 44 K.⁸⁵

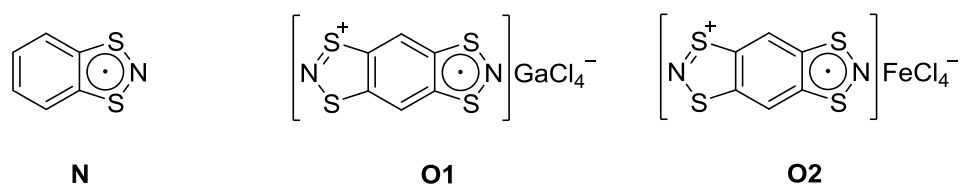


Figure 1.5.3.3: Benzo-fused DTA radicals.

Sulfur-nitrogen radicals which are not derived from compounds isoelectronic to **J**, namely thioaminyl radicals [RSNR' \cdot], have also been extensively studied but require bulky substituents (*e.g.* **P** - Figure 1.5.3.4) to be stable and isolable.^{86,87} Cyclic and fused-ring thioaminyls such as **Q** and **R** are generally only persistent at low temperatures, although some perhalogenated derivatives are sufficiently stable to be isolated.⁸⁸⁻⁹⁰

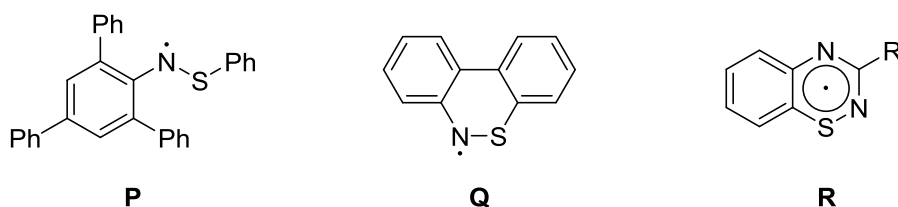


Figure 1.5.3.4: Thioaminyl radicals.

The 1,2,4-benzothiadiazinyl (BTDA) radicals of type **R** are a potentially versatile class of compound as they allow facile alteration of the substituents about the fused-ring and

of the pendant R group. Nevertheless, these have received considerably less attention than the DTDA and DTA based radicals, and very few examples have been reported.^{90,91} More recent work by Oakley into the related, resonance delocalised *bis*-benzothiadiazinyl radicals **S** (Figure 1.5.3.5) has shown these species to be remarkably stable and monomeric in the solid-state.^{92,93} The choice of substituent was found to dramatically alter the magnetic properties, with **S1** exhibiting paramagnetic behaviour whilst susceptibility measurements of **S2** indicated a strongly antiferromagnetically coupled system.⁹³ Subtle substituents affects have also been observed in the hybrid BTDA-DTA radicals **T**.⁹⁴

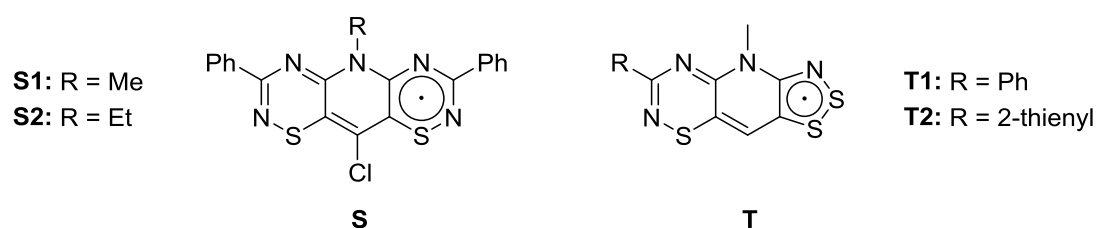


Figure 1.5.3.4: Resonance stabilised BTDA radicals.

1.5.4 – Selenium-Nitrogen Radicals

The replacement of sulfur with selenium into heterocyclic radicals affords the heavier congeners which often exhibit enhanced conducting and magnetic properties due to increased SOMO overlap.^{49,95,96} A family of isostructural radicals **U** (Figure 1.5.4.1) based on 1,2,3-dithiazolyls has been successfully isolated and characterised, and allowed for a direct comparison of the effect of selenium incorporation on the physical properties.⁹⁶ Like many selenazyl radicals, these species were found to form Se-Se σ -bonded dimers in the solid state,^{97–100} however careful choice of substituents afforded the desired monomeric species. The incorporation of heavy heteroatoms was shown to enhance the magnetic properties; **U4a** and **U3a** behave as spin-canted antiferromagnets with ordering temperatures of 27 K and 18 K respectively, whilst **U4b** and **U2b** exhibit bulk ferromagnetic order at 17.0 K and 12.8 K respectively.^{101,102}

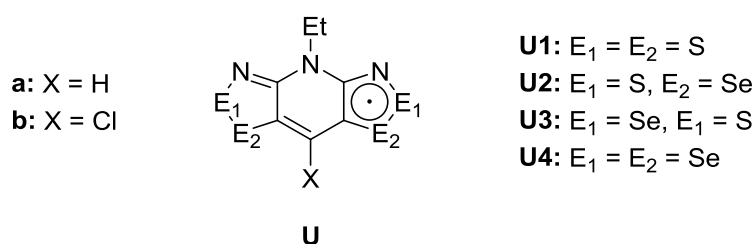


Figure 1.5.4.1: Selenium-nitrogen radicals derived from 1,2,3-dithiazolyls.

1.5.5 – Phosphorus-Centred Radicals

The involvement of phosphorus-centred radicals in many organic reactions has been recognised and investigated for many years,¹⁰³⁻¹⁰⁵ and was directly observed *via* EPR spectroscopy in 1969.¹⁰⁶ The phosphinyl species $[R_2P\cdot]$ ($R = N(SiMe_3)_2$ or $CH(SiMe_3)_2$) were amongst the first class of persistent phosphorus-centred radicals to be studied, and were generated by photolysis of the parent R_2PCl species in the presence of an electron-rich olefin.¹⁰⁷ Many other persistent sterically encumbered phosphinyl radicals (**V** – Figure 1.5.5.1) can also be prepared by reduction of the corresponding halophosphine with an alkali metal.¹⁰⁸ These radicals dimerise in the solid-state to give constrained diphosphines $[R_2P-PR_2]$, but dissociate into monomeric radicals in solution and in the gas-phase, which has led to their description as “Jack-in-the-box” compounds.^{109,110} The P-P bond dissociation process has been thoroughly examined for a number of species including cyclic and acyclic tetra-amino-diphosphines.^{111,112}

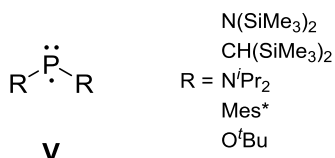


Figure 1.5.5.1: Persistent phosphinyl radicals.

There has been a growing interest in the study of persistent and stable phosphorus radicals since this time, and several neutral two-coordinate species have been isolated. Nitridovanadium metalloligands¹¹³ **V1** (Figure 1.5.5.2) are able to stabilise phosphinyl radicals by delocalisation of the spin density, as are *N*-heterocyclic carbene (NHC) derivatives^{114,115} **V2**, although to a lower extent (*i.e.* more spin density resides on phosphorus). The bulky cyclic species **V3** represents the first neutral dialkylphosphinyl radical that is monomeric in the solid-state.¹¹⁶

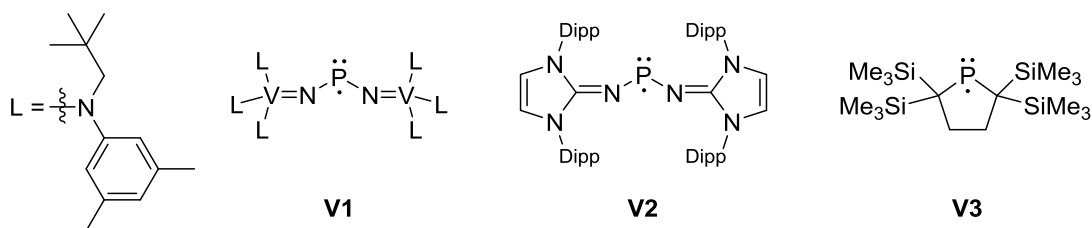


Figure 1.5.5.2: Monomeric, stable phosphinyl radicals.

Isolated cases of other classes of stable phosphorus radicals have also been reported. The 1,3-diphosphacyclobutenyl radical¹¹⁷ **V4** (Figure 1.5.5.3) is monomeric in the solid-state, unlike analogues bearing less bulky substituents,¹¹⁸ but EPR and DFT studies revealed that the majority of the SOMO is localised on the two carbon atoms in the P_2C_2

ring. Several other examples of phosphorus-containing radicals with inverse spin densities have also been recently reported.^{119,120} The electrochemical and chemical reduction of triarylphosphine oxides to give the corresponding radical anions $[\text{Ar}_3\text{PO}\cdot]^-$ dates back to the 1950s¹²¹⁻¹²³ and were studied as analogues to the ketyl radical anion.¹²⁴ These species were found to be short-lived, and early studies were solely based on EPR spectroscopy. Recently, however, a stable P^{V} radical anion **W** was isolated by one electron reduction of a bridged triarylphosphine oxide decorated with bulky fluorenyl moieties. Two-coordinate P^{III} radical anions have also been reported by the alkali metal reduction of phosphalkenes.¹²⁵⁻¹²⁷

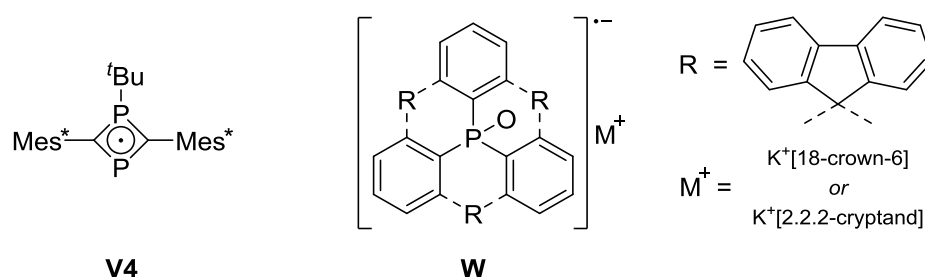


Figure 1.5.5.3: Neutral and anionic phosphorus radicals.

The redox properties of triarylphosphines can be modulated by the choice of substituents, and can be reversibly oxidised to give stable radical cations when extremely bulky aryl groups are employed.^{128,129} The use of weakly coordinating anions (WCA)^{130,131} has recently allowed $[\text{Ar}_3\text{P}\cdot]^+$ species (**X1** – Figure 1.5.5.4) to be isolated in the solid-state,¹³² and this approach has been extended to the tetraaryldiphosphines, **X2**.¹³³ Cyclophosphadiazines and cyclotetraphosphines bearing bulky and electron-rich substituents are also readily oxidised to afford the corresponding radical cations.¹³⁴ Whilst EPR and DFT studies show that the spin density is delocalised across the P_2N_2 core in **X3**, the all phosphorus four-membered ring system **X4** shows inverse spin density distribution with the SOMO delocalised onto the four exocyclic nitrogen atoms with little contribution on phosphorus.

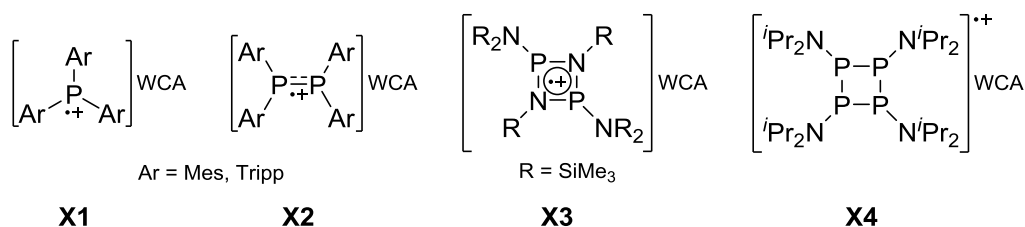


Figure 1.5.5.4: Phosphorus radical cations.

The synthesis of stable phosphorus-centred radicals remains a significant chemical challenge. Kinetic stabilisation and shielding of the radical centre through the

Elucidation of the solid-state structure, typically *via* single-crystal X-ray diffraction (SCXRD), is necessary for the physical properties to be understood. UV-Vis spectroscopy is also commonly used to gain information about HOMO-LUMO transitions. Finally, electrochemical methods such as cyclic voltammetry (CV) are routinely used to probe the redox properties of radicals (*vide infra*).

1.6.1 – Electron Paramagnetic Resonance Spectroscopy

Electron paramagnetic resonance (EPR) spectroscopy is a powerful technique for the study of systems containing unpaired electrons, and is well suited for the characterisation of organic radicals. The fundamental basis of EPR spectroscopy involves the observation of electron spin transitions in the presence of an external magnetic field. Like all spectroscopic techniques, excitation between two states or energy levels is induced by the absorption of electromagnetic (EM) radiation. In EPR spectroscopy, the magnetic field component of EM radiation interacts with permanent magnetic dipole moments arising from the unpaired electrons in the sample. These dipoles are aligned in the presence of an applied external magnetic field meaning that when EM radiation of the correct frequency is available, resonance absorption will occur. In continuous wave (CW) EPR spectroscopy, the sample is exposed to EM radiation of fixed frequency, usually in the microwave region (GHz), and the external magnetic field is swept.

1.6.1.1 – Background Theory

Electrons are negatively charged particles possessing an intrinsic property called spin, characterised by the *spin angular momentum* \mathbf{S} . This property is a vector with magnitude quantised in units of \hbar :

$$|\mathbf{S}| = \sqrt{S(S + 1)} \quad (1)$$

where S is the electron spin quantum number. There are $2S + 1$ projections allowed onto an arbitrarily chosen z axis, which coincides with the direction of the applied magnetic field vector \mathbf{B} . The allowed orientations of \mathbf{S} along the z axis are consequently given by the m_S values of the spin; m_S is the electron spin angular momentum quantum number with $2S + 1$ integral steps between $+S$ and $-S$. An electron with $S = \frac{1}{2}$ therefore has two possible spin states denoted as ‘spin-up’ (α spin, m_S value = $+\frac{1}{2}$) and ‘spin-down’ (β spin, m_S value = $-\frac{1}{2}$). In the absence of a magnetic field, the two electron spin states are degenerate, and the probability of the electron being in either spin state is equal.

It is convenient to consider the electron as a particle of mass m_e and charge e rotating about an axis with spin angular momentum \mathbf{S} which produces a circulating current. This generates a magnetic dipole moment μ_S related to the gyromagnetic ratio γ by:

$$\mu_S = -\gamma \mathbf{S} \hbar = -g_e \frac{e\hbar}{2m_e} \mathbf{S} \quad (2)$$

where g_e is the free-electron g -factor (≈ 2.0023).¹³⁸ Equation 2 is more commonly expressed in terms of the Bohr magneton ($\mu_B = e\hbar/2m_e$). The z -component of the magnetic moment μ_z along the magnetic field \mathbf{B} direction can be related to the m_s electron spin states, resulting in two electron magnetic dipole moments given by:

$$\mu_z = -g_e \mu_B m_s \quad (3)$$

In the absence of a magnetic field the electron spin states are degenerate. This degeneracy is removed in the presence of an external magnetic field. The energy of the electron magnetic moment is directly proportional to the magnitude of the applied magnetic field such that:

$$E = -g_e \mu_B m_s B \quad (4)$$

The two components of the magnetic dipole moment along the z -direction give two states of differing energy, referred to as the *electron Zeeman levels* (Figure 1.6.1.1.1). The lowest energy β spin state corresponds to the electron magnetic moment aligned parallel to the applied magnetic field, and the high energy α spin state arises due to the anti-parallel alignment.

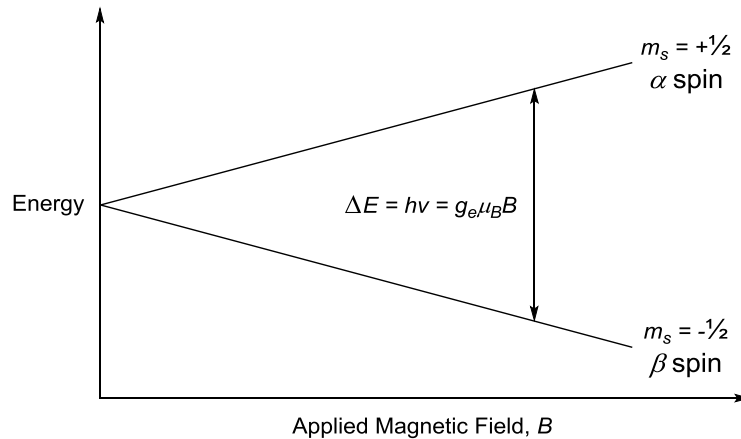


Figure 1.6.1.1.1: Electron Zeeman levels for an unpaired electron in an external magnetic field of increasing magnitude B .

In EPR spectroscopy, a sample containing unpaired electrons is irradiated with electromagnetic radiation $h\nu$ in the presence of an external magnetic field. When the energy difference between the two energy levels matches the supplied energy, absorption occurs which leads to an EPR resonance. The selection rule in EPR spectroscopy is $\Delta m_s = \pm 1$ so that the resulting resonance condition is:

$$\Delta E = h\nu = g_e \mu_B B \quad (5)$$

A key parameter of interest is the g -value, since this determines the resonant field position and is influenced by the chemical environment of the electron. For organic radicals, the g -value is usually close to free spin ($g_e \approx 2.0023$) whilst deviations are observed for systems with large orbital angular momenta contributions such as main-group radicals and transition metal ions.

The presence of nuclei with magnetic spin I adds further magnetic interactions to the electron spin systems, which give multi-line EPR spectra that contain a wealth of information. The interactions of the nuclear spin with \mathbf{B} results in *nuclear Zeeman splitting*, and the resulting interaction between the electron and nuclear magnetic moments is referred to as the *hyperfine interaction*.

In analogy with μ_s (Equation 2), nuclei that possess a non-zero spin quantum number I will also have an associated magnetic moment μ_I . The magnitude of the nuclear spin moments are also quantised in units of \hbar and given as:

$$|I| = \sqrt{I(I + 1)} \quad (6)$$

As a result, the vector I can assume $2I + 1$ discrete orientations which are given by the magnetic quantum number m_I . In analogy to the electron spin, the z -component of the nuclear magnetic dipole moment is related to the m_I nuclear spin states by:

$$\mu_z = -g_N \mu_N m_I \quad (7)$$

where g_N is the effective nuclear g -factor and μ_N is the nuclear magneton. In the absence of an applied magnetic field, the permitted z -components of nuclei with $I \geq \frac{1}{2}$ will have the same energy; the degeneracy of the $2I + 1$ *nuclear Zeeman energy levels* is removed in the presence of an applied external magnetic field.

The interaction between the electron and nuclear magnetic dipole moments gives rise to a *hyperfine interaction*. This leads to a perturbation of the *nuclear Zeeman energy levels* towards higher or lower energy, the extent of which is described by the *hyperfine*

coupling constant a (i.e. the magnitude of the magnetic interaction between the electron and nuclear spin). In CW EPR spectroscopy, the transitions from one state to another which occur with the highest probabilities are the ones corresponding to $\Delta m_s \pm 1$ and $\Delta m_l \pm 0$ – i.e. the electron spin state must change whilst the nuclear spin state remains the same. Different energy quanta are required to induce these transitions, which results in two resonance lines in the EPR spectrum. The magnitude of the separation between these two lines is given by the *hyperfine coupling constant, a*. There are two contributions to the *hyperfine interaction* that arise from the regions of space inside and outside the nuclear volume; the *isotropic* and *anisotropic* interactions.

The *isotropic*, or *Fermi contact* interaction, is a direct measure of the interaction between the electron and nuclear magnetic dipole moments as a result of the finite probability that the unpaired electron will be located at the nucleus. This arises exclusively for *s* orbitals and the magnitude of the experimentally observed *isotropic hyperfine coupling constant* can thus be related to the electron spin density located at the nucleus.

The second contribution to the *hyperfine interaction* arises from classical dipole-dipole interactions. The energy of this *anisotropic hyperfine interaction* is dependent on the relative orientation and distance between the electron and nuclear magnetic dipole moments. The terms of this relationship must be averaged over the entire probability of the spin distribution such that the energy is zero for *s* orbitals, or for rapidly tumbling molecules where the anisotropy with respect to the external field is motionally averaged – i.e. small organic radicals in low viscosity solvents. Spectra arising from *anisotropic interactions* are observed in the solid-state and for frozen solutions.

1.6.1.2 – The EPR Spectrum

An EPR spectrum is a plot of microwave absorption as a function of applied magnetic field intensity. In the CW experiment, the resonance absorption signal is plotted as the first derivative rather than in absorption mode. The EPR spectrum for an arbitrary $S = \frac{1}{2}$ radical is shown in Figure 1.6.1.2.1.

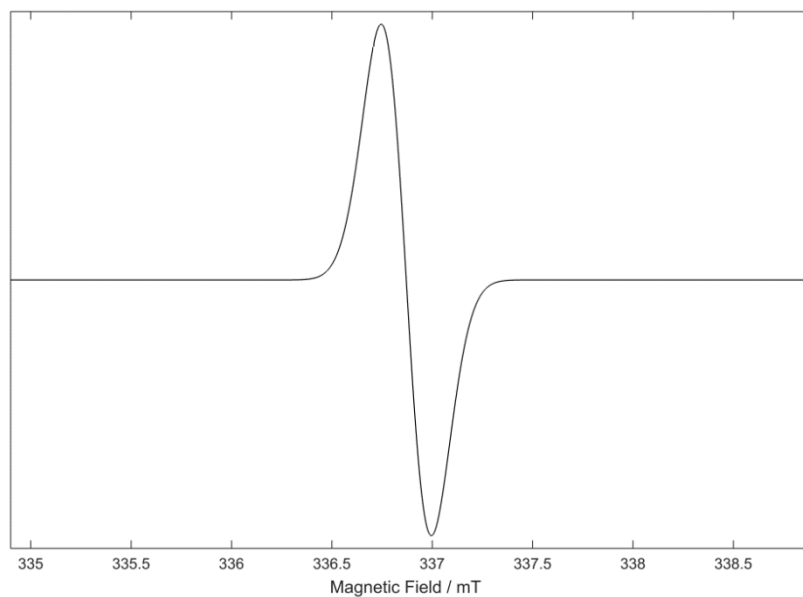


Figure 1.6.1.2.1: CW EPR spectrum for an arbitrary $S = \frac{1}{2}$ radical.

The EPR spectra of real systems are typically more complex compared to the simple spectrum shown in in Figure 1.6.1.2.1. Such multi-line EPR spectra contain a wealth of information that make it possible to not only identify and unambiguously assign a structure to a particular radical, but also obtain further geometrical details about the spin system including the distribution of electron density in both organic and inorganic systems containing unpaired electrons. The EPR spectra for a $S = \frac{1}{2}$ radical coupling to two non-equivalent $I = 1$ nuclei is shown in Figure 1.6.1.2.2.

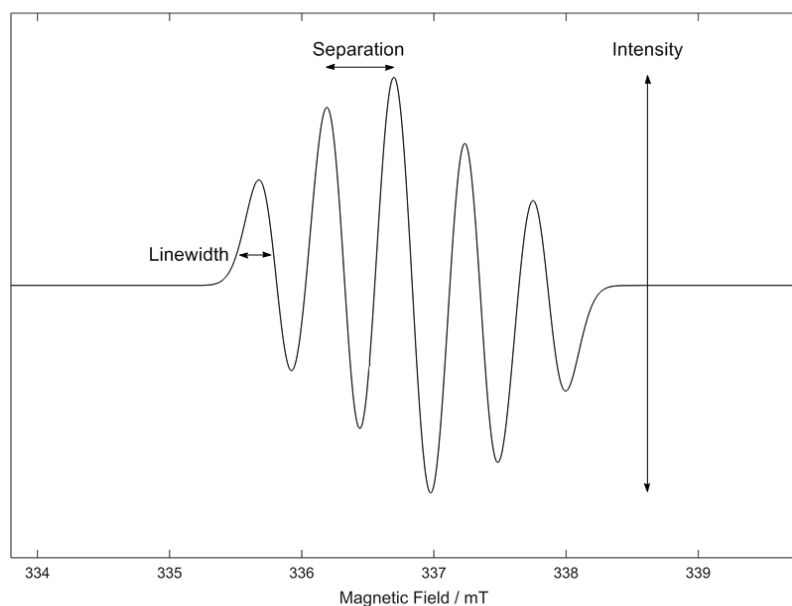


Figure 1.6.1.2.2: CW EPR spectrum for a $S = \frac{1}{2}$ radical coupling to two non-equivalent $I = 1$ nuclei.

The position of the EPR signal is determined by the g -value. This is usually close to that of a free electron ($g_e \approx 2.0023$) for organic radicals and provides limited structural information. The separation between the lines is determined by the *hyperfine coupling constant*, a , whilst the number of lines in the *hyperfine splitting pattern* is dictated by the nuclear spin, I . The linewidth is influenced by a number of factors including dynamic effects and unresolved *hyperfine interactions*. The differing line intensities depends primarily on the multiplicity of the *hyperfine* lines caused by interactions with nuclei of $I \geq \frac{1}{2}$, or the anisotropy of the paramagnetic systems.

1.6.2 - Electrochemical Studies

Electrochemistry is a powerful tool to probe reactions involving the transfer of electrons, and is therefore routinely used in the characterisation and study of radicals. Knowledge of the reduction and oxidation potentials required to access radicals, and the window within which the radical is stable, provides good guidelines for the choice of appropriate reducing or oxidising agent. The potentials may also be related to ionisation energies of the system, which are in turn useful for estimating the *Coulombic* repulsion, U , for the design of conducting materials. In addition, electrochemistry data are useful when considering the formation of charge-transfer salts or the stability of metal complexes. The potentials of these redox processes may be probed by various techniques of which cyclic voltammetry is the most common for organic radicals and the one employed in this thesis.

1.6.2.1 - Cyclic Voltammetry

In a standard cyclic voltammetry experiment, a circuit is prepared by placing two electrodes into a solution containing a small amount of the analyte and a supporting electrolyte. A varying potential is placed across the cathode and anode within the solution and the current that flows is recorded. The supporting electrolyte serves to carry the current between the electrodes when a voltage is applied. When the potential across the electrodes corresponds to a redox process, there is an increase in current associated with the flow of electrons. The analyte will undergo reduction (accept an electron from the electrode) when the potential energy of the electrons in the electrode is higher than the lowest unoccupied molecular orbital (LUMO) of the analyte. Conversely, the analyte will undergo oxidation (lose an electron to the electrode) when the potential energy of the highest occupied molecular orbital (HOMO) is higher than the potential energy of the electrons in the electrode. The plot of measured current against the applied potential is called a cyclic voltammogram (CV); the CV trace for the reversible ferrocene/ferrocenium (Fc/Fc⁺) couple is shown in Figure 1.6.2.1.1.

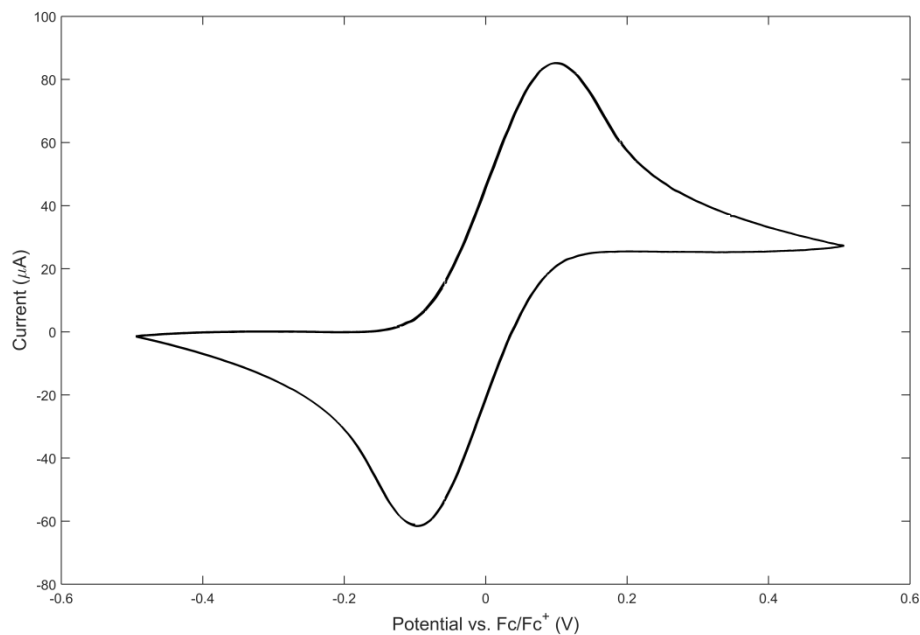


Figure 1.6.2.1.1: Cyclic voltammogram for the reversible Fc/Fc⁺ redox couple.

The Nernst equation relates the potential of an electrochemical cell E to the standard potential of a species E^0 and the relative activities of the oxidised (Ox) and reduced (Red) analyte in the system at equilibrium. The activities are typically replaced with concentrations, which are more experimentally accessible, such that for a one electron process:

$$E = E^0 + \frac{RT}{F} \ln \frac{(\text{Ox})}{(\text{Red})} \quad (8)$$

where R is the universal gas constant, T is the temperature, and F is Faraday's constant. The Nernst equation thus provides a powerful way to predict how a system will respond to a change of concentration of the species in solution, or a change in the electrode potential.

The cathodic and anodic peaks are separated due to the diffusion of the analyte to and from the electrode. For this reason, it is imperative that the experiment is performed under diffusion controlled conditions and without stirring. If the electron transfer process is chemically and electrochemically reversible, the difference between the peak potentials (ΔE_p) is 57 mV at standard temperature and pressure.¹³⁹ Chemical reversibility refers to the stability of the analyte upon reduction and whether it can be subsequently be reoxidised. Electrochemical reversibility describes the electron transfer kinetics between the analyte and the electrode; these processes are fast and have a low barrier to electron transfer. In contrast, electrochemical irreversibility refers to slow electron transfer processes and require more negative (or positive)

applied potentials to observe subsequent reduction (or oxidation), which results in peak-to-peak separations larger than 57 mV.

Asymmetric voltammograms are often observed when an electron transfer is coupled to a chemically irreversible process, E_rC_i . If the irreversible chemical reaction is slow compared to the electron transfer, then the symmetry will be preserved and the voltammogram appears reversible. For a rapid irreversible chemical reaction however, the ratio of cathodic and anodic peak currents will differ significantly until just a single peak is observed. For sufficiently fast scan rates, the electrochemical feature will regain reversibility as the electron transfer process out-competes the irreversible chemical reaction. Variable scan-rate studies can therefore be used to extract information about the kinetics and mechanisms involved in E_rC_i reactions.

While the current flows between a working and counter electrode in a cyclic voltammetry experiment, a third reference electrode is used to accurately measure the applied potential relative to a stable and well-defined redox process. In non-aqueous solvents, reference electrodes are typically based on the Ag/Ag⁺ couple. This potential however can vary significantly between experiments due to a number of factors, and it is therefore recommended to instead reference potentials to an internal reference compound with a known E^0 , such as ferrocene.^{140,141}

The solvent and supporting electrolyte employed must be stable towards reduction and oxidation within the potential range of the experiment, as well as being chemically inert with the analyte. It is crucial that the solvent and electrolyte are free of impurities and rigorously dried whilst performing the experiments under an inert atmosphere, to prevent the occurrence of additional and unwanted redox processes. Further details and practical guides on cyclic voltammetry are given by Dempsey¹⁴² and Graham.¹⁴³

1.7 – Conclusions

Organic radicals are promising candidates for the development of new molecular materials exhibiting interesting properties such as magnetism and conductivity. This field is dominated by sulfur-nitrogen radicals, primarily those derived from DTDA and DTA radicals, whilst comparatively little research has been published on other systems such as the 1,2,4-benzothiadiazinyl (BTDA) radicals. Prior work in the Clark group has explored the synthesis and chemistry of BTDA radicals and their precursors,¹⁴⁴ and this thesis aims to expand on this earlier work to further investigate the magnetic and electrochemical behaviour of this versatile class of radicals. The synthesis of stable phosphorus-centred radicals remains a significant challenge and no data to date have

been published on the magnetic properties of neutral phosphorus radicals. The latter half of this thesis will therefore focus on the development of new synthetic routes to novel phosphorus-nitrogen heterocyclic radicals, which are isoelectronic to the 1,2,4-benzothiadiazinyl radicals and are heavier congeners of the well-established 1,2,4-benzotriazinyl radicals.

1.8 – References

- 1 P. Muller, *Int. Union Pure Appl. Chem.*, 1994, **66**, 1077–1184.
- 2 E. Demarçay, *Compt. Rend.*, 1880, **91**, 854.
- 3 R. G. Hicks, *Org. Biomol. Chem.*, 2007, **5**, 1321.
- 4 D. Griller and K. U. Ingold, *Acc. Chem. Res.*, 1976, **9**, 13–19.
- 5 P. P. Power, *Chem. Rev.*, 2003, **103**, 789–809.
- 6 M. Gomberg, *J. Am. Chem. Soc.*, 1902, **22**, 597–628.
- 7 P. Anderson and B. Klewe, *Acta Chem. Scand.*, 1967, 2599–2607.
- 8 M. Ballester, J. Riera, J. Castafier, C. Badía and J. M. Monsó, *J. Am. Chem. Soc.*, 1971, **93**, 2215–2225.
- 9 R. Ghadwal, D. Rottschäfer, B. Neumann, H. G. Stammler, M. Van Gastel and D. Andrada, *Angew. Chem. Int. Ed.*, 2018, **57**, 4765–4768.
- 10 L. J. Berliner, *Spin Labelling: Theory and Applications*, Academic Press, New York, 1979.
- 11 D. Rehorek, *Chem. Soc. Rev.*, 1991, **20**, 341–353.
- 12 M. J. Davies, *Methods*, 2016, **109**, 21–30.
- 13 J. M. Rawson, A. Alberola and A. Whalley, *J. Mater. Chem.*, 2006, **16**, 2560.
- 14 J. S. Miller and A. J. Epstein, *Angew. Chem. Int. Ed.*, 1994, **33**, 385–415.
- 15 J. Wosnitza, *Curr. Opin. Solid State Mater. Sci.*, 2001, **5**, 131–141.
- 16 I. Ratera and J. Veciana, *Chem. Soc. Rev.*, 2012, **41**, 303–349.
- 17 G. R. Desiraju, *Crystal Engineering*, Elsevier, Amsterdam, 1989.
- 18 C. B. Aakeröy, *Acta Cryst. Sect. B*, 1997, **53**, 569–586.
- 19 G. R. Desiraju, *Angew. Chem. Int. Ed.*, 1995, **34**, 2311–2327.
- 20 J. S. Miller, *Mater. Today*, 2014, **17**, 224–235.
- 21 J. A. Crayston, J. N. Devine and J. C. Walton, *Tetrahedron*, 2000, **56**, 7829–7857.
- 22 R. G. Hicks, *Nat. Chem.*, 2011, **3**, 189–191.
- 23 D. A. Haynes, *CrystEngComm*, 2011, **13**, 4793–4805.
- 24 A. F. Orchard, *Magnetochemistry*, Oxford Chemistry Primers, Oxford, 2003.
- 25 H. D. Young, *University Physics*, Addison Wesley, 7th edn., 1992.
- 26 H. E. Hall and J. R. Hook, *Solid State Physics*, John Wiley & Sons, Chichester, 2nd edn., 1991.
- 27 R. Winpenney, *Molecular Cluster Magnets*, World Scientific, 2011.
- 28 O. Sato, *Nat. Chem.*, 2016, **8**, 644–656.
- 29 O. Kahn, *Science*, 1998, **279**, 44–48.
- 30 M. A. Halcrow, *Spin-Crossover Materials: Properties and Applications*, John Wiley & Sons, 1st edn., 2013.

- 31 L. Cambi and A. Cagnasso, *Atti. Accad. Naz. Lincei.*, 1931, **13**, 809.
- 32 L. Cambi, L. Szego and A. Cagnasso, *Atti. Accad. Naz. Lincei.*, 1932, **15**, 266.
- 33 A. Alberola, D. J. Eisler, L. Harvey and J. M. Rawson, *CrystEngComm*, 2011, **13**, 1794–1796.
- 34 A. Alberola, O. P. Clements, R. J. Collis, L. Cubbitt, C. M. Grant, R. J. Less, R. T. Oakley, J. M. Rawson, R. W. Reed and C. M. Robertson, *Cryst. Growth Des.*, 2008, 2–8.
- 35 A. Alberola, R. J. Collis, S. M. Humphrey, R. J. Less and J. M. Rawson, *Inorg. Chem.*, 2006, **45**, 1903–1905.
- 36 G. D. McManus, J. M. Rawson, N. Feeder, J. van Duijn, E. J. L. McInnes, J. J. Novoa, R. Burriel, F. Palacio and P. Oliete, *J. Mater. Chem.*, 2001, **11**, 1992–2003.
- 37 T. M. Barclay, A. W. Cordes, N. A. George, R. C. Haddon, R. T. Oakley, T. M. Palstra, G. W. Patenaude, R. W. Reed, F. Richardson and H. Zhang, *Chem. Commun.*, 1997, 873–874.
- 38 J. L. Brusso, O. P. Clements, R. C. Haddon, M. E. Itkis, A. A. Leitch, R. T. Oakley, R. W. Reed and J. F. Richardson, *J. Am. Chem. Soc.*, 2004, **126**, 8256–8265.
- 39 J. L. Brusso, O. P. Clements, R. C. Haddon, M. E. Itkis, A. A. Leitch, R. T. Oakley, R. W. Reed and J. F. Richardson, *J. Am. Chem. Soc.*, 2004, **126**, 14692–14693.
- 40 W. Fujita, *Science*, 1999, **286**, 261–262.
- 41 T. M. Barclay, A. W. Cordes, N. A. George, R. C. Haddon, M. E. Itkis, M. S. Mashuta, R. T. Oakley, G. W. Patenaude, R. W. Reed, J. F. Richardson and H. Zhang, *J. Am. Chem. Soc.*, 1998, **120**, 352–360.
- 42 D. Bates, C. M. Robertson, A. A. Leitch, P. A. Dube and R. T. Oakley, *J. Am. Chem. Soc.*, 2018, **140**, 3846–3849.
- 43 P. Atkins and J. De Paula, *Physical Chemistry*, Oxford University Press, 9th edn., 2010.
- 44 R. Hoffmann, *Angew. Chem. Int. Ed.*, 1987, **26**, 846–878.
- 45 R. C. Haddon, *Nature*, 1975, **256**, 394–396.
- 46 R. G. Hicks, *Stable Radicals: Fundamentals and Applied Aspects of Odd-Electron Compounds*, John Wiley & Sons, Wiltshire, 2010.
- 47 N. F. Mott, *Metal-insulator Transitions*, Taylor & Francis, London, 1990.
- 48 R. T. Oakley, *Can. J. Chem.*, 1993, **71**, 1775–1784.
- 49 L. Beer, J. L. Brusso, R. C. Haddon, M. E. Itkis, R. T. Oakley, R. W. Reed, J. F. Richardson, R. A. Secco and X. Yu, *Chem. Commun.*, 2005, 5745–5747.
- 50 Y. Takano, T. Taniguchi, H. Isobe, T. Kubo, Y. Morita, K. Yamamoto, K. Nakasuji, T. Takui and K. Yamaguchi, *J. Am. Chem. Soc.*, 2002, **124**, 11122–11130.

- 51 N. M. Shishlov, *Russ. Chem. Rev.*, 2007, **75**, 863–884.
- 52 W. C. Danen and F. A. Neugebauer, *Angew. Chem. Int. Ed.*, 1975, **14**, 783–789.
- 53 T. Barth, B. Kanellakopoulos, C. Krieger and F. A. Neugebauer, *J. Chem. Soc., Chem. Commun.*, 1993, **50**, 1626–1628.
- 54 G. E. Jeromin, *Tetrahedron Lett.*, 2001, **42**, 1863–1865.
- 55 A. R. Forrester, J. M. Hay and R. H. Thomson, *Organic Chemistry of Stable Free Radicals*, Academic Press, London, 1968.
- 56 H. M. Blatter and H. Lukaszewski, *Tetrahedron Lett.*, 1968, **9**, 2701–2705.
- 57 P. Kaszyński, C. P. Constantinides and V. G. Young, *Angew. Chem. Int. Ed.*, 2016, **55**, 11149–11152.
- 58 C. P. Constantinides, A. A. Berezin, M. Manoli, G. M. Leitus, M. Bendikov, J. M. Rawson and P. A. Koutentis, *New J. Chem.*, 2014, **38**, 949–954.
- 59 C. P. Constantinides, A. A. Berezin, M. Manoli, G. M. Leitus, G. A. Zissimou, M. Bendikov, J. M. Rawson and P. A. Koutentis, *Chem. Eur. J.*, 2014, **20**, 5388–5396.
- 60 Y. Miura and N. Yoshioka, *Chem. Phys. Lett.*, 2015, **626**, 11–14.
- 61 C. P. Constantinides, P. A. Koutentis, H. Krassos, J. M. Rawson and A. J. Tasiopoulos, *J. Org. Chem.*, 2011, **76**, 2798–2806.
- 62 C. P. Constantinides, P. A. Koutentis and J. M. Rawson, *Chem. Eur. J.*, 2012, **18**, 15433–15438.
- 63 R. Kuhn and H. Trischmann, *Angew. Chem. Int. Ed.*, 1963, **2**, 155.
- 64 F. A. Neugebauer, H. Fischer and R. Siegel, *Chem. Ber.*, 1988, **121**, 815–822.
- 65 A. Caneschi, D. Gatteschi, R. Sessoli and P. Rey, *Acc. Chem. Res.*, 1989, **22**, 392–398.
- 66 B. D. Koivisto and R. G. Hicks, *Coord. Chem. Rev.*, 2005, **249**, 2612–2630.
- 67 J. B. Gilroy, B. D. Koivisto, R. McDonald, M. J. Ferguson and R. G. Hicks, *J. Mater. Chem.*, 2006, **16**, 2618–2624.
- 68 F. Pointillart, C. Train, P. Herson, J. Marrot and M. Verdaguer, *New J. Chem.*, 2007, **31**, 1001–1006.
- 69 E. G. Rozanstev, *Free Nitroxyl Radicals*, Plenum, New York, 1970.
- 70 S. Nakatsuji and H. Anzai, *J. Mater. Chem.*, 1997, **7**, 2161–2174.
- 71 O. L. Lebedev and S. N. Kazarnovskii, *Zhur. Obs. Khim.*, 1960, **30**, 1631–1635.
- 72 S. S. Kim and H. C. Jung, *Synthesis*, 2003, 2135–2137.
- 73 E. F. Ullman, J. H. Osiecki, D. G. B. Boocock and R. Darcy, *J. Am. Chem. Soc.*, 1972, **94**, 7049–7059.
- 74 M. Tamura, Y. Nakazawa, D. Shiomi, K. Nozawa, Y. Hosokoshi, M. Ishikawa, M. Takahashi and M. Kinoshita, *Chem. Phys. Lett.*, 1991, **186**, 401–404.

- 75 A. Vegas, A. Perez-Salazar, A. J. Banister and R. G. Hey, *J. Chem. Soc., Dalt. Trans.*, 1980, 1812–1815.
- 76 A. J. Banister, N. Bricklebank, W. Clegg, M. R. J. Elsegood, C. Gregory, I. Lavender, J. M. Rawson and B. K. Tanner, *J. Chem. Soc., Chem. Commun.*, 1995, 679–680.
- 77 A. J. Banister, N. Bricklebank, I. Lavender, J. M. Rawson, C. I. Gregory, B. K. Tanner, W. Clegg, M. R. J. Elsegood and F. Palacio, *Angew. Chem. Int. Ed.*, 1996, **35**, 2533–2535.
- 78 G. Antorrena, J. E. Davies, M. Hartley, F. Palacio, J. M. Rawson, J. N. B. Smith and A. Steiner, *Chem. Commun.*, 1999, 1393–1394.
- 79 A. Alberola, R. J. Less, C. M. Pask, J. M. Rawson, F. Palacio, P. Oliete, C. Paulsen, A. Yamaguchi, R. D. Farley and D. M. Murphy, *Angew. Chem. Int. Ed.*, 2003, **42**, 4782–4785.
- 80 M. Mito, T. Kawae, K. Takeda, S. Takagi, Y. Matsushita, H. Deguchi, J. M. Rawson and F. Palacio, *Polyhedron*, 2001, **20**, 1509–1512.
- 81 W. Fujita, K. Awaga, Y. Nakazawa, K. Saito and M. Sorai, *Chem. Phys. Lett.*, 2002, **352**, 348–352.
- 82 G. Wolmershauser, M. Schnauber, T. Wilhelm and L. H. Sutcliffe, *Synth. Met.*, 1986, **14**, 239–244.
- 83 W. Fujita and K. Awaga, *Chem. Phys. Lett.*, 2002, **357**, 385–388.
- 84 W. Fujita and K. Awaga, *Chem. Phys. Lett.*, 2004, **388**, 186–189.
- 85 W. Fujita, K. Awaga, M. Takahashi, M. Takeda and T. Yamazaki, *Chem. Phys. Lett.*, 2002, **362**, 97–102.
- 86 Y. Miura, E. Yamano, A. Tanaka and J. Yamauchi, *J. Org. Chem.*, 1994, **59**, 3294–3300.
- 87 Y. Miura, A. Yamamoto, Y. Katsura and M. Kinoshita, *J. Chem. Soc., Chem. Commun.*, 1980, **0**, 37.
- 88 V. Benin and P. Kaszynski, *J. Org. Chem.*, 2000, **65**, 8086.
- 89 P. Kaszynski, *Molecules*, 2004, **9**, 716–724.
- 90 J. Zienkiewicz, P. Kaszynski and V. G. Young, *J. Org. Chem.*, 2004, **69**, 7525–7536.
- 91 J. Zienkiewicz, A. Fryszkowska, K. Zienkiewicz, F. Guo, P. Kaszynski, A. Januszko and D. Jones, *J. Org. Chem.*, 2007, **72**, 3510–3520.
- 92 L. Beer, R. C. Haddon, M. E. Itkis, A. A. Leitch, R. T. Oakley, R. W. Reed, J. F. Richardson, D. G. VanderVeer, L. Beer, J. L. Brusso, A. W. Cordes, R. C. Haddon, M. E. Itkis, K. Kirschbaum, D. S. MacGregor, R. T. Oakley, A. A. Pinkerton and R. W. Reed, *Chem. Commun.*, 2005, **124**, 1218–1220.
- 93 A. Leitch, R. T. Oakley, R. W. Reed and L. K. Thompson, *Inorg. Chem.*, 2007, **46**,

- 6261–70.
- 94 S. M. Winter, A. R. Balo, R. J. Roberts, K. Lakin, A. Assoud, P. A. Dube and R. T. Oakley, *Chem. Commun.*, 2013, **49**, 1603.
- 95 J. L. Brusso, K. Cvrkalj, A. A. Leitch, R. T. Oakley, R. W. Reed and C. M. Robertson, *J. Am. Chem. Soc.*, 2006, **128**, 15080–15081.
- 96 C. M. Robertson, A. A. Leitch, K. Cvrkalj, D. J. T. Myles, R. W. Reed, P. A. Dube and R. T. Oakley, *J. Am. Chem. Soc.*, 2008, **130**, 14791–14801.
- 97 N. Feeder, R. J. Less, J. M. Rawson, P. Oliete and F. Palacio, *Chem. Commun.*, 2000, **2**, 2449–2450.
- 98 A. W. Cordes, R. C. Haddon, R. G. Hicks, R. T. Oakley, T. T. M. Palstra, L. F. Schneemeyer and J. V. Waszczak, *J. Am. Chem. Soc.*, 1992, **114**, 1729–1732.
- 99 A. W. Cordes, R. C. Haddon, R. T. Oakley, L. F. Schneemeyer, J. V. Waszczak, K. M. Young and N. M. Zimmerman, *J. Am. Chem. Soc.*, 1991, **113**, 582–588.
- 100 M. P. Andrews, A. W. Cordes, D. C. Douglass, R. M. Fleming, S. H. Glarum, R. C. Haddon, P. Marsh, R. T. Oakley, T. T. M. Palstra, L. F. Schneemeyer, G. W. Trucks, R. Tycko, J. V. Waszczak, K. M. Young, N. M. Zimmerman, A. W. Cordes, R. T. Oakley and K. M. Young, *J. Am. Chem. Soc.*, 1991, **113**, 3559–3568.
- 101 A. A. Leitch, J. L. Brusso, K. Cvrkalj, R. W. Reed, C. M. Robertson, P. A. Dube and R. T. Oakley, *Chem. Commun.*, 2007, **4**, 3368–3370.
- 102 C. M. Robertson, D. J. T. Myles, A. A. Leitch, R. W. Reed, B. M. Dooley, N. L. Frank, P. A. Dube, L. K. Thompson and R. T. Oakley, *J. Am. Chem. Soc.*, 2007, **129**, 12688–12689.
- 103 C. Walling and M. S. Pearson, *Top. Phosphorus Chem.*, 1966, **3**, 1.
- 104 W. G. Bentrude, *The Chemistry of Organophosphorus Compounds*, Wiley, Chichester, 1990.
- 105 D. Leca, L. Fensterbank, E. Lacôte and M. Malacria, *Chem. Soc. Rev.*, 2005, **34**, 858–865.
- 106 J. K. Kochi and P. J. Krusic, *J. Am. Chem. Soc.*, 1969, **91**, 3944–3946.
- 107 M. J. S. Gynane, A. Hudson, M. F. Lappert and P. P. Power, *J. Chem. Soc., Chem. Commun.*, 1976, 623–624.
- 108 M. J. S. Gynane, A. Hudson, M. F. Lappert, P. P. Power and H. Goldwhite, *J. Chem. Soc., Dalt. Trans.*, 1980, 2428–2433.
- 109 S. L. Hinchley, C. A. Morrison, D. W. H. Rankin, C. L. B. Macdonald, R. J. Wiacek, A. H. Cowley, M. F. Lappert, G. Gundersen, J. A. C. Clyburne and P. P. Power, *Chem. Commun.*, 2000, 2045–2046.
- 110 S. L. Hinchley, C. A. Morrison, D. W. H. Rankin, C. L. B. Macdonald, R. J. Wiacek, A.

- Voigt, A. H. Cowley, M. F. Lappert, G. Gundersen, J. A. C. Clyburne and P. P. Power, *J. Am. Chem. Soc.*, 2001, **123**, 9045–9053.
- 111 M. Blum, O. Puntigam, S. Plebst, F. Ehret, J. Bender, M. Nieger and D. Gudat, *Dalton Trans.*, 2016, **45**, 1987–1997.
- 112 D. M. C. Ould, A. C. Rigby, L. C. Wilkins, S. J. Adams, J. A. Platts, S. J. A. Pope, E. Richards and R. L. Melen, *Organometallics*, 2018, **37**, 712–719.
- 113 P. Agarwal, N. A. Piro, K. Meyer, P. Müller and C. C. Cummins, *Angew. Chem. Int. Ed.*, 2007, **46**, 3111–3114.
- 114 O. Back, B. Donnadieu, M. von Hopffgarten, S. Klein, R. Tonner, G. Frenking and G. Bertrand, *Chem. Sci.*, 2011, **2**, 858–861.
- 115 C. D. Martin, M. Soleilhavoup and G. Bertrand, *Chem. Sci.*, 2013, **4**, 3020–3030.
- 116 S. Ishida, F. Hirakawa and T. Iwamoto, *J. Am. Chem. Soc.*, 2011, **133**, 12968–12971.
- 117 S. Ito, M. Kikuchi, M. Yoshifuji, A. J. Arduengo, T. A. Konovalova and L. D. Kispert, *Angew. Chem. Int. Ed.*, 2006, **45**, 4341–4345.
- 118 M. Sebastian, O. Schmidt, A. Fuchs, M. Nieger, D. Szieberth, L. Nyulaszi and E. Niecke, *Phosphorus, Sulfur Silicon Relat. Elem.*, 2004, **179**, 779–783.
- 119 X. Pan, X. Wang, Z. Zhang and X. Wang, *Dalton Trans.*, 2015, **44**, 15099–15102.
- 120 F. Biaso, T. Cantat, N. Mézailles, L. Ricard, P. Le Floch and M. Geoffroy, *Angew. Chem. Int. Ed.*, 2006, **45**, 7036–7039.
- 121 V. F. Hein, H. Plust and H. Pohlemann, *Z. Anorg. Allg. Chem.*, 1953, **272**, 25–31.
- 122 A. K. Hoffmann and A. G. Tesch, *J. Am. Chem. Soc.*, 1959, **81**, 5519–5520.
- 123 A. H. Cowley and M. H. Hnoosh, *J. Am. Chem. Soc.*, 1966, **88**, 2595–2597.
- 124 E. Beckmann and T. Paul, *Justus Liebigs Ann. Chem.*, 1891, **266**, 1–28.
- 125 S. Sasaki, F. Murakami and M. Yoshifuji, *Angew. Chem. Int. Ed.*, 1999, **38**, 340–343.
- 126 X. Pan, X. Weng, Y. Zhao, Y. Sui and X. Wang, *J. Am. Chem. Soc.*, 2014, **136**, 9834–9837.
- 127 G. Tan, S. Li, S. Chen, Y. Sui, Y. Zhao and X. Wang, *J. Am. Chem. Soc.*, 2016, **138**, 6735–6738.
- 128 S. Sasaki, K. Sutoh, F. Murakami and M. Yoshifuji, *J. Am. Chem. Soc.*, 2002, **124**, 14830–14831.
- 129 R. T. Boéré, A. M. Bond, S. Cronin, N. W. Duffy, P. Hazendonk, J. D. Masuda, K. Pollard, T. L. Roemmele, P. Tran and Y. Zhang, *New J. Chem.*, 2008, **32**, 214–231.
- 130 I. Krossing and I. Raabe, *Angew. Chem. Int. Ed.*, 2004, **43**, 2066–2090.
- 131 I. M. Riddlestone, A. Kraft, J. Schaefer and I. Krossing, *Angew. Chem. Int. Ed.*, 2018, **57**, 2–45.

- 132 X. Pan, X. Chen, T. Li, Y. Li and X. Wang, *J. Am. Chem. Soc.*, 2013, **135**, 3414–3417.
- 133 X. Pan, Y. Su, X. Chen, Y. Zhao, Y. Li, J. Zuo and X. Wang, *J. Am. Chem. Soc.*, 2013, **135**, 5561–5564.
- 134 X. Wang, Y. Su, X. Zheng, X. Wang, X. Zhang and Y. Sui, *J. Am. Chem. Soc.*, 2014, **136**, 6251–6254.
- 135 G. Tan and X. Wang, *Chinese J. Chem.*, 2018, **36**, 573–586.
- 136 R. Edge, R. J. Less, E. J. L. McInnes, K. Müther, V. Naseri, J. M. Rawson and D. S. Wright, *Chem. Commun.*, 2009, **2**, 1691–1693.
- 137 V. Chechik, E. Carter and D. Murphy, *Electron Paramagnetic Resonance*, Oxford Chemistry Primers, 2015.
- 138 W. M. Haynes, *CRC Handbook of Chemistry and Physics*, CRC Press, 93rd edn., 2012.
- 139 A. J. Bard and L. R. Faulkner, *Electrochemical Methods: Fundamental and Applications*, John Wiley & Sons, NJ, 2nd edn., 2001.
- 140 G. Gritzner and J. Kuta, *Int. Union Pure Appl. Chem.*, 1984, **1**, 462–466.
- 141 N. G. Tsierkezos, *J. Solution Chem.*, 2007, **36**, 289–302.
- 142 N. Elgrishi, K. J. Rountree, B. D. McCarthy, E. S. Rountree, T. T. Eisenhart and J. L. Dempsey, *J. Chem. Educ.*, 2018, **95**, 197–206.
- 143 D. J. Graham, *Standard Operating Procedures for Cyclic Voltammetry*, 2018.
- 144 E. R. Clark, *Synthesis and Chemistry of 1,2,4-Benzothiadiazines*, University of Cambridge, 2008.

Chapter 2

1,2,4-Benzothiadiazine 1-Chlorides

"If it bleeds, we can kill it."

Predator (1987)

2.1 - Introduction to 1,2,4-Benzothiadiazines

1,2,4-Benzothiadiazines in various oxidation states (Figure 2.1.1) have been known for many years.¹ Early studies focused on the S^{VI} 1,1-dioxides (**A**) for their medicinal properties² and this framework now lies at the core of commercially available pharmaceuticals used to treat osteoporosis and hypertension.^{3,4} S^{II} derivatives (**B**) may undergo one electron oxidation to form stable benzothiadiazinyl radicals,^{1,5,6} and appropriately functionalised S^{II} 1,2,4-benzothiadiazines can act as bidentate *N,N'*-chelating ligands to afford first row transition metal^{7,8} and Ir^{III} complexes.⁹ Whilst reports of the S^{IV} heterocycles (**C-D**) are limited,^{1,10-12} their facile synthesis allows hitherto inaccessible S^{II} and S^{VI} analogues to be prepared.⁶

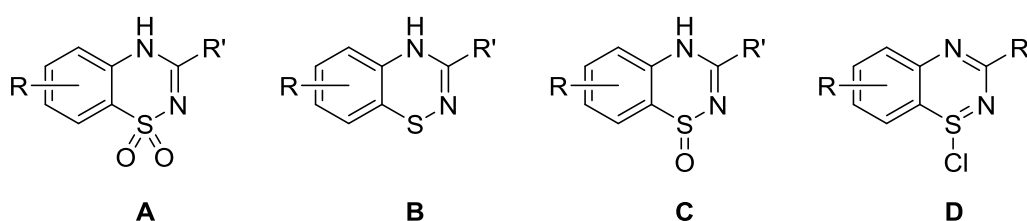
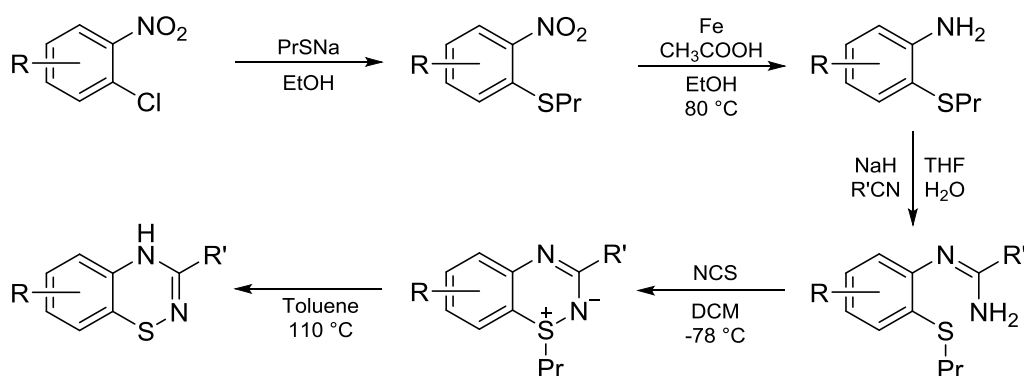
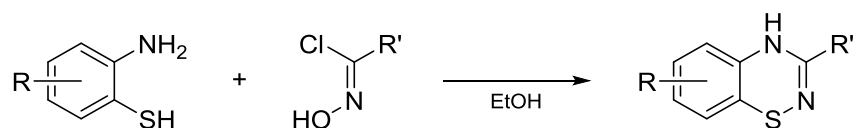


Figure 2.1.1: Various oxidation states of 1,2,4-benzothiadiazines.

Early synthetic routes to S^{II} 1,2,4-benzothiadiazines relied on the preparation and subsequent reduction of S^{IV} 1-oxides,¹² whilst more recent approaches have utilised the thermolysis and intramolecular elimination of *S*-alkyl ylides (Scheme 2.1.1).⁵ The use of microwave synthesis has been shown to afford high yields and short reaction times in several key reaction steps.¹³ The only direct methods to these species however, involve the condensation of *ortho*-aminothiophenols with hydroxamoyl chlorides (Scheme 2.1.2)¹⁴ which, despite having high reported yields, suffers from a limited range of suitable starting materials. The multi-step reactions, sensitivity to substituents, and lack of a general method for the synthesis of S^{II} 1,2,4-benzothiadiazines therefore prompted us to focus on S^{IV} 1-chlorides (**D**) as suitable precursors to neutral S^{III} 1,2,4-benzothiadiazinyl radicals.



Scheme 2.1.1: Synthesis of S^{II} 1,2,4-benzothiadiazines *via* thermal elimination.

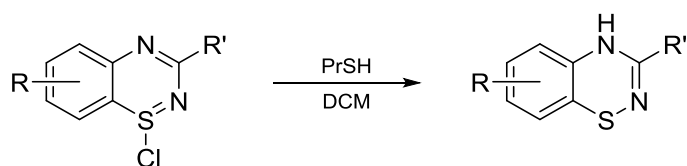


Scheme 2.1.2: Direct synthesis of S^{II} 1,2,4-benzothiadiazines *via* condensation of *ortho*-aminothiophenols and hydroxamoyl chlorides.

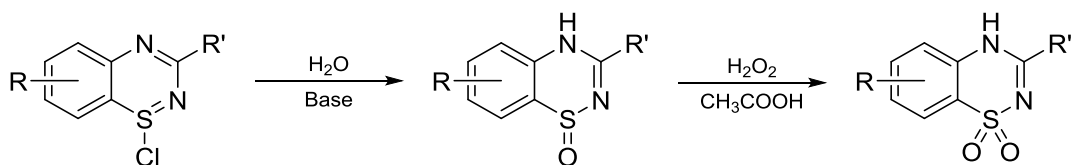
2.2 – Introduction to 1,2,4-Benzothiadiazine 1-Chlorides

The relatively short synthetic pathway and tolerance to substitutional variation make the S^{IV} 1-chlorides advantageous precursors to the corresponding radicals. These are a potentially extremely versatile as they allow fine-tuning of the molecular structure, and hence physical properties, by altering the substituents around the fused-ring and changing the nature of the pendant groups. The 1,2,4-benzothiadiazine 1-chlorides were first synthesised in 1981 utilising SCl_2 as the source of sulfur as well as the oxidising and chlorinating agent.¹⁵ The strongly chlorinating nature of the reaction conditions however, resulted in substitution of labile functional groups by chlorine, and varying degrees of chlorination of the benzo-fused ring.

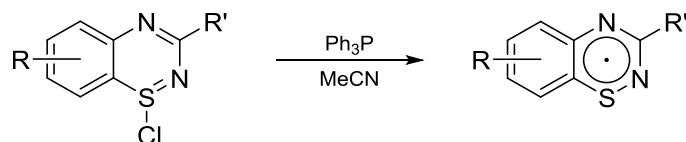
The 1,2,4-benzothiadiazine 1-chlorides may undergo facile $2e^-$ reduction,⁶ typically using a thiol (Scheme 2.2.1), to afford the corresponding S^{II} heterocycles, making hitherto inaccessible analogues available as valid synthetic targets. The S^{IV} 1-chlorides are also susceptible to hydrolysis to form the S^{IV} 1-oxides,¹⁰ which may be further oxidised up to the S^{VI} 1,1-dioxide (Scheme 2.2.2).¹² Finally, $1e^-$ reduction of 1,2,4-benzothiadiazine 1-chlorides, under mild conditions (Scheme 2.2.3), yields the target neutral S^{III} benzothiadiazinyl radicals [Discussed in Chapter 3].



Scheme 2.2.1: Two electron reduction of 1,2,4-benzothiadiazine 1-chlorides.



Scheme 2.2.2: Hydrolysis of 1,2,4-benzothiadiazine 1-chlorides and subsequent two electron oxidation.

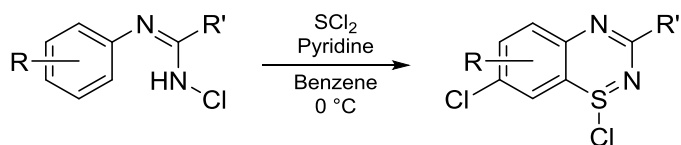


Scheme 2.2.3: One electron reduction of 1,2,4-benzothiadiazine 1-chlorides.

2.2.1 – Prior Synthesis of 1,2,4-Benzothiadiazine 1-Chlorides

2.2.1.1 – Route 1 – SCl₂

The first detailed study of the synthesis of 1,2,4-benzothiadiazine 1-chlorides was carried out by Levchenko in 1984,¹⁰ by the reaction of *N*-chloroamidines with SCl₂ in the presence of base (Scheme 2.2.1.1.1). This was found to give ring-closed and oxidised benzothiadiazine 1-chlorides with varying degrees of chlorination on the benzo-fused ring. Their experiments revealed that the position *para* to the amidine nitrogen was always chlorinated suggesting that chlorination occurred either at the same time as or prior to ring-closure. 1,2,3-Dithiazolylum salts prepared by Herz cyclisation are also prone to chlorination at this position.^{16,17} No additional chlorination was observed on the pendant aryl groups (R') despite the fact that the products were recrystallised from solvents saturated with Cl₂.



Scheme 2.2.1.1.1: Synthesis of 1,2,4-benzothiadiazine 1-chlorides *via* Route 1.

Levchenko reported that careful control of the quantity of SCl₂ and reaction conditions could offer access to selectively chlorinated derivatives.¹⁰ However, previous work by Clark¹⁸ found this approach to be unreproducible and all attempts to prepare partially-chlorinated derivatives or form those based upon methyl-substituted amidine precursors were unsuccessful. Further studies into this route revealed that in the absence of base, the *N*-protonated S^{IV} benzothiadiazine 1-chloride (**E**) (Figure 2.2.1.1.1) was isolated, whilst utilising the hindered base, EtNⁱPr₂, afforded the S^{II} benzothiadiazine (**F**). This indicates that the S^{II} species is the initial product and that ring chlorination *para* to the nitrogen must be more facile than chlorination at the heterocyclic sulfur centre. Other experiments revealed that the amidine precursor itself is the initial base during the reaction, suggesting that a large excess is required in relation to SCl₂ to form the neutral S^{IV} benzothiadiazine 1-chloride. However, in the absence of excess SCl₂ the reaction mixtures were observed to decay to dark-green EPR active solutions suggesting either partial oxidation to the corresponding S^{III} radical or

comproportionation of the S^{II} and S^{IV} states. Thus in order to stabilise the desired S^{IV} product, an excess of SCl₂ or additional chlorinating agent such as SO₂Cl₂ is required.

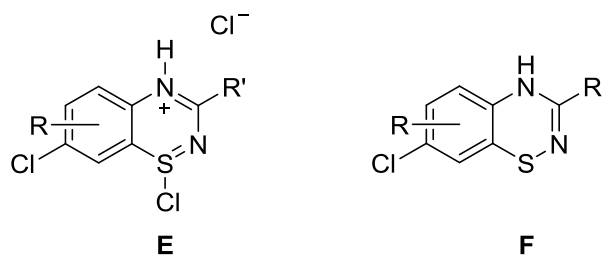
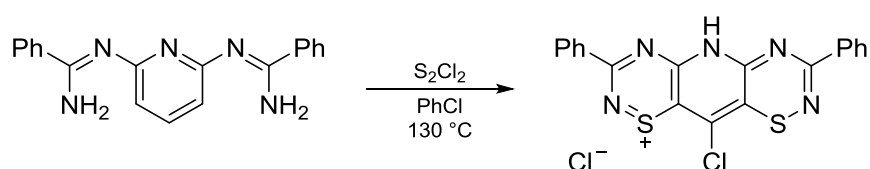


Figure 2.2.1.1.1: Intercepted intermediates *via* Route 1.

In light of these observations, Clark developed a modified procedure, using NaH as a strong, non-nucleophilic base and performing the reaction at room temperature to prevent further ring chlorination. Trace SO₂Cl₂ was added during recrystallization to stabilise the S^{IV} state, and this was successfully employed to prepare substituted 1,2,4-benzothiadiazine 1-chlorides.

2.2.1.2 - Route 2 - S₂Cl₂

More recent research by Oakley^{19,20} into the related, symmetrical *bis*-thiadiazines has made use of the milder, less oxidising S₂Cl₂, which yielded mixed valence S^{II}/S^{IV} compounds (Scheme 2.2.1.2.1). Unlike Route 1, the starting amidine is unoxidised and no base is present. Instead the reaction is performed under reflux in high boiling solvents to drive off the HCl. This initial step occurs with chlorination of the fused ring, whilst the pendant aryl-groups remain unaffected. The ionic character of the S^{IV} chloride is reflected in the subsequent facile anion metathesis step, the stability of which is ascribed to the high symmetry of the resonance stabilised cation. Further transformations are necessary however to remove the acidic proton and alkylate the species prior to reduction to the target radical.



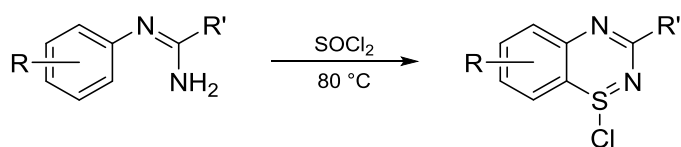
Scheme 2.2.1.2.1: Synthesis of *bis*-1,2,4-benzothiadiazines *via* Route 2.

2.2.1.3 - Route 3 - SOCl₂

The complications involving S^{II} intermediates prompted Clark to explore the use of SOCl₂ as a S^{IV} source in the synthesis of 1,2,4-benzothiadiazine 1-chlorides. Despite the

well-established chemistry of thionyl chloride with primary amines,²¹ first investigated in 1890, its reactions with *N*-arylamidines has received less attention. Benzothiadiazine 1-oxides have been prepared by the reaction of *N*-phenyl-benzamidine with SOCl₂ followed by an aqueous work-up, but this approach was low-yielding.¹² Initial attempts to react thionyl chloride with *N*-phenyl-benzamidine were unsuccessful, yielding a fine colourless precipitate of *N*-phenyl-benzamidine hydrochloride, and a dark red supernatant which swiftly discoloured regardless of the choice of base or solvent.

The use of thionyl chloride as both the reagent and high-boiling solvent circumvented the poor solubility of amidinium hydrochloride salts, whilst performing the reaction under reflux to drive off HCl eliminated the need for additional base. These conditions (Scheme 2.2.1.3.1) afforded a family of substituted 1,2,4-benzothiadiazine 1-chlorides in good yield, crystallised by layering dry hexane onto the reaction mixture. It is believed that the 1,2,4-benzothiadiazine 1-oxide is the initial ring-closed product, which then reacts with a second equivalent of SOCl₂, with the loss of SO₂ and HCl gas, to give the desired S^{IV} 1-chloride. Additional chlorination to the fused-ring and substituents is also observed due to the strongly chlorinating conditions, but the exact stage at which this occurs is unknown.



Scheme 2.2.1.3.1: Synthesis of 1,2,4-benzothiadiazines 1-chlorides *via* Route 3.

This chapter will further expand on this synthetic approach to prepare a library of substituted 1,2,4-benzothiadiazine 1-chlorides as suitable precursors to the neutral S^{III} benzothiadiazinyl radicals.

2.3 – Synthesis of New Compounds

2.3.1 – Synthesis of Substituted *N*-Arylamidines

A large family of substituted *N*-arylamidines **1a-q** (Figure 2.3.1.1) were prepared *via* standard methods, through condensation of lithiated anilines with suitable carbonitriles followed by aqueous work-up,²² or by Lewis-acid mediated condensation in the melt.²³

	Aniline R	Nitrile R'	Synthetic Route	Yield %
1a	H	Ph	A	89.7
1b	2-Me	Ph	A	70.8
1c	2,3-Me ₂	Ph	A	86.8
1d	2,5-Me ₂	Ph	A	78.7
1e	3,5-Me ₂	Ph	A	77.8
1f	3-OMe	Ph	A	64.5
1g	H	<i>o</i> -Tolyl	A	62.8
1h	2,3-Me ₂	<i>o</i> -Tolyl	A	66.1
1i	H	<i>p</i> -Pyridyl	A	87.9
1j	2,3-Me ₂	<i>p</i> -Pyridyl	A	84.5
1k	H	<i>p</i> -OMe-C ₆ H ₄	A	77.0
1l	2,3-Me ₂	<i>p</i> -OMe-C ₆ H ₄	A	73.7
1m	4-Me	Ph	A	70.8
1n	2,4-Me ₂	Ph	A	72.2
1o	2-Ph	Ph	A	67.5
1p	H	^t Bu	B	41.0
1q	H	<i>p</i> -NO ₂ -C ₆ H ₄	A or B	0

Figure 2.3.1.1: Target substituted *N*-arylamidines.

The syntheses of amidines **1a-o** proceeded in good yield to give colourless crystalline solids. Attempts to prepare *p*-nitro-substituted amidine **1q** by the standard routes were unsuccessful, and both the base and acid-catalysed Pinner reaction^{24,25} were likewise found to be ineffective, yielding only free aniline or substituted methyl benzoate respectively, the latter due to hydrolysis of the intermediate iminoether.

2.3.2 – Synthesis of Substituted 1,2,4-Benzothiadiazine 1-Chlorides

Substituted 1,2,4-benzothiadiazine 1-chlorides were prepared according to Route 3, by refluxing the corresponding *N*-arylamididine in neat thionyl chloride. This approach was successfully employed to prepare compounds **2a-h** and **2k-l** (Figure 2.3.2.1). In all instances, the benzo-fused ring was partially chlorinated, and for compounds **2b-e** the methyl groups at the 5 or 6 position were also singly chlorinated whilst methyl groups at the 8 position were unaffected. This is in contrast to the milder conditions of Route 1, where the methyl groups remain unchlorinated.¹⁸

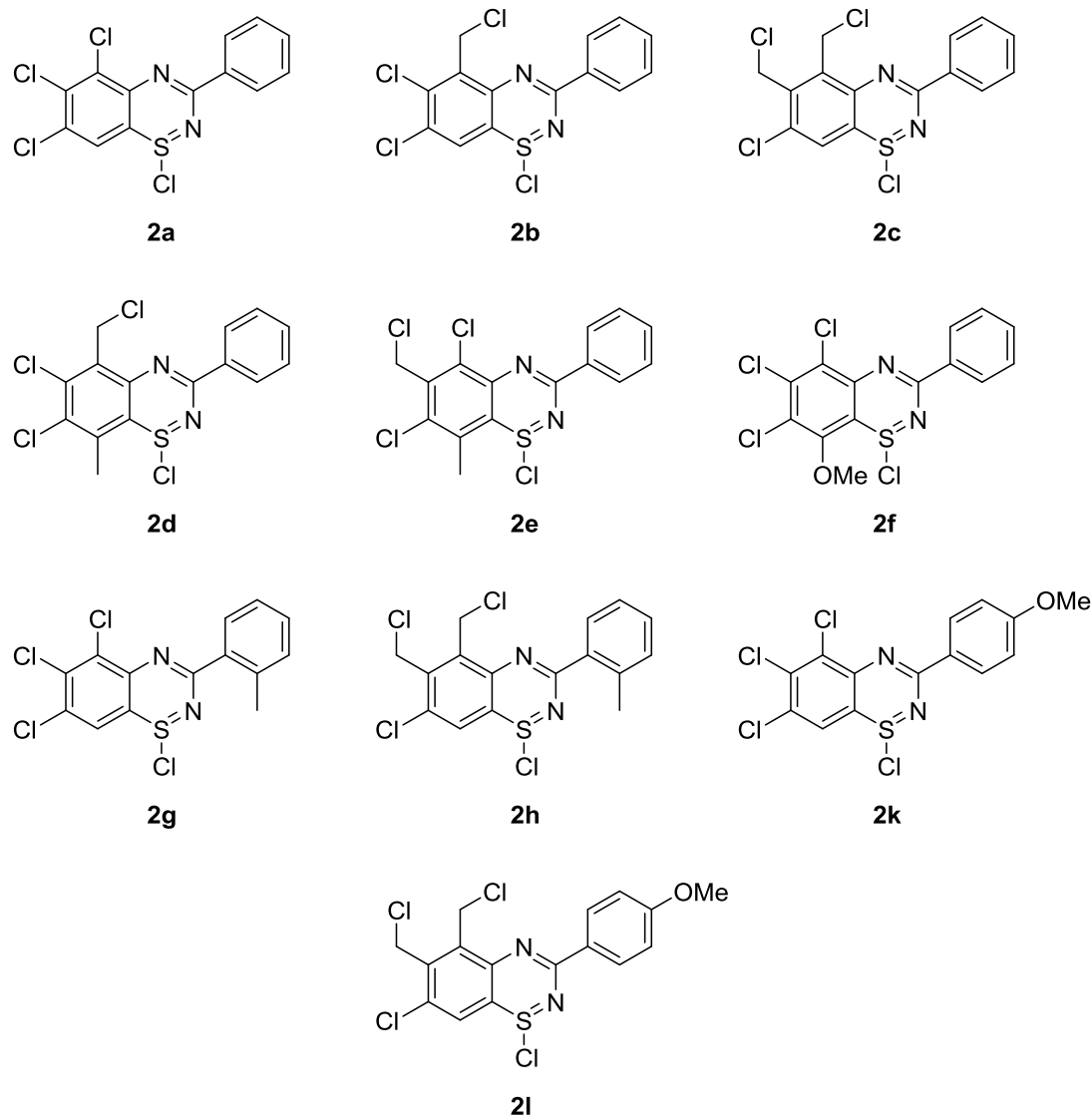


Figure 2.3.2.1: Substituted 1,2,4-benzothiadiazine 1-chlorides synthesised in this thesis.

The 1,2,4-benzothiadiazine 1-chlorides were isolated as yellow to red solids that were poorly soluble in most organic solvents (DCM, THF, toluene), but readily dissolved in thionyl chloride. Crystals suitable for single-crystal X-ray diffraction were grown by slow diffusion of hexane into a saturated solution of the product in SOCl_2 or by slow cooling from boiling SOCl_2 . Derivative **2e** was isolated in high purity by NMR and elemental analysis, but no crystals suitable for SCXRD analysis were obtained.

Initial attempts to prepare **2i** under standard conditions resulted in partial chlorination ($X = \text{Cl} \approx 45\%$) at position X, *ortho* to the OMe moiety (Figure 2.3.2.2). Nevertheless, the minor product, **2r**, was still fully characterised by ^1H and ^{13}C NMR spectroscopy using a range of 2D experiments. Repeating the reaction with decreased reflux times cleanly afforded compound **2i**. The red solid was observed to slowly discolour to green in both solution and solid-state over the course of several days, even

in the absence of light. The addition of trace SO_2Cl_2 during recrystallisation to help stabilise the S^{IV} state afforded crystals identified as **2s** by SCXRD ($X = \text{Cl} \approx 58\%$), demonstrating the susceptibility of these species to further chlorination. Attempts to isolate **2r** and **2s** as analytically pure compounds were unsuccessful.

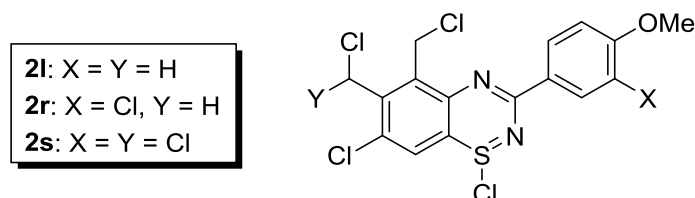


Figure 2.3.2.2: Variable chlorination species observed for 1,2,4-benzothiadiazine 1-chlorides derived from **1l**.

Attempts to prepare **2i** yielded a yellow solid that was practically insoluble in most organic solvents and only poorly soluble in SOCl_2 , suggesting that the pyridinium hydrochloride salt had formed. NMR data indicated that position X (Figure 2.3.2.3) was partially chlorinated ($X = \text{Cl} \approx 40\%$), which implies that the position *ortho* to the amidine functionality is the second position on the benzo-fused ring to be chlorinated. This is expected to occur rapidly after chlorination of the position *para* to the amidine functionality which is believed to be chlorinated prior to, or at the same time as ring-closure (*vide infra*). Prolonged reflux in the presence of excess SO_2Cl_2 and larger volumes of SOCl_2 only increased chlorination at position X to $\approx 60\%$ due to the poor solubility of the salt, whilst shorter refluxing times afforded other unidentified species.

In contrast, no partial chlorination was observed for compound **2j** by ^1H and $^{13}\text{C}\{^1\text{H}\}$ NMR spectroscopy despite also suffering from limited solubility. Crystals of **[2j.H][HCl₂]** grown from SOCl_2 and hexane indicated that the $[\text{Cl-H-Cl}]^-$ salt had formed whilst elemental analysis values were between that expected for the HCl and $\text{H}[\text{HCl}_2]$ salts even after recrystallisation, likely due to the poor stability of the $[\text{HCl}_2]^-$ anion and tendency to readily lose HCl . It is possible that compound **2i** also exists as both the Cl^- and $[\text{HCl}_2]^-$ salts but elemental analysis results were inconclusive.

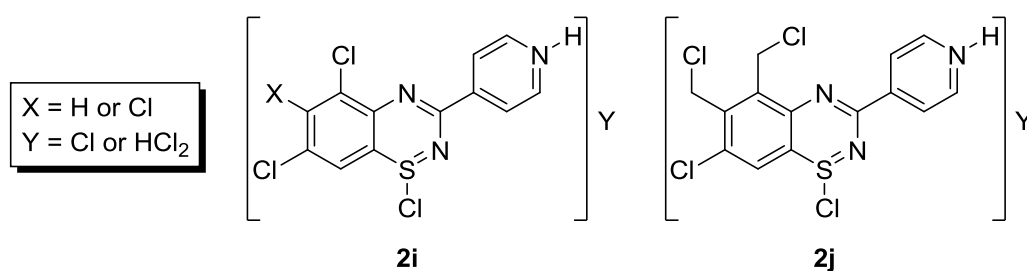


Figure 2.3.2.3: Synthesis of 1,2,4-benzothiadiazine 1-chloride pyridinium salts.

Attempts to deprotonate compound **2i** with basic amines (pyridine, Et₃N, DABCO) resulted in the immediate formation of a dark blue EPR active solution consistent with the formation of the neutral BTDA radical (*vide infra*), which indicates that these species are highly oxidising. Crystals of **3i** suitable for SCXRD analysis (Figure 2.3.2.4), grown by slow cooling of the reaction mixture, confirmed the formation of the neutral radical, which unlike the parent 1,2,4-benzothiadiazine 1-chloride, is only partially chlorinated around 17 % at position X.

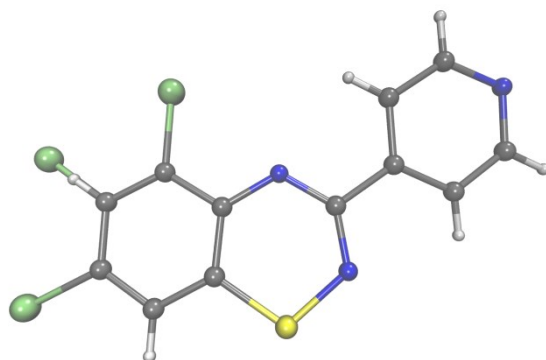


Figure 2.3.2.4: Crystal structure of **3i** showing the partial chlorination of fused-ring.

Following the synthesis of **2d**, slow cooling of the reserved supernatant afforded orange needles of the isomeric compound **2t** with partial chlorination at position X (X = Cl \approx 12 %) (Figure 2.3.2.5). This finding suggests that the rate of the second chlorination step of the methyl group *ortho* to the amidine nitrogen is comparable to the chlorination of the fused ring at position X as seen for **2d**; the former process is expected to dramatically suppress further chlorination at position X due to steric constraints.

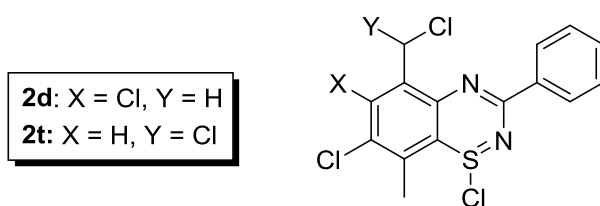


Figure 2.3.2.5: Isomeric forms of 1,2,4-benzothiadiazine 1-chlorides derived from **1d**.

No crystalline products could be isolated for the reactions of **1m-n** with SOCl₂. Since chlorination occurs *para* to the amidine functionality prior to or at the same time as ring-closure, it is believed that the presence of a methyl-group at this position inhibits the formation of the desired 1,2,4-benzothiadiazine 1-chloride. Attempts to prepare **2o** were unsuccessful; yielding a dark brown insoluble solid assigned as a mixture of partially chlorinated species by ¹H NMR. A low yield of pale peach solid was obtained

during the attempted synthesis of **2p** and colourless crystals were grown by recrystallization of the crude solid from boiling SOCl₂. This was identified as partially chlorinated **1p.HCl** (Figure 2.3.2.6) by SCXRD suggesting that chlorination of the aryl-ring is more rapid than ring-closure; chlorination at both positions *ortho* to the amidine nitrogen inhibits the formation of the fused-ring.

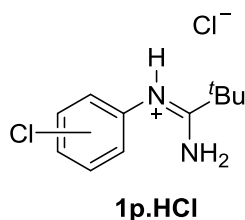


Figure 2.3.2.6: Isolated products from the reaction of **1p** with SOCl₂.

2.4 – Structural Studies of 1,2,4-Benzothiadiazine 1-Chlorides

The structures of the crystallographically characterised 1,2,4-benzothiadiazine 1-chlorides are labelled according to the general scheme shown in Figure 2.4.1.

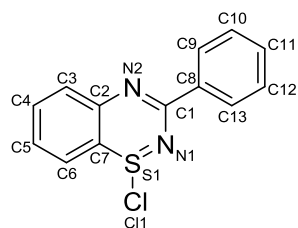


Figure 2.4.1: Structural labelling scheme.

The deviation from planarity of the heterocyclic ring, measured as the difference in angles between the mean planes of the benzo-fused ring (C2-C7) and the S1-N1-C1-N2 fragment, shows significant variation in the formally 10 π aromatic chlorides (Table 2.4.1). In all instances, N1 lies considerably above or below the plane of the fused-ring depending on the orientation of the S-Cl bond (Figure 2.4.2). The S^{IV} 1,2,4-benzothiadiazine 1-chlorides are however more planar than the 12 π protonated S^{II} derivatives.¹³ The torsion angles also show variety, reflecting the degree of twisting of the pendant aryl ring with respect to the heterocyclic ring. This is most noticeable for the *o*-tolyl substituted compounds, **2g-h**, where steric interactions of the methyl-group with either N1 or N2 disfavour a coplanar orientation. Compounds with larger N1-C1-C8-C13 and N2-C1-C8-C9 torsion angles (Table 2.4.1) were found to have a greater deviation from planarity.

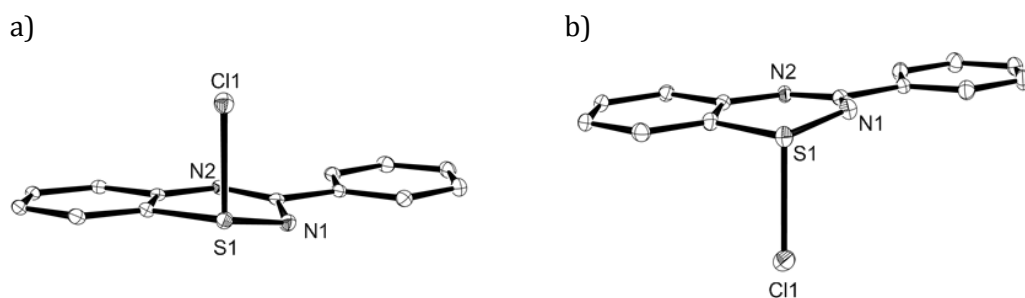


Figure 2.4.2: Idealised geometry showing the orientation of the S-Cl bond with respect to the benzo-fused ring: a) Above the plane; b) Below the plane.

	Deviation from Planarity / °	Torsion Angles / °		S-Cl Bond Length / Å	S-Cl Angle / ° N2-S1-Cl1
		N1-C1-C8-C13	N2-C1-C8-C9		
2a	9.38	6.00(3)	2.42(3)	2.2572(7)	102.64(4)
2b	11.13	11.90(3)	9.05(3)	2.2811(8)	102.58(4)*
2c	7.17	6.65(3)	4.18(3)	2.3412(7)	106.11(4)*
2d-α	12.88	8.64(4)	6.16(4)	2.2974(9)	102.32(5)
2f	8.07	3.83(2)	0.89(2)	2.2759(6)	104.06(3)*
2g	8.96	19.80(1)	16.08(1)	2.309(2)	106.23(1)
	15.07	10.51(1)	9.96(1)	2.229(3)	99.97(1)
2h	18.33	30.90(3)	28.91(3)	2.2689(9)	99.84(5)
2j.H[HCl₂]	14.28	20.56(2)	18.15(2)	2.238(4)	100.25(2)
2k	8.60	9.59(3)	5.89(3)	2.3205(8)	106.80(5)
2l	7.71	8.25(5)	5.10(5)	2.279(1)	105.33(7)
2s	7.75	9.98(1)	8.45(1)	2.264(4)	103.42(2)
2t	12.63	7.01(9)	4.03(9)	2.287(2)	104.89(1)

* S-Cl bond orientated below the plane of the benzo-fused ring.

Table 2.4.1: Structural parameters of 1,2,4-benzothiadiazine 1-chlorides.

The variation in S-Cl bond lengths weakly correlate with the electronegativity of the fused-ring, with **[2j.H][HCl₂]** having the shortest at 2.238(4) Å whilst **2c**, which bears two mildly electron-donating chloromethyl-groups, has the longest S-Cl bond length at 2.3412(7) Å. No apparent correlation is observed for the N2-S1-Cl1 angles, and these differences are likely to arise through external packing forces. On average, the S-Cl bonds (2.281 Å) are longer than the literature value for a single covalent S-Cl bond (2.072 Å)²⁶ and are more comparable to those seen in thiatriazines (2.283-2.357 Å).^{27,28} These benzothiadiazine 1-chlorides clearly show a significantly covalent S-Cl bond and should not be classed as salts. For example, DTDA salts are considered ionic but exhibit long S...Cl contacts (2.906-2.962 Å)²⁹ within the sum of the van der Waals radii (3.55 Å).³⁰ The strength of the S-Cl bond is of particular interest here because it largely reflects the ease with which the system may undergo anion metathesis reactions or be reduced to the neutral radical.

2.4.1 – Crystal Structure of 2a

Compound **2a** crystallises as large orange blocks in the monoclinic space group $P2_1/n$ with a single molecule in the asymmetric unit (Figure 2.4.1.1). The heterocyclic ring deviates considerably from planarity at 9.38° , largely due to the position of N1, whilst the pendant phenyl ring only deviates from coplanarity of the fused ring by 4.02° . Despite providing satisfactory elemental and NMR analysis, crystals of **2a**, grown by slow cooling of a saturated SOCl_2 solution, showed partial additional chlorination (ca. 12.5 %) at C6. Interestingly, previous crystallographic studies by Clark have showed that crystals of **2a**, grown by slow diffusion of hexane into a saturated solution of the compound in thionyl chloride, crystallises with two molecules in the asymmetric unit, also in the monoclinic space group $P2_1/n$. This partial chlorination results in a crystal structure that is instead isostructural with the perchlorinated analogue.¹⁸

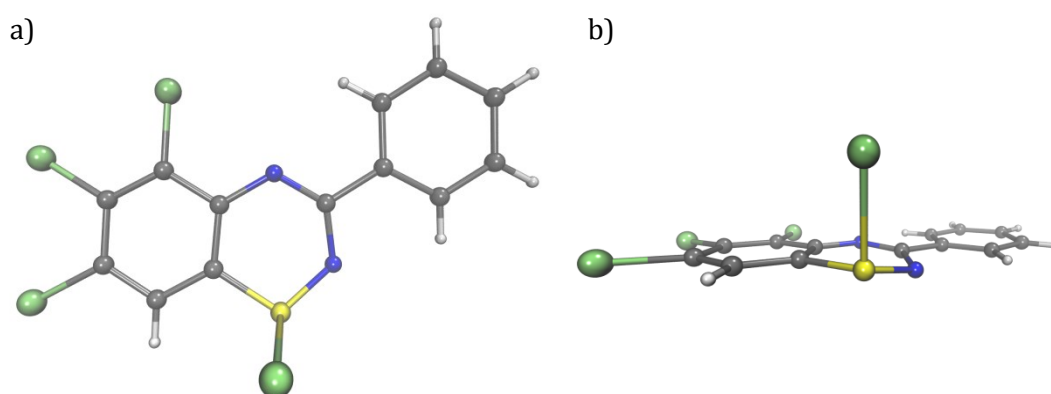


Figure 2.4.1.1: Crystal structure of **2a**: a) Top-down view. b) Side view.

2.4.2 – Crystal Structure of 2b

Compound **2b** crystallises as yellow blocks in the triclinic space group $P\bar{1}$ with a single molecule in the asymmetric unit (Figure 2.4.2.1). The heterocyclic ring deviates from planarity with respect to the fused ring by 11.13° , whilst the pendant phenyl ring remains relatively coplanar at 3.10° . The harsh ring-closing conditions results in chlorination of the methyl-group, which is orientated above the plane of the fused-ring *trans* to the S-Cl bond.

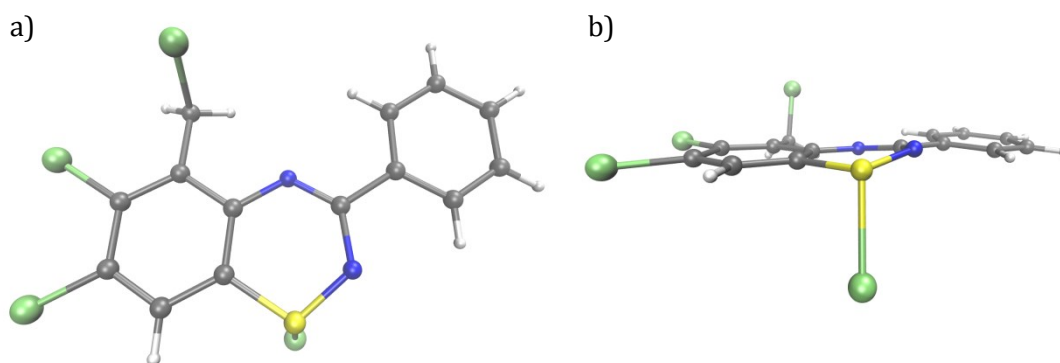


Figure 2.4.2.1: Crystal structure of **2b**: a) Top-down view. b) Side view.

2.4.3 – Crystal Structure of **2c**

Compound **2c** crystallises as yellow plates in the triclinic space group $P\bar{1}$ with a single molecule in the asymmetric unit (Figure 2.4.3.1). The deviation from planarity (7.17°) is lower than other structurally characterised 1,2,4-benzothiadiazine 1-chlorides, and the pendant phenyl ring is essentially coplanar with the benzo-fused-ring at 0.63° . Both CH_2Cl groups are orientated above the plane in a *cis* conformation, and *trans* to the S-Cl bond. Additional chlorination (*ca.* 3.5 %) is observed at C6, whilst minor unmodelled residual electron density in close proximity to the methyl-protons suggests that these positions are also sensitive to further chlorination.

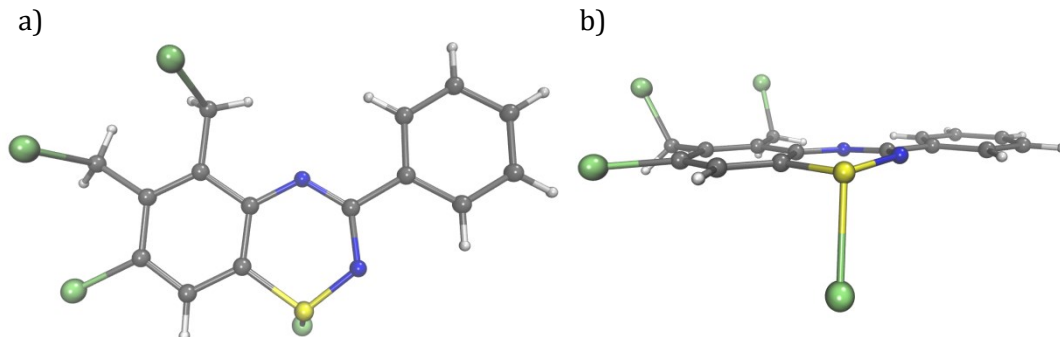


Figure 2.4.3.1: Crystal structure of **2c**: a) Top-down view. b) Side view.

2.4.4 – Crystal Structure of **2d- α**

Crystallisation of compound **2d** from boiling SOCl_2 afforded orange needles that crystallise in the monoclinic space group $P2_1/c$ with a single molecule in the asymmetric unit (Figure 2.4.4.1). The heterocyclic ring deviates significantly from planarity at 12.88° whilst the pendant phenyl ring is relatively coplanar at 2.98° despite comparatively large torsion angles. The CH_2Cl group on C3 is orientated below the plane of the fused-ring and *trans* to the S-Cl bond; the methyl group at C6 is not chlorinated under these conditions.

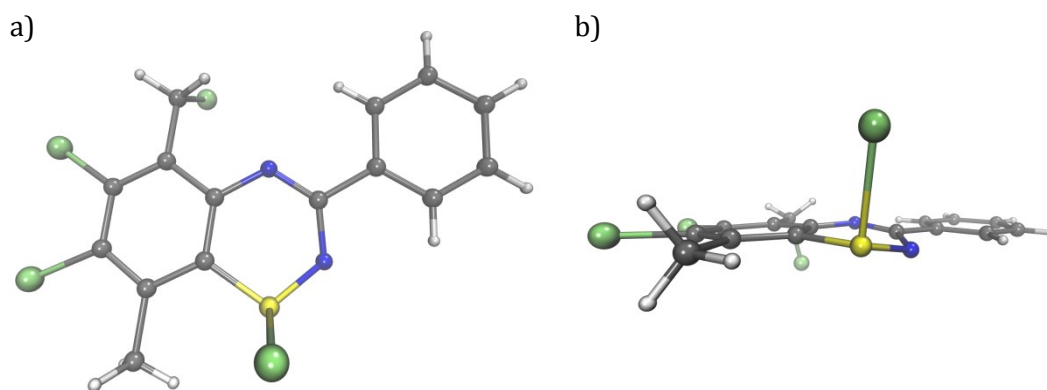


Figure 2.4.4.1: Crystal structure of **2d-α**: a) Top-down view. b) Side view.

Previous studies by Clark has shown that slow diffusion of hexane into a saturated solution of **2d** in thionyl chloride produced two distinct crystal morphologies, predominately orange needles (α -phase) with red blocks (β -phase) as the minor product. These two forms differ in the orientation of the CH_2Cl group relative to the S-Cl bond, a phenomenon known as conformational polymorphism.³¹ Attempts to grow crystals of the β -phase however, to permit direct and precise structural metric comparisons with the other 1,2,4-benzothiadiazine 1-chlorides at the same temperature, were unsuccessful.

2.4.5 – Crystal Structure of **2f**

Compound **2f** crystallises as dark orange blocks in the triclinic space group $P\bar{1}$ with a single molecule in the asymmetric unit (Figure 2.4.5.1). The deviation from planarity of the heterocyclic ring (8.07°) and coplanarity of the pendant phenyl ring (2.76°) is comparable to **2a** whilst the torsion angles are considerably smaller. The methoxy group is disordered such that it is orientated equally above and below the plane of the benzo-fused ring. The twisting of the methoxy group out of conjugation of the fused ring is necessary to minimise steric interactions resulting from chlorination. Despite potential steric clash, the methoxy group is located on C6 and acts as a *ortho*-directing electron donating group during the ring-closure, and not at C3 as a *para*-directing group, as previously anticipated and observed for similar systems discussed in Chapter 4.

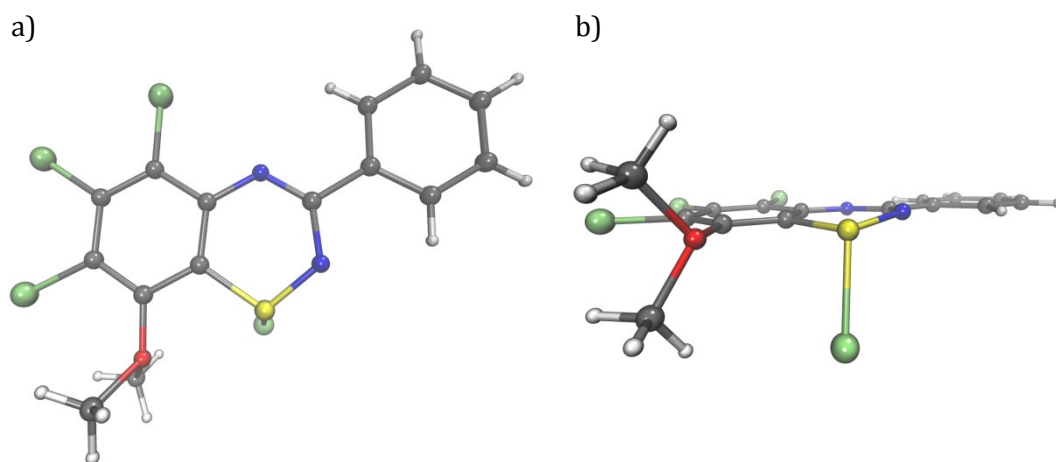


Figure 2.4.5.1: Crystal structure of **2f**: a) Top-down view. b) Side view.

2.4.6 – Crystal Structure of **2g**

Compound **2g** crystallises as orange rods in the monoclinic space group $P2_1$ with two molecules in the asymmetric unit (Figure 2.4.6.1). The deviation from planarity of the heterocyclic ring is considerably larger in molecule two (15.07° vs. 8.96° for molecule one) whilst the torsion angles are significantly greater in molecule one ($19.80(1)^\circ$ and $16.08(1)^\circ$ vs. $10.51(1)^\circ$ and $9.96(1)^\circ$ for molecule two). The pendant *ortho*-tolyl ring in molecule one is twisted out of the plane by 12.61° with respect to the benzo-fused ring to minimise steric hindrance between the methyl-group and N2 of the heterocyclic ring. In contrast, the pendant *ortho*-tolyl ring in molecule two is essentially coplanar with only a minor deviation of 0.39° . The dramatic difference in the conformations observed for the two molecules suggests that external packing forces have a significant influence on their solid-state structure.

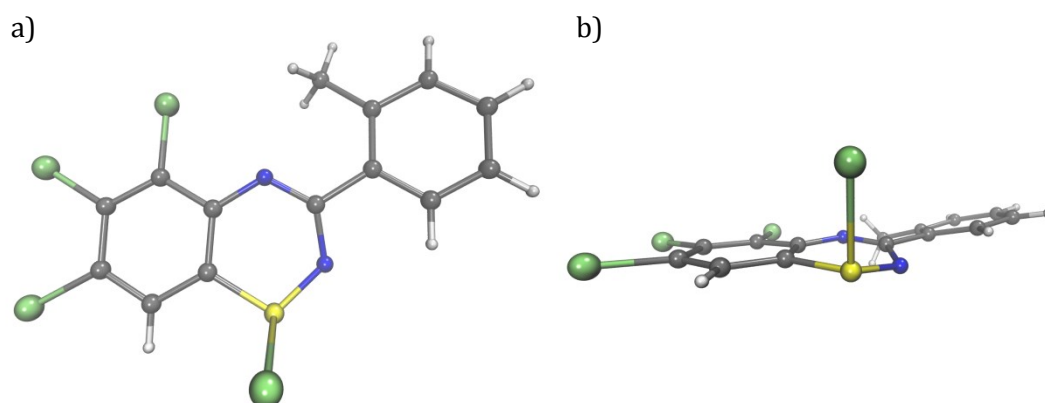


Figure 2.4.6.1: Crystal structure of **2g**, molecule one: a) Top-down view. b) Side view. Molecule two omitted for clarity.

2.4.7 – Crystal Structure of **2h**

Compound **2h** crystallises as dark yellow blocks in the orthorhombic space group *Pbca* with a single molecule in the asymmetric unit (Figure 2.4.7.1). The heterocyclic ring is severely distorted and deviates significantly from planarity at 18.33°. The pendant *ortho*-tolyl ring is twisted out of the plane of the fused-ring by 18.56°, resulting in large N1-C1-C8-C13 and N2-C1-C8-C9 torsion angles. Unlike compound **2g**, the pendant *ortho*-tolyl ring is orientated such that the methyl-group is closer to N1, presumably to minimise steric hindrance with the CH₂Cl group at C3. As with **2c**, both CH₂Cl groups are orientated above the plane of the fused-ring in a *cis* conformation, and *trans* to the S-Cl bond.

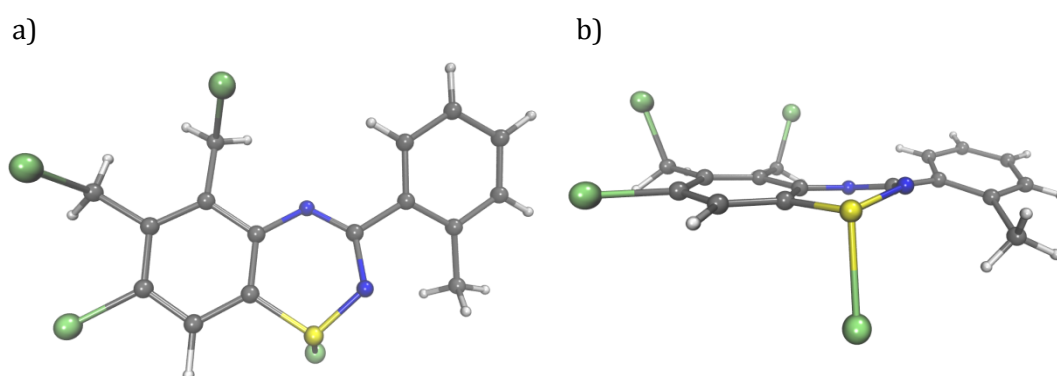


Figure 2.4.7.1: Crystal structure of **2h**: a) Top-down view. b) Side view.

2.4.8 – Crystal Structure of [2j.H][HCl₂]

Compound [2j.H][HCl₂] crystallises as yellow rods in the triclinic space group *P* $\bar{1}$ with a single ion pair in the asymmetric unit (Figure 2.4.8.1). The heterocyclic ring and pendant pyridyl ring deviate significantly from planarity/coplanarity with respect to the benzo-fused ring (14.28° and 14.59° respectively), and the torsion angles are larger than all of the other structural characterised 1,2,4-benzothiadiazine 1-chlorides except **2h**. The CH₂Cl groups adopt a *trans* conformation, with one CH₂Cl group orientated above the plane of the fused-ring and the other orientated below, contrary to the conformations adopted by both **2c** and **2h**.

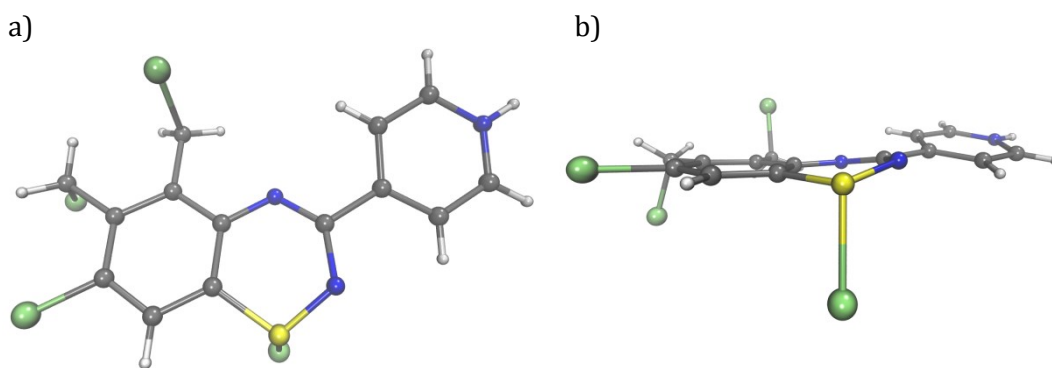


Figure 2.4.8.1: Crystal structure of $[2j.H][HCl_2]$: a) Top-down view. B) Side-view. HCl_2 counterion omitted for clarity.

The HCl_2 anion adopts a severely bent geometry ($113.70(6)^\circ$) with asymmetric and elongated H-Cl bond lengths ($2.001(1)$ and $1.809(1)$ Å) (Figure 2.4.8.2). This deviation from the model symmetric-linear geometry, which is typically observed for isolated ion pairs ($H-Cl \approx 1.57$ Å),³² is consistent with strong anion-cation interactions in the solid-state.³³

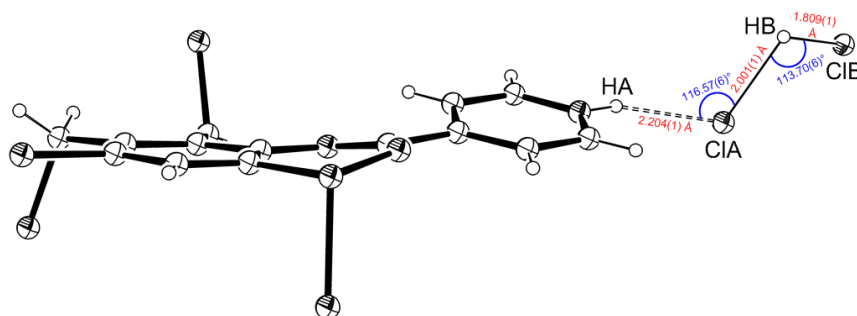


Figure 2.4.8.2: Crystal structure of $[2j.H][HCl_2]$ highlighting the HCl_2 counterion.

2.4.9 – Crystal Structure of **2k**

Compound **2k** crystallises as dark red rods in the triclinic space group $P\bar{1}$ with a single molecule in the asymmetric unit (Figure 2.4.9.1). The heterocyclic ring deviates from planarity at 8.60° and the torsion angles are similar to the other 1,2,4-benzothiadiazine 1-chlorides. The methoxy group is coplanar with the associated aryl-ring, which itself is essentially coplanar with the benzo-fused ring, with only a minor deviation of 0.91° . Whilst these features are reminiscent to **2a**, the S-Cl bond length is significantly elongated ($2.3205(8)$ vs $2.2572(7)$ Å), likely due to the addition of a more electron-rich pendant aryl ring.

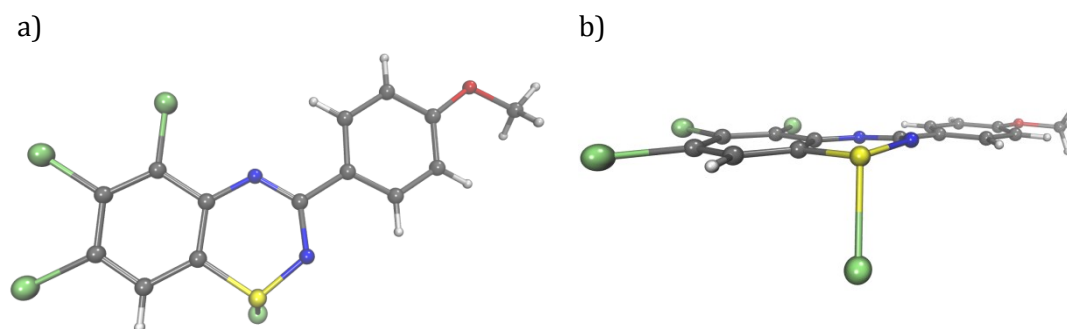


Figure 2.4.9.1: Crystal structure of **2k**: a) Top-down view. b) Side view.

2.4.10 – Crystal Structure of **2l**

Compound **2l** crystallises as orange needles in the triclinic space group $P\bar{1}$ with a single molecule in the asymmetric unit (Figure 2.4.10.1). The deviation from planarity of the heterocyclic ring is similar to **2c** (7.71° vs. 7.17°), as are the torsion angles and coplanarity of the pendant aryl ring (1.78° vs. 0.63° for **2c**). As with **2k**, the methoxy group is coplanar with the associated aryl ring. The CH_2Cl groups adopt a *cis* orientation below the plane of the fused-ring, and *trans* to the S-Cl bond. The S-Cl bond length is surprisingly short at $2.279(1)$ Å; this is counter to expectations since there is an increase in S-Cl bond length from **2a** to **2l**, whilst the longest distance observed across the 1,2,4-benzothiadiazine 1-chlorides is for **2c**. This again indicates that external packing forces have a significant influence on many of the structural features.

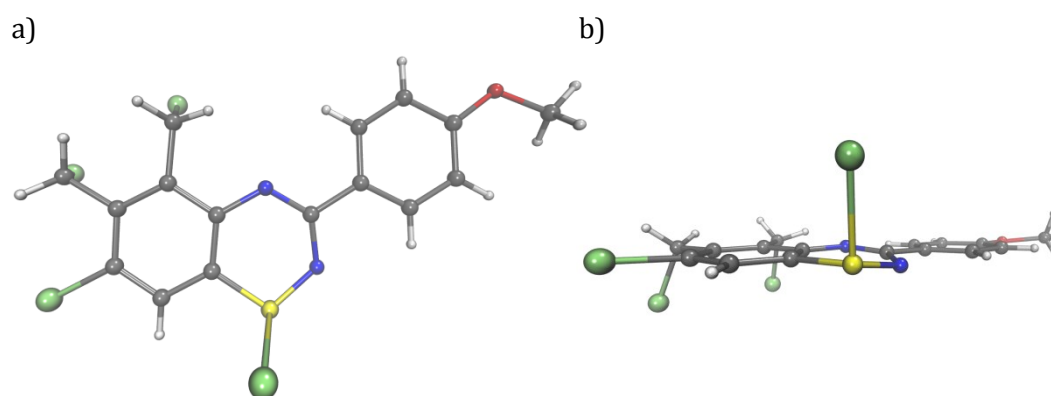


Figure 2.4.10.1: Crystal structure of **2l**: a) Top-down view. b) Side view.

2.4.11 – Crystal Structure of **2s**

Compound **2s** crystallises as red blocks in the monoclinic space group $P2_1/n$ with a single molecule in the asymmetric unit (Figure 2.4.11.1). The deviation from planarity of the heterocyclic ring is 7.75° , comparable to **2c** and **2l**, whilst the pendant aryl ring is twisted slightly with a deviation of 4.93° . The partial chlorination ($\approx 58\%$) at the position *ortho* to the methoxy group causes it to flip 180° to minimise steric hindrance,

however it still remains coplanar with the associated aryl ring to allow conjugation of the oxygen lone pairs into the aromatic system. This also suppresses additional chlorination at the other *ortho* position.

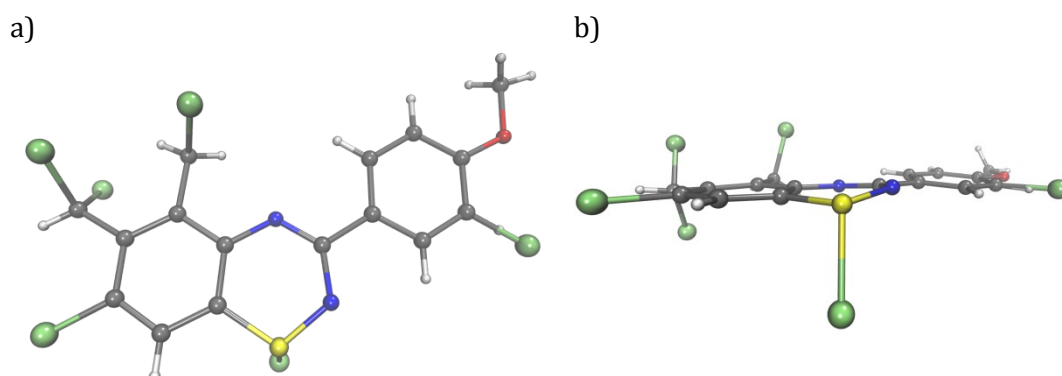


Figure 2.4.11.1: Crystal structure of **2s**: a) Top-down view. b) Side view. Shown with partial chlorination.

2.4.12 – Crystal Structure of **2t**

Compound **2t** crystallises as orange rods in the monoclinic space group $P2_1/n$ with a single molecule in the asymmetric unit (Figure 2.4.12.1). The deviation from planarity of the heterocyclic ring is similar to the isomeric **2d- α** (12.63° vs. 12.88°) whilst the pendant phenyl ring is twisted slightly (5.21° vs. 2.98° for **2d- α**). The position *meta* to the amidine nitrogen is partially chlorinated ($\approx 12\%$) and the CHCl_2 group is orientated to minimise steric hindrance.

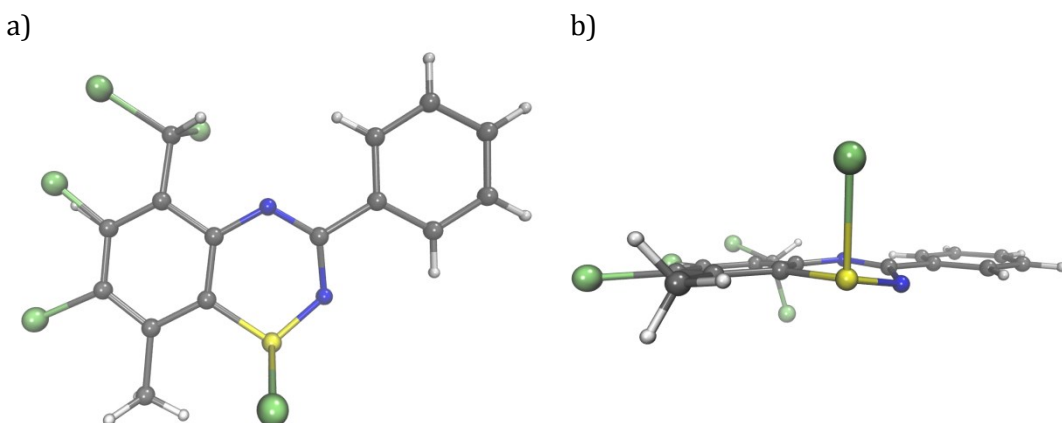


Figure 2.4.12.1: Crystal structure of **2t**: a) Top-down view. b) Side view. Shown with partial chlorination.

2.4.13 – Conformational Polymorphism

The variation in deviations from planarity for the heterocyclic ring and pendant aryl-ring, as well as the range of torsion angles and S-Cl bond lengths in the solid-state, clearly reflects the conformational flexibility of the 1,2,4-benzothiadiazine 1-chlorides. Previous studies by Clark¹⁸ found that compound **2d** adopts two distinct crystal

morphologies that differ in the conformation of the CH₂Cl group relative to the S-Cl bond. *Ab initio* computational studies were employed to further understand the conformational polymorphism; the favourable energies in the gas-phase for **2d- α** suggest that it is the thermodynamic product and that **2d- β** is the kinetic product. However, the barrier to interconversion between the two conformers, performed *via* single-point calculations, was found to be negligible. This result is consistent with the rapid interconversion observed by NMR and suggests that the conformation adopted in solid-state depends significantly on external packing forces.

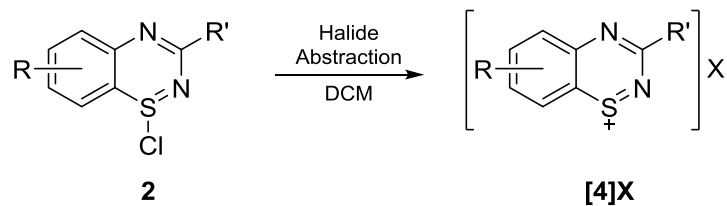
Interestingly, no indication of polymorphism was observed for any of the other 1,2,4-benzothiadiazine 1-chlorides, with only one distinct crystal morphology formed even when grown *via* different methods and using alternative solvents. This is despite the fact that differing conformations were observed for the two CH₂Cl groups in **2c/2h** vs. **[2j.H][HCl₂]**, and for the *o*-tolyl rings in **2g** vs. **2h**.

2.5 – Transformations of 1,2,4-Benzothiadiazine 1-Chlorides

The relatively short synthetic pathway and tolerance to substitution that is offered by Route 3, presents the opportunity to synthesise previously unknown or inaccessible 1,2,4-benzothiadiazines in different oxidation states. For example, the reaction of 1,2,4-benzothiadiazine 1-chlorides with two equivalents of morpholine gives the corresponding 1-morpholino derivative,¹⁰ whilst reduction with *p*-chlorothiophenol or 1-propanethiol affords the S^{II} benzothiadiazine.⁶ Besides the hydrolysis or one electron reduction of the S^{IV} chlorides, further transformations of these species have not been explored.

2.5.1 – Anion Metathesis

Anion metathesis reactions of S-N heterocyclic cations are typically performed to improve solubility and therefore yield higher purity material after recrystallization. Classically employed metathesis agents include AlCl₃ and the sodium or silver salts of BF₄⁻, ClO₄⁻, AsF₆⁻ and PF₆⁻ although GaCl₃ and OTf salts are now also commonly used.^{17,29,34} Anion metathesis reactions may also be used to probe the degree of covalency of S-Cl bond, with shorter and more covalent S-Cl bonds being less likely to undergo metathesis reactions than the ionic chloride salts. A general scheme for the proposed metathesis of 1,2,4-benzothiadiazine 1-chlorides is shown in Scheme 2.5.1.1.



Scheme 2.5.1.1: Metathesis of 1,2,4-benzothiadiazine 1-chlorides.

The addition of GaCl_3 to a suspension of **2a** in DCM immediately afforded a dark purple solution of **[4a]GaCl₄**. The ^1H NMR data differs significantly from the parent chloride, with the sole fused-ring proton being shifted *ca.* 1 ppm downfield on removal of the chloride indicative of the increased electron withdrawing effects from the formal positive charge at sulfur. Crystallisation of the product from DCM and hexane confirmed its proposed identity.

Compound **[4a]GaCl₄** crystallises as purple hexagonal plates in the monoclinic space group $P2_1/c$ with a single ion pair in the asymmetric unit (Figure 2.5.1.1). The molecule is essentially planar with only minor deviations from planarity for the heterocyclic (2.03°) and pendant phenyl ring (1.93°) with respect to the benzo-fused ring. This also leads to much smaller N1-C1-C8-C13 and N2-C1-C8-C9 torsion angles ($0.36(6)^\circ$ and $2.57(6)^\circ$ respectively) compared to the 1,2,4-benzothiadiazine 1-chlorides. Two long cation-anion interactions of $3.341(1)\text{\AA}$ and $3.463(1)\text{\AA}$ are observed between S1 and the chlorine atoms of two adjacent GaCl_4 anions.

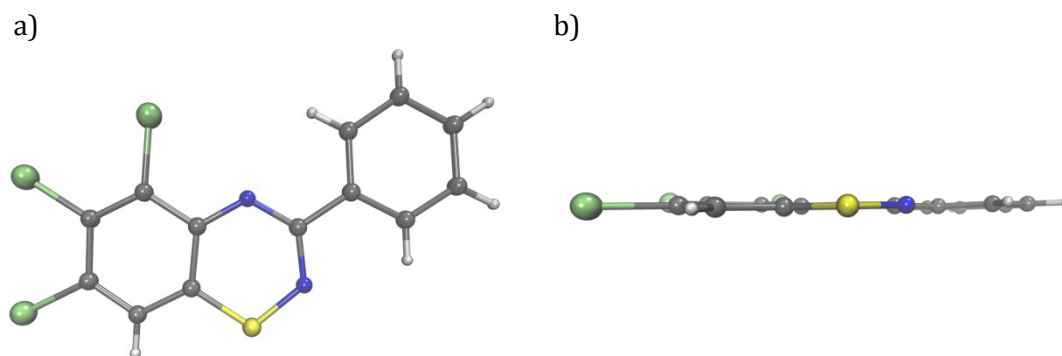


Figure 2.5.1.1: Crystal structure of **[4a]GaCl₄**: a) Top-down view. b) Side view. Anion omitted for clarity.

Attempts to prepare **[4]OTf** derivatives by treatment of **2a** with TMSOTf were unsuccessful, yielding a dark red solid which was extremely insoluble in all organic solvents. SCXRD analysis of poor quality crystals grown by slow cooling of a saturated SOCl_2 solution showed the formation of the *N*-protonated OTf salt, **[2a.H]OTf** (Figure 2.5.1.2). The true nature of the compound prior to treatment with thionyl chloride

however is unknown. In contrast, the treatment of **2a** with NaBAr^{Cl} in DCM resulted in a deep blue EPR active solution consistent with the formation of the neutral S^{III} benzothiadiazinyl radical, **3a**. More oxidatively stable fluorinated *tetra*-aryl boronates were not explored.

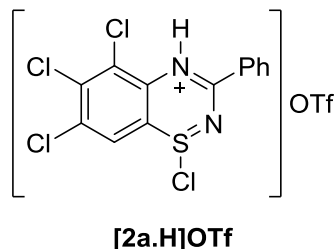
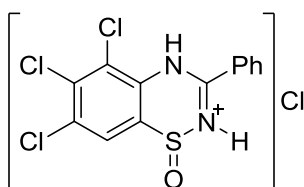


Figure 2.5.1.2: Isolated compound from the treatment of **2a** with TMSOTf.

2.5.2 - Hydrolysis

1,2,4-benzothiadiazine 1-oxides are known to be formed from the hydrolysis of the corresponding S^{IV} chlorides.^{10,12} 1,2,4-benzothiadiazine 1-oxides have received considerably less attention than S^{II} benzothiadiazines since published attempts to reduce them to the S^{III} benzothiadiazinyl radical have shown poor success;¹⁰ they can however be readily converted to S^{VI} species such as the 1,1-dioxide or 1-oxo-1-fluoride.³⁵ Since the hydrolysis is essentially reversible, conversion of 1,2,4-benzothiadiazine 1-oxides derived *via* alternative routes to the corresponding 1,2,4-benzothiadiazine 1-chlorides, may allow the synthesis of derivatives inaccessible *via* the standard routes. This therefore offers the potential to synthesise non-chlorinated (at carbon) derivatives or those with sensitive substituents.

Although the hydrolysis of 1,2,4-benzothiadiazine 1-chlorides to give the corresponding 1-oxides has been documented,^{10,12} this was merely reported as an observation and no procedure or conditions for a controlled hydrolysis accompanied the statement. Initial attempts to controllably hydrolyse **2a** with aqueous base showed limited success and consistently gave a low yield of light green oil containing a mixture of products on concentration of the organic extracts. When **2a** was suspended in wet methanol, an off-white, poorly soluble solid readily formed, assigned as **5a.HCl** (Figure 2.5.2.1). Attempts to deprotonate this species with triethylamine, aqueous NaOH or K₂CO₃ however were unsuccessful. Attempts to convert this species back to **2a** *via* dehydration were not performed.

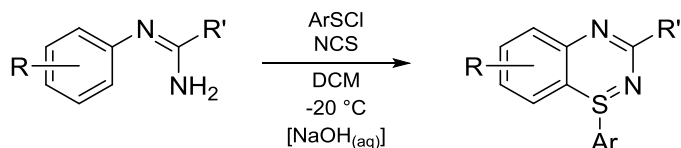


5a.HCl

Scheme 2.5.2.1: Protonated hydrolysis product.

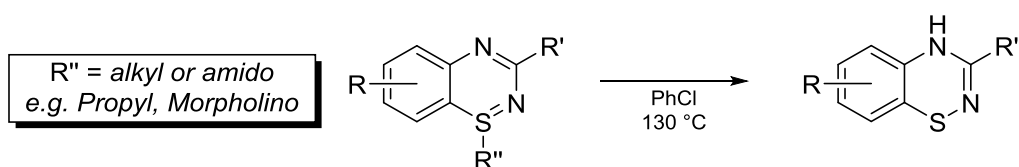
2.6 – *S*-Aryl 1,2,4-Benzothiadiazines

The facile synthesis of S^{IV} 1,2,4-benzothiadiazines bearing alkyl, aryl and amido substituents at sulfur directly from *N*-arylamidines was first reported in 1978 by Rees and coworkers,³⁶ and further expanded in 1983.³⁷ The preparation of *S*-aryl derivatives from sulfonyl chlorides in the presence of *N*-chlorosuccinimide, followed by a basic aqueous work-up, gives the fused-ring S^{IV} heterocycles in good yield (Figure 2.6.1). The required sulfonyl chlorides can conveniently be prepared *in situ* by treatment of corresponding disulphide with SO_2Cl_2 .



Scheme 2.6.1: Synthesis of *S*-aryl substituted 1,2,4-benzothiadiazines.

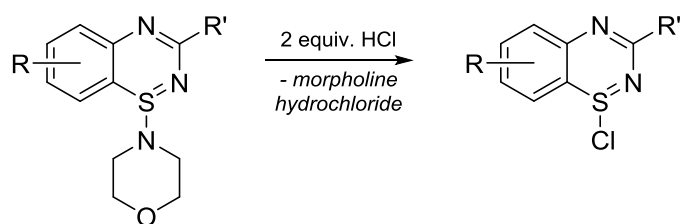
S-alkyl benzothiadiazines can be prepared in the same way, whilst amido-substituted derivatives use sulfoxylic diamides or sulfenamides as the source of sulfur. Appropriately substituted *S*-alkyl and *S*-amido species may undergo thermally induced cycloelimination reactions to afford the S^{II} benzothiadiazines (Scheme 2.6.2). This presents a more direct approach to S^{II} analogues that typically require cumbersome and multi-step syntheses.



Scheme 2.6.2: Conversion to S^{II} 1,2,4-benzothiadiazines.

The *S*-aryl benzothiadiazines are of particular interest since the introduction of a 2-pyridyl moiety at sulfur presents the opportunity to develop new bidentate or tridentate chelating ligands. Hitherto unknown S^{IV} chlorides should be accessible by the treatment of *S*-amido benzothiadiazines with anhydrous acid (Scheme 2.6.3), in a

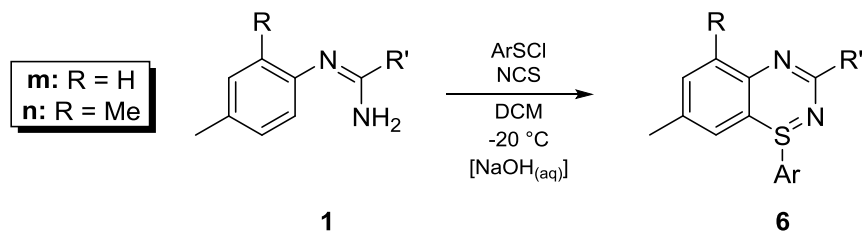
reaction analogous to the deprotection of phosphorus-nitrogen bonds,³⁸ giving access to unchlorinated (at carbon) derivatives.



Scheme 2.6.3: Conversion of *S*-amido 1,2,4-benzothiadiazines to S^{IV} 1-chlorides.

2.6.1 – Structural Studies of *S*-Aryl 1,2,4-Benzothiadiazines

Independent syntheses of **6m-n** were carried out according to Scheme 2.6.1.1 to probe the solid-state structure of the *S*-aryl benzothiadiazines. These were both isolated as pale yellow crystalline solids that were stable to air and moisture.



Scheme 2.6.1.1: Synthesis of *S*-aryl substituted 1,2,4-benzothiadiazines.

2.6.1.1 – Crystal Structure of **6m**

Compound **6m** crystallises as pale yellow blocks in the monoclinic space group $P2_1/n$ with a single molecule in the asymmetric unit (Figure 2.6.1.1.1). The heterocyclic ring adopts a bent conformation, folded along the $S1 \cdots N2$ axis and deviates significantly from planarity with respect to the benzo-fused ring at 26.69° . The $N1-C1-C8-13$ and $N2-C1-C8-C9$ torsion angles are small ($3.56(2)^\circ$ and $2.05(2)^\circ$ respectively) but the pendant aryl-ring is non-planar with the heterocyclic ring, deviating by 7.44° . The *S*-phenyl ring is essentially perpendicular with the mean plane of the heterocyclic ring (88.22°) with a $N2-S1-C_{ipso}$ angle of $92.49(5)^\circ$. The *S*-phenyl ring is considerably twisted with a $N1-S1-C_{ipso}-C_{ortho}$ torsion of $24.22(1)^\circ$ whilst the $S-C_{ipso}$ bond length at $1.808(1) \text{ \AA}$ is slightly elongated compared to a typical $S^{IV}-C_{Ar}$ single bond (1.790 \AA).³⁶

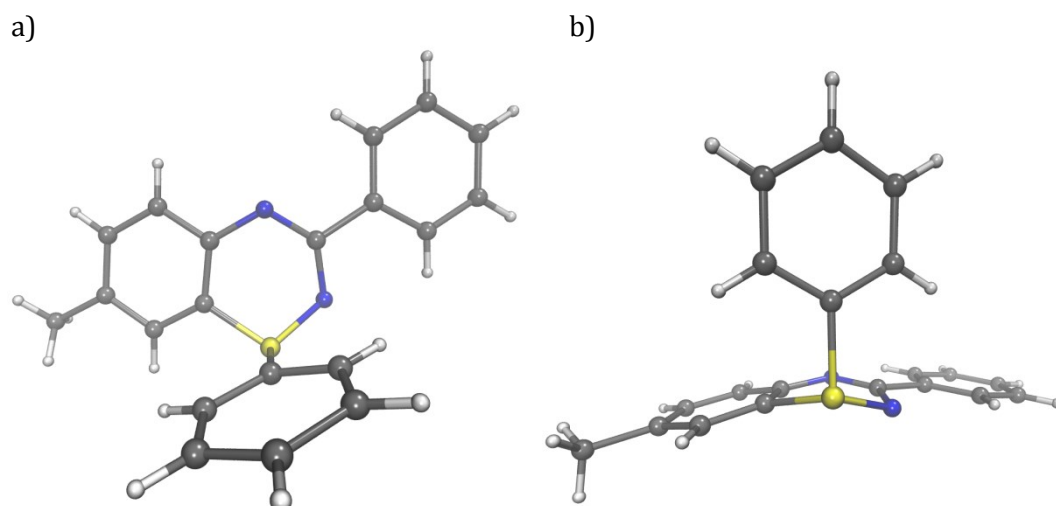


Figure 2.6.1.1.1: Crystal structure of **6m**: a) Top-down view. b) Side view.

2.6.1.2 – Crystal Structure of **6n**

Compound **6n** crystallises as pale yellow blocks in the monoclinic space group $P2_1/n$ with a single molecule in the asymmetric unit (Figure 2.6.1.2.1). The heterocyclic ring again adopts a bent conformation, folded along the S1...N2 axis, but deviates from planarity with respect to the fused-ring to a lesser extent compared to **6m** (17.62° vs. 26.69°). The pendant aryl-ring however is significantly twisted; the deviation from coplanarity compared to the heterocyclic ring is 32.11° and the N1-C1-C8-13 and N2-C1-C8-C9 torsion angles are $29.22(2)^\circ$ and $24.19(2)^\circ$ respectively. Again, the *S*-phenyl ring is essentially perpendicular with the mean plane of the heterocyclic ring (88.02°) but the N2-S1-C_{ipso} angle is $98.05(5)^\circ$. The *S*-phenyl ring is less twisted compared to **6m** with a N1-S1-C_{ipso}-C_{ortho} torsion of $9.19(1)^\circ$ and the S-C_{ipso} bond length is marginally shorter at $1.803(1)$ Å, but still longer than a typical S^{IV}-C_{Ar} single bond (1.790 Å).³⁶

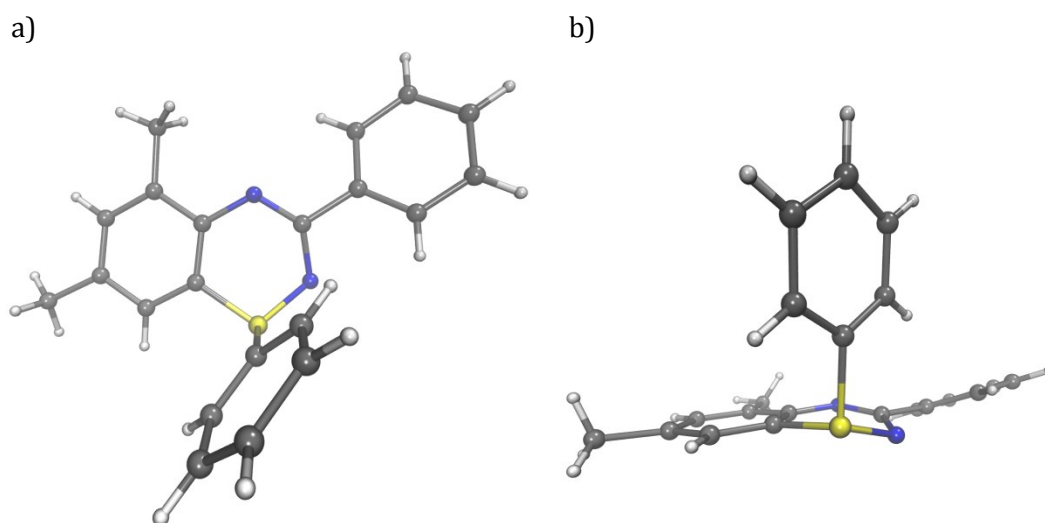
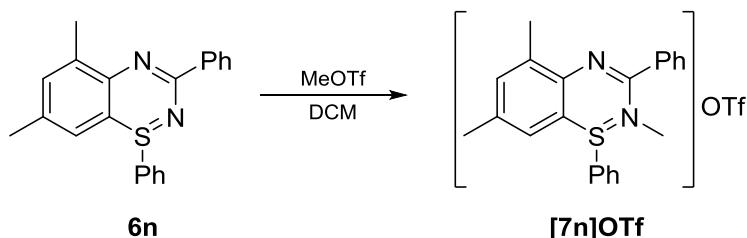


Figure 2.6.1.2.1: Crystal structure of **6n**: a) Top-down view. b) Side view.

2.6.2 – N-Methylation

The treatment of **6n** with one equivalent of MeOTf in DCM (Scheme 2.6.2.1) leads to an immediate loss of colour and clean conversion to **[7n]OTf**. The position of N-methylation could not be easily assigned *via* 2D NMR experiments but was successfully determined by SCXRD analysis.



Scheme 2.6.2.1: N-methylation of S-aryl 1,2,4-benzothiadiazines.

Compound **[7n]OTf** crystallises as colourless plates in the triclinic space group $P\bar{1}$ with a single ion pair in the asymmetric unit (Figure 2.6.2.1). The heterocyclic ring is severely distorted and folded along the S1...N2 axis; the deviation from planarity with respect to the benzo-fused ring is 35.04°. The pendant aryl ring is considerably twisted to minimise steric hindrance with the N-methyl group and deviates from coplanarity of the heterocyclic ring by 43.83° with N1-C1-C8-13 and N2-C1-C8-C9 torsion angles of 36.66(2)° and 33.63(2)° respectively. The S-phenyl ring is again close to perpendicular relative to the mean plane of the heterocyclic ring (86.07°) and the N2-S1-C_{ipso} angle is 84.48(5)°. The S-phenyl ring is also twisted considerably compared to **6n** such that the N1-S1-C_{ipso}-C_{ortho} torsion angle is 58.66(1)° and the S-C_{ipso} distance contracts (1.793(1) Å). A close contact is observed between S1 and one of the oxygens of the OTf anion (2.813(1) Å) within the sum of the van der Waals radii (3.22 Å)³⁰ which suggests that this structure is better described as a sulfur cation.

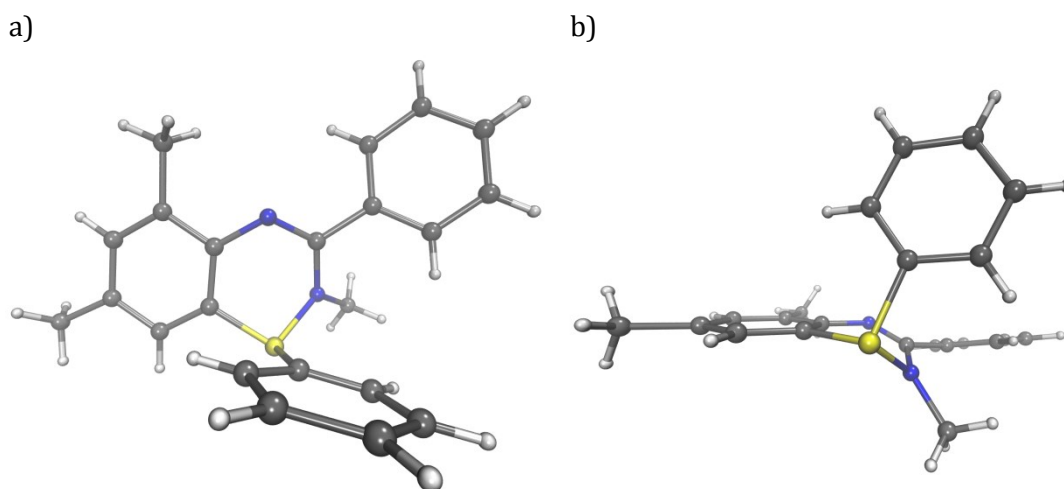


Figure 2.6.2.1: Crystal structure of **[7n]OTf**: a) Top-down view. b) Side view.

Counterion omitted for clarity.

Attempts to reduce **[7n]OTf** to the neutral S^{III} radical with ferrocene afforded a green solution that swiftly discoloured before any EPR spectroscopic measurements could be taken. Electrochemical studies should first be performed to determine if this radical is accessible and sufficiently long-lived, followed by controlled reductions under more rigorous conditions.

2.7 – Conclusions

Substituted 1,2,4-benzothiadiazines 1-chlorides are readily prepared by the treatment of *N*-arylamidines with neat thionyl chloride. Whilst the harsh ring-closing conditions result in partial chlorination of the benzo-fused ring and methyl groups at C3 and C4, the relatively short synthetic pathway and tolerance to substitution make this a versatile route to the S^{IV} chlorides as precursors to the S^{III} radicals. The 1,2,4-benzothiadiazine framework is extremely flexible as it allows fine-tuning of the substituents around the fused-ring and pendant groups; this has important implications for crystal engineering and the physical properties of the corresponding radical.

The crystallographically characterised benzothiadiazine 1-chlorides show considerable variation in the degree of planarity of the heterocyclic ring and pendant aryl ring with respect to the fused-ring. In the case of *o*-tolyl substituted **2g-h** systems, the deviation away from coplanarity was severe; this may potentially be exploited to develop neutral benzothiadiazinyl radicals that suppress dimerisation in the solid-state (*vide infra*). The range of S-Cl bond lengths observed weakly correlate with the electronic donating or withdrawing ability of substituents, although external packing forces are also likely to be an influencing factor. Despite showing significant covalency in the solid-state, the S-Cl bonds undergo halide abstraction with GaCl₃, whilst NaBAR^{Cl} resulted in reduction to the neutral radical.

Attempts to prepare the 1,2,4-benzothiadiazine 1-oxides *via* controlled hydrolysis of the S^{IV} chlorides were unsuccessful. Further work is thus necessary to optimise the reaction conditions for this transformation, as well as the reconversion of the S^{IV} 1-oxides back to S^{IV} chlorides. The synthesis of *S*-aryl 1,2,4-benzothiadiazines operates under mild conditions and may potentially be exploited to prepare hitherto inaccessible S^{II} and S^{IV} species.

2.8 - Experimental

2.8.1 - Synthesis of Amidines

The substituted *N*-arylamidines **1a-o** were prepared *via* standard methods through condensation of lithiated anilines with suitable carbonitriles, followed by aqueous work-up.²² Compound **1p** was synthesised by Lewis-acid mediated condensation in the melt.²³ The syntheses of **1a** and **1p** are given as exemplars. All amidines were isolated as colourless crystalline solids in good yield. 4-methoxybenzotrile was prepared according to known literature procedures.³⁹

2.8.1.1 - Synthesis of *N*-phenylbenzamidine, **1a**:

Aniline (4.56 cm³, 50 mmol) was dissolved in THF (50 cm³) and ⁿBuLi in hexane (20 cm³, 2.5 M, 50 mmol) was added dropwise at 0 °C. The reaction mixture was allowed to slowly warm to room temperature and stir for 1 hour. Benzotrile (4.84 cm³, 50 mmol) was then added yielding a straw-coloured solution thick with off-white precipitate. After 12 hours, the mixture was quenched with ice water (50 cm³) and the organics extracted into DCM (3 x 50 cm³). The combined organic extracts were washed with water and brine (50 cm³ each), dried over MgSO₄, filtered and concentrated *in vacuo*. The off-white solids were recrystallized from DCM and hexanes and stored at -20 °C for two hours. The colourless microcrystalline powder was collected at the pump, washed with cold hexanes and dried *in vacuo*. Yield - 8.80 g (44.8 mmol, 89.7 %). ¹H NMR (400 MHz, DCM, 19.8 °C) δ: 7.87 (bs, 2H), 7.45 (m, 3H), 7.35 (t, *J* = 7.3 Hz, 2H), 7.04 (t, *J* = 7.3 Hz, 1H), 6.94 (d, *J* = 7.3 Hz, 2H), 3.91 (s, 2H). ¹³C{¹H} NMR (100.5 MHz, DCM, 18.4 °C) δ: 154.4, 150.2, 136.0, 130.6, 129.6, 128.5, 126.8, 122.9, 121.5.

Analytical data in accordance with the literature.⁴⁰⁻⁴²

2.8.1.2 - Synthesis of *N*-(*o*-tolyl)-benzamidine, **1b**:

Colourless needles, 70.8 % yield. ¹H NMR (400 MHz, DCM, 19.3 °C) δ: 7.89 (d, *J* = 6.4 Hz, 2H), 7.46 (m, 3H), 7.22 (d, *J* = 7.3 Hz, 1H), 7.17 (t, *J* = 7.3, 7.8 Hz, 1H), 6.97 (t, *J* = 7.3 Hz, 1H), 6.82 (d, *J* = 7.8 Hz), 4.76 (bs, 2H), 2.15 (s, 3H). ¹³C{¹H} NMR (100.5 MHz, DCM, 18.5 °C) δ: 153.5, 148.5, 135.9, 130.8, 130.5, 129.6, 128.5, 126.9, 126.8, 123.0, 120.8, 17.5.

Analytical data in accordance with the literature.^{42,43}

2.8.1.3 - Synthesis of *N*-(2,3-dimethylphenyl)-benzamidine, **1c**:

Colourless needles, 86.8 % yield. ¹H NMR (400 MHz, DCM, 19.8 °C) δ: 7.90 (d, *J* = 6.4 Hz, 2H), 7.47 (m, 3H), 7.05 (t, *J* = 7.3, 7.8 Hz, 1H), 6.87 (d, *J* = 7.3 Hz, 1H), 6.68 (d, *J* = 7.8 Hz,

1H), 4.72 (bs, 2H), 2.28 (s, 3H), 2.07 (s, 3H). $^{13}\text{C}\{^1\text{H}\}$ NMR (100.5 MHz, DCM, 18.4 °C) δ : 153.5, 148.3, 138.1, 136.0, 130.5, 128.5, 128.0, 126.8, 126.2, 124.6, 118.5, 20.3, 13.4.

Analytical data in accordance with the literature.^{41,44}

2.8.1.4 – Synthesis of *N*-(2,5-dimethylphenyl)-benzamidine, 1d:

Colourless needles, 78.7 % yield. ^1H NMR (400 MHz, DCM, 19.8 °C) δ : 7.89 (d, J = 6.9 Hz, 2H), 7.46 (m, 3H), 7.09 (d, J = 7.8 Hz, 1H), 6.79 (d, J = 7.3 Hz, 1H), 6.65 (s, 1H), 4.75 (bs, 1H), 2.29 (s, 3H), 2.10 (s, 3H). $^{13}\text{C}\{^1\text{H}\}$ NMR (100.5 MHz, DCM, 18.3 °C) δ : 153.5, 148.3, 136.6, 136.0, 130.6, 130.5, 128.5, 126.8, 126.3, 123.7, 121.4, 20.9, 17.0.

Analytical data in accordance with the literature.⁴¹

2.8.1.5 – Synthesis of *N*-(3,5-dimethylphenyl)-benzamidine, 1e:

Colourless needles, 77.8 % yield. ^1H NMR (400 MHz, DCM, 19.9 °C) δ : 7.85 (d, J = 6.9 Hz, 2H), 7.45 (m, 3H), 6.70 (s, 1H), 6.55 (s, 2H), 4.89 (bs, 2H), 2.29 (s, 6H). $^{13}\text{C}\{^1\text{H}\}$ NMR (100.5 MHz, DCM, 18.4 °C) δ : 154.2, 150.0, 139.3, 136.1, 130.5, 128.5, 126.8, 124.6, 119.0, 21.2.

Analytical data in accordance with the literature.^{41,42}

2.8.1.6 – Synthesis of *N*-(3-methoxyphenyl)-benzamidine, 1f:

Synthesised in the absence of light. Colourless microcrystalline solid, 64.5 % yield. ^1H NMR (400 MHz, DCM, 17.1 °C) δ : 7.86 (d, J = 5.7 Hz, 2H), 7.46 (m, 3H), 7.24 (t, J = 8.0 Hz, 1H), 6.60 (d, J = 7.8 Hz, 1H), 6.52 (d, J = 8.7 Hz, 2H), 4.93 (bs, 2H), 3.78 (s, 3H). $^{13}\text{C}\{^1\text{H}\}$ NMR (100.5 MHz, DCM, 18.4 °C) δ : 161.0, 154.3, 151.7, 135.9, 130.6, 130.4, 128.5, 126.8, 113.7, 108.7, 107.0, 55.3.

Analytical data in accordance with the literature.^{44,45}

2.8.1.7 – Synthesis of *N*-phenyl-2-methylbenzamidine, 1g:

Colourless microcrystalline solid, 62.8 % yield. ^1H NMR (400 MHz, DCM, 18.7 °C) δ : 7.28 (m, 6H), 6.95 (bs, 3H), 4.84 (bs, 2H), 2.50 (bs, 3H). $^{13}\text{C}\{^1\text{H}\}$ NMR (100.5 MHz, DCM, 18.8 °C) δ : 156.2, 149.6, 137.2, 135.7, 130.7, 129.3, 129.1, 127.9, 125.7, 122.6, 121.6, 19.6.

Analytical data in accordance with the literature.⁴²

2.8.1.8 – Synthesis of *N*-(2,3-dimethylphenyl)-2-methylbenzamidine, 1h:

Colourless microcrystalline solid, 66.1 % yield. ^1H NMR (400 MHz, DCM, 18.8 °C) δ : 7.49 (bs, 1H), 7.28 (m, 3H), 7.06 (bs, 1H), 6.87 (bs, 1H), 6.73 (bs, 1H), 2.55 (s, 3H), 2.30

(s, 3H), 2.14 (s, 3H). $^{13}\text{C}\{^1\text{H}\}$ NMR (100.5 MHz, DCM, 19.0 °C) δ : 155.3, 148.1, 138.0, 137.4, 135.9, 130.8, 129.1, 128.0, 126.3, 125.8, 124.5, 118.6, 20.3, 19.8, 13.6.

2.8.1.9 – Synthesis of *N*-phenylisonicotinamide, **1i**:

Colourless microcrystalline powder, 87.9 % yield. ^1H NMR (400 MHz, DCM, 18.4 °C) δ : 8.68 (d, J = 4.6 Hz, 2H), 7.73 (d, J = 4.6 Hz, 2H), 7.36 (t, J = 6.4, 6.9 Hz, 2H), 7.07 (t, J = 6.9 Hz, 1H), 6.93 (d, J = 6.9 Hz, 2H), 5.01 (bs, 2H). $^{13}\text{C}\{^1\text{H}\}$ NMR (100.5 MHz, DCM, 18.7 °C) δ : 152.4, 150.4, 149.5, 143.2, 129.7, 123.4, 121.2, 121.0.

2.8.1.10 – Synthesis of *N*-(2,3-dimethylphenyl)-isonicotinamide, **1j**:

Colourless microcrystalline powder, 84.5 % yield. ^1H NMR (400 MHz, DCM, 18.8 °C) δ : 8.68 (d, J = 4.6 Hz, 2H), 7.76 (d, J = 4.6 Hz, 2H), 7.06 (t, J = 7.3, 7.8 Hz, 1H), 6.89 (d, J = 7.3 Hz, 1H), 6.67 (d, J = 7.8 Hz, 1H), 4.87 (bs, 2H), 2.29 (s, 3H), 2.05 (s, 3H). $^{13}\text{C}\{^1\text{H}\}$ NMR (100.5 MHz, DCM, 18.8 °C) δ : 151.6, 150.4, 147.6, 143.1, 138.2, 127.8, 126.3, 125.0, 121.0, 118.1, 20.2, 13.4.

2.8.1.11 – Synthesis of *N*-phenyl-4-methoxybenzamide, **1k**:

Colourless microcrystalline powder, 77.0 % yield. ^1H NMR (400 MHz, DCM, 19.6 °C) δ : 7.82 (d, J = 6.9 Hz, 2H), 7.33 (t, J = 6.6, 7.1 Hz, 2H), 7.03 (t, J = 6.6, 7.3 Hz, 1H), 6.93 (t, J = 7.3, 8.2 Hz, 4H), 4.81 (bs, 2H), 3.84 (s, 3H). $^{13}\text{C}\{^1\text{H}\}$ NMR (100.5 MHz, DCM, 19.2 °C) δ : 161.6, 153.7, 150.4, 129.6, 128.3, 122.7, 121.6, 113.7, 55.5.

Analytical data in accordance with the literature.^{22,42,45}

2.8.1.12 – Synthesis of *N*-(2,3-dimethylphenyl)-4-methoxybenzamide, **1l**:

Colourless microcrystalline powder, 73.7 % yield. ^1H NMR (400 MHz, DCM, 18.3 °C) δ : 7.85 (d, J = 8.2 Hz, 2H), 7.04 (t, J = 7.6, 7.8 Hz, 1H), 6.94 (d, J = 8.7 Hz, 2H), 6.86 (d, J = 7.3 Hz, 1H), 6.66 (d, J = 7.6 Hz, 1H), 4.68 (bs, 2H), 3.84 (s, 3H), 2.28 (s, 3H), 2.06 (s, 3H). $^{13}\text{C}\{^1\text{H}\}$ NMR (100.5 MHz, DCM, 19.3 °C) δ : 161.6, 153.0, 148.5, 138.0, 128.3, 128.1, 126.2, 124.4, 118.7, 113.7, 55.5, 20.3, 13.4.

2.8.1.13 – Synthesis of *N*-(*p*-tolyl)-benzamide, **1m**:

Colourless needles, 70.8 % yield. ^1H NMR (400 MHz, DCM, 19.3 °C) δ : 7.89 (d, J = 6.4 Hz, 2H), 7.46 (m, 3H), 7.22 (d, J = 7.3 Hz, 1H), 7.17 (t, J = 7.3, 7.8 Hz, 1H), 6.97 (t, J = 7.3 Hz, 1H), 6.82 (d, J = 7.8 Hz, 1H), 4.91 (bs, 2H), 2.16 (s, 3H). $^{13}\text{C}\{^1\text{H}\}$ NMR (100.5 MHz, DCM, 19.3 °C) δ : 153.5, 148.5, 135.9, 130.8, 130.5, 129.6, 128.5, 126.9, 126.8, 123.0, 120.8, 17.5.

Analytical data in accordance with the literature.^{42,44}

2.8.1.14 – Synthesis of *N*-(2,4-dimethylphenyl)-benzamidine, **1n**:

Colourless needles, 72. % yield. $^1\text{H NMR}$ (400 MHz, DCM, 18.9 °C) δ : 7.87 (d, J = 7.1 Hz, 2H), 7.45 (m, 3H), 7.06 (s, 1H), 6.99 (d, J = 7.9 Hz, 1H), 6.71 (d, J = 7.8 Hz, 1H), 4.78 (bs, 2H), 2.31 (s, 3H), 2.13 (s, 3H). $^{13}\text{C}\{^1\text{H}\}$ NMR (100.5 MHz, DCM, 18.9 °C) δ : 153.8, 145.7, 136.0, 132.3, 131.5, 130.4, 129.3, 128.5, 127.5, 126.8, 120.7, 20.7, 17.5.

Analytical data in accordance with the literature.⁴²

2.8.1.15 – Synthesis of *N*-(2-biphenyl)-benzamidine, **1o**:

Colourless needles, 67.5 % yield. $^1\text{H NMR}$ (400 MHz, DCM, 19.3 °C) δ : 7.70 (d, J = 7.2 Hz, 2H), 7.50 (d, J = 7.4 Hz, 2H), 7.46-7.29 (m, 7H), 7.24 (t, J = 7.3, 7.4 Hz, 1H), 7.16 (t, J = 7.4 Hz, 1H), 6.98 (d, J = 7.6 Hz, 1H), 4.81 (bs, 2H). $^{13}\text{C}\{^1\text{H}\}$ NMR (100.5 MHz, DCM, 19.7 °C) δ : 153.7, 147.4, 140.4, 135.9, 133.9, 130.9, 130.5, 129.1, 128.7, 128.5, 127.9, 126.8, 126.7, 123.5, 122.1.

2.8.1.16 – Synthesis of *N*-phenylpivalamidine, **1p**:

Aniline (2.05 cm³, 22.5 mmol), pivalonitrile (2.49 cm³, 22.5 mmol) and AlCl₃ (3.00 g, 22.5 mmol) were combined and heated to 130 °C under argon. After 1 hour, the molten mixture was poured into a 12.5 % aqueous NaOH (50 cm³) and ice (50 g) mixture, and allowed to stir for 15 minutes. The suspension was extracted into DCM (3 x 50 cm³) and the combined organic extracts were washed with water and brine (50 cm³ each), dried over MgSO₄, filtered and concentrated *in vacuo*. The crude solids were recrystallised from DCM and hexanes, and stored at -20 °C for 2 hours. The colourless needles were collected at the pump, washed with cold hexanes and dried *in vacuo*. Yield: 1.63 g (9.25 mmol, 41.0 %). $^1\text{H NMR}$ (400 MHz, DCM, 25.0 °C) δ : 7.28 (t, J = 7.6, 8.0 Hz, 2H), 6.97 (t, J = 7.4 Hz, 1H), 6.77 (d, J = 7.4 Hz, 2H), 4.38 (bs, 2H), 1.26 (s, 9H). $^{13}\text{C}\{^1\text{H}\}$ NMR (100.5 MHz, DCM, 25.0 °C) δ : 164.1, 150.9, 129.5, 122.3, 121.4, 36.9, 28.4.

Analytical data in accordance with the literature.⁴⁶

2.8.1.17 – Attempted Synthesis of **1q** *via* Base-Catalysed Pinner reaction:

4-Nitrobenzonitrile (1.00 g, 6.75 mmol) was degassed, flushed with argon and dissolved in a freshly prepared solution of MeONa (3.48 mmol) in anhydrous MeOH (20 cm³). The pale peach solution was heated and maintained at reflux for 12 hours. Once cooled, the reaction was quenched with glacial acetic acid (0.2 cm³, 3.48 mmol) and allowed to stir for 1 hour. Aniline (0.63 cm³, 6.75 mmol) was added and the solution was returned to reflux for 16 hours. The solvent was removed *in vacuo*, and the residues were redissolved in DCM (50 cm³). The organic extracts were washed with

water, saturated NaHCO₃ solution and brine (25 cm³ each), dried over MgSO₄, filtered and evaporated to dryness yielding 0.58 g of pale amber liquid that was identified as aniline by ¹H NMR.

2.8.1.18 – Attempted Synthesis of **1q** via Acid-Catalysed Pinner reaction:

4-Methoxybenzotrile (1.00 g, 6.75 mmol) was dissolved in MeOH (25 cm³) and cooled to 0 °C. TMSCl (2.5 cm³, 19.70 mmol) was added dropwise and the solution was slowly warmed to room temperature, then heated to reflux and maintained for 18 hours. The volatiles were removed *in vacuo* and the residues were redissolved in fresh MeOH (25 cm³). Aniline (0.63 cm³, 6.75 mmol) was added and the bronze solution was returned to reflux for 20 hours. The solvent was removed *in vacuo*, and the residues were dissolved in DCM (50 cm³). The organic extracts were washed with water, saturated NaHCO₃ solution and brine (25 cm³ each), dried over MgSO₄, filtered and evaporated to dryness yielding an off-white oily solid. Recrystallisation from DCM and hexanes afforded 0.41 g of colourless crystals that were identified as methyl-2,4-dihydroxybenzoate by ¹H NMR and SCXRD.

2.8.2 – Synthesis of **1,2,4-Benzothiadiazine 1-Chlorides**

The S^{IV} heterocycles were prepared by refluxing the corresponding *N*-arylamidine in excess thionyl chloride. The synthesis of **2a** is given as exemplar. Crystals suitable for X-ray diffraction studies were grown *via* slow diffusion of hexane into a saturated solution of the product in SOCl₂. NMR spectra recorded in SOCl₂ were arbitrarily referenced to DMSO-*d*₆ in the capillary.

2.8.2.1 – Synthesis of **1,5,6,7-tetrachloro-3-phenyl-benzo-1,2,4-thiadiazine, 2a**:

1a (1.500 g, 7.64 mmol) was degassed, flushed with argon and cooled to -95 °C. SOCl₂ (15 cm³, 207 mmol) was added slowly and the reaction mixture was gradually warmed to room temperature then heated at reflux for 12 hours. Once cooled to room temperature, hexane (30 cm³) was added with rapid stirring producing a fine orange precipitate. The supernatant was removed *via* filter cannula and the solids were washed with hexane (2 x 10 cm³) then dried *in vacuo*. Yield: 1.980 g (5.44 mmol, 71.1 %). *Anal.* Calc. for C₁₃H₆Cl₄N₂S: C, 42.9; H, 1.7; N, 7.7. Found: C, 42.7; H, 1.8; N, 7.4. ¹H NMR (400 MHz, SOCl₂, 19.4 °C) δ: 8.46 (d, *J* = 7.3 Hz, 2H), 7.92 (s, 1H), 7.52 (m, 3H). ¹³C{¹H} NMR (100.5 MHz, SOCl₂, 18.7 °C) δ: 158.3, 140.4, 139.5, 135.3, 134.6, 132.9, 132.6, 129.2, 128.7, 122.1, 116.5.

2.8.2.2 – Synthesis of 1,6,7-trichloro-5-(chloromethyl)-3-phenyl-benzo-1,2,4-thiadiazine, 2b:

Orange solid, 60.8 % yield. *Anal. Calc.* for $C_{14}H_8Cl_4N_2S$: C, 44.5; H, 2.1; N, 7.4. Found: C, 44.3; H, 2.1; N, 7.5. 1H NMR (400 MHz, $SOCl_2$, 18.4 °C) δ : 8.43 (d, $J = 7.1$ Hz, 2H), 8.01 (s, 1H), 7.53 (m, 3H), 5.36 (s, 2H). $^{13}C\{^1H\}$ NMR (100.5 MHz, $SOCl_2$, 18.6 °C) δ : 141.7, 141.4, 136.6, 135.6, 132.7, 132.6, 129.0, 128.8, 124.3, 116.3, 37.2.

2.8.2.3 – Synthesis of 1,7-dichloro-5,6-bis(chloromethyl)-3-phenyl-benzo-1,2,4-thiadiazine, 2c:

Orange solid, 75.9 % yield. *Anal. Calc.* for $C_{15}H_{10}Cl_4N_2S$: C, 45.9; H, 2.6; N, 7.1. Found: C, 45.8; H, 2.4; N, 7.2. 1H NMR (400 MHz, $SOCl_2$, 19.6 °C) δ : 8.44 (d, $J = 8.2$ Hz, 2H), 7.97 (s, 1H), 7.52 (m, 3H), 5.38 (s, 2H), 4.96 (s, 2H). $^{13}C\{^1H\}$ NMR (100.5 MHz, $SOCl_2$, 19.6 °C) δ : 157.5, 142.4, 141.3, 137.9, 135.6, 134.0, 132.6, 129.0, 128.7, 124.4, 118.1, 38.6, 35.2.

2.8.2.4 – Synthesis of 1,6,7-trichloro-5-(chloromethyl)-8-methyl-3-phenyl-benzo-1,2,4-thiadiazine, 2d:

Pale yellow solid, 30.9 % yield. *Anal. Calc.* for $C_{15}H_{10}Cl_4N_2S$: C, 45.9; H, 2.6; N, 7.1. Found: C, 45.7; H, 2.6; N, 7.2. 1H NMR (400 MHz, $SOCl_2$, 16.6 °C) δ : 8.44 (d, $J = 7.3$ Hz, 2H), 7.52 (m, 3H), 5.37 (s, 2H), 2.85 (s, 3H). $^{13}C\{^1H\}$ NMR (100.5 MHz, $SOCl_2$, 19.1 °C) δ : 157.5, 141.8, 141.6, 135.5, 133.9, 133.5, 133.0, 132.7, 129.0, 128.8, 116.8, 37.7, 16.7.

2.8.2.5 – Synthesis of 1,5,7-trichloro-6-(chloromethyl)-8-methyl-3-phenyl-benzo-1,2,4-thiadiazine, 2e:

Orange solid, 39.8 % yield. *Anal. Calc.* for $C_{15}H_{10}Cl_4N_2S$: C, 45.9; H, 2.6; N, 7.1. Found: C, 45.8; H, 2.4; N, 7.3. 1H NMR (400 MHz, $SOCl_2$, 17.7 °C) δ : 8.49 (d, $J = 7.3$ Hz, 2H), 7.55 (m, 3H), 5.07 (s, 2H), 2.81 (s, 3H). $^{13}C\{^1H\}$ NMR (100.5 MHz, $SOCl_2$, 18.7 °C) δ : 157.6, 140.6, 139.6, 135.2, 134.3, 133.4, 132.8, 130.7, 129.1, 128.8, 119.0, 41.3, 16.0.

2.8.2.6 – Synthesis of 1,5,6,7-tetrachloro-8-methoxy-3-phenyl-benzo-1,2,4-thiadiazine, 2f:

Red solid, 45.5 % yield. *Anal. Calc.* for $C_{14}H_8Cl_4N_2OS$: C, 42.7; H, 2.0; N, 7.1. Found: C, 42.5; H, 1.9; N, 7.2. 1H NMR (400 MHz, $SOCl_2$, 18.5 °C) δ : 8.47 (d, $J = 8.0$ Hz, 2H), 7.52 (m, 3H), 4.24 (s, 3H). $^{13}C\{^1H\}$ NMR (100.5 MHz, $SOCl_2$, 18.3 °C) δ : 159.1, 149.3, 140.6, 140.4, 135.4, 132.8, 129.2, 128.7, 124.7, 112.5, 62.4.

2.8.2.7 – Synthesis of 1,5,6,7-tetrachloro-3-(*o*-tolyl)-benzo-1,2,4-thiadiazine, 2g:

Pale orange solid, 45.8 % yield. *Anal. Calc.* for $C_{14}H_8Cl_4N_2S$: C, 44.5; H, 2.1; N, 7.4. Found: C, 44.4; H, 2.1; N, 7.5. 1H NMR (400 MHz, $SOCl_2$, 18.4 °C) δ : 8.02 (d, $J = 7.3$ Hz, 1H), 7.95

(s, 1H), 7.43 (t, $J = 6.4, 7.3$ Hz, 1H), 7.33 (t, $J = 6.0$ Hz, 7.3 Hz, 2H), 2.76 (s, 3H). $^{13}\text{C}\{^1\text{H}\}$ NMR (100.5 MHz, SOCl_2 , 18.9 °C) δ : 160.3, 139.6, 139.4, 135.2, 134.3, 132.8, 132.0, 131.6, 131.5, 126.1, 122.1, 116.1, 22.4.

2.8.2.8 – Synthesis of 1,7-dichloro-5,6-bis(chloromethyl)-3-(*o*-tolyl)-benzo-1,2,4-thiadiazine, 2h:

Turmeric-coloured solid, 53.2 % yield. *Anal.* Calc. for $\text{C}_{16}\text{H}_{12}\text{Cl}_4\text{N}_2\text{S}$: C, 47.3; H, 3.0; N, 6.9. Found: C, 47.2; H, 2.9; N, 6.7. ^1H NMR (400 MHz, SOCl_2 , 18.5 °C) δ : 8.00 (s, 1H), 7.96 (d, $J = 7.8$ Hz, 1H), 7.41 (t, $J = 7.3, 7.6$ Hz, 1H), 7.33 (t, $J = 6.0, 7.3$ Hz, 2H), 5.32 (s, 2H), 4.98 (s, 2H), 2.71 (s, 3H). $^{13}\text{C}\{^1\text{H}\}$ NMR (100.5 MHz, SOCl_2 , 19.2 °C) δ : 159.9, 142.5, 140.9, 138.8, 138.0, 136.0, 134.4, 131.8, 131.5, 131.3, 126.1, 124.5, 117.4, 38.7, 35.4, 22.0.

2.8.2.9 – Synthesis of 1,7-dichloro-5,6-bis(chloromethyl)-3-(*p*-pyridinium)-benzo-1,2,4-thiadiazine hydrogen dichloride, 2j.H.HCl₂:

Yellow solid, 86.8 % yield. ^1H NMR (400 MHz, SOCl_2 , 18.2 °C) δ : 8.86 (d, $J = 5.3$ Hz, 2H), 8.77 (d, $J = 5.3$ Hz, 2H), 8.03 (s, 1H), 5.33 (s, 2H), 4.96 (s, 2H). $^{13}\text{C}\{^1\text{H}\}$ NMR (100.5 MHz, SOCl_2 , 19.0 °C) δ : 152.2, 151.7, 142.9, 141.4, 139.8, 138.3, 136.8, 125.4, 124.8, 116.3, 38.4, 35.1.

2.8.2.10 – Synthesis of 1,5,6,7-tetrachloro-3-(4-methoxyphenyl)-benzo-1,2,4-thiadiazine, 2k:

Dark red solid, 81.1 % yield. *Anal.* Calc. for $\text{C}_{14}\text{H}_8\text{Cl}_4\text{N}_2\text{OS}$: C, 42.7; H, 2.1; N, 7.1. Found: C, 42.3; H, 2.1; N, 7.1. ^1H NMR (400 MHz, SOCl_2 , 18.5 °C) δ : 8.44 (d, $J = 8.6$ Hz, 2H), 7.92 (s, 1H), 7.01 (d, $J = 8.6$ Hz, 2H), 3.88 (s, 3H). $^{13}\text{C}\{^1\text{H}\}$ NMR (100.5 MHz, SOCl_2 , 25.0 °C) δ : 163.5, 158.1, 140.6, 139.4, 134.2, 131.8, 131.3, 127.8, 122.1, 116.6, 114.1, 55.3.

2.8.2.11 – Synthesis of 1,7-dichloro-5,6-bis(chloromethyl)-3-(4-methoxyphenyl)-benzo-1,2,4-thiadiazine, 2l:

Red solid, 62.5 % yield. *Anal.* Calc. for $\text{C}_{16}\text{H}_{12}\text{Cl}_4\text{N}_2\text{OS}$: C, 45.5; H, 2.9; N, 6.6. Found: C, 45.4; H, 2.8; N, 6.8. ^1H NMR (400 MHz, SOCl_2 , 18.0 °C) δ : 8.42 (d, $J = 8.8$ Hz, 2H), 7.97 (s, 1H), 7.02 (d, $J = 8.8$ Hz, 2H), 5.39 (s, 2H), 4.97 (s, 2H), 3.88 (s, 3H). $^{13}\text{C}\{^1\text{H}\}$ NMR (100.5 MHz, SOCl_2 , 19.0 °C) δ : 163.4, 157.4, 142.4, 141.5, 137.6, 133.5, 131.2, 128.1, 124.5, 118.3, 114.2, 55.4, 38.7, 35.4.

2.8.2.12 – NMR Characterisation of 1,7-dichloro-5,6-bis(chloromethyl)-3-(3-chloro-4-methoxyphenyl)-benzo-1,2,4-thiadiazine, 2r:

^1H NMR (400 MHz, SOCl_2 , 18.7 °C) δ : 8.45 (s, 1H), 8.36 (m, 1H), 7.97 (s, 1H), 7.08 (d, $J = 8.7$ Hz, 1H), 5.39 (s, 2H), 4.98 (s, 2H), 3.96 (s, 3H). $^{13}\text{C}\{^1\text{H}\}$ NMR (100.5 MHz, SOCl_2 ,

18.3 °C) δ : 158.8, 156.7, 142.8, 138.0, 133.9, 131.1, 129.9, 129.4, 124.9, 123.2, 118.4, 112.3, 56.6, 39.1, 35.7.

2.8.3 – Synthesis of S^{IV} Cations

S^{IV} cations were prepared by combination of 1,2,4-benzothiadiazine 1-chloride, **2**, and halide abstraction agent in DCM. Attempts to isolate analytically pure samples of **[4a]GaCl₄** were unsuccessful. This species was found to be extremely air and moisture sensitive, and crystals of **[5a.H]GaCl₄** were isolated on a number of occasions.

2.8.3.1 – Synthesis of 5,6,7-trichloro-3-phenyl-benzo-1,2,4-thiadiazinium tetrachlorogallate, **[4a]GaCl₄**:

2a (30 mg, 0.08 mmol) was suspended in DCM (2.5 cm³) and GaCl₃ (14.5 mg, 0.08 mmol) was added giving a dark purple solution and solids. An additional 2.5 cm³ of DCM was added and the reaction mixture was filtered to remove undissolved material. Layering of the filtrate with hexane (10 cm³) and storage at – 20 °C afforded purple crystals, that were filtered and dried *in vacuo*. Yield: 27 mg (0.05 mmol, 61.0 %). ¹H NMR (400 MHz, DCM, 25.0 °C) δ : 8.92 (s, 1H), 8.70 (d, *J* = 7.4 Hz, 2H), 7.84 (t, *J* = 7.4, 7.6 Hz, 1H), 7.73 (t, *J* = 7.4, 7.6 Hz, 2H).

2.8.4 – Synthesis of 1,2,4-Benzothiadiazine 1-Oxides

The 1,2,4-benzothiadiazine 1-chlorides rapidly hydrolyse to give off-white solids believed to be the corresponding 1-oxide as it's hydrochloride salt. The poor solubility prevented its characterisation, and all attempts to deprotonate these species were unsuccessful.

2.8.4.1 – Synthesis of 1-oxo-5,6,7-trichloro-3-phenyl-benzo-1,2,4-thiadiazine hydrochloride, **5a.HCl**:

2a (0.25 g, 0.69 mmol) was suspended in a mixture of H₂O (1 cm³) and MeOH (15 cm³) and stirred for 30 minutes. The off-white suspension was filtered and the solids were with MeOH (5 cm³) then dried *in vacuo*. Yield: 0.22 g (0.58 mmol, 84.0 %).

2.8.5 – Synthesis of S-Aryl 1,2,4-Benzothiadiazines

S-aryl benzothiadiazines were prepared according to the general procedure developed by Rees.^{36,37} The synthesis of **6m** is provided as an exemplar. Compound **[7n]OTf** was prepared by treatment of **6n** with methyl triflate.

2.8.5.1 – Synthesis of 7-methyl-1,3-diphenyl-benzo-1,2,4-thiadiazine, 6m:

PhSSPh (0.268 g, 1.23 mmol) was dissolved in DCM (10 cm³) and SO₂Cl₂ (0.1 cm³, 1.23 mmol) was slowly added. After 5 minutes, the orange solution of PhSCl was added dropwise to a solution of **1m** (0.516 g, 2.46 mmol) in DCM (10 cm³) at -20 °C and maintained at this temperature for 30 mins. *N*-bromosuccinimide (0.437 g, 2.46 mmol) in DCM (10 cm³) was then added and the reaction mixture was allowed to warm to room temperature and stir for 18 hours. The orange solution was transferred to a separatory funnel along with 10% aqueous NaOH (50 cm³) and the organic phase was collected. The aqueous layer was further extracted with DCM (2 x 30 cm³) and the combined organic extracts were washed with water (50 cm³), dried over MgSO₄, filtered and evaporated to dryness. Recrystallisation of the crude residue from DCM and hexanes gave the product as pale yellow crystals that were washed with hexane and dried *in vacuo*. Yield: 0.464 g (1.47 mmol, 59.8 %). ¹H NMR (400 MHz, DCM, 18.4 °C) δ: 8.34 (d, *J* = 6.4 Hz, 2H), 7.47-7.33 (m, 9H), 7.30 (d, *J* = 8.2 Hz, 1H), 7.25 (s, 1H), 2.41 (s, 3H). ¹³C{¹H} NMR (100.5 MHz, DCM, 18.5 °C) δ: 163.4, 142.8, 140.9, 139.1, 135.9, 134.5, 131.5, 130.5, 129.7, 128.3, 128.0, 126.6, 126.0, 125.7, 106.8, 20.9.

Analytical data in accordance with the literature.³⁷

2.8.5.2 – Synthesis of 5,7-dimethyl-1,3-diphenyl-benzo-1,2,4-thiadiazine, 6n:

Pale yellow crystals, 52.8 % yield. ¹H NMR (400 MHz, DCM, 18.9 °C) δ: 8.38 (d, *J* = 7.6 Hz, 2H), 7.46-7.32 (m, 8H), 7.30 (s, 1H), 7.12 (s, 1H), 2.50 (s, 3H), 2.38 (s, 3H). ¹³C{¹H} NMR (100.5 MHz, DCM, 19.3 °C) δ: 162.7, 141.0, 140.9, 139.6, 135.4, 135.0, 134.9, 131.3, 130.4, 129.6, 128.5, 127.9, 125.6, 123.6, 106.4, 20.9, 17.0.

2.9 – References

- 1 N. Finch, S. J. Ricca, L. H. Werner and R. Rodebaugh, *J. Org. Chem.*, 1980, 3416–3421.
- 2 L. H. Werner, A. Halamandaris, S. Ricca, L. Dorfman and G. deStevens, *J. Am. Chem. Soc.*, 1960, **82**, 1161–1166.
- 3 A. Fretheim, *BMC Fam. Pract.*, 2003, **4**, 1–4.
- 4 P. G. Welling, *Biopharm. Drug Dispos.*, 1986, **7**, 501–535.
- 5 J. Zienkiewicz, P. Kaszynski and V. G. Young, *J. Org. Chem.*, 2004, **69**, 2551–2561.
- 6 J. Zienkiewicz, P. Kaszynski and V. G. Young, *J. Org. Chem.*, 2004, **69**, 7525–7536.
- 7 E. R. Clark, M. U. Anwar, B. J. Leontowicz, Y. Beldjoudi, J. J. Hayward, W. T. K. Chan, E. L. Gavey, M. Pilkington, E. Zysman-Colman and J. M. Rawson, *Dalton Trans.*, 2014, **43**, 12996.
- 8 K. Pringouri, M. U. Anwar, B. J. Leontowicz and J. M. Rawson, *Polyhedron*, 2018, **150**, 110–117.
- 9 A. K. Pal, D. B. Cordes, K. Pringouri, M. U. Anwar, A. M. Z. Slawin, J. M. Rawson and E. Zysman-Colman, *J. Coord. Chem.*, 2016, **69**, 1924–1937.
- 10 E. S. Levchenko, G. S. Borovikova, E. I. Borovik and V. V. Kalinin, *Russ. J. Org. Chem.*, 1984, **20**, 176–181.
- 11 D. D. Ross and D. Lednicer, *J. Heterocycl. Chem.*, 1982, 975.
- 12 V. G. Kresze, C. Seyfried and A. Trede, *Liebigs. Ann. Chem.*, 1968, 223–237.
- 13 E. R. Clark, J. J. Hayward, B. J. Leontowicz, D. J. Eisler and J. M. Rawson, *CrystEngComm*, 2014, **16**, 1755–1762.
- 14 A. O. Abdelhamid, F. A. Khalifa and S. S. Ghabrial, *Phosphorus Sulfur Relat. Elem.*, 2006, **40**, 41–46.
- 15 L. N. Markovskii, V. S. Talanov, O. M. Polumbrik and Y. G. Shermolovich, *Russ. J. Org. Chem.*, 1981, **17**, 2338–2339.
- 16 P. Hope and L. A. Wiles, *J. Chem. Soc.*, 1967, 1965–1967.
- 17 J. M. Rawson and G. D. McManus, *Coord. Chem. Rev.*, 1999, **189**, 135–168.
- 18 E. R. Clark, *Synthesis and Chemistry of 1,2,4-Benzothiadiazines*, University of Cambridge, 2008.
- 19 L. Beer, R. C. Haddon, M. E. Itkis, A. A. Leitch, R. T. Oakley, R. W. Reed, J. F. Richardson, D. G. VanderVeer, L. Beer, J. L. Brusso, A. W. Cordes, R. C. Haddon, M. E. Itkis, K. Kirschbaum, D. S. MacGregor, R. T. Oakley, A. A. Pinkerton and R. W. Reed, *Chem. Commun.*, 2005, **124**, 1218–1220.
- 20 A. a Leitch, R. T. Oakley, R. W. Reed and L. K. Thompson, *Inorg. Chem.*, 2007, **46**, 6261–70.

- 21 G. Kresze and W. Wucherpennig, *Angew. Chem. Int. Ed.*, 1967, **6**, 149–167.
- 22 I. K. Khanna, Y. Yu, R. M. Huff, R. M. Weier, X. Xu, F. J. Koszyk, P. W. Collins, J. N. Cogburn, P. C. Isakson, C. M. Koboldt, J. L. Masferrer, W. E. Perkins, K. Seibert, A. W. Veenhuizen, J. Yuan, D. Yang and Y. Y. Zhang, *Synthesis*, 2000, 3168–3185.
- 23 S. I. R. Alexander, *J. Chem. Soc.*, 1949, 449–456.
- 24 F. C. Schaefer and G. A. Peters, *J. Org. Chem.*, 1961, **26**, 412–418.
- 25 S. Caron, L. Wei, J. Douville and A. Ghosh, *J. Org. Chem.*, 2010, **75**, 945–947.
- 26 A. G. Orpen, L. Brammer, F. H. Allen, O. Kennard, D. G. Watson and R. Taylor, *J. Chem. Soc., Dalt. Trans.*, 1987, S1–S83.
- 27 A. W. Cordes, P. J. Hayes, P. D. Josephy, H. Koenig, R. T. Oakley and W. T. Pennington, *J. Chem. Soc., Chem. Commun.*, 1984, 1021–1022.
- 28 N. Burford, T. Chivers, M. Hojo, W. G. Laidlaw, J. F. Richardson and M. Trsic, *Inorg. Chem.*, 1985, **24**, 709–715.
- 29 J. M. Rawson, A. J. Banister and I. Lavender, *Adv. Heterocycl. Chem.*, 1995, **62**, 137–247.
- 30 A. Bondi, *J. Phys. Chem.*, 1964, **68**, 441–451.
- 31 J. Bernstein and A. T. Hagler, *J. Am. Chem. Soc.*, 1978, **100**, 673–681.
- 32 J. L. Atwood, S. G. Bott, C. M. Means, A. W. Coleman, H. Zhang and M. T. May, *Inorg. Chem.*, 1990, **29**, 467–470.
- 33 B. H. Ward, G. E. Granroth, K. A. Abboud, M. W. Meisel and D. R. Talham, *Chem. Mater.*, 1998, **10**, 1102.
- 34 C. M. Robertson, A. A. Leitch, K. Cvrkalj, D. J. T. Myles, R. W. Reed, P. A. Dube and R. T. Oakley, *J. Am. Chem. Soc.*, 2008, **130**, 14791–14801.
- 35 N. P. Kolesnik, A. B. Rozhenko, V. Kinzhybalov, T. Lis and Y. G. Shermolovich, *J. Fluor. Chem.*, 2014, **160**, 16–19.
- 36 T. L. Gilchrist, C. W. Rees and D. Vaughan, *J. Chem. Soc., Chem. Commun.*, 1978, 1049–1050.
- 37 T. L. Gilchrist, C. W. Rees and D. Vaughan, *J. Chem. Soc., Perkin Trans.*, 1983, 49–54.
- 38 W. Voskuil and J. F. Arens, *Recl. des Trav. Chim. des Pays-Bas*, 1962, **81**, 993–1008.
- 39 C. S. Chang, Y. T. Lin, S. R. Shih, C. C. Lee, Y. C. Lee, C. L. Tai, S. N. Tseng and J. H. Chern, *J. Med. Chem.*, 2005, **48**, 3522–3535.
- 40 M. Cortes-Salva, C. Garvin and J. C. Antilla, *J. Org. Chem.*, 2011, **76**, 1456–1459.
- 41 T. B. Nguyen, L. Ermolenko and A. Al-Mourabit, *Heterocycles*, 2012, **86**, 555–563.
- 42 Y. Wang, H. Wang, J. Peng and Q. Zhu, *Org. Lett.*, 2011, **13**, 4604–4607.
- 43 J. I. Clodt, V. D. Hack, R. Fröhlich and E. U. Würthwein, *Synthesis*, 2010, 1485–

1492.

- 44 B. L. Korbadi and S. Lee, *Bull. Korean Chem. Soc.*, 2013, **34**, 1266–1268.
- 45 T. Yao, *Tetrahedron Lett.*, 2015, **56**, 4623–4626.
- 46 J. C. Zhuo, A. H. Soloway, J. C. Beeson, W. Ji, B. A. Barnum, F. G. Rong, W. Tjarks, G. T. Jordan IV, J. Liu and S. G. Shore, *J. Org. Chem.*, 1999, **64**, 9566–9574.

Chapter 3

1,2,4-Benzothiadiazinyl Radicals

“Gee, did you make a movie mistake? You forgot to reload the damn gun.”

Last Action Hero (1993)

3.1 - Introduction

Short-lived persistent radicals are usually generated by homolytic bond cleavage through the application of heat or UV irradiation. Other high energy radiation or electron sources can also be used to produce free radicals.¹ Stable radicals, on the other hand, are commonly prepared by one electron oxidation or reduction of a closed-shell precursor. Single electron processes typically produce charged radicals (unless the precursor is charged) which may then be protonated or deprotonated to form neutral radicals. Common methods of achieving single electron transfer are synthetic electrochemical methods or reactions with redox-active transition-metals.² A wide variety of oxidising and reducing agents are available, depending on the electrochemical requirement of the system and whether the radical is unstable in the presence of the by-products.

Open-shell compounds are rarely air or moisture stable, and are usually extremely reactive, making radical purification problematic. Typical methods such as column chromatography are unsuitable for all but the most stable systems,³ whilst recrystallization can be difficult due to the increased sensitivity of radicals in solution. Vacuum sublimation is the favoured method for purifying radicals,⁴ especially for sulfur-nitrogen systems, but this is limited to those with high thermal stabilities.

3.2 - 1,2,4-Benzothiadiazinyl Radicals

1,2,4-Benzothiadiazinyl radicals were first reported in 1981 by Shermolovich⁵ and were generated by the oxidation of the corresponding S^{II} benzothiadiazines or reduction of the appropriate S^{IV} benzothiadiazine 1-chlorides. The radicals were reported to persist in solution but their isolation was not attempted. Later work by Kaszynski and co-workers in 2004 investigated 1,2,4-benzothiadiazinyl radicals as potential structural elements of liquid crystalline materials.³ They were successful in isolating and characterising the tetrachloro- and tetrafluoro-derivatives in solution and the solid-state (Figure 3.2.1).

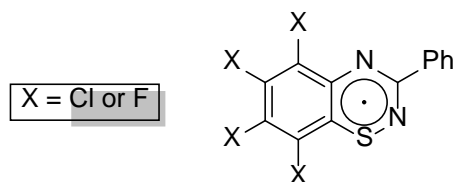


Figure 3.2.1: Isolated halogenated 1,2,4-benzothiadiazinyl radicals.

These halogenated-derivatives are sufficiently stable to be purified by chromatography and vacuum sublimation, whilst other electron-poor 1,2,4-benzothiadiazinyl radicals persist only at low temperatures (< -80 °C) and rapidly oxidise to form the S^{IV} 1-oxides.

The related *bis*-thiadiazinyl radicals show exceptional air and thermally stability in both solution and the solid-state, allowing their physical properties to be examined in great detail.^{4,6,7} This stability is ascribed to resonance delocalisation of the unpaired electron across the heterocyclic rings. The magnetic properties of 1,2,4-benzothiadiazinyl radicals however, remains to be explored.

3.2.1 – Radical Generation *via* Oxidation

The one electron oxidation of S^{II} benzothiadiazines is the most common method of generating 1,2,4-benzothiadiazinyl radicals in the literature. This is despite the fact that the synthesis of the S^{II} species^{8,9} typically requires many steps in comparison to the S^{IV} 1-chlorides.¹⁰ A wide variety of oxidising agents and solvents have been investigated,³ with oxidation and subsequent radical decay occurring more rapidly in polar solvents, likely due to the inherently high H₂O and O₂ content. Initial studies utilised a large excess of PbO₂ or AgO with K₂CO₃ in a 9:1 mixture of dry, degassed toluene and acetonitrile. The reaction mixture is filtered after a suitable length of time (30-90 minutes), which is primarily and subjectively determined by a visual inspection of colour, followed by removal of solvent under vacuum. Unsurprisingly, these methods gave impure material with low spin yields. Reproducible and high spin yields were achieved using SO₂Cl₂ and pyridine in dry toluene although the isolated yield of radical after purification remained low at about 10 %.

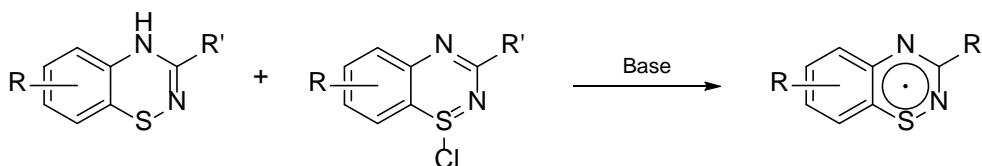
3.2.2 – Radical Generation *via* Reduction

The generation of 1,2,4-benzothiadiazinyl radicals by one electron reduction of the S^{IV} chloride⁵ has received considerably less attention, despite the fact that the majority of sulfur-nitrogen radicals are typically prepared from the parent S^{IV} cation.¹¹ The chloride salts, which are the primary products after heterocyclic ring closure with SCl₂ or S₂Cl₂, are often converted through to more soluble salts *via* anion metathesis prior to reduction.^{6,11} Typical reducing agents include ferrocene derivatives,⁶ metallic silver,^{12,13} zinc/copper couple^{12,14} and triphenyl antimony.¹⁵

Previous studies by Clark¹⁶ found that attempted reductions of 1,2,4-benzothiadiazine 1-chlorides with silver metal or a zinc/copper couple did not proceed smoothly; the slow reactions resulted in discoloured supernatants and no radical could be isolated. Reductions with Ph₃Sb and Fe(η⁵-C₅H₅)₂ proceeded smoothly, and removal of solvent yielded dark blue-green EPR active solids. Attempts to purify the crude material by recrystallization or vacuum sublimation to remove the Ph₃SbCl₂ or [Fe(η⁵-C₅H₅)₂]Cl by-products were unsuccessful.

3.2.3 – Radical Generation *via* Comproportionation

1,2,4-Benzothiadiazinyl radicals can also be prepared by comproportionation of the S^{II} benzothiadiazines and S^{IV} 1-chlorides in the presence of base (Scheme 3.2.3.1).¹⁶

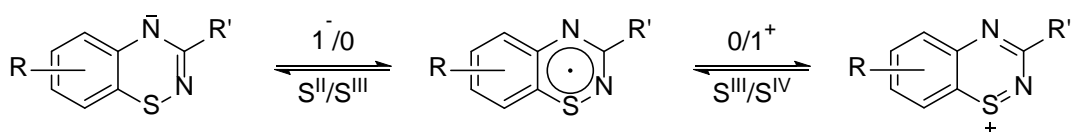


Scheme 3.2.3.1: Radical formation *via* comproportionation.

3.3 – Electrochemical Studies

The electrochemistry of many sulfur-nitrogen radicals has been studied in great detail, and a thorough summary is found in the review by Boeré.¹⁷ Far less is known about the electrochemical properties of redox-active six-membered S-N heterocycles, and these have generally received less study since they are often less stable and more difficult to prepare in comparison to the numerous five-membered systems known. The redox potentials are in principle however tunable to a much greater degree than five-membered systems due to the potential for alteration of substituents at multiple positions.¹⁷ In addition, six-membered thiazines and benzothiadiazines show significant covalency in their S-Cl bonds (*vide infra*), meaning that their electrochemical behaviour is not directly comparable to that of formal S^{IV} cations.¹⁸

The expected redox couples for the 1,2,4-benzothiadiazinyls are shown in Scheme 3.3.1. The reduction of the S^{IV} chloride to the S^{III} neutral radical, denoted as the 0/1⁺ couple, is of particular interest for this chapter.



Scheme 3.3.1: Redox scheme for 1,2,4-benzothiadiazinyls.

Cyclic voltammetry studies were performed under an argon atmosphere in anhydrous and degassed DCM with [ⁿBu₄N][PF₆] electrolyte, glassy carbon working-electrode, platinum wire counter-electrode and silver-wire *pseudo*-reference electrode. The internal potentials were referenced and reported against the Fc/Fc⁺ couple as an internal standard.¹⁹ The 1,2,4-benzothiadiazine 1-chlorides **2a-h** and **2k-l** studied by cyclic voltammetry, whose syntheses are discussed in Chapter 2, are shown in Figure 3.3.1.

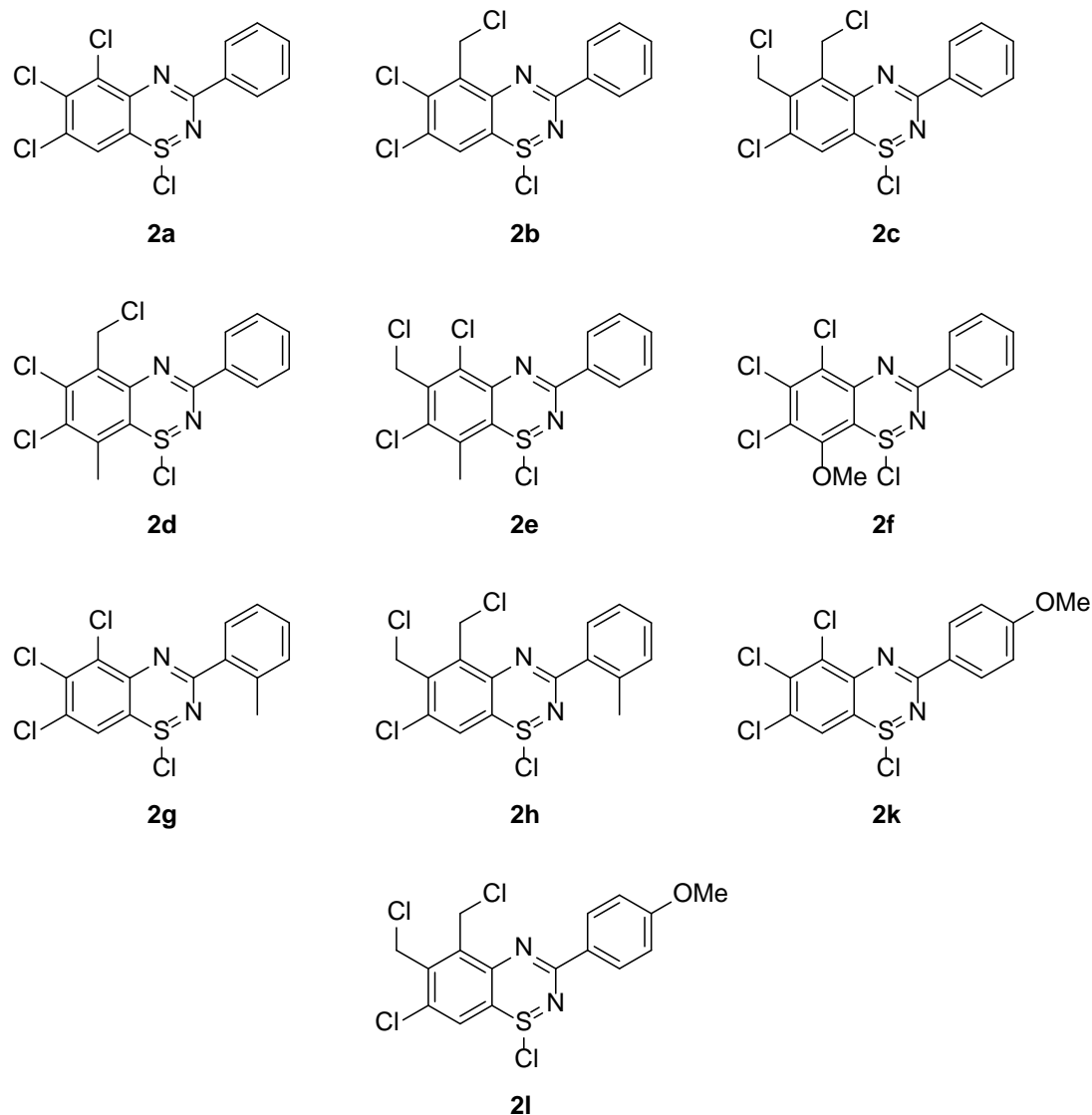


Figure 3.3.1: 1,2,4-benzothiadiazine 1-chlorides studied *via* cyclic voltammetry.

3.3.1 - Cyclic Voltammetry Results

The 1,2,4-benzothiadiazine 1-chlorides all displayed similar electrochemical behaviour, and the cyclic voltammogram of **2a** is typical of this (Chart 3.3.1.1). The two, often-overlapping, reversible processes at 0.096 and 0.444 V are assigned to the 0/1⁺ (S^{III}/S^{IV}) couple, whilst the irreversible process at -1.457 V is attributed to the 1-/0 (S^{II}/S^{III}) couple. The redox potentials of the 1,2,4-benzothiadiazines 1-chlorides are shown in Table 3.3.1.1. The difference in peak reduction and oxidation potentials for an ideal *Nernstian* process is 57/*n* mV at 25 °C, where *n* is the number of electrons transferred.²⁰ Although the values indicate significant deviation from *Nernstian* behaviour, likely due to Ohmic drop as a result of high resistance,²¹ the observation of values larger than 57 mV indicate that they are all associated with 1e⁻ transfer processes.

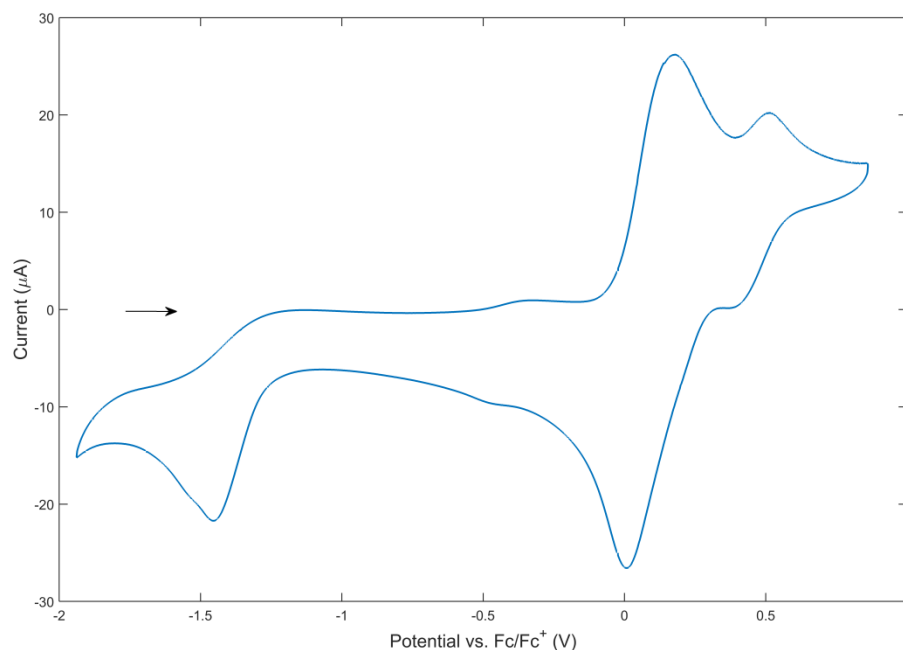


Chart 3.3.1.1: Cyclic voltammogram of **2a**.

	$1/0$	$0/1^+$ (Dimer)			$0/1^+$ (Monomer)		
	E_{red}/V	E_{red}/V	E_{ox}/V	$E_{1/2}/V$	E_{red}/V	E_{ox}/V	$E_{1/2}/V$
2a	-1.457	0.013	0.179	0.096	0.371	0.518	0.444
2b	-1.511	-0.112	0.084	-0.014	/	0.449	/
2c	-1.649	-0.094	0.054	-0.020	/	0.501	/
2d	-1.654	-0.084	0.036	-0.024	/	0.441	/
2e	-1.473	-0.027	0.142	0.057	0.336	0.469	0.403
2f	-1.557	-0.083	0.111	0.014	0.379	0.508	0.443
2g	-1.446	-0.011	0.226	0.108	0.400	0.481	0.440
2h	-1.599	-0.040	0.123	0.041	/	0.479	/
2k	-1.450	0.028	0.144	0.086	0.300	0.397	0.349
2l	-1.620	-0.071	0.035	-0.018	/	0.558	/

Table 3.3.1.1: Redox potentials for 1,2,4-benzothiadiazine 1-chlorides. Potentials referenced against the Fc/Fc⁺ couple.

The two 0/1⁺ redox couples indicate the presence of radical monomers and dimers in solution. This monomer-dimer equilibrium has also been observed for 6-membered thiatriazines¹⁷ and independently confirmed by quantitative EPR measurements.²² The radical monomer-dimer equilibria was qualitatively assessed *via* variable concentration studies on **2a** (Chart 3.3.1.2). These studies confirmed the initial assignment of the two 0/1⁺ redox couples; it is assumed that the one electron reduction potential on the monomer is positive relative to the dimer.¹⁷ At low concentrations the monomer is favoured whilst at high concentrations the CV is dominated by signals for the dimer. In addition, the 0/1⁻ reduction wave splits into two well resolved peaks at

low concentrations, further confirming the presence of radical monomers and dimers in solution.

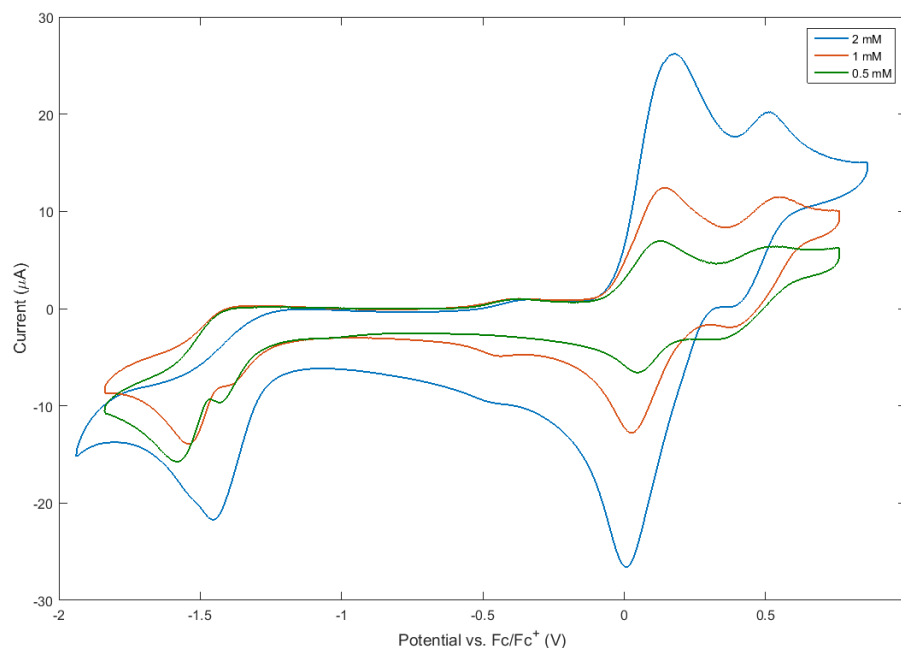


Chart 3.3.1.2: Cyclic voltammogram of **2a** at various concentrations.

The irreversible process at -1.457 V is attributed to the reduction of the neutral S^{III} radical to the S^{II} anion. This process is expected to be irreversible if there is an *EC* process (*i.e.* chemical reaction after an electrochemical process). If a salt of the cation is used as the source of bulk material in the electrochemical cell, the $0/1^+$ process is always reversible whilst the $1/0$ process is always irreversible.²³ This electrochemical irreversibility is attributed to a rapid comproportionation reaction between the electro-generated S^{II} anion and bulk S^{IV} cation, and has been observed for several sulfur-nitrogen systems.¹⁷ This process is thermodynamically favourable if there is sufficient cation at the electrode to quench the anion generated, or if the rate of diffusion of the cation from the bulk solution to the electrode is fast on the electrochemical timescale. Use of the middle species of the redox triad, the neutral radical, prevents this comproportionation reaction and electrochemical studies on pure neutral radical are important to assess the stability of various redox states.

The $E_{1/2}$ potentials for the $0/1^+$ (dimer) couples follow the expected trend, with 1,2,4-benzothiadiazine 1-chlorides bearing electron-withdrawing groups (Cl) such as **2a**, **2g** and **2k** being more easily reduced than those with electron-donating groups (Me) such as **2b-d**. The substituents on the benzo-fused ring were found to have a greater influence on the electrochemical behaviour and redox potentials compared to substituents on

the pendant aryl ring. This is supported by DFT studies (section 3.6.2) which indicate that there is negligible delocalisation of the unpaired electron onto the pendant aryl ring but significant π -delocalisation across the benzo-fused and heterocyclic ring. There are, however, only minor changes observed across the $0/1^+$ $E_{1/2}$ potentials for the substituted benzothiadiazine 1-chlorides, spanning 0.132 V. A slightly larger potential range of 0.208 V is observed for the reduction of the neutral radical to the S^{II} anion, and these follow the same trend as the $E_{1/2}$ potentials for the $0/1^+$ couple.

In several cases, additional peaks were also observed around -0.80 V and -0.45 V which are attributed to the daughter products resulting from trace water and/or oxygen contamination.

Further insight into the electrochemical behaviour was provided by recording multiple CV at different scan-rates for **2f** (Chart 3.3.1.3). These can be superimposed upon one another, although the peak-to-peak separation increases with scan-rate, suggesting that the redox chemistry for the $0/1^+$ couple is *quasi*-reversible.²¹ The $1/0$ couple is believed to be associated with an E_rC_i process; a reversible electron transfer followed by an irreversible chemical reaction. For a typical E_rC_i mechanism, the ratio of the anodic to cathodic peak currents decreases because the reduced species (*i.e.* the S^{II} anion) is consumed by a subsequent chemical reaction (*i.e.* comproportionation), resulting in fewer species to oxidise on the anodic scan. As the scan rate is increased, the time scale of the experiment competes with the time scale of the chemical step. This results in relatively more reduced species left for reoxidation, and for sufficiently fast scan rates, the electrochemical feature will regain reversibility. No evidence of *quasi*-reversibility was observed for the $1/0$ couple for scan rates up to 2 V/s, indicating that the comproportionation reaction is extremely rapid.

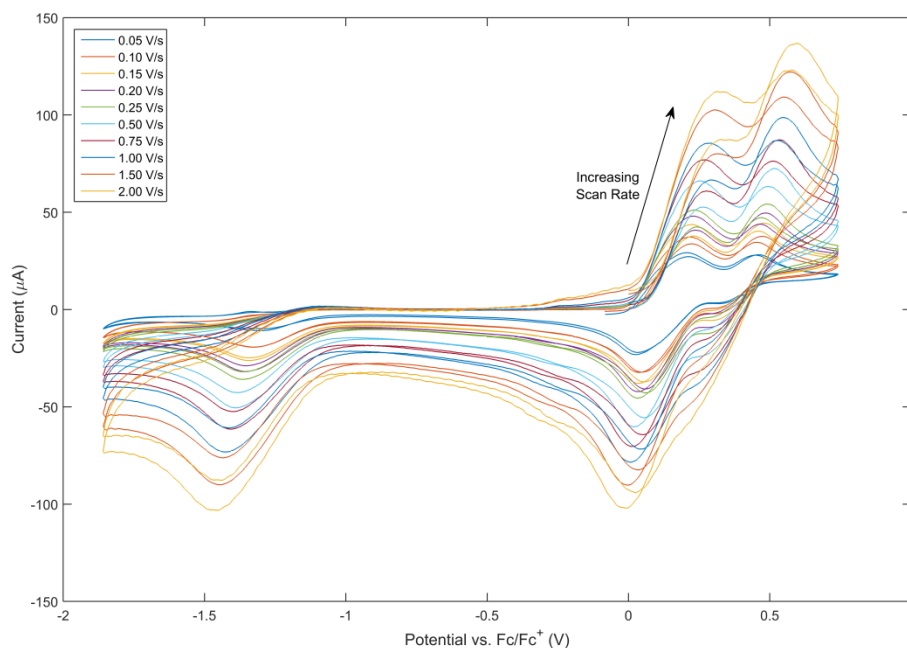
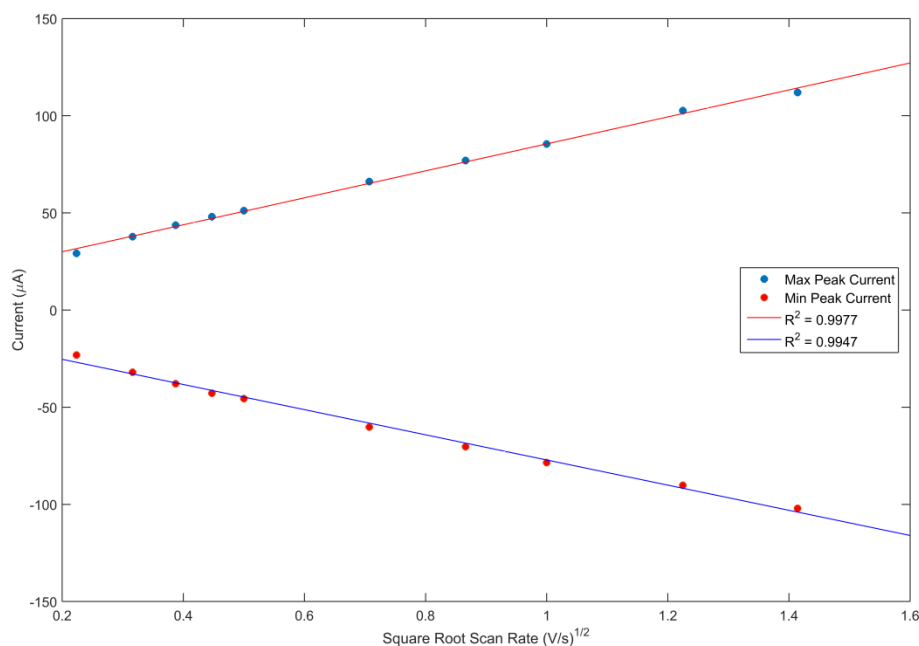


Chart 3.3.1.3: Cyclic voltammogram of **2f** at variable scan rates.

A plot for each of the maximum and minimum peak currents against the square root of the scan rate gave a linear correlation with R^2 values close to 1. The plots for the 0/1⁺ dimer redox couple are shown in Graph 3.3.1.1. This indicates an electrochemically reversible electron transfer process involving a freely diffusing redox species according to the Randles-Sevcik equation, and confirms that the analyte is not adsorbed to the electrode surface.²⁴



Graph 3.3.1.1: Peak current as a function of the square root of the scan rate.

3.3.2 – Computational Studies of the Redox Process

Theoretical calculations, performed at the UB3LYP/6-31g level, indicate that the form of the single occupied molecular orbital (SOMO) is independent of the substitution around the benzo-fused and pendant aryl rings. The SOMO geometry for radical **3a**, which is typical of all the 1,2,4-benzothiadiazinyls, is shown in Figure 3.2.2.1.

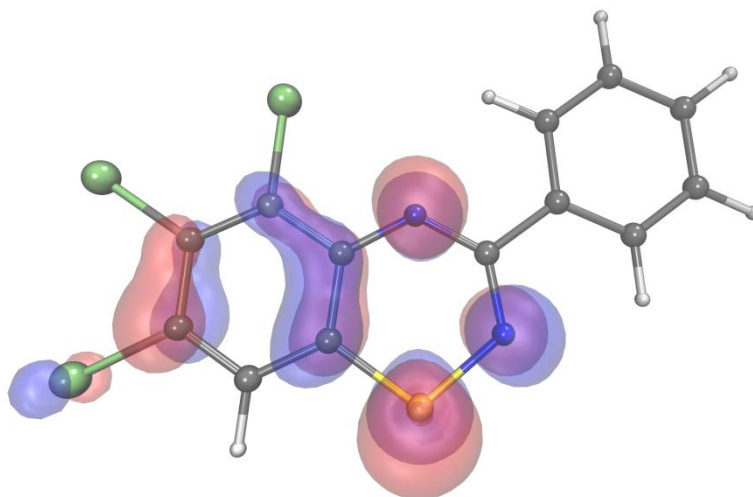


Figure 3.3.2.1: SOMO geometry for **3a** (isovalue = 0.04).

Many studies on the redox properties of sulfur-nitrogen radicals have found good correlation between the $E_{1/2}$ potentials for the 0/1⁺ couple with both the calculated energies of the LUMO of the S^{IV} cations, and the SOMO of the radical.²⁵ DFT (UB3LYP/6-31g) gas-phase optimised geometries of the 1,2,4-benzothiadiazine 1-chlorides **2a-h** and **2k-l** were calculated, along with their corresponding free radicals **3a-h** and **3k-l**. The results, summarised in Table 3.3.2.1, were found to give poor correlation with experimental electrochemical results although systems bearing electron-withdrawing groups did tend to have SOMOs with lower (more negative) energies, whilst those bearing electron-donating groups had SOMOs with higher (less negative) energies. As with the $E_{1/2}$ potentials for the 0/1⁺ couple, the range of values observed for the calculated LUMO and SOMO energies was small, further indicating that the substituents on the benzo-fused and pendant aryl ring have only a minor influence on the electronic structure of the radical.

	LUMO Energy / eV	SOMO Energy / eV	$E_{1/2}$ / V
a	-4.5013	-6.1177	0.096
b	-4.5165	-6.1231	-0.014
c	-4.4951	-6.0913	-0.020
d	-4.4836	-6.0477	-0.024
e	-4.4733	-6.0447	0.057
f	-4.2687	-6.0371	0.014
g	-4.4997	-6.0872	0.108
h	-4.4970	-6.0700	0.041
k	-4.3974	-6.0273	0.086
l	-4.5413	-6.0037	-0.018

Table 3.3.2.1: Calculated LUMO and SOMO energies of the 1,2,4-benzothiadiazine 1-chlorides and the corresponding radicals. Potentials referenced $E_{1/2}$ against the Fc/Fc⁺ couple.

3.4 – Synthesis and Isolation of 1,2,4-Benzothiadiazinyl Radicals

Previous attempts to generate the 1,2,4-benzothiadiazinyl radicals *via* one electron reduction of the S^{IV} 1-chloride found both Ph₃Sb and Fe(η^5 -C₅H₅) to be effective reducing agents, but attempts to remove the by-products and isolate the pure radical were unsuccessful.¹⁶ Preliminary small-scale studies utilising Ph₃P as the reducing agent in a variety of common organic solvents were promising, immediately yielding dark blue-green EPR active solutions, with the formation of Ph₃PCl₂ or [Ph₃PCl]Cl observed by ³¹P NMR spectroscopy depending on the choice of solvent.²⁶ Solutions of the radicals generated in DCM, toluene and THF swiftly discoloured to give cloudy yellow-brown suspensions, whilst the radicals were only poorly soluble in MeCN. The solutions of the radical were observed to become a rich blue colour on cooling in liquid nitrogen which is believed to originate from the monomer-dimer equilibrium, with the formation of closed-shell dimers being favoured at low temperatures.

A family of substituted 1,2,4-benzothiadiazinyl radicals, **3a-h** and **3k-l** (Figure 3.4.1), were prepared by the treatment of the parent S^{IV} chlorides, **2a-h** and **2k-l**, with Ph₃P in thoroughly degassed and anhydrous MeCN (Scheme 3.4.1). Despite the poor solubility of the S^{IV} chlorides in MeCN, the radicals formed cleanly and rapidly, and precipitated as dark purple-green solids that were subsequently isolated by filtration and washed prior to drying under vacuum. The washings were found to swiftly discolour, even when stored at -20 °C, and in several cases crystals of the S^{IV} 1-chloride, S^{IV} 1-oxide or S^{II} benzothiadiazine were isolated from the mother liquor.

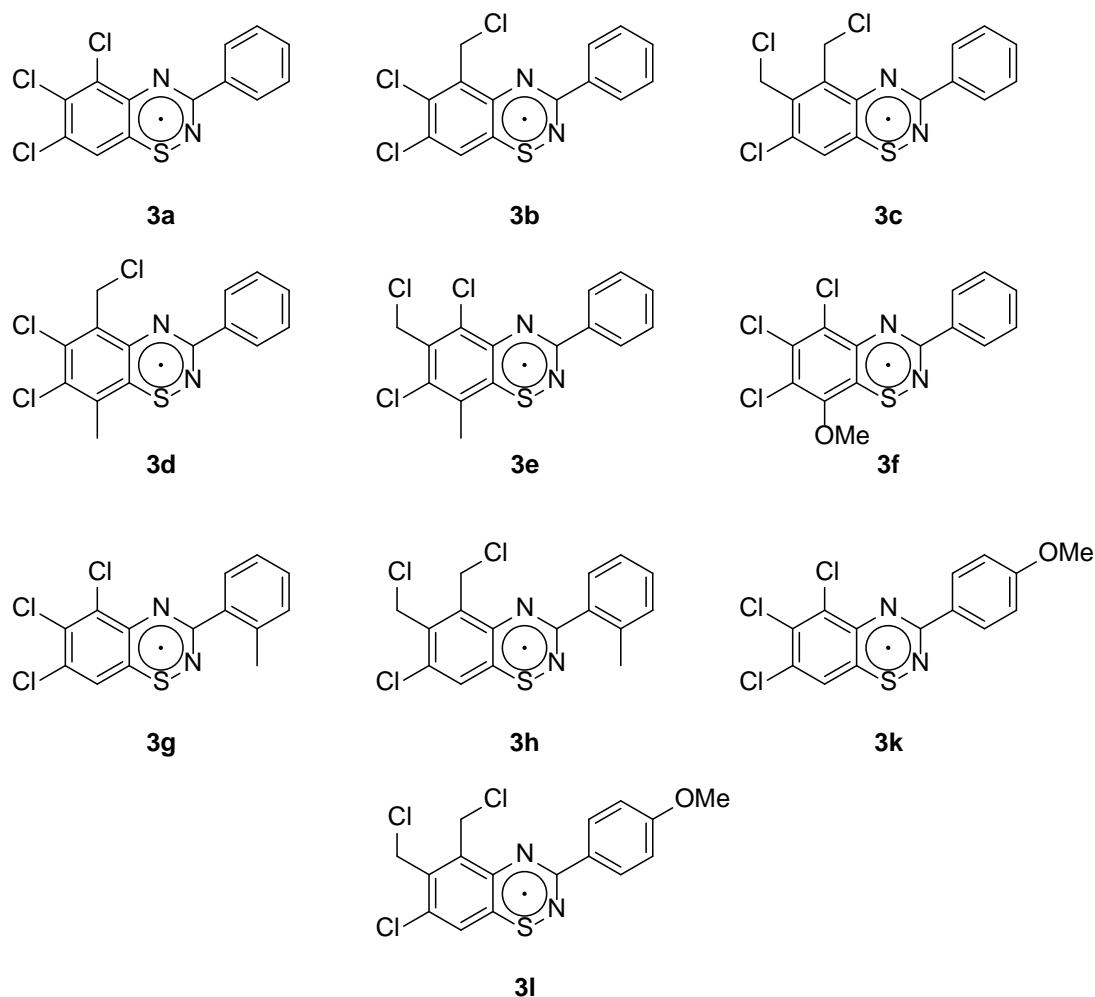
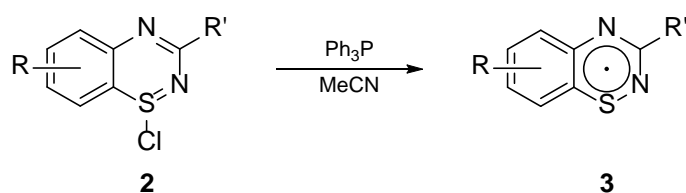


Figure 3.4.1: Substituted 1,2,4-benzothiadiazinyl radicals studied in this chapter.



Scheme 3.4.1: Synthesis of substituted 1,2,4-benzothiadiazinyl radicals.

3.5 – Structural Studies of 1,2,4-Benzothiadiazinyl Radicals

The growth of crystals suitable for SCXRD analysis was severely hampered by the poor stability of the 1,2,4-benzothiadiazinyl radicals in solution, with several approaches (slow cooling, vapour diffusion) and solvents (DCM, THF, toluene, pyridine, hexane, Et₂O) giving only rapid discolouration and formation of yellow/brown precipitates. Single crystals suitable for SCXRD analysis of **3a** and **3c** were successfully grown by rapidly mixing the parent S^{IV} 1-chloride and reducing agent in DCM, and allowing the radical to slowly crystallise out of solution. This method however, was found to be

extremely unreproducible and often afforded micro-crystalline material unsuitable for diffraction studies. Crystals of **3e** on the other hand, readily grew from saturated toluene solutions.

3.5.1 – Crystal Structure of **3a**

Compound **3a** crystallises as dark purple blocks in the orthorhombic space group *Pbcn* with a single radical molecule in the asymmetric unit and half a molecule of DCM (Figure 3.5.1.1). The molecule is essentially planar with only minor deviations of 1.76° for the heterocyclic ring and 2.53° for the pendant phenyl ring with respect to the benzo-fused ring; the N1-C1-C8-C13 and N2-C1-C8-C9 torsion angles are 1.14(5)° and 0.67(5)°.

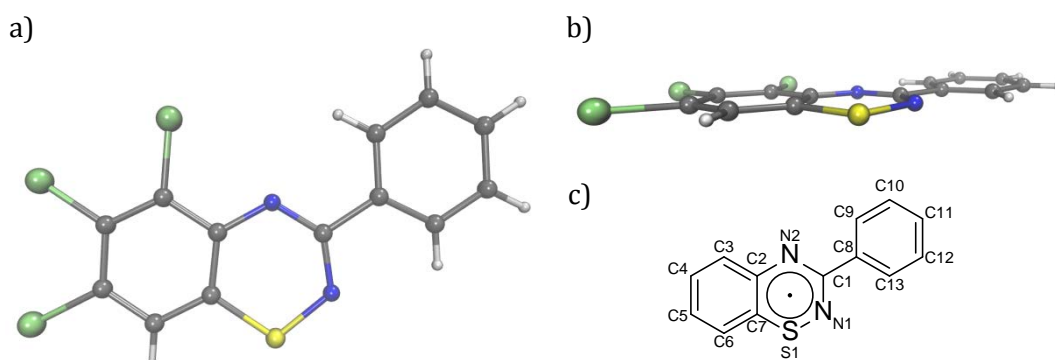


Figure 3.5.1.1: Crystal structure of **3a**: a) Top-down view; b) Side view; c) Structural labelling scheme. Solvents of crystallisation omitted for clarity.

Molecules of **3a** form non-parallel dimer pairs with short S1...N1 contacts (2.866(4) Å) between the heterocyclic rings within the sum of the van der Waals radii (3.26 Å)²⁷ (Figure 3.5.1.2). The angle between the mean planes of the heterocyclic rings is 7.82°. The molecules are further associated through π -stacking of the chlorinated fused-ring and pendant aryl rings (Figure 3.5.1.3), reminiscent of the electron-rich/electron-poor stacking in the C₆F₆/C₆H₆ co-crystal,²⁸ which is favoured by the anti-parallel alignment of molecular dipoles. This results in offset distorted π -stacks of alternating parallel and non-parallel planes; the distance between parallel planes is 3.281 Å, within the upper limit for true π -stacking of 3.40 Å.²⁹ The 1D chain propagates along the crystallographic *c* axis through the centre of the unit cell, with neighbouring offset chains located along the unit cell edges that are non-parallel by 23.41° and 24.72°.

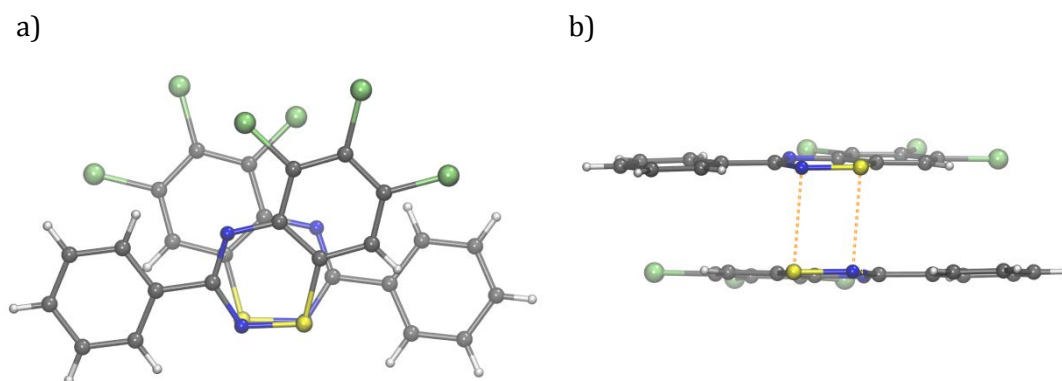


Figure 3.5.1.2: Dimer pairs of **3a**: a) Top-down view; b) Side view.

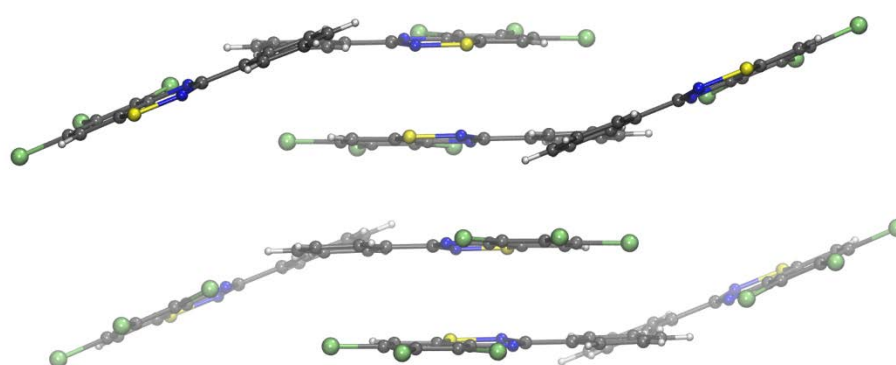


Figure 3.5.1.3: Crystal packing of **3a** looking down the crystallographic *b* axis.

3.5.2 – Crystal Structure of **3c**

Compound **3c** crystallises as dark purple rods in the monoclinic space group $P2_1/c$ with a single molecule in the asymmetric unit (Figure 3.5.2.1). The deviation from planarity of the heterocyclic ring with respect to the fused-ring is marginally smaller than the parent S^{IV} chloride (6.38° vs. 7.17° for **2c**) whilst the pendant aryl ring is less coplanar with both the heterocyclic and fused-ring despite the smaller N1-C1-C8-C13 and N2-C1-C8-C9 torsion angles. The CH_2Cl groups adopt a *trans* conformation with one orientated below the plane and the other above, contrary to **2c** where the two CH_2Cl groups adopt a *cis* conformation.

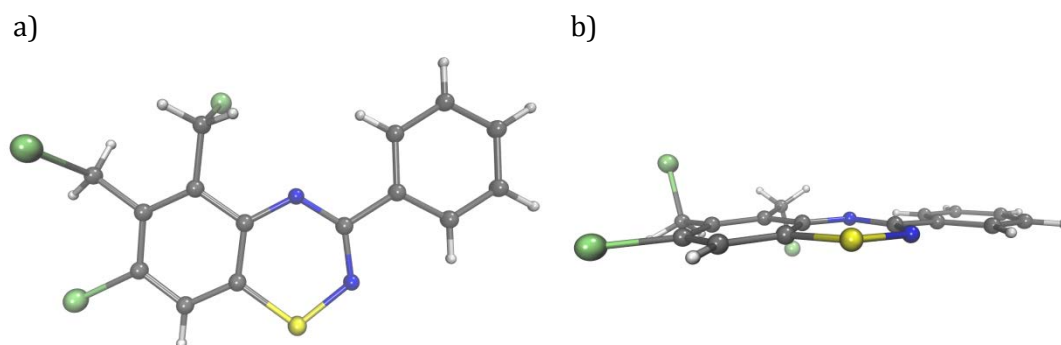


Figure 3.5.2.1: Crystal structure of **3c**: a) Top-down view; b) Side view.

Molecules of **3c** form parallel dimer pairs related through an inversion centre with $S1\cdots N2$ contacts between the heterocyclic rings of $3.087(2)$ Å, within the sum of the van der Waals radii (3.26 Å)²⁷ (Figure 3.5.2.2). The dimer pairs propagate through the lattice to form offset parallel π -stacks along the crystallographic b axis with alternating interplanar distances of 3.104 Å and 3.585 Å (Figure 3.5.2.3). Independent 1D chains of molecule run diagonally through the lattice at 59.53° , perpendicular to the crystallographic ab plane.

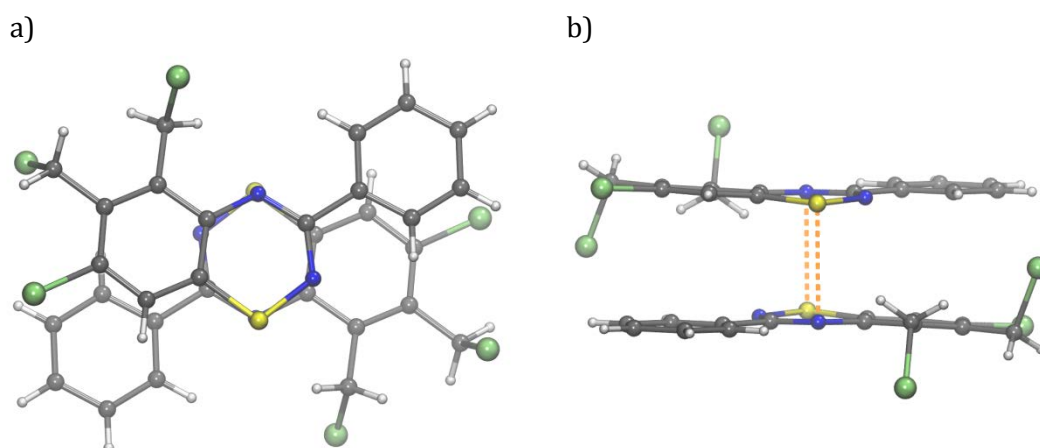


Figure 3.5.2.2: Dimer pairs of **3c**: a) Top-down view; b) Side view.

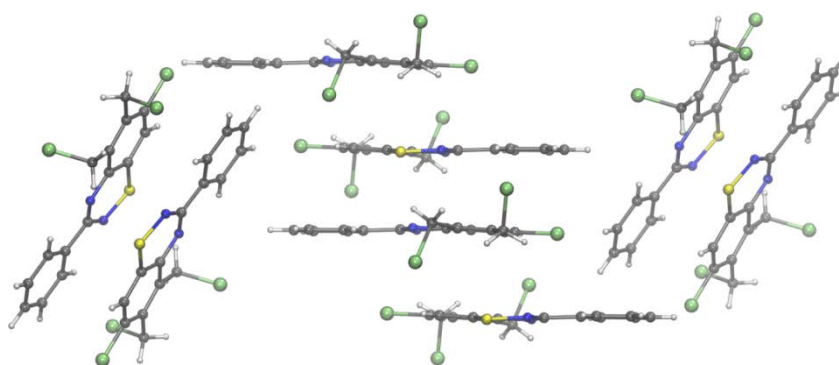


Figure 3.5.2.3: Crystal packing of **3c** looking down the crystallographic c axis.

3.5.3 – Crystal Structure of 3e

Compound **3e** crystallises as purple parallelepipeds in the triclinic space group $P\bar{1}$ with two molecules in the asymmetric unit (Figure 3.5.3.1). The heterocyclic rings deviate from planarity at 5.38° and 5.55° and the pendant aryl ring is twisted compared to **3a** and **3c** such that the deviations from coplanarity with respect to the fused ring are 6.31° and 10.94° for molecules one and two respectively.

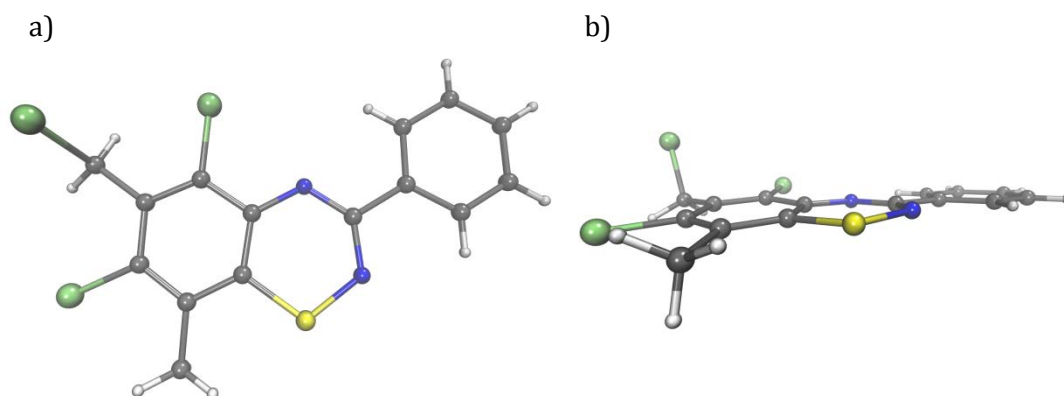


Figure 3.5.3.1: Crystal structure of **3e**: a) Top-down view; b) Side view. One molecule of the asymmetric unit omitted for clarity.

Molecules of **3e** form non-parallel dimer pairs associated through $S1\cdots S1$ contacts ($2.846(1)$ Å) between the heterocyclic rings, within the sum of the van der Waals radii (3.60 Å)²⁷ (Figure 3.5.3.2). The angle between the mean planes of the heterocyclic rings is 10.45° . Molecules are further associated through π -stacking of the chlorinated fused-ring and pendant aryl rings, as seen in **3a**, resulting in offset distorted π -stacks of alternating parallel and non-parallel planes; the distance between parallel planes is 3.231 Å (Figure 3.5.3.3). The 1D chains propagate diagonally through the crystallographic a and b axes, running parallel to neighbouring chains such that the parallel and anti-parallel planes of molecules intersect.

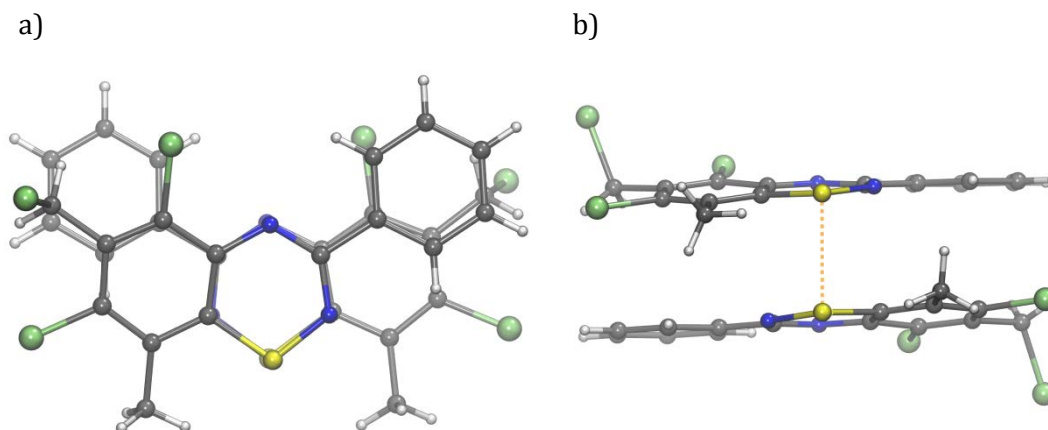


Figure 3.5.3.2: Dimer pairs of **3e**: a) Top-down view; b) Side view.

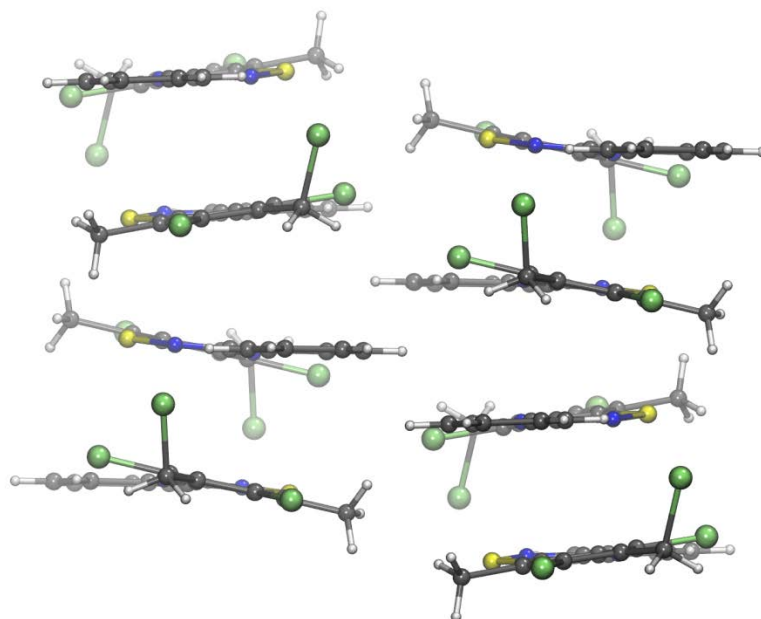


Figure 3.5.3.3: Crystal packing of **3e** looking down the crystallographic *c* axis.

3.5.4 – Comparison of Solid-State Structures

The crystallographically characterised 1,2,4-benzothiadiazinyl radicals are all dimeric in the solid-state and feature short contacts between the heteroatoms. Different configurations of dimer (Figure 3.5.4.1) were observed for each of the radicals, all of which involve a π^* - π^* bonding interaction between the single occupied molecular orbitals. Compound **3a** dimerises in a twisted suprafacial motif (**A**) with two short identical S1...N1 contacts (2.866(4) Å); the heterocyclic rings are non-parallel with an interplanar angle of 7.82°. Compound **3c** adopts a *trans*-antarafacial dimer motif (**B**) featuring two short identical S1...N2 contacts (3.087(2) Å) and parallel heterocyclic rings. Compound **3e** dimerises in a *trans*-suprafacial motif (**C**) with a single short S1...S1 contact (2.846(1) Å) and a non-parallel arrangement of the heterocyclic rings; the angle between the planes is 10.45°.

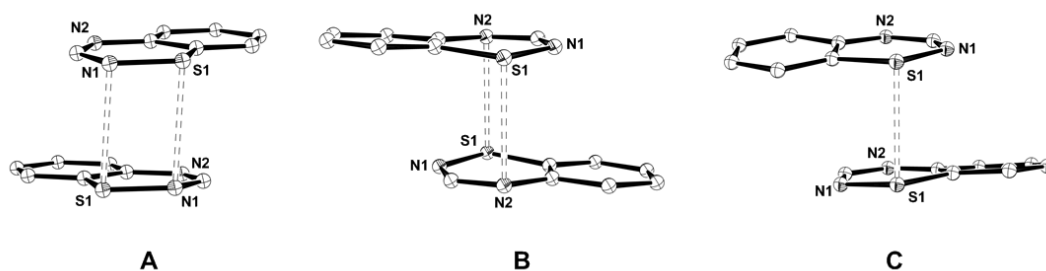


Figure 3.5.4.1: Dimerisation motifs observed for 1,2,4-benzothiadiazinyl radicals: (**A**) twisted suprafacial; (**B**) *trans*-antarafacial; (**C**) *trans*-suprafacial.

The solid-state structures of the two previously crystallographically characterised 1,2,4-benzothiadiazinyl radicals, **3x** and **3y** (Figure 3.5.4.2), are essentially planar with only minor deviations from planarity for the heterocyclic rings of 0.18° and 1.14° respectively.³

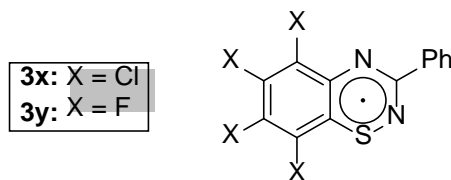


Figure 3.5.4.2: Previously reported structurally characterised 1,2,4-benzothiadiazinyl radicals.

Compound **3x** adopts parallel offset planes associated through π -stacking of the perchlorinated-fused ring and the pendant aryl ring; the interplanar spacing is almost equal at 3.398 Å and 3.395 Å, which is approaching the upper limit for true π -stacking (3.40 Å).²⁹ Each molecule forms a weak dimer pair with an inversion related molecule within a neighbouring slipped stack, with a single long S1...S1 contact of 3.365(6) Å within the sum of the van der Waals radii. This dimerisation motif may be regarded as a pseudo-*cis*-oid (**D**) (Figure 3.5.4.3) due to the presence of two additional long S1...N1 contacts of 3.530(1) Å. Molecules of **3y** adopt equally spaced non-parallel stacks associated through the heterocyclic rings with two non-identical S1...N1 contacts of 3.193(4) Å and 3.213(4) Å. The molecules are further associated with neighbouring molecules in a slightly offset stack through two equal S1...N1 contacts of 3.269(3) Å, resulting in a ladder-type structure. Each molecule thus forms a single *cis*-oid and two twisted suprafacial heterocyclic associations (**E**) with neighbouring molecules.

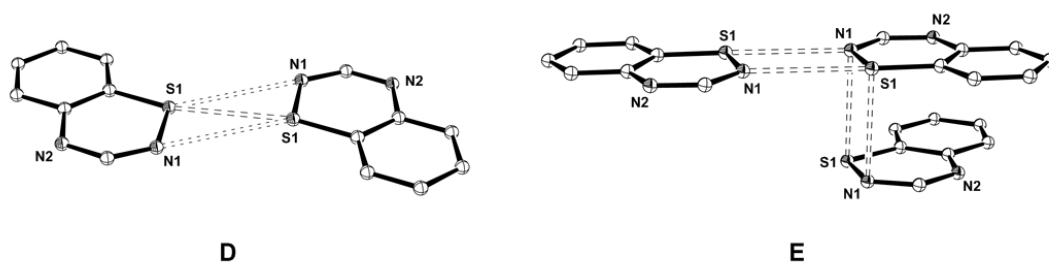


Figure 3.5.4.3: Heterocyclic association motifs observed for 1,2,4-benzothiadiazinyl radicals: (**D**) pseudo-*cis*-oid; (**E**) *cis*-oid, twisted suprafacial.

Sulfur-nitrogen radicals are well known to dimerise in the solid-state, especially those based on less delocalised five-membered ring systems such as dithiadiazolylys (DTDA)s for which several dimer configurations have been observed.³⁰ Since dimerisation

results in spin-pairing, rendering the material diamagnetic, a great deal of effort has been directed at overcoming dimerisation in the solid-state. Steric shielding through the introduction of bulky substituents is most commonly employed, but this can also prevent magnetic communication in the solid-state as orbital overlap is diminished. Similarly, increasing the degree of delocalisation of the unpaired electron can have both positive and negative effects, and the balance is often subtle and unpredictable.³¹

The *trans* configuration of the CH₂Cl groups in **3c** helps to prevent close contact of the fused-rings such that the contacts between heteroatoms is significantly longer than those observed for **3a** and **3e**. The addition of substituents to the pendant aryl ring is also likely to have a significant influence on the solid-state structure. Radicals **3g** and **3h** in particular are potentially promising candidates since the *o*-tolyl ring is expected to twist considerably with respect to the fused-ring, as observed for the parent S^{IV} chlorides, and suppress close contact of radical centres. However, attempts to crystallise these radicals were unsuccessful.

The three radicals may be considered as *Peierls* distorted π -stacks with alternating short and long intermolecular contacts along the stacking direction. This packing motif is thermodynamically favourable and all one-dimensional stacks have an inherent instability with respect to spin-Peierls.³² For such systems however, a transition to a configuration featuring evenly spaced π -stacks may be accessible at high temperatures. This transition between the enthalpically favoured low temperature phase and entropically favoured high temperature has been observed in a number of benzodithiazolyis (BDTAs)³³ resulting in magnetic bistability with a well-defined hysteresis.^{34,35} Variable temperature X-ray diffraction studies on the 1,2,4-benzothiadiazyl radicals are therefore highly desirable to explore these potential properties.

3.6 – Electron Paramagnetic Resonance

Preliminary EPR studies of the 1,2,4-benzothiadiazinyl radicals were performed by *in situ* reduction of the parent S^{IV} chloride with ferrocene in toluene. The later isolation of pure samples of the radicals allowed consistent measurements at a set concentration of radical to be performed. Prior attempts to collect frozen-solution spectra to obtain anisotropic data for orbital coefficient studies were unsuccessful, resulting in loss of resolution such that no spectral features could be extracted.¹⁶ This is attributed to rapid dimerisation on cooling.

3.6.1 – EPR Results

The EPR spectra of the 1,2,4-benzothiadiazinyl radicals **3a-h** and **3k-l** were recorded in toluene at ambient temperature on a continuous wave (CW) X-band spectrometer. EPR spectral simulation and analysis were performed using the EasySpin computational package.³⁶ The experimental and simulated spectra are shown in Figures 3.6.1.1 to 3.6.1.10.

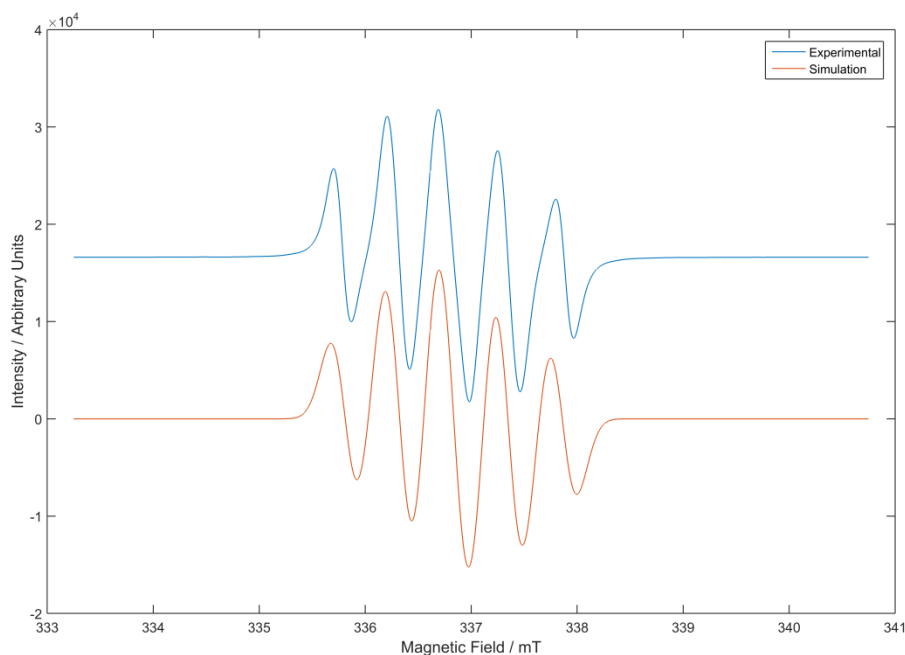


Figure 3.6.1.1: EPR spectra of **3a**.

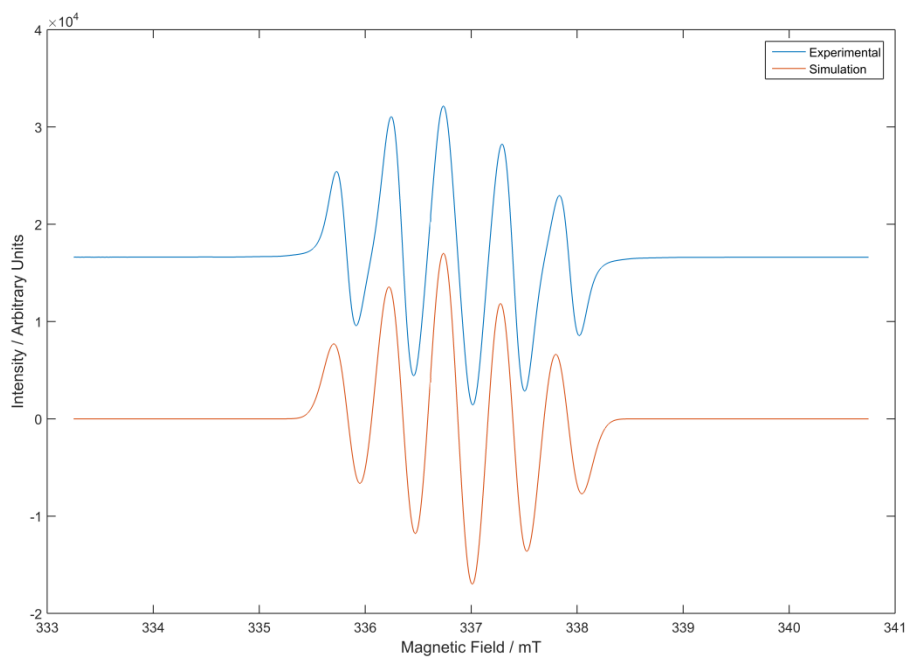


Figure 3.6.1.2: EPR spectra of **3b**.

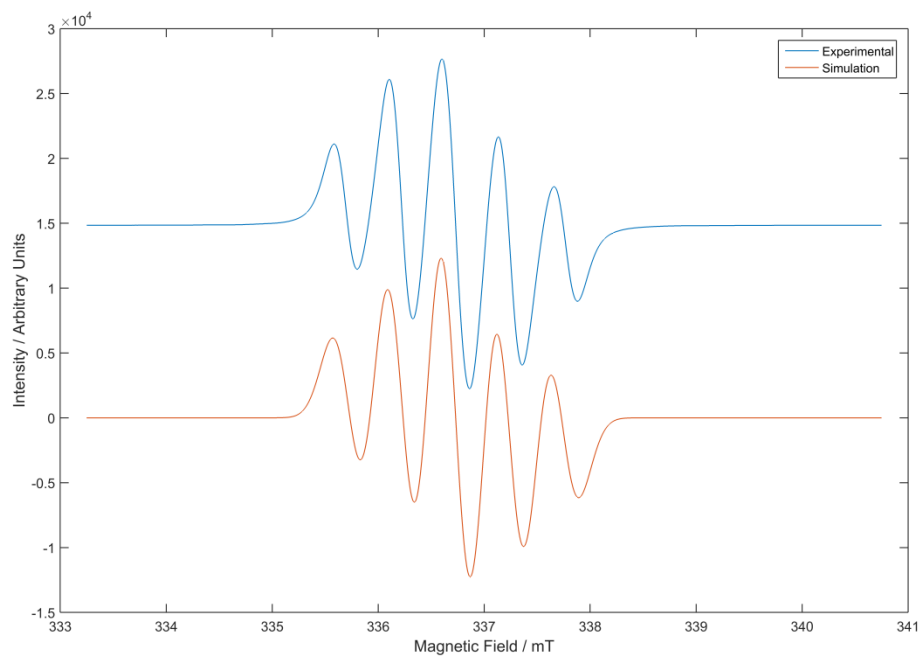


Figure 3.6.1.3: EPR spectra of **3c**.

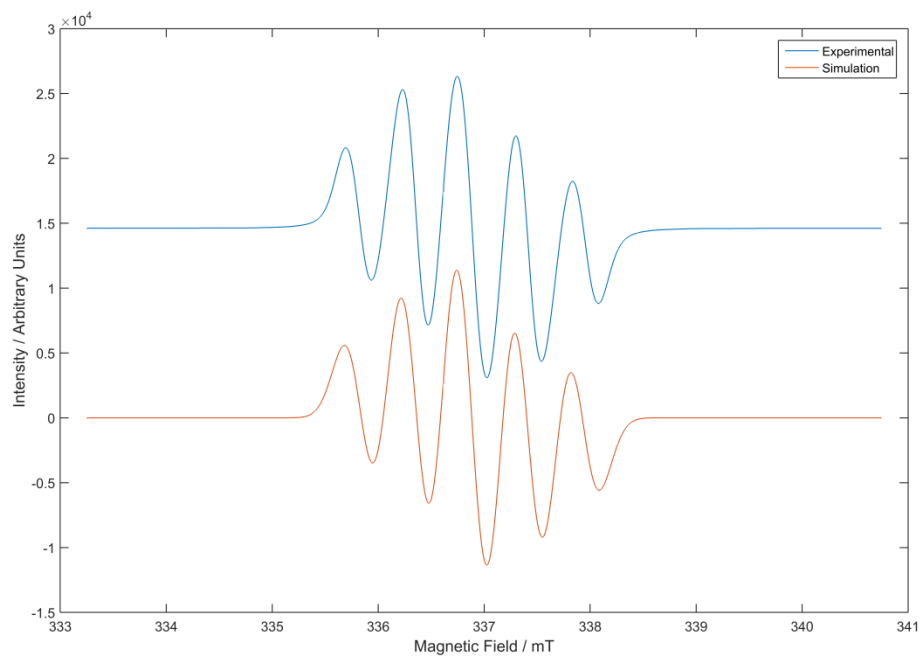


Figure 3.6.1.4: EPR spectra of **3d**.

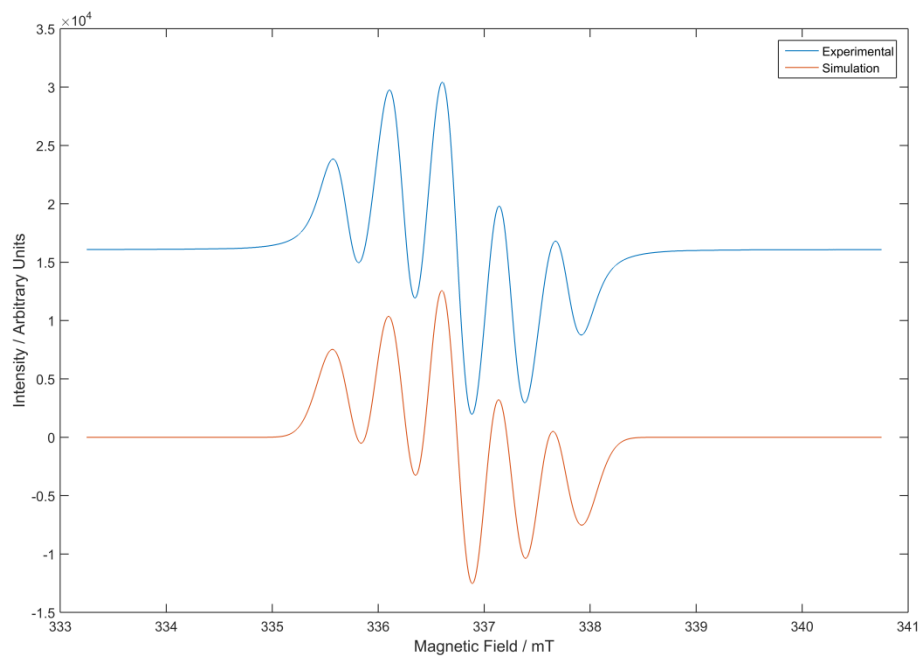


Figure 3.6.1.5: EPR spectra of 3e.

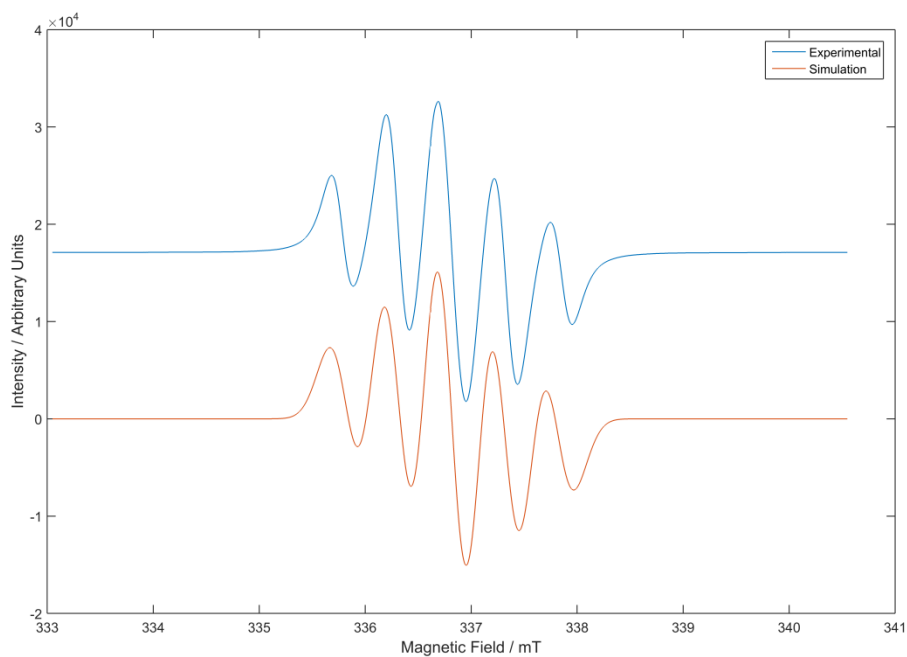


Figure 3.6.1.6: EPR spectra of 3f.

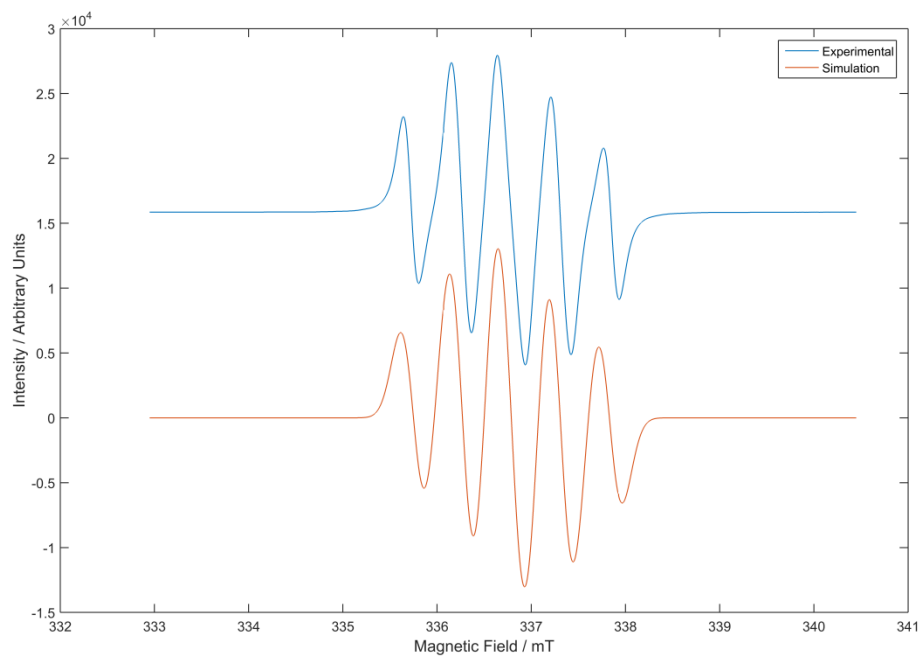


Figure 3.6.1.7: EPR spectra of 3g.

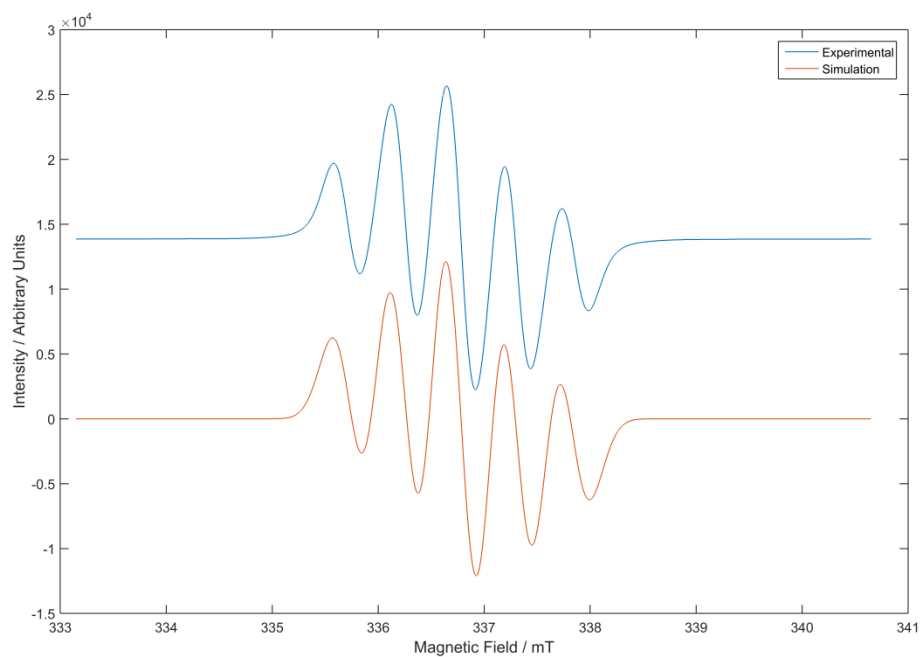


Figure 3.6.1.8: EPR spectra of 3h.

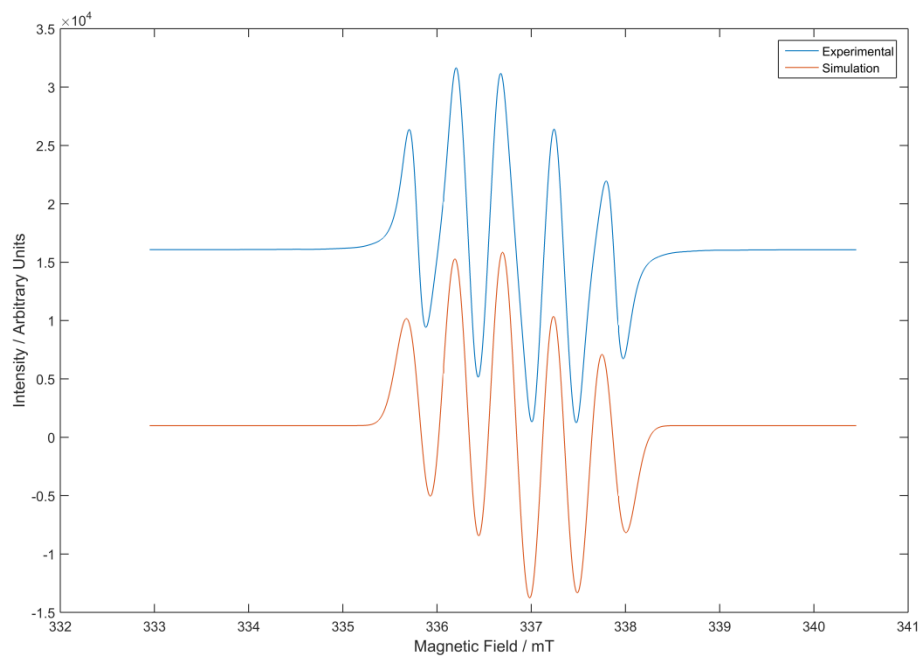


Figure 3.6.1.9: EPR spectra of 3k.

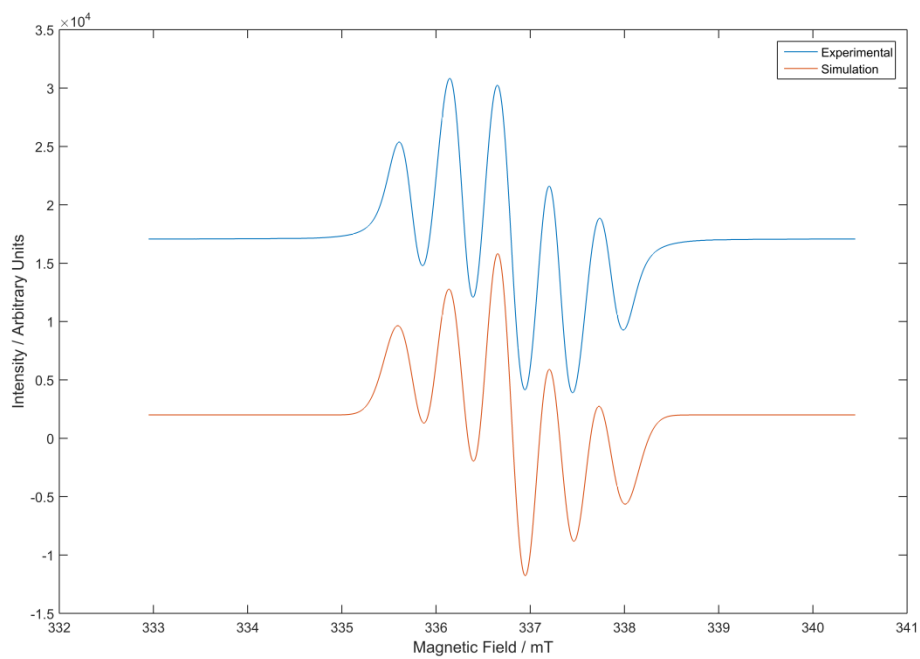


Figure 3.6.1.10: EPR spectra of 3l.

The EPR spectra for the 1,2,4-benzothiadiazinyl radicals are all based upon distorted 1:2:3:2:1 quintets arising from coupling to two similar but non-identical nitrogens within the heterocyclic ring. Significant line-broadening is observed in all cases arising from chlorination of the fused ring. Since both ^{35}Cl and ^{37}Cl are quadrupolar nuclei with $I = 3/2$, the spectra consist of multiple superimposed spectra for each possible isotopologue resulting in net loss of resolution and increased-line broadening, and so all features beyond nitrogen coupling are lost.⁴ A summary of EPR results and parameters for the radicals are shown in Table 3.6.1.1.

	<i>g</i>-value	Line-Width / MHz	a_{N1} / MHz	a_{N2} / MHz
3a	2.00369	0.2696	15.662	13.132
3b	2.00346	0.2633	15.635	13.505
3c	2.00341	0.3097	15.804	13.599
3d	2.00431	0.3106	15.102	13.102
3e	2.00463	0.3694	14.687	13.298
3f	2.00453	0.3258	14.561	13.226
3g	2.00461	0.2689	15.883	13.354
3h	2.00449	0.3388	15.606	13.705
3k	2.00410	0.2904	15.821	12.892
3l	2.00411	0.3767	14.731	13.980

Table 3.6.1.1: EPR parameters for the 1,2,4-benzothiadiazinyl radicals.

The similarity in the *g*-values and nitrogen hyperfine coupling constants across the 1,2,4-benzothiadiazinyl radicals indicates that the electronic structure is only slightly perturbed by substitution of the benzo-fused and pendant aryl ring. This is in good agreement with electrochemical studies where the variation in $E_{1/2}$ potentials for the 0/1⁺ redox couple was small. Indeed, the SOMO geometry (Figure 3.6.1.11), calculated at the UB3LYP/cc-pVDZ level at the UB3LYP/6-31G geometry, reveals that it is largely independent of the substitution around the benzo-fused and pendant aryl rings. Although significant delocalisation is observed across the benzo-fused ring framework, the low abundance (1.1 %) of ^{13}C nuclide ($I = 1/2$) will have negligible contribution to the EPR spectra and was therefore excluded from simulations of experimental data. In addition, the hyperfine coupling constants to H atoms on the benzo-fused or pendant aryl ring are small and further contribute to line broadening.³

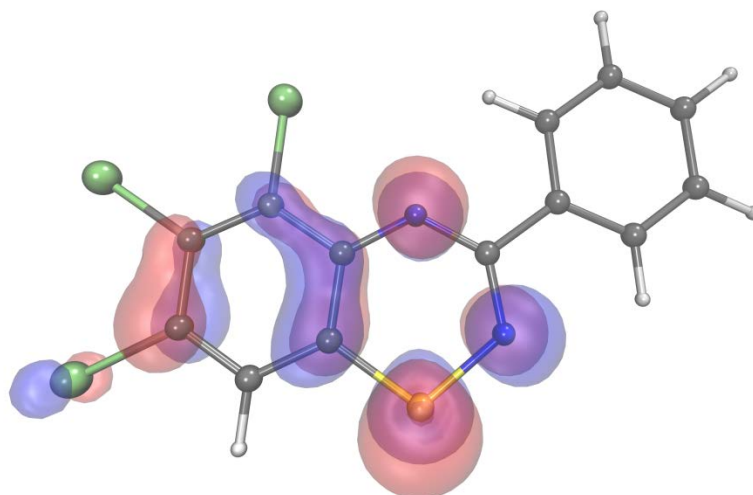


Figure 3.6.1.11: SOMO geometry for **3a** (isovalue = 0.04).

3.6.2 – Computational Studies

Systematic and comprehensive studies of sulfur-nitrogen radicals has shown that DFT calculations using the UB3LYP/6-31G* method gives excellent correlation to experimental EPR parameters.^{37,38} However, the absolute accuracy of the calculated hyperfine coupling constants were typically poor and showed significant basis set sensitivity. As such, appropriate scaling factors have been developed for each nuclei and basis set. Calculations were performed at the UB3LYP/cc-pVDZ level of theory at the UB3LYP/6-31G optimised geometry following established methods for 1,2,4-benzothiadiazinyl radicals.³ The hyperfine coupling constants were found to be significantly overestimated even after scaling (0.73 for ¹⁴N) whilst the ratio of a_{N1} to a_{N2} was inconsistent and gave poor correlation to experimental data. A table of unscaled calculated hyperfine coupling constants and the estimated spin densities on N1, N2 and S1 are shown in Table 3.6.2.1.

	a_{N1} / MHz	a_{N2} / MHz	Spin Densities		
			N1	N2	S1
3a	23.181	20.460	0.3766	0.3359	0.2389
3b	22.772	20.328	0.3694	0.3293	0.2427
3c	23.043	20.633	0.3750	0.3348	0.2358
3d	22.604	20.437	0.3679	0.3313	0.2359
3e	23.320	20.851	0.3810	0.3432	0.2261
3f	23.122	20.436	0.3752	0.3361	0.2457
3g	21.362	21.433	0.3500	0.3514	0.2323
3h	21.922	21.269	0.3588	0.3449	0.2302
3k	23.949	19.921	0.3886	0.3272	0.2396
3l	23.787	20.144	0.3866	0.3269	0.2364

Table 3.6.2.1: Calculated hyperfine coupling constants and spin densities for the 1,2,4-benzothiadiazinyl radicals.

The correlation between the calculated hyperfine coupling constants and spin densities on N1 and N2 are close to linear ($R^2 = 0.9938$ for N1 and $R^2 = 0.9175$ for N2) in accordance with the McConnell relationship,³⁹ however considerable variation across the radicals was observed. The calculated spin density and hence hyperfine coupling constant for N1 in **3g** was found to be less than N2, and only marginally larger in **3h**. This is contrary to radicals **3a-f**, where the spin density on N1 is typically $\approx 11-12\%$ greater than N2 whilst this increases to $\approx 18-19\%$ for **3k-l**. This suggests that whilst substitution on the pendant aryl ring has little effect on the energy of the SOMO and hence electrochemical behaviour, it may have a marked effect on the spin distribution of the radicals which, in combination with the added sterics or alternative packing interactions, could have a significant influence on the association of radical centres in the solid-state and any resultant magnetic communication.

The poor correlation between theoretical and experimental EPR results may be attributed to a number of factors. Primarily, the calculations are all performed in the gas-phase on a static optimised model. In contrast, EPR measurements were recorded in the solution-state on a dynamic system and represent a weighted average of all contributing geometries. This will have an amplified impact for the 1,2,4-benzothiadiazinyl radicals for which the conformational preference of both the pendant aryl ring and the substituents on the benzo-fused ring must be considered. Additionally, hyperfine coupling constants are sensitive to experimental conditions as well the geometry.³⁸

3.7 – Magnetic Studies

The magnetic properties of a selection of the 1,2,4-benzothiadiazinyl radicals obtained in a pure form based on elemental analysis, were examined through a combination of experimental and theoretical studies. Whilst the crystallographic data indicates that these radicals form dimer pairs in the solid-state, the observation of a magnetic phase-transition at a finite temperature is not uncommon for other dimeric sulfur-nitrogen radicals.^{31,34,40}

3.7.1 – SQUID Results

Variable temperature magnetic susceptibility measurements were recorded between 2-300 K in either a 1000 Oe or 10000 Oe applied magnetic field. The poor magnetic response of the radicals became evident during sample centring, with each sample giving a very weak signal unless cooled to 5 K in a 10 kOe applied field. Preliminary studies on **3c** (Chart 3.7.1.1) displayed what appeared to be paramagnetic behaviour

with a slight increase in the magnetic susceptibility on warming to 47 K and 57 K, which then steadily decreases as the sample approaches room temperature. On cooling in the presence of the applied field, the magnetic susceptibility begins to steadily increase towards 65 K before a brief plateau followed by a rapid increase on further cooling. This feature was maintained for several cycles of heating and cooling in the absence or presence of the field.

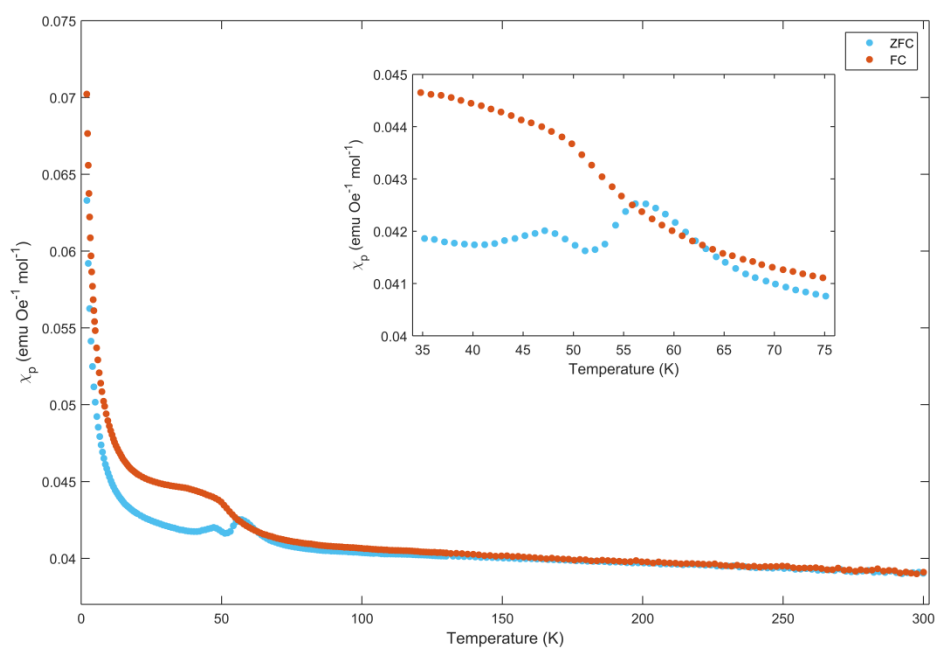


Chart 3.7.1.1: Paramagnetic susceptibility as a function of temperature for **3c**.

This behaviour was observed for duplicate measurements of a freshly prepared sample of **3c**, as well as for radicals **3a** and **3e** (Charts 3.7.1.2 and 3.7.1.3). The origin of this behaviour is attributed to the antiferromagnetic transition of trace oxygen contamination within the sample.⁴¹

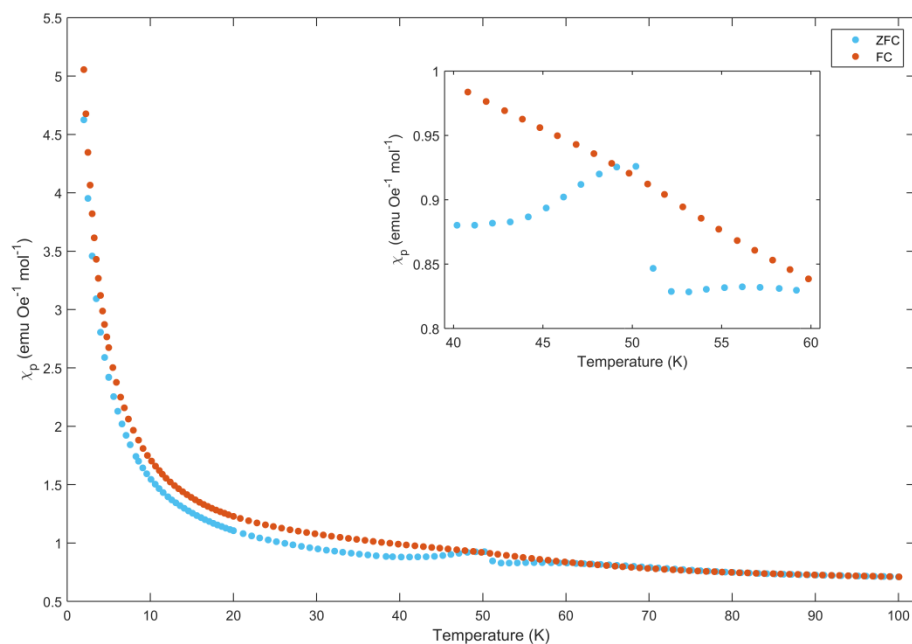


Chart 3.7.1.2: Paramagnetic susceptibility as a function of temperature for **3a**.

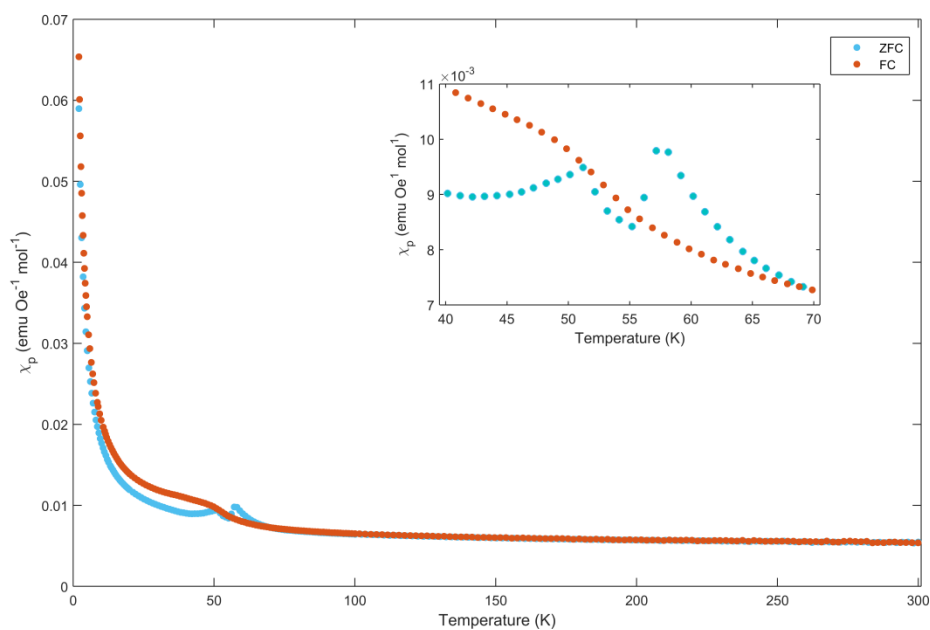


Chart 3.7.1.3: Paramagnetic susceptibility as a function of temperature for **3e**.

This feature was not observed during magnetic measurements of **3d**, which was not structurally characterised, but the magnitude of the response is significantly lower than that for **3a**, **3c** and **3e**. Initial examination of the data showed that the magnetic susceptibility was directly proportional to the temperature (Chart 3.7.1.4). The *Curie-Weiss* plot (Chart 3.7.1.5) however was non-linear, as would be expected for an ideal *Curie* paramagnet with $S = \frac{1}{2}$.⁴² Extrapolation of the high temperature data above 150

K gave a *Curie* constant of $C = 0.0369 \text{ emu K mol}^{-1}$ and θ value of -370 K which is consistent with extremely strong AFM interactions between radicals pairs such that they are spin-paired and hence essentially diamagnetic. The paramagnetic shape of the magnetic susceptibility plot may be attributed either to residual unpaired spins at the surface of the finely ground material or due to a trace paramagnetic impurity. These would explain the poor magnetic response from this sample and the calculated effective magnetic moment of $0.54 \mu\text{B}$, which is much lower than expected for a spin $S = \frac{1}{2}$ centre.

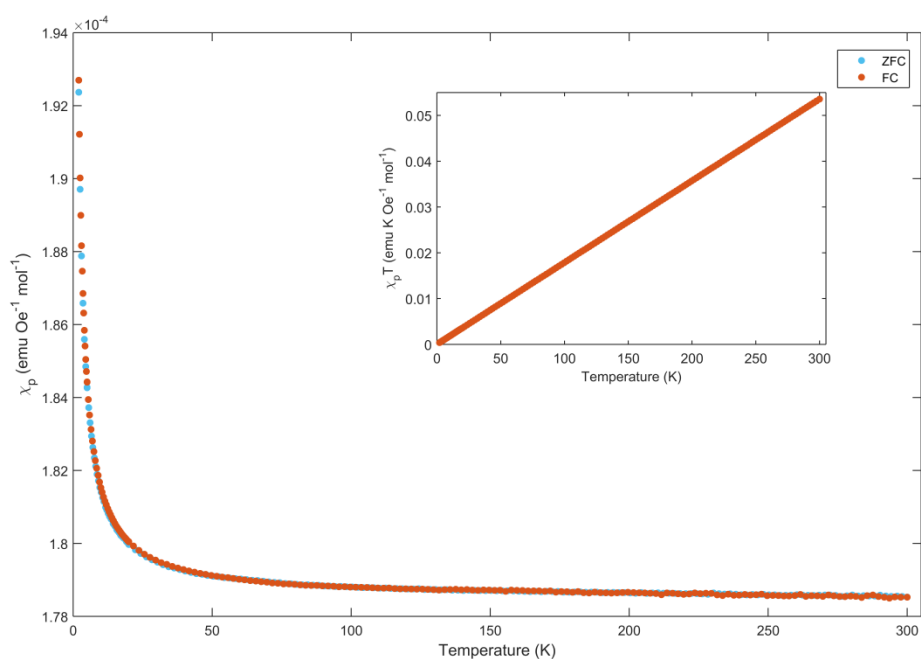


Chart 3.7.1.4: Paramagnetic susceptibility as a function of temperature for **3d**. $\chi_p T$ vs. T plot shown in inset. T

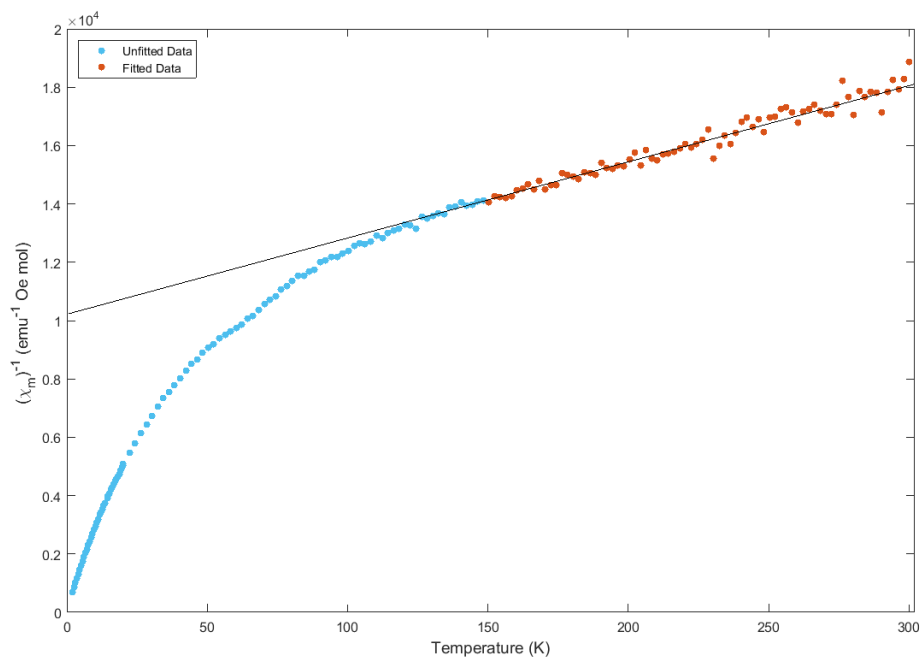


Chart 3.7.1.5: Curie-Weiss plot for **3d**.

Magnetic measurements were also performed on radical **3e**. Although structural data were not obtained, it was reasoned that the methoxy-group may prevent close contact of radical centres and suppress dimerisation in the solid-state. The magnetic susceptibility plot (Figure 3.7.1.6) is similar to **3d**, however an additional feature was observed at approximately 225 K. On warming in the applied magnetic field (zero-field cooled, ZFC), there is a sudden increase in the magnetic susceptibility, albeit very small, followed by a steady decline on further heating. As the sample is cooled back down towards 2 K in the field (field-cooled, FC) however, there is no concomitant decrease in the magnetic susceptibility around 225 K. This behaviour may be indicative of a minor structural phase transition which is locked in the presence of an applied magnetic field. This feature was observable on repeated ZFC-FC cycles indicating that the removal of the external magnetic field returns the material to its original state. Further studies on this compound, primarily *via* variable temperature X-ray diffraction, are highly desirable to further investigate this phenomenon.

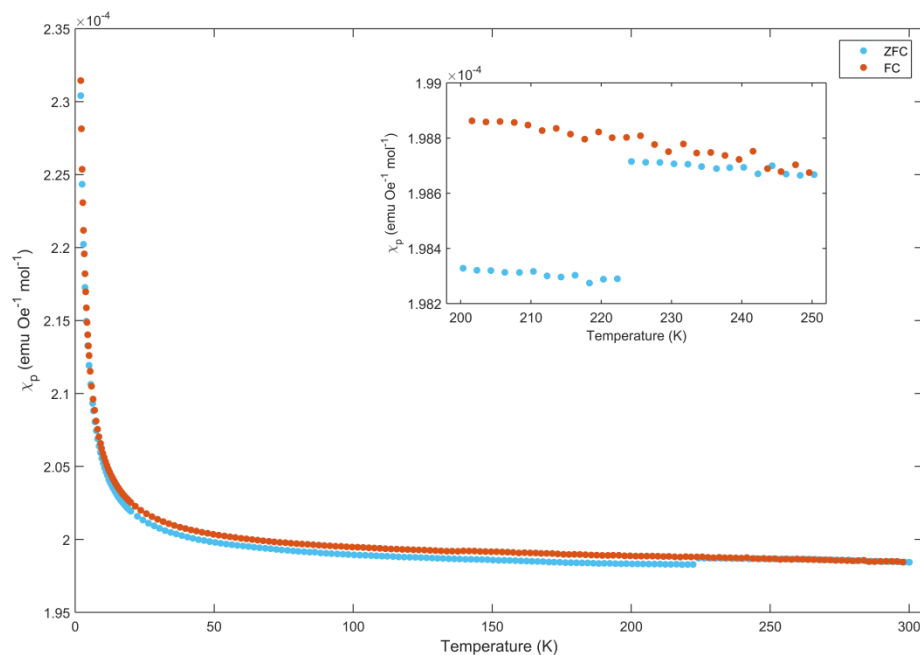


Chart 3.7.1.6: Paramagnetic susceptibility as a function of temperature for **3f**.

3.7.2 – Magnetic Exchange Interactions

Broken-symmetry calculations were performed to estimate the single-triplet exchange energies for closely interacting pairs of radicals, and to explore the origins of the magnetic properties in the structurally characterised 1,2,4-benzothiadiazinyl radicals.^{43,44,45} This approach has been successfully applied to a variety of heterocyclic sulfur-nitrogen radicals.^{7,35,46} Individual pairwise exchange energies, J , based on the *Heisenberg Hamiltonian* $H_{ex} = -2J\{S_1 \cdot S_2\}$, were estimated in terms of the difference between the UB3LYP/6-311G(d,p) total energies of the triplet (TS) and broken symmetry singlet (BSS) states and the respective expectation values of the two states according to the expression:

$$J = - \frac{(E_{TS} - E_{BSS})}{\langle S^2 \rangle_{TS} - \langle S^2 \rangle_{BSS}} \quad (1)$$

Exchange energies were calculated with a simple dinuclear nearest-neighbour exchange model using a variety of pairwise combinations of radicals, with atomic coordinates taken from crystallographic data. For radical **3a**, there are strong antiferromagnetic (AFM) interactions along the $J_{\pi 1}$ exchange pathway, indicative of spin-pairing arising through two short S...N contacts between the heterocyclic rings (Figure and Table 3.7.2.1). A much weaker, but still relatively strong AFM interaction⁴⁷ is estimated for the $J_{\pi 2}$ exchange pathway whilst both J_3 and J_3 are essentially zero.

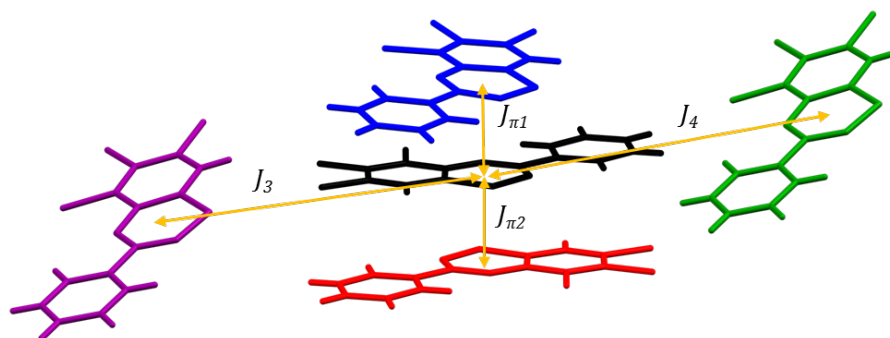


Figure 3.7.2.1: Magnetic exchange pathways in 3a.

	E_{TS} / Hartrees	$\langle S^2 \rangle_{TS}$	E_{BSS} / Hartrees	$\langle S^2 \rangle_{BSS}$	J' / cm^{-1}
J_{π_1}	-4774.51052355	2.0263	-4774.52988085	0.9989	-4135.138
J_{π_2}	-4774.53000748	2.0273	-4774.53044164	0.9994	-92.701
J_3	-4774.53327083	2.0290	-4774.53327407	1.0000	-0.691
J_4	-4774.53468043	2.0291	-4774.53468038	1.0000	0.011

Table 3.7.2.1: Calculated exchange energies for 3a.

Similar results were obtained for 3c, but the larger interplanar spacing between radical pairs results in significantly smaller exchange energies compared to 3a, especially for J_{π_1} , but these are still strongly antiferromagnetic and indicative of spin-pairing and overall diamagnetism (Figure and Table 3.7.2.2).

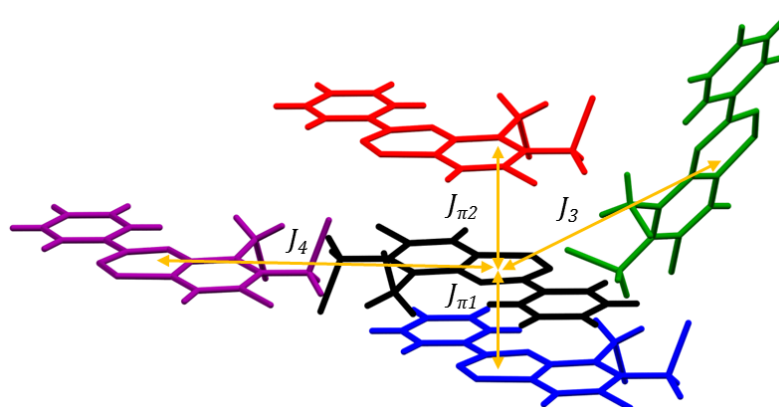


Figure 3.7.2.2: Magnetic exchange pathways in 3c.

	E_{TS} / Hartrees	$\langle S^2 \rangle_{TS}$	E_{BSS} / Hartrees	$\langle S^2 \rangle_{BSS}$	J' / cm^{-1}
J_{π_1}	-4931.92924166	2.0329	-4931.93785381	0.9984	-1827.115
J_{π_2}	-4931.94238034	2.0330	-4931.94253497	0.9996	-32.841
J_3	-4931.94504518	2.0348	-4931.94504480	1.0000	0.081
J_4	-4931.94527360	2.0347	-4931.94527371	1.0000	-0.023

Table 3.7.2.2: Calculated exchange energies for 3c.

For radical **3e**, the exchange along the $J_{\pi 1}$ pathway is again strongly antiferromagnetic due to the short S...S contacts between radicals (Figure and Table 3.7.2.3). The magnetic exchange along the $J_{\pi 2}$ and $J_{\pi 3}$ pathways are also very large and negative, whilst both J_4 and J_5 are negligible.

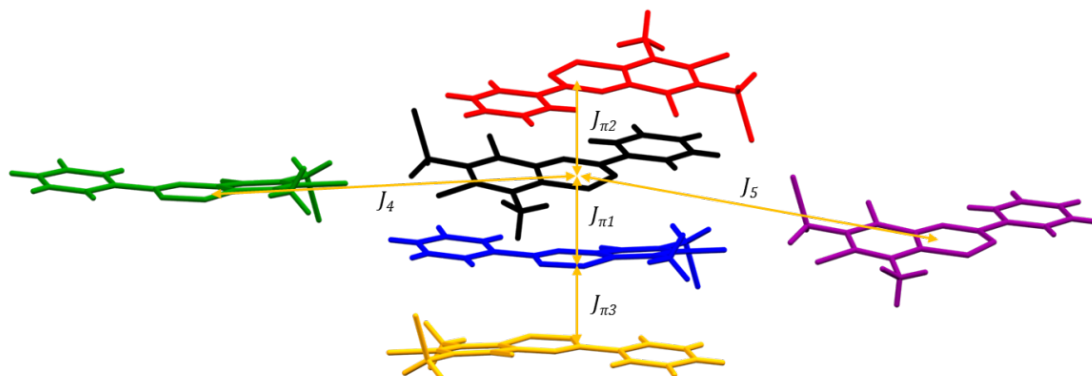


Figure 3.7.2.3: Magnetic exchange pathways in **3e**.

	E_{TS} / Hartrees	$\langle S^2 \rangle_{TS}$	E_{BSS} / Hartrees	$\langle S^2 \rangle_{BSS}$	J' / cm^{-1}
$J_{\pi 1}$	-4931.83391003	2.0309	-4931.85623662	0.9934	-4723.013
$J_{\pi 2}$	-4931.89695375	2.0319	-4931.89802333	0.9987	-227.203
$J_{\pi 3}$	-4931.81925623	2.0310	-4931.81968459	0.9989	-91.090
J_4	-4931.86338358	2.0330	-4931.86338389	1.0000	-0.066
J_5	-4931.82426099	2.0324	-4931.82426100	1.0000	-0.002

Table 3.7.2.3: Calculated exchange energies for **3e**.

Variable temperature single-crystal X-ray diffraction studies for **3e** at 100 K, 150 K and 200 K were performed to examine the effect of temperature on the solid-state structure and the resulting magnetic properties. As expected, the unit cell parameters increase on heating, as does the S...S distance between radical centres and interplanar spacing. This results in a decrease in the AFM interactions along each of the exchange pathways (Table 3.7.2.4). Given that this decrease is small over the measured 100 K temperature range, it is unlikely that the entropically-favoured arrangement of equally spaced π -stacks will exist below 400 K, however further experimental studies are required to confirm this.

Temperature / K	S-S Distance / Å	$J_{\pi 1}$ / cm^{-1}	$J_{\pi 2}$ / cm^{-1}	$J_{\pi 3}$ / cm^{-1}
100	2.846(1)	-4723.013	-227.203	-91.090
150	2.853(8)	-4596.365	-212.739	-82.557
200	2.864(8)	-4388.673	-202.020	-68.238

Table 3.7.2.4: Calculated exchange energies and S-S distances at variable temperatures for **3e**.

Calculations were also performed on the perchlorinated, **3x**, and perfluorinated, **3y**, derivatives previously reported by Kaszynski³ to compare the magnetic exchange pathways of the crystallographically known systems. These were both observed to form slipped π -stacks in the solid-state at 173 K with additional long contacts to neighbouring molecules through S1...S1 or S1...N1 contacts. The calculations for **3x** differ considerably to the other radicals, and features two, almost equal and weak antiferromagnetic interactions along the $J_{\pi 1}$ and $J_{\pi 2}$ exchange pathways, consistent with a 1D AFM chain (Figure and Table 3.7.2.5). Surprisingly, the exchange energy along the J_3 pathway, associated with the single S...S contact between molecules, is close to zero suggesting that the interchain interaction is minimal due to the poor SOMO overlap.

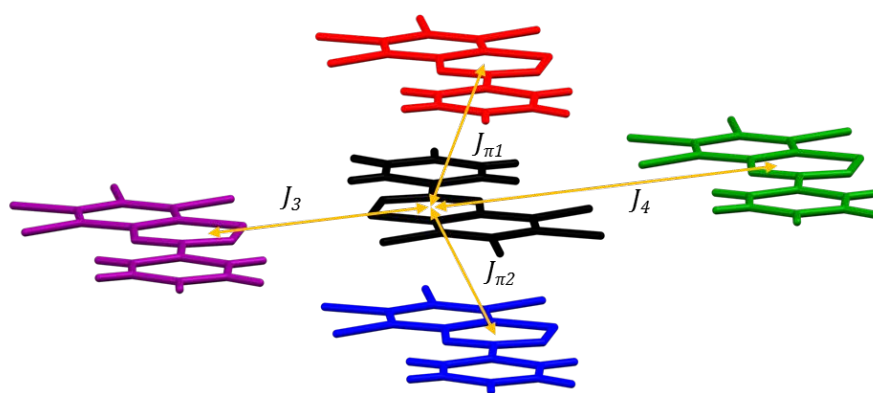


Figure 3.7.2.5: Magnetic exchange pathways in **3x**.

	E_{TS} / Hartrees	$\langle S^2 \rangle_{TS}$	E_{BSS} / Hartrees	$\langle S^2 \rangle_{BSS}$	J' cm^{-1}
$J_{\pi 1}$	-5693.991834	2.0301	-5693.991900	0.9998	-14.066
$J_{\pi 2}$	-5693.991559	2.0301	-5693.991626	0.9997	-14.147
J_3	-5693.993244	2.0312	-5693.993247	0.9998	-0.726
J_4	-5693.994372	2.0314	-5693.994372	1.0000	-0.111

Table 3.7.2.5: Calculated exchange energies for **3x**.

In contrast, the antiferromagnetic interactions along the π -stack for **3y** are extremely strong, with essentially equal exchange energies for both $J_{\pi 1}$ and $J_{\pi 2}$ (Figure and Table 3.7.2.6). The AFM interchain interactions along the J_3 pathway is of significant strength whilst J_4 is negligible resulting in an offset ladder structure; the infinite $J_{\pi 1}$ and $J_{\pi 2}$ stacks form 1D AFM chains representing the side-rails whilst the J_3 pathway represent the rungs of the ladder.

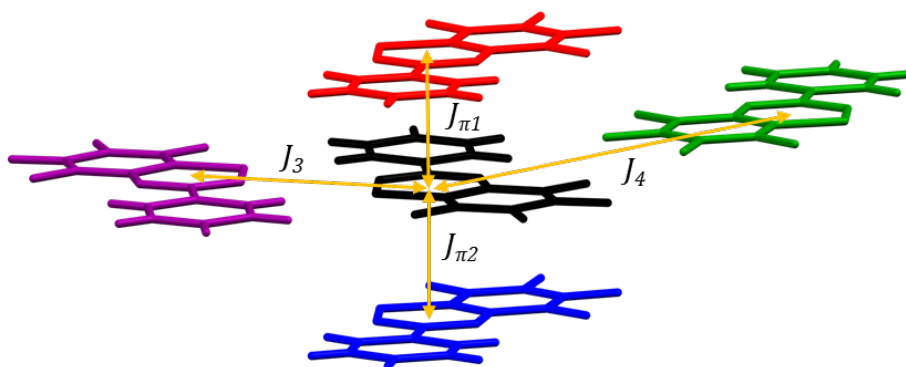


Figure 3.7.2.6: Magnetic exchange pathways in **3y**.

	E_{TS} / Hartrees	$\langle S^2 \rangle_{TS}$	E_{BSS} / Hartrees	$\langle S^2 \rangle_{BSS}$	J' / cm^{-1}
$J_{\pi 1}$	-2811.148837	2.0314	-2811.157064	0.9994	-1749.632
$J_{\pi 2}$	-2811.148869	2.0314	-2811.157097	0.9994	-1749.985
J_3	-2811.156895	2.0321	-2811.157033	1.0000	-29.326
J_4	-2811.158509	2.0329	-2811.158509	1.0000	-0.002

Table 3.7.2.6: Calculated exchange energies for **3y**.

The solid-state structures adopted by **3x** and **3y** may give rise to interesting magnetic effects. For radical **3x**, the regular π -stacks of weakly interacting molecules is likely to result in paramagnetic behaviour, whilst the strong interaction along the π -stacks in **3y** may lead to antiferromagnetic ordering at a finite temperature. Similarly, radicals **3x** and **3y** may exhibit conductivity as a result of a non-zero density of states at the *Fermi* level due to the regular bands of half-filled orbitals (SOMOs).⁴⁸ Experimental magnetic and conductivity measurements of both compounds are therefore highly desirable.

3.8 – Conclusions

Electrochemical studies on the 1,2,4-benzothiadiazine 1-chlorides showed that there is little variation in the redox potentials across the prepared derivatives, which indicate that the substituents on the benzo-fused and pendant aryl rings have little effect on the electronic structure. The electrochemical behaviour was further examined *via* variable concentration studies to qualitatively assess the radical monomer-dimer equilibria, and *via* variable scan rate studies to probe the reversibility of the electron transfer processes.

1,2,4-Benzothiadiazine 1-chlorides are reduced under mild conditions to afford analytically pure samples of the corresponding radical. These were found to be short-lived in solution and thermally unstable, severely hampering the growth of crystals suitable for SCXRD studies. The solid-state structures of **3a**, **3c** and **3e** consisted of

dimer pairs of planar radicals, which lead to distorted π -stacks with alternating short and long interplanar contacts.

The EPR spectra for the 1,2,4-benzothiadiazinyl radicals all show distorted 1:2:3:2:1 quintets due to coupling to two non-identical but similar nitrogens within the heterocyclic ring. The minor variation in experimental g -values and hyperfine coupling constants across the series of radicals further indicates that the substituents have little effect on the electronic structure. The correlation between experimental and DFT UB3LYP/cc-pVDZ/6-31G calculated EPR parameters was poor, and showed considerable variation especially for the radicals bearing substituents on the pendant aryl ring. Further studies are required to develop a more suitable model for these complex systems.

Magnetic studies showed that the crystallographically characterised radicals are dimeric in the solid-state; the *pseudo*-paramagnetic behaviour is attributed to residual free spins or trace paramagnetic impurities. Broken-symmetry single-point calculations at the DFT UB3LYP/6-311G(d,p) level confirmed that the interactions between radical dimer pairs are strongly antiferromagnetic, consistent with spin pairing and overall diamagnetism. Theoretical examination of the known crystalline radicals, **3x** and **3y**, suggest that these materials may exhibit interesting magnetic properties which result from regular 1D π -stacks with either weak (**3x**) or strong (**3y**) interactions between radical centres.

3.9 – Future Work

The substituents on the benzo-fused and pendant aryl ring were shown to have little effect on the electronic properties of the radicals but have a significant influence on the solid-state structure. The examination of the crystal structures of the remaining radicals is thus highly desirable and requires the successful growth of single crystals suitable for analysis. The *o*-tolyl systems, **3g** and **3h**, in particular are likely to be promising candidates for systems that overcome the tendency to dimerise and hence display interesting magnetic behaviour.

Co-crystallisation with other π -stacking species is an alternative approach that is being employed to suppress dimerisation in sulfur-nitrogen radicals,^{30,49,50} and samples of the 1,2,4-benzothiadiazinyl radicals have been sent to Professor Delia Haynes at the University of Stellenbosch to investigate their co-crystallisation with DTDA radicals.

3.10 – Experimental

3.10.1 – Synthesis of 1,2,4-Benzothiadiazinyl Radicals

The radicals **3a-h** and **3k-l** were prepared by one electron reduction of the corresponding 1,2,4-benzothiadiazine 1-chloride with triphenylphosphine. The synthesis of **3a** is given as exemplar. Ph₃P was recrystallised prior to use from DCM and hexanes.

3.10.1.1 – Synthesis of 1,5,6,7-tetrachloro-3-phenyl-benzo-1,2,4-thiadiazinyl, **3a**:

2a (0.400 g, 1.10 mmol) was suspended in MeCN (5 cm³) and degassed with three freeze-thaw-pump cycles and backfilled with argon. A solution of Ph₃P (0.145 g, 0.55 mmol) in degassed MeCN (5 cm³) was added resulting in an immediate darkening of colour. After 5 minutes of rapid stirring, the supernatant was removed *via* filter cannula and the solids were washed with MeCN (5 cm³) and dried *in vacuo* to afford a dark purple powder. Yield 0.247 g (0.75 mmol, 68.3 %).

3.10.1.2 – Synthesis of 1,6,7-trichloro-5-(chloromethyl)-3-phenyl-benzo-1,2,4-thiadiazinyl, **3b**:

Dark blue powder, 51.1 % yield.

3.10.1.3 – Synthesis of 1,7-dichloro-5,6-bis(chloromethyl)-3-phenyl-benzo-1,2,4-thiadiazinyl, **3c**:

Dark purple powder, 71.8 % yield. *Anal.* Calc. for C₁₅H₁₀Cl₃N₂S: C, 50.5; H, 2.8; N, 7.9. Found: C, 50.4; H, 2.7; N, 8.0.

3.10.1.4 – Synthesis of 1,6,7-trichloro-5-(chloromethyl)-8-methyl-3-phenyl-benzo-1,2,4-thiadiazinyl, **3d**:

Dark purple powder, 59.7 % yield. *Anal.* Calc. for C₁₅H₁₀Cl₃N₂S: C, 50.5; H, 2.8; N, 7.9. Found: C, 50.5; H, 2.9; N, 8.0.

3.10.1.5 – Synthesis of 1,5,7-trichloro-6-(chloromethyl)-8-methyl-3-phenyl-benzo-1,2,4-thiadiazinyl, **3e**:

Dark purple powder, 67.5 % yield. *Anal.* Calc. for C₁₅H₁₀Cl₃N₂S: C, 50.5; H, 2.8; N, 7.9. Found: C, 50.3; H, 2.7; N, 7.9.

3.10.1.6 – Synthesis of 1,5,6,7-tetrachloro-8-methoxy-3-phenyl-benzo-1,2,4-thiadiazinyl, **3f**:

Dark purple/green powder, 58.3 % yield.

3.10.1.7 – Synthesis of 1,5,6,7-tetrachloro-3-(*o*-tolyl)-benzo-1,2,4-thiadiazinyl, 3g:

Dark green powder, 64.1 % yield.

3.10.1.8 – Synthesis of 1,7-dichloro-5,6-bis(chloromethyl)-3-(*o*-tolyl)-benzo-1,2,4-thiadiazinyl, 3h:

Dark purple powder, 57.4 % yield.

3.10.1.9 – Synthesis of 1,5,6,7-tetrachloro-3-(4-methoxyphenyl)-benzo-1,2,4-thiadiazinyl, 3k:

Dark blue powder, 48.6 % yield.

3.10.1.10 – Synthesis of 1,7-dichloro-5,6-bis(chloromethyl)-3-(4-methoxyphenyl)-benzo-1,2,4-thiadiazinyl, 3l:

Dark blue powder, 67.7 % yield.

3.10.2 – Computational Methods

DFT calculations were performed using the Gaussian16⁵¹ suite of programs. Structures were optimised from single-crystal X-ray diffraction data at the DFT⁵² UB3LYP/6-31G⁵³ level of theory. The Fermi contacts and spin densities were calculated at the UB3LYP/cc-pVDZ⁵⁴ level of theory from previously optimised geometries. Single-point broken symmetry calculations were performed at the UB3LYP/6-311G(d,p)⁵⁵ level of theory, with pairwise exchange interactions based on atomic coordinates from SCXRD data.

3.11 – References

- 1 M. J. Perkins, *Radical Chemistry: The Fundamentals*, Oxford Chemistry Primers, 2000.
- 2 V. Chechik, E. Carter and D. Murphy, *Electron Paramagnetic Resonance*, Oxford Chemistry Primers, 2015.
- 3 J. Zienkiewicz, P. Kaszynski and V. G. Young, *J. Org. Chem.*, 2004, **69**, 7525–7536.
- 4 A. a Leitch, R. T. Oakley, R. W. Reed and L. K. Thompson, *Inorg. Chem.*, 2007, **46**, 6261–70.
- 5 L. N. Markovskii, V. S. Talanov, O. M. Polumbrik and Y. G. Shermolovich, *Russ. J. Org. Chem.*, 1981, **17**, 2338–2339.
- 6 L. Beer, R. C. Haddon, M. E. Itkis, A. A. Leitch, R. T. Oakley, R. W. Reed, J. F. Richardson, D. G. VanderVeer, L. Beer, J. L. Brusso, A. W. Cordes, R. C. Haddon, M. E. Itkis, K. Kirschbaum, D. S. MacGregor, R. T. Oakley, A. A. Pinkerton and R. W. Reed, *Chem. Commun.*, 2005, **124**, 1218–1220.
- 7 S. M. Winter, K. Cvrkalj, P. A. Dube, C. M. Robertson, M. R. Probert, J. A. K. Howard and R. T. Oakley, *Chem. Commun.*, 2009, 7306.
- 8 J. Zienkiewicz, P. Kaszynski and V. G. Young, *J. Org. Chem.*, 2004, **69**, 2551–2561.
- 9 E. R. Clark, J. J. Hayward, B. J. Leontowicz, D. J. Eisler and J. M. Rawson, *CrystEngComm*, 2014, **16**, 1755–1762.
- 10 E. S. Levchenko, G. S. Borovikova, E. I. Borovik and V. V. Kalinin, *Russ. J. Org. Chem.*, 1984, **20**, 176–181.
- 11 J. M. Rawson and G. D. McManus, *Coord. Chem. Rev.*, 1999, **189**, 135–168.
- 12 J. M. Rawson, A. J. Banister and I. Lavender, *Adv. Heterocycl. Chem.*, 1995, **62**, 137–247.
- 13 A. Alberola, R. J. Collis, S. M. Humphrey, R. J. Less and J. M. Rawson, *Inorg. Chem.*, 2006, **45**, 1903–1905.
- 14 A. Alberola, D. Eisler, R. J. Less, E. Navarro-Moratalla and J. M. Rawson, *Chem. Commun.*, 2010, **46**, 6114–6116.
- 15 T. M. Barclay, L. Beer, A. W. Cordes, R. T. Oakley, K. E. Preuss, J. Nicholas and R. W. Reed, 1999, **175**, 531–532.
- 16 E. R. Clark, *Synthesis and Chemistry of 1,2,4-Benzothiadiazines*, University of Cambridge, 2008.
- 17 T. Boere, T. L. Roemmele and C. T. K. M, *Coord. Chem. Rev.*, 2000, **210**, 369–445.
- 18 A. W. Cordes, P. J. Hayes, P. D. Josephy, H. Koenig, R. T. Oakley and W. T. Pennington, *J. Chem. Soc., Chem. Commun.*, 1984, 1021–1022.
- 19 G. Gritzner and J. Kuta, *Int. Union Pure Appl. Chem.*, 1984, **1**, 462–466.

- 20 P. Atkins and J. De Paula, *Physical Chemistry*, Oxford University Press, 9th edn., 2010.
- 21 N. Elgrishi, K. J. Rountree, B. D. McCarthy, E. S. Rountree, T. T. Eisenhart and J. L. Dempsey, *J. Chem. Educ.*, 2018, **95**, 197–206.
- 22 R. T. Oakley, R. W. Reed, A. W. Cordes, S. L. Craig and J. B. Graham, *J. Am. Chem. Soc.*, 1987, **109**, 7745–7749.
- 23 A. J. Banister, I. Lavender, J. M. Rawson, W. Clegg, B. K. Tanner and R. J. Whitehead, *J. Chem. Soc., Dalton Trans.*, 1993, 1421–1429.
- 24 A. J. Bard and L. R. Faulkner, *Electrochemical Methods: Fundamental and Applications*, John Wiley & Sons, NJ, 2nd edn., 2001.
- 25 R. T. Boeré, K. H. Moock and M. Parvez, *ZAAC - J. Inorg. Gen. Chem.*, 1994, **620**, 1589–1598.
- 26 D. B. Denney, D. Z. Denney and B. C. Chang, *J. Am. Chem. Soc.*, 1968, **90**, 6332–6335.
- 27 A. Bondi, *J. Phys. Chem.*, 1964, **68**, 441–451.
- 28 J. S. W. Overell and G. S. Pawley, *Acta Cryst.*, 1982, **38**, 1966–1972.
- 29 G. R. Desiraju, *Crystal Engineering*, Elsevier, Amsterdam, 1989.
- 30 D. A. Haynes, *CrystEngComm*, 2011, **13**, 4793–4805.
- 31 C. P. Constantinides and P. A. Koutentis, *Adv. Heterocycl. Chem.*, 2016, **119**, 173–207.
- 32 R. C. Peierls, *Quantum Theory of Solids*, Oxford University Press, London, 1953.
- 33 T. M. Barclay, A. W. Cordes, N. A. George, R. C. Haddon, M. E. Itkis and R. T. Oakley, *Chem. Commun.*, 1999, 2269–2270.
- 34 G. D. McManus, J. M. Rawson, N. Feeder, J. van Duijn, E. J. L. McInnes, J. J. Novoa, R. Burriel, F. Palacio and P. Oliete, *J. Mater. Chem.*, 2001, **11**, 1992–2003.
- 35 D. Bates, C. M. Robertson, A. A. Leitch, P. A. Dube and R. T. Oakley, *J. Am. Chem. Soc.*, 2018, **140**, 3846–3849.
- 36 S. Stoll and A. Schweiger, *J. Magn. Reson.*, 2006, **178**, 42–55.
- 37 P. Kaszynski, *J. Phys. Chem. A*, 2001, **105**, 7626–7633.
- 38 P. Kaszynski, *J. Phys. Chem. A*, 2001, **105**, 7615–7625.
- 39 H. M. McConnell and D. B. Chesnut, *J. Chem. Phys.*, 1958, **28**, 107–117.
- 40 J. L. Brusso, O. P. Clements, R. C. Haddon, M. E. Itkis, A. A. Leitch, R. T. Oakley, R. W. Reed and J. F. Richardson, *J. Am. Chem. Soc.*, 2004, **126**, 14692–14693.
- 41 N. Feeder, R. J. Less, J. M. Rawson, P. Oliete and F. Palacio, *Chem. Commun.*, 2000, **2**, 2449–2450.
- 42 A. F. Orchard, *Magnetochemistry*, Oxford Chemistry Primers, Oxford, 2003.

- 43 L. Noodleman and E. R. Davidson, *Chem. Phys.*, 1986, **109**, 131–143.
- 44 L. Noodleman, *J. Chem. Phys.*, 1981, **74**, 5737–5743.
- 45 N. Deumal, M. A. Robb and J. J. Novoa, in *Topics in the Theory Of Chemical and Physical Systems*, Springer US, 2007, pp. 271–289.
- 46 S. M. Winter, A. R. Balo, R. J. Roberts, K. Lekin, A. Assoud, P. A. Dube and R. T. Oakley, *Chem. Commun.*, 2013, **49**, 1603.
- 47 C. P. Constantinides, A. A. Berezin, M. Manoli, G. M. Leitus, M. Bendikov, J. M. Rawson and P. A. Koutentis, *New J. Chem.*, 2014, **38**, 949–954.
- 48 R. Hoffmann, *Angew. Chem. Int. Ed.*, 1987, **26**, 846–878.
- 49 S. Domagała, K. Kosc, S. W. Robinson, D. A. Haynes and K. Woźniak, *Cryst. Growth Des.*, 2014, **14**, 4834–4848.
- 50 S. W. Robinson, D. A. Haynes and J. M. Rawson, *CrystEngComm*, 2013, **15**, 10205–10211.
- 51 M. J. Frisch, G. W. Trucks, H. B. Schlegel, G. E. Scuseria, M. A. Robb, G. A. Cheeseman, J. R. Scalmani, G.; Barone, V. Petersson, X. Nakatsuji, H.; Li, M. Caricato, A. V. Marenich, J. Bloino, B. G. Janesko, R. Gomperts, B. Mennucci, H. P. Hratchian, J. V. Ortiz, A. F. Izmaylov, J. L. Sonnenberg, D. Williams-Young, F. Ding, F.; Lipparini, F. Egidi, J. Goings, B. Peng, A. Petrone, T. Henderson, D. Ranasinghe, V. G. Zakrzewski, J. Gao, N. Rega, G. Zheng, W. Liang, M. Hada, M. Ehara, K. Toyota, R. Fukuda, J. Hasegawa, M. Ishida, T. Nakajima, Y. Honda, O. Kitao, H. Nakai, T. Vreven, K. Throssell, J. Montgomery, J. A., J. E. Peralta, F. Ogliaro, M. J. Bearpark, J. J. Heyd, E. N. Brothers, K. N. Kudin, V. N. Staroverov, T. A. Keith, R. Kobayashi, J. Normand, K. Raghavachari, A. P. Rendell, J. C. Burant, S. S. Iyengar, J. Tomasi, M. Cossi, J. M. Millam, M. Klene, C. Adamo, R. Cammi, J. W. Ochterski, R. L. Martin, K. Morokuma, O. Farkas, J. B. Foresman and D. J. Fox, Gaussian 16, Revision B.01 2016.
- 52 R. G. Parr and W. Yang, *Density-functional theory of atoms and molecules*, Oxford University Press, 1989.
- 53 R. Ditchfield, W. J. Hehre and J. A. Pople, *J. Chem. Phys.*, 1971, **54**, 724–728.
- 54 T. H. Dunning, *J. Chem. Phys.*, 1989, **90**, 1007–1023.
- 55 A. D. McLean and G. S. Chandler, *J. Chem. Phys.*, 1980, **72**, 5639–5648.

Chapter 4

1,2,4-Benzophosphadiazines

“I’m afraid that my condition has left me cold to your pleas of mercy.”

Batman & Robin (1997)

4.1 – Introduction to Fused-Ring Phosphorus Nitrogen Heterocycles

Fused-ring phosphorus-nitrogen heterocycles have found emerging applications in ligands for catalysis, pesticides, and flame-retardant materials, and are important building blocks for drug discovery.¹ Phosphorus-carbon bond formation is an important step in the construction of these molecules, and the development of general, mild reaction conditions with good functional group tolerance is highly desirable. The most common method of P-*C_{aryl}* bond formation involves the addition of an organic nucleophile to a phosphorus electrophile, typically a chlorophosphine. Since these are poor electrophiles, strong organic nucleophiles such as Grignard² or aryl-lithium reagents³ are often needed. The direct phosphination of electron-rich aromatics/heteroaromatics has also been shown to be a straightforward method to access fused-ring phosphorus-heterocycles.⁴

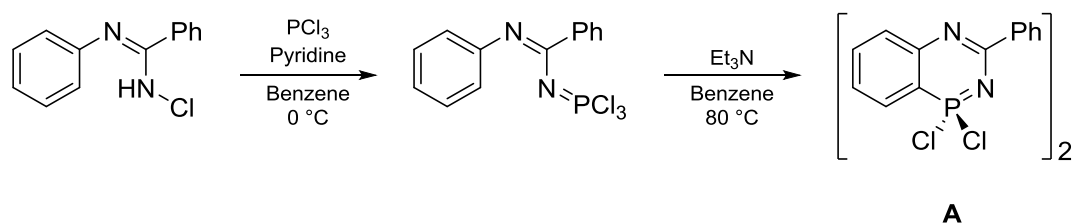
Alternatively, the electrophilicity of phosphorus can be enhanced *via* chloride abstraction, which results in a highly reactive and Lewis-acidic phosphonium intermediate. This approach has been applied to the Friedel-Crafts addition of phosphine units to aromatic substrates and has been established for over a century.⁵ Nevertheless, the harsh conditions, long reaction times, and low yields mean that this approach has found limited use. Substitution of AlCl₃ or ZnCl₂, the typical superstoichiometric Lewis acids employed in phospho-Friedel-Crafts chemistry, with catalytic quantities of superacid has however considerably lowered the reaction temperatures and improved product isolation for fused-ring derivatives.⁶ The use of ionic liquids in phospho-Friedel-Crafts chemistry has also been investigated.⁷

4.1.1 – An Overview of 1,2,4-Benzophosphadiazines

The incorporation of larger or heavier heteroatoms into stable radicals has been shown to improve both the conductivity and magnetic exchange interactions, due to a greater intermolecular orbital overlap in the solid-state.^{8,9} This prompted us to prepare 1,2,4-benzophosphadiazines, as phosphorus containing analogues of the 1,2,4-benzothiadiazines discussed in Chapters 2 and 3, and heavier congeners of the well-known Blatter radicals.¹⁰⁻¹⁵

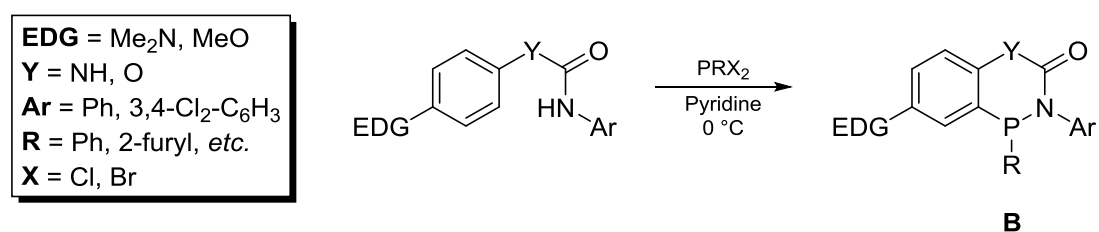
The synthesis of 1,2,4-benzophosphadiazines was first reported in 1984 by Levchenko,¹⁶ by treatment of *N*-chloroarylamidines with PCl₃ in the presence of base (Scheme 4.1.1.1) to give the P^V 1,1-dichloro 1,2,4-benzophosphadiazine (**A**), analogous to their earlier work on the preparation of 1,2,4-benzothiadiazines.¹⁷ This was reported to be the dimeric heterocycle based on molecular mass measurements;

crystals suitable for single-crystal X-ray analysis could not be grown. However, the lack of additional reported analytical data for this compound, such as NMR or IR spectra, leaves some doubt as to the true nature of the product.



Scheme 4.1.1.1: Reported synthesis of 1,2,4-benzophosphadiazines.

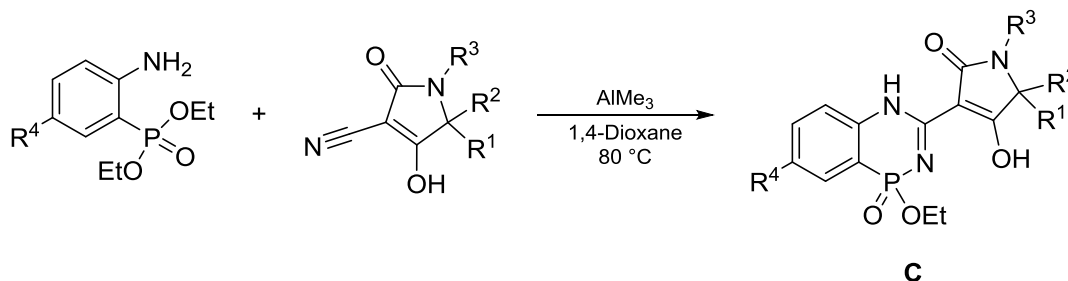
The synthesis of 1,2,4-benzophosphadiazines (**B**) through phosphination of electron-rich substituted *N,N'*-diarylureas was reported in 2001 by Volochnyuk¹⁸ and later extended to *N*-arylamidines and *N,O*-diarylcarbamates.⁴ The synthesis proceeds under mild conditions for systems bearing electron-donating groups (EDG) *para* to the *C*-nucleophilic centre, giving facile access to a family of substituted 1,2,4-benzophosphadiazines (Scheme 4.1.1.2). Attempted cyclisations with trihalophosphines were unsuccessful for ureas (Y = NH), where the resulting benzophosphadiazine (R = X) is believed to polymerise due to the presence of an additional nucleophilic NH fragment. Conversely, the reaction of PBr₃ or PCl₃ with *N,O*-diarylcarbamates (Y = O) gave the corresponding 1-halo-1,2,4-benzophosphazines, which react with alcohols or secondary amines to afford *P*-substituted derivatives. Attempts to extend the reaction to the corresponding thioureas were unsuccessful, which was attributed to the affinity of the phosphorus atom for sulfur in such reactions.



Scheme 4.1.1.2: Synthesis of substituted 1,2,4-benzophosphazines from *N,N'*-diarylureas and *N,O*-diarylcarbamates.

1,2,4-benzophosphadiazine derivatives (**C**) have recently found applications in medicinal chemistry as novel hepatitis C allosteric NS5B RdRp inhibitors, by replacement of sulfur in the 1,2,4-benzothiadiazine pharmacophore with phosphorus.¹⁹ The potential of phosphorus chemistry as a bioisostere strategy is an important tool in medicinal chemistry that has been shown to improve potency, selectivity, physicochemical properties, and the pharmacokinetic profile of key compounds.²⁰ The

synthetic approach to this fused-ring heterocycle relied on the condensation of a 2-aminoarylphosphonate with a substituted nitrile in the presence of AlMe₃, the former phosphonate being prepared by the palladium-catalysed phosphorylation of the corresponding 2-bromoaniline (Scheme 4.1.1.3).

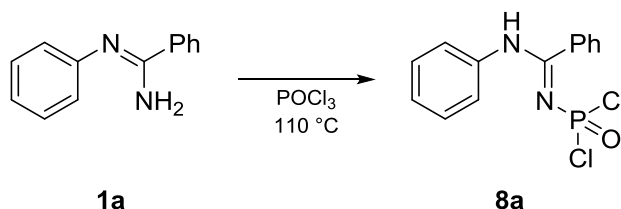


Scheme 4.1.1.3: Synthesis of non-nucleoside inhibitors containing the 1,2,4-benzophosphadiazine scaffold.

4.2 – Attempted Syntheses of 1,2,4-Benzophosphadiazines

4.2.1 – Initial Studies with P^V Sources

Following the facile synthesis of 1,2,4-benzothiadiazine 1-chlorides from the reaction of *N*-arylamidines with neat SOCl₂, the analogous reaction was attempted with phosphorus oxychloride. Refluxing *N*-phenylbenzamidine, **1a**, in neat POCl₃ for 16 hours, followed by layering with dry hexane afforded colourless crystals of the phosphoramidic dichloride **8a** (Scheme 4.2.1.1). Attempts to encourage cyclisation through the use of an electron rich *N*-arylamidine such as **1r** (*vide infra*) and prolonged refluxing were unsuccessful.



Scheme 4.2.1.1: Reaction of *N*-arylamidines with POCl₃.

Compound **8a** was found to be poorly soluble in most organic solvents but dissolved readily in pyridine. NMR analysis exhibited a major singlet ($\approx 85\%$ by integration) at $\delta + 1.2$ ppm in the ³¹P NMR spectrum, assigned to **8a**, and a minor peak at -7.0 ppm (Figure 4.2.1.1). Heating this solution at 100 °C overnight resulted in complete consumption of **8a**, and conversion through to a single new major species, along with a few minor products. This is postulated to be the 1,2,4-benzophosphadiazine 1-chloro-1-oxide, **9a**, based on the ³¹P NMR chemical shift,²¹ resulting from the loss of one equivalent of HCl from **8a** according to Scheme 4.2.1.2. Repeated attempts to isolate the product to enable further characterisation were unsuccessful.

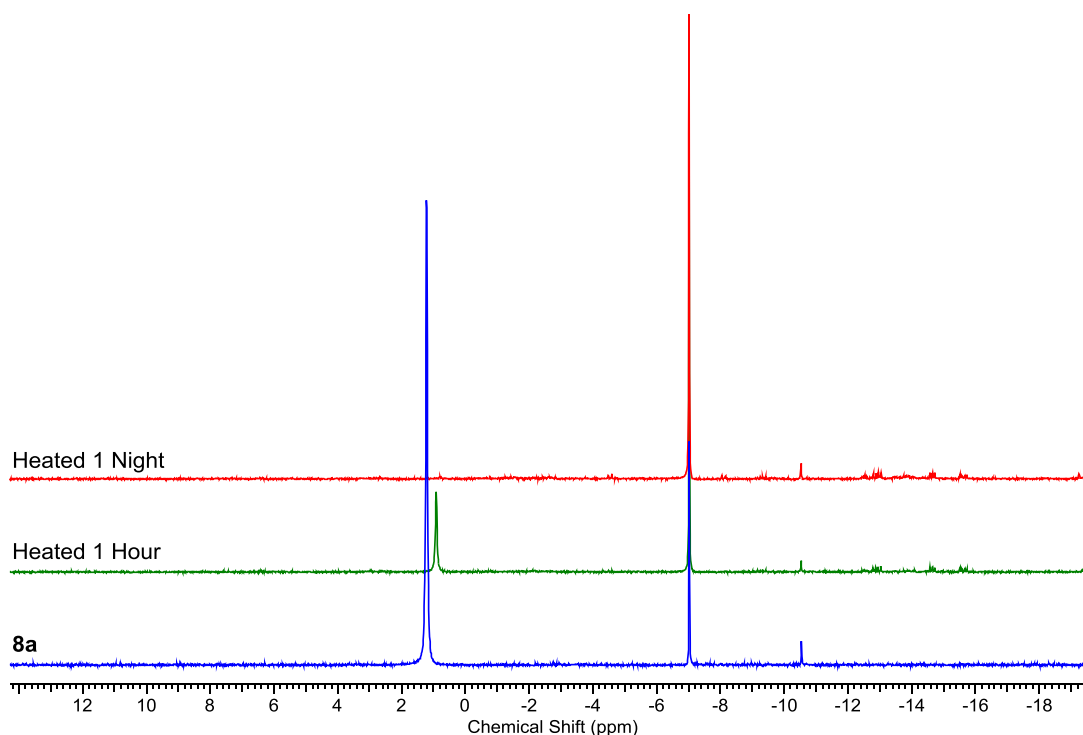
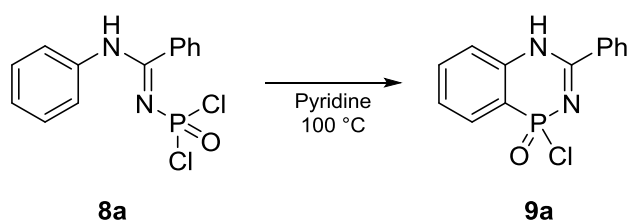
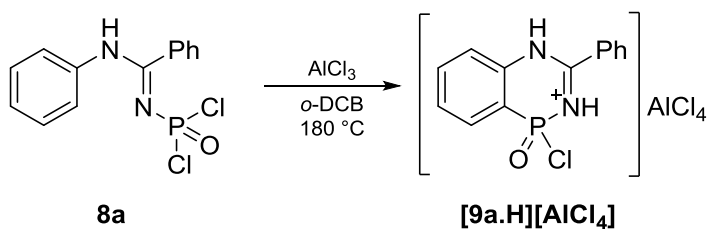


Figure 4.2.1.1: ^{31}P NMR spectra of **8a** in pyridine.



Scheme 4.2.1.2: Proposed scheme for the reaction of **8a** with excess pyridine.

When **8a** is refluxed in *o*-DCB for 72 hours at 180 °C with excess AlCl_3 , the resulting ^{31}P NMR spectrum exhibits a major doublet at $\delta + 24.1$ ppm with $^2J_{\text{P-H}} = 21.8$ Hz, assigned as **[9a.H][AlCl₄]**. The AlCl_3 is believed to promote cyclisation through the formation of an intermediate Lewis-acidic phosphonium; whilst proton-migration results in the formation of the *N*-protonated heterocycle as the AlCl_4 salt (Scheme 4.2.1.3). A single sharp peak at $\delta + 105.9$ ppm in the ^{27}Al NMR spectrum confirmed the presence of the AlCl_4^- anion. Attempts to deprotonate this species to confirm its proposed relationship with **9a** gave a mixture of unidentified products.



Scheme 4.2.1.3: Proposed scheme for the reaction of **8a** with excess AlCl_3 .

Although there was evidence to suggest that cyclisation of the intermediate **8a** does occur under these conditions, it was evident that further steps would be necessary to first optimise the ring-closing step, and then transform the 1,2,4-benzophosphadiazine 1-oxide into a suitable radical precursor. Reactions of *N*-arylamidines with PCl_5 were also fraught with problems, and yielded a mixture of products when performed in range of solvents (DCM, THF, toluene) with and without base (Et_3N , pyridine, DABCO). In light of these observations, further reactions with P^{V} species were not attempted.

4.2.2 –Initial Studies with P^{III} Sources

Given the utility of S^{II} sources for the direct synthesis of S^{IV} radical precursors,²² P^{III} halides were examined as phosphinating agents for the construction of 1,2,4-benzophosphadiazines. For the initial attempts, we opted for harsh reaction conditions given the literature precedence of P-C_{aryl} bond-formation for unactivated species.²³ Refluxing *N*-phenylbenzamidine in neat PCl_3 afforded a poorly soluble material that exhibited a number of phosphorus-containing species by ^{31}P NMR ranging from δ - 7 to + 220 ppm. Stoichiometric reactions were repeated in a range of solvents (THF, DCM, DMF, PhCl) with and without base (NaH, DABCO, pyridine), but repeatedly gave intractable and insoluble materials. These are believed to be polymeric materials arising from the rapid formation of three P-N bonds, with either of the two amidine nitrogens, to give compounds such as **D** shown in Figure 4.2.2.1.

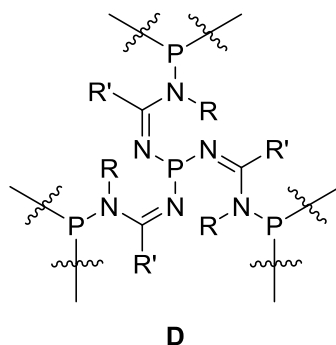
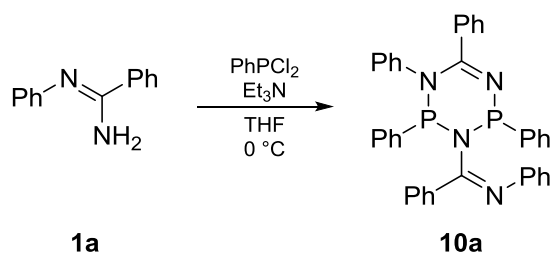


Figure 4.2.2.1: Potential polymeric material resulting from the reaction of *N*-arylamidines with PCl_3 .

Analogous reactions with aryldichlorophosphines also provided limited success. The treatment of *N*-phenylbenzamidine with PhPCl_2 under mild conditions in the presence of Et_3N however, afforded the six-membered heterocyclic species, **10a** (Scheme 4.2.2.1). Further discussion of **10a**, along with the synthesis of other non-fused ring phosphorus-nitrogen heterocycles is provided in Chapter 5. This result further indicates that the formation of a second P-N bond is much more rapid than P-C_{aryl} bond formation and cyclisation.



Scheme 4.2.2.1: Reaction of *N*-phenylbenzamidine with PhPCl₂ under mild conditions.

4.3 – *N,N*-Substituted Amidines

The initial reactions of *N*-arylamidines with PCl₃ and PhPCl₂ suggested that cyclisation is unfavourable in the presence of the second nucleophilic N-H fragment, since P-N bond formation is rapid, especially in the presence of base. To prevent this, we investigated the reactions of aryldichlorophosphines with *N,N'*- (**E**) and *N,N*-substituted (**F**) amidines (Figure 4.3.1).

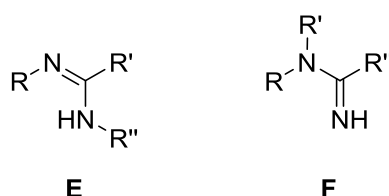


Figure 4.3.1: *N,N'*- and *N,N*-substituted amidines.

4.3.1 – Synthesis of *N,N*-substituted Amidines

N-methyl and *N*-phenyl derivatives (Figure 4.3.1.1) were prepared according to known literature procedures: **11a** *via* condensation of a primary amine with a *N*-substituted nitrilium salt;²⁴ **12a** *via* condensation of a primary amine with a substituted imidoyl chloride;²⁵ and **13a** *via* Lewis-acid mediated condensation of a secondary amine and nitrile in the melt.²⁶

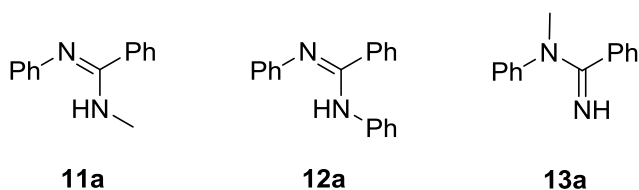


Figure 4.3.1.1: *N,N'*- and *N,N*-substituted amidines prepared in this thesis.

4.3.2 – Reactions with PhPCl₂

The reaction of **11a**, **12a** and **13a** with PhPCl₂ and Et₃N in THF resulted in clean conversion to the monosubstituted products (Figure 4.3.2.1) which all exhibited a major single sharp peak in the ³¹P NMR spectra.

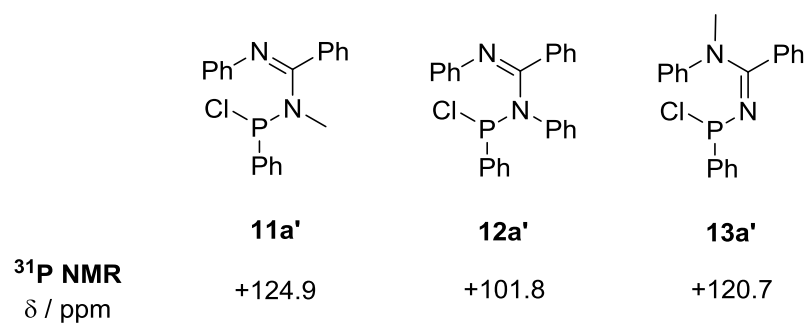


Figure 4.3.2.1: Monosubstituted products from the reaction of *N,N'*- or *N,N*-substituted amidines with PhPCl₂, and their ³¹P NMR chemical shifts.

A number of different approaches were attempted to form the corresponding fused-ring 1,2,4-benzophosphadiazine from compounds **11a'**, **12a'** and **13a'**. Heating solutions of these species with and without base lead only to slow decomposition and formation of cyclic [PhP]_n species. No changes were observed by ³¹P NMR on the addition of Lewis acid (AlCl₃, GaCl₃, TMSOTf, NaBAR^{Cl}) to **11a'** or **13a'**, whilst the addition of GaCl₃ to **12a'** resulted in an immediate downfield shift to δ + 161.5 ppm (Figure 4.3.2.2). This is consistent with the formation of the four-membered heterocycle **[14a][GaCl₄]**, analogous to Grubbs' 1,3,2-diazophosphetene salts (**G**) (Figure 4.3.2.3), derived from the corresponding formamidine and which are precursors to stable four-membered *N*-heterocyclic carbenes.²⁷ On heating at 60 °C for one hour, the signal for **[14a][GaCl₄]** is lost and several minor peaks are observed between δ + 37 and - 37 ppm in the ³¹P NMR spectrum. Heating overnight resulted in clean conversion to a single major phosphorus-containing species at δ + 16.6 ppm. Attempts to isolate this species and **[14a][GaCl₄]** to allow for further characterisation were unsuccessful, affording colourless crystals of **12a.HCl** on a number of occasions, likely due to P-N bond cleavage through contamination with trace air or moisture.

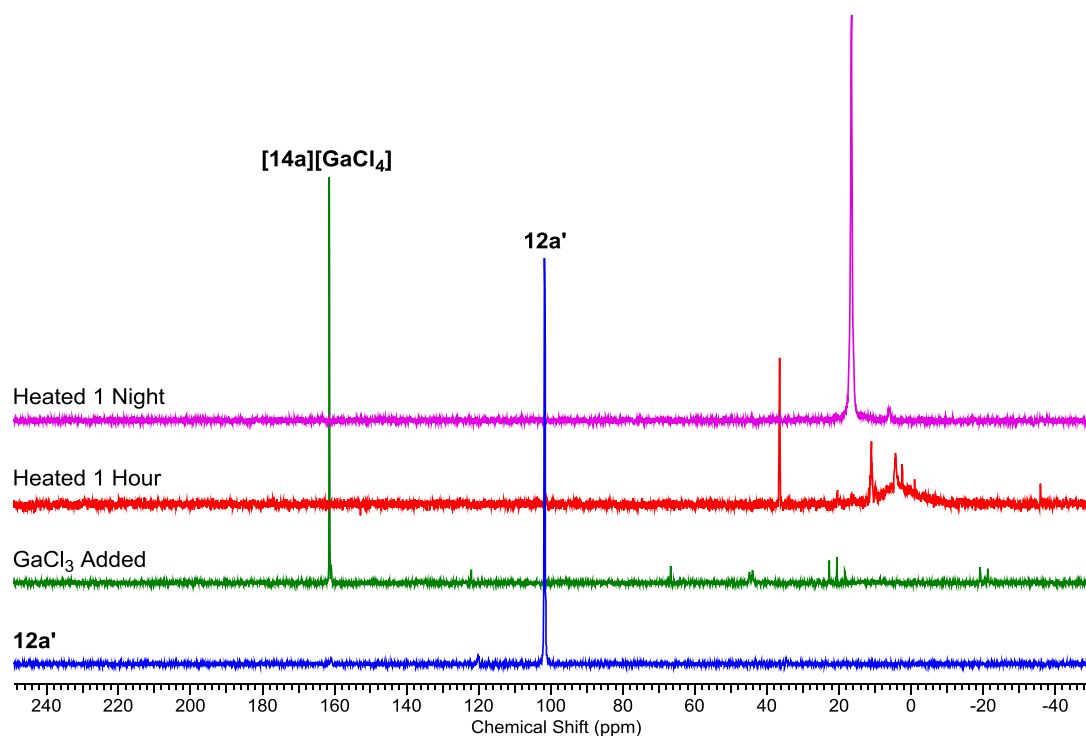


Figure 4.3.2.2: ^{31}P NMR spectra showing the addition of GaCl_3 to **12a'**.

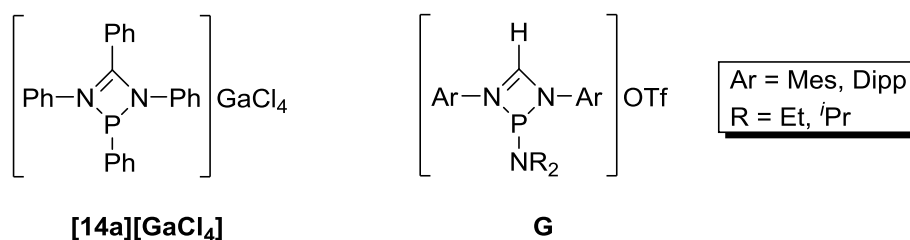
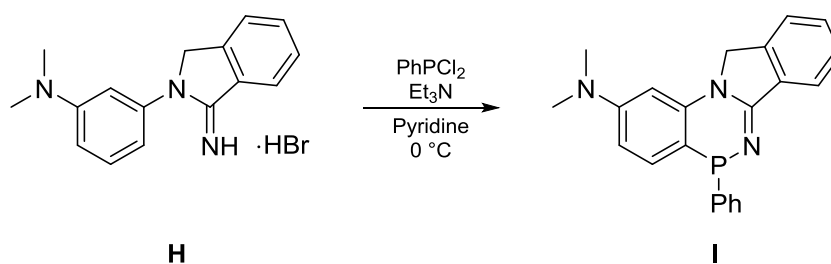


Figure 4.3.2.3: Four-membered 1,3,2-diazophosphetines.

4.4 - Electron-Rich Aromatics

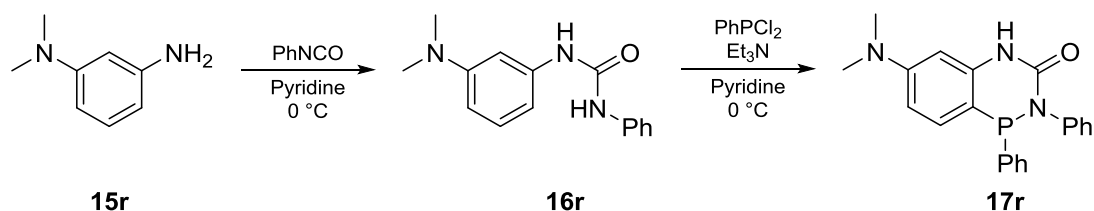
Following the poor success of these amidines derived from aniline itself at forming the desired 1,2,4-benzophosphadiazine, we turned our attention to alternative methods. Rather than increasing the electrophilicity at phosphorus through the addition of Lewis-acid to form an intermediate phosphonium, the nucleophilicity at C_{aryl} can be increased through the introduction of electron-donating groups. This has in the past been successfully applied to a range of N,N' -diarylureas and N,O -diarylcarbamates to give the corresponding 1,2,4-benzophosphadiazines,^{4,18} although the synthesis of benzo-fused P-N heterocycles from N -arylamidines is limited to a single example (Scheme 4.4.1).²⁸ The introduction of a Me_2N group *meta* to the amidine nitrogen (**H**) acts as electron donating and *para*-directing substituent, allowing the 1,2,4-benzophosphadiazine (**I**) to be formed under mild conditions. The isoindole framework also avoids complications that may arise due to the presence of a second nucleophilic N-H fragment.



Scheme 4.4.1: Literature precedence for the construction of 1,2,4-benzophosphadiazines from amidines.

4.4.1 - Initial Studies with Electron-Rich *N,N'*-Diarylureas

The synthesis of 1,2,4-benzophosphadiazines from electron-rich *N,N'*-diarylureas was initially attempted to confirm the applicability of established methods. The reaction of electron-rich urea **16r**, derived from 3-amino-*N,N'*-dimethylaniline **15r** and phenyl isocyanate, with PhPCl_2 under standard literature procedures¹⁸ afforded the fused-ring heterocycle **17r** in low yield (Scheme 4.4.1.1). A similar species has been prepared by Volochnyuk by using 5-methyl-2-furyl-dibromophosphine as the phosphinating agent.



Scheme 4.4.1.1: Synthesis of 1,2,4-benzophosphadiazines from electron-rich *N,N'*-diarylureas.

Single crystals of **17r**, grown by slow diffusion of hexane into a saturated solution of the product in DCM, confirmed the formation of the fused-ring heterocycle. Compound **17r** crystallises as colourless blocks in the triclinic space group $P\bar{1}$ with two enantiomers in the asymmetric unit (Figure 4.4.1.1). These two crystallographically inequivalent molecules differ in the relative orientation of the *P*-phenyl ring. The heterocyclic ring is non-planar and is folded along the $\text{P}\cdots\text{NH}$ axis by 37.3° and 32.9° for the two isomers. The *P*-phenyl rings are close to perpendicular to the heterocyclic rings with $\text{NH}\cdots\text{P-C}_{\text{isop}}$ angles of $79.5(4)^\circ$ and $84.9(4)^\circ$.

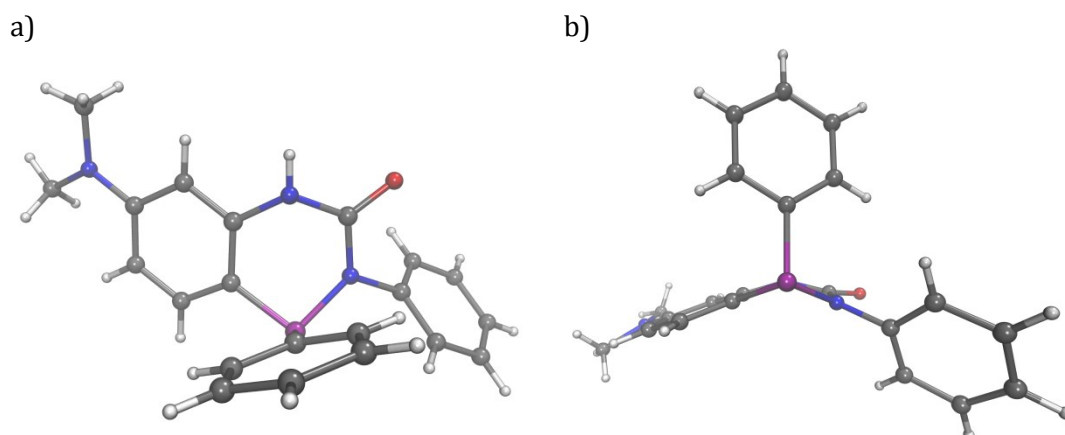
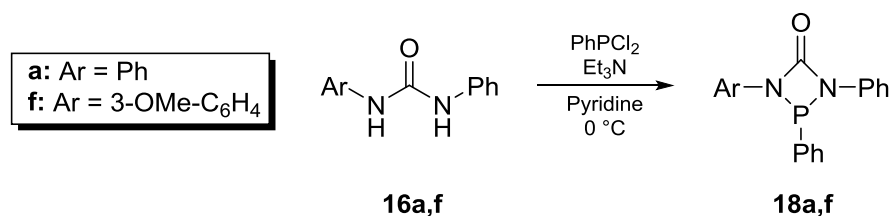


Figure 4.4.1.1: Crystal structure of **17r**; a) Top-down view; b) Side view. Single molecule (*S* isomer) shown for clarity.

Repeating the reaction with *N,N'*-diphenylurea **16a** or the asymmetric system derived from *m*-anisidine **16f** under identical conditions afforded the *N,N'*-chelating four-membered heterocycle **18** (Scheme 4.4.1.2). These species were hypothesised to be intermediates in the formation of the fused-ring species **17** but could not be detected by ^{31}P NMR; this was attributed to rapid equilibrium between the open and cyclic species. If a stronger base such as Et_3N is used for the reaction of electron-rich urea **16r** with PhPCl_2 , the four-membered heterocycle **18r** is instead formed as the sole product. This species was observed to slowly isomerise to give the fused-ring 1,2,4-benzophosphadiazines (see section 5.6).



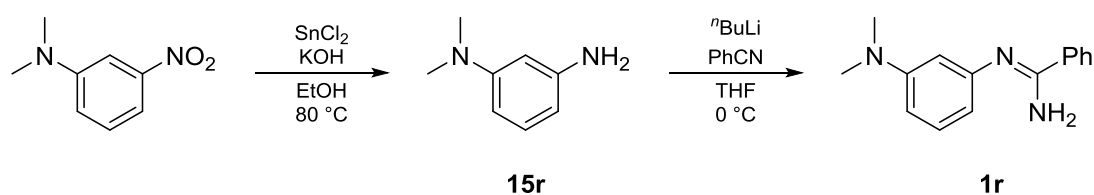
Scheme 4.4.1.2: Synthesis of 1,3,2-diazophosphetines from *N,N'*-diarylureas.

The four-membered heterocycle is also obtained when the electron-rich urea **16r** is treated with $\text{N}^i\text{Pr}_2\text{PCl}_2$ with no evidence of the fused-ring species (see section 5.6). These results indicate that there are three major factors that influence whether the benzo-fused or non-fused, *N,N'*-chelating heterocycle is formed; the *C*-nucleophilicity of the aromatic ring, the electrophilicity of the phosphine, and the strength of the base employed in the reaction. The desired 1,2,4-benzophosphadiazine is formed for electron-rich aromatics and electrophilic phosphines when a moderately weak base such as pyridine is used. The synthesis of non-fused phosphorus-nitrogen heterocycles derived from *N,N'*-diarylureas is further discussed in Chapter 5.

4.4.2 –Electron-Rich *N*-Arylamidines

4.4.2.1 –Synthesis of *N*-Arylamidines

The novel electron rich *N*-arylamidine **1r** was synthesised *via* standard literature procedures *via* condensation of lithiated 3-amino-*N,N*-dimethylaniline with benzonitrile followed by aqueous work-up,²⁹ according to Scheme 4.4.2.1. The aniline **15r** was first prepared by reduction³⁰ of the commercially available 3-nitro-*N,N*-dimethylaniline, yielding a colourless oil that rapidly polymerises on exposure to air. In contrast, the amidine was isolated as an air- and moisture-stable, colourless crystalline solid.



Scheme 4.4.2.1: Synthesis of electron-rich *N*-arylamidines.

4.4.2.2 – Synthesis of 1,2,4-Benzophosphadiazines

The treatment of electron-rich *N*-arylamidine **1r** with PhPCl_2 and Et_3N in pyridine at $0\text{ }^\circ\text{C}$, following the reaction conditions employed for compound **J**,²⁸ afforded a dark amber solution containing a mixture of products ranging from $\delta + 5$ to $+ 133$ ppm in the ^{31}P NMR spectrum. Conversely, when the reaction was repeated without Et_3N , a bright yellow solution immediately formed that contained a major product exhibiting a multiplet at $\delta + 4.1$ ppm in the ^{31}P NMR spectrum, that collapsed to a sharp singlet in the $^{31}\text{P}\{^1\text{H}\}$ NMR spectrum. This again suggests that in the presence of the stronger base Et_3N , secondary phosphorus-nitrogen bond forming reactions are more rapid than cyclisation to give the desired 1,2,4-benzophosphadiazine as previously observed.

Attempts to isolate this major species by removal of solvent under vacuum followed by extraction into toluene or THF were unsuccessful due to the poor solubility of the product; no signal was observed in the ^{31}P NMR spectra of the extracts. Dissolution of the residues in DCM followed by aqueous workup to remove the pyridinium hydrochloride resulted in a mixture of hydrolysis products. The reaction was also performed using NaH as the base, reasoning that the by-products would be either gaseous (H_2) or insoluble in DCM (NaCl), allowing for easy product isolation. This however was found to produce other phosphorus-containing species likely due to the competing P-N bond forming reactions.

The poor solubility of the product suggested that it was the hydrochloride salt of the 1,2,4-benzophosphadiazine (**J**) (Figure 4.4.2.2.1). This was confirmed by repeating the

reaction in THF with a single equivalent of pyridine; dissolution of the yellow precipitate in DCM gave a complex multiplet at $\delta + 4.6$ ppm in the ^{31}P NMR spectra with several P-H couplings. The addition of Et_3N however resulted in a mixture of products by ^{31}P NMR – subsequent isolation of the neutral fused ring (*vide infra*) indicated that none of these peaks corresponded to the desired species.

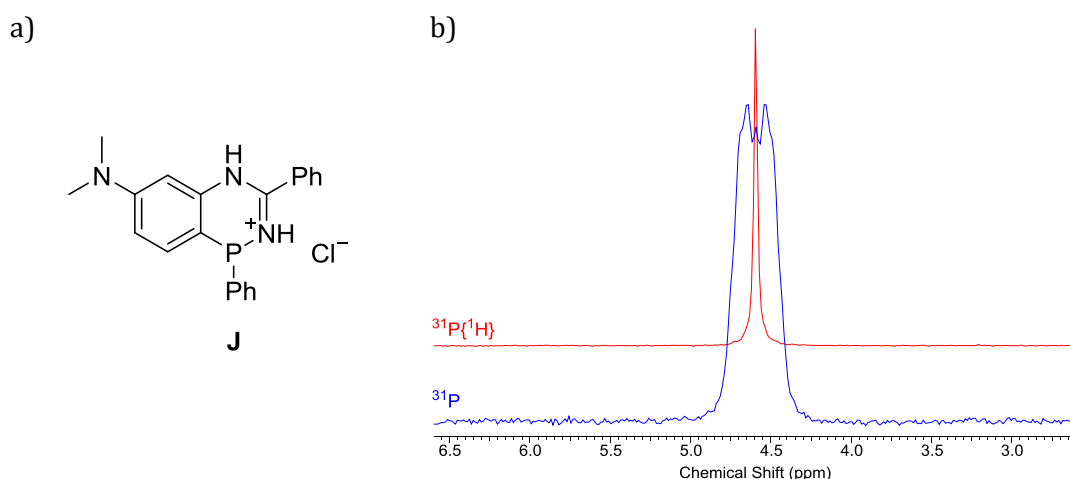
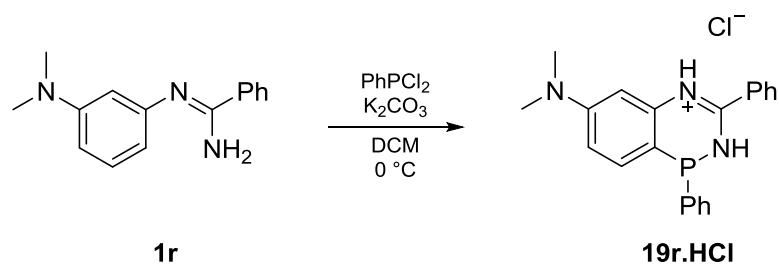


Figure 4.4.2.2.1: a) Proposed identity of the product; b) ^{31}P and $^{31}\text{P}\{^1\text{H}\}$ NMR spectra in DCM showing the complex P-H coupling.

Since it was evident that a mild base was sufficient to form the 1,2,4-benzophosphadiazine, we chose to use an excess of finely ground and dried potassium carbonate whilst performing the reaction in DCM. The dropwise addition of PhPCl_2 to a mixture of **1r** and K_2CO_3 in DCM at 0°C (Scheme 4.4.2.2.1) afforded a bright yellow suspension, which after 1 hour had consumed approximately 50 % of the PhPCl_2 . After stirring at room temperature overnight, the suspension was filtered through Celite to remove KCl and excess K_2CO_3 , then concentrated to give a yellow solid which could be thoroughly washed and dried to give the target 1,2,4-benzophosphadiazine **19r.HCl** in high yields. The ^{31}P NMR spectrum of **19r.HCl** was consistent with the spectra shown in Figure 4.4.2.2.1.



Scheme 4.4.2.2.1: Synthesis of 1,2,4-benzophosphadiazines under mild conditions.

4.4.2.3 – Crystal Structure of 19r.HCl

Crystals of **19r.HCl** suitable for SCXRD analysis, grown by slow cooling of a saturated solution of the product in DCM, confirmed the formation of the benzo-fused P-N heterocycle. Compound **19r.HCl** crystallises as yellow hexagonal rods in the chiral monoclinic space group $P2_1$ with two ion pairs and two molecules of DCM in the asymmetric unit. A single ion pair and the corresponding structural labelling scheme are shown in Figure 4.4.2.3.1.

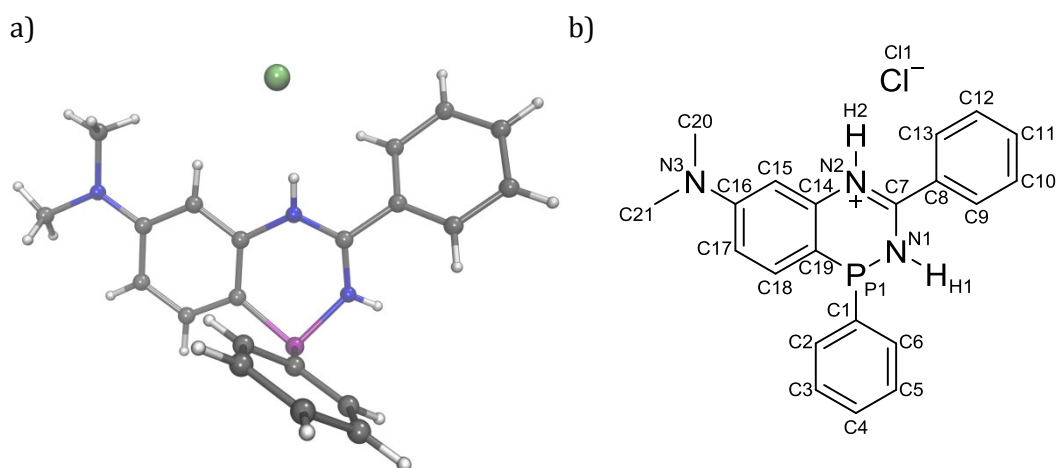


Figure 4.4.2.3.1: a) Single ion pair of **19r.HCl**. Solvents of crystallisation omitted for clarity; b) Structural labelling scheme.

Compound **19r.HCl** crystallises as an equal mixture of both enantiomers; these isomers differ in the relative orientation of the *P*-phenyl ring (Figure 4.4.2.3.2). The two crystallographically inequivalent enantiomers in the asymmetric unit are associated through a hydrogen bonded network with H1...Cl1 and H2...Cl1 contacts ranging from 2.17(9) Å to 2.39(8) Å, leading to infinite chains that propagate along the crystallographic *a* axis.

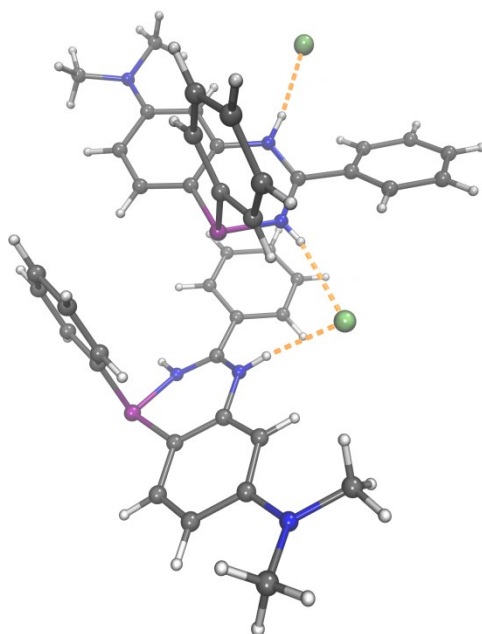


Figure 4.4.2.3.2: Asymmetric unit of **19r.HCl** showing the H \cdots Cl contacts. Solvents of crystallisation omitted for clarity.

In both molecules, the C7-N2 distance is marginally shorter (1.311(9) Å and 1.317(9) Å) than the C7-N1 distance (1.329(1) Å for both molecules) indicating that the former has slightly more double bond character and that the structure is better represented as **19r.HCl** and not as **J** (Figure 4.4.2.3.3) as was earlier hypothesised based on the structure of **8a** and the analogous S^{II} 1,2,4-benzothiadiazines. This was further confirmed by the isolation of the corresponding neutral 1,2,4-benzophosphadiazine in which the hydrogen atom is located on N1 (*vide infra*).

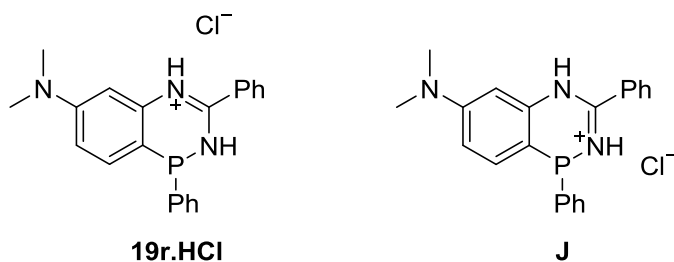


Figure 4.4.2.3.3: Representations of protonated 1,2,4-benzophosphadiazines.

The heterocyclic and benzo-fused rings deviate significantly from planarity at 19.5° and 13.1°, with a fold along the P1 \cdots N2 axis such that the phosphorus atom sits slightly above or below the mean plane (Figure 4.4.2.3.4). The pendant phenyl rings are considerably twisted relative to the heterocyclic ring with deviations from coplanarity 38.2° and 42.6°, and N2-C7-C8-C13 and N1-C7-C8-C9 torsion angles of 35.7(9)°/37.4(1)° and 39.6(1)°/40.7(1)° for the two molecules respectively. The *P*-

phenyl rings are essentially perpendicular to the heterocyclic ring with deviations of 87.8° and 87.0°, with C2-C1-P1-C19 torsion angles close to 0°.

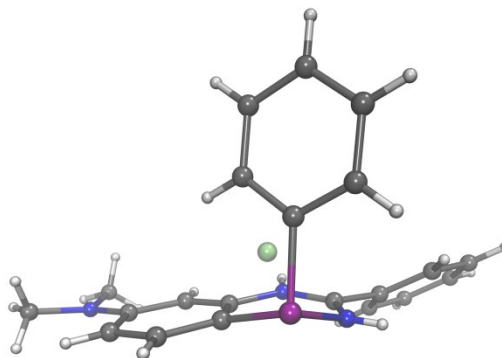


Figure 4.4.2.3.4: Side view of a single ion pair (*S* isomer) of **19r.HCl** showing the deviation from planarity. Solvents of crystallisation omitted for clarity.

4.5 – Electron-Neutral Aromatics

Having established optimal conditions for the synthesis of 1,2,4-benzophosphadiazines from electron-rich *N*-arylamidines, the reactions were attempted with weaker nucleophiles to test the necessity of electron-donating groups in the formation of the fused-ring P-N heterocycle. The reaction of *N*-phenylbenzamidine **1a** with PhPCl₂ and K₂CO₃ in DCM resulted in several pairs of doublets in the ³¹P NMR spectrum, indicative of the formation of P-P coupled species (Figure 4.5.1). These P-P species are believed to be related to compounds discussed in Chapter 5 (see section 5.2), but attempts to isolate and identify these were unsuccessful. The consumption of PhPCl₂ was extremely slow, taking three weeks to convert 92% of the chlorophosphine. The major species after this time however, had chemical shifts similar to **19r.HCl** ($\delta + 4.6$ ppm) suggesting that ring-closure may be achievable under similar conditions. Heating the reaction to help drive the reaction to completion lead primarily to the formation of [PhP]_n species, with minor peaks around $\delta + 5.5$, $+ 3.4$ and $+ 3.1$ ppm in the ³¹P NMR spectrum. The reductive coupling of PhPCl₂ to form the [PhP]_n species implies that the amidine is either oxidised to the *N*-chloroarylamidine or that an aryl-carbon is chlorinated to give a protonated amidine hydrochloride.

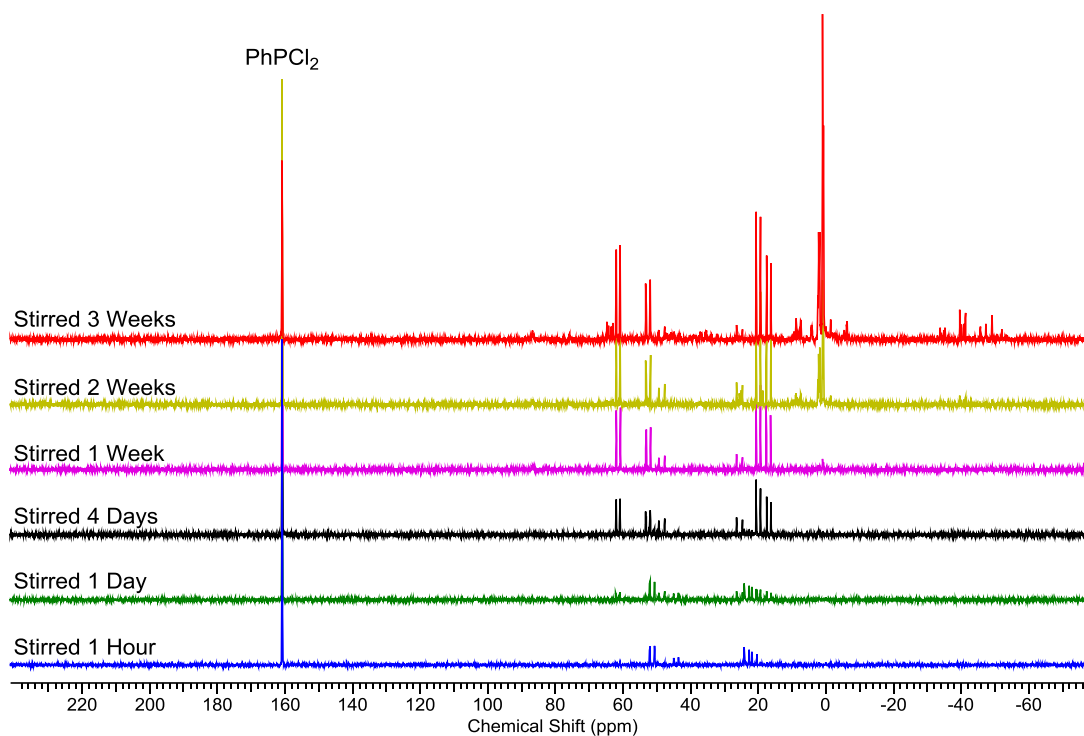


Figure 4.5.1: ^{31}P NMR spectra of the reaction of *N*-phenylbenzamidinium **1a** with PhPCl_2 in the presence of K_2CO_3 .

The reaction of the more nucleophilic *N*-arylamidinium, **1f**, derived from *m*-anisidine, under the same conditions showed promise but was again extremely slow. After two weeks, the PhPCl_2 was fully consumed to give two major species in the ^{31}P NMR spectrum at $\delta + 10.0$ and $+ 6.3$ ppm (Figure 4.5.2). These peaks are believed to be the two isomers of the corresponding protonated fused-ring heterocycle, **19f.HCl** and **19f'.HCl** (Figure 4.5.3); the ratio of these two products is approximately 0.82:1 for the peaks at $\delta + 10.0$ and $+ 6.3$ ppm respectively for the isolated material.

The considerably slower reaction times of the methoxy-substituted amidinium **1f** compared to the dimethylamino amidinium **1r** is expected due to the decreased *C*-nucleophilicity of the former species. The related phosphination of *N,N'*-diarylureas bearing alkoxy groups *para* to the *C*-nucleophilic centre require more activated phosphorus electrophiles such as PBr_3 to form the fused-ring 1,2,4-benzophosphadiazine.⁴ The reaction does not occur with aryldibromophosphines for *N,N'*-diarylureas whilst *N,O*-diarylcarbamates simply required increased reaction times. No evidence for the formation of two isomers were observed for either of these species and the alkoxy-group was assigned to be *para* to the C-P bond in all cases based on ^1H NMR data. Attempted reactions of **1f** with PBr_3 favoured the formation of non-fused ring heterocyclic species [see Chapter 5].

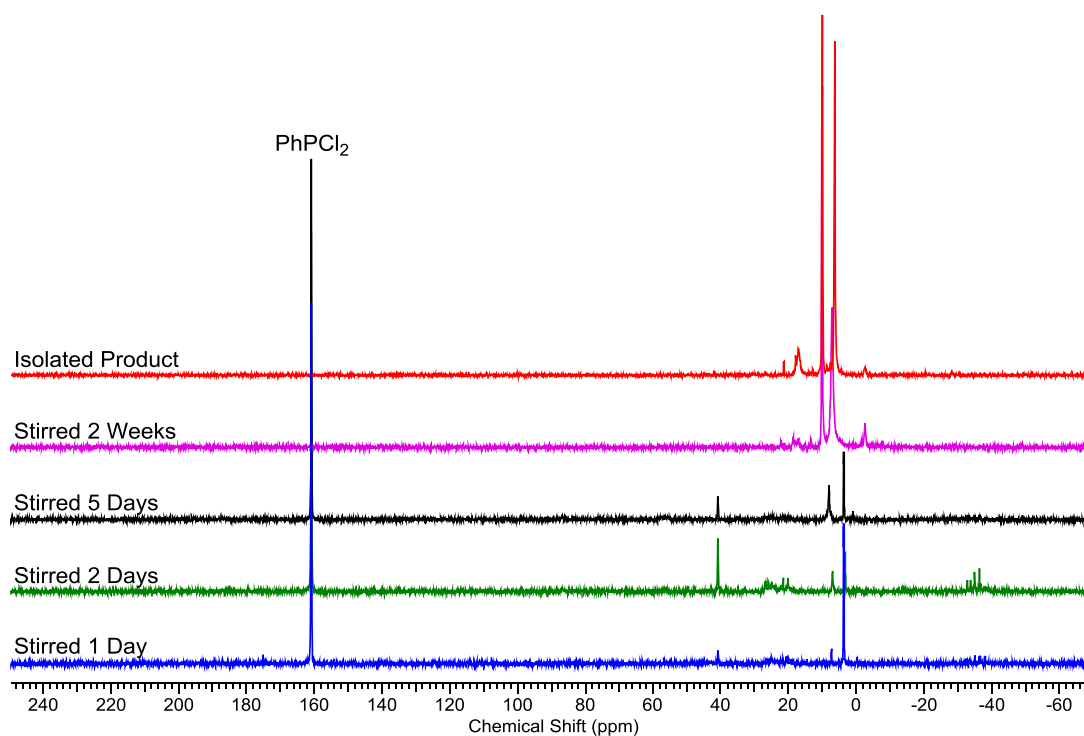


Figure 4.5.2: ^{31}P NMR spectra of the reaction of *N*-(3-methoxyphenyl)-benzamidinium **1f** with PhPCl_2 in the presence of K_2CO_3 .

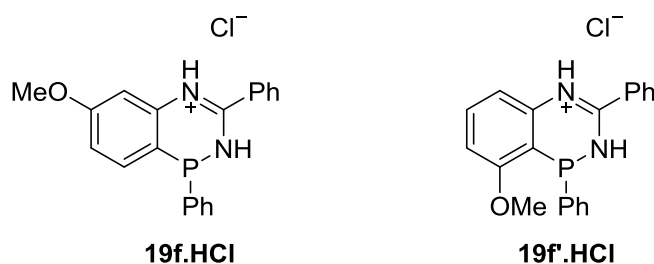


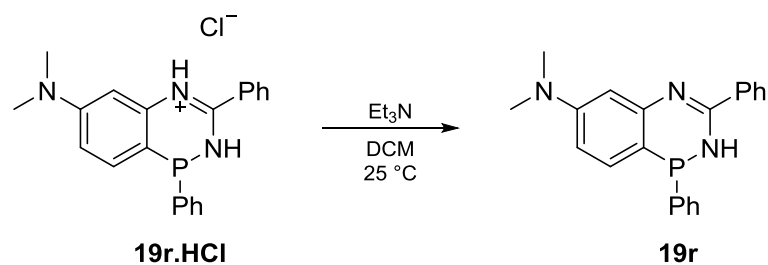
Figure 4.5.3: Proposed isomeric forms of **19f.HCl**.

4.6 – Functionalisation of 1,2,4-Benzophosphadiazines

Having developed synthetic routes to prepare the protonated fused-ring P-N heterocycle **19r.HCl** in high yields under mild conditions, further steps were necessary to transform this parent compound into a suitable radical precursor, as the presence of the *protic* N-H fragments is expected to lead to additional potential degradation pathways.³¹

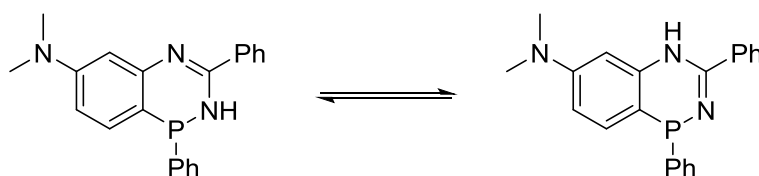
4.6.1 – Deprotonation

Compound **19r.HCl** is readily deprotonated with Et_3N in DCM to give the neutral 1,2,4-benzophosphadiazine **19r** (Scheme 4.6.1.1).



Scheme 4.6.1.1: Synthesis of neutral 1,2,4-benzophosphadiazines.

The ^{31}P NMR spectrum exhibits a broad singlet at $\delta + 0.2$ ppm, which is upfield shifted relative to **19r.HCl** ($\delta + 4.6$ ppm). The broadening of this signal and lack of observable P-H coupling is thought to arise through rapid tautomerism in solution (Scheme 4.6.1.2), leading to a time-averaged signal in the NMR spectrum.



Scheme 4.6.1.2: Tautomerism of 1,2,4-benzophosphadiazines.

Single crystals suitable for X-ray diffraction analysis were grown by slow diffusion of hexane into a saturated solution of the product in DCM at -20 °C. Compound **19r** crystallises as colourless plates in the monoclinic space group $P2_1/n$ with a single molecule in the asymmetric unit (Figure 4.6.1.1). The heterocyclic ring deviates from planarity relative to the fused ring at 17.8° , folded along the $\text{P1}\cdots\text{N2}$ axis such that the nitrogen adjacent to phosphorus, N1, and C7 of the heterocyclic ring are raised significantly above the plane of the fused ring. The pendant phenyl ring is disordered equally across two sites and twisted by 41.5° relative to each site. In both positions, the pendant phenyl ring deviates significantly from coplanarity relative to heterocyclic ring at 25.2° and 31.9° , with N2-C7-C8-C13 and N1-C7-C8-C9 torsion angles of $19.4(3)^\circ/10.4(4)^\circ$ and $30.1(3)^\circ/21.7(4)^\circ$ respectively for the two sites. The *P*-phenyl ring is orientated below the plane of the molecule (*R* isomer) and is essentially perpendicular to the heterocyclic ring at 84.8° . Many of the structural features are similar to the parent HCl salt excluding the C2-C1-P1-C19 torsion angle which is $73.6(2)^\circ$ (*cf.* $6.5(7)^\circ$ and $8.3(7)^\circ$ for **19r.HCl**).

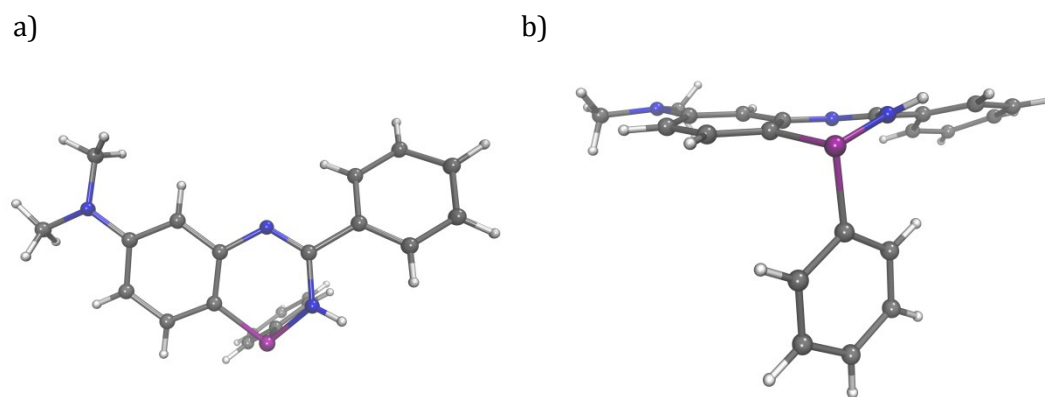
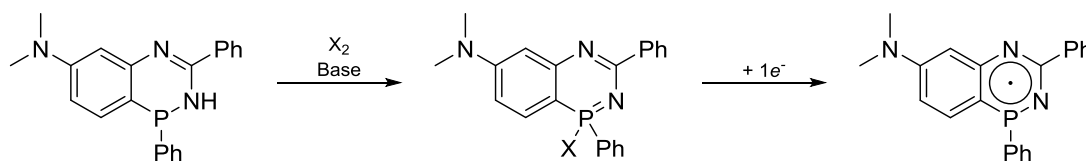


Figure 4.6.1.1: Crystal structure of **19r**: a) Top-down view; b) Side view.

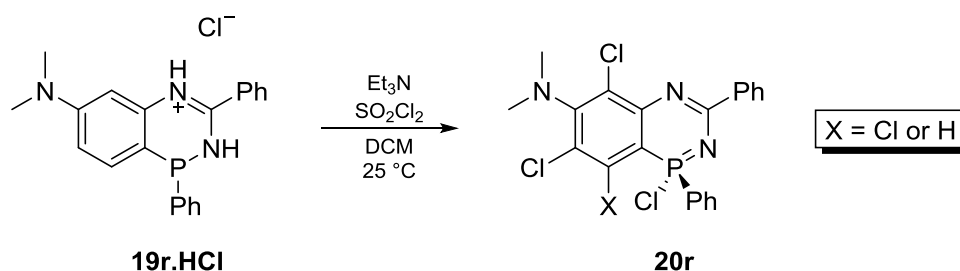
4.6.2 - Oxidation

Two electron oxidation of the P^{III} 1,2,4-benzophosphadiazine in the presence of base, followed by one electron reduction may afford a neutral P^{IV} radical, analogous to the reduction of 1,2,4-benzothiadiazine 1-chlorides discussed in Chapter 3. A general scheme for the proposed synthetic pathway is shown in Scheme 4.6.2.1.



Scheme 4.6.2.1: Proposed scheme for the synthesis of neutral 1,2,4-benzophosphadiazinyl radicals.

The treatment of **19r.HCl** with a slight excess of SO_2Cl_2 in the presence of Et_3N (Scheme 4.6.2.2) gave a number of species by ^{31}P NMR, with a major multiplet (approximately 69% by integration) at $\delta + 42.8$ ppm, and minor multiplets at $\delta + 40.9$, $+ 39.3$ and $+ 35.0$ ppm, which all collapsed to sharp singlets in the $^{31}\text{P}\{^1\text{H}\}$ NMR spectrum. Layering of this solution with hexane afforded colourless crystals identified as **20r**; the excess SO_2Cl_2 results in chlorination of the fused ring and partial chlorination at position X ($\text{X} = \text{Cl} \approx 17\%$). The major species observed by ^{31}P NMR at $\delta + 42.8$ ppm can therefore be assigned tentatively as **20r** with $\text{X} = \text{H}$, whilst the next major species at $\delta + 40.9$ ppm is **20r** with $\text{X} = \text{Cl}$. The other minor species are believed to be other partially chlorinated and protonated systems.



Scheme 4.6.2.2: Oxidation of **19r.HCl** with SO_2Cl_2 .

Compound **20r** crystallises as pale yellow blocks in the monoclinic space group $P2_1/n$ with a single molecule in the asymmetric unit (Figure 4.6.2.1). The heterocyclic ring again deviates from the plane of the fused-ring by 15.9° as does the pendant phenyl ring at 21.1° , similarly to **15r** and **15r.HCl**. The *P*-phenyl ring is essentially perpendicular to the fused ring with a deviation from coplanarity at 89.1° . Unlike **15r** and **15r.HCl**, the NMe_2 group is twisted out conjugation with the association ring due to the increased steric hindrance that arises through chlorination of the fused-ring.

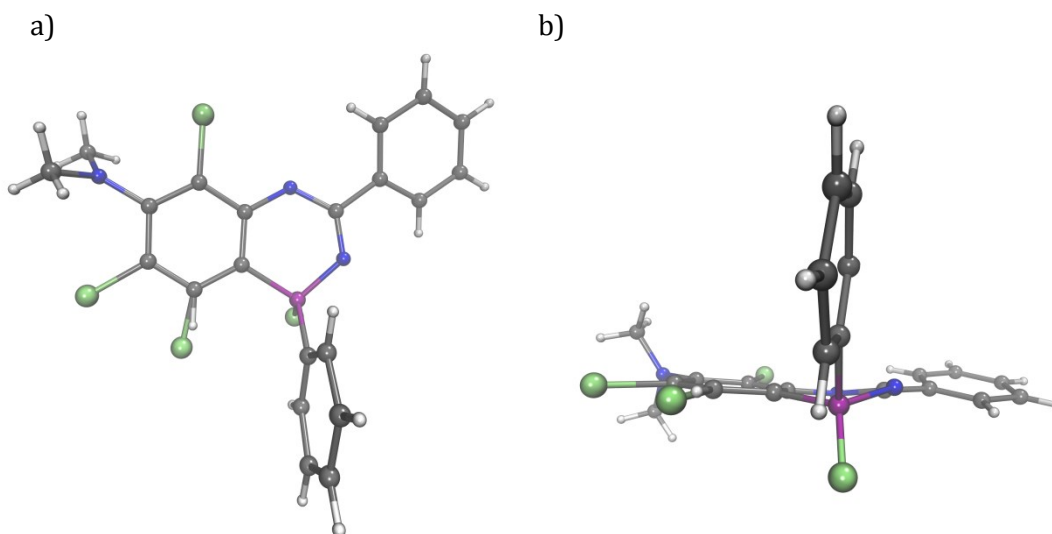
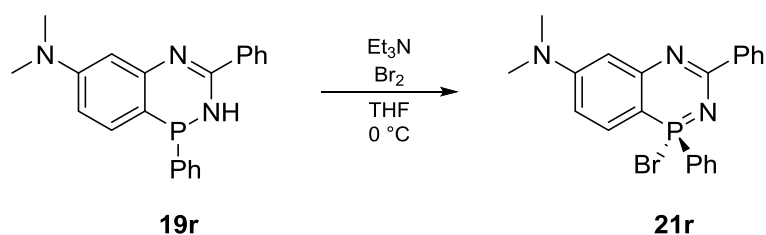


Figure 4.6.2.1: Crystal structure of **20r** shown with partial chlorination: a) Top-down view; b) Side view.

Reactions performed with controlled addition of stoichiometric SO_2Cl_2 at 0°C gave a mixture of products suggesting that chlorination at phosphorus and of the fused-ring are competitive. The addition of excess SO_2Cl_2 was found to change the product distribution but a single species could not be obtained even in the presence of excess base. A mixture of unidentified products, inconsistent with **20r**, was obtained with PhICl_2 as oxidant.

Oxidations with elemental bromine gave better results provided that the neutral fused-ring heterocycle **19r** was used as the starting material, to avoid halogen exchange problems that may arise in the presence of both HCl and HBr salts. The treatment of **19r** with a single equivalent of Br₂ and Et₃N according to Scheme 4.6.2.3 gave a single major species in the ³¹P NMR spectrum at δ + 36.8 ppm assigned as **21r** but attempts to isolate this compound were unsuccessful, likely due to hydrolysis.

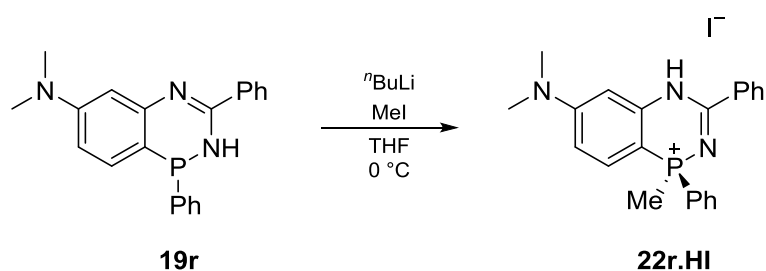


Scheme 4.6.2.3: Oxidation of **19r** with Br₂.

4.6.3 – N-Functionalisation

4.6.3.1 – N-Methylation

N-Methylation has been shown to be a necessary step prior to one electron reduction for Oakley's bis-1,2,4-thiadiazinyl radicals; reduction of the former N-H containing species led to proton-migration and degradation of the resulting radical.³¹ The treatment of **19r** with ⁿBuLi followed by MeI according to Scheme 4.6.3.1.1 afforded air- and moisture-stable crystals of **22r.HI**. The formation of the phosphonium species indicates that the P^{III} centre is more nucleophilic than either of the two heterocyclic nitrogens, despite initial deprotonation by ⁿBuLi. Attempted reactions in DMF with excess NaH yielded identical results.



Scheme 4.6.3.1.1: Attempted N-methylation of **19r**.

Compound **22r.HI** crystallises as pale yellow parallelepipeds in the triclinic space group $P\bar{1}$ with a single ion pair in the asymmetric unit (Figure 4.6.3.1.1). The deviation from planarity of the heterocyclic ring with respect to the benzo-fused ring is significantly smaller than the P^{III} or P^{IV} 1,2,4-benzophosphadiazines at 7.3° and the pendant phenyl ring is essentially coplanar with the heterocyclic ring (deviation of

2.3°). The *P*-phenyl ring is non-perpendicular with respect to the heterocyclic ring such that the $\text{HN}\cdots\text{P-C}_{\text{ispo}}$ angle ($125.1(2)^\circ$) is more obtuse and further from 90° compared to the P^{III} species. The phosphonium center adopts a tetrahedral geometry with angles between the four substituents ranging from $107.7(1)^\circ$ to $110.0(1)^\circ$, close to the idealised $\approx 109.5^\circ$ for a perfect tetrahedron.

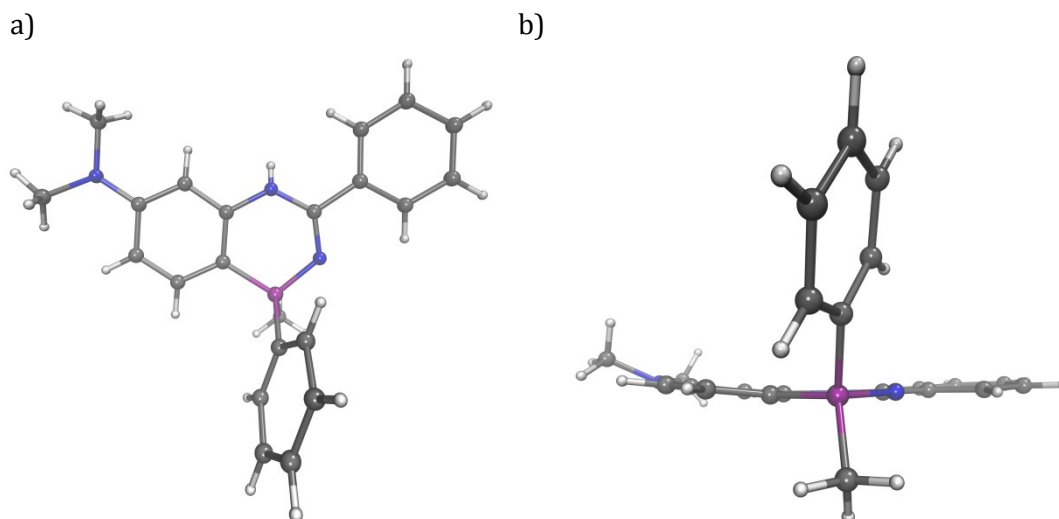


Figure 4.6.3.1.1: Crystal structure of **22r.HI**: a) Top-down view; b) Side view. Counterion omitted for clarity.

The DFT optimised geometry of **19r**, performed at the M062X-6-311g(d,p) level of theory, indicates that HOMO -2 (Figure 4.6.3.1.2) is largely localised (24.2 %) on phosphorus and suggests that *P*-methylation is driven by the nucleophilicity of the electron-rich phosphorus centre. The HOMO -1 is significantly more delocalised across the fused-ring, such that the orbital populations on N1 and N2 are 10.5 % and 17.3 % respectively; the HOMO is solely delocalised across the fused-ring and Me_2N group.

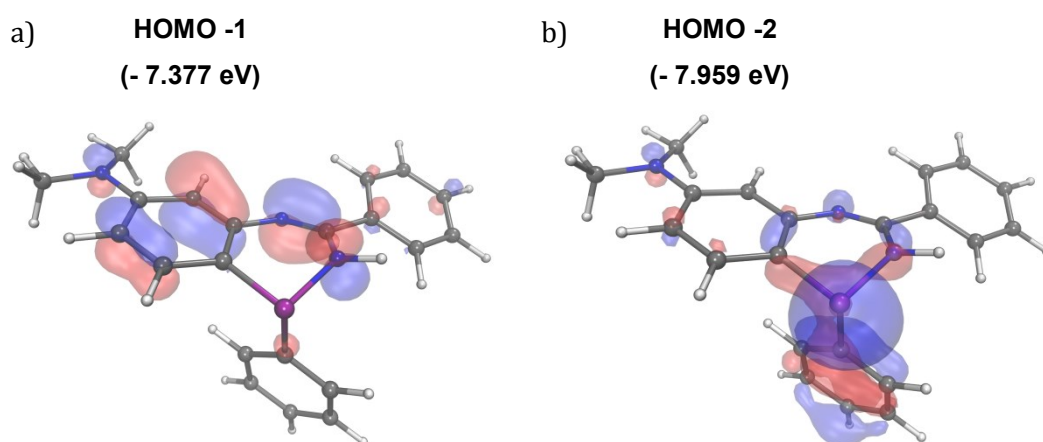


Figure 4.6.3.1.2: Frontier molecular orbitals and energies of **19r**: a) HOMO -1; b) HOMO -2 (isovalue = 0.05).

Nucleus independent chemical shift (NICS⁰) calculations³² (Figure 4.6.3.1.3) show that *P*-methylation (**22r.H⁺**) results in increased anti-aromaticity for the heterocyclic ring compared to **19r**, given by an increase and positive number for the isotropic magnetic shielding tensor, whilst the hypothetical *N*-methylated analogues **X** and **Y** are both calculated to be weakly aromatic (negative chemical shift). *P*-methylation does however lead to a greater increase in the aromaticity of the benzo-fused ring (*cf.* -8.50 ppm for benzene) and **22r.H⁺** is significantly lower in energy than both **X** and **Y**. This indicates that formation of the P-Me bond is enthalpically favoured and that *N*-methylation is not likely to be achieved.

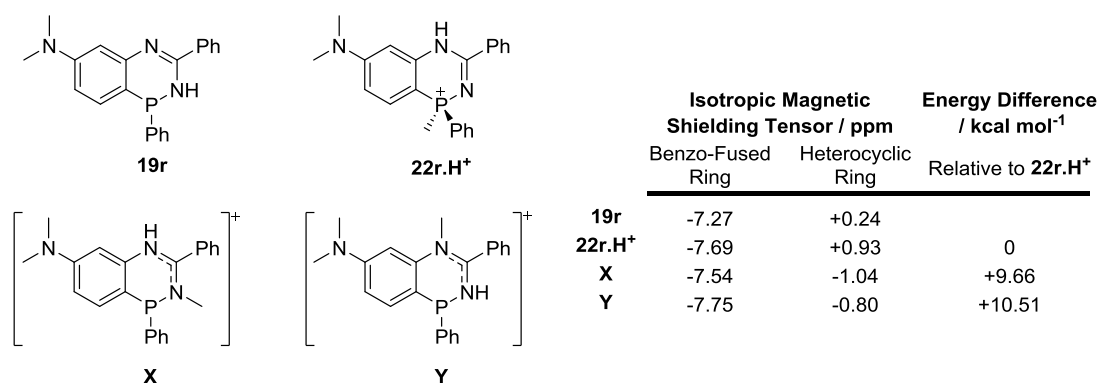
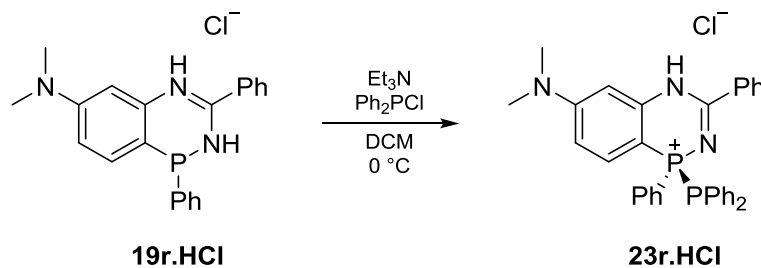


Figure 4.6.3.1.3: Calculated isotropic magnetic shielding tensors and energy differences for *P*- and *N*-methylated systems.

4.6.3.2 - *N*-Phosphination

The use of bulkier R-X species to favour functionalisation of one of the heterocyclic nitrogens over the phosphorus atom and remove the N-H proton was also attempted. The reaction of **19r**, generated *in situ* by deprotonation of **19r.HCl** with excess Et₃N, with Ph₂PCl (Scheme 4.6.3.2.1) resulted in a pair of doublets in the ³¹P{¹H} NMR spectrum at δ + 21.9 and - 18.9 ppm with ¹J_{P-P} = 269.0 Hz.



Scheme 4.6.3.2.1: Attempted *N*-phosphination of **15r**.

Crystals suitable for SCXRD analysis, grown by slow diffusion of Et₂O into a solution of the product in DCM, confirmed the formation of the P-P coupled 1,2,4-

benzophosphadiazine as the chloride salt, **23.HCl**. This can be regarded as an autoionisation product which results from the electron-rich phosphane activating Ph_2PCl , followed by tautomerism. Autoionisation of P-Cl bonds is not typically observed for phosphines, suggesting that **19r** may potentially be exploited as a strong σ -donating ligand.

Compound **23r.HCl** crystallises as yellow plates in the monoclinic space group $P2_1/n$ with a single ion pair in the asymmetric unit (Figure 4.6.3.2.1). The deviation from planarity of the heterocyclic ring relative to the benzo-fused ring is 8.0° and similar to **22r.HI** at 7.3° . The pendant phenyl ring deviates marginally from coplanarity to the heterocyclic ring at 10.7° whilst the $\text{HN}\cdots\text{P-C}_{\text{isop}}$ angle increases to $136.8(6)^\circ$ (cf. $92.5(7)^\circ$ for the parent P^{III} 1,2,4-benzophosphadiazine, **19r**). The heterocyclic phosphorus atom adopts a *pseudo*-tetrahedral geometry with A-P-B (where A and B are any two of the four substituents) angles in the range of $101.8(5)^\circ$ to $115.9(5)^\circ$. This distortion away from uniform values close to $\approx 109.5^\circ$ as observed for **18r.HI** is expected due to the increased steric bulk of the $-\text{PPh}_2$ fragment. The P-P bond length is $2.2022(6) \text{ \AA}$ which is at the lower end of the range of other P-P systems ($2.197\text{--}2.249 \text{ \AA}$).³³

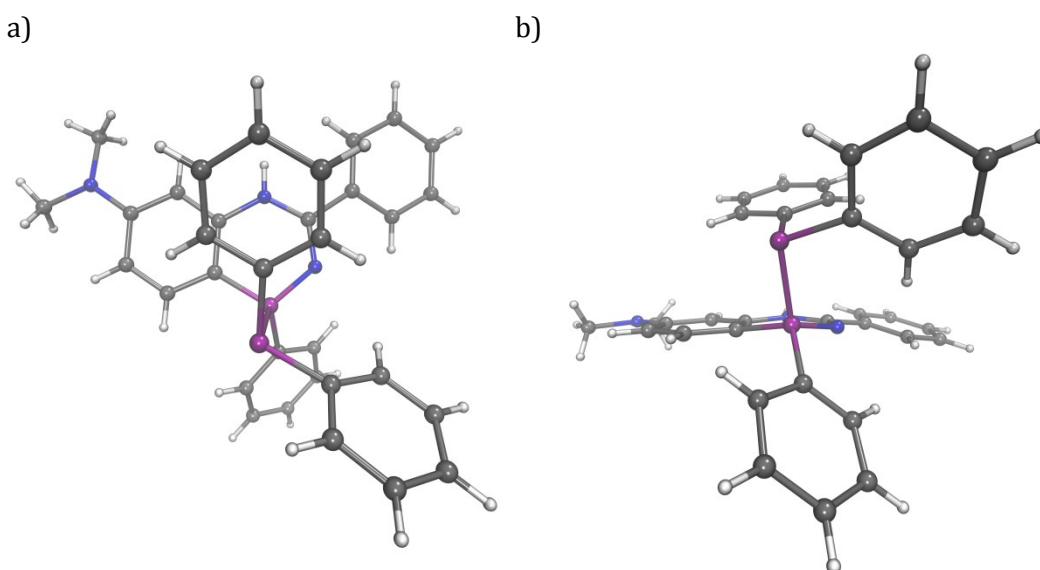
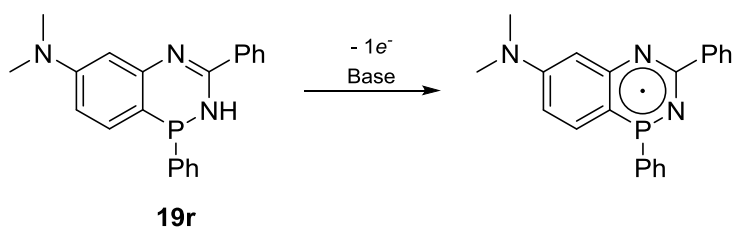


Figure 4.6.3.2.1: Crystal structure of **19r.HCl**: a) Top-down view; b) Side view.

Counterion omitted for clarity.

4.6.4 – One Electron Oxidation

In light of the failure to obtain an *N*-methylated derivative, the one electron oxidation of the neutral 1,2,4-benzophosphadiazine **19r** in the presence of base was attempted according to the Scheme 4.6.4.1.



Scheme 4.6.4.1: Proposed one electron oxidation of **19r** in the presence of base.

No reaction was observed with AgBAR^{F} in the presence of Et_3N . The use of NOBF_4 as the oxidising agent afforded a deep red solution that was EPR inactive and showed a number of species by ^{31}P NMR spectroscopy. An immediate deep blue solution formed on addition of DDQ to a solution of **19r** and Et_3N in DCM at $-95\text{ }^\circ\text{C}$, but swiftly decolourised on warming to room temperature to afford a dark brown solution. The ^{31}P NMR of this solution displayed a single major phosphorus species at $\delta + 38.2\text{ ppm}$ which is believed to be the phosphine-oxide of **19r** resulting from deoxygenation of the DDQ radical anion.

4.7 – Conclusions

The methods developed for the sulfur-nitrogen heterocycles discussed in Chapter 2 were found to not be directly transferable to the isoelectronic phosphorus systems and attempts to prepare 1,2,4-benzophosphadiazines directly from *N*-arylamidines with P^{V} or P^{III} sources were unsuccessful. The use of electron-rich *N,N'*-diarylureas or *N*-arylamidines however allowed the desired fused-ring heterocycles to be prepared under mild conditions, whilst the use of a stronger base resulted in the formation of non-fused P-N heterocycles; these species are discussed in detail in Chapter 5.

The protonated 1,2,4-benzophosphadiazine **19r.HCl** is readily deprotonated to give the neutral heterocycle **19r** but attempts at further transforming this species into a suitable radical precursor showed poor success. Oxidation of **19r** with SO_2Cl_2 or Br_2 to form the corresponding P^{V} heterocycle showed promise but a single species could not be isolated. Attempts to *N*-methylate instead gave the *P*-methylated phosphonium species **22r.HI**, whilst similar reactions with Ph_2PCl resulted in the formation of a phosphane-stabilised phosphonium cation **23r.HCl**. Direct one electron oxidation of **19r** with a range of oxidising agents was unsuccessful.

4.8 – Future Work

Whilst the utility of the reaction conditions developed for the synthesis of 1,2,4-benzophosphadiazines was found to be limited to the more electron-rich aromatics, a library of compounds of type **K** (Figure 4.8.1) may nevertheless be accessible by

changing the carbonitrile used in the preparation of the *N*-arylamidine, or the substituent on phosphorus.

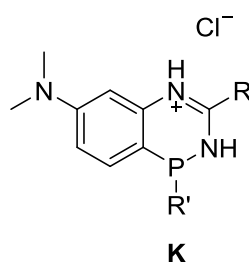


Figure 4.8.1: Accessible 1,2,4-benzophosphadiazines *via* the routes developed in this chapter.

Further optimisation of reaction conditions are necessary to obtain the P^V 1,2,4-benzophosphadiazine *via* oxidation of the neutral heterocycle **19r**. Following this, investigations into the electrochemical behaviour are required to determine whether the corresponding neutral P^{IV} radical, formed *via* one electron reduction, is accessible and stable. *N*-methylation of an electron-rich *N*-arylamidine prior to the synthesis of the fused-ring P-N heterocycle may be a viable approach to overcome the problems encountered with attempted post-synthetic modifications of the 1,2,4-benzophosphadiazines.

4.9 – Experimental

4.9.1 – Synthesis of *N*-Arylamidines

The electron rich *N*-arylamidine **1r** was prepared *via* standard methods, through condensation of lithiated aniline **14r** with benzonitrile, followed by aqueous work-up. The aniline **14r** was synthesised by reduction of the corresponding nitro-derivative according to known literature procedures.

4.9.1.1 – Synthesis of 3-amino-*N,N*-dimethylaniline, **14r**;

3-nitro-*N,N*-dimethylaniline (5.00 g, 30.1 mmol) was partially dissolved in degassed EtOH (100 cm³) and heated to 80 °C. SnCl₂ (22.80 g, 120.4 mmol) was added slowly under a blanket of argon. The dark purple suspension was maintained at reflux for 16 hours and then carefully quenched with a solution of KOH (13.50 g, 240.8 mmol) in degassed H₂O (100 cm³) at 0 °C. The reaction mixture was extracted into Et₂O (3 x 50 cm³) and the combined organic extracts were dried over degassed MgSO₄, filtered and evaporated to dryness. Vacuum distillation of the crude red oil (120-130 °C at $\approx 1 \times 10^{-3}$ Tor) afforded the product as a colourless, air-sensitive liquid. Yield: 2.41 g (17.7 mmol, 58.8 %). ¹H NMR (400 MHz, DMSO-*d*₆, 26.0 °C) δ : 6.87 (t, *J* = 7.9 Hz, 1H), 6.04-5.98 (m, 3H), 4.76 (bs, 2H), 2.83 (s, 6H). ¹³C{¹H} NMR (100.5 MHz, DCM, 26.6 °C) δ : 152.1, 147.9, 129.8, 104.1, 103.5, 99.5, 40.5.

4.9.1.2 – Synthesis of *N*-(3-dimethylamino-phenyl)-benzamidines, **1r**:

14r (1.47 g, 10.8 mmol) was dissolved in THF (30 cm³) and cooled to 0 °C. ⁿBuLi (2.5M in hexane, 4.32 cm³, 10.8 mmol) was added dropwise and the yellow solution was warmed to room temperature. After two hours, benzonitrile (1.04 cm³, 10.8 mmol) was slowly added and allowed to stir for 12 hours. The thick cream reaction mixture was quenched with water (25 cm³) and extracted into DCM (3 x 25 cm³). The combined organic extracts were washed with water and brine (25 cm³ each), dried over MgSO₄, filtered and concentrated *in vacuo*. The crude off-white solids were recrystallised from DCM and hexanes to give the product as a colourless microcrystalline powder. Yield: 2.19 g (9.1 mmol, 84.5 %). ¹H NMR (400 MHz, DCM, 20.1 °C) δ : 7.86 (d, *J* = 7.0 Hz, 2H), 7.52-7.39 (m, 3H), 7.22 (t, *J* = 7.9, 8.0 Hz, 1H), 6.48 (dd, *J* = 2.4, 8.3 Hz, 1H), 6.35-6.29 (m, 2H), 5.07 (bs, 2H), 2.94 (s, 6H). ¹³C{¹H} NMR (100.5 MHz, DCM, 20.3 °C) δ : 154.3, 152.2, 150.9, 136.1, 130.4, 130.0, 128.5, 126.8, 109.4, 107.5, 105.6, 40.5.

4.9.2 – Synthesis of *N,N'*- and *N,N'*-Substituted Arylamidines

N,N'- and *N,N*-substituted arylamidines were prepared according to known literature procedures: **11a** *via* condensation of a primary amine with a *N*-substituted nitrilium

salt;²⁴ **12a** *via* condensation of a primary amine with a substituted imidoyl chloride;²⁵ and **13a** *via* Lewis-acid mediated condensation of a secondary amine and nitrile in the melt.²⁶ *N*-methylbenzotriilium triflate was synthesised *via* standard literature procedures and recrystallized from DCM and hexanes prior to use.²⁴

4.9.2.1 – Synthesis of *N*-methyl-*N'*-phenylbenzamidine, **11a**:

Aniline (0.5 cm³, 5.5 mmol) was added dropwise to a suspension of *N*-methylbenzotriilium triflate (1.47 g, 5.5 mmol) in toluene (15 cm³) and allowed to stir for 90 minutes. The supernatant was removed *via* filter cannula and the solids were washed with hexane (10 cm³) then dried *in vacuo*. The solids were dissolved in DCM (20 cm³) and quenched with a solution of KOH (0.50 g, 8.9 mmol) in H₂O (20 cm³). The organic layer was collected and the aqueous phase was further extracted with portions of DCM (2 x 20 cm³). The combined organic extracts were washed with water (20 cm³), dried over MgSO₄, filtered and evaporated to dryness. The residues were crystallised from DCM and hexane to give **11a** as colourless needles. Yield: 0.82 g (3.9 mmol, 71.3 %). ¹H NMR (400 MHz, DCM, 17.8 °C) δ: 7.31-7.16 (m, 5H), 7.03 (t, *J* = 6.9, 7.3 Hz, 2H), 6.78 (t, *J* = 6.4, 6.9 Hz, 1H), 6.59 (d, *J* = 6.9 Hz, 2H), 4.74 (bs, 1H), 3.01 (s, 3H). ¹³C{¹H} NMR (100.5 MHz, DCM, 18.3 °C) δ: 158.1, 151.6, 135.6, 129.1, 128.7, 128.4, 128.2, 123.0, 121.0, 28.7.

Analytical data in accordance with the literature.²⁴

4.9.2.2 – Synthesis of *N,N'*-diphenylbenzamidine, **12a**:

Benzanilide (5.0 g, 25.4 mmol) was partially dissolved in SOCl₂ (11.1 cm³, 152.1 mmol) and heated at reflux for 15 hours. The dark yellow solution was cooled to room temperature and volatiles were removed *in vacuo*. The residues were redissolved in toluene (15 cm³) and evaporated to dryness. The off-white solids were dissolved in DCM (20 cm³) and added slowly to a solution of aniline (4.6 cm³, 50.8 mmol) and Et₃N (10.6 cm³, 76.2 mmol) in DCM (20 cm³). The colourless suspension was heated to 50 °C for 2 hours. Once cooled to room temperature, the reaction mixture was poured into brine (100 cm³) and extracted into DCM (3 x 50 cm³). The combined organic extracts were washed with brine (50 cm³), dried over MgSO₄, filtered and concentrated *in vacuo*. The crude residues were recrystallised from DCM and hexane to afford **12a** as an off-white solid. Yield: 5.07 g (18.6 mmol, 73.4 %). ¹H NMR (400 MHz, DMSO, 19.6 °C) δ: 9.10 (bs, 1H), 7.82 (d, *J* = 6.3 Hz, 2H), 7.29-7.18 (m, 7H), 7.04-6.89 (m, 3H), 6.70 (m, 1H), 6.52 (d, *J* = 6.0 Hz, 2H). ¹³C{¹H} NMR (100.5 MHz, DMSO, 20.3 °C) δ: 155.2, 151.1, 141.9, 135.3, 129.4, 128.8, 128.5, 122.8, 122.4, 121.4, 120.0.

Analytical data in accordance with the literature.²⁵

4.9.2.3 – Synthesis of *N*-methyl-*N*-phenylbenzamidine, **13a**:

N-methylaniline (2.0 cm³, 18.5 mmol), benzonitrile (1.9 cm³, 18.5 mmol) and AlCl₃ (2.46 g, 18.5 mmol) were combined under argon and heated to 100 °C for 13 hours. The purple melt was allowed to cool to room temperature, crushed into a fine powder and slurried in 12.5 % NaOH (6.25 g in 50 cm³ H₂O). The organics were extracted into DCM (50 cm³ + 2 x 25 cm³), washed with 12.5 % NaOH, water and brine (25 cm³ each), dried over MgSO₄, filtered and concentrated *in vacuo*. The crude purple oil was crystallised from toluene to give **13a** as colourless needles. Yield: 2.45 g (11.7 mmol, 66.0 %). ¹H NMR (400 MHz, DCM, 19.5 °C) δ: 7.32-7.27 (m, 2H), 7.22-7.17 (m, 3H), 7.14 (t, *J* = 7.8, 7.9 Hz, 2H), 7.02-6.95 (m, 3H), 3.45 (s, 3H). ¹³C{¹H} NMR (100.5 MHz, DCM, 20.3 °C) δ: 168.3, 147.3, 139.0, 128.8, 128.1, 127.9, 126.5, 124.7, 39.9.

Analytical data in accordance with the literature.²⁶

4.9.3 – Synthesis of *N'*-Phosphanyl-*N*-Arylamidines

N'-phosphanyl-*N*-arylamidines, **11-13a'**, were prepared by treating the corresponding *N,N'*- or *N,N*-substituted arylamidines, **11-13a**, with PhPCl₂ in the presence of base. The synthesis of **11a** is given as exemplar.

4.9.3.1 – Synthesis of *N*-(chlorophenylphosphanyl)-*N*-methyl-*N'*-phenylbenzamidine, **11a'**:

PhPCl₂ (0.2 cm³, 1.5 mmol) was added dropwise to a solution of **11a** (0.35 g, 1.6 mmol) and Et₃N (0.21 cm³, 1.5 mmol) in THF (15 cm³) at 0 °C. The colourless suspension was warmed to room temperature and allowed to stir for 20 hours. The solvent was removed *in vacuo* and the residues were extracted into hexane (2 x 10 cm³) then filtered through celite. Removal of the solvent *in vacuo* afforded **11a'** as a colourless paste. Yield: 0.27 g (0.8 mmol, 51.9 %). ¹H NMR (400 MHz, DCM, 17.6 °C) δ: 7.72 (t, *J* = 6.6 Hz, 2H), 7.57-7.47 (m, 3H), 7.35-7.26 (m, 5H), 7.09 (t, *J* = 7.6, 8.0 Hz, 2H), 6.85 (t, *J* = 7.3 Hz, 1H), 6.66 (d, *J* = 7.8 Hz, 2H), 3.04 (s, 3H). ³¹P NMR (161.8 MHz, DCM, 17.9 °C) δ: 123.9 (s). ¹³C{¹H} NMR (100.5 MHz, DCM, 18.5 °C) δ: 161.1 (d, *J*_{C-P} = 36.4 Hz), 149.8 (s), 138.1 (d, *J*_{C-P} = 32.6 Hz), 133.6 (d, *J*_{C-P} = 5.8 Hz), 130.4 (d, *J*_{C-P} = 1.9 Hz), 130.2 (d, *J*_{C-P} = 22.5 Hz), 129.5 (d, *J*_{C-P} = 5.3 Hz), 129.3 (s), 128.9 (d, *J*_{C-P} = 4.3 Hz), 128.5 (s), 128.4 (s), 122.3 (s), 121.9 (s), 33.1 (d, *J*_{C-P} = 8.2 Hz).

4.9.3.2 – Synthesis of *N*-(chlorophenylphosphanyl)-*N*',*N*'-diphenylbenzamidine, **12a'**:

Off-white solid, 86.1 % yield. $^1\text{H NMR}$ (400 MHz, DCM, 25.0 °C) δ : 7.52 (t, $J = 7.5, 7.9$ Hz, 2H), 7.366 (t, $J = 7.0$ Hz, 1H), 7.29 (t, $J = 7.1, 8.0$ Hz, 2H), 7.17-7.10 (m, 5H), 7.08-6.99 (m, 6H), 6.89-6.80 (m, 2H), 6.70-6.62 (m, 2H). $^{31}\text{P NMR}$ (161.8 MHz, DCM, 25.0 °C) δ : 101.7 (s).

4.9.3.3 – Synthesis of *N*-(chlorophenylphosphanyl)-*N*'-methyl-*N*'-phenylbenzamidine, **13a'**:

Off-white solid, 72.3 % yield. $^1\text{H NMR}$ (400 MHz, THF, 23.0 °C) δ : 7.82-7.77 (m, 2H), 7.33-7.28 (m, 2H), 7.17-7.09 (m, 6H), 7.09-7.04 (m, 2H), 6.98 (t, $J = 1.5, 7.1$ Hz, 1H), 3.29 (s, 3H). $^{31}\text{P NMR}$ (161.8 MHz, DCM, 17.9 °C) δ : 123.7 (s).

4.9.4 – Synthesis of *N,N'*-Diarylureas

N,N'-diarylureas were prepared *via* standard literature procedures through condensation of a substituted aniline with phenylisocyanate.³⁴ The synthesis of **16a** is given as exemplar.

4.9.4.1 – Synthesis of *N,N'*-diphenylurea, **16a**:

Phenylisocyanate (5.0 cm³, 46 mmol) and Et₃N (13.0 cm³, 93 mmol) were dissolved in DCM (30 cm³) and cooled to 0 °C. Aniline (5 cm³, 55 mmol) was added dropwise affording a fine colourless precipitate. The reaction mixture was stirred at room temperature for 15 hours, after which the supernatant was removed *via* filter cannula and the colourless solids were washed with DCM (2 x 10 cm³) and dried *in vacuo*. Yield: 9.34 g (44 mmol, 95.7 %). $^1\text{H NMR}$ (400 MHz, THF, 25.0 °C) δ : 7.71 (bs, 2H), 7.40 (d, $J = 7.8$ Hz, 4H), 7.14 (t, $J = 7.7, 8.3$ Hz, 4H), 6.85 (t, $J = 7.3, 7.4$ Hz, 2H).

Analytical data in accordance with the literature.³⁴

4.9.4.2 – Synthesis of *N*-3-methoxyphenyl-*N'*-diphenylurea, **16f**:

Colourless solid, 87.4 % yield. $^1\text{H NMR}$ (400 MHz, THF, 25.7 °C) δ : 7.75 (d, $J = 6.9$ Hz, 2H), 7.41 (d, $J = 7.8$ Hz, 2H), 7.24 (t, $J = 2.1, 2.2$ Hz, 1H), 7.15 (t, $J = 7.7, 8.2$ Hz, 2H), 7.03 (t, $J = 8.0, 8.2$ Hz, 1H), 6.87 (t, $J = 7.3, 7.6$ Hz, 1H), 6.83 (m, 1H), 6.45 (dd, $J = 2.4, 8.2$ Hz, 1H), 3.68 (s, 3H). $^{13}\text{C}\{^1\text{H}\}$ NMR (100.5 MHz, THF, 26.8 °C) δ : 160.7, 152.5, 141.5, 140.3, 129.3, 128.7, 122.0, 118.6, 110.7, 107.7, 104.5, 54.6.

Analytical data in accordance with the literature.³⁴

4.9.4.3 – Synthesis of *N*-3-dimethylaminophenyl-*N'*-diphenylurea, **16r**:

Colourless solid, 73.6 % yield. $^1\text{H NMR}$ (400 MHz, THF, 19.2 °C) δ : 7.75 (bs, 1H), 7.68 (bs, 1H), 7.41 (d, $J = 7.7$ Hz, 2H), 7.14 (t, $J = 7.6, 8.3$ Hz, 2H), 7.05 (t, $J = 2.2$ Hz, 1H), 6.96 (t, $J = 8.0, 8.2$ Hz, 1H), 6.85 (t, $J = 7.3, 7.4$ Hz, 1H), 6.57 (dd, $J = 1.7, 7.6$ Hz, 1H), 6.29 (dd, $J = 2.4, 8.3$ Hz, 1H), 2.84 (s, 6H). $^{13}\text{C}\{^1\text{H}\}$ NMR (100.5 MHz, THF, 20.3 °C) δ : 152.7, 151.6, 140.9, 140.5, 129.0, 128.7, 121.8, 118.5, 107.2, 106.9, 103.3, 40.0.

4.9.5 – Synthesis of 1,2,4-Benzophosphadiazines

The 1,2,4-benzophosphadiazine **17r** derived from electron-rich *N,N'*-diarylurea **16r** was prepared according to literature procedures. All other 1,2,4-benzophosphadiazines were synthesised *via* alternative methods. Attempts to prepare and isolate clean samples of **20r** and **21r** were unsuccessful.

4.9.5.1 – Synthesis of 1,2-diphenyl-6-dimethylamino-4-hydro-1,2,4-benzophosphadiaz-3-one, **17r**:

16r (94 mg, 0.37 mmol) was dissolved in pyridine (1.5 cm³) and added dropwise to a solution of PhPCl₂ (50 μm^3 , 0.37 mmol) in pyridine (1.5 cm³) at 0 °C. The yellow reaction mixture was warmed to room temperature and after 3 days, Et₃N (150 μm^3 , 1.08 mmol) was added. The solvent was removed *in vacuo* and the residues were extracted into toluene (2 x 5 cm³) and decanted *via* filter cannula. The filtrate was evaporated to dryness and the crude solids were washed with MeCN (2 x 2.5 cm³) to give **17r** as a colourless solid. Yield: 26 mg (0.07 mmol, 19.8 %). $^1\text{H NMR}$ (400 MHz, DCM, 18.5 °C) δ : 8.55 (bs, 1H), 7.44-7.21 (m, 11H), 6.51 (d, $J = 8.0$ Hz, 1H), 6.21 (bs, 1H), 2.91 (s, 6H). $^{31}\text{P NMR}$ (161.8 MHz, DCM, 18.2 °C) δ : 35.6 (s). $^{13}\text{C}\{^1\text{H}\}$ NMR (100.5 MHz, DCM, 18.4 °C) δ : 155.9 (d, $J_{\text{C-P}} = 7.7$ Hz), 152.6 (s), 143.5 (d, $J_{\text{C-P}} = 18.2$ Hz), 142.5 (s), 140.8 (d, $J_{\text{C-P}} = 26.8$ Hz), 132.3 (d, $J_{\text{C-P}} = 46.0$ Hz), 129.7 (d, $J_{\text{C-P}} = 20.1$ Hz), 129.3 (s), 128.9 (s), 128.7 (d, $J_{\text{C-P}} = 5.8$ Hz), 127.6 (d, $J_{\text{C-P}} = 6.7$ Hz), 126.4 (s), 107.6 (d, $J_{\text{C-P}} = 14.4$ Hz), 98.9 (s), 40.4 (s).

4.9.5.2 – Synthesis of 1,3-diphenyl-6-dimethylamino-2,4-dihydro-1,2,4-benzophosphadiazine chloride, **19r.HCl**:

1r (0.71 g, 2.95 mmol) and K₂CO₃ (0.82 g, 5.90 mmol) were combined in DCM (35 cm³) and cooled to 0 °C. PhPCl₂ (0.4 cm³, 2.95 mmol) was added dropwise, giving an immediate yellow suspension. The reaction mixture was slowly warmed to room temperature and stirred for 14 hours. The suspension was filtered through celite and the solids were washed with DCM (2 x 10 cm³). The combined filtrate was evaporated to dryness and the resulting oil was triturated with hot MeCN (5 cm³), washed with

Et₂O (2 x 5 cm³) and dried *in vacuo* to give a pale yellow solid. Yield: 0.99 g (2.59 mmol, 87.7 %). **¹H NMR** (400 MHz, DCM, 25.0 °C) δ: 13.30 (bs, 1H), 10.96 (d, *J*_{H-P} = 26.6 Hz, 1H), 8.32 (s, 1H), 8.06 (d, *J* = 7.6 Hz, 2H), 7.39-7.08 (m, 10H), 3.00 (s, 6H). **³¹P NMR** (161.8 MHz, DCM, 25.0 °C) δ: 4.6 (m).

4.9.5.3 – Synthesis of 1,3-diphenyl-6-dimethylamino-2-hydro-1,2,4-benzophosphadiazine, **19r**:

19r.HCl (0.66 g, 1.73 mmol) was partially dissolved in DCM (20 cm³) and Et₃N (0.24 cm³, 1.73 mmol) was added. The yellow solution was stirred for 30 minutes and then evaporated to dryness. The residues were extracted into hot toluene (2 x 15 cm³) and filtered, concentrated to *ca.* 5 cm³ *in vacuo* and stored at -20 °C overnight. The supernatant was removed *via* filter cannula, and the pale yellow crystalline solids were washed with Et₂O (5 cm³) and dried *in vacuo*. Yield: 0.32 g (0.91 mmol, 52.8 %). **¹H NMR** (400 MHz, DCM, 25.0 °C) δ: 7.88 (d, *J* = 7.5 Hz, 2H), 7.50-7.40 (m, 3H), 7.30-7.20 (m, 5H), 6.77 (bs, 1H), 6.66 (d, *J* = 8.1 Hz, 1H), 6.07 (bs, 1H), 3.01 (s, 6H). **³¹P NMR** (161.8 MHz, DCM, 25.0 °C) δ: 0.2 (bs). **¹³C{¹H} NMR** (100.5 MHz, DCM, 19.4 °C) δ: 153.0 (s), 152.7 (d, *J*_{C-P} = 8.8 Hz), 143.7 (d, *J*_{C-P} = 27.9 Hz), 137.0 (s), 132.6 (d, *J*_{C-P} = 44.8 Hz), 130.8 (s), 129.8 (d, *J*_{C-P} = 19.8 Hz), 129.0 (s), 128.7 (s), 128.4 (d, *J*_{C-P} = 5.9 Hz), 127.2 (s), 110.1 (d, *J*_{C-P} = 14.7 Hz), 40.3 (s).

4.9.5.4 – Synthesis of 1-methyl-1,3-diphenyl-6-dimethylamino-4-hydro-1,2,4-benzodiazaphosphonium iodide, **22r.HI**:

To a suspension of NaH (0.24 g, 10.0 mmol) in DMF (15 cm³) was dropwise added a solution of **19r.HCl** (0.76 g, 2.0 mmol) in DMF (15 cm³) at 0 °C. The yellow reaction mixture was allowed to warm to room temperature and stir for 1 hour, then cooled back down to 0 °C. MeI (0.13 cm³, 2.0 mmol) was added dropwise and the yellow reaction mixture was again allowed to warm to room temperature and stir for 1 hour. The solvent was removed *in vacuo* and the residues were extracted into DCM (2 x 15 cm³) and filtered through celite. The combined filtrate was washed with water and brine (15 cm³), dried over MgSO₄, filtered and evaporated to dryness. Recrystallisation of the crude solids from DCM and Et₂O afforded **22r.HI** as pale yellow needles. Yield: 0.14 g (0.3 mmol, 15.0 %). **¹H NMR** (400 MHz, DCM, 20.4 °C) δ: 11.35 (bs, 1H), 8.50 (d, *J*_{H-H} = 7.8 Hz, 2H), 8.13 (dd, *J*_{H-H} = 2.3 Hz, *J*_{H-P} = 5.1 Hz, 1H), 7.75 (d, *J*_{H-P} = 13.6 Hz, 1H), 7.73 (dd, *J*_{H-H} = 1.5 Hz, *J*_{H-P} = 13.6 Hz, 1H), 7.66 (m, 1H), 7.62-7.54 (m, 3H), 7.47 (t, *J*_{H-H} = 7.5, 7.8 Hz, 2H), 7.35 (d, *J*_{H-H} = 8.9 Hz, *J*_{H-P} = 11.9 Hz, 1H), 6.74 (dt, *J*_{H-H} = 2.2, 8.9 Hz, 1H), 3.09 (s, 6H), 2.40 (d, *J*_{H-P} = 13.9 Hz, 3H). **³¹P NMR** (161.8 MHz, DCM, 19.7 °C) δ: 17.8 (m). **¹³C{¹H} NMR** (100.5 MHz, DCM, 20.5 °C) δ: 161.6 (d, *J*_{C-P} = 8.8 Hz), 154.7 (d, *J*_{C-P} = 1.5

Hz), 142.6 (d, $J_{C-P} = 4.4$ Hz), 133.9 (d, $J_{C-P} = 2.9$ Hz), 133.2 (s), 132.4 (d, $J_{C-P} = 16.9$ Hz), 130.6 (d, $J_{C-P} = 11.7$ Hz), 130.2 (d, $J_{C-P} = 8.1$ Hz), 129.6 (d, $J_{C-P} = 13.2$ Hz), 129.5 (d, $J_{C-P} = 1.5$ Hz), 128.9 (d, $J_{C-P} = 107.8$ Hz), 128.5 (s), 111.9 (d, $J_{C-P} = 11.7$ Hz), 102.0 (d, $J_{C-P} = 5.9$ Hz), 84.2 (d, $J_{C-P} = 94.6$ Hz), 40.5 (s), 16.6 (d, $J_{C-P} = 78.5$ Hz).

4.9.5.5 – Synthesis of 1-diphenylphosphanyl-1,3-diphenyl-6-dimethylamino-4-hydro-1,2,4-benzodiazaphosphonium chloride, 23r.HCl:

19r.HCl (0.21 g, 0.56 mmol) and Et₃N (0.16 cm³, 1.12 mmol) were dissolved in DCM (15 cm³) and cooled to 0 °C. Ph₂PCl (0.1 cm³, 0.56 mmol) was added dropwise and the yellow solution was allowed to warm to room temperature and stir for 12 hours. The solvent was removed *in vacuo* and the residues extracted into toluene (2 x 10 cm³) and filtered. Concentration of the combined filtrate to *ca.* 5 cm³ gave a pale yellow precipitate that was isolated by filtration and dried *in vacuo*. Yield: 0.03 g (0.05 mmol, 8.6 %). ¹H NMR (400 MHz, DCM, 23.0 °C) δ: 12.68 (bs, 1H), 8.40 (d, $J = 7.4$ Hz, 2H), 7.90 (d, $J = 7.3$ Hz, 1H), 7.87 (d, $J = 7.3$ Hz, 1H), 7.79 (t, $J = 7.9, 8.3$ Hz, 2H), 7.61-7.33 (m, 10H), 7.28 (d, $J = 8.8$ Hz, 1H), 7.26 (d, $J = 8.9$ Hz, 1H), 7.14 (t, $J = 4.5, 4.8$ Hz, 4H), 6.66 (dt, $J = 2.4, 8.9$ Hz, 1H), 3.04 (s, 6H). ³¹P{¹H} NMR (161.8 MHz, DCM, 23.0 °C) δ: 21.9 (d, $^1J_{P-P} = 267.7$ Hz), -19.1 (d, $^1J_{P-P} = 267.7$ Hz).

4.10 - References

- 1 R. Engel and J. I. Cohen, *Synthesis of Carbon-Phosphorus Bonds*, CRC Press, Raton, 2004.
- 2 H. R. Pickard and J. Kenyon, *J. Chem. Soc.*, 1906, 262–273.
- 3 E. S. S. A and W. Chodkiewicz, *J. Organomet. Chem.*, 1984, **273**, 55–56.
- 4 D. M. Volochnyuk, A. O. Pushechnikov, D. G. Krotko, A. M. Pinchuk and A. A. Tolmachev, *Synthesis*, 2005, 3124–3134.
- 5 Michaelis, *Ber.*, 1879, **12**, 1009.
- 6 T. Ito, T. Iwai, T. Nakai, M. Mihara, T. Mizuno, T. Ohno, A. Ishikawa and J. ichi Kobayashi, *Heteroat. Chem.*, 2016, **27**, 336–342.
- 7 Z. W. Wang and L. S. Wang, *Green Chem.*, 2003, **5**, 737–739.
- 8 J. M. Rawson, A. Alberola and A. Whalley, *J. Mater. Chem.*, 2006, **16**, 2560.
- 9 R. G. Hicks, *Org. Biomol. Chem.*, 2007, **5**, 1321.
- 10 C. P. Constantinides, P. A. Koutentis and J. M. Rawson, *Chem. Eur. J.*, 2012, **18**, 15433–15438.
- 11 C. P. Constantinides, A. A. Berezin, M. Manoli, G. M. Leitus, M. Bendikov, J. M. Rawson and P. A. Koutentis, *New J. Chem.*, 2014, **38**, 949–954.
- 12 C. P. Constantinides, A. A. Berezin, M. Manoli, G. M. Leitus, G. A. Zissimou, M. Bendikov, J. M. Rawson and P. A. Koutentis, *Chem. Eur. J.*, 2014, **20**, 5388–5396.
- 13 C. P. Constantinides, P. A. Koutentis, H. Krassos, J. M. Rawson and A. J. Tasiopoulos, *J. Org. Chem.*, 2011, **76**, 2798–2806.
- 14 P. Kaszyński, C. P. Constantinides and V. G. Young, *Angew. Chem. Int. Ed.*, 2016, **55**, 11149–11152.
- 15 Y. Miura and N. Yoshioka, *Chem. Phys. Lett.*, 2015, **626**, 11–14.
- 16 G. S. Borovikova, F. Tsymbal, I. E. C. Levchenko and E. I. Borovik, *Zhurnal Org. Khimii*, 1984, **20**, 1784–1790.
- 17 E. S. Levchenko, G. S. Borovikova, E. I. Borovik and V. V. Kalinin, *Russ. J. Org. Chem.*, 1984, **20**, 176–181.
- 18 A. O. Pushechnikov, D. G. Krotko, D. M. Volochnyuk and A. A. Tolmachev, *Chem. Heterocycl. Compd.*, 2001, **37**, 710–712.
- 19 J. L. Paporin, A. Amador, E. Badaroux, S. Bot, C. Caillet, T. Convard, D. Da Costa, D. Dukhan, L. Griffe, J. F. Griffon, M. LaColla, F. Leroy, M. Liuzzi, A. Giulia Loi, J. McCarville, V. Mascia, J. Milhau, L. Onidi, C. Pierra, R. Rahali, E. Rosinosky, E. Sais, M. Seifer, D. Surleraux, D. Standring and C. B. Dousson, *Bioorganic Med. Chem. Lett.*, 2017, **27**, 2634–2640.
- 20 C. Pierra Rouvière, A. Amador, E. Badaroux, T. Convard, D. Da Costa, D. Dukhan, L.

- Griffe, J. F. Griffon, M. LaColla, F. Leroy, M. Liuzzi, A. G. Loi, J. McCarville, V. Mascia, J. Milhau, L. Onidi, J. L. Paporin, R. Rahali, E. Sais, M. Seifer, D. Surleraux, D. Standing and C. Dousson, *Bioorganic Med. Chem. Lett.*, 2016, **26**, 4536–4541.
- 21 J. P. Harger, Martin and R. Sreedharan-Menon, *J. Chem. Soc., Perkin Trans.*, 1994, 3261–3267.
- 22 J. M. Rawson and G. D. McManus, *Coord. Chem. Rev.*, 1999, **189**, 135–168.
- 23 G. M. Kosolapoff and W. Frederick Huber, *J. Am. Chem. Soc.*, 1947, **69**, 2020–2021.
- 24 B. L. Booth, K. O. Jibodu and M. F. Proença, *J. Chem. Soc., Chem. Commun.*, 1980, 1151–1153.
- 25 Z. C. Shen, P. Yang and Y. Tang, *J. Org. Chem.*, 2016, **81**, 309–317.
- 26 S. I. R. Alexander, *J. Chem. Soc.*, 1949, 449–456.
- 27 E. Despagnet-Ayoub and R. H. Grubbs, *J. Am. Chem. Soc.*, 2004, **126**, 10198–10199.
- 28 A. O. Pushechnikov, D. M. Volochnyuk, D. G. Krotko, A. K. Tyltin and A. A. Tolmachev, *Chem. Heterocycl. Compd.*, 2001, **37**, 656–658.
- 29 I. K. Khanna, Y. Yu, R. M. Huff, R. M. Weier, X. Xu, F. J. Koszyk, P. W. Collins, J. N. Coghburn, P. C. Isakson, C. M. Koboldt, J. L. Masferrer, W. E. Perkins, K. Seibert, A. W. Veenhuizen, J. Yuan, D. Yang and Y. Y. Zhang, *Synthesis*, 2000, 3168–3185.
- 30 F. D. Bellamy and K. Ou, *Tetrahedron Lett.*, 1984, **25**, 839–842.
- 31 L. Beer, R. C. Haddon, M. E. Itkis, A. A. Leitch, R. T. Oakley, R. W. Reed, J. F. Richardson, D. G. VanderVeer, L. Beer, J. L. Brusso, A. W. Cordes, R. C. Haddon, M. E. Itkis, K. Kirschbaum, D. S. MacGregor, R. T. Oakley, A. A. Pinkerton and R. W. Reed, *Chem. Commun.*, 2005, **124**, 1218–1220.
- 32 Z. Chen, C. S. Wannere, C. Corminboeuf, R. Puchta and P. V. R. Schleyer, *Chem. Rev.*, 2005, **105**, 3842–3888.
- 33 A. G. Orpen, L. Brammer, F. H. Allen, O. Kennard, D. G. Watson and R. Taylor, *J. Chem. Soc., Dalt. Trans.*, 1987, S1–S83.
- 34 M. Blain, H. Yau, L. Jean-Gérard, R. Auvergne, D. Benazet, P. R. Schreiner, S. Caillol and B. Andrioletti, *ChemSusChem*, 2016, **9**, 2269–2272.

Chapter 5

Structural Diversity in Phosphorus-Nitrogen Heterocycles

"I need your clothes, your boots and your heterocycles."

Terminator 2: Judgement Day (1991) [Paraphrased]

Whilst the chemistry of cyclophosphazines bearing alkoxy, aryloxy and amide functionalities is extensive, prepared by nucleophilic substitution of the P-X precursor, systems bearing P-R bonds have received considerably less attention. These are mostly restricted to aryl and alkyl derivatives, and are prepared from the corresponding RPCl_2 species. Substitution reactions of the P-X precursors with RLi and RMgX reagents may also be used, but these are known to often cleave P-N bonds.²¹ This approach however has been successfully employed to prepare alkynyl-functionalised cyclophosphadiazines which on treatment with $[\text{Rh}(\text{CO})_2\text{Cl}]_2$ afforded a rhodium(I) pentameric macrocycle.²²

Cyclophosphadiazines are known to exist as geometrical isomers (Figure 5.1.1.1), with the *cis* isomer being more thermodynamically favoured while the *trans* isomer is the kinetic product.⁷ The *cis* isomers tend to form puckered P_2N_2 rings, whereas the *trans* isomers are planar. The choice of substituent on both phosphorus and nitrogen is the major factor in determining which isomer is formed, with bulky substituents favouring the *trans* isomer.²¹ Solution state NMR studies provide a simple way to differentiate between the isomers, as well as a means of probing the *cis-trans* equilibrium, due to the markedly different ^{31}P NMR chemical shifts observed.²³

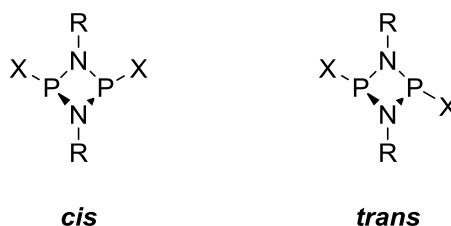


Figure 5.1.1.1: Geometrical isomers of cyclophosphadiazines.

Despite being perhaps the simplest class of $\text{P}^{\text{III}}\text{-N}$ heterocycle, the chemistry of cyclophosphazines illustrates the complex and diverse library of compounds that are accessible for simple primary amines and halophosphines.²¹ The tendency for P-N systems to form oligomeric species may however be exploited to form polymers of the type $[-\text{XPNR-}]_n$ which, due to their remarkable tunability, have found well-established uses as high-performance elastomers and flame-retardant coatings,²⁴ with emerging uses in biomedical applications.²⁵ The pioneering work of Wright into the P_2N_2 -based macrocycles continues, with current work focusing on developing reliable synthetic methodologies and further exploring their coordination chemistry.²⁶

5.1.2 – Cyclophosph(V)azenes

Cyclophosph(V)azenes, cyclic species made up of alternating P^V and N single and double bonds, were first synthesised by Liebig in 1832 through the reaction of PCl₅ and NH₃. This yielded a mixture of the trimeric (**D**) and tetrameric (**E**) species (Figure 5.1.2.1), which can be separated by fractional sublimation. The trimeric species undergoes ring-opening polymerisation at elevated temperatures (> 250 °C) to afford poly(dichlorophosphazenes) of the formula [NPCl₂]_n.²⁷ Replacement of the chlorine groups by organic substituents gives polyphosphazenes which have found use in a plethora of applications and are the subject of several reviews.^{24,25} The utility of cyclophosph(V)azenes themselves has also been explored, primarily as flame-retardant materials²⁸ and as ligands to metals.²⁹

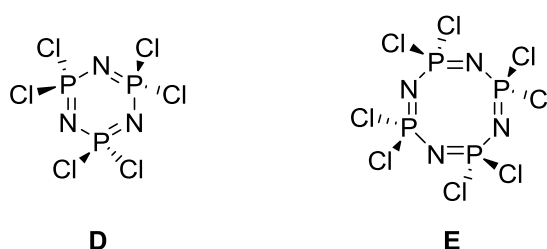


Figure 5.1.2.1: Trimeric and tetrameric cyclophosph(V)azenes.

5.1.3 – Urea-Ligated Phosphorus Heterocycles

The first reported phosphorus-urea heterocycle was synthesised in 1964 through the reaction of *N,N'*-disubstituted ureas with PCl₅ to give either **F** (Figure 5.1.3.1) or the chloroformamidine hydrochloride depending on the nature of the substituents.³⁰ This four-membered heterocycle was later treated with a second equivalent of 1,3-disubstituted urea to give the spirocyclic compound **G**;³¹ there are no reports of the octahedral anion which may be accessible when R = R' = Me.

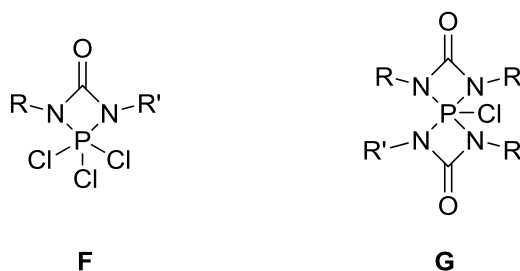


Figure 5.1.3.1: Phosphorus(V)-urea heterocycles.

In contrast, the reaction of *N,N'*-disubstituted silylated-ureas with aryl-dichlorophosphines afforded the spirobicyclic compound **H** (Figure 5.1.3.2) with the first reported $\lambda^3\text{P}-\lambda^5\text{P}$ bond.^{31,32} It is presumed that compound **I** is initially formed, one molecule of which undergoes phosphorus-nitrogen bond cleavage followed by oxidative addition to an intact ring. It was originally hypothesised that the phosphorus-

substituent only influenced the chemical and thermal-stability but not the constitution of the compound formed, however the use of strongly electron withdrawing groups ($R'' = C_2F_5$) produced the four-membered monocycle **I** as a distillable liquid.³³ Later reports claimed that the reaction of *protio-N,N'*-diphenylurea with $PhPCl_2$ in the presence of base gave a different λ^3P - λ^5P heterocycle, **J**, which must also yield one equivalent of the corresponding carbodiimide through deoxygenation.³

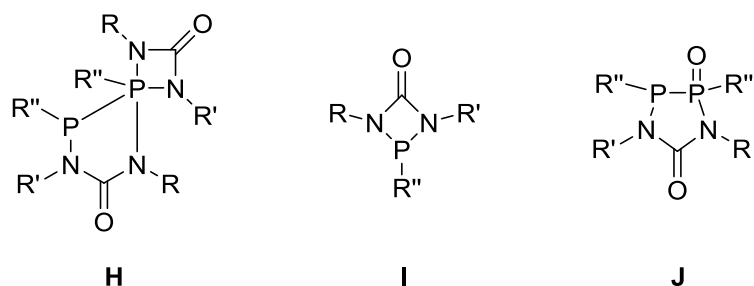


Figure 5.1.3.2: Phosphorus(III) and mixed P^{III}/P^V -urea heterocycles derived from $RPCL_2$.

The reaction of *N,N'*-disubstituted silylated-ureas with PCl_3 was initially believed to form a bicyclic compound with a P-O-P bridge³¹ but was later shown to form compound **K** (Figure 5.1.3.3) through variable temperature NMR and X-ray crystallography.³³ When $R = Me$, the formation of **L** was instead observed along with a solid residue which contained the six-membered heterocycle **M**. When the order of addition of the reagents was reversed, compounds **K** and **N** were formed.³³ The four-membered monocycle, **O**, has not been observed. The bicyclic λ^3P - λ^5P heterocycle, **K**, may also be formed from the *protio-N,N'*-diphenylurea and PCl_3 at reflux in the presence of base.³

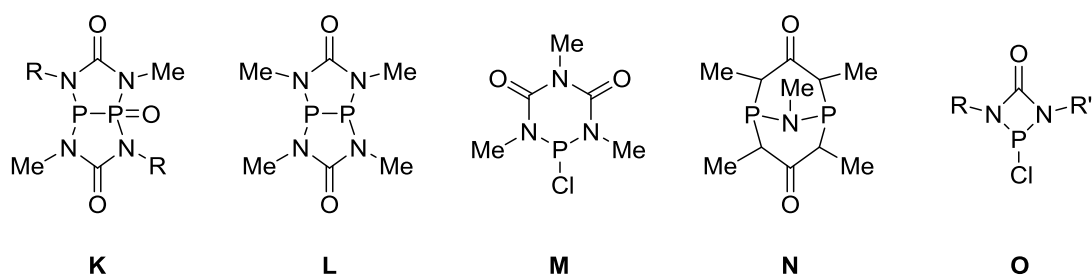


Figure 5.1.3.3: Phosphorus(III) and mixed P^{III}/P^V -urea heterocycles derived from PCl_3 .

Despite later papers describing the herbicidal activity³ of phosphorus-urea heterocycles, they have found limited application and hence received little attention in recent years. Whilst the structural diversity of the compounds produced was the primary point of interest, binding towards metal carbonyls and further reactivity has also been explored.³⁴ *N,N'*-diarylureas have more recently been employed in the

construction of fused-ring phosphorus-nitrogen heterocycles under mild conditions (See Chapter 4).³⁵

5.1.4 – Phosphorus-Amidinate Chemistry

The coordination chemistry of *N,N'*-disubstituted amidinates is well established for the transition metals, with the bridging **P** and chelating **Q** binding modes being the most common (Figure 5.1.4.1).³⁶⁻³⁸ These are typical for symmetric *mono*-anionic ligands although for the latter considerable steric strain occurs in the four-membered ring. In contrast, much less is known about complexes involving the main-group elements.³⁹ Earlier studies investigated the group 13 elements and aimed to determine how the variation in R groups of the amidinate ligand affects the degree of association of the complexes. The group 13 trihalides (M = B, Al, Ga, In) formed monomeric chelating complexes for amidines bearing sufficiently bulky groups (R = SiMe₃, Ph; R' = SiMe₃, Ph).⁴⁰ Monomeric species were also observed for the MMe₃ derived complexes (M = Ga, Al) but formed bridging dimers **R** featuring an eight-membered puckered ring when R = R' = Me.⁴¹ The MMe-*bis*-amidinate and M-*tris*-amidinate complexes can also be accessed through controlled sequential addition of *protio*-amidine, although forcing conditions are required.

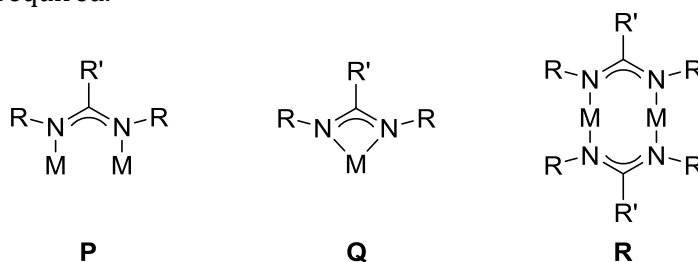


Figure 5.1.4.1: Binding modes of amidinate ligands.

The amidinate ligand can act as both a bridging and chelating ligand simultaneously to magnesium depending on the ligand substituents, and these complexes have found use in bond forming catalytic reactions and to promote the Tishchenko reaction.⁴² Amidinates have also been employed in the synthesis of four-membered *N*-heterocyclic silylenes and germylenes, which have been used to prepare catalytically active metal complexes or can act as catalysts in their own right.^{43,44} Sterically bulky amidinates can impart significant kinetic stability to low-valent group 14 (I) dimers, including the first tin (I) dimer, which are potentially useful for small molecule activation.⁴⁵

Despite their promising chemistry with main-group elements, the binding of amidines to phosphorus has yet to be explored. The closest examples were by Grubbs in 2004 who produced the first four-membered *N*-heterocyclic carbene **S** (Figure 5.1.4.2) from

the corresponding silylated-formamidine and amidodichlorophosphine followed by deprotonation. Related systems have been prepared by Wright in 2015 with dichlorodiphosphadiazines to give hybrid phosphazine/NHC systems **T**.

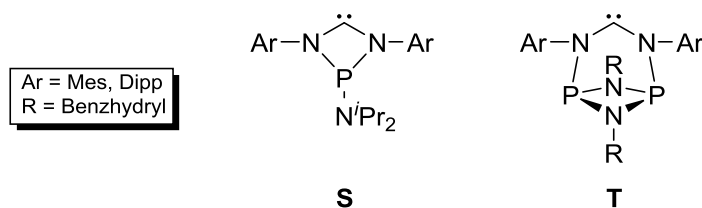


Figure 5.1.4.2: Phosphorus-formamidinate NHCs.

Mono-substituted *N*-arylamidines, on the other hand, have found limited use as asymmetric *di*-anionic ligands. The coordination mode adopted by amidinates is largely dependent on the steric bulk on the nitrogen atoms, with bulkier substituents favouring chelation, and smaller substituents favouring a bridging motif. As such, the range of coordination modes accessible to asymmetric *di*-anionic amidinates is expected to lead to considerable structural diversity; a selection of possible coordination modes are shown in Figure 5.1.4.3.

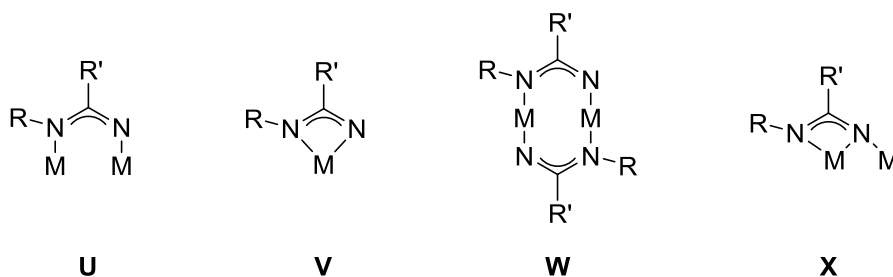
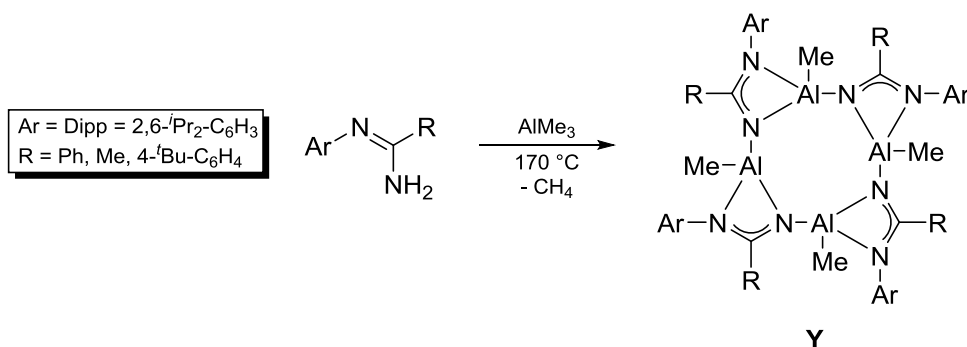


Figure 5.1.4.3: Possible coordination modes of asymmetric *di*-anionic amidinates.

The reactions of *mono*-substituted *N*-arylamidines with AlMe_3 was first reported in 2010 by Reddy⁴⁶ and later expanded the following year.⁴⁷ For bulky amidines the formation of tetrameric aluminium amidinates **Y** were observed (Scheme 5.1.4.1), adopting the **X** coordination mode ($\mu_2\text{-}\eta^1\text{-}\eta^2$).

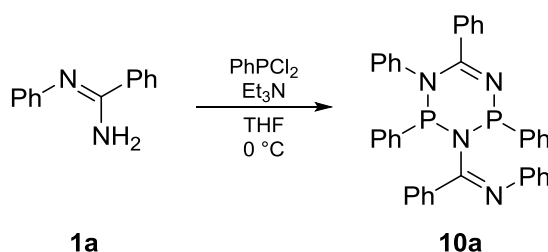


Scheme 5.1.4.1: Reaction of *N*-arylamidines with AlMe_3 .

When the bulky aryl group is replaced by a phenyl ring, the formation of tetracyclic triazaalanes, comprised of fused six-membered Al_2CN_3 rings is observed as a mixture of isomers. Replacement of AlMe_3 with $\text{GaMe}_3\cdot\text{OEt}_2$ gave analogous compounds in most cases, whilst the use of AlMeCl_2 gave bicyclic triazaalanes.⁴⁸ These studies highlight the complex E-N-C (E = Al, Ga) frameworks that can be formed from *mono*-substituted *N*-arylamidines and illustrate that the steric bulk of the *N*-aryl group significantly influences the coordination mode adopted.

5.2 – Reactions of *N*-Arylamidines with PhPCl_2

During the attempted syntheses of fused-ring 1,2,4-benzophosphadiazines, discussed in Chapter 4, the reaction of *N*-phenylbenzamidine **1a** with PhPCl_2 under mild conditions unexpectedly gave the six-membered heterocycle **10a** (Scheme 5.2.1). Similar systems have been observed for the reaction of chlorostannylenes and chlorogermolenes with diimidosulfinates.⁴⁹



Scheme 5.2.1: Reaction of *N*-phenylbenzamidine **1a** with PhPCl_2 .

In light of this interesting result, we decided to further explore this behaviour and examine whether similar reactivity would be observed with other *mono*-substituted *N*-arylamidines.

5.2.1 – *N*-Phenylbenzamidine

The reaction of *N*-phenylbenzamidine with PhPCl_2 in the presence of base cleanly affords a single species which exhibits two sharp singlets of equal intensity in the ^{31}P NMR spectrum at $\delta + 54.2$ and $+ 39.1$ ppm. Single crystals suitable for X-ray diffraction, grown by slow diffusion of hexane into a saturated solution of the product in DCM, revealed the formation of a six-membered P_2CN_3 heterocycle **10a** from two equivalents each of amidine and phosphine.

Compound **10a** crystallises as pale yellow plates in the triclinic space group $P\bar{1}$ with a single molecule in the asymmetric unit (Figure 5.2.1.1). The P_2CN_3 heterocyclic ring adopts a distorted envelope conformation, folded along the $\text{P}2\cdots\text{N}1$ axis by 36.4° , with the two *P*-phenyl rings in a *cis*-orientation. The $\text{P}2\text{-N}2$ and $\text{P}2\text{-N}3$ bond lengths are similar at $1.723(2)$ Å and $1.729(2)$ Å whilst the $\text{P}1\text{-N}1$ and $\text{P}1\text{-N}3$ bond lengths differ

significantly at 1.679(2) Å and 1.765(2) respectively; these values are still within the typical range of values observed for phosphorus-nitrogen single bonds.⁵⁰

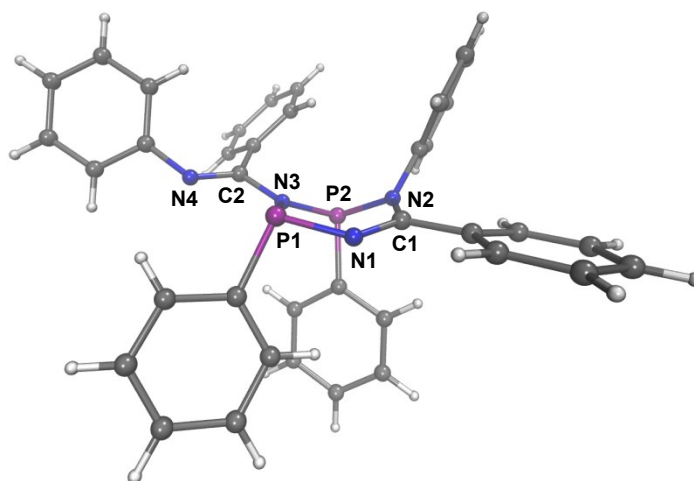


Figure 5.2.1.1: Crystal structure of **10a**.

One of the amidinate ligands (N1-C1-N2) in **10a** coordinates to two phosphorus atoms via a $\mu_2\text{-}\eta^1\text{-}\eta^1$ coordination mode whilst the second ligand binds in a $\mu_2\text{-}\eta^0\text{-}\eta^2$ monodentate fashion such that a single nitrogen centre (N3) is bonded to the two different phosphorus atoms. Both phosphorus atoms possess distorted trigonal-pyramidal geometries; the sum of bond angles around phosphorus are 310.1° and 302.3° for P1 and P2 respectively, and comparable to other N-P(R)-N fragments in cyclic structures.⁵¹

The DFT optimised geometry of **10a**, performed at the M062X/6-311g(d,p) level of theory, is in good agreement with the experimental crystallographic data. Whilst the calculated and experimental C-N bond lengths show excellent correlation, the P-N bond lengths are typically overestimated (Table 5.2.1.1). The Mayer bond indices are consistent with the assignment of single and double bonds within the structure.

	Bond Lengths / Å		Bond Index
	Experimental	Calculated	Mayer
C1-N1	1.281(3)	1.275	1.834
C1-N2	1.422(2)	1.412	0.965
N1-P1	1.679(2)	1.694	1.009
N2-P2	1.723(2)	1.740	0.890
N3-P1	1.765(2)	1.779	0.774
N3-P2	1.729(2)	1.744	0.846
N3-C2	1.399(2)	1.397	0.999
C2-N4	1.279(2)	1.279	1.784

Table 5.2.1.1: Selected experimental and calculated bond lengths, and Mayer bond indices for **10a**.

5.2.2 - *N*-3-Dimethylaminophenyl-benzamidine

When the electron-rich *N*-arylamidine **1r** was treated with PhPCl_2 under identical conditions, no evidence of the six-membered heterocycle **10r** was observed. Instead, the ^{31}P NMR spectrum exhibited a major pair of doublets at $\delta + 52.2$ and $+ 10.2$ ppm ($^1J_{\text{P-P}} = 245.1$ Hz), a minor pair of doublets at $\delta + 56.8$ and $+ 21.4$ ppm ($^1J_{\text{P-P}} = 232.6$ Hz), and other minor species. Initial attempts to grow crystals of these unknown species were unsuccessful and repeatedly gave crystals of the fused-ring 1,2,4-benzophosphadiazine **19r**. Subsequent NMR scale experiments showed that this species converts through to **19r** ($\delta - 0.1$ ppm) over the space of three days in solution at ambient temperature, and within 1 hour at 100 °C in PhCl (Figure 5.2.2.1). The disappearance of both pairs of doublets to form a single product **19r** initially suggested that these species may be conformational isomers, whilst later experiments instead suggested that the minor species was a protonated analogue (*vide infra*).

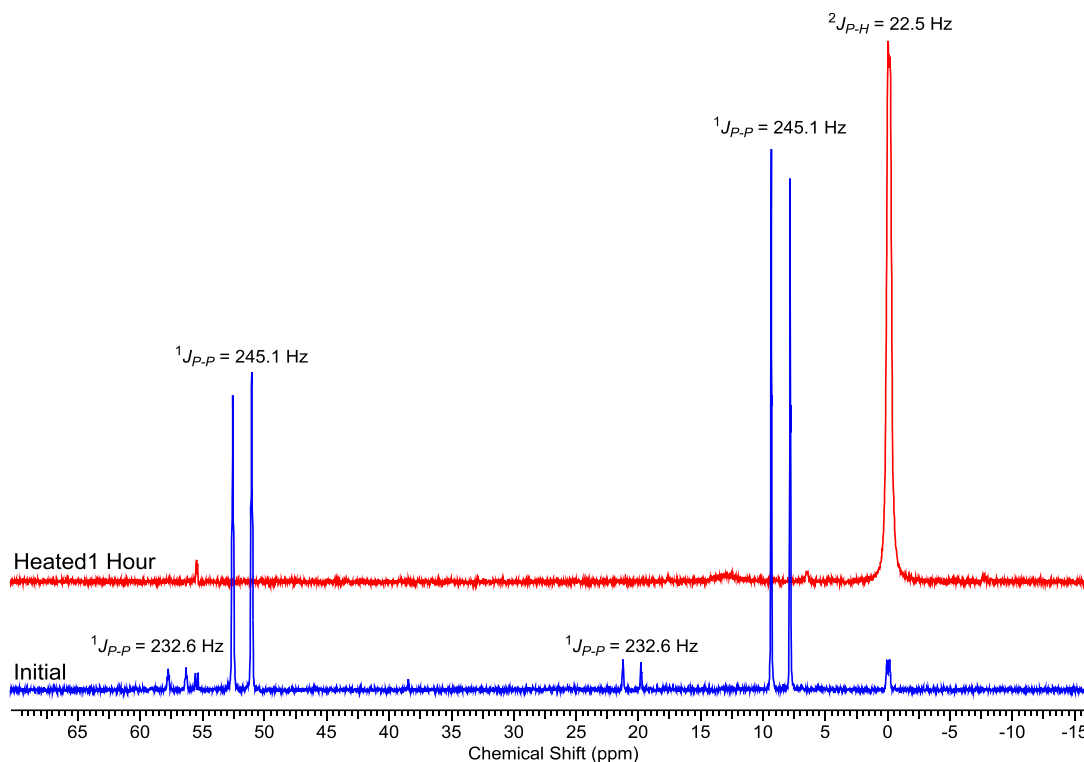
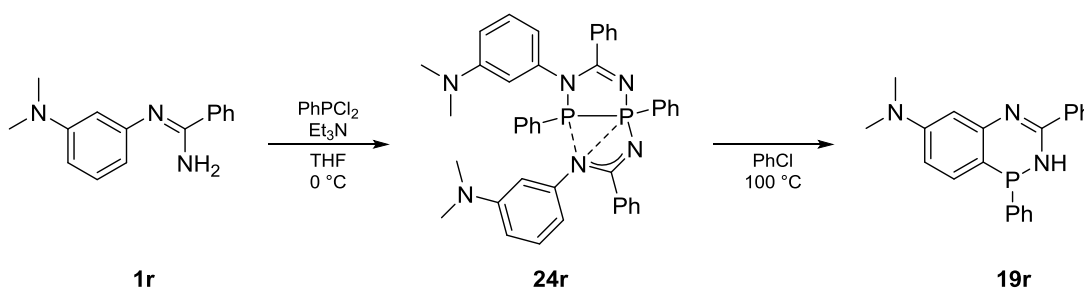


Figure 5.2.2.1: ^{31}P NMR spectra showing conversion through to the neutral 1,2,4-benzophosphadiazine **19r**.

Poor quality crystals of the unknown species, grown from a saturated toluene solution at $-20\text{ }^\circ\text{C}$, revealed the formation of the *pseudo*-bicyclic species **24r**. An overall scheme for the reaction of **1r** with PhPCl_2 is shown in Scheme 5.2.2.1.



Scheme 5.2.2.1: Reaction of electron-rich *N*-arylamidine **1r** with PhPCl_2 .

Compound **24r** crystallises as colourless plates in the triclinic space group $P\bar{1}$ with a single molecule in the asymmetric unit (Figure 5.2.2.2). The structure features a five-membered P_2CN_2 ring, in which both nitrogen atoms (N1 and N2) adopt a $\mu_2\text{-}\eta^1\text{-}\eta^1$ coordination mode, with a second amidinate fragment tethering from P1 in a η^1 monodentate fashion at N3. There are additional long contacts between $\text{N4}\cdots\text{P2}$ and $\text{N4}\cdots\text{P1}$ at $2.89(3)\text{ \AA}$ and $2.69(3)\text{ \AA}$ respectively, within the sum of the van der Waals

radii.⁵² The *P*-phenyl rings again adopt a *cis*-conformation, whilst the P1-P2 bond length is typical of P-P single bonds at 2.22(1) Å.⁵⁰

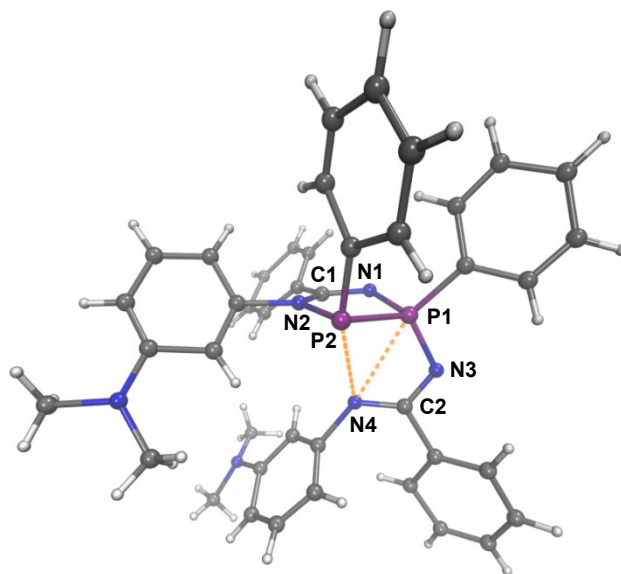


Figure 5.2.2.2: Crystal structure of **24r**.

The DFT optimised geometry is in good agreement with the experimental structure (Table 5.2.2.1) and replicates the connectivity and overall conformation of **24r**. The Mayer bond indices indicate that there is double-bond character delocalised across the tethered P1-N3-C2-N4 fragment and suggests that the N2-P2 and P1-P2 bonds are relatively weak (bond order < 1) such that P1 has a total bond order of 4.39 compared to P2 at 2.78. The N4...P2 and N4...P1 contacts are calculated to be longer than observed experimentally but still show small but significant N-P σ -bond character despite both N-P- C_{phenyl} angles deviating from linearity (experimental: 161.9(1)° / 162.8(1)°; calculated: 157.6°/162.2° for N4...P2- C_{phenyl} and N4...P1- C_{phenyl} respectively).

	Bond Lengths / Å		Bond Index
	Experimental	Calculated	Mayer
C1-N1	1.33(4)	1.300	1.708
C1-N2	1.43(4)	1.372	1.103
N1-P1	1.75(4)	1.676	1.079
N2-P2	1.74(4)	1.765	0.853
P1-P2	2.22(1)	2.242	0.807
P1-N3	1.63(3)	1.610	1.356
N3-C2	1.25(5)	1.362	1.342
C2-N4	1.30(4)	1.299	1.598
N4...P1	2.69(3)	2.761	0.059
N4...P2	2.89(3)	2.985	0.058

Table 5.2.2.1: Selected experimental and calculated bond lengths, and Mayer bond indices for **24r**.

The HOMO and HOMO -1 of **24r** are both delocalised over the electron-rich aryl rings, with significant electron density (22.8 % and 17.8 % respectively) at the positions *para* to the NMe₂ groups (Figure 5.2.2.3). This indicates that these positions are likely to be nucleophilic and supports the facile transformation to give the fused ring 1,2,4-benzophosphadiazine **19r**.

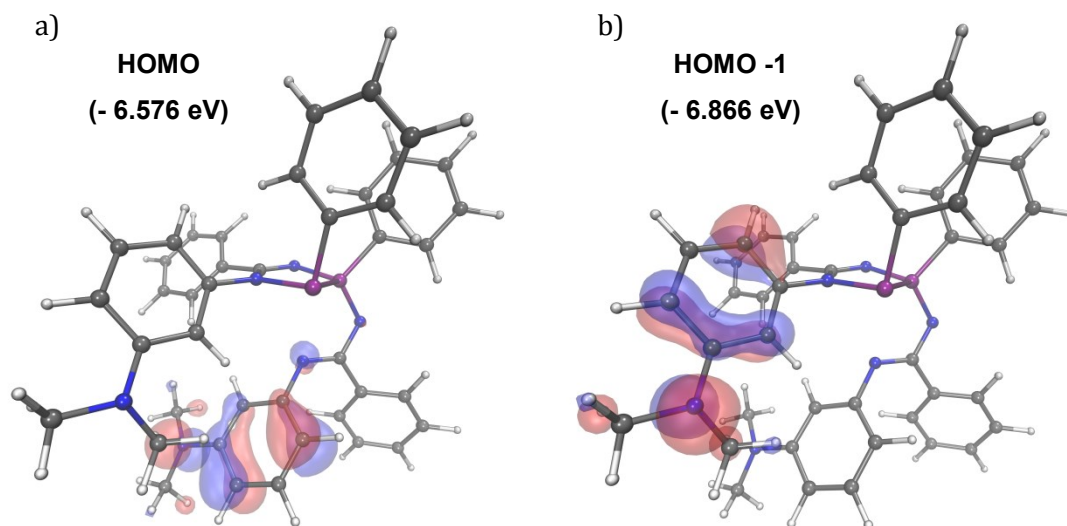


Figure 5.2.2.3: Highest occupied molecular orbitals and energies for **24r**: a) HOMO; b) HOMO -1 (isovalue = 0.05).

In contrast, the LUMO is delocalised across the P₂CN₂ heterocyclic ring whilst the LUMO +1 corresponds to a P2-P1 antibonding interaction (Figure 5.2.2.4)

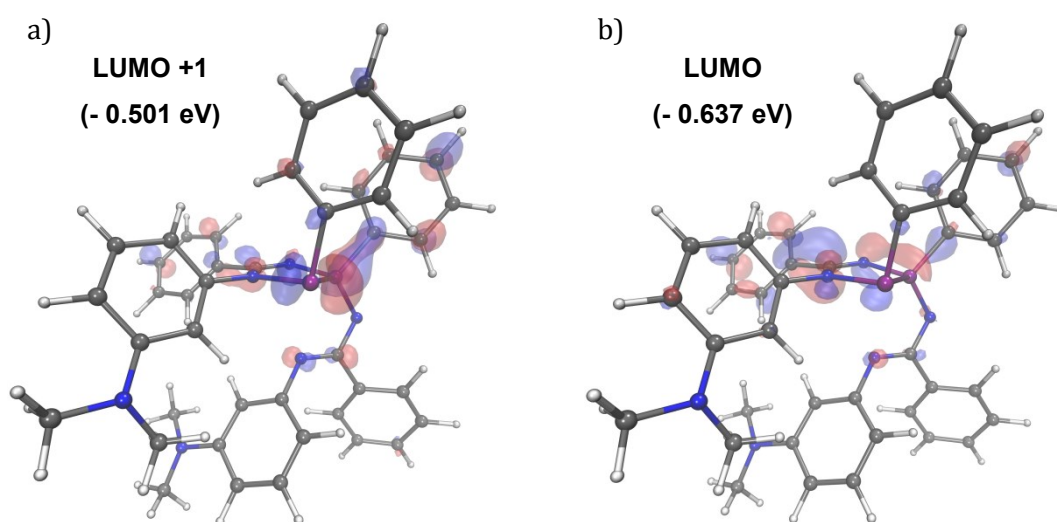
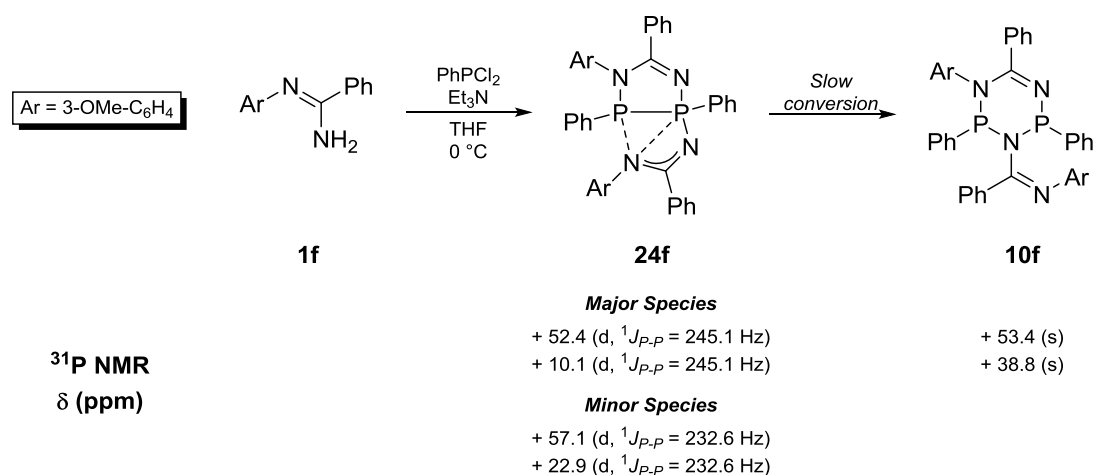


Figure 5.2.2.4: Lowest unoccupied molecular orbitals and energies for **24r**: a) LUMO +1; b) LUMO (isovalue = 0.05).

5.2.3 – N-3-Methoxyphenyl-benzamidine

The reaction of the less electron-rich *N*-arylamidine **1f** with PhPCl₂ under mild conditions (Scheme 5.2.3.1) gave **24f** as the major product with *ca.* 10 % of **10f** after 1 hour. The ratio of **24f** to **10f** decreases over time, with approximately 45 % of the six-membered heterocycle after 24 hours, increasing up to 57 % after 48 hours. This indicates that **24f** is in fact the initial product and that conversion through to either the six-membered heterocycle **10f** or the corresponding fused-ring 1,2,4-benzophosphadiazine **19f** is largely dependent on the *C*-nucleophilicity of *N*-aryl ring.



Scheme 5.2.3.1: Reaction of **1f** with PhPCl₂ and the ³¹P NMR chemical shifts of the products.

The percentage of **10f** ceased at approximately 60 % after 5 days and heating the reaction mixture at this stage was found to have no effect on the product distribution. However, if the reaction mixture was heated at reflux shortly after addition of PhPCl₂, the formation of the fused-ring 1,2,4-benzophosphadiazine was observed, giving two multiplets at δ = 2.0 at - 13.1 ppm as the major species, assigned as the two possible isomers, **19f** and **19f'** (Figure 5.2.3.1).

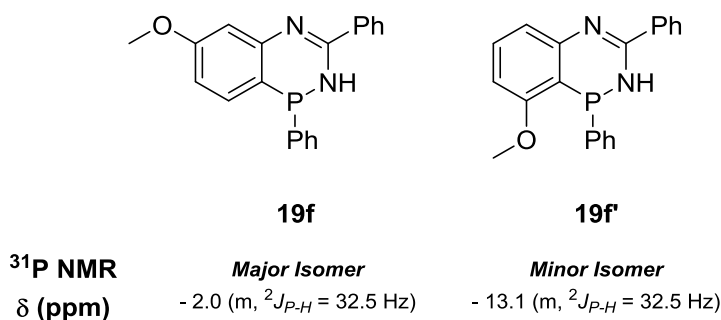
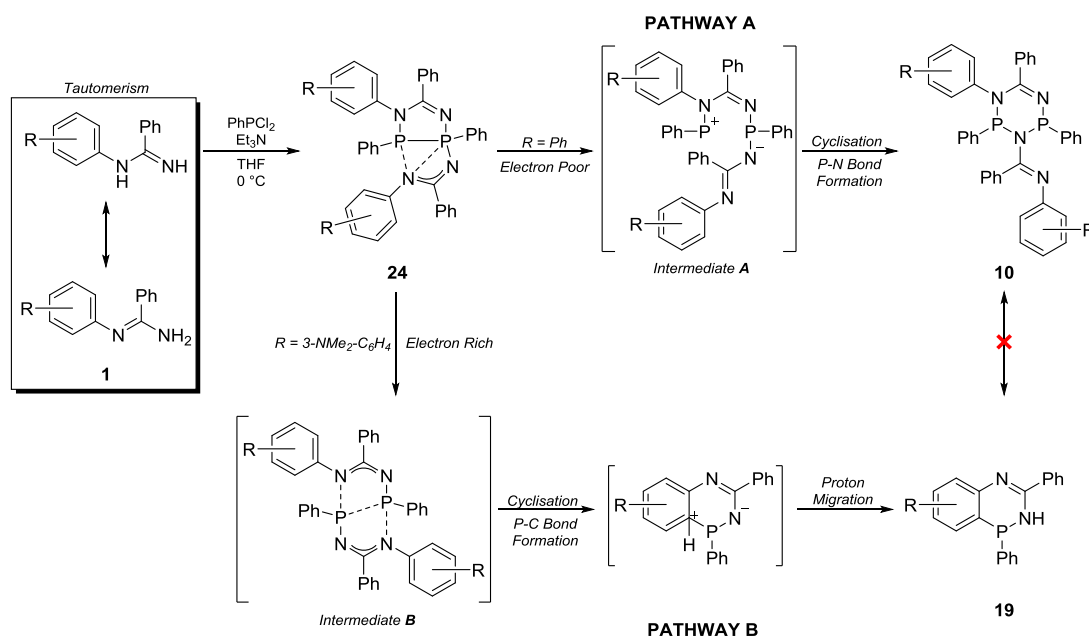


Figure 5.2.3.1: Isomeric 1,2,4-benzophosphadiazines derived from **1f**.

After 24 hours of heating, four major species were present by ^{31}P NMR spectroscopy: **24f** ($\approx 50\%$ by integration), **10f** ($\approx 22\%$), **19f** ($\approx 10\%$) and **19f'** ($\approx 3\%$). After 5 days, **24f** had fully converted to give **19f** ($\approx 45\%$) and **19f'** ($\approx 13.5\%$), amongst other unidentified minor species. The amount of **10f** decreased to $\approx 16\%$, but this is believed to be due to decomposition rather than conversion/rearrangement to give **19f** and **19f'**.

These results confirm that **24** is the initial product in the reaction of *N*-arylamidines with PhPCl_2 in the presence of Et_3N . For electron-poor *N*-arylamidines such as **1a**, this species is not observed and **24a** is believed to rapidly convert through to give the six-membered P_2CN_3 heterocycle **10a**, with no evidence of **19a**. In contrast, **24r** can be isolated for the electron-rich *N*-arylamidine **1r** and converts through to give the fused-ring 1,2,4-benzophosphadiazine **19r**, but no evidence of **10r** is observed. For the moderately electron-rich *N*-arylamidine **1f**, the distribution of products can be driven by changing the reaction conditions, but no single species could be isolated.

Proposed pathways for the formation of **10** and **19** from **24** are shown in Scheme 5.2.3.2; unisolated, tentatively postulated intermediates are shown in square brackets. Compound **24** rapidly forms from the reaction of *N*-arylamidines with PhPCl_2 in the presence of Et_3N , and no other species are observed by ^{31}P NMR prior to this. For the six-membered P_2CN_3 heterocycle **10** to form, the P-P bond in **24** must break whilst the tethered amidine decoordinates from phosphorus, followed by P-N bond formation (Pathway A). In contrast, for the fused-ring heterocycle **19** to form, **24** is proposed to rearrange to give a symmetrical dimeric intermediate, which then potentially splits to give monomeric four-membered heterocyclic intermediates, that undergo cyclisation followed by proton migration to give the 1,2,4-benzophosphadiazine **19r** (Pathway B). No interconversion between **19** and **10** was observed, and extended heating resulted only in slow decomposition of both species.



Scheme 5.2.3.2: Proposed pathway for the conversion of **24** into **10** or **19**.

A geometry optimisation of **24a** was performed to further probe the differing pathways observed for electron-poor and electron-rich *N*-arylamidines. Although the structural parameters and conformation are essentially identical to **24r**, the HOMO and HOMO -1 are localised heavily on the heteroatoms (Figure 5.2.3.2) and not on the *N*-aryl rings as calculated for **24r**. This suggests that the nitrogen and phosphorus atoms of **24a**, particularly N3, N4 and P2, are much stronger nucleophiles compared to the aromatic carbon, and this is likely to be the origin of the formation of **10a** in which a new P-N bond is formed. In addition, **10a** is calculated to be lower in energy than **24a** by $9.60 \text{ kcal mol}^{-1}$ whilst **19a** (not observed) is calculated to be less favourable than **10a** by $3.50 \text{ kcal mol}^{-1}$. In contrast, **19r** is lower in energy than **24r** by $5.87 \text{ kcal mol}^{-1}$ whilst **10r** (not observed) is calculated to be less favourable than **19r** by $1.57 \text{ kcal mol}^{-1}$.

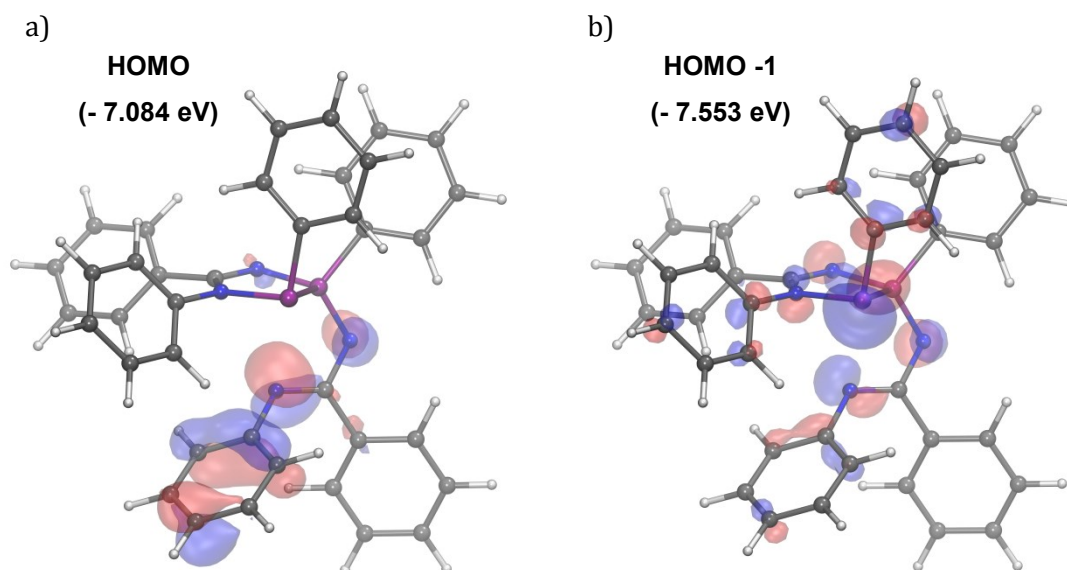


Figure 5.2.2.3: Highest occupied molecular orbitals and energies for **24r**: a) HOMO; b) HOMO -1 (isovalue = 0.05).

5.2.4 – *N*-4-Chlorophenyl-benzamidine

In light of these results, we decided to test other substituted *N*-arylamidines to probe which other factors influence whether the six-membered P₂CN₃ heterocycle or fused-ring 1,2,4-benzophosphadiazine is formed. The electron-poor *N*-4-chlorophenyl-benzamidine **1u** gave a mixture of both **10u** and **24u** (\approx 60:40 ratio by integration of ³¹P NMR chemical shifts), suggesting that the steric bulk of the *N*-aryl ring decreases the rate of conversion of **24u** to **10u**; formation of **10a** is rapid for the unsubstituted and less electron-poor *N*-phenylbenzamidine **1a**. A single species could not be obtained, however single crystals of **10u** suitable for X-ray diffraction were isolated during attempted recrystallisations from DCM and hexane.

Compound **10u** crystallises as colourless blocks in the triclinic space group $P\bar{1}$ with a single molecule of **10u** and DCM in the asymmetric unit (Figure 5.2.4.1). The bond metrics are identical within errors to the isostructural **10a**, with the P₂CN₃ heterocyclic ring adopting a distorted envelope conformation, folded along the P2...N1 axis by 36.2°, with the two *P*-phenyl rings in a *cis*-orientation.

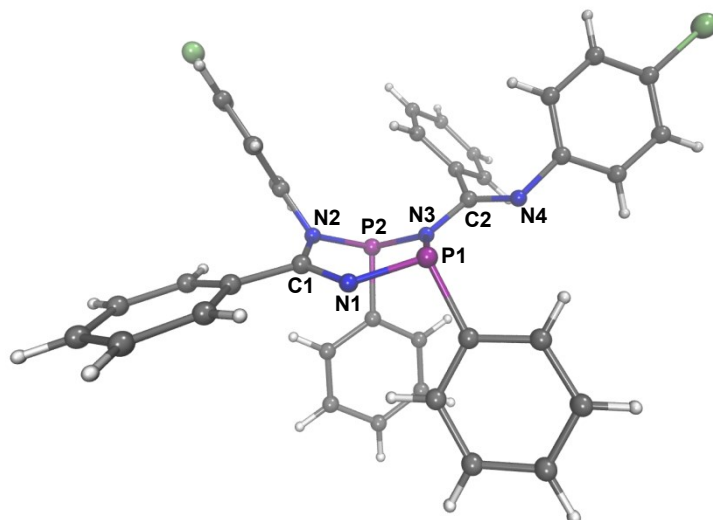
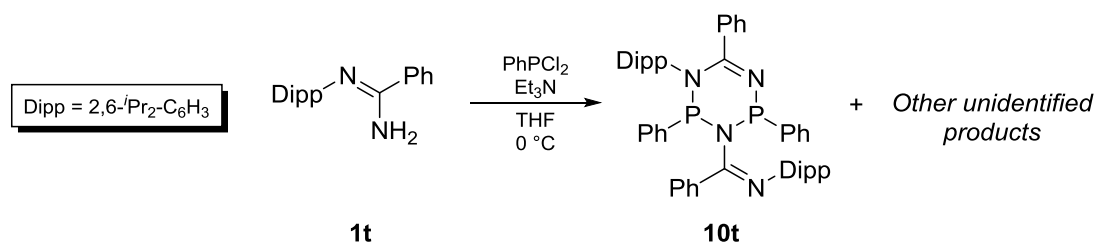


Figure 5.2.4.1: Crystal structure of **10u**. Solvents of crystallisation omitted for clarity.

5.2.5 – *N*-2,6-Diisopropylphenyl-benzamidine

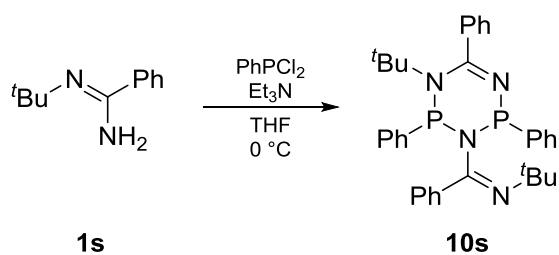
Following this, we investigated the reaction of the bulky *N*-2,6-diisopropylphenyl-benzamidine **1t** with PhPCl_2 and Et_3N (Scheme 5.2.5.1). The presence of *iso*-propyl groups at both positions *ortho* to the *N*-aryl nitrogen however prevents the formation of the fused-ring 1,2,4-benzophosphadiazine. After 1 hour, peaks in the ^{31}P NMR spectrum consistent with **10t** were observed at $\delta + 52.8$ and $+ 41.8$ ppm, together with a second pair of singlets of equal intensity at $\delta + 76.9$ and $+ 54.6$ ppm, along with several unidentified minor pairs of doublets (*i.e.* P-P coupled species). No change in the product distribution was observed on further stirring at room temperature, but heating the reaction mixture at $100\text{ }^\circ\text{C}$ resulted in complete loss of the signals at $\delta + 76.9$ and $+ 54.6$ ppm, and conversion through to **10t**. It is therefore postulated that the former species is an intermediate along pathway A (see Scheme 5.2.3.2) despite not being observed for other systems. Attempts to isolate this species however were unsuccessful and a single product could not be obtained.



Scheme 5.2.5.1: Reaction of **1t** with PhPCl_2 .

5.2.6 – *N*-*tert*-Butyl-benzamidine

The reaction of the alkyl-substituted *N*-*tert*-butyl-benzamidine **1s** with PhPCl₂ under standard conditions (Scheme 5.2.6.1) was also performed to further examine the effect of *N*-substituents on the product distribution. This gave clean and rapid formation of the six-membered P₂CN₃ heterocycle **10s** with no evidence of **24s** or additional species by ³¹P NMR. Compound **10s** exhibits a pair of doublets in the ³¹P{¹H} NMR spectrum at δ + 43.1 and + 38.6 ppm with ²J_{P-P} = 11.4 Hz; this is marginally upfield shifted compared to **10a** which gives two singlets at δ + 54.2 and + 39.1 ppm.



Scheme 5.2.6.1: Reaction of **1s** with PhPCl₂.

Compound **10s** crystallises as pale yellow blocks in the monoclinic space group *P*2₁/*n* with a single molecule in the asymmetric unit (Figure 5.2.6.1). The overall conformation of **10s** is essentially identical to **10a** and **10u** but the bond lengths within the heterocyclic ring are marginally longer, and the fold angle along the N1⋯P2 axis is slightly more obtuse at 37.3°.

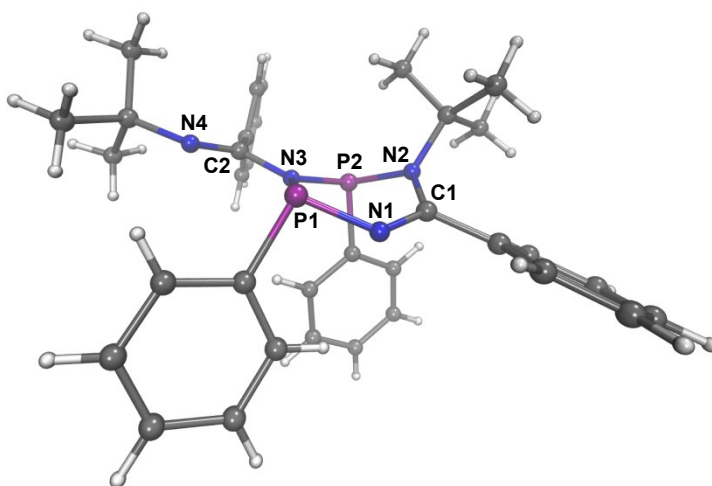
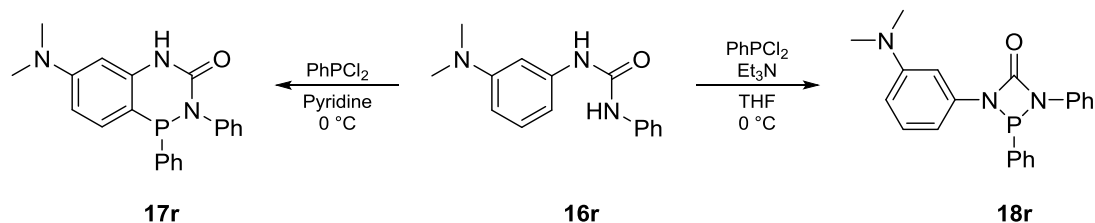


Figure 5.2.6.1: Crystal structure of **10s**.

5.2.7 – The Influence of Base

In Chapter 4, the synthesis of 1,2,4-benzophosphadiazines from electron-rich *N*-arylamidines and *N,N'*-diaryllureas under mild conditions was investigated. During these studies, it was evident that the use of a mild base was a key factor in forming the fused-ring heterocycle, since stronger bases favoured the formation of undesired P-N

heterocycles. This was particularly emphasised for the electron-rich *N,N'*-diaryllurea **16r** which gives the 1,2,4-benzophosphadiazine **17r** when pyridine is employed as the base and solvent, or the four-membered 1,3,2-diazophosphetene **18r** (*vide infra*) when the reaction is performed in THF with Et₃N (Scheme 5.2.7.1).



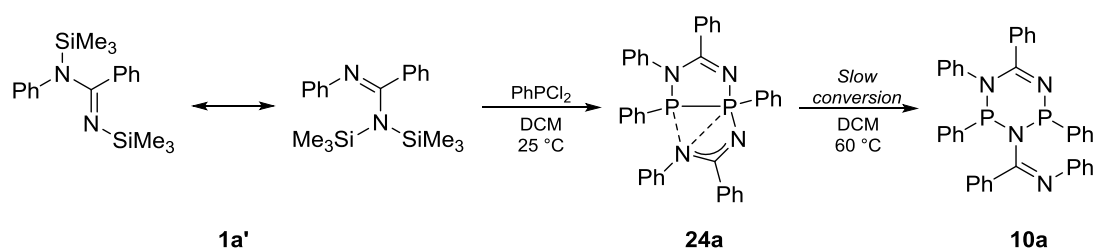
Scheme 5.2.7.1: Influence of base strength on the reaction of electron-rich *N,N'*-diaryllurea **16r** with PhPCl_2 .

When *N*-phenylbenzamidine **1a** was treated with PhPCl_2 in neat pyridine at $0\text{ }^\circ\text{C}$, two major species were observed by ^{31}P NMR which both gave broad pairs of doublets at $\delta + 53.7$ and $+ 20.9$ ppm ($^1J_{\text{P-P}} = 257.7$ Hz), and at $\delta + 45.3$ and $+22.5$ ppm ($^1J_{\text{P-P}} = 255.2$ Hz). These peaks are similar to but inconsistent with **24a** and are instead proposed to be protonated analogues based on earlier studies which showed that pyridine is insufficiently basic to deprotonate **19.HCl**; the poor solubility of these unknown species in toluene and THF further supports this. No change in product distribution was observed on prolonged stirring at room temperature, whereas the addition of Et_3N cleanly gave **10a**.

In contrast, heating the reaction mixture (without Et_3N) at $100\text{ }^\circ\text{C}$ for two hours gave a new roofed pair of doublets at $\delta + 56.9$ and $+ 55.1$ ($^1J_{\text{P-P}} = 225.1$ Hz) as the major species with concomitant loss of signals corresponding to the earlier species. Attempts to isolate and identify this new species were unsuccessful. Further heating gave an approximately equal mixture of $[\text{PhP}]_n$ species and a multiplet at $\delta + 2.9$ ppm in the ^{31}P NMR spectrum. The latter species is believed to be the protonated fused-ring 1,2,4-benzophosphadiazine **19a.HCl**, implying that the intermediates undergo some form of sacrificial redox ring-closing step. Similar behaviour was also observed for *N*-3-methoxyphenyl-benzamidine **1f**. The electron-rich *N*-3-dimethylaminophenyl-benzamidine **1r** on the other hand, cleanly gave the protonated fused-ring 1,2,4-benzophosphadiazine **19r.HCl** but could not be separated from the pyridinium hydrochloride. This prompted us to use K_2CO_3 as the base and allowed **19r.HCl** to be isolated in high yields (see section 4.4.2.2).

The omission of base, by using the *bis*-silylated *N*-arylamidine **1a'** supports the hypothesis that **24a** is the initial product prior to forming the six-membered

heterocycle **10a** (Scheme 5.2.7.2). The *bis*-silylated *N*-arylamidine **1a'** exists as a mixture of both tautomers in solution but crystallises as the *N,N*-disubstituted tautomer, analogous to the *protio-N*-arylamidines (See Supplementary Chapter 1). On addition of PhPCl_2 , immediate formation of Me_3SiCl was observed by ^1H and ^{29}Si NMR spectroscopy, and the ^{31}P NMR spectrum displays signals corresponding to **24a** ($\approx 60\%$ by integration) and **10a** ($\approx 30\%$), as well as several minor peaks (Figure 5.2.7.1). Surprisingly, the product distribution did not change significantly on standing at room temperature despite the earlier assumption that **24a** was rapidly converted through to **10a** and hence could not be observed. Heating the reaction mixture at $60\text{ }^\circ\text{C}$ did however result in slow conversion of **24a** into **10a** as expected.



Scheme 5.2.7.2: Reaction of *bis*-silylated *N*-phenylbenzamidinium **1a'** with PhPCl_2 .

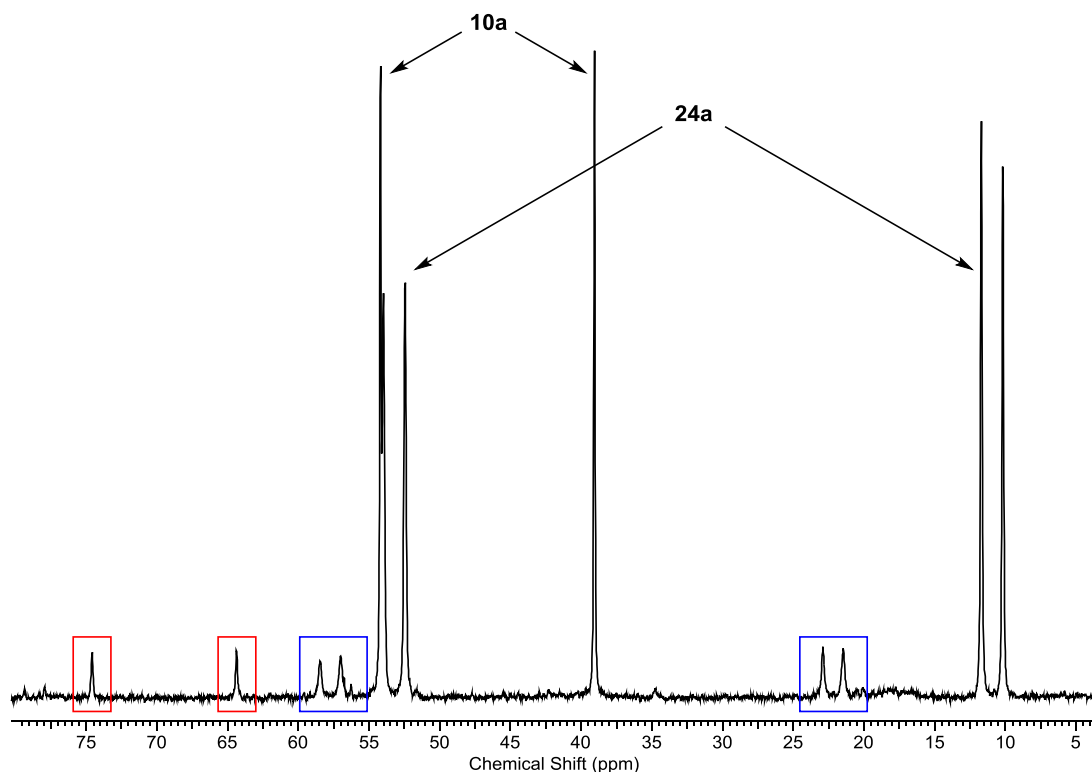
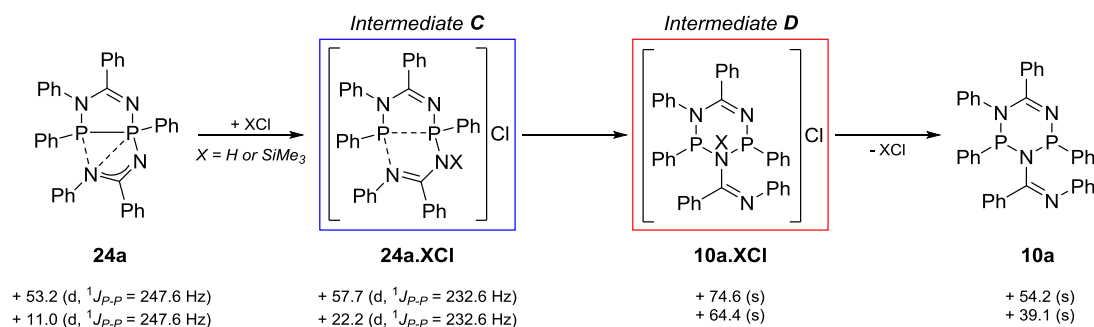


Figure 5.2.7.1: ^{31}P NMR spectrum showing the distribution of products from the reaction of **1a'** with PhPCl_2 .

The significantly slower rate of conversion of **24a** to **10a** observed under these conditions suggests that proton transfer plays a critical role in the rearrangement. This requires that the basicity of the *N*-arylamidine or intermediate phosphino-amidine species such as **24a** is comparable to the base employed in the reaction. Indeed, substituted amidines such as DBU have a similar pK_{aH} to Et_3N (*cf.* 12.0 vs. 10.8 respectively). This supports the observation that **10a** does not form when weaker bases such as pyridine ($pK_{aH} = 5.2$) are employed, as well as K_2CO_3 where the pK_a of H_2O is significantly higher at 15.7. For reactions with NaH , the evolution of H_2 means that proton transfer is not possible under those conditions.

A proposed pathway for the conversion of **24a** to **10a** is shown in Scheme 5.7.2.3. The additional peaks in the ^{31}P NMR spectrum (see Figure 5.2.7.1) were observed on a number of occasions during the reactions of substituted *N*-arylamidines with PhPCl_2 in the presence of Et_3N . The minor pair of doublets at $\delta + 57.7$ and $+ 22.2$ ppm ($^1J_{P-P} = 232.6$ Hz) were initially attributed to a conformational isomer of **24a**, which results from the orientation of the substituted *N*-aryl ring (*i.e.* for **1f** and **1r**). However, the appearance of these doublets when amidines with symmetrical or unsubstituted *N*-aryl rings were employed suggested that it was instead a protonated derivative of **24a**, assigned as **24a.HCl**, resulting from proton transfer from $[\text{Et}_3\text{NH}]\text{Cl}$ to **24a**. This species is believed to rearrange to give the protonated six-membered heterocycle **10a.HCl** which is then deprotonated by Et_3N to give **10a**.



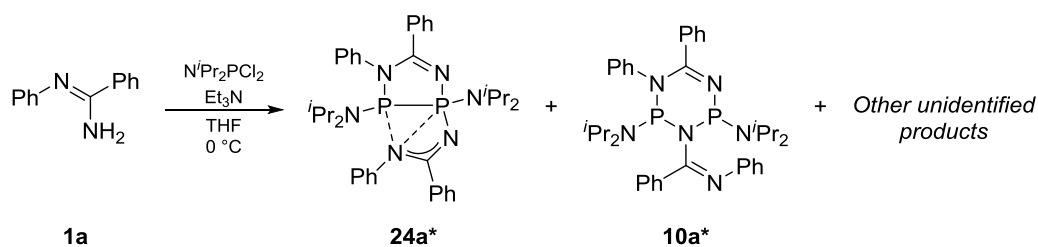
Scheme 5.2.7.3: Proposed scheme for the conversion of **24a** to **10a**, including ^{31}P NMR chemical shifts for the intermediates.

This process is rapid for the reaction of *N*-phenylbenzamidine **1a** with PhPCl_2 in the presence of Et_3N , and intermediate species, including **24a**, cannot be observed by ^{31}P NMR spectroscopy. In contrast, the rearrangement of **24a** to **10a** is significantly slower but still observed for the *bis*-silylated *N*-arylamidine **1a'** in the absence of base, suggesting that X can be either H or SiMe_3 – the latter resulting from reversible *N*-silylation. The quantity of the two proposed intermediates is minor at any given time

(*ca.* < 5 %) and there is limited information in the ^1H and ^{29}Si NMR spectra to aid in their assignment. The position of the *N*-silylation or protonation in intermediates **C** and **D** were assigned based on the relative chemical shifts in the ^{31}P NMR spectrum. The protonated/silylated analogues **24a.XCl** and **10a.XCl** are downfield shifted compared to the neutral species, consistent with deshielding due to the removal of electron density from the phosphorus centres.

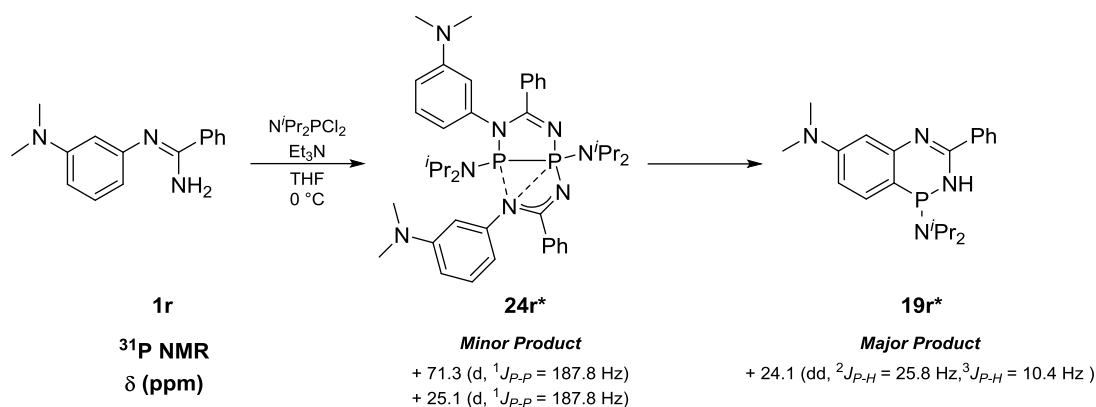
5.3 – Reactions of *N*-Arylamidines with $\text{N}^i\text{Pr}_2\text{PCL}_2$

The reaction of *N*-arylamidines with the less electrophilic amido-substituted phosphine $\text{N}^i\text{Pr}_2\text{PCL}_2$ was also investigated to further understand the factors affecting product distribution. The treatment of *N*-phenylbenzamidine **1a** with $\text{N}^i\text{Pr}_2\text{PCL}_2$ in the presence of Et_3N (Scheme 5.3.1) gave a mixture of products including **24a*** and **10a*** as minor species; these are downfield shifted compared to the *P*-phenyl analogues. The other unidentified species, primarily consisting of a broad peak at $\delta + 144.0$ ppm in the ^{31}P NMR spectrum, are believed to arise through the cleavage of the $\text{P-N}^i\text{Pr}_2$ bond which results from the HCl generated from the formation of other, more favourable $\text{P-N}_{\text{amidine}}$ bonds. This leads to reactive P-Cl fragments in the presence of nucleophilic N-H moieties and may lead to polymeric materials.



Scheme 5.3.1: Reaction of *N*-phenylbenzamidine **1a** with $\text{N}^i\text{Pr}_2\text{PCL}_2$.

In contrast, when the reaction is performed with the electron-rich *N*-arylamidine **1r**, the major product is the fused ring 1,2,4-benzophosphadiazine **19r***, with minor quantities of **24r*** (Scheme 5.3.2). Attempts to isolate **19r*** and remove residual **24r*** were however unsuccessful.



Scheme 5.3.2: Reaction of electron-rich *N*-arylbenzamidines **1r** with $N^iPr_2PCl_2$.

The cleavage of P- N^iPr_2 bonds observed during the reaction of **1a** with $N^iPr_2PCl_2$ is consistent with the proposed proton-transfer mediated rearrangement of **24** to **10**. The clean reactivity of the electron-rich *N*-arylamidines **1r** with $N^iPr_2PCl_2$, and lack of degradation products compared to **1a**, suggests that the rearrangement of **24** to **19** does not involve proton-transfer. No intermediate species were observed by ³¹P NMR spectroscopy however, and the true mechanism for this rearrangement is unknown.

5.4 – Reactions of *N*-Arylamidines with Phosphorus Trihalides

5.4.1 – Phosphorus Trichloride

Initial reactions of *N*-arylamidines with PCl_3 , either neat or stoichiometrically in the presence of a range of bases and solvents, repeatedly gave intractable and insoluble materials believed to be polymeric in nature (see section 4.2.2). In light of the findings discussed in section 5.2, we decided to reinvestigate the reactions of *N*-arylamidines with PCl_3 under mild conditions.

The treatment of *N*-phenylbenzamidines **1a** with PCl_3 under standard conditions (THF, Et_3N , 0 °C) gave several P-P coupled species by ³¹P NMR (Figure 5.4.1.1). The major species (**A**, red boxes) exhibited a pair of doublets at $\delta + 79.2$ and $+ 33.5$ ppm ($^1J_{P-P} = 245.1$ Hz); accurate coupling constants could not be measured for the broad doublet at $\delta + 79.2$ ppm, but the relative integrals of this doublet and the sharper doublet at $\delta + 33.5$ ppm was approximately 1:1 on a number of occasions (repeated reactions, multiple recrystallisations, *etc.*) suggesting that these two doublets were correlated. The next major species (**B**, blue boxes) exhibited a pair of sharp doublets in the ³¹P NMR spectrum at $\delta + 73.6$ and $+ 24.8$ ppm ($^1J_{P-P} = 192.6$ Hz). A minor pair of doublets of triplets (**C**, green asterisks) was also observed at $\delta + 74.5$ and $+ 28.5$ ppm ($^1J_{P-P} = 192.6$ Hz, $^2J_{P-P} = 15.0, 17.5$ Hz), together with a singlet (**D**, orange box) at $\delta + 18.7$ ppm.

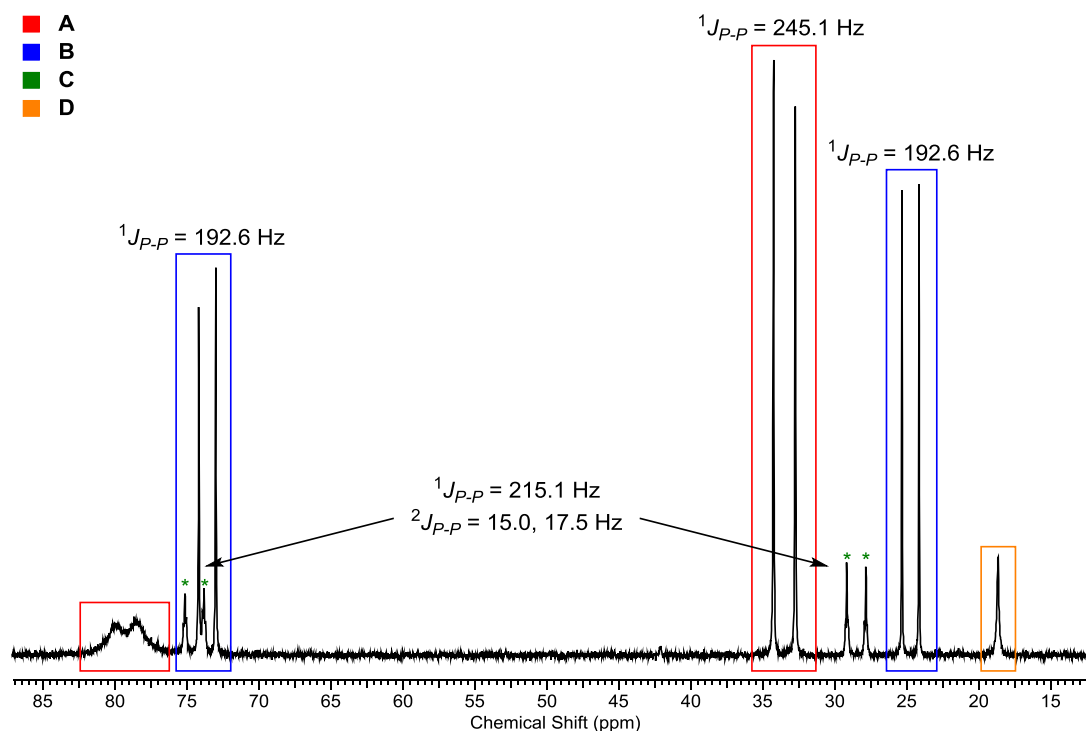
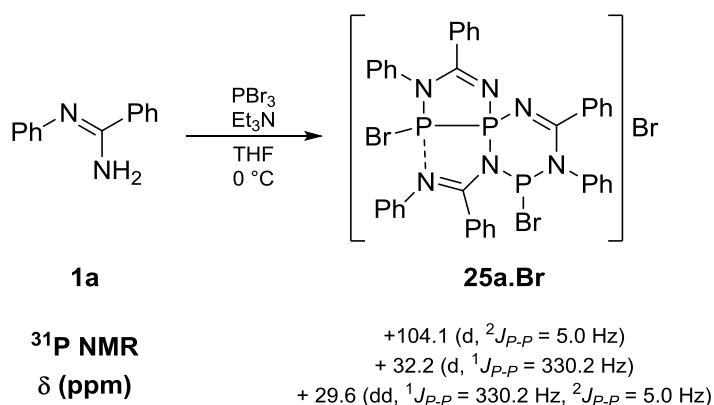


Figure 5.4.1.1: ^{31}P NMR spectrum showing the major species from the reaction of *N*-phenylbenzamidinium **1a** with PCl_3 .

Heating the reaction mixture resulted in a decrease in intensity for the signals assigned to species **A** and **D** and a concomitant increase in intensity for species **B** and **C**. In contrast, performing the reaction at $-95\text{ }^\circ\text{C}$ gave species **B** as the major species (*ca.* 46 % by integration) with an equal amount of species **A** and **D** (*ca.* 27 % each). Attempts to isolate and identify any of these species by repeated recrystallisations were unsuccessful.

5.4.2 - Phosphorus Tribromide

Having established that the electrophilicity of the phosphine was also a significant factor in determining which product was formed, we tested the reactions of *N*-arylamidines with PBr_3 under mild conditions. Unlike the reaction of *N*-phenylbenzamidinium **1a** with PCl_3 which gave a mixture of unidentified products, the treatment of **1a** with PBr_3 in the presence of Et_3N afforded the *pseudo*-spirotricyclic cationic species **25a.Br** (Scheme 5.4.2.1). Whilst no evidence of **25a.Cl** was observed when PCl_3 was used, a minor pair of doublets in the ^{31}P NMR spectrum at $\delta + 73.5$ and $+ 24.7$ ($^1J_{\text{P-P}} = 192.6$ Hz) consistent with species **B** (see Figure 5.4.1.1) was present when PBr_3 was used, suggesting that a P-P coupled species related to **24** may form prior to or after **25.X**.



Scheme 5.4.2.1: Reaction of *N*-phenylbenzamidine **1a** with PBr₃ under mild conditions.

Compound **25a.Br** crystallises as pale yellow blocks in the monoclinic space group $P2_1/n$ with a single ion pair and a single molecule of DCM in the asymmetric unit (Figure 5.4.2.1). The structure is reminiscent of both **10a** and **24r** and features a five-membered P_2CN_2 ring, in which both nitrogen atoms (N1 and N2) adopt a $\mu_2\text{-}\eta^1\text{-}\eta^1$ coordination mode. The N3 atom of the second amidinate fragment is bonded to two different phosphorus atoms, P1 and P3, in a $\mu_2\text{-}\eta^2$ monodentate fashion whilst N4 exhibits a close contact to P2 of 2.440(2) Å with a $\text{N4}\cdots\text{P4-Br1}$ angle of 163.5(6)°. A third amidinate fragment (N5-C3-N6) coordinates to P1 and P3 in a $\mu_2\text{-}\eta^1\text{-}\eta^1$ fashion to form a six-membered P_2CN_3 ring. The P_2CN_2 ring is planar whilst the P_2CN_3 ring adopts a distorted envelope conformation, folded along the $\text{P3}\cdots\text{N5}$ axis by 26.1°; the two heterocyclic rings are spirocyclic at P1 and twisted by 87.4° (deviation of mean planes). The bromide counterion (Br3) weakly coordinates to P2 with a distance of 3.083(7) Å, well within the sum of van der Waals radii (3.73 Å), and a $\text{N2-P2}\cdots\text{Br3}$ angle of 161.6(7)°.

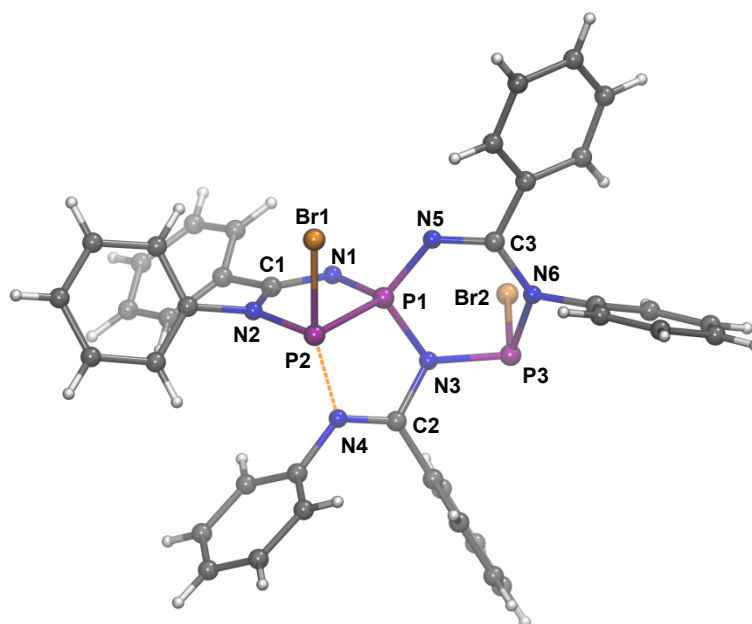


Figure 5.4.2.1: Crystal structure of **25a.Br**. Counterion and solvents of crystallisation omitted for clarity.

The DFT optimised geometry of **25a.Br** is in excellent agreement with the experimental crystal structure (Table 5.4.2.1). The positive charge is largely localised on P1 to give a λ^4 -phosphonium species with additional charge density on P2 and P3. The N4 \cdots P2 contact exhibits significant N-P σ -bond character (bond order = 0.175) suggesting that the P1-P2 bond may be better represented as a phosphane-stabilised phosphonium given the observed electrophilic nature of P2.

	Bond Lengths / Å		Bond Index
	Experimental	Calculated	Mayer
C1-N1	1.319(3)	1.309	1.651
C1-N2	1.368(3)	1.374	1.110
N1-P1	1.628(2)	1.635	1.189
N2-P2	1.777(2)	1.759	0.873
P1-P2	2.210(9)	2.230	0.777
P2-Br1	2.316(7)	2.368	0.742
P1-N3	1.693(2)	1.707	0.825
C2-N3	1.406(3)	1.409	0.954
C2-N4	1.269(3)	1.275	1.647
P1-N5	1.610(2)	1.611	1.212
P3-N3	1.723(2)	1.738	0.844
P3-N6	1.729(2)	1.744	0.870
P3-Br2	2.256(6)	2.271	0.974
C3-N5	1.299(3)	1.302	1.677
C3-N6	1.377(3)	1.377	1.058
N4 \cdots P2	2.440(2)	2.362	0.175

Table 5.4.2.1: Selected experimental and calculated bond lengths and Mayer bond indices for **25a.Br**.

The highest occupied molecular orbital (HOMO) of **25a.Br** is largely ligand based and delocalised across the C1 and N2 phenyl groups (Figure 5.4.2.2). The HOMO -1 on the other hand corresponds to an N4...P4-Br1 anti-bonding interaction and a π -bonding orbital on the N3-phenyl ring.

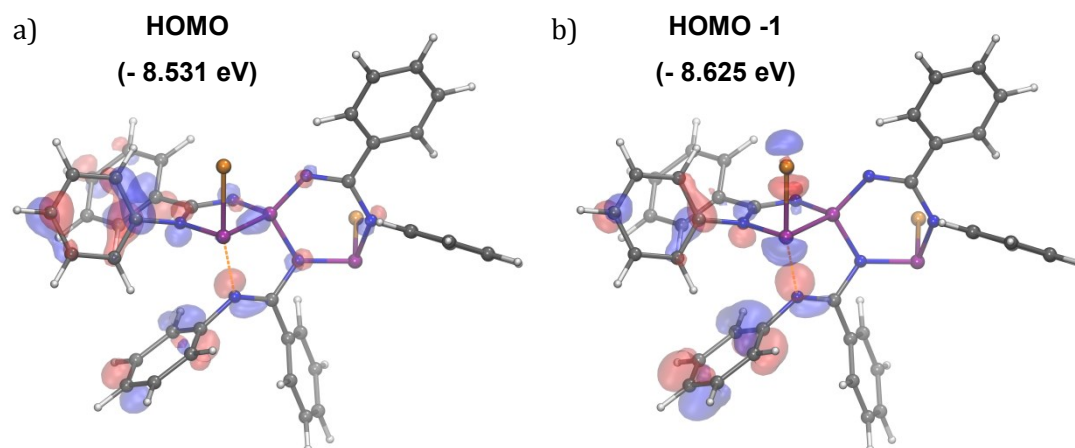


Figure 5.4.2.2: Highest occupied molecular orbitals and energies for **25a.Br**: a) HOMO; b) HOMO -1 (isovalue = 0.05).

The lowest unoccupied molecular orbital (LUMO) is delocalised across the P₂CN₃ ring and corresponds to a π -bonding orbital and a P3-Br2 anti-bonding interaction (Figure 5.4.2.3). The LUMO +1 is a π -bonding orbital delocalised across N1-P1-P2-N2 of the P₂CN₂ five-membered heterocyclic ring, with nodes at C1-N1 and C1-N2, and another P2-Br1 anti-bonding interaction.

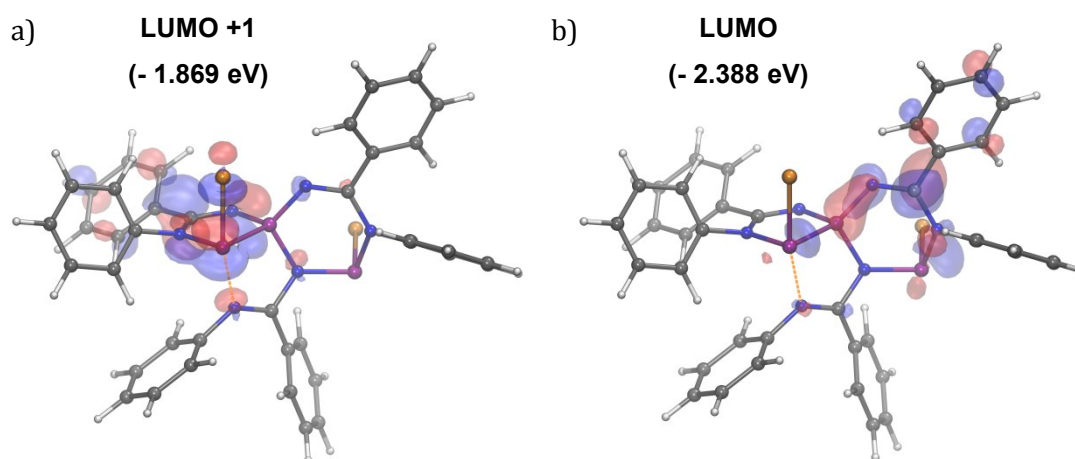


Figure 5.4.2.3: Lowest unoccupied molecular orbitals and energies for **25a.Br**: a) LUMO; b) LUMO +1 (isovalue = 0.05).

When the reaction of **1a** with PBr₃ in the presence of Et₃N was repeated at 75 °C, **25a.Br** was fully consumed and two new P-P coupled species were formed and

observed by $^{31}\text{P}\{^1\text{H}\}$ NMR (Figure 5.4.2.4). The major species (**F**, red dots) exhibits a pair of doublets of triplets resulting from direct $^1J_{\text{P1-P2}}$ coupling together with two additional $^2J_{\text{P1-P2}}$ couplings, whilst the minor species (**G**, blue asterisks) exhibits a pair of doublets with direct $^1J_{\text{P1-P2}}$ coupling only. Similar species were observed during the reaction of **1a** with PCl_3 (see Figure 5.4.1.1), albeit in different ratios, indicating that **25a.Cl** maybe the initial product but is too short-lived to be observed. The similarity of the chemical shifts of species **F** and **G** suggests that they are related, whilst the additional P-P coupling observed for species **F** implies it may be dimeric or oligomeric in nature. Prolonged heating at $75\text{ }^\circ\text{C}$ or repeating the reaction at $110\text{ }^\circ\text{C}$, converted species **G** into **F**, however, several minor peaks were also observed, likely due to product decomposition.

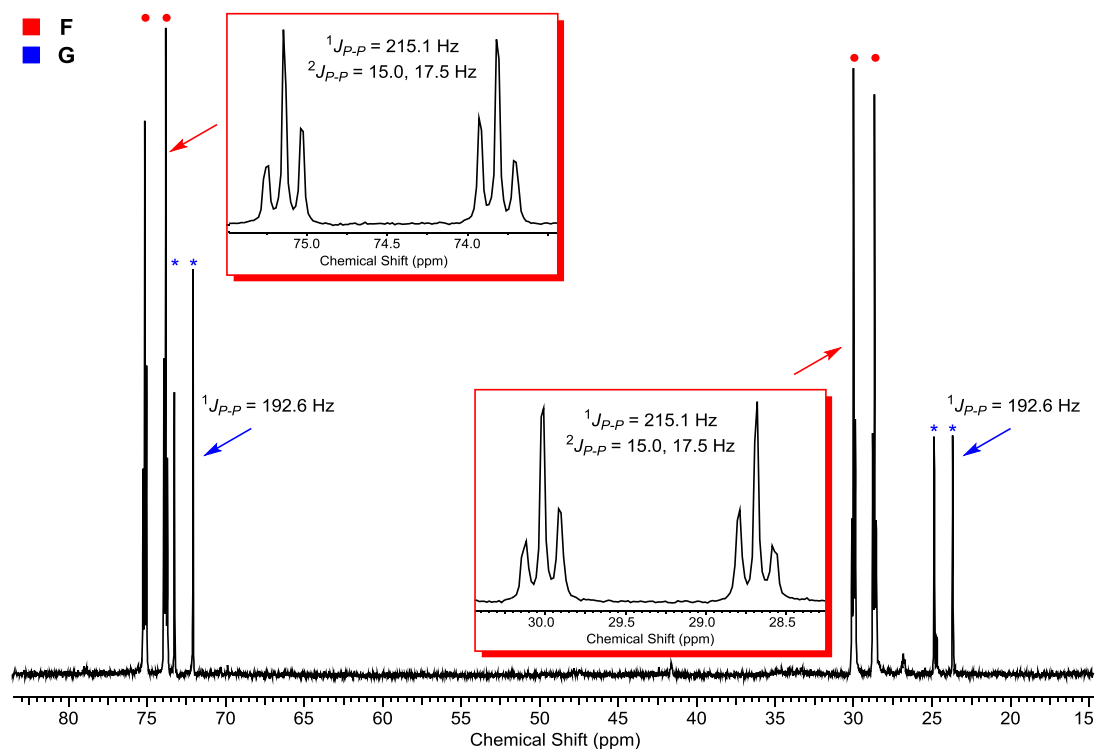
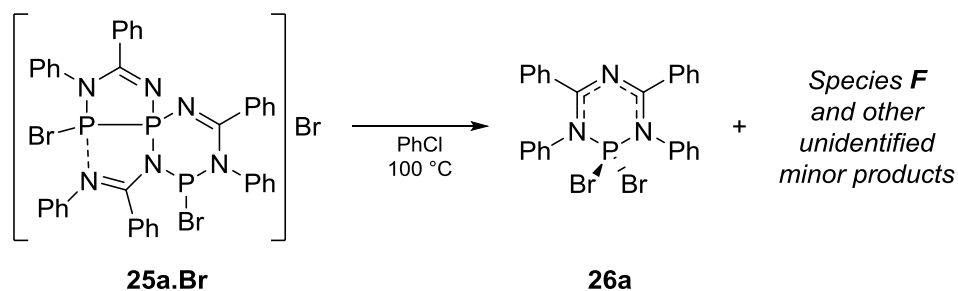


Figure 5.4.2.4: $^{31}\text{P}\{^1\text{H}\}$ NMR spectrum from the reaction of *N*-phenylbenzamidinium **1a** with PBr_3 in the presence of Et_3N at $75\text{ }^\circ\text{C}$.

Despite extensive attempts and recrystallisations, single crystals suitable for X-ray diffraction studies could not be grown, and the identity of species **F** remains unknown. ^1H NMR data provided limited information on the structure of **F** whilst elemental analysis gave higher percentage values of carbon, nitrogen and hydrogen than expected (and calculated for **25a.Br**), suggesting that bromine (in some form) is lost on heating. Further analysis, including mass spectrometry, is required to obtain further information on the identity of species **F**.

When an isolated sample of **25a.Br** was dissolved and heated at 100 °C in chlorobenzene, the solution rapidly darkened from pale yellow to deep orange and afforded large orange crystals on cooling. Single-crystal X-ray diffraction analysis revealed the formation of the six-membered heterocycle **26a** (Scheme 5.4.2.2), which must result from the breaking and making of C-N bonds.



Scheme 5.4.2.2: Thermal rearrangement of **25a.Br**.

³¹P NMR analysis of the supernatant indicated the presence of species **F** as the major product remaining in solution, along with several other unidentified minor species. When the orange crystals of **26a** were redissolved in DCM and analysed by ³¹P NMR, a major singlet was present at δ + 54.6 ppm; this is significantly upfield shifted compared to a typical amido-dibromophosphine (NⁱPr₂PBr₂ = δ + 170.8 ppm)⁵³ and is consistent with the drastic change in geometry at phosphorus. A minor pair of doublets at δ + 159.6 and + 48.6 ppm (²J_{P-P} = 57.5 Hz) were also observed. Neither of these two species were observed by ³¹P NMR spectroscopy when **1a** was heated with PBr₃ in the presence of Et₃N suggesting that proton-transfer again has a significant role in this rearrangement. In the presence of [Et₃NH]Br, nucleophilic amidine nitrogens are expected to be sufficiently basic to deprotonate [Et₃NH]Br; these intermediate species must then thermally rearrange to give species **F** and **G**. In the absence of acidic-protons, the nucleophilic amidine nitrogen instead attacks an electrophilic amidine carbon which ultimately results in C-N bond breaking and making to give **26a** and species **F** (species **G** is rapidly converted to **F** at elevated temperatures). Further insight into the mechanism involved would first require knowledge of the identities of species **F** and **G**.

Compound **26a** crystallises as orange blocks in the monoclinic space group *P2*₁/*n* with a single molecule in the asymmetric unit (Figure 5.4.2.5). The PC₂N₃ heterocyclic ring adopts a twisted conformation (13.2° twist angle) such that P1 and N3 lie in the mean plane whilst N1 and C2 lie slightly above the plane, and N2 and C1 sit slightly below the plane. The Br1-P1-Br2 angle is close to linear at 178.6(4)° and is orthogonal to the plane of the heterocyclic ring; however, the P1-Br1 and P1-Br2 distances are

inequivalent at 2.676(1) Å and 2.464(1) Å respectively, likely due to external packing forces. The phosphorus centre adopts a *pseudo*-distorted trigonal bipyramidal geometry; the N1-P1-N2 angle is 97.7(1)° and the N-P-Br angles are close to 90° (range: 87.4(9)-94.1(9)°).

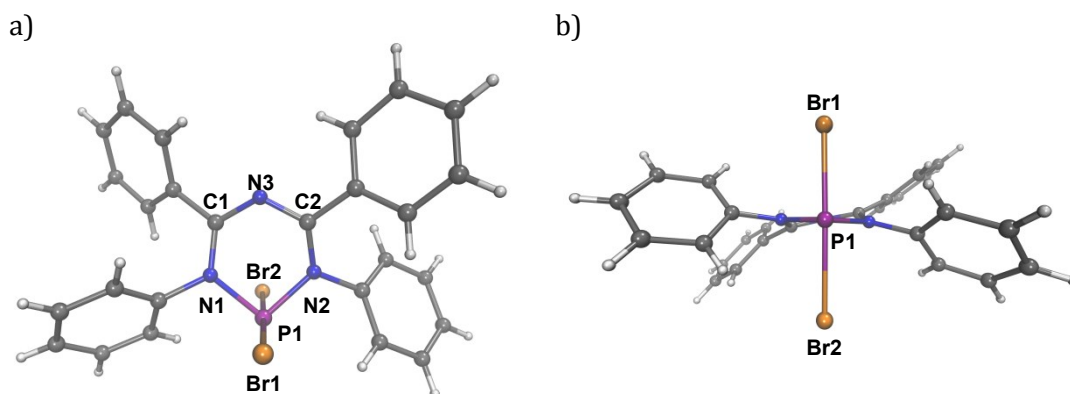


Figure 5.4.2.5: Crystal structure of **26a**: a) Top-down view; b) Side view.

The DFT optimised geometry of **26a** is in good agreement with the experimental crystal structure, and predicts C_2 symmetry about the P1...N3 axis of the heterocyclic ring (Table 5.4.2.2). The Mayer bond indices show that the double-bond character is spread across the C1-N3-C2 backbone of the triazapentadienyl ligand, with partial double-bond character (bond order > 1) in the N1-C1 and N2-C2 bonds.

	Bond Lengths / Å		Bond Index
	Experimental	Calculated	Mayer
P1-Br1	2.676(1)	2.605	0.547
P1-Br2	2.464(1)	2.607	0.545
P1-N1	1.744(3)	1.750	0.825
P1-N2	1.736(3)	1.749	0.825
N1-C1	1.358(4)	1.345	1.164
N2-C2	1.340(4)	1.345	1.163
N3-C1	1.326(4)	1.321	1.484
N3-C2	1.328(4)	1.321	1.486

Table 5.4.2.2: Selected experimental and calculated bond lengths and Mayer bond indices for **26a**.

The P-Br bond orders are close to 0.5 indicative of 3-centre 4-electron ($3c4e^-$) bonding across the near-linear Br1-P1-Br2 moiety. The HOMO of **26a** illustrates this bonding interaction as well as showing the phosphorus lone pair of electrons that lies in the plane of the heterocyclic ring (Figure 5.4.2.6). The HOMO -1 is again largely localised on the bromine atoms with electron density on N1 and N2 and their associated *N*-phenyl rings.

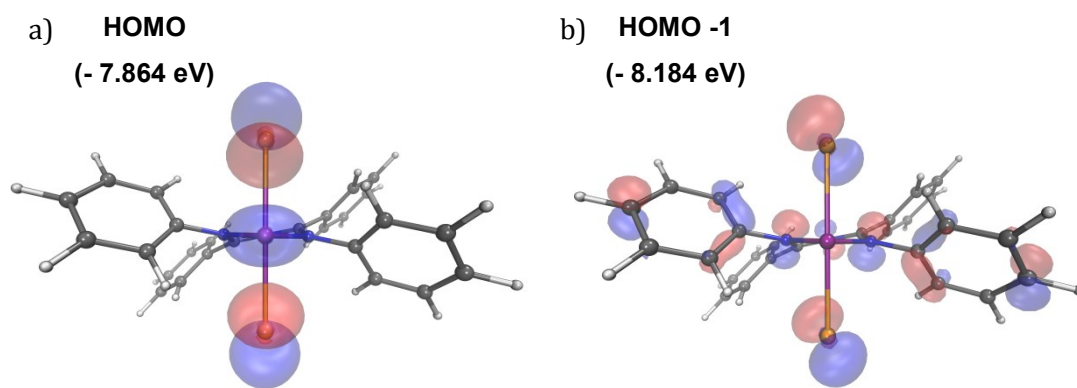


Figure 5.4.2.6: Highest occupied molecular orbitals and energies for **26a**: a) HOMO; b) HOMO -1 (isovalue = 0.05).

The LUMO of **26a** is ligand based and corresponds to a π^* -antibonding interaction with orthogonal nodes along the P1...N3 axis and the N1-C1/N1-C2 bonds (Figure 5.4.2.7). The LUMO +1 is largely localised on P1 and corresponds to a Br1-P1-Br2 anti-bonding interaction, with additional orbital population at N3.

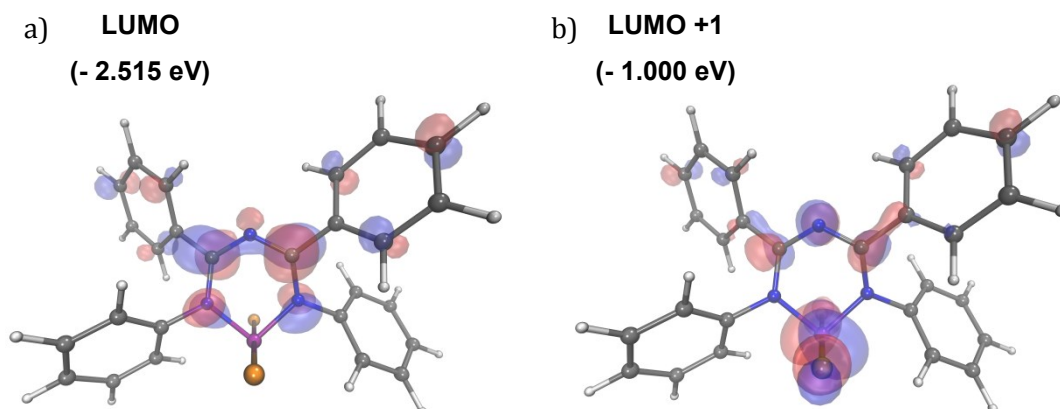


Figure 5.4.2.7: Lowest unoccupied molecular orbitals and energies for **26a**: a) LUMO; b) LUMO +1 (isovalue = 0.05).

Several transition-metal⁵⁴ and main-group complexes⁵⁵ of the electron-rich monoanionic *N,N'*-chelating triazapentadienyl ligand (α , Figure 5.4.2.8) have previously been reported. The related β -diketimate ligand (β) has been used extensively,⁵⁶ most notably in the stabilisation of low-valent metal complexes which have found a host of applications.⁵⁷ Attempts to prepare the analogous phosphorus complexes however have resulted solely in γ -phosphino- β -diketimates (γ).⁵⁸ A single *N,N'*-chelated β -diketimate P^{III} complex is known,⁵⁹ but this was prepared *via* non-traditional methods through insertion of nitriles into unstrained P-C bonds, essentially constructing the ligand around the main-group metal centre. Compound **26a** therefore represents the first true example of a symmetric *N,N'*-chelated β -diketimate-type P^{III}

complex. Further work is necessary to establish whether P^{III} complexes can be prepared directly from the triazapentadienyl ligand *via* traditional methods such as salt metathesis or σ -bond metathesis.

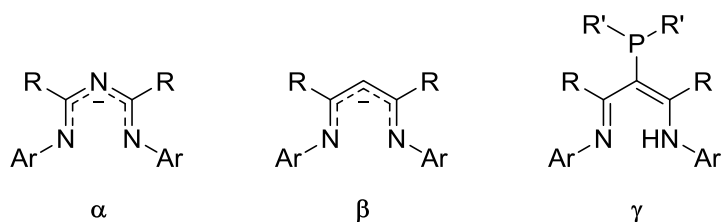


Figure 5.4.2.8: β -diketiminato-type complexes.

5.4.3 – Phosphorus Triiodide

When *N*-phenylbenzamidinium **1a** was treated with a solution of PI_3 in the presence of Et_3N under standard conditions (THF, 0 °C), a dark amber suspension immediately formed. ^{31}P NMR analysis of the mother liquor gave a major pair of doublets (species **H**, Figure 5.4.3.1) at δ + 129.7 and + 109.8 ppm ($^1J_{P,P} = 225.1$ Hz). A minor peak at + 19.4 ppm (species **I**) was also observed, along with a small quantity of **25a.I**, however, this converted through to species **H** on further stirring.

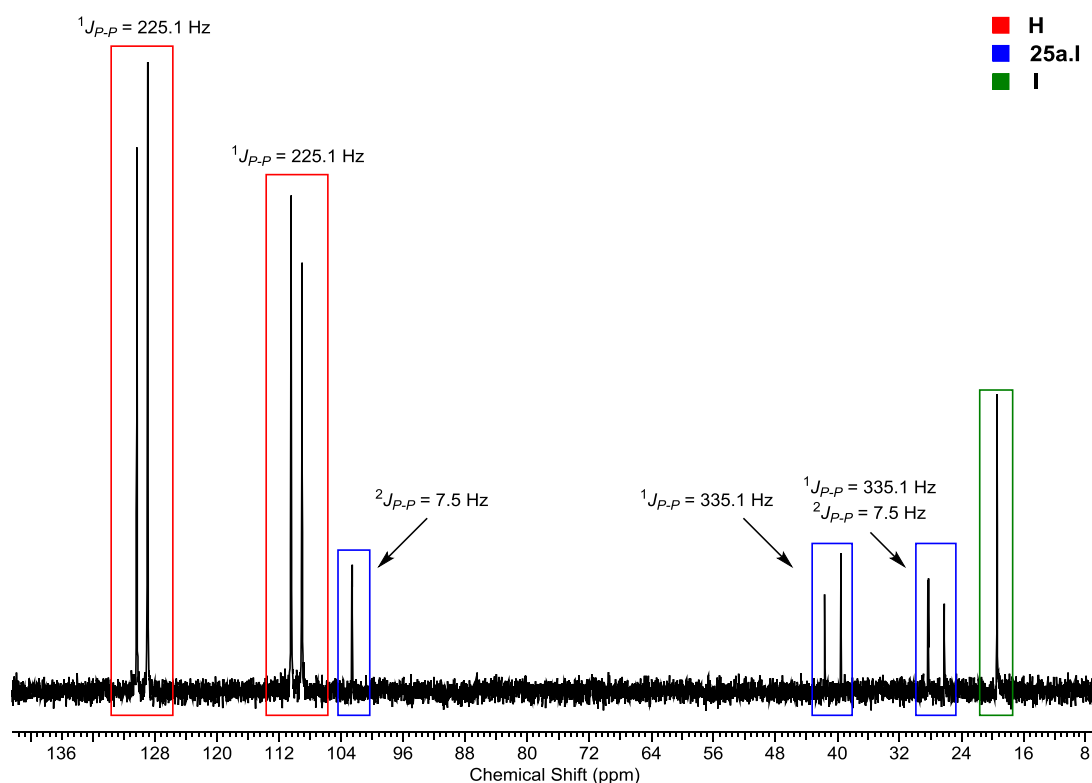


Figure 5.4.3.1: ^{31}P NMR spectrum showing the major products from the reaction of *N*-phenylbenzamidinium **1a** with PI_3 .

Additional ^{31}P NMR analysis over a wider spectral range (+ 700 to - 700 ppm) revealed the formation of P_4 (δ - 527.5 ppm) resulting from the reduction of PI_3 . The orange solid deposited from solution is therefore suspected to be red phosphorus and other polymeric material. No spectroscopic evidence was observed however for the formation of PI_4^+ , P_2I_4 or P_2I_5^+ .⁶⁰ Attempts to isolate and identify species **H** were unsuccessful.

5.5 - Transformations of Phosphorus-Amidine Heterocycles

The synthesis of the novel compound **10a** from the reaction of *N*-phenylbenzamidine **1a** with PhPCl_2 under mild conditions, prompted us to briefly explore further transformations. Reactions with the other novel P-N heterocycles described in this chapter were not attempted as they were not isolated as analytically pure samples.

5.5.1 - Thermal Rearrangement

Several phosphorus(III)-nitrogen heterocycles have been observed to thermally rearrange to give larger oligomeric, or mixed P^{III} - P^{IV} heterocycles.²⁰ Our studies with phosphorus-amidine heterocycles has also shown that heating the reaction mixture or isolated products will often lead to new P-N species (*vide supra*). No clean reactivity was observed by ^{31}P NMR spectroscopy when a solution of **10a** in DCM was heated at 60 °C for 4 days, giving only several minor species likely arising through product decomposition; this decomposition was accelerated at higher temperatures.

Following this, we repeated the reaction with a catalytic amount of AlCl_3 (25 %); Lewis-acid mediated rearrangements of dimeric to trimeric cyclophosph(III)azines are also established.¹⁹ After two days of heating at 60 °C, a new pair of doublets was observed by ^{31}P NMR spectroscopy at δ + 73.9 and + 17.2 ppm ($^1J_{\text{P-P}} = 230.1$ Hz). The integration of these peaks were approximately 25 % (with 75 % of **10a**) and no further conversion was seen on further heating. Performing the reaction with 100 % AlCl_3 in a higher boiling point solvent such as chlorobenzene gave relatively clean conversion through to the new species after 1 hour at 100 °C (Figure 5.5.1.1).

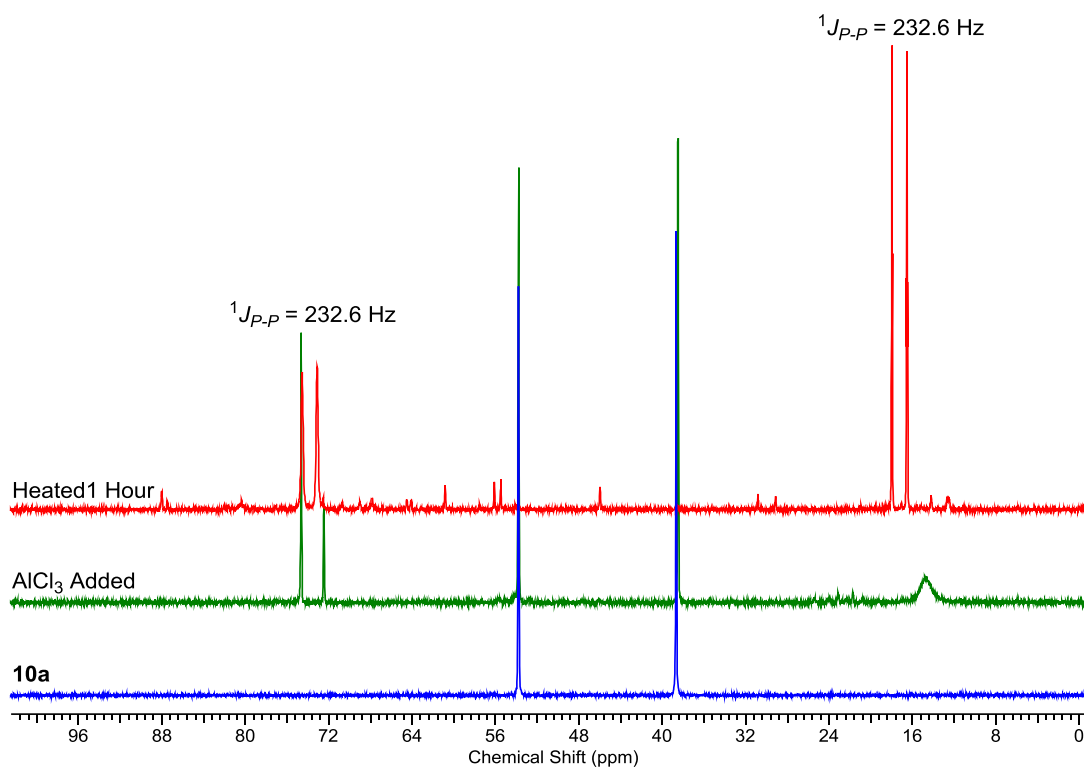
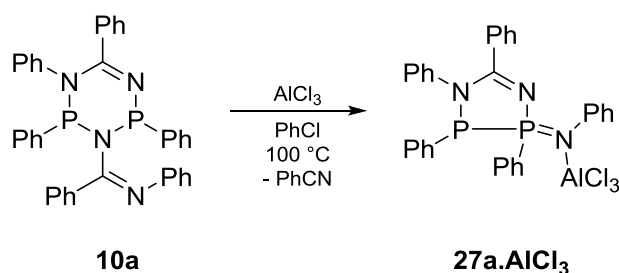


Figure 5.5.1.1: ^{31}P NMR spectrum showing the reaction of **10a** with AlCl_3 at $100\text{ }^\circ\text{C}$.

Slow diffusion of hexane into the reaction mixture afforded colourless crystals identified as **27a**. AlCl_3 by single-crystal X-ray diffraction (Scheme 5.5.1.1). Compound **27a**. AlCl_3 is a mixed P^{III} - P^{V} five-membered heterocyclic Lewis-adduct resulting from the loss of benzonitrile from **10a**. This was confirmed by monitoring the reaction by $^{13}\text{C}\{^1\text{H}\}$ NMR spectroscopy; no evidence for the formation of the cyclotrimerisation product of benzonitrile, 2,4,6-triphenyl-1,3,5-triazine, was observed.



Scheme 5.5.1.1: Reaction of **10a** with AlCl_3 at $100\text{ }^\circ\text{C}$.

Compound **27a**. AlCl_3 crystallises as colourless plates in the triclinic space group $P\bar{1}$ with two molecules in the asymmetric unit and a single molecule of PhCl (Figure 5.5.1.2). The P_2CN_2 heterocyclic rings adopt a non-planar twisted conformation (twist angle = 10.5° and 9.0°) with the two *P*-phenyl rings in a *cis*-orientation. The $\text{P}^{\text{I}}\text{-N}^3$ bond lengths are $1.625(1)\text{ \AA}$ and $1.628(1)\text{ \AA}$ for the two molecules, and intermediate of a $\text{P}^{\text{V}}=\text{N}$ double bond (range: $1.571\text{-}1.599\text{ \AA}$) and $\text{P}^{\text{V}}\text{-N}$ single bond (1.652 \AA for planar $N\text{-}sp^2$).⁵⁰ The $\text{N}^3\cdots\text{Al}^1$ distances ($1.868(1)\text{ \AA}$ and $1.871(1)\text{ \AA}$) are shorter than observed

for typical nitrogen-aluminium adducts (*e.g.* Py-AlCl₃ = 1.930(2) Å; 4-DMAP-AlCl₃ = 1.900(5) Å)^{61,62} suggesting that N3 is electron-rich.

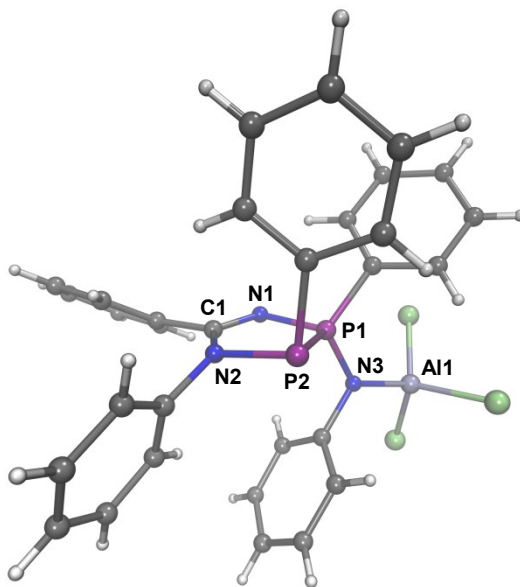


Figure 5.5.1.2: Crystal structure of **27a·AlCl₃**. Single molecule shown and solvents of crystallisation omitted for clarity.

The DFT optimised geometry of **27a·AlCl₃** is in good agreement with the experimental structure (Table 5.5.1.1). Despite the observed short P1-N3 bond lengths, which implies P=N double bond character, the bond order is only marginally above 1, and comparable to the N1-P1 bond order. The total bond valence for P1 is 4.22 and there is significant positive charge localised on P1 with negative charge on N3; this indicates that **27a·AlCl₃** is better described as a P-N ylide.

	Bond Lengths / Å		Bond Index
	Experimental	Calculated	Mayer
C1-N1	1.312(2)	1.300	1.723
	1.305(2)		
C1-N2	1.370(2)	1.384	1.073
	1.388(2)		
N1-P1	1.650(1)	1.667	1.086
	1.660(1)		
N2-P2	1.761(1)	1.760	0.873
	1.754(1)		
P1-P2	2.214(5)	2.242	0.809
	2.230(6)		
P1-N3	1.625(1)	1.635	1.143
	1.628(1)		
N3-Al1	1.868(1)	1.886	0.597
	1.871(1)		

Table 5.5.1.1: Selected experimental and calculated bond lengths and Mayer bond indices for **27a·AlCl₃**.

5.5.2 – Methylation

It was reasoned that *N*-methylation of **10a**, ideally at N1, followed by one-electron reduction might afford a neutral phosphorus-nitrogen heterocyclic radical. An immediate shift in the peak positions in the ^{31}P NMR spectrum was observed on addition of MeOTf to a solution of **10a** in DCM, to give a narrow doublet at $\delta + 71.7$ ppm and a narrow multiplet at $\delta + 30.6$ ppm (Figure 5.5.2.1). This multiplet collapsed to a narrow doublet in the $^{31}\text{P}\{^1\text{H}\}$ NMR spectrum to reveal weak $^2J_{\text{P-P}}$ coupling (7.5 Hz). The ^1H NMR spectrum showed a small but clear shift for the aromatic protons, and a new doublet at $\delta + 2.84$ ppm ($^2J_{\text{H-P}} = 14.3$ Hz) corresponding to the methyl-group; this indicates that similarly to **19r** (see section 4.6.3.1), methylation had occurred at phosphorus and not on nitrogen.

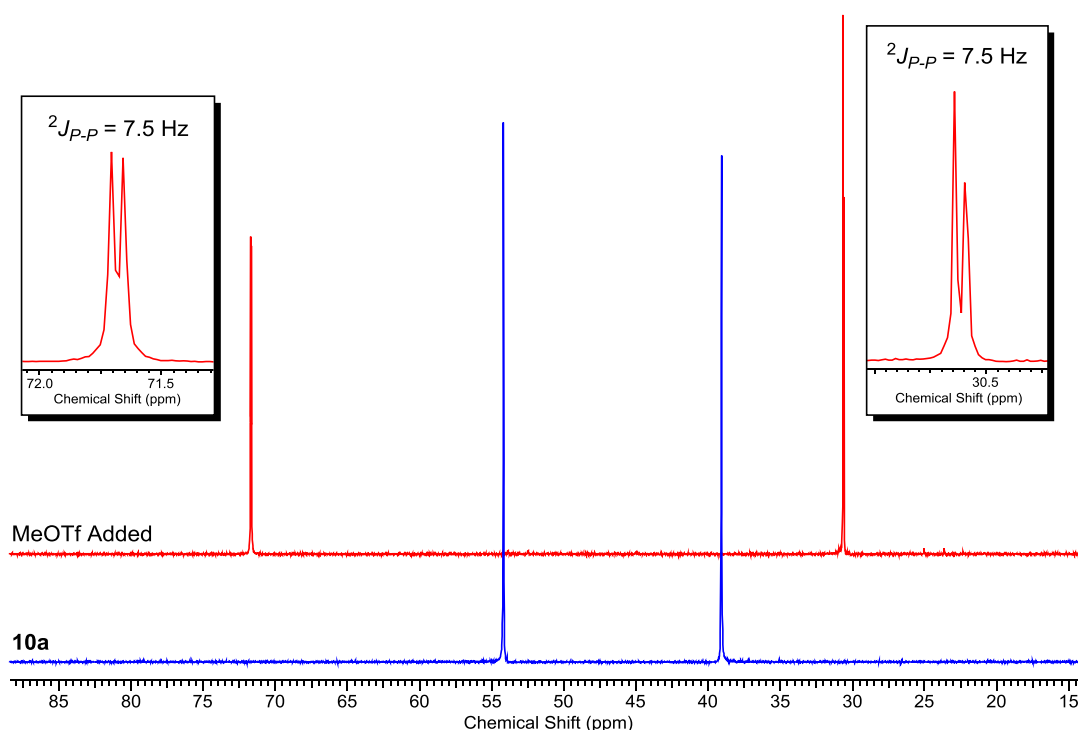
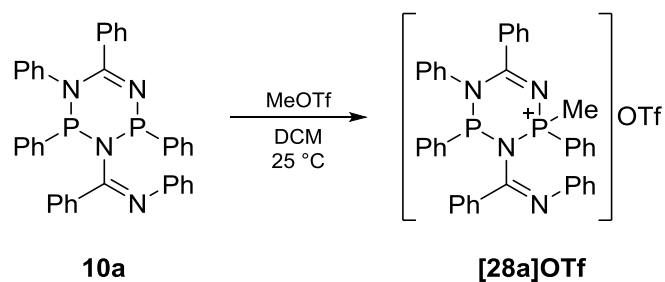


Figure 5.5.2.1: $^{31}\text{P}\{^1\text{H}\}$ NMR spectrum showing the reaction of **10a** with MeOTf.

Single crystals suitable for X-ray diffraction, grown by slow diffusion of hexane into the DCM reaction mixture, revealed the formation of **[28a]OTf** (Scheme 5.5.2.1). This confirmed that methylation had occurred at the least sterically hindered and most nucleophilic phosphorus centre; the HOMO of **10a** is largely localised on P1.



Scheme 5.5.2.1: The reaction of **10a** with MeOTf.

Compound **[28a]OTf** crystallises as colourless plates in the monoclinic space group $P2_1$ with a single ion pair in the asymmetric unit (Figure 5.5.2.2). The P_2CN_3 heterocyclic ring retains a distorted envelope conformation, folded along the $P2 \cdots N1$ axis by 31.2° (*cf.* 36.4° for **10a**) with the two *P*-phenyl rings in a *cis*-orientation. The λ^4 -phosphonium P1 adopts a distorted tetrahedral geometry with R-P-R' angles ranging from $106.1(2)^\circ$ to $114.2(2)^\circ$ whilst P2 possesses a distorted trigonal-pyramidal geometry; the sum of bond angles around P2 is 301.6° (*cf.* 302.26° for **10a**). On *P*-methylation the N1-P1 and N3-P1 bond lengths contract significantly compared to **10a** whilst the N2-P2 and N3-P2 increase marginally (Table 5.5.2.1). Minor deviations are also observed for other bond-lengths within the two amidine fragments.

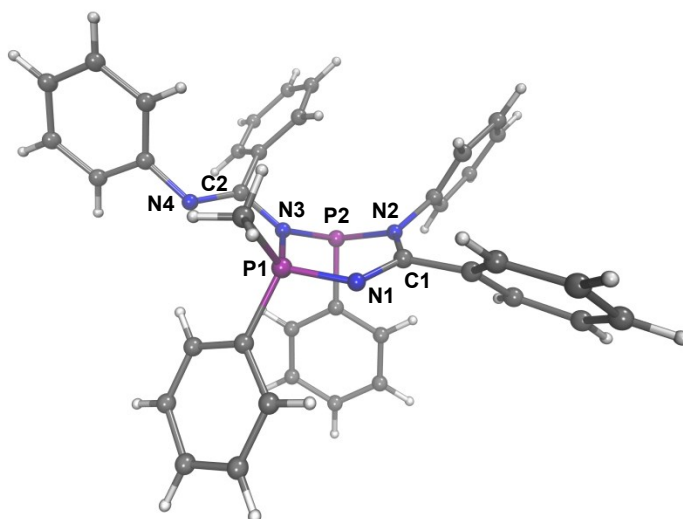


Figure 5.5.2.2: Crystal structure of **[28a]OTf**. Counterion omitted for clarity.

	Bond Lengths / Å	
	10a	[28a]OTf
C1-N1	1.281(3)	1.298(7)
C1-N2	1.422(2)	1.376(7)
N1-P1	1.679(2)	1.623(4)
N2-P2	1.723(2)	1.752(4)
N3-P1	1.765(2)	1.685(5)
N3-P2	1.729(2)	1.740(5)
N3-C2	1.399(2)	1.429(7)
C2-N4	1.279(2)	1.273(7)

Table 5.5.2.1: Selected experimental bond lengths for **10a** and [28a]OTf.

5.5.3 – One-Electron Oxidation

Attempts were also made to directly oxidise **10a** to give the corresponding radical cation. This approach has successfully been applied to electron-rich cyclodiphosphazines and cyclotetraphosphines, as well as bulky *tri*-aryl phosphines.^{63,64} No reaction was observed when **10a** was treated with AgBAR^F or NOBF₄/NaBAR^F whilst a deep blue solution formed when DDQ was used (DCM, -95 °C) despite being a weaker oxidant.⁶⁵ This solution however swiftly discoloured on warming to room temperature before EPR measurements could be recorded. Cyclic voltammetry studies of **10a** revealed an irreversible oxidation at +0.743 V which suggests that a stable radical cation of **10a** may not be isolable; the irreversible peak at -1.236 V is attributed to the reduction of trace oxygen (Chart 5.5.3.1).

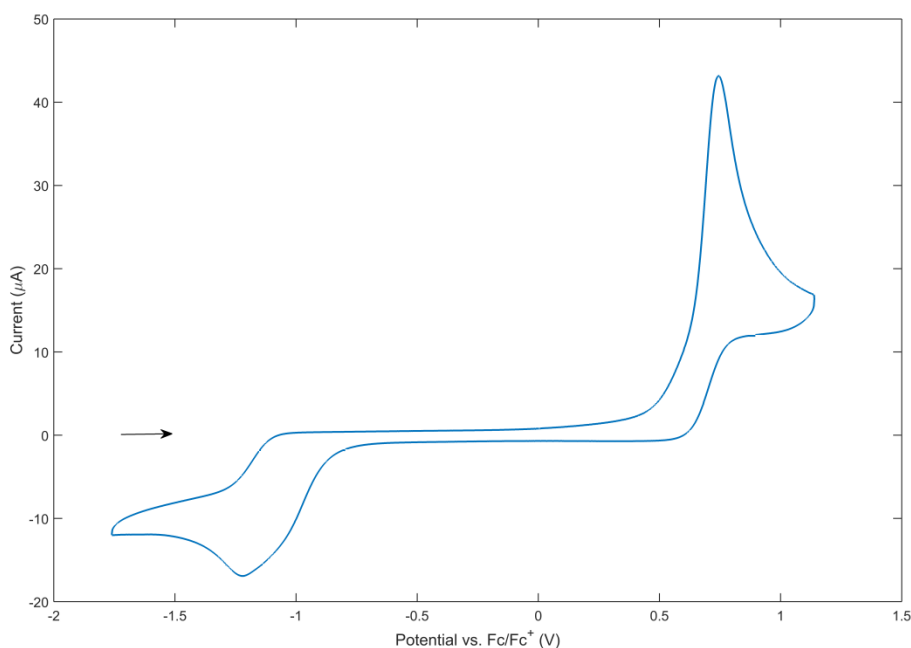


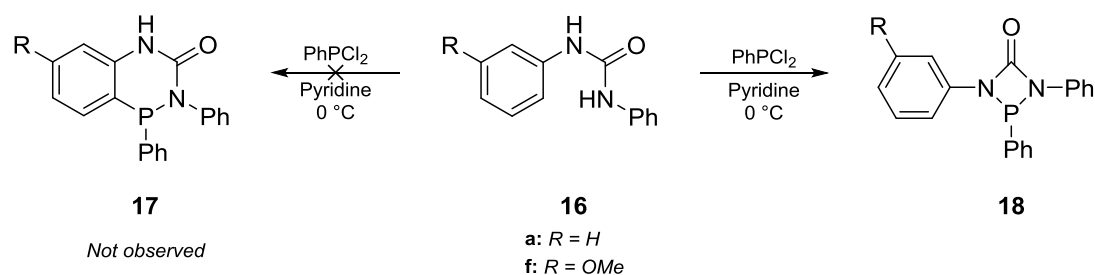
Chart 5.5.3.1: Cyclic voltammogram of **10a**.

5.6 – Reactions of *N,N'*-Diarylureas with Chlorophosphines

In Chapter 4, the syntheses of fused-ring 1,2,4-benzophosphadiazines from electron-rich *N,N'*-diarylureas was investigated. These studies indicated that there are three major factors that influence whether the benzo-fused or non-fused heterocycle is formed; namely the *C*-nucleophilicity of the aromatic ring, the electrophilicity of the phosphine, and the strength of the base employed in the reaction.

5.6.1 – Electron-Poor *N,N'*-Diarylureas

When electron-poor or electron-neutral *N,N'*-diarylureas are used, the four-membered heterocycles **18** are formed instead of the corresponding fused-ring 1,2,4-benzophosphadiazine **17** (Scheme 5.6.1.1). This four-membered heterocycle is believed to be an intermediate species for both the fused-ring heterocycles⁶⁶ and other phosphorus-urea heterocycles,^{31,32} but have only been isolated (as distillable liquids) from *bis*-silylated ureas when electron-withdrawing groups on phosphorus and nitrogen are employed.³³



Scheme 5.6.1.1: Reaction of *N,N'*-diarylureas with PhPCl_2 .

Compound **18a** crystallises as colourless plates in the monoclinic space group $P2_1/c$ with a single molecule in the asymmetric unit (Figure 5.6.1.1). The PCN_2 heterocyclic ring is planar but the N1- and N2-phenyl rings deviate slightly from this plane by 2.6° and 4.3° respectively, whilst the *P*-phenyl ring is almost perpendicular at 81.1° . The internal bond angles for P1-N1-C1, N1-C1-N2 and P1-N2-C1 are similar and range from $94.5(1)^\circ$ to $97.3(1)^\circ$ whilst the N1-P1-N2 angle is considerably smaller at $73.4(7)^\circ$. The bond lengths within the heterocyclic ring are non-symmetrical; notably, the P1-N2 distance is marginally shorter than P1-N1 ($1.746(1) \text{ \AA}$ vs. $1.756(2) \text{ \AA}$). This is likely to arise due to the torsion (N-P-*C*_{ipso}-*C*_{ortho}) of the *P*-phenyl ring which is almost 0° for N2 ($0.6(2)^\circ$) and $75.8(2)^\circ$ for N1. External packing forces may also influence this asymmetry.

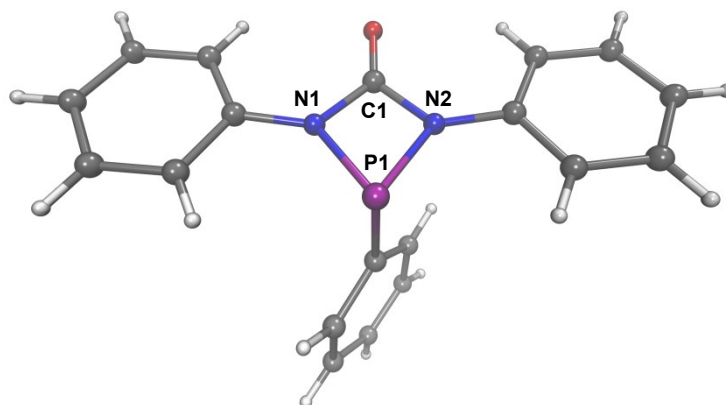
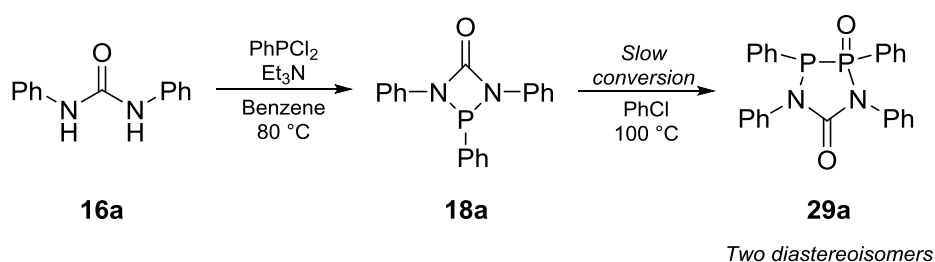


Figure 5.6.1.1: Crystal structure of **18a**.

The reaction of *N,N'*-diphenylurea **16a** with PhPCl_2 under reflux in the presence of base has been documented.³ This was postulated to form compound **29a** however all attempts to replicate this under identical published conditions cleanly afforded **18a** (Scheme 5.6.1.2). In addition, the reported ^{31}P NMR spectral data is inconsistent with the published data for the isolated and crystallographically characterised *N,N'*-dimethylurea derived heterocycle, prepared *via* alternative methods, which exists as a mixture of two diastereoisomers in solution.³³ When an isolated sample of **18a** was heated at $100\text{ }^\circ\text{C}$ in PhCl , very slow conversion (2 weeks) to **29a** was observed by ^{31}P NMR spectroscopy to give two pairs of doublets attributed to the two diastereoisomers (Figure 5.6.1.2). This draws some doubt over the published synthesis and characterisation of compound **29a**.³



Scheme 5.6.1.2: Reaction of *N,N'*-diphenylurea with PhPCl_2 .

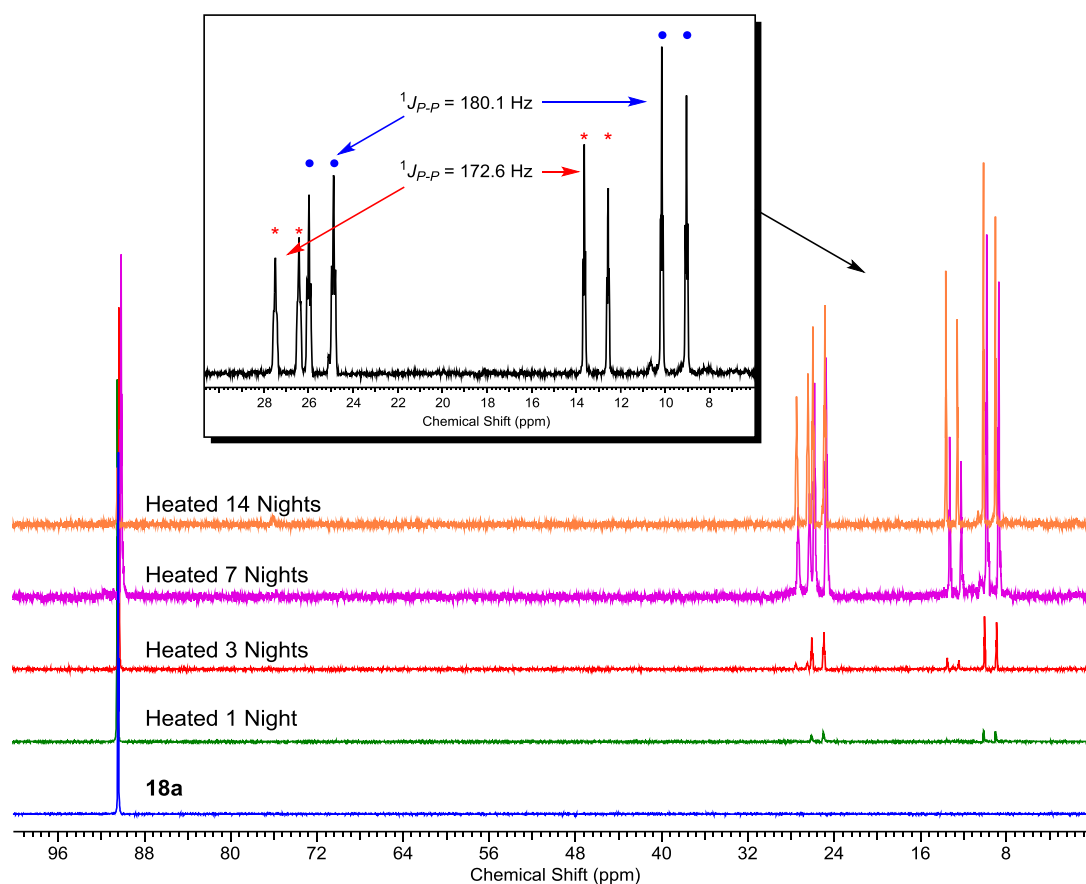
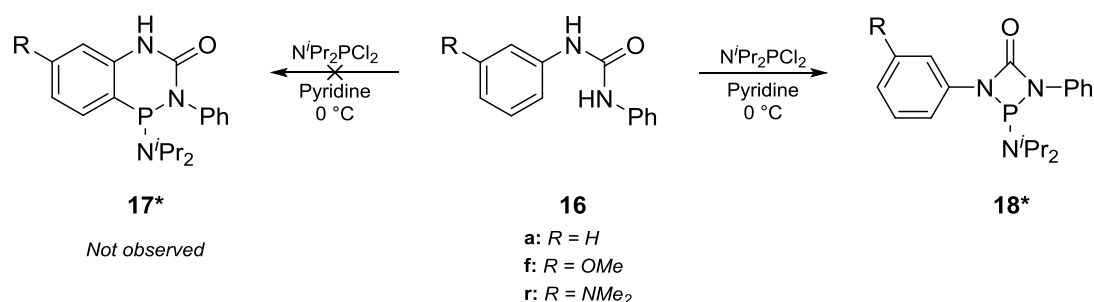


Figure 5.6.1.2: ^{31}P NMR spectra showing the thermal rearrangement of **18a**.

5.6.2 – Poorly Electrophilic Chlorophosphines

When a poorly electrophilic chlorophosphine such as $\text{N}^i\text{Pr}_2\text{PCl}_2$ was employed instead of PhPCl_2 , the four-membered heterocycle **18*** is formed regardless of the nucleophilicity of the N,N' -diarylurea **16** (Scheme 5.6.2.1).



Scheme 5.6.2.1: Reaction of N,N' -diarylureas with $\text{N}^i\text{Pr}_2\text{PCl}_2$.

Compound **18r*** crystallises as colourless blocks in the monoclinic space group $P2_1/c$ with a single molecule in the asymmetric unit (Figure 5.6.2.1). Unlike **18a**, the PCN_2 heterocyclic ring is non-planar and is folded along the $\text{P1}\cdots\text{C1}$ axis by 11.3° . The N -aryl

rings lie above the mean plane of the heterocyclic ring and are twisted in opposite directions by 5.8° and 13.4° respectively for N1 and N2. The internal bond angles for the heterocyclic ring are similar to **18a** and range from 94.1(7)° to 97.0(9)° for the P1-N1-C1, N1-C1-N2 and P1-N2-C1 angles and are again significantly more acute for N1-P1-N2 at 72.7(5)°. The heterocyclic bond lengths are moderately shorter for N1-C1 (1.390(2) Å) and N1-P1 (1.758(1) Å) than for N2-C1 (1.402(1) Å) and N2-P1 (1.770(1) Å) due to the increased electron-donating capability of the dimethylamino-substituted aryl ring.

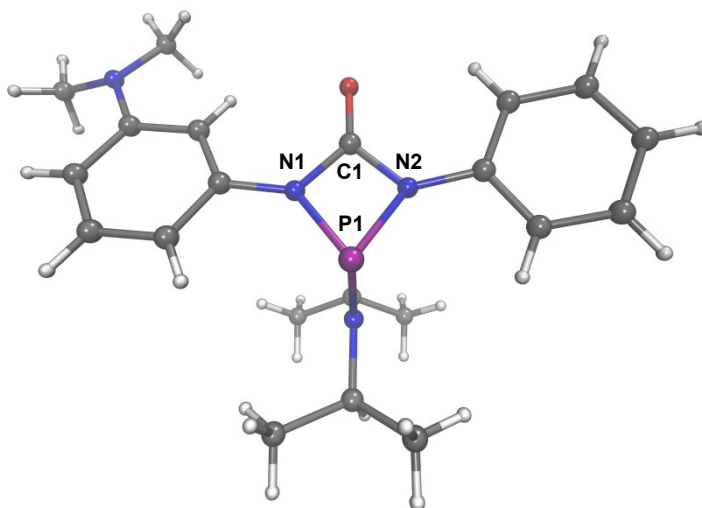
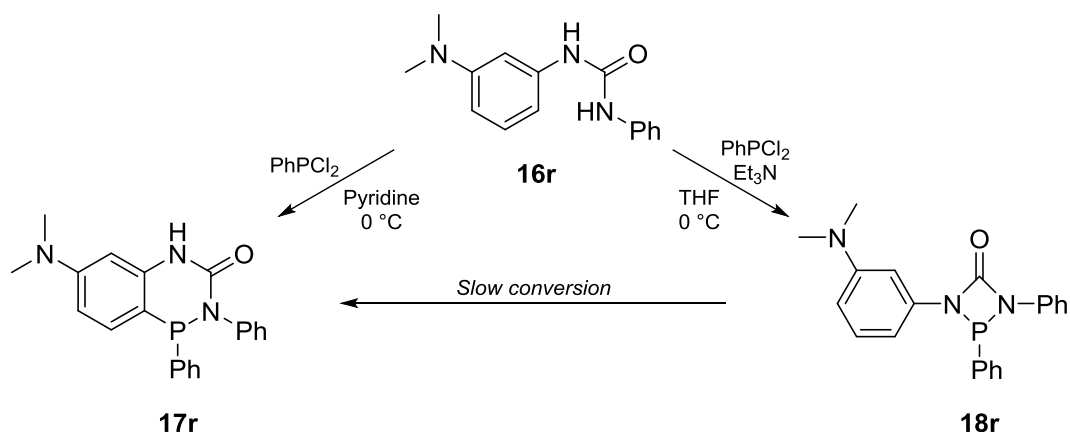


Figure 5.6.2.1: Crystal structure of **18r***.

5.6.3 – Base Strength

The strength of the base employed in the reactions of *N*-arylamidines with halophosphines was shown to be a major influence in determining which product is formed, with stronger bases favouring the formation of non-fused phosphorus-nitrogen heterocycles. Whilst the fused-ring 1,2,4-benzophosphadiazine **17r** is formed when electron rich *N,N'*-diarylurea **16r** is treated with PhPCl₂ in pyridine, the four-membered heterocycle **18r** is obtained when the reaction is performed in THF in the presence of Et₃N (Scheme 5.6.3.1).



Scheme 5.6.3.1: The influence of base on the reaction of electron-rich *N,N'*-diarylurea **16r** with PhPCl₂.

Compound **18r** however, was observed to slowly rearrange to the fused-ring heterocycle **17r** in solution by ³¹P NMR spectroscopy; this was accelerated on heating but lead to minor pairs of doublets attributed to the two diastereoisomers of **29r** (Figure 5.6.3.1). The additional minor peaks at δ + 104.0 and + 31.6 ppm are believed to be phosphine-oxides of **18r** and **17r** respectively.

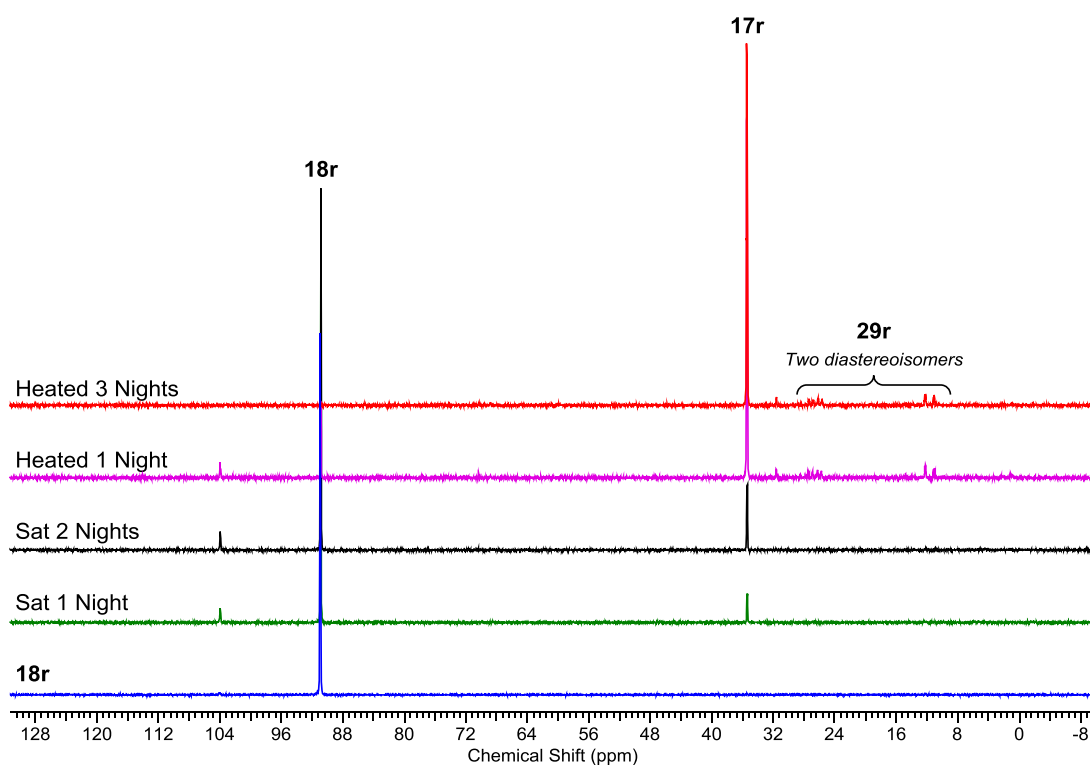


Figure 5.6.3.1: ³¹P NMR spectra showing the thermal rearrangement of **18r** to **17r**.

DFT optimised geometries for compounds **18r** and **17r** at the M06-2X/6-311g(d,p) level of theory show that the fused-ring 1,2,4-benzophosphadiazine **17r** is calculated to be significantly lower in energy (14.22 kcal mol⁻¹) than the four-membered heterocycle

18r. This rearrangement can also be justified by examination of the frontier molecular orbitals of **18r**: the highest occupied molecular orbital (HOMO) corresponds to the nucleophilic C_{aryl} centre *para* to the electron-donating dimethylamino-group, whilst the lowest unoccupied molecular orbital (LUMO) is largely localised (36.1 %) on the electrophilic phosphorus centre (Figure 5.6.3.2). This rearrangement is not observed however for **18a**, **18f** or **18r***, likely due to the increased HOMO-LUMO gap (*cf.* 6.35 eV for **18a** vs. 5.81 eV for **18r**) and less localised HOMOs, rendering the C_{aryl} sites less nucleophilic.

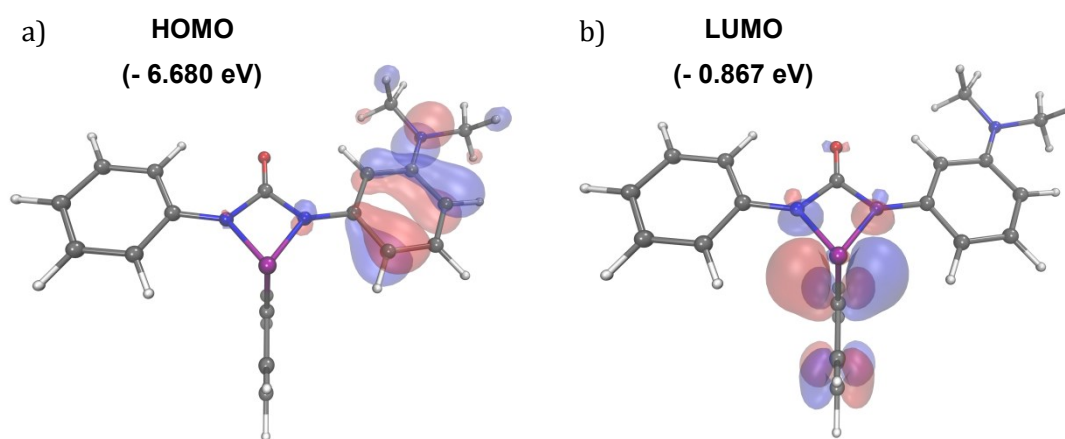
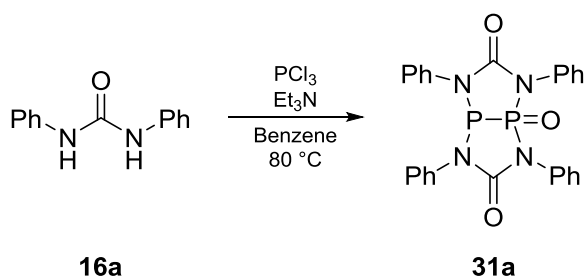


Figure 5.6.3.2: Frontier molecular orbitals and energies of **18r**: a) HOMO; b) LUMO (isovalue = 0.05).

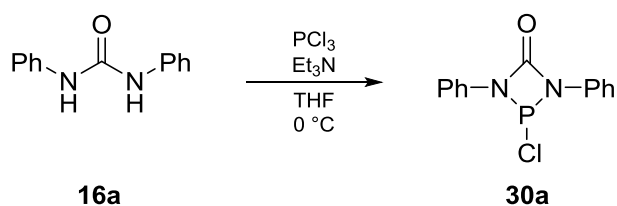
5.6.4 – Phosphorus Trichloride

The reactions of *bis*-silylated N,N' -diarylureas with PCl_3 have been studied in great detail, and are highly sensitive to both the substituents and reaction conditions, including the order in which reagents are added. For electron-rich *protio*- N,N' -diarylureas in the presence of weak base, where fused-ring heterocycles are targeted, polymeric materials are formed due to the additional free nucleophilic N-H and electrophilic P-Cl fragments. The reaction of N,N' -diphenylurea with PCl_3 is reported to give the bicyclic heterocycle **31a** when performed under reflux (Scheme 5.6.4.1).³



Scheme 5.6.4.1: Reaction of N,N' -diphenylurea **16a** with PCl_3 in the presence of base at $80\text{ }^\circ\text{C}$.

Given that this species must result from the deoxygenation of an urea fragment to give the corresponding carbodiimide, and is analogous to **29a** (see Scheme 5.6.1.2), it was reasoned that the four-membered P-Cl heterocycle must again be the initial product. Repeating the reaction at 0 °C gave a major species by ^{31}P NMR spectroscopy at $\delta + 140.1$ ppm, assigned as **30a**, amongst other unidentified minor species (Scheme 5.6.4.2). Attempts to isolate an analytically pure sample of **30a** or grow single crystals suitable for X-ray diffraction studies were unsuccessful.



Scheme 5.6.4.2: Reaction of *N,N'*-diphenylurea **16a** with PCl_3 in the presence of base at 0 °C.

Heating a PhCl solution of **30a** at 100 °C overnight resulted in complete conversion through to **31a**, which crystallised out of solution on cooling. Several other species were observed by ^{31}P NMR spectroscopy (Figure 5.6.4.1) including PCl_3 confirming that 3 equivalents of **30a** are converted to a single equivalent each of **31a**, PCl_3 and *N,N'*-diphenylcarbodiimide³³ according to Scheme 5.6.4.3.

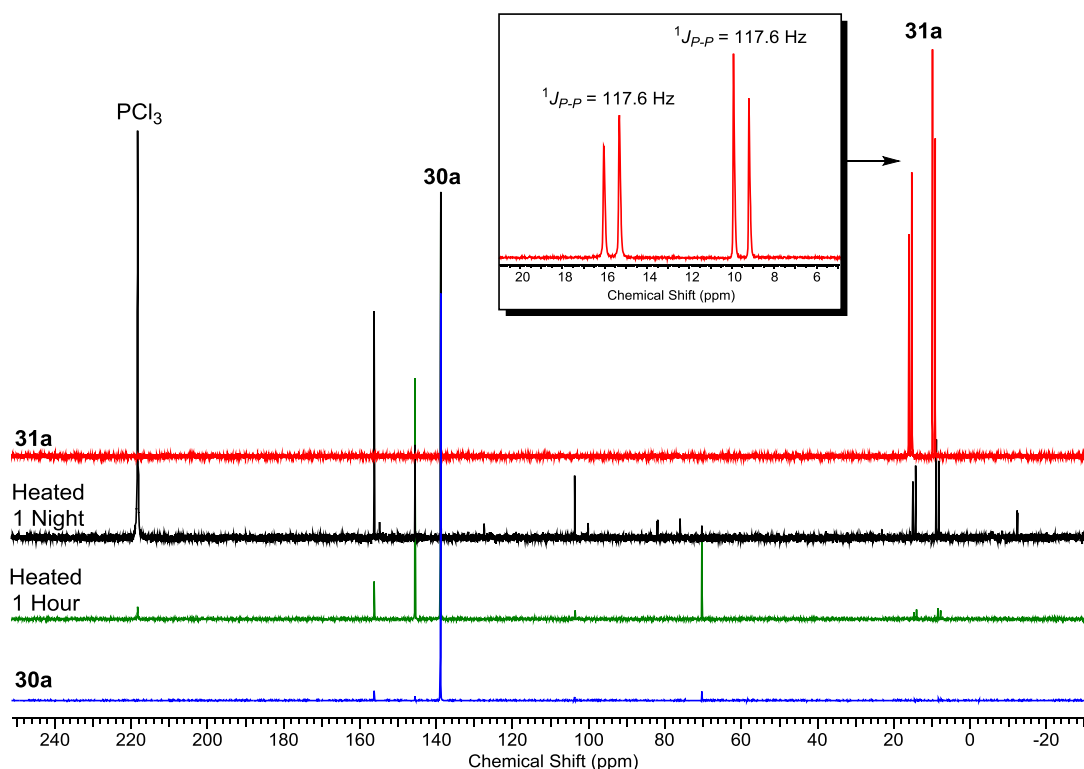
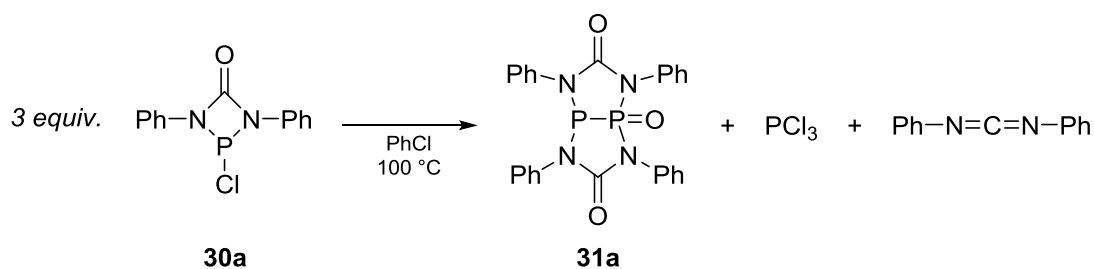


Figure 5.6.4.1: ^{31}P NMR spectra showing the thermal rearrangement of **30a** to **31a**.



Scheme 5.6.4.3: Thermal rearrangement of **30a** to give **31a** with loss of PCl₃ and *N,N'*-diphenylcarbodiimide.

Compound **31a** crystallises as colourless parallelepipeds in the triclinic space group $P\bar{1}$ with a single molecule in the asymmetric unit (Figure 5.6.4.2). The heterocyclic rings adopt an “open-book” arrangement consisting of two fused planar P₂CN₂ rings; the angle between the fused P₂CN₂ rings is 71.4°. The bond lengths and angles for the two heterocyclic rings are identical within errors, however the differing oxidation states and coordination numbers of P1 and P2 results in shorter P-N distances (*cf.* 1.682(1) Å for P1-N1 vs. 1.740(1) Å for P2-N2). The P1-P2 bond length (2.191(6) Å) is typical of other P-P bond lengths⁵⁰ despite the small ¹J_{P-P} coupling observed by ³¹P NMR; this is likely due to the strongly electron-withdrawing nature of the urea and P=O moieties.

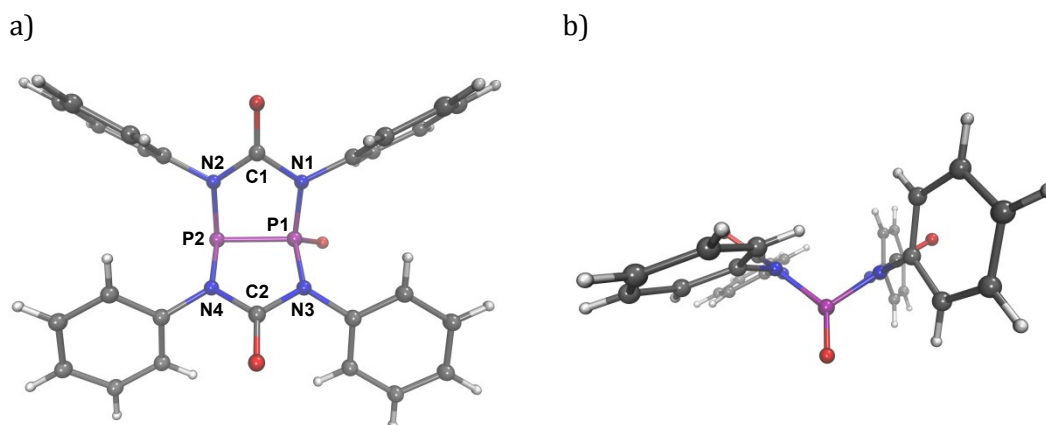


Figure 5.6.4.2: Crystal structure of **31a**; a) Top-down view; b) Side view.

5.7 – Conclusions

The reactions of *N*-arylamidines with halophosphines were shown to be highly sensitive to a number of factors including the nucleophilicity of the *N*-aryl ring, the electrophilicity of the phosphine, the strength of the base employed, and the temperature at which the reaction was performed. The formation of fused-ring 1,2,4-benzophosphadiazines **19** and six-membered P₂CN₃ heterocycles **10** were found to proceed *via* a common short-lived intermediate **24**. DFT studies were performed to provide insight into the differing pathways observed for the electron-rich and electron-poor *N*-arylamidines. The formation of the six-membered P₂CN₃ heterocycle **10** is

postulated to involve a proton-transfer mechanism, whilst the mechanism for the cyclisation of **24** to give **19** is unknown.

Complex behaviour was also observed for the phosphorus trihalides. Several species were formed on treatment of *N*-phenylbenzamidine **1a** with PCl₃ whilst PBr₃ cleanly afforded a *pseudo*-spirotricyclic cation **25a.Br** when the reaction was performed at 0 °C. When the reaction was performed at 75 °C, two new P-P coupled species are observed by ³¹P NMR spectroscopy, however all attempts to isolate these products were unsuccessful. In contrast, heating an isolated sample of **25a.Br** gave crystals of **26a** on cooling; this product must result from the breaking and making of carbon-nitrogen bonds.

N,N'-diarylureas were also shown to be highly sensitive to many of these factors. The fused-ring *P*-phenyl 1,2,4-benzophosphadiazine **17** is formed for electron-rich *N,N'*-diarylureas in the presence of weak base, whilst less nucleophilic systems gave the corresponding four-membered PCN₂ heterocycle **18**. Substitution of PhPCl₂ with the less electrophilic *N*'Pr₂PCl₂ also gave the PCN₂ heterocycle as did the use of stronger bases such as Et₃N. **18r** was found to thermally rearrange to give the fused-ring heterocycle **17r** but analogous behaviour was not observed for other systems. These findings were further supported by DFT studies.

5.8 – Future Work

Detailed computational studies in tandem with additional experiments are required to gain further insight into the mechanisms involved in the formation of fused-ring and six-membered P₂CN₃ heterocycles. This includes deuterium-labelling and kinetic isotope experiments to support the postulated proton-transfer mechanism for **10**. Isolation and identification of unknown species **F** and **G** (section 5.4.2) are highly desirable and may help justify the formation of **26a** which was observed when an isolated sample of **25a.Br** was heated in solution.

5.9 – Experimental

5.9.1 – Synthesis of *N*-Arylamidines

N-arylamidines were prepared *via* standard methods, through condensation of lithiated anilines with benzonitrile, followed by aqueous work-up. Further details are given in Chapter 2.

5.9.1.1 – Synthesis of *N*-*tert*-butyl-benzamidine, **1s**:

Amber oil, 89.6 % yield. $^1\text{H NMR}$ (400 MHz, DCM, 25.0 °C) δ : 7.50-7.44 (m, 2H), 7.39-7.33 (m, 3H), 6.40 (bs, 1H), 4.47 (bs, 1H), 1.45 (s, 9H). $^{13}\text{C}\{^1\text{H}\}$ NMR (100.5 MHz, DCM, 25.0 °C) δ : 164.0, 140.5, 129.6, 128.7, 125.9, 51.3, 28.7.

Analytical data in accordance with the literature.⁶⁷

5.9.1.2 – Synthesis of *N*-(2,6-diisopropylphenyl)-benzamidine, **1t**:

Colourless microcrystalline solid, 76.0 % yield. $^1\text{H NMR}$ (400 MHz, DCM, 25.0 °C) δ : 7.94 (d, $J = 6.8$ Hz, 2H), 7.54-7.44 (m, 3H), 7.20 (d, $J = 7.6$ Hz, 2H), 7.10 (t, $J = 7.4, 7.8$ Hz, 1H), 7.41 (bs, 2H), 3.04 (sep, $J = 6.8, 6.9$ Hz, 2H), 1.22 (d, $J = 6.9$ Hz, 6H), 1.19 (d, $J = 6.8$ Hz, 6H). $^{13}\text{C}\{^1\text{H}\}$ NMR (100.5 MHz, DCM, 25.0 °C) δ : 153.2, 144.6, 139.2, 135.9, 130.5, 128.6, 126.9, 123.5, 28.4, 23.6, 23.4.

Analytical data in accordance with the literature.⁶⁸

5.9.1.3 – Synthesis of *N*-(4-chlorophenyl)-benzamidine, **1u**:

Colourless microcrystalline solid, 86.0 % yield. $^1\text{H NMR}$ (400 MHz, DCM, 25.0 °C) δ : 7.84 (bs, 2H), 7.52-7.40 (m, 3H), 7.30 (d, $J = 7.9$ Hz, 2H), 6.88 (d, $J = 7.9$ Hz, 2H). $^{13}\text{C}\{^1\text{H}\}$ NMR (100.5 MHz, DCM, 25.0 °C) δ : 154.7, 148.9, 135.7, 130.7, 129.6, 128.6, 127.8, 126.9, 123.1.

Analytical data in accordance with the literature.⁶⁹

5.9.1.4 – Synthesis of *N*-phenyl-*N',N'*-bis-trimethylsilyl-benzamidine, **1a'**:

Aniline (2.9 cm³, 25 mmol) was dissolved in THF and cooled to -95 °C. *n*BuLi (2.5 M, 10 cm³, 25 mmol) was added dropwise and the pale pink suspension was allowed to warm to room temperature and stir for 1 hour. The reaction mixture was cooled to 0 °C and Me₃SiCl (3.2 cm³, 25 mmol) was slowly added. The resulting yellow suspension was stirred at room temperature for 1 hour and then cooled to -95 °C. A second portion of *n*BuLi (2.5 M, 10 cm³, 25 mmol) was added dropwise to give a bronze solution that was slowly warmed to room temperature. After 2 hours, benzonitrile (2.7 cm³, 25 mmol) was added and the reaction mixture was allowed to stir for 12 hours. The peach

suspension was recooled to 0 °C and a second portion of Me₃SiCl (3.2 cm³, 25 mmol) was slowly added. The reaction mixture was stirred at room temperature for 4 hours and then evaporated to dryness. The residues were extracted into Et₂O (2 x 25 cm³) and filtered through celite. The filtrate was removed *in vacuo* and residues recrystallised twice from hexane to give **1a'** as an off-white solid. Yield 4.7 g (13.8 mmol, 55.2 %). **¹H NMR** (400 MHz, DCM, 25.0 °C) δ: *Tautomer 1* (*N,N'*-(SiMe₃)₂ - ≈ 36 %): 7.80 (d, *J* = 6.8 Hz, 2H), 7.32 (t, *J* = 7.6, 7.8 Hz, 2H), 7.11-7.08 (m, 2H), 6.97 (d, *J* = 7.8 Hz, 2H), 6.88 (t, *J* = 7.1, 7.3 Hz), -0.01 (s, 18H). *Tautomer 2* (*N*-SiMe₃-*N'*-SiMe₃ - ≈ 64 %): 7.46-7.38 (m, 1H), 7.16-7.02 (m, 7H), 6.70 (bs, 2H), 0.11 (bs, 18H). **²⁹Si{¹H} INEPT NMR** (79.5 MHz, DCM, 25.0 °C) δ: 4.5 (s).

5.9.2 – Synthesis of Phosphorus-Amidine Heterocycles

The phosphorus-amidine heterocycles were typically prepared by treating an *N*-arylamidine with a halophosphine in the presence of Et₃N. Representative examples for each class of compound are given. Many of the compounds discussed in this chapter were found to rapidly convert through to new species and could not be isolated as analytically pure samples; ¹H and ³¹P NMR spectral data of the crude compounds is therefore provided where necessary. Crystals suitable for X-ray diffraction were grown by slow diffusion of hexane into a saturated solution of the product in DCM or toluene at 20 °C.

5.9.2.1 – Synthesis of **10a**:

1a (0.72 g, 3.7 mmol) and Et₃N (1.0 cm³, 7.4 mmol) were dissolved in THF (30 cm³) and cooled to 0 °C. PhPCl₂ (0.5 cm³, 3.7 mmol) was added dropwise and the resulting yellow suspension was warmed to room temperature and allowed to stir for 16 hours. The reaction mixture was filtered through celite and the filtrate concentrated *in vacuo*. The residues were recrystallised from DCM (5 cm³) and hexane (20 cm³) at -20 °C to give a pale yellow crystalline solid that was isolated by filtration, washed with hexane (2 x 5 cm³) and dried *in vacuo*. Yield: 0.82 g (1.4 mmol, 73.6 %). *Anal. Calc.* for C₃₈H₃₀N₄P₂: C, 75.5; H, 5.0; N, 9.3. Found: C, 74.0; H, 5.1; N, 9.2. **¹H NMR** (400 MHz, DCM, 25.0 °C) δ: 7.85 (d, *J* = 6.5 Hz, 2H), 7.48 (t, *J* = 6.0, 6.8 Hz, 2H), 7.37-7.24 (m, 7H), 7.18-7.02 (m, 10H), 7.00 (t, *J* = 7.6, 7.9 Hz, 2H), 6.94-6.84 (m, 5H), 6.75 (d, *J* = 7.4 Hz, 2H). **³¹P NMR** (162 MHz, DCM, 25.0 °C) δ: 54.2 (s), 39.1 (s). **¹³C{¹H} NMR** (100.5 MHz, DCM, 25.0 °C) δ: 161.9 (d, *J*_{C-P} = 13.9 Hz), 161.5 (d, *J*_{C-P} = 14.7 Hz), 157.1 (d, *J*_{C-P} = 3.7 Hz), 149.4 (s), 146.6 (d, *J*_{C-P} = 3.7 Hz), 146.4 (d, *J*_{C-P} = 3.7 Hz), 141.2 (d, *J*_{C-P} = 28.6 Hz), 137.7 (d, *J*_{C-P} = 11.0 Hz), 137.6 (d, *J*_{C-P} = 8.1 Hz), 133.9 (d, *J*_{C-P} = 3.7 Hz), 133.1 (d, *J*_{C-P} = 18.3 Hz), 129.9 (d, *J*_{C-P} = 48.4 Hz), 129.7 (d, *J*_{C-P} = 3.7 Hz), 129.4 (d, *J*_{C-P} = 31.5 Hz), 129.2 (d, *J*_{C-P} = 44.0 Hz),

128.7 (d, $J_{C-P} = 1.5$ Hz), 128.2 (d, $J_{C-P} = 5.1$ Hz), 128.1 (d, $J_{C-P} = 26.4$ Hz), 128.0 (s), 127.4 (d, $J_{C-P} = 5.1$ Hz), 124.6 (s), 124.5 (d, $J_{C-P} = 5.9$ Hz), 122.7 (s), 122.3 (s).

5.9.2.2 – Synthesis of 10s:

Pale yellow crystalline solid, 37.1 % yield. *Anal.* Calc. for $C_{34}H_{38}N_4P_2$: C, 72.3; H, 6.8; N, 9.9. Found: C, 72.1; H, 6.9; N, 9.8. 1H NMR (400 MHz, DCM, 18.5 °C) δ : 7.82-7.77 (m, 2H), 7.54 (d, $J = 6.7$ Hz, 2H), 7.46-7.35 (m, 3H), 7.33-7.21 (m, 9H), 7.11-7.03 (m, 2H), 6.99 (td, $J = 1.9, 7.8$ Hz, 2H), 1.33 (s, 9H), 1.08 (s, 9H). ^{31}P NMR (162 MHz, DCM, 18.7 °C) δ : 43.1 (d, $^2J_{P-P} = 11.4$ Hz), 38.7 (d, $^2J_{P-P} = 11.4$ Hz). $^{13}C\{^1H\}$ NMR (100.5 MHz, DCM, 19.4 °C) δ : 160.9 (d, $J_{C-P} = 5.9$ Hz), 160.8 (d, $J_{C-P} = 4.4$ Hz), 157.8 (d, $J_{C-P} = 11.7$ Hz), 157.4 (d, $J_{C-P} = 11.7$ Hz), 143.0 (d, $J_{C-P} = 2.2$ Hz), 142.7 (d, $J_{C-P} = 2.2$ Hz), 142.3 (d, $J_{C-P} = 6.6$ Hz), 139.5 (d, $J_{C-P} = 9.5$ Hz), 138.7 (d, $J_{C-P} = 4.4$ Hz), 138.6 (d, $J_{C-P} = 3.7$ Hz), 132.6 (d, $J_{C-P} = 18.3$ Hz), 130.6 (d, $J_{C-P} = 21.3$ Hz), 129.2 (d, $J_{C-P} = 71.9$ Hz), 128.7 (d, $J_{C-P} = 4.4$ Hz), 128.5 (d, $J_{C-P} = 1.5$ Hz), 128.4 (d, $J_{C-P} = 26.4$ Hz), 128.3 (d, $J_{C-P} = 5.1$ Hz), 127.8 (s), 127.7 (d, $J_{C-P} = 5.1$ Hz), 127.4 (d, $J_{C-P} = 5.1$ Hz), 127.3 (d, $J_{C-P} = 5.1$ Hz), 59.3 (d, $J_{C-P} = 3.7$ Hz), 59.1 ((d, $J_{C-P} = 3.7$ Hz), 54.8 (s), 32.3 (d, $J_{C-P} = 2.2$ Hz), 32.2 (d, $J_{C-P} = 2.2$ Hz), 32.1 (s).

5.9.2.3 – Synthesis of 24r:

1r (0.53 g, 2.2 mmol) and Et_3N (0.62 cm³, 4.5 mmol) were dissolved in toluene (25 cm³) and cooled to 0 °C. $PhPCl_2$ (0.3 cm³, 2.2 mmol) was added dropwise and the bright yellow suspension was allowed to warm to room temperature and stir for 3 hours. The solids were removed *via* filtration through celite and washed with toluene (2 x 5 cm³). The filtrate was concentrated *in vacuo* and the residues recrystallised from DCM and hexane at -20 °C. The pale yellow solids were isolated by filtration, washed with hexane and Et_2O (5 cm³ each) and dried *in vacuo*. Yield: 0.45 g (0.66 mmol, 59.7 %). 1H NMR (400 MHz, DCM, 25.0 °C) δ : 7.61 (d, $J = 7.4$ Hz, 4H), 7.57 (dd, $J = 8.0, 11.4$ Hz), 7.32-7.21 (m, 10H), 7.13-7.07 (m, 5H), 6.82 (t, $J = 7.9, 8.0$ Hz, 2H), 6.25 (dd, $J = 1.6, 8.4$ Hz, 2H), 6.14 (d, $J = 7.6$ Hz, 2H), 6.02 (s, 2H), 2.52 (s, 12H). ^{31}P NMR (162 MHz, DCM, 25.0 °C) δ : 52.2 (d, $^1J_{P-P} = 245.1$ Hz), 10.2 2 (d, $^1J_{P-P} = 245.1$ Hz).

5.9.2.4 – Synthesis of 25a.Br:

1a (1.04 g, 5.3 mmol) and Et_3N (1.5 cm³, 10.8 mmol) were partially dissolved in toluene (40 cm³) and cooled to 0 °C. PBr_3 (0.5 cm³, 5.3 mmol) was added dropwise and the pale orange suspension was allowed to stir at room temperature for 1 hour then filtered through celite. The solids were washed with toluene (2 x 10 cm³) and the combined filtrate was evaporated to dryness. The residues were redissolved in DCM (5 cm³) and hexane (30 cm³) was added with strong stirring to give a pale cream precipitate. After

1 hour, the supernatant was removed *via* filter cannula, the solids were washed with hexane and Et₂O (5 cm³ each), and dried *in vacuo*. Yield: 1.14 g (1.25 mmol, 70.2 %). **¹H NMR** (400 MHz, DCM, 25.0 °C) δ: 7.69 (d, *J* = 7.5 Hz, 3H), 7.45-7.09 (m, 23H), 7.06 (d, *J* = 7.8 Hz, 3H), 6.51 (d, *J* = 6.4 Hz, 1H). **³¹P NMR** (162 MHz, DCM, 25.0 °C) δ: 104.1 (d, ²*J*_{P-P} = 5.0 Hz), 31.5 (d, ¹*J*_{P-P} = 330.2 Hz), 29.2 (dd, ¹*J*_{P-P} = 330.2 Hz, ²*J*_{P-P} = 5.0 Hz).

5.9.2.5 – NMR Scale Synthesis of **27a**.AlCl₃:

To a J. Young's NMR tube fitted with a *d*₆-DMSO capillary was added **10a** (30.2 mg, 0.05 mmol), AlCl₃ (6.7 mg, 0.05 mmol) and PhCl (0.6 cm³). The NMR tube was heated at 100 °C for 1 hour to give a yellow solution of **27a**.AlCl₃. Attempts to isolate **27a**.AlCl₃ were unsuccessful. **³¹P NMR** (162 MHz, PhCl, 19.8 °C) δ: 73.8 (d, ¹*J*_{P-P} = 232.6 Hz), 17.2 (d, ¹*J*_{P-P} = 232.6 Hz).

5.9.2.6 – NMR Scale Synthesis of **[28a]**OTf:

To a J. Young's NMR tube fitted with a *d*₆-DMSO capillary was added **10a** (32.1 mg, 0.053 mmol) and DCM (0.6 cm³). MeOTf (0.006 cm³, 0.053 mmol) was added to give a colourless solution of **[28a]**OTf. Attempts to isolate **[28a]**OTf were unsuccessful. **¹H NMR** (400 MHz, DCM, 25.0 °C) δ: 7.80 (d, *J* = 7.3 Hz, 2H), 7.67 (d, *J* = 7.3 Hz, 1H), 7.63 (d, *J* = 7.4 Hz, 1H), 7.51 (q, *J* = 7.4 Hz, 2H), 7.42-7.22 (m, 17H), 7.17 (td, *J* = 2.4, 7.8 Hz, 2H), 7.11 (t, *J* = 7.6, 7.9 Hz, 2H), 7.06 (t, *J* = 7.4 Hz, 1H), 6.91 (d, *J* = 7.4 Hz, 2H), 2.84 (d, ²*J*_{H-P} = 14.3 Hz, 3H). **³¹P{¹H} NMR** (162 MHz, DCM, 25.0 °C) δ: 71.7 (d, ²*J*_{P-P} = 7.5 Hz), 30.6 (d, ²*J*_{P-P} = 7.5 Hz). **¹⁹F NMR** (376.5 MHz, DCM, 25.0 °C) δ: -79.3 (s).

5.9.3 – Synthesis of *N,N'*-Diarylureas

N,N'-diarylureas were prepared *via* standard literature procedures through condensation of a substituted aniline with phenylisocyanate. Further details are given in Chapter 4.

5.9.4 – Synthesis of Phosphorus-Urea Heterocycles

The phosphorus-urea heterocycles were typically prepared by treating an *N*-arylamidine with a halophosphine in the presence of base. The synthesis of **18a** is given as exemplar. Crystals suitable for X-ray diffraction were grown by slow diffusion of hexane into a saturated solution of the product in DCM or toluene at 20 °C.

5.9.4.1 – Synthesis of **18a**:

16a (0.47g, 2.2 mmol) and Et₃N (0.6 cm³, 4.4 mmol) were dissolved in THF (20 cm³) and cooled to 0 °C. PhPCl₂ (0.3 cm³, 2.2 mmol) was added dropwise to give a colourless suspension that was slowly warmed to room temperature and allowed to stir for 24

hours. The supernatant was removed *via* filter cannula and the solids washed with THF (5 cm³). The combined filtrate was concentrated *in vacuo* and the residues recrystallised from DCM and hexane to give **16a** as a colourless solid. Yield: 0.31 g (0.97 mmol, 43.9 %). **¹H NMR** (400 MHz, DCM, 25.0 °C) δ : 7.88 (t, J = 8.1, 8.4 Hz, 2H), 7.58 (t, J = 7.3, 7.5 Hz, 1H), 7.50 (t, J = 7.4, 7.5 Hz, 2H), 7.31-7.22 (m, 8H), 7.01 (t, J = 6.8 Hz, 2H). **³¹P NMR** (162 MHz, DCM, 25.0 °C) δ : 91.8 (t, J_{P-H} = 7.5, 10.0 Hz). **¹³C{¹H} NMR** (100.5 MHz, DCM, 25.0 °C) δ : 150.0 (d, J_{C-P} = 9.1 Hz), 139.8 (s), 138.0 (d, J_{C-P} = 5.3 Hz), 135.3 (d, J_{C-P} = 39.3 Hz), 133.9 (s), 132.2 (d, J_{C-P} = 26.8 Hz), 129.4 (s), 128.9 (s), 123.5 (s), 122.4 (s), 119.1 (s), 117.4 (d, J_{C-P} = 4.8 Hz).

5.9.4.2 – Synthesis of **18r**:

Pale yellow solid, 68.2 % yield. **¹H NMR** (400 MHz, DCM, 25.0 °C) δ : 7.89 (td, J = 1.3, 8.6 Hz, 2H), 7.58 (td, J = 1.5, 7.3 Hz, 1H), 7.5 (t, J = 7.3 Hz, 2H), 7.31-7.21 (m, 4H), 7.06 (t, J = 8.2 Hz, 1H), 7.01 (tt, J = 1.7, 6.9 Hz, 1H), 6.76 (s, 1H), 6.51 (dd, J = 1.3, 7.8 Hz, 1H), 6.40 (dd, J = 2.2, 8.4 Hz, 1H), 2.89 (s, 6H). **³¹P NMR** (162 MHz, DCM, 25.0 °C) δ : 90.9 (t, J_{P-H} = 8.4, 8.9 Hz). **¹³C{¹H} NMR** (100.5 MHz, DCM, 25.0 °C) δ : 153.5 (s), 151.6 (s), 150.2 (d, J_{C-P} = 9.5 Hz), 139.5 (s), 138.7 (d, J_{C-P} = 5.9 Hz), 138.2 (d, J_{C-P} = 5.9 Hz), 135.7 (d, J_{C-P} = 38.9 Hz), 133.8 (s), 132.0 (d, J_{C-P} = 26.4 Hz), 129.8 (s), 129.5 (d, J_{C-P} = 8.1 Hz), 129.4 (s), 128.9 (s), 123.4 (s), 122.7 (s), 119.5 (s), 117.5 (d, J_{C-P} = 5.9 Hz), 108.1 (s), 105.5 (d, J_{C-P} = 5.9 Hz), 101.7 (d, J_{C-P} = 5.1 Hz), 40.4 (s).

5.9.4.3 – Synthesis of **18r***:

16r (0.26 g, 1 mmol) was dissolved in pyridine (2.5 cm³) and cooled to 0 °C. NⁱPr₂PCl₂ (0.18 cm³, 1 mmol) was added dropwise and the pale orange solution was slowly warmed to room temperature and allowed to stir. After 15 hours Et₃N (0.42 cm³, 3 mmol) was added to give a colourless precipitate. The solvent was removed *in vacuo* and the residues extracted into toluene (2 x 10 cm³) and filtered. The filtrate was evaporated to dryness and the residues were recrystallised from MeCN at -20 °C to give **18r*** as a colourless solid. Yield: 0.21 g (0.55 mmol, 55.0 %). **¹H NMR** (400 MHz, DCM, 26.0 °C) δ : 7.45 (d, J = 7.9 Hz, 2H), 7.30 (t, J = 7.5, 7.9 Hz, 2H), 7.13 (t, J = 8.0, 8.3 Hz, 1H), 7.01 (t, J = 7.4 Hz, 1H), 6.82 (d, J = 7.9 Hz, 2H), 6.78 (s, 1H), 6.41 (d, J = 8.4 Hz, 1H), 3.88-3.77 (m, 1H), 3.61-3.48 (m, 1H), 2.93 (s, 6H), 1.56 (d, J = 5.8 Hz, 6H), 0.94 (d, J = 6.4 Hz, 3H), 0.90 (d, J = 6.4 Hz, 3H). **³¹P NMR** (162 MHz, DCM, 26.0 °C) δ : 78.8 (d, J_{P-H} = 18.1 Hz). **¹³C{¹H} NMR** (100.5 MHz, DCM, 26.0 °C) δ : 151.6 (s), 151.1 (d, J_{C-P} = 11.6 Hz), 139.8 (d, J_{C-P} = 6.5 Hz), 139.1 (d, J_{C-P} = 6.5 Hz), 129.7 (s), 129.3 (s), 122.8 (s), 117.4 (d, J_{C-P} = 5.1 Hz), 107.5 (s), 105.9 (d, J_{C-P} = 5.1 Hz), 101.4 (d, J_{C-P} = 5.8 Hz), 45.0 (d, J_{C-P} = 30.5 Hz), 44.3

(d, $J_{C-P} = 7.3$ Hz), 40.5 (s), 26.8 (d, $J_{C-P} = 13.8$ Hz), 26.7 (d, $J_{C-P} = 13.8$ Hz), 21.0 (d, $J_{C-P} = 10.2$ Hz).

5.9.4.4 – Synthesis of 30a:

Colourless solid, 38.9 % yield. $^1\text{H NMR}$ (400 MHz, DCM, 26.0 °C) δ : 7.44-7.37 (m, 8H), 7.21-7.16 (m, 2H). $^{31}\text{P NMR}$ (162 MHz, DCM, 26.0 °C) δ : 140.1 (s).

5.9.4.5 – NMR Scale Synthesis of 31a:

To a J. Young's NMR tube fitted with a d_6 -DMSO capillary was added **30a** (27.7 mg, 0.1 mmol) and PhCl (0.6 cm³). The NMR tube was heated at 100 °C for 16 hours and then slowly cooled to room temperature to give colourless crystals of **31a**. The supernatant was decanted and the crystals were dried *in vacuo*. $^1\text{H NMR}$ (400 MHz, DCM, 20.3 °C) δ : 7.42-7.10 (m, 20H). $^{31}\text{P NMR}$ (162 MHz, DCM, 20.1 °C) δ : 15.7 (d, $^1J_{P-P} = 117.6$ Hz), 9.5 (d, $^1J_{P-P} = 117.6$ Hz).

5.10 – References

- 1 F. Mathey, *Phosphorus-Carbon Heterocyclic Chemistry*, Elsevier, 2001.
- 2 R. Engel and J. I. Cohen, *Synthesis of Carbon-Phosphorus Bonds*, CRC Press, Raton, 2004.
- 3 H. Liangnian, Z. Renxi, C. Fei and L. Alhong, *Wuhan Univ. J. Nat. Sci.*, 1998, **3**, 126–128.
- 4 J. L. Paparin, A. Amador, E. Badaroux, S. Bot, C. Caillet, T. Convard, D. Da Costa, D. Dukhan, L. Griffe, J. F. Griffon, M. LaColla, F. Leroy, M. Liuzzi, A. Giulia Loi, J. McCarville, V. Mascia, J. Milhau, L. Onidi, C. Pierra, R. Rahali, E. Rosinosky, E. Sais, M. Seifer, D. Surleraux, D. Standring and C. B. Dousson, *Bioorganic Med. Chem. Lett.*, 2017, **27**, 2634–2640.
- 5 D. Da Costa, A. Roland and C. B. Dousson, *Tetrahedron Lett.*, 2017, **58**, 194–196.
- 6 C. Pierra Rouvière, A. Amador, E. Badaroux, T. Convard, D. Da Costa, D. Dukhan, L. Griffe, J. F. Griffon, M. LaColla, F. Leroy, M. Liuzzi, A. G. Loi, J. McCarville, V. Mascia, J. Milhau, L. Onidi, J. L. Paparin, R. Rahali, E. Sais, M. Seifer, D. Surleraux, D. Standring and C. Dousson, *Bioorganic Med. Chem. Lett.*, 2016, **26**, 4536–4541.
- 7 L. Stahl, *Coord. Chem. Rev.*, 2000, **210**, 203–250.
- 8 R. Suter, Z. Benkő, M. Bispinghoff and H. Grützmacher, *Angew. Chem. Int. Ed.*, 2017, **56**, 11226–11231.
- 9 M. Papke, L. Dettling, J. A. W. Sklorz, D. Szieberth, L. Nyulászi and C. Müller, *Angew. Chem. Int. Ed.*, 2017, **56**, 16484–16489.
- 10 S. S. Chitnis, H. A. Sparkes, V. T. Annibale, N. E. Pridmore, A. M. Oliver and I. Manners, *Angew. Chem. Int. Ed.*, 2017, **56**, 9536–9540.
- 11 M. S. Balakrishna, V. S. Reddy, S. S. Krishnamurthy, J. F. Nixon and J. C. T. R. B. S. Laurent, *Coord. Chem. Rev.*, 1994, **129**, 1–90.
- 12 A. Bashall, E. L. Doyle, C. Tubb, S. J. Kidd, M. McPartlin, A. D. Woods and D. S. Wright, *Chem. Commun.*, 2001, **0**, 2542–2543.
- 13 D. S. Wright, *Host-Guest Chemistry - p-Block Systems*, Elsevier Ltd., 2013, vol. 1.
- 14 M. S. Balakrishna, *Dalton Trans.*, 2016, **45**, 12252–12282.
- 15 W. Zeiss, W. Schwarz and H. Hess, *Angew. Chem. Int. Ed.*, 1977, **16**, 407–408.
- 16 R. T. Oakley, S. J. Rettig, N. L. Paddock and J. Trotter, *J. Am. Chem. Soc.*, 1985, **107**, 6923–6936.
- 17 E. Niecke, M. Nieger and F. Reichert, *Angew. Chem. Int. Ed.*, 1988, **27**, 1715–1716.
- 18 M. Lehmann, A. Schulz and A. Villinger, *Struct. Chem.*, 2011, **22**, 35–43.
- 19 N. Burford, S. T. Cameron, K. D. Conroy, B. Ellis, M. Lumsden, C. L. B. Macdonald, R. McDonald, A. D. Phillips, P. J. Ragogna, R. W. Schurko, D. Walsh and R. E.

- Wasylishen, *J. Am. Chem. Soc.*, 2002, **124**, 14012–14013.
- 20 F. Garcia, R. A. Kowenicki, D. S. Wright and L. Riera, *Dalton Trans.*, 2005, **2**, 2495–2496.
- 21 M. S. Balakrishna, D. J. Eisler and T. Chivers, *Chem. Soc. Rev.*, 2007, **36**, 650–664.
- 22 M. M. Siddiqui, J. T. Mague and M. S. Balakrishna, *Inorg. Chem.*, 2015, **54**, 1200–1202.
- 23 S. S. Kurnaravel, S. S. Krishnamurthy, T. S. Cameron and A. Lindenib, *Inorg. Chem.*, 1988, **27**, 4546.
- 24 P. Potin and R. De Jaeger, *Eur. Polym. J.*, 1991, **27**, 341–348.
- 25 I. Teasdale and O. Brüggemann, *Polymers*, 2013, **5**, 161–187.
- 26 H. C. Niu, A. J. Plajer, R. Garcia-Rodriguez, S. Singh and D. S. Wright, *Chem. Eur. J.*, 2018, **24**, 3073–3082.
- 27 H. N. Stokes, *Am. Chem. J.*, 1895, **17**, 275.
- 28 Y. J. Shin, Y. R. Ham, S. H. Kim, D. H. Lee, S. B. Kim, C. S. Park, Y. M. Yoo, J. G. Kim, S. H. Kwon and J. S. Shin, *J. Ind. Eng. Chem.*, 2010, **16**, 364–367.
- 29 V. Chandrasekhar and K. R. J. Thomas, *Appl. Organomet. Chem.*, 1993, **7**, 1–31.
- 30 H. Ulrich and A. A. R. Sayigh, *Angew. Chem. Int. Ed.*, 1964, 647–648.
- 31 H. W. Roesky, K. Ambrosius, M. Banek and W. S. Sheldrick, *Chem. Ber*, 1980, **113**, 1847.
- 32 H. W. Roesky, K. Ambrosius and W. S. Sheldrick, *Chem. Ber*, 1979, **112**, 1365.
- 33 H. W. Roesky, H. Zamankhan, W. S. Sheldrick, A. H. Cowley and S. K. Mehrotra, *Inorg. Chem.*, 1981, **20**, 2910–2915.
- 34 J. Lucas, D. Amirzadeh-asl, H. Djarrah and H. W. Roesky, *Phosphorus Sulfur Relat. Elem.*, 1983, **18**, 69–72.
- 35 A. O. Pushechnikov, D. M. Volochnyuk, D. G. Krotko, A. K. Tyltin and A. A. Tolmachev, *Chem. Heterocycl. Compd.*, 2001, **37**, 656–658.
- 36 J. Barker and M. Kilner, *Coord. Chem. Rev.*, 1994, **133**, 219–300.
- 37 M. P. Coles, *J. Chem. Soc., Dalt. Trans.*, 2006, **60**, 985985–10011001.
- 38 F. T. Edelman, *Chem. Soc. Rev.*, 2009, **38**, 2253–2268.
- 39 F. T. Edelman, *Coord. Chem. Rev.*, 1994, **137**, 403–481.
- 40 C. Ergezinger, F. Weller and K. Dehnicke, *Z. Naturforsch.*, 1988, **43b**, 1621–1627.
- 41 J. Barker, N. C. Blacker, P. R. Phillips, N. W. Alcock, W. Errington and M. G. H. Wallbridge, *Dalton Trans.*, 1996, 431–437.
- 42 B. M. Day, W. Knowelden and M. P. Coles, *Dalton Trans.*, 2012, **41**, 10930–10933.
- 43 S. Pahar, S. Karak, M. Pait, K. V. Raj, K. Vanka and S. S. Sen, *Organometallics*, 2018, **37**, 1206–1213.

- 44 B. Blom, D. Gallego and M. Driess, *Inorg. Chem. Front.*, 2014, **1**, 134–148.
- 45 C. Jones, S. J. Bonyhady, N. Holzmann, G. Frenking and A. Stasch, *Inorg. Chem.*, 2011, **50**, 12315–12325.
- 46 K. Maheswari, N. M. Rajendran, J. Meyer and N. D. Reddy, *Organometallics*, 2010, **29**, 3799–3807.
- 47 K. Maheswari and N. D. Reddy, *Organometallics*, 2012, **31**, 197–206.
- 48 K. Maheswari, A. R. Rao and N. D. Reddy, *Inorg. Chem.*, 2015, **54**, 2000–2008.
- 49 N. Nakata, N. Hosoda, S. Takahashi and A. Ishii, *Dalton Trans.*, 2018, **47**, 481–490.
- 50 A. G. Orpen, L. Brammer, F. H. Allen, O. Kennard, D. G. Watson and R. Taylor, *J. Chem. Soc., Dalt. Trans.*, 1987, S1–S83.
- 51 T. Chivers and R. S. Laitinen, *Dalton Trans.*, 2017, **46**, 1357–1367.
- 52 A. Bondi, *J. Phys. Chem.*, 1964, **68**, 441–451.
- 53 S. Stadlbauer, R. Frank, L. Maulana, P. Lönnecke, B. Kirchner and E. Hey-Hawkins, *Inorg. Chem.*, 2009, **48**, 6072–6082.
- 54 I. Häger, R. Fröhlich and E.-U. Würthwein, *Eur. J. Inorg. Chem.*, 2009, 2415–2428.
- 55 I. Pernik, B. J. Maitland, A. Stasch and C. Jones, *Can J. Chem.*, 2017, 1–34.
- 56 T. B. Rauchfuss, in *Inorganic Syntheses*, John Wiley & Sons, 2010.
- 57 M. Asay, C. Jones and M. Driess, *Chem. Rev.*, 2011, **111**, 354–396.
- 58 P. B. Hitchcock, M. F. Lappert and J. E. Nycz, *Chem. Commun.*, 2003, **129**, 1142–1143.
- 59 M. Schiffer and M. Scheer, *Angew. Chem. Int. Ed.*, 2001, **40**, 3413–3416.
- 60 M. Kaupp, C. Aubauer, G. Engelhardt, T. M. Klapotke and O. L. Malkina, *J. Chem. Phys.*, 1999, **110**, 3897–3902.
- 61 F. Thomas, T. Bauer, S. Schulz and M. Nieger, *Z. Anorg. Allg. Chem.*, 2003, **629**, 2018–2027.
- 62 A. Dimitrov, D. Heidemann and E. Kemnitz, *Inorg. Chem.*, 2006, **45**, 10807–10814.
- 63 X. Pan, X. Wang, Z. Zhang and X. Wang, *Dalton Trans.*, 2015, **44**, 15099–15102.
- 64 X. Pan, X. Chen, T. Li, Y. Li and X. Wang, *J. Am. Chem. Soc.*, 2013, **135**, 3414–3417.
- 65 N. G. Connelly and W. E. Geiger, *Chem. Rev.*, 1996, **96**, 877–910.
- 66 D. M. Volochnyuk, A. O. Pushechnikov, D. G. Krotko, A. M. Pinchuk and A. A. Tolmachev, *Synthesis*, 2005, 3124–3134.
- 67 R. Navrátil, J. Tarábek, I. Linhart and T. Martinů, *Org. Lett.*, 2016, **18**, 3734–3737.
- 68 M. Cortes-Salva, C. Garvin and J. C. Antilla, *J. Org. Chem.*, 2011, **76**, 1456–1459.
- 69 Y. Wang, H. Wang, J. Peng and Q. Zhu, *Org. Lett.*, 2011, **13**, 4604–4607.

Chapter 6

Donor-Functionalised Diiodophosphanes

"I'll be back!"

The Terminator (1984)

6.1 – Introduction

6.1.1 – A Brief Introduction to Main Group Lewis Acids

The Lewis acidity of main-group species may be modulated by the choice of substituents and overall charge, which leads to exploitable reactivities. Work by Stephan,¹ Ingleson,² and Crudden³ has shown that appropriately substituted and stabilised borenium cations are able to activate dihydrogen, in some cases catalytically, and Stephan has successfully extended this to catalysis by phosphonium cations.⁴ Hudnall⁵ and Gabbaï⁶ have exploited stibonium cations as Lewis acids to activate aldehydes, and Alcarazo has used carbene-stabilised sulfenyl cations to mimic the reactivity of λ^3 iodanes, which lead to new C-C bond forming reactions.⁷ In all cases, the careful choice of substituents was key to controlling reactivity and the nature of the interaction of main-group Lewis acids with donor species is therefore of fundamental importance.

Previous work in the Clark group has found that, contrary to expectations, tri-aryl phosphanes bearing an *ortho*-donor functionality to permit chelation form less stable phosphane-phosphenium adducts with the diphenylphosphenium [Ph_2P^+] cation in comparison to the unsubstituted Lewis base triphenylphosphane.⁸ Computational studies, coupled with crystallographic characterisation, showed that the donor phosphanes adopted an internally coordinated configuration, raising the energy of the phosphorus lone pairs, but nevertheless produced less stable adducts, which implies significant steric influence on complex stability. This is in marked contrast to the behaviour of these phosphanes in transition-metal complexes, wherein they behave as chelate ligands,^{9,10} or with hard main-group Lewis acids, where competitive binding with the donor functionality is observed.¹¹ Diiodophosphoranes, which may be regarded as phosphane-diiodine Lewis adducts, are highly crystalline species and so were selected as suitable targets to provide structural information on the behaviour of these phosphanes with soft, low steric demand Lewis acids.

6.1.2 – Introduction to Diiodophosphoranes

Molecules of the formula R_3PX_2 ($\text{X} = \text{F}, \text{Cl}, \text{Br}, \text{I}$) have been known for many years and their solid-states structures are now well established, and adopt three major structural motifs (Figure 6.1.2.1). When $\text{X} = \text{F}$,¹² the molecular five-coordinate trigonal bipyramidal species (**A**) is preferred and this structure is also observed when $\text{X} = \text{Cl}$, where R is an electron-withdrawing group ($\text{R} = \text{Ph}, \text{C}_6\text{F}_5$).^{13,14} The ionic halo-phosphonium halide salts (**B**), represented as $[\text{R}_3\text{PX}^+]\text{X}^-$, are largely dominated by $\text{X} =$

Cl¹⁵ or X = Br¹⁶⁻¹⁹ species, whilst the molecular charge-transfer “spoke” motif (C), R₃P-X-X, is frequently encountered when X = Br,^{16,18} but is most commonly observed for X = I adducts.²⁰⁻²³ The particular structure adopted is largely dependent on the identity of the halogen and the R groups, but also depends on the solvent and the crystallisation conditions employed.²⁴

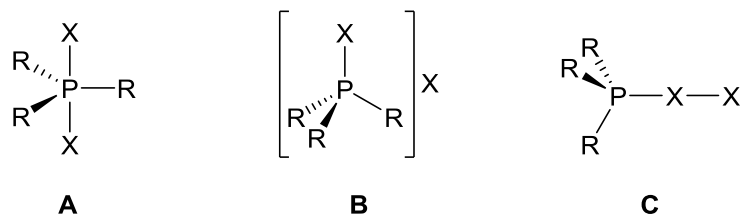


Figure 6.1.2.1: Structural motifs adopted by R₃PX₂ adducts: (A) Molecular five-coordinate trigonal bipyramidal species; (B) Ionic halo-phosphonium halide salts; (C) Charge-transfer molecular “spoke” structure.

The charge-transfer “spoke” structure adopted when X = I may be regarded as a P^{III} Lewis base adduct of the very soft, linear Lewis acid, I₂. Diiodine adducts may also be regarded as iodophosphonium iodide salts which exhibit strong cation-anion interactions between the phosphorus-bound iodine atom and I⁻ anion, and therefore the true interpretation of bonding in R₃PI₂ systems is somewhat ambiguous. Regardless, it is evident that the P-I and I-I bond lengths are highly sensitive to the electron donating capacity and steric demand about the phosphorus centre.^{22,25} The length of the I-I interaction in particular varies considerably, ranging from 3.021(1) Å²⁶ for (Me-carb)ⁱPr₂PI₂ [Me-carb = 1-(2-Me-1,2-C₂B₁₀H₁₀)] to 3.6389(14) Å²⁷ for [(ⁿPr₂N)₃PI]I, and is significantly longer than the I-I bond lengths observed in the arsenic analogues [Ph₃AsI₂ (3.005(1) Å)²⁸ vs. Ph₃PI₂ (3.161(2) Å)²¹] and I₂ (2.660 Å),²⁹ but still within the sum of the Van der Waals radii (3.96 Å).²⁹ This elongation of the I-I bond in the adducts relative to diiodine is a result of electron density being transferred into the σ* orbital of I₂ by the Lewis base, R₃P. Therefore, the I-I bond length can be regarded as highly indicative of the degree of charge transfer and thus phosphine donor strength.

The magnitude of the P-I and I-I bond lengths in diiodophosphoranes are also significantly impacted by steric effects, in particular, the P-I distances show greater susceptibility to steric influence than the I-I bond. As expected, the P-I bond length elongates as the size of the R group increases with ^tBu₃PI₂ (2.461(2) Å)²⁰ exhibiting a greater P-I separation than ⁱPr₃PI₂ (2.409(2) Å/2.420(2) Å).²³ For aryl-substituted Ar₃PI₂ adducts, the effects of sterics becomes more apparent since the orientation and

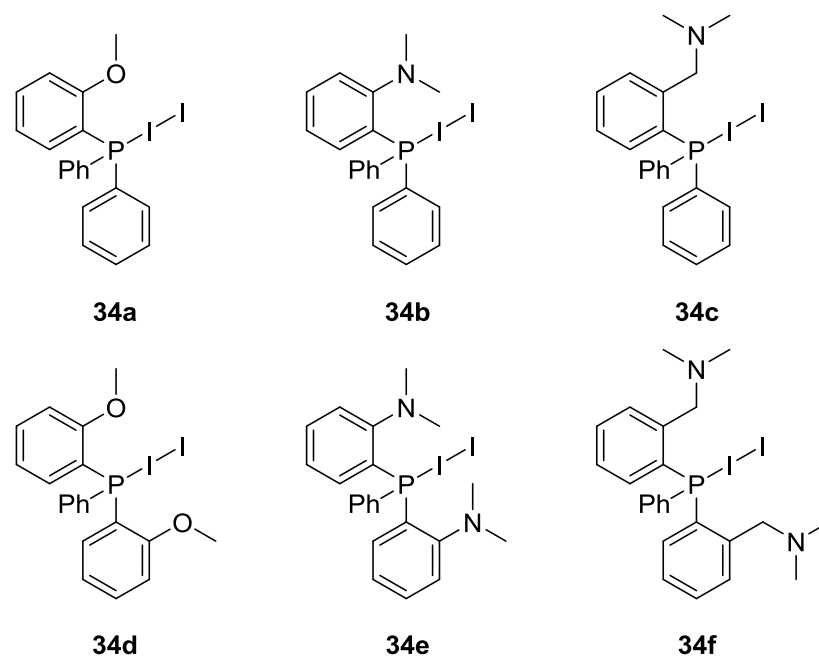


Figure 6.2.1: Selected donor-functionalised Ar_3PI_2 targets.

Compounds **34a-e** and **34g** (Ph_3PI_2) were all isolated as free flowing yellow powders. Where necessary, products were purified by recrystallisation from DCM and Et_2O . Compound **34c** was found to contain *ca.* 25% phosphine oxide impurity by ^{31}P NMR which suggests extreme moisture/air sensitivity. Attempts to prepare and purify **33f** were unsuccessful, and yielded a viscous amber oil that was found to contain an unknown phosphorus-containing impurity (*ca.* 5% by ^{31}P NMR) that interfered with all attempts to synthesise **34f**. Crystals suitable for single-crystal X-ray diffraction studies were successfully grown by slow diffusion of diethyl ether into a saturated solution of the product in dichloromethane.

6.3 – Structural Studies of Donor-Functionalised Diiodophosphoranes

As expected, the charge-transfer molecular “spoke” structure is adopted in the solid-state for the five novel donor-functionalised Ar_3PI_2 adducts. The P1-I1-I2 angles are close to linear, ranging from $171.0(3)^\circ$ for **34e** to $178.3(2)^\circ$ for **34a**. The P1-I1 and I1-I2 bond lengths fall within the large range observed for Ar_3PI_2 and R_3PI_2 adducts, but the greater electron donating capacity results in an elongated I1-I2 bond. Single-crystal X-ray diffraction data was also collected for the known unsubstituted Ph_3PI_2 adduct, **34g**, at 100K to permit direct and precise bond metric comparisons with the donor-functionalised diiodophosphoranes at the same temperature. Selected bond lengths and angles are displayed in Table 6.3.1.

The phosphorus-iodine bond length is similar to that of Ph_3PI_2 (**34g**) (*cf.* 2.4753(6) vs. 2.4690(8) Å), but the I1-I2 distance is elongated at 3.2022(3) Å. This is therefore well described as an adduct with increased phosphane donor strength, as demonstrated by the increased I1-I2 bond length, which arises from π -conjugation of the oxygen lone pairs rather than hypervalent bond formation (*vide infra*). The close oxygen-phosphorus contact must therefore arise of steric necessity, supported by the lack of contraction of the P1-I1 bond compared to the donor free structure due to steric constraint.

Molecules of **34a** form side-to-side anti-parallel pairs in which the near-linear P-I-I spoke is directed diagonally through the crystallographic *a* and *b* axes (Figure 6.3.1.2). The aryl rings adopt a staggered propeller conformation with I1-P1-C_P-C_{ortho} torsion angles ranging from 49.8(2)° to 61.3(2)°. The back-to-back sextuple phenyl embrace of molecules commonly adopted for Ar_3P containing species³⁶ is not observed, presumably due to the unsymmetrical nature of the adduct. There is however, a single long offset face-to-face (OFF) embrace between pairs of molecules and two consequent edge-to-face (EF) embraces (Figure 6.3.1.3), together with much shorter OFF embraces to diagonally neighbouring anti-parallel molecules which link to form chains that propagate along the crystallographic *b* axis. Importantly however, the donor-moiety does not electronically contribute to the packing observed in **34a**.

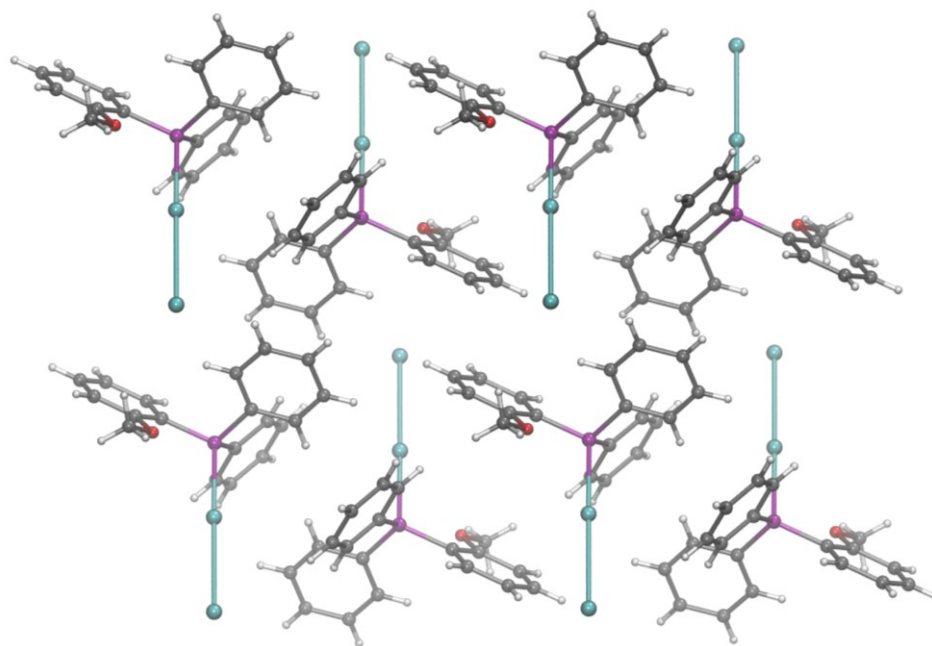


Figure 6.3.1.2: Crystal packing of **34a** looking down the crystallographic *a* axis, showing the anti-parallel arrangement of molecules.

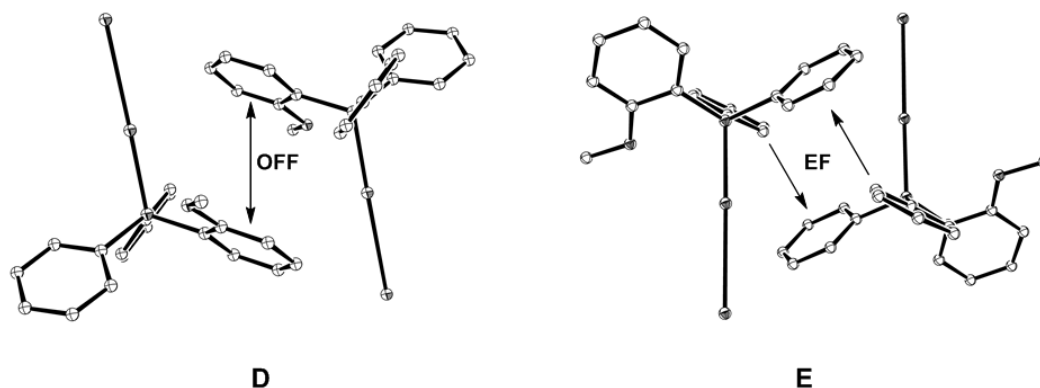


Figure 6.3.1.3: (D) The offset face-to-face (OFF) and (E) edge-to-face (EF) interactions of aromatic molecules and substituents.

6.3.2 – Crystal Structure of **34b**

Compound **34b** crystallises as yellow blocks in the triclinic space group $P\bar{1}$, with a single molecule in the asymmetric unit (Figure 6.3.2.1). The geometry of the molecule can be considered a distorted trigonal bipyramid, with a close nitrogen-phosphorus contact (2.898(1) Å) within the sum of the van der Waals radii. The donor NMe₂ fragment is rotated such that the lone pair is orthogonal to the π -system, directed towards the phosphorus centre and *trans* to the apical phenyl substituent. Furthermore, the sum of the equatorial angles is 336.51°, greater than that seen for **34g** (330.42°), although the N1-P1-C1 angle still deviates significantly from linearity at 161.9(7)°. This deviation presumably stems from the rigidity of the chelate tether. The P1-I1 bond (2.4913(5) Å) is significantly longer than that of **34g**, whilst the I1-I2 distance is considerably shorter at 3.1238(3) Å. Despite the donation of the lone pair into phosphorus, the contraction of the I1-I2 bond indicates that the overall degree of charge transfer is in fact less than that of **34g**.

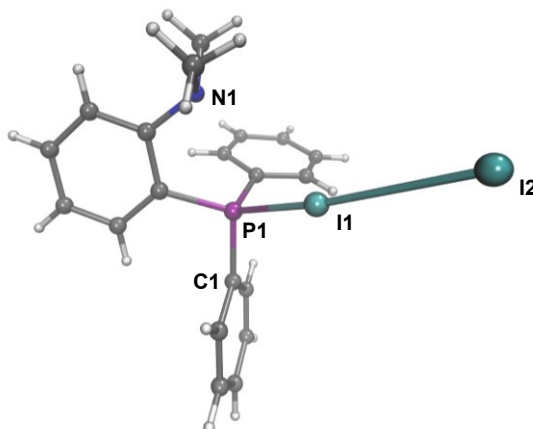


Figure 6.3.2.1: Crystal structure of **34b**.

Molecules of **34b** form dimer pairs linked by six EF embraces between the aryl rings (Figure 6.3.2.2). The aryl rings are twisted in the same direction adopting a staggered propeller conformation; the I1-P1-C_{p-Ortho} torsion angles are 58.8(2)°, 57.4(2)° and 38.0(2)°, with the lowest torsion belonging to the equatorial phenyl ring. The sextuple phenyl embrace observed for this molecule suggests that the asymmetry of the phosphane does not necessarily prevent this packing arrangement as previously hypothesised for **34a**, but does highlight the unpredictability of crystal packing within these systems.

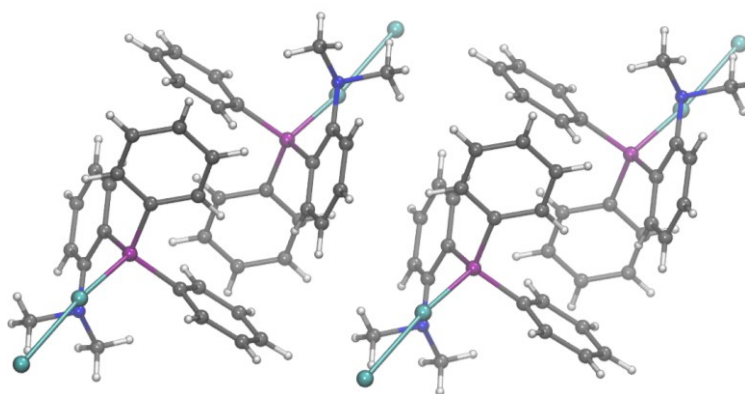


Figure 6.3.2.2: Crystal packing of **34b** looking down the crystallographic *a* axis, showing the sextuple phenyl embrace adopted between molecules.

6.3.3 – Crystal Structure of **34c**

Compound **34c** crystallises as yellow blocks in the monoclinic space group $P2_1/c$ with a single molecule with unambiguous distorted trigonal bipyramidal geometry (Figure 6.3.3.1) in the asymmetric unit. The sum of angles about the equatorial plane is 339.7° and the nitrogen-phosphorus contact (2.951(3) Å) is slightly elongated relative to **34b**. Despite the flexibility of the methylene linker which, in theory, allows the NMe₂ group to twist away from the phosphorus centre to minimise steric clashes, it adopts an apical position, linearly *trans* to a phenyl ring – the N1-P1-C1 angle is 177.8(1)°. The P1-I1 bond length is comparable to **34g** at 2.4791(7) Å, whilst the I1-I2 contact is elongated at 3.1884(3) Å, which indicates a greater degree of charge transfer.

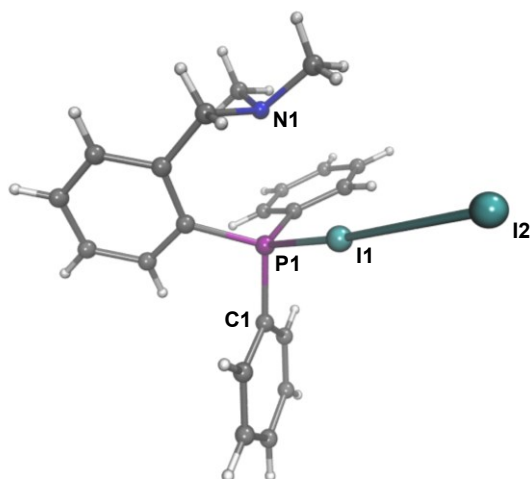


Figure 6.3.3.1: Crystal structure of **34c**.

The aryl rings in **34c** adopt a staggered propeller conformation but the phenyl ring in the equatorial plane has a small torsion angle ($4.1(3)^\circ$ compared to $47.5(3)^\circ$ and $56.3(2)^\circ$) such that an *ortho*-hydrogen is orientated upwards towards the P1-I1 bond. This molecule can therefore be termed as having an exo_1 conformation using the notation of Howell.³⁷ Molecules of **34c** form side-to-side parallel and anti-parallel pairs in which the P-I-I spoke is directed diagonally along the crystallographic *a* and *c* axes (Figure 6.3.3.2). Parallel pairs are linked by a single EF embrace with a I1-P1...P1-I1 torsion of $3.35(3)^\circ$, whilst anti-parallel pairs are linked by a single OFF embrace.

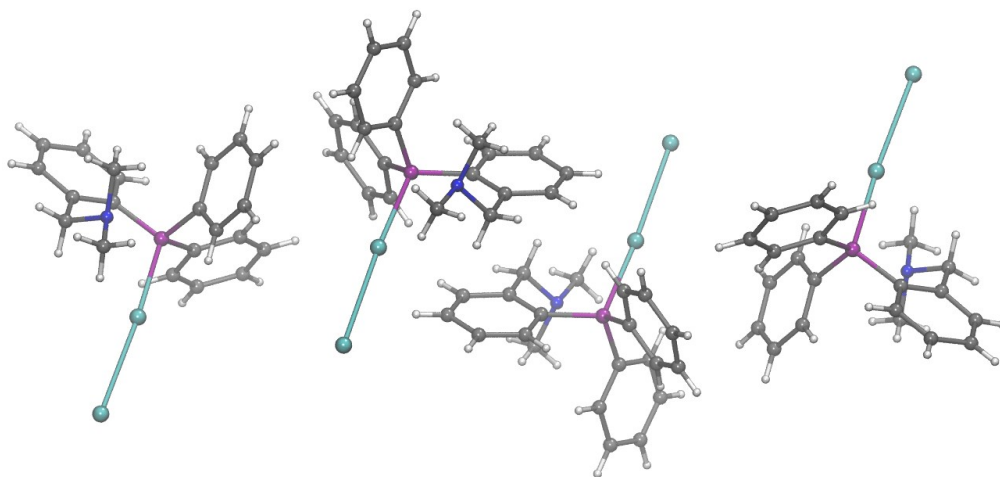


Figure 6.3.3.2: Crystal packing of **34c** looking down the crystallographic *a* axis, showing the parallel and anti-parallel pairs of molecules.

6.3.4 – Crystal Structure of 34d

Compound **34d** crystallises as yellow rhombohedra in the triclinic space group $P\bar{1}$, with a single molecule in the asymmetric unit (Figure 6.3.4.1). The molecules adopt a distorted tetrahedral geometry with both OMe fragments coplanar with their associated aryl rings, and short oxygen-phosphorus contacts ($O1\cdots P1 = 2.896(2)$ Å; $O2\cdots P1 = 2.898(1)$ Å) which arise through steric necessity. The primary methoxy moiety adopts an apical position, *trans* to the unsubstituted phenyl ring whilst the secondary OMe is *trans* to the primary anisole fragment, with both O-P- C_{trans} angles deviating significantly from linearity. Despite the addition of a second *ortho*-donor, the sum of equatorial angles (329.20°) is smaller than **34a** and the other Ar_3PI_2 adducts. Both C_{ortho} -O bonds are contracted ($C_{ortho}-O1 = 1.354(2)$ Å; $C_{ortho}-O2 = 1.358(3)$ Å) relative to free anisole, which indicates a significant degree of π -conjugation of the oxygen lone pairs into the ring. This leads to an elongation of the I1-I2 bond to $3.2648(3)$ Å and a concomitant reduction of the P1-I1 bond length ($2.4610(6)$ Å) compared to **34g**, due to increased donor strength, despite the increase in steric bulk which arises through the addition a second *ortho*-donor.

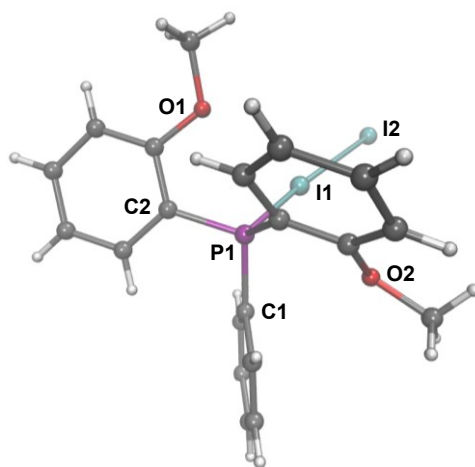


Figure 6.3.4.1: Crystal structure of **34d**.

Molecules of **34d** form side-to-side antiparallel pairs along the crystallographic c axes linked by two EF embraces; parallel neighbours are also linked by a single EF embrace along the crystallographic a axes (Figure 6.3.4.2). The P-I-I spoke is orientated diagonally through the crystallographic a and b axes. Each molecule adopts a staggered propeller conformation with I1-P1- C_P - C_{ortho} torsions ranging from $41.9(2)^\circ$ to $64.8(2)^\circ$.

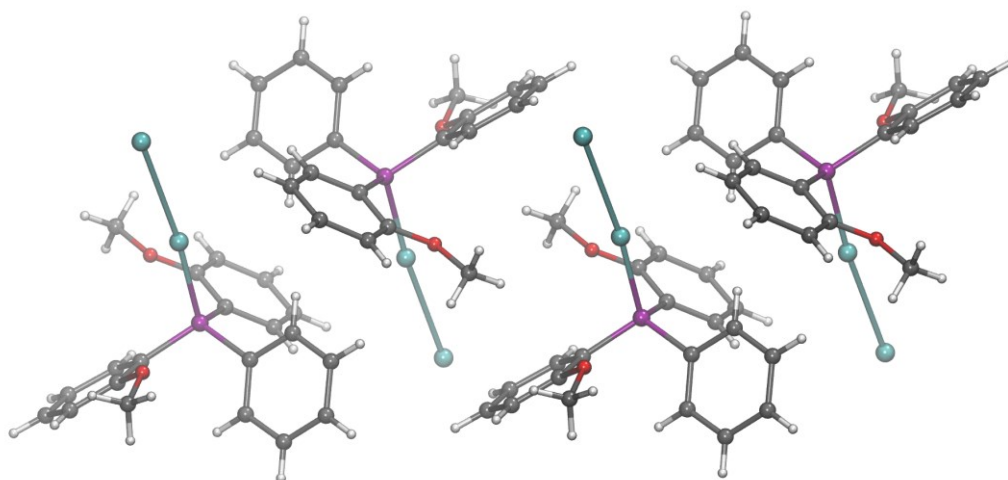


Figure 6.3.4.2: Crystal packing of **34d** looking down the crystallographic *a* axis, showing the anti-parallel pairs of molecules.

6.3.5 – Crystal Structure of **34e**

Compound **34e** crystallises as yellow blocks in the monoclinic space group $P2_1/c$ with two molecules in the asymmetric unit; both adopt distorted octahedral geometries with formally six-coordinate P^{III} centres (Figure 6.3.5.1). Both NMe_2 fragments are twisted out of conjugation with the adjacent π -system, which makes them available for donation into the phosphorus centre. In each molecule, there are two $3c4e$ hypervalent bonding interactions with one NMe_2 moiety adopting an apical position, *trans* to a phenyl ring as with **34b** whilst the second is *trans* to the I1-I2 spoke.

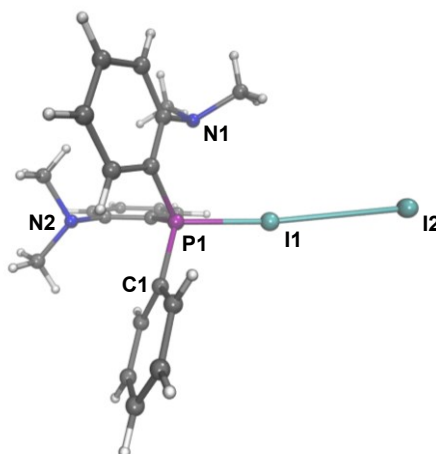


Figure 6.3.5.1: Crystal structure of **34e**.

The $N\cdots P$ contacts are again short (molecule 1, $N1\cdots P1 = 2.883(3)$ Å, $N2\cdots P1 = 2.945(3)$ Å; molecule 2, $N1'\cdots P1' = 2.904(3)$ Å, $N2'\cdots P1' = 2.933(2)$ Å), with the $N1\cdots P1$ distances comparable to **34b** but the $N2\cdots P1$ distances are slightly longer. The $N1-P1-C1$ and $N2-P1-I1$ hypervalent interactions deviate from linearity ($165.3(1)^\circ$ and $169.2(6)^\circ$

respectively) but are still expected to be strongly bonding. The significant contraction of the P1-I1 bond despite increased steric hindrance, and concomitant elongation of the I1-I2 bond, indicate increased overall donor strength for the phosphane relative to Ph_3P .

Compound **34e** adopts an $endo_1$ conformation in which the secondary NMe_2 *ortho*-substituted aryl ring is orientated such that the donor is pointing away from the P-I-I spoke and the I-P-C_{P-C_{ortho}} torsions approach 180° . The remaining two aryl rings are twisted in the same direction and have similar I-P-C_{P-C_{ortho}} torsions ranging from $59.0(2)^\circ$ to $68.6(2)^\circ$. The unit cell of **34e** contains eight molecules that form two 'up' and 'down' facing sets of four which are diagonally offset in a zigzag arrangement (Figure 6.3.5.2). Each quartet contains two pairs of parallel molecules that are further coupled with anti-parallel molecules through an inversion centre. Molecules are linked by a single EF embrace and a long-range OFF embrace along the crystallographic *c* axes.

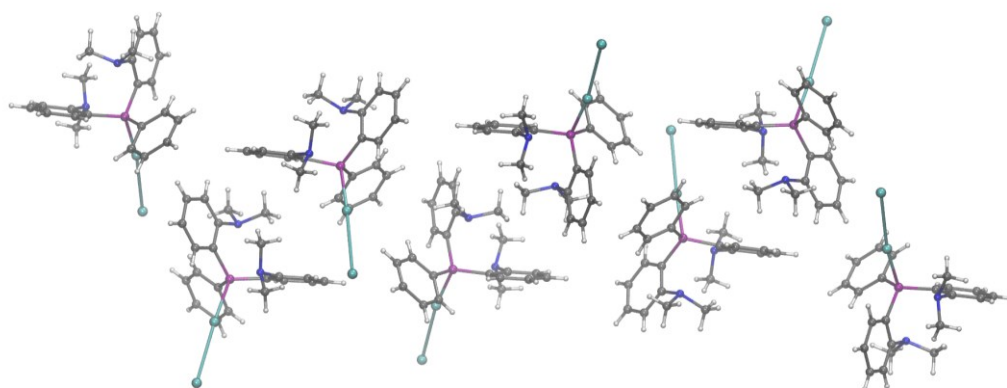
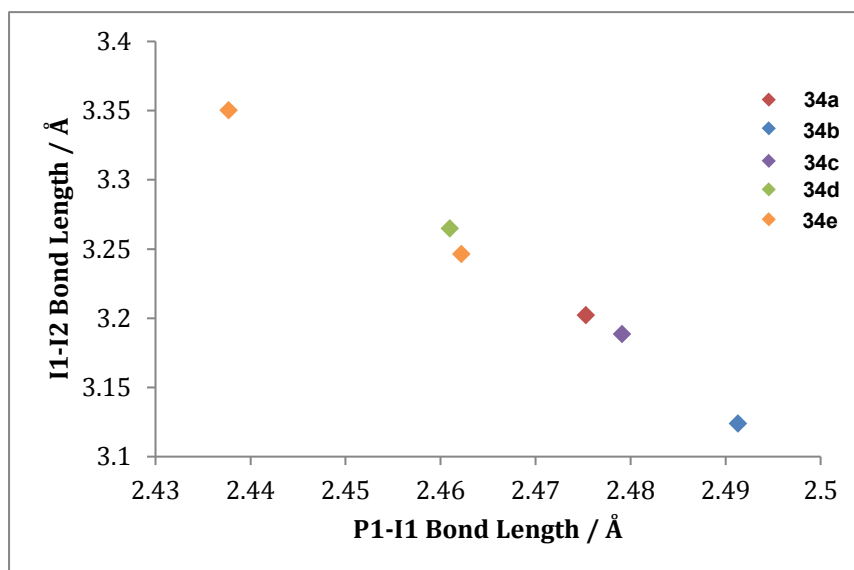


Figure 6.3.5.2: Crystal packing of **34e** looking down the crystallographic *a* axis, showing the anti-parallel pairs of molecules.

Comparison of the bond metrics between the donor-functionalised diiodophosphoranes and unsubstituted Ph_3PI_2 donor allows the relative “phosphane donor strength” to be determined and the electronic and steric effects to be understood. As the P1-I1 bond length increases, there is a linear decrease in the I1-I2 distance (Graph 6.3.1) despite the substantial variance in the sum of the P1-I1 and I1-I2 bond lengths within the internally solvated set. The P1-I1 distances show greater susceptibility to the steric influences of the donor moieties, whilst the I1-I2 distances are highly indicative of the degree of charge transfer and thus overall donor strength. From this, we can see that of the singly substituted phosphanes, **33a** is a stronger donor than both **33c** and **33b**, despite **34a** having a longer P1-I1 bond length when compared to **34g**. The short I1-I2

distances observed for **34b** and **34c** suggests that the steric demand is significant even for a single additional substituent.



Graph 6.3.1: A scatterplot of the I1-I2 bond lengths versus the P1-I1 bond lengths observed crystallographically for the donor-functionalised diiodophosphoranes.

Addition of a second donor moiety results in reduced P1-I1 bond lengths despite the increased steric demand at the phosphorus centre, with a concomitant increase in the I1-I2 distance which indicates a greater degree of charge transfer. Gratifyingly, **34b** and **34c** both show N1-P1-C1 $3c4e$ bonding interactions in preference to the potential N1-P1-I1 motif – it is only for **34e** that both become observed – this is perhaps unsurprising considering that hypervalent bonding is stabilised by electronegative apical elements.

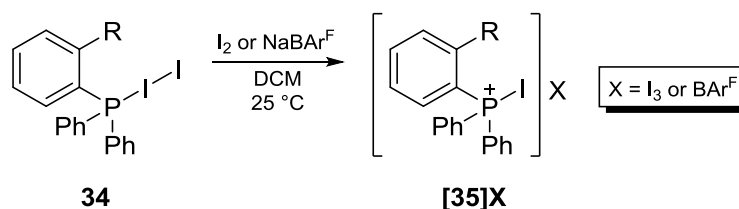
That the additional donor capacity of **34a** and **34d** arises from conjugation through the aromatic systems is further supported by examination of the known structure for *tris*-(2,4,6-trimethoxyphenyl)-diiodophosphorane,¹⁴ which shows greater P1-I1 separation (2.482(1) Å) than **34e**, but comparable I1-I2 distances (3.3394(5) Å) and no evidence of any O1-P1-I1 alignment, with all methoxy fragments essentially coplanar with the aromatic rings – the additional potential donor strength is therefore significantly offset by the increased steric bulk of additional *ortho* substituents.²⁵

6.4 – Synthesis and Structural Studies of Iodophosphonium Salts

6.4.1 – Initial Synthesis

Addition of one equivalent of NaBAR^F or I₂ to the donor-functionalised Ar₃PI₂ adducts in dichloromethane afforded the corresponding iodophosphonium salts (Scheme 6.4.1.1). The reactions were monitored by ³¹P NMR spectroscopy and formation of the product

was indicated by a downfield shift in the ^{31}P NMR spectra. As with triphenylphosphine and diiodine, where the chemical shifts changes continuously as the ratio of I_2 is increased,³⁸ a smooth shift to higher frequencies is observed when NaBAR^{F} or I_2 is added to the diiodophosphorane, and discrete reagent/product peaks are not observed due to rapid exchange on the NMR time scale.



Scheme 6.4.1.1: Synthesis of iodophosphonium salts.

The majority of the iodophosphonium salts were isolated as pure free flowing solids, and were characterised by elemental analysis and multinuclear NMR spectroscopy. Addition of I_2 to **34b** in DCM resulted in a downfield shift in the ^{31}P NMR spectrum, indicative of the formation of **[35b]I₃**. Attempts to isolate the product by precipitation with diethyl ether afforded a dark viscous oil that readily hydrolysed, and yielded a new major ^{31}P NMR peak at $\delta + 41.3$ ppm, consistent with the formation of the corresponding phosphine oxide.

Addition of I_2 to **34c** in DCM also resulted in an initial downfield shift in the ^{31}P NMR spectrum. Upon heating, to encourage dissolution of the iodine and to drive the reaction to completion, a new major signal emerged at $\delta + 51.9$ ppm, and the original signal at $- 0.7$ ppm, corresponding to **[35c]I₃**, was no longer observed. Attempts to crystallise the unknown species *via* slow diffusion of diethyl ether into a saturated solution in DCM yielded poor quality red crystals immersed in an intractable oil. Nevertheless, a suitable crystal was selected and the identity of the product was established as **[36]I₃** (Figure 6.4.1.1). The elimination of CH_3I and formation of a new nitrogen-phosphorus bond upon heating validates the strong donating capability provided by the CH_2NMe_2 fragment. Similar behaviour was also observed spectroscopically when preparing **[35c]BAR^F**, although attempts to grow single crystals for X-ray diffraction studies were unsuccessful.

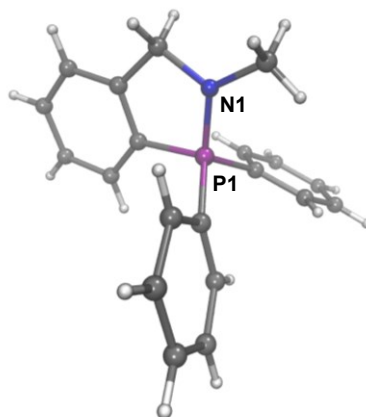


Figure 6.4.1.1: Crystal structure of the thermal degradation product **[36]I₃**.
Counterion omitted for clarity.

6.4.2 - Structural Studies

Single crystals of the iodophosphonium salts **[35]X** were grown by slow diffusion of diethyl ether or hexane into a saturated solution of the product in dichloromethane. Out of the seven crystallographically characterised **[Ar₃PI]X** salts, the observed internal structural changes upon ionisation are minor when compared to the corresponding parent diiodophosphorane. The P1-I1 bond lengths however are significantly contracted, with the **BAr^F** salts having slightly shorter P1-I1 distances than the triiodides due to weak contacts between the phosphorus-bound iodine and the I₃ anion. Selected bond lengths and angles for the iodophosphonium salts are displayed in Table 6.4.2.1.

	Bond Lengths / Å				Bond Angles / °		
	P1-I1	D1... P1	D2... P1	I1... I ₃	D1-P1-C1	D2-P1-C2	D2-P1-I1
[35a]BAr^F	2.376(1)	2.855(5)			164.3(2)		
[35b]BAr^F	2.379(6)	2.920(3)			164.8(1)		
[35d]BAr^F	2.385(1)	2.875(5)	2.898(4)		163.1(1)	161.94(1)	
	2.382(1)	2.877(5)	2.902(3)		163.3(1)	161.37(1)	
[35g]BAr^F	2.379(6)						
[35d]I₃	2.407(1)	2.895(3)	2.901(3)	3.5167(5)	161.8(2)	163.1(2)	
	2.411(1)	2.870(3)	2.886(3)	3.4872(5)	163.0(1)	163.5(2)	
[35e]I₃	2.427(1)	2.892(3)	2.845(3)	3.5802(4)	166.7(1)		167.9(6)
[35g]I₃	2.408(2)			3.4837(2)			

Table 6.4.2.1: Selected bond lengths and angles for the donor-functionalised iodophosphonium salts.

6.4.2.1 – Crystal Structure of [35a]BAr^F

Compound [35a]BAr^F crystallises in the triclinic space group $P\bar{1}$ with a single ion pair in the asymmetric cell (Figure 6.4.2.1.1). The trifluoromethyl-groups of the BAr^F counterion are disordered and a single molecule of both hexane and dichloromethane crystallises in the unit cell. The P1-I1 bond length is significantly contracted relative to **34a** (2.376(1) Å vs. 2.4753(6) Å) but is equivalent within errors to the other crystallographically characterised iodophosphonium BAr^F salts. The C_{ortho} -O1 distance (1.344(7) Å) contracts in comparison to **34a** to accommodate the reduced P1-I1 bond length, and the C_{ortho} -C_P-P1 angle decreases slightly resulting in a reduced O1...P1 contact and increased O1-P1-C1 angle (164.3(2)° vs. 159.2(1)° for **34a**). The sum of equatorial angles decreases (330.85°) as the system approaches a more tetrahedral geometry but the cation maintains a staggered propeller conformation with I1-P1-C_P- C_{ortho} torsion angles ranging from 45.8(4)° to 60.9(4)°.

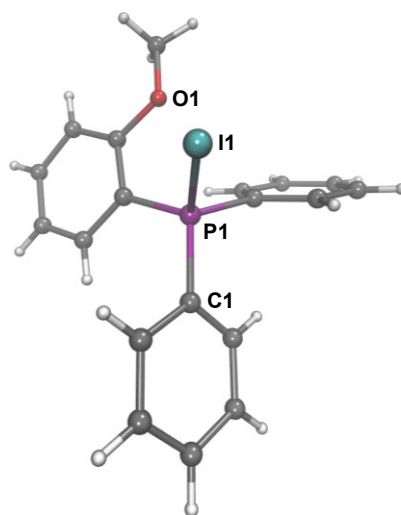


Figure 6.4.2.1.1: Crystal structure of [35a]BAr^F. Disordered counterion and solvent molecules omitted for clarity.

6.4.2.2 – Crystal Structure of [35b]BAr^F

Compound [35b]BAr^F crystallises in the triclinic space group $P\bar{1}$ with a single ion pair in the asymmetric unit (Figure 6.4.2.2.1). Again, the BAr^F counterion is disordered and there is a single molecule of dichloromethane in the unit cell. The P1-I1 bond length is comparable to [35a]BAr^F despite the P1-I1 distance for the corresponding parent diiodophosphoranes, **34a** and **34b**, being dissimilar. The C_{ortho} -N1 distance remains unchanged whilst the N1- C_{ortho} -C_P and C_{ortho} -C_P-P angles increase relative to **34b** which results in a slightly elongated N1...P1 contact (2.920(3) Å vs. 2.898(1) Å). This differs

from **[35a]BAR^F** and reflects the second mode in which steric congestion about the phosphorus centre is minimised. The cation adopts a staggered propeller conformation with the equatorial phenyl ring approaching an *exo*₁ configuration - the I1-P1-C_p-C_{ortho} torsion angles range from 17.5(3)° to 67.3(2)°. The sum of equatorial angles is slightly smaller than **34b** (334.17°) but the structure is still best described as a distorted trigonal bipyramid.

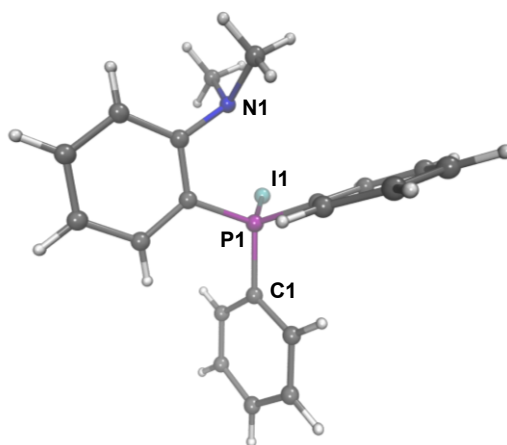


Figure 6.6.2.2.1: Crystal structure of **[35b]BAR^F**. Disordered counterion and solvent molecule omitted for clarity.

6.4.2.3 – Crystal Structure of **[35d]BAR^F**

Compound **[35d]BAR^F** crystallises in the monoclinic space group $P2_1$ with two ion pairs in the asymmetric cell along with a single molecule of dichloromethane and disordered counterions (Figure 6.4.2.3.1). The O1...P1 contacts shorten upon ionisation (molecule 1, 2.875(5) Å; molecule 2, 2.877(5) Å vs. 2.896(2) Å for **34d**) whilst the O2...P1 distances are unchanged. Unlike **[35a]BAR^F**, the C_{ortho}-O1 bond length and O1-C_{ortho}-C_p angle remain constant whilst the C_p-P1 distances contract significantly (molecule 1, 1.782(5) Å; molecule 2, 1.780(5) Å vs. 1.790(5) Å) and results in a reduced oxygen-phosphorus contact. The C_{ortho}-O2 distance in molecule 1 of **[35d]BAR^F** is abnormally short (1.337(6) Å) but the O2...P1 contact remains unchanged due to a slight contraction of the C_p-P1 bond length (1.787(5) Å). The C_{ortho}-O2 distance is longer than a typical carbon-oxygen double bond (1.2183 Å for benzoquinone)³⁹ and a carbon-oxygen single bond that has substantial double bond character (1.2813 Å for benzoic acid at 100 K)⁴⁰ which confirms that there is significant π -conjugation of the oxygen lone pairs into the aryl ring. For molecule 1, the three I1-P1-C_p-C_{ortho} torsions have a smaller range (48.6(4)° to 60.7(4)°) compared to **34d** whilst molecule 2 has a slightly larger range of torsions (33.1(5)° to 64.0(4)°). Both molecules maintain a staggered

propeller conformation with the lowest I1-P1-C_p-C_{ortho} torsion belonging to the unsubstituted aryl ring.

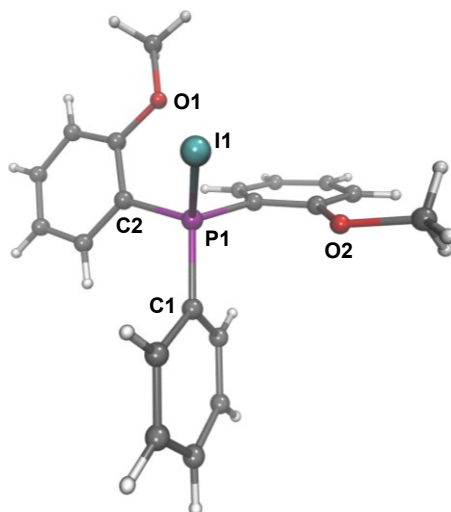


Figure 6.4.2.3.1: Crystal structure of **[35d]BAR^F**. Disordered counterion and solvent molecule omitted for clarity.

6.4.2.4 – Crystal Structure of **[35g]BAR^F**

Compound **[35g]BAR^F** crystallises in the triclinic space group $P\bar{1}$ with a single ion pair in the asymmetric cell along with a disordered molecule of dichloromethane (Figure 6.4.2.4.1). The molecule adopts a staggered propeller conformation with I1-P1-C_p-C_{ortho} torsion angles ranging from 44.2(3)° to 64.5(3)°. This is slightly larger than the range of torsions observed in **34g** (39.1(3)° to 59.5(2)°) which suggests that the aryl rings twist upon ionisation to reduce the steric demands that result from a contracted P1-I1 bond. Overall, the three C_p-P1 bonds are also marginally shorter than **34g** (1.787-1.792(4) Å vs. 1.792-1.798(3) Å) which is consistent with a change of oxidation state at phosphorus.

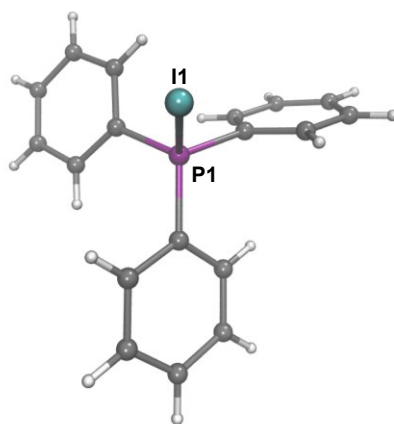


Figure 6.4.2.4.1: Crystal structure of **[35g]BAR^F**. Disordered counterion and solvent molecule omitted for clarity.

6.4.2.5 – Crystal Structure of [35d]I₃

Compound [35d]I₃ crystallises in the monoclinic space group $P2_1/n$ with two ion pairs in the asymmetric cell, together with two molecules of dichloromethane (Figure 6.4.2.5.1). Both molecules adopt comparable structures and bond metrics, with the O1...P1 contacts, C_{ortho} -O1 and C_P -P1 bond lengths, and the O1- C_{ortho} - C_P angles being identical within errors for the two molecules, and for the parent diiodophosphorane, **34d**, despite significant contraction of the P1-I1 bonds. A minor reduction of the O1- C_{ortho} - C_P and the C_{ortho} - C_P -P1' angles results in a shorter O1'...P1' contact in molecule 2 (2.870(3) Å).

The I1-P1- C_P - C_{ortho} torsion angle decreases slightly upon ionisation, with both molecules sharing similar torsion angles in the range of 39.3(4)° to 62.1(3)° such that the staggered propeller conformation is maintained. [35d]I₃ adopts a Z-shaped structural isomer in which two crystallographically inequivalent cations strongly interact with opposite ends of a single triiodide anion. The bridging and interstitial I₃⁻ anions form offset perpendicular planes that weakly interact with one another *via* the terminal atoms (4.5359(6) Å and 4.6707(6) Å); this distance is considerably longer than the sum of the van der Waals radii (3.96 Å) and the I1...I₃ contacts observed in the analogous (Ph₃PI)₃ polymorph.⁴¹

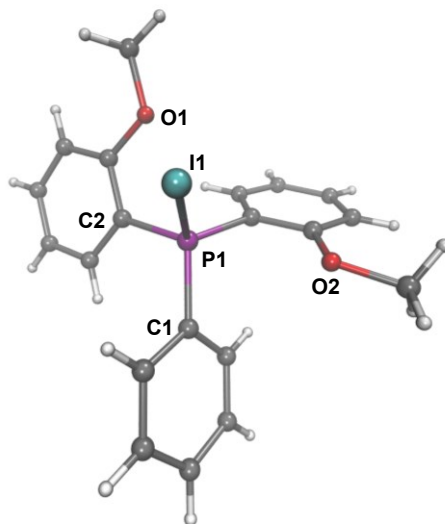


Figure 6.4.2.5.1: Crystal structure of [35d]I₃. Counterion and solvent molecules omitted for clarity.

6.4.2.6 – Crystal Structure of [35e]I₃

Compound [35e]I₃ crystallises in the monoclinic space group $P2_1/n$ with a single ion pair in the asymmetric unit (Figure 6.4.2.6.1). Upon ionisation, the N2- C_{ortho} - C_P and

C_{ortho} -C $_P$ -P1 angles decrease leading to a significantly contracted N2...P1 contact (2.845(3) Å vs. 2.945(3) Å and 2.933(2) Å for **34e**). This reduction suggests that the strength of the N2-P1-I1 $3c4e$ hypervalent interaction increases for the iodophosphonium salt whilst the remaining bond lengths and angles do not significantly differ from the parent diiodophosphorane.

The $endo_1$ conformation is also maintained for **[35e]I₃** with the I1-P1-C $_P$ -C $_{ortho}$ torsion angle for the secondary NMe₂ *ortho*-substituted aryl ring closely approaching 180°. Again, the remaining two aryl rings are twisted in the same direction with I1-P1-C $_P$ -C $_{ortho}$ torsion angles (59.9(3)° and 71.6(3)°) that do not deviate significantly from **34e**. Compound **[35e]I₃** adopts the 1:1 structural motif such that each Ar₃PI⁺ fragment interacts strongly with a single I₃⁻ anion (3.5802(4) Å). The opposing end of the asymmetric triiodide counterion also shows contacts to the *N*-methyl hydrogens on an adjacent cation (closest cation *ca.* 3.254 Å) but does not appear to interact with any additional phosphorus-bound iodine atoms or I₃⁻ anions.

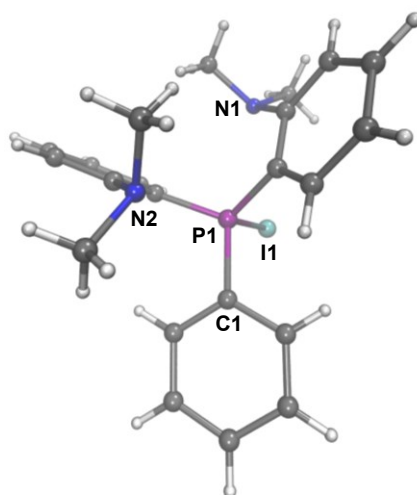


Figure 6.4.2.6.1: Crystal structure of **[35e]I₃**. Counterion omitted for clarity.

6.4.2.7 – Polymorphism in Ar₃PI₄ Systems

The known compound **[35g]I₃** was prepared and single-crystal X-ray diffraction data was collected at 100K to permit direct and precise bond metric comparisons with the donor-functionalised iodophosphonium triiodides. Slow diffusion of Et₂O into a saturated solution of **[35g]I₃** in DCM yielded single crystals of the [(Ph₃PI)₂I₃]₃ polymorph⁴¹ which consists of parallel zigzag chains of [(Ph₃PI)₂I₃]⁺ cations sandwiched between layers of I₃⁻ anions. The phosphorus-bound iodine of both Ph₃PI fragments interact with the same terminal atoms of the triiodide anion (I1...I₃ = 3.4837 Å). This is in contrast with the (Ph₃PI)₃ polymorph, crystallised from toluene by Cotton,

which forms a network of parallel infinite chains where the terminal atom of I_3^- strongly interacts with a single Ph_3PI^+ fragment (3.551(1) Å) whilst the opposite end of I_3^- binds weakly with a second Ph_3PI^+ fragment (4.337(1) Å), and further linked into a polymeric network by weak interactions between the triiodide anions (3.741(1) Å).

This structural isomerism is well documented for R_3PI_4 adducts⁴² and three isomers are commonly observed (Figure 6.4.2.7.1); the simple 1:1 ion pair, $[R_3PI][I_3]$ (Isomer **A**); a 2:1 $[(R_3PI)_2I_3][I_3]$ compound where two R_3PI^+ fragments are linked to the same terminal atom of one I_3^- anion giving a Y-shaped motif (Isomer **B**); and an alternative 2:1 $[(R_3PI)_2I_3][I_3]$ compound where the two R_3PI^+ fragments are linked to opposite ends of the triiodide anion giving a Z-shaped motif (Isomer **C**). The structural isomer obtained is dependent on the choice of solvent used for crystallisation and the nature of the R groups. Compound **[35d]** I_3 adopts the structural isomer **C** whilst compound **[35e]** I_3 adopts the structural isomer **A**. Due to the limited quantity of product, no attempts were made to grow crystals from different solvent systems to explore further polymorphism.

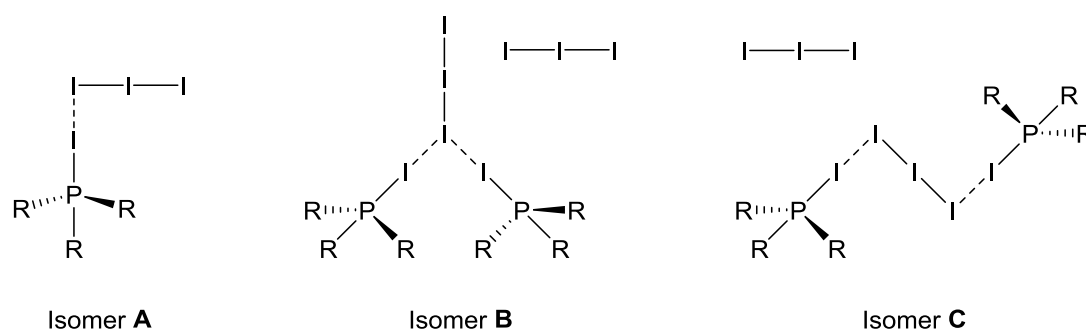


Figure 6.4.2.7.1: Structural isomers of R_3PI_4 adducts.

6.5 – Computational Studies

Computational studies were performed to provide further insight into the mechanism by which the apparent donor strength of the phosphanes varies between the diiodophosphanes and iodophosphonium salts. Initial calculations using the LanL2DZ^{43,44} effective core potential (ECP) to model the iodine atoms gave poor correlations with observed experimental data, and so the more computationally demanding def2TZVP split valence, triple- ζ basis set was employed.⁴⁵ This gave reasonable correlation with experimental structural data.

6.5.1 – Bonding and Lewis Basicity of Functionalised Phosphanes

The counterintuitively weak Lewis basicity observed experimentally for the diiodophosphanes clearly reflects the delicate balance between electronic and steric

effects in the adducts. These factors were quantified by examining the energy of the highest occupied molecular orbitals (HOMO) of the free phosphanes, which in all cases was found to correspond to an orbital with considerable phosphorus lone pair character, and through buried volume analysis^{46,47} ($\% V_{Bur}$) of the optimised Ar_3PI_2 adducts - these can be compared to the I1-I2 bond length as a measure of overall donor strength. Neglecting steric effects, phosphanes with a less negative HOMO energy should, in principle, be stronger donors relative to Ph_3P , which results in an elongation of the I1-I2 distance in the corresponding diiodophosphorane.

The computational studies also confirm that two possible modes exist by which phosphane donor strength is enhanced, namely π -conjugation or direct lone pair donation to phosphorus, and allow clear differences to be established for the oxygen and nitrogen donors. Examination of the Mayer bond indices between the donor atoms and the phosphorus center, and comparison of the occupied molecular orbitals of the free phosphanes provide good evidence for the origin of the different behaviour.

Table 6.5.1.1 shows the clear trend that substitution leads to an increase in both the HOMO energy and steric demand of the free phosphane, as seen in the increase in calculated buried volumes. At the same time, the nitrogen donors show a greater increase in steric demand than the oxygen donors, which may be understood in terms of coplanarity of the OMe fragments with the arene rings in comparison to the twisting out of the ring plane seen for the nitrogen fragments. Examination of the C_{ortho} -O bond lengths and Mayer bond indices for **33a^c** (C_{ortho} -O = 1.356 Å, bond index 1.049) and **33d^c** (C_{ortho} -O = 1.357 Å each, bond indices 1.046 and 1.052) confirm the presence of π donation of the oxygen lone pairs into the arene rings (bond indices >1), albeit with a slight reduction in C_{ortho} -O bond index in comparison to free anisole (1.065), likely as a result of steric congestion. Nevertheless, the calculated O \cdots P bond indices are low (**33a^c**, 0.046; **33d^c**, 0.047 and 0.043) despite the close O \cdots P contacts. In contrast, the orientations of the nitrogen lone pairs in **33b^c** and **33e^c** preclude such conjugation and the NMe_2 fragments would thus be expected to act as electron withdrawing groups *via* the σ -bonding network - a significant increase in bond length (**33b^c**, C_{ortho} -N = 1.436 Å, bond index 1.018; **33e^c**, C_{ortho} -N = 1.430 Å and 1.436 Å, bond indices 1.032 and 1.019) and decrease in bond indices are observed in comparison to free *N,N*-dimethylaniline (C_{ortho} -N = 1.383 Å, bond index 1.077). The nitrogen lone pairs of **33b^c**, **33c^c**, and **33e^c** are all oriented toward the phosphorus center, as seen in available crystallographic data^{48,49} with comparatively short N \cdots P contacts (**33b^c**, 2.887 Å; **33c^c**, 2.878 Å; **33e^c**,

2.945 Å and 2.890 Å). The energy change of the lone pair must therefore, as previously reported,⁸ arise from a small but significant degree of N...P bonding and leads to rehybridization at phosphorus - this is reflected in the calculated N...P bond indices (**33b^c**, 0.063; **33c^c**, 0.049; **33e^c**, 0.051 and 0.063) and, in each case, the HOMO -1 is identified as showing N...P σ -bonding character (Figure 6.5.1.1). Ligand **33c^c** shows both greater buried volume and a higher energy lone pair in comparison to **3b^c**, which may be understood as arising from the transition toward a *pseudo*-trigonal-bipyramidal, five-coordinate geometry; the effect of this rehybridization may be seen in the lone pair of **33c^c** being raised above that of **33d^c**, despite the presence of two strongly conjugated donor moieties in the latter case.

	HOMO Energy (eV)	%V _{Bur}	D...P Distance / Å	D...P Bond Index	C _{ortho} -D Distance / Å	C _{ortho} -D Bond Index
33a^c	-0.268	23.5	2.852	0.046	1.356	1.049
33b^c	-0.265	26.2	2.888	0.063	1.436	1.018
33c^c	-0.262	28.8	2.878	0.049	1.453	0.964
33d^c	-0.263	25.2	2.857	0.047	1.357	1.046
			2.846	0.043	1.357	1.052
33e^c	-0.257	27.3	2.945	0.051	1.430	1.032
			2.890	0.063	1.436	1.019
33g^c	-0.273	21.8				
Anisole^c					1.358	1.065
DMA^c					1.383	1.077

Table 6.5.1.1: Selected parameters for the computed free phosphanes, showing calculated separations and Mayer bond indices for donor-phosphorus contacts and donor-arene bonds.

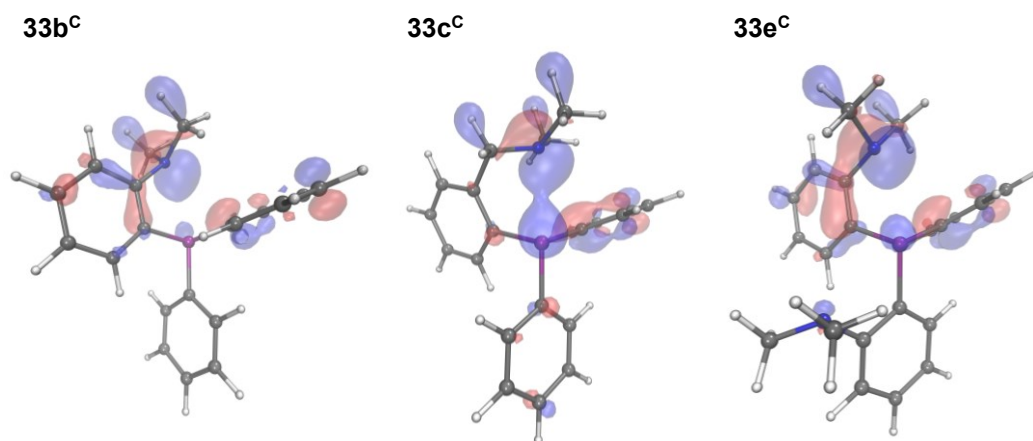


Figure 6.5.1.1: Visualisation of the HOMO -1 orbitals for **33b^c**, **33c^c** and **33e^c** (isovalue = 0.05), showing the N...P σ -bonding interaction.

6.5.2 – Diiodophosphanes

Geometry optimisation of the diiodophosphanes confirmed the increase in donor strength of the phosphanes, with increased I1-I2 bond lengths relative to **34g^c** seen for all cases and shorter P1-I1 contacts for all save **34c^c**, as shown in Table 6.5.2.1. The same trend is seen in the P1-I1 and I1-I2 Mayer bond indices, though here the P1-I1 bond index is nevertheless increased for **34c^c** relative to **34g^c**, which shows that the P1-I1 bond elongation arises from steric grounds. Considering first the *mono*-substituted phosphorane series, the trends clearly show that despite the increase in lone pair energy indicating an expected donor strength of **33c^c** > **33b^c** > **33a^c**, instead **33a^c** > **33b^c** \approx **33c^c** is found by both I1-I2 bond length and bond index comparison (the experimentally observed order is **33a** > **33c** > **33b** by I1-I2 contacts in **34**). Instead, this trend in donor strength follows the order dictated by the steric demand of the phosphane as measured by buried volume, with longer P1-I1 and shorter I1-I2 bonds as buried volume increases. Further substitution leads to a proportionately smaller change in buried volume, and so unsurprisingly, donor strength is found to increase such that **33d^c** > **33a^c** and **33e^c** > **33b^c**. Interestingly, despite the increase in donor strength seen in the increase in I1-I2 bond lengths (3.192 Å vs. 3.173 Å) and decrease in I1-I2 bond indices (0.314 vs. 0.332) for **33d^c** relative to **33a^c**, the P1-I1 bond lengths and bond indices are essentially invariant, which confirms that this metric is more sensitive to steric demand than the I1-I2 bond length.

	Bond Lengths / Å				Bond Indices			
	P1-I1	I1-I2	D1... P1	D2... P1	P1-I1	I1-I2	D1... P1	D2... P1
34a^c	2.483	3.173	2.858		0.929	0.332	0.037	
34b^c	2.485	3.150	2.889		0.930	0.350	0.065	
34c^c	2.491	3.149	2.943		0.925	0.350	0.075	
34d^c	2.484	3.192	2.876	2.856	0.930	0.314	0.036	0.037
34e^c	2.467	3.244	2.906	2.971	0.987	0.272	0.061	0.059
34g^c	2.487	3.138			0.921	0.361		

Table 6.5.2.1: Selected bond lengths and bond indices for the computed diiodophosphanes, showing calculated separations and Mayer bond indices for donor-phosphorus contacts and donor-arene bonds.

On binding of I₂, the computed O...P bond indices decrease for **34a^c** and **34d^c** relative to the free phosphanes (*e.g.* **34a^c**: 0.037 vs **33a^c**: 0.046) whilst the *C_{ortho}*-O bond indices increase. This demonstrates that conjugation through the arene rings dominates over direct donation to phosphorus in these systems, whilst an increase in N...P bond index

is observed for the *mono*-substituted nitrogen donor species. This increase is comparatively small for **34b^c** (**34b^c**: 0.065 vs. **33b^c**: 0.063), but substantially larger for **34c^c** (**34c^c**: 0.075 vs. **33c^c**: 0.049), despite both **34b^c** and **34c^c** showing a simultaneous increase in N...P bond length (Δ N...P **34b^c**: 0.001 Å; **34c^c** 0.065 Å). The increase in N...P separation likely arises from the increased steric bulk about phosphorus, but this is concomitant with a change in bond angle towards linearity (**34c^c** N1-P1-C1 angle: 171.4° to 177.1°) which nevertheless improves orbital overlap and thus bonding. For the *bis*-substituted donors, the same trends are evident, albeit with a slight decrease observed for the N...P contact in the N2-P1-I1 hypervalent interaction of **34e^c**. Overall, it can therefore be seen that whilst the internal solvation might be predicted to have a greater influence on donor strength than more remote conjugation, the steric demands imposed by the N...P bonding weaken the effect, with the bonding in **34c^c** indicating that **33c^c** is the weakest of the substituted donors despite having the second greatest lone pair energy. **34c^c** not only shows the smallest increase in I1-I2 separation but also manifests a P1-I1 contact slightly greater in length than that of **34g^c** (**34c^c**: 2.491 Å vs. **34g^c**: 2.487 Å).

6.5.3 – Iodophosphonium Salts

The optimised iodophosphonium series, shown in Table 6.5.3.1, however, tells a very different story. All of the substituted cations exhibit longer P1-I1 bonds than **35g^c**, but nevertheless are still shorter than the P1-I1 contacts seen in the diiodophosphanes, which implies weaker donor strength and the reverse of the trend seen for the diiodophosphanes. Interestingly, whilst the steric demands clearly dominate in this situation, the efficiency of direct N...P donation at enhancing donor strength can clearly be seen in that the P1-I1 contact of **35c^c** is essentially identical to that of **35a^c**, despite the enormous increase in steric bulk between **33c^c** and **33a^c**. Furthermore, the nitrogen donor systems **35b^c**, **35c^c** and **35e^c** show P1-I1 bond indices greater than that for **35g^c**, whilst the oxygen donor systems **35a^c** and **35d^c** show reduced P1-I1 bond indices. This is mirrored in the bond indices for *C_{ortho}*-O, O...P and N...P contacts. The O...P bond indices for **35a^c** (0.039) and **35d^c** (0.038 and 0.040) do show a small increase relative to the diiodophosphanes, but do not rise to the levels seen in the free phosphanes. There is also a significant increase in *C_{ortho}*-O bond index (**35a^c**: 1.084; **35d^c**: 1.079 and 1.081) commensurate with a greater degree of charge transfer to phosphorus through the arene ring. The N...P bonds indices for **35b^c**, **35c^c** and **35e^c**, (**35b^c**: 0.070; **35c^c**: 0.088; **35e^c**: 0.064 and 0.083) on the other hand, are increased relative to the diiodophosphanes, with the greatest increase seen for **35c^c** despite a

slight associated increase in bond length ($\Delta N\cdots P$ **35c^C** 0.005 Å). Unfortunately, since complete crystallographic data could not be obtained for either I₃⁻ or BAr^F salts, it is not possible to directly and generally compare computational and experimental results, though the invariance of the P1-I1 bond length observed for **[35]BAr^F** suggests that packing effects, not computationally modelled, may be significant.

	Bond Lengths / Å			Bond Indices		
	P1-I1	D1... P1	D2... P1	P1-I1	D1... P1	D2... P1
35a^C	2.399	2.866		1.036	0.039	
35b^C	2.393	2.904		1.047	0.070	
35c^C	2.398	2.949		1.044	0.088	
35d^C	2.403	2.886	2.859	1.029	0.038	0.040
35e^C	2.410	2.915	2.858	1.056	0.064	0.083
35g^C	2.392			1.040		

Table 5.5.3.1: Selected bond lengths and bond indices for the computed iodophosphonium cations, showing calculated separations and Mayer bond indices for donor-phosphorus contacts and donor-arene bonds.

6.5.4 – Summary of Computational Studies

The computational results give good correlation with experimental data and allow the relative donor strength of the donor-functionalised phosphanes to be explained in terms of electronic and steric effects. However, the apparent dramatically weak Lewis basicity observed experimentally in **34b**, which could not be fully predicted computationally, suggests that there are additional factors to consider. The crystal packing of the Ar₃PI₂ adducts, as discussed in section 6.3, will also influence the observed donor strength since favourable supramolecular interactions will alter the conformation and orientation of the aryl rings, which in turn affects the magnitude of the P-I and I-I bond lengths.²⁵ Out of the six crystallographically characterised diiodophosphoranes, **34b** is the only diiodophosphorane in which the back-to-back sextuple phenyl embrace is observed. This conformation, which is commonly adopted for Ar₃P containing species,¹⁹ contains six attractive edge-to-face (EF) interactions between aryl groups and contributes to a significant attraction between molecules. Given that this intermolecular embrace is only seen for **34b**, and since crystal packing has not been considered computationally, it is plausible that this is responsible for the long P-I and short I-I bond lengths observed experimentally for this adduct.

6.6 – Conclusions

Analysis of the reported diiodophosphoranes, supplemented by computational studies, shows that the phosphorus centres of the nitrogen-donor substituted phosphanes are themselves internally solvated and act simultaneously as Lewis acid and Lewis base. In contrast, no significant internal solvation is observed for the oxygen-donor substituted phosphanes, with their increased donor ability arising from delocalisation of oxygen lone pairs onto phosphorus *via* an aromatic system. Comparison of the I₂ adduct structures reveals a counterintuitively weak Lewis basicity for **33c**, indicated by a decrease in the I-I bond length when compared to the unsubstituted Ph₃P donor, shown to derive from a delicate balance between steric and electronic effects within the adducts.

Synthesis of the corresponding iodophosphonium salts, in tandem with further computational studies, reveals that the impact of the steric bulk on donor strength is more significant for the cationic species, but also that internal solvation is more efficient at increasing donor strength than through-ring conjugation. These observations imply that this internal solvation may be general to soft Lewis acid adducts of these donor-functionalized phosphanes, with implications for their utility in stabilizing main-group cations - the assumption that more donating substituents leads to better cation stabilization may not hold. Finally, the marked difference in behaviour between neutral adduct and cation clearly indicates that, when the donor strengths of ligands are compared, a single probe Lewis acid is insufficient to understand the overall trends in ligand behaviour

6.7 – Experimental

6.7.1 – Synthesis of Aryl-Lithiums

The *ortho*-donor functionalised aryl-lithiums **32a-c** were all prepared according to known literature procedures.³²⁻³⁴ The synthesis of **32a** is given as an example. All products were isolated as pyrophoric solids that were extremely sensitive to air and moisture.

6.7.1.1 – Synthesis of (*o*-OMe-C₆H₄)Li, **32a**:

Anisole (4 cm³, 36.8 mmol) and TMEDA (6.1 cm³, 40.5 mmol) were dissolved in Et₂O (15 cm³) and cooled to 0 °C. ⁿBuLi in hexane (16.2 cm³, 2.5 M, 40.5 mmol) was added dropwise over 30 minutes producing an off-white precipitate that was allowed to slowly warm to room temperature and stir for 17 hours. The yellow supernatant was removed by filtration and the pale pink solid product was washed with hexane (2 x 10 cm³) and dried *in vacuo*. Yield: 2.747 g (24.1 mmol, 65.4 %).

6.7.1.2 – Synthesis of (*o*-NMe₂-C₆H₄)Li, **32b**:

Off-white solid, 87.6 % yield. ¹H NMR (400 MHz, THF, 18.3°C): δ 7.93 (d, *J* = 5.5 Hz, 1H, *Ph*), 6.70-6.80 (m, 3H, *Ph*), 3.45 (s, 2H, CH₂NMe₂), 2.14 (s, 6H, CH₂NMe₂).

6.7.1.3 – Synthesis of (*o*-CH₂NMe₂-C₆H₄)Li, **32c**:

Colourless solid, 84.5 % yield. ¹H NMR (400 MHz, DCM, 18.6 °C): δ 7.92 (d, *J* = 5.7 Hz, *Ph*, 1H), 6.78-6.71 (m, *Ph*, 3H), 3.43 (s, CH₂NMe₂, 2H), 2.12 (s, CH₂NMe₂, 6H).

6.7.2 – Synthesis of Donor Functionalised Phosphanes

The tri-aryl phosphines **33a-e** were all prepared according to the same general unoptimised procedure using the appropriate aryl-lithium and chlorophosphine.⁸ The synthesis of **33a** is given as exemplar. Compounds **33a**, **33b** and **33e** were purified by recrystallization from boiling ethanol. Compound **33c** was extracted into boiling hexane and filtered before removal of solvent under prolonged vacuum – this was found to remove any polar or ionic impurities. Compound **33d** was recrystallised from DCM and hexanes. Attempts to purify **33f** were unsuccessful, yielding a viscous amber oil which was found to contain an unknown phosphorus-containing impurity (*ca.* 5 % by ³¹P NMR) that interfered with subsequent experiments. Compound **33f** was also found to rapidly oxidise on contact with trace air or moisture, preventing alternative purification *via* column chromatography from being employed.

6.7.2.1 – Synthesis of Ph₂P(*o*-OMe-C₆H₄), 33a:

Ph₂P(OMe)Cl (0.6 cm³, 3.3 mmol) was dissolved in THF (10 cm³) and cooled to -95 °C. A solution of **32a** (0.400 g, 3.5 mmol) in THF (15 cm³) was added dropwise yielding a cloudy yellow reaction mixture that was allowed to slowly warm to room temperature and stir overnight. The solvent was removed *in vacuo* and the residues were extracted into DCM (2 x 10 cm³) and filtered through celite. The filtrate was quenched with ice water (20 cm³) and extracted into DCM (3 x 15 cm³). The combined organic extracts were washed with water and brine (15 cm³ each), dried over MgSO₄, filtered and evaporated to dryness. The crude solids were recrystallised from boiling EtOH, and washed with cold hexanes to give **33a** as colourless needles. Yield: 0.145 g (0.5 mmol, 15.2 %). ¹H NMR (400 MHz, DCM, 18.1 °C): δ 7.38-7.29 (m, *Ph*, 7H), 7.28-7.22 (m, *Ph*, 4H), 6.91 (dd, *J* = 4.8, 8.2 Hz, *Ph*, 1H), 6.84 (t, *J* = 7.6 Hz, *Ph*, 1H), 6.67-6.61 (m, *Ph*, 1H), 3.73 (s, *OMe*, 3H). ³¹P NMR (161.8 MHz, DCM, 18.2 °C): δ -16.6 (s).

6.7.2.2 – Synthesis of Ph₂P(*o*-NMe₂-C₆H₄), 33b:

Yellow needles, 43.6 % yield. ¹H NMR (400 MHz, DCM, 20.1 °C): δ 7.37-7.19 (m, *Ph*, 12H), 6.99 (t, *J* = 7.8 Hz, *Ph*, 1H), 6.76 (ddd, *J* = 1.0, 3.7, 7.3 Hz, *Ph*, 1H), 2.60 (s, *NMe*₂, 6H). ³¹P NMR (161.8 MHz, DCM, 20.1 °C): δ -13.7 (s).

6.7.2.3 – Synthesis of Ph₂P(*o*-CH₂NMe₂-C₆H₄), 33c:

Amber oil, 78.7 % yield. ¹H NMR (400 MHz, DCM, 20.5 °C): δ 7.44 (dd, *J* = 4.6, 7.3 Hz, *Ph*, 1H), 7.35-7.22 (m, *Ph*, 11H), 7.15 (t, *J* = 7.3 Hz, *Ph*, 1H), 6.92 (dd, *J* = 4.6, 7.8 Hz, *Ph*, 1H), 3.60 (s, *CH*₂*NMe*₂, 2H), 2.01 (s, *CH*₂*NMe*₂). ³¹P NMR (161.8 MHz, DCM, 20.5 °C): δ -15.7 (s).

6.7.2.4 – Synthesis of PhP(*o*-OMe-C₆H₄)₂, 33d:

Colourless needles, 92.6 % yield. ¹H NMR (400 MHz, DCM, 20.9 °C): δ 7.37-7.28 (m, *Ph*, 5H), 7.22 (t, *J* = 7.3, 8.0 Hz, *Ph*, 2H), 6.91 (dd, *J* = 4.6, 8.0 Hz, *Ph*, 2H), 6.83 (t, *J* = 7.3, 7.6 Hz, *Ph*, 2H), 6.64-6.59 (m, *Ph*, 2H), 3.73 (s, *OMe*, 6H). ³¹P NMR (161.8 MHz, DCM, 18.6 °C): δ -27.7 (s).

6.7.2.5 – Synthesis of PhP(*o*-NMe₂-C₆H₄)₂, 33e:

Colourless needs 29.0 % yield. ¹H NMR (400 MHz, DCM, 20.1 °C): δ 7.34-7.26 (m, *Ph*, 5H), 7.22-7.12 (m, *Ph*, 4H), 6.96 (t, *J* = 7.3 Hz, *Ph*, 2H), 6.75 (ddd, 1.8, 3.2, 7.8 Hz, *Ph*, 2H), 2.65 (s, *NMe*₂, 12H). ³¹P NMR (161.8 MHz, DCM, 20.1 °C): δ -21.8 (s).

6.7.3 – Synthesis of Diiodophosphoranes

The Ar_3PI_2 adducts **34a-g** were all prepared by the reaction of donor-functionalised phosphane with 1 equivalent of diiodine in anhydrous diethyl ether. The synthesis of **34a** is given as an example. All products were isolated as free-flowing yellow powders. Crystals suitable for single-crystal X-ray diffraction were grown by slow diffusion of Et_2O into a concentrated solution of the product in DCM.

6.7.3.1 – Synthesis of $[\text{Ph}_2\text{P}(o\text{-OMe-C}_6\text{H}_4)]\text{I}_2$, **34a**:

To a stirred solution of **33a** (0.200 g, 0.68 mmol) in Et_2O (10 cm^3) was added dropwise a solution of I_2 (0.165 g, 0.65 mmol) in Et_2O (10 cm^3), generating an immediate yellow precipitate. The reaction mixture was stirred overnight, the pale yellow supernatant removed by filtration and the solid product washed with Et_2O (10 cm^3) before being dried *in vacuo* to give the product as a bright yellow powder. Yield: 0.247 g (0.45 mmol, 70 %). *Anal. Calc.* for $\text{C}_{19}\text{H}_{17}\text{I}_2\text{OP}$: C, 41.79; H, 3.14. Found: C, 41.89; H, 3.17. $^1\text{H NMR}$ (400 MHz, DCM, 20.9 °C): δ 7.76-7.67 (bm, *Ph*, 3H), 7.59-7.55 (m, *Ph*, 8H), 7.14-7.06 (m, *Ph*, 2H), 6.98 (dd, $J = 14.7$ Hz, 7.8 Hz, *Ph*, 1H), 3.76 (s, *OMe*, 3H). $^{31}\text{P NMR}$ (161.8 MHz, DCM, 20.9 °C): δ -23.4 (s). $^{13}\text{C}\{^1\text{H}\}$ NMR (100.5 MHz, DCM, 19.3 °C): δ 161.7 (d, $J_{\text{C-P}} = 1.9$ Hz, *Ph*), 137.2 (d, $J_{\text{C-P}} = 1.9$ Hz, *Ph*), 135.0 (d, $J_{\text{C-P}} = 5.8$ Hz, *Ph*), 133.9 (d, $J_{\text{C-P}} = 2.9$ Hz, *Ph*), 133.4 (d, $J_{\text{C-P}} = 10.5$ Hz, *Ph*), 127.9 (d, $J_{\text{C-P}} = 10.5$ Hz, *Ph*), 122.6 (d, $J_{\text{C-P}} = 65.2$ Hz, *Ar-P*), 121.8 (d, $J_{\text{C-P}} = 12.5$ Hz, *Ph*), 112.7 (d, $J_{\text{C-P}} = 6.7$ Hz, *Ph*), 109.3 (d, $J_{\text{C-P}} = 64.0$ Hz, *Ar-P*), 65.1 (s, *OMe*).

6.7.3.2 – Synthesis of $[\text{Ph}_2\text{P}(o\text{-NMe}_2\text{-C}_6\text{H}_4)]\text{I}_2$, **34b**:

Yellow solid, 85 % yield. *Anal. Calc.* for $\text{C}_{20}\text{H}_{20}\text{I}_2\text{NP}$: C, 42.96; H, 3.61; N, 2.50. Found: C, 42.92; H, 3.73; N, 2.65. $^1\text{H NMR}$ (400 MHz, DCM, 20.5 °C): δ 7.76 (t, $J = 7.3$ Hz, *Ph*, 1H), 7.65-7.50 (m, *Ph*, 11H), 7.35 (d of t, $J = 7.8, 2.7$ Hz, *Ph*, 1H), 7.18 (dd, $J = 13.3, 7.8$ Hz, *Ph*, 1H), 2.24 (s, *NMe}_2*, 6H). $^{31}\text{P NMR}$ (161.8 MHz, DCM, 20.5 °C): δ -25.8 (s). $^{13}\text{C}\{^1\text{H}\}$ NMR (100.5 MHz, DCM, 20.5 °C): δ 159.2 (d, $J_{\text{C-P}} = 6.7$ Hz, *Ph*), 136.3 (d, $J_{\text{C-P}} = 2.9$ Hz, *Ph*), 134.6 (d, $J_{\text{C-P}} = 7.7$ Hz, *Ph*), 133.6 (s, *Ph*), 133.5 (s, *Ph*), 133.4 (singlet, *Ph*), 129.6 (d, $J_{\text{C-P}} = 11.5$ Hz, *Ph*), 127.4 (d, $J_{\text{C-P}} = 11.5$ Hz, *Ph*), 126.5 (d, $J_{\text{C-P}} = 7.7$ Hz, *Ph*), 124.4 (d, $J_{\text{C-P}} = 63.3$ Hz, *Ar-P*), 122.7 (d, $J_{\text{C-P}} = 67.0$ Hz, *Ar-P*), 45.6 (s, *NMe}_2*).

6.7.3.2 – Synthesis of $[\text{Ph}_2\text{P}(o\text{-CH}_2\text{NMe}_2\text{-C}_6\text{H}_4)]\text{I}_2$, **34c**:

Yellow solid, 93 % yield. *Anal. Calc.* for $\text{C}_{21}\text{H}_{22}\text{I}_2\text{NP}$: C, 44.00; H, 3.87; N, 2.44. Found: C, 43.89; H, 3.95; N, 2.56. $^1\text{H NMR}$ (400 MHz, DCM, 20.9 °C): δ 7.75-7.34 (bm, *Ph*, 13H),

7.15 (dd, $J = 14.2, 7.3$ Hz, *Ph*, 1H), 3.57 (bs, CH_2NMe_2 , 2H), 1.65 (bs, CH_2NMe_2 , 6H). ^{31}P NMR (161.8 MHz, DCM, 20.9 °C): δ -23.1 (s). $^{13}\text{C}\{^1\text{H}\}$ NMR (100.5 MHz, DCM, 18.1 °C): δ 145.8 (d, $J_{\text{C-P}} = 9.6$ Hz, *Ph*), 136.1 (d, $J_{\text{C-P}} = 5.3$ Hz, *Ph*), 134.6 (d, $J_{\text{C-P}} = 12.0$ Hz, *Ph*), 134.0 (d, $J_{\text{C-P}} = 7.2$ Hz, *Ph*), 132.9 (d, $J_{\text{C-P}} = 8.6$ Hz, *Ph*), 131.8 (d, $J_{\text{C-P}} = 11.5$ Hz, *Ph*), 129.5 (d, $J_{\text{C-P}} = 11.5$ Hz, *Ph*), 128.0 (d, $J_{\text{C-P}} = 12.0$ Hz, *Ph*), 125.8 (d, $J_{\text{C-P}} = 62.8$ Hz, *Ar-P*), 120.6 (d, $J_{\text{C-P}} = 57.0$ Hz, *Ar-P*), 59.4 (s, CH_2NMe_2), 43.8 (s, NMe_2).

6.7.3.4 – Synthesis of $[\text{PhP}(o\text{-OMe-C}_6\text{H}_4)]_2\text{I}_2$, **34d**:

Yellow solid, 84.9 % yield. *Anal.* Calc. for $\text{C}_{20}\text{H}_{19}\text{I}_2\text{O}_2\text{P}$: C, 41.69; H, 3.32. Found: C, 41.51; H, 3.36. ^1H NMR (400 MHz, DCM, 19.7 °C): δ 7.62 (m, *Ph*, 7H), 7.08 (m, *Ph*, 6H), 3.75 (s, *OMe*, 6H). ^{31}P NMR (161.8 MHz, DCM, 20.0 °C): δ -32.1 (s). $^{13}\text{C}\{^1\text{H}\}$ NMR (100.5 MHz, DCM, 18.7 °C): δ 161.0 (d, $J_{\text{C-P}} = 2.9$ Hz, *Ph*), 136.1 (d, $J_{\text{C-P}} = 2.9$ Hz, *Ph*), 134.2 (d, $J_{\text{C-P}} = 6.7$ Hz, *Ph*), 132.9 (d, $J_{\text{C-P}} = 2.9$ Hz, *Ph*), 132.7 (d, $J_{\text{C-P}} = 9.6$ Hz, *Ph*), 128.8 (d, $J_{\text{C-P}} = 13.4$ Hz, *Ph*), 122.1 (d, $J_{\text{C-P}} = 69.0$ Hz, *Ar-P*), 121.0 (d, $J_{\text{C-P}} = 12.5$ Hz, *Ph*), 112.1 (d, $J_{\text{C-P}} = 6.7$ Hz, *Ph*), 108.6 (d, $J_{\text{C-P}} = 67.1$ Hz, *Ar-P*), 55.4 (s, *OMe*).

6.7.3.5 – Synthesis of $[\text{PhP}(o\text{-NMe}_2\text{-C}_6\text{H}_4)]_2\text{I}_2$, **34e**:

Yellow solid, 82 % yield. *Anal.* Calc. for $\text{C}_{22}\text{H}_{25}\text{N}_2\text{PI}_2$: C, 43.88; H, 4.18; N, 4.65. Found: C, 43.75; H, 4.02; N, 4.62. ^1H NMR (400 MHz, DCM, 20.4 °C): δ 7.84-7.73 (m, *Ph*, 4H), 7.60-7.45 (m, *Ph*, 9H), 2.14 (s, NMe_2 , 12H). ^{31}P NMR (161.8 MHz, DCM, 20.9 °C): δ -22.7 (s). $^{13}\text{C}\{^1\text{H}\}$ NMR (100.5 MHz, DCM, 19.3 °C): δ 158.7 (d, $J_{\text{C-P}} = 3.8$ Hz, *Ph*), 135.9 (d, $J_{\text{C-P}} = 2.9$ Hz, *Ph*), 135.5 (d, $J_{\text{C-P}} = 9.6$ Hz, *Ph*), 133.0 (d, $J_{\text{C-P}} = 3.8$ Hz, *Ph*), 132.3 (d, $J_{\text{C-P}} = 9.6$ Hz, *Ph*), 129.2 (d, $J_{\text{C-P}} = 13.4$ Hz, *Ph*), 127.4 (d, $J_{\text{C-P}} = 13.4$ Hz, *Ph*), 127.3 (d, $J_{\text{C-P}} = 61.4$ Hz, *Ar-P*), 125.9 (d, $J_{\text{C-P}} = 7.7$ Hz, *Ph*), 121.9 (d, $J_{\text{C-P}} = 72.9$ Hz, *Ar-P*), 45.8 (s, NMe_2).

6.7.3.6 – Synthesis of Ph_3PI_2 , **34g**:

Yellow solid, 94.9 % yield. ^1H NMR (400 MHz, DCM, 18.7 °C): δ 7.71 (m, *Ph*, 3H), 7.58 (m, *Ph*, 12H). ^{31}P NMR (161.8 MHz, DCM, 18.8 °C): δ -19.8 (s).

6.7.4 – Synthesis of Iodophosphonium Salts

NMR scale samples of the iodophosphonium salts **[35a-g]X** were prepared by combination of appropriate donor-functionalised diiodophosphorane and NaBAR^{F} or I_2 in DCM unless stated otherwise. The synthesis of **[35a]BAR^F** is given as exemplar. All reactions were monitored *via* NMR at each stage. Crystals suitable for X-ray diffraction were grown by slow diffusion of hexane or Et_2O into a saturated solution of the product in DCM.

6.7.4.1 – Synthesis of [Ph₂P(*o*-OMe-C₆H₄)I][BAR^F] [35a]BAR^F:

To a J. Young's NMR tube fitted with a d₆-DMSO capillary was added **34a** (20 mg, 0.037 mmol) and DCM (0.7 cm³). NaBAR^F (33 mg, 0.037 mmol) was added and the reaction mixture was heated to reflux for 1 hour. The supernatant was decanted into a crystallisation tube and layered with hexane. After 24 hours, the colourless crystals were filtered, washed with hexane (5 cm³) and dried *in vacuo*. Yield: 27.3 mg (0.021 mmol, 58.2 %). *Anal. Calc.* for C₅₁H₂₉BF₂₄IOP: C, 47.77; H, 2.28. Found: C, 47.86; H, 2.40. ¹H NMR (400 MHz, DCM, 18.9 °C): δ 7.85 (t, *J* = 7.3, 7.8 Hz, 1H, *Ph*), 7.79 (t, *J* = 7.8 Hz, 2H, *Ph*), 7.71 (s, 8H, ArH (BAR^F)), 7.66 (q, *J* = 5.0, 7.3, 8.2 Hz, 4H, *Ph*), 7.58 (dd, *J* = 7.3, 16.5 Hz, 4H, *Ph*), 7.54 (s, 4H, ArH (BAR^F)), 7.17 (q, *J* = 7.8 Hz, 2H, *Ph*), 6.93 (dd, *J* = 7.8, 16.5 Hz, 1H, *Ph*), 3.8 (s, 3H, *OMe*). ³¹P NMR (161.8 MHz, DCM, 18.9 °C): δ 2.6 (s). ¹³C{¹H} NMR (100.5 MHz, DCM, 19.0 °C): δ 162.3 (d, *J*_{C-P} = 1.9 Hz, *Ph*), 161.9 (q, *J*_{C-B} = 49.8 Hz, aromatic C (BAR^F)), 140.0 (d, *J*_{C-P} = 2.9 Hz, *Ph*), 136.3 (d, *J*_{C-P} = 2.9 Hz, *Ph*), 135.6 (d, *J*_{C-P} = 9.6 Hz, *Ph*), 134.9 (bs, aromatic C (BAR^F)), 133.5 (d, *J*_{C-P} = 12.5 Hz, *Ph*), 130.5 (d, *J*_{C-P} = 14.4 Hz, *Ph*), 129.0 (qq, *J*_{C-F} = 31.6 Hz, *J*_{C-B} = 2.9 Hz, C-CF₃ (BAR^F)), 124.7 (q, *J*_{C-F} = 272.2, 272.7 Hz, CF₃ (BAR^F)), 122.5 (d, *J*_{C-P} = 14.4 Hz, *Ph*), 119.9 (d, *J*_{C-P} = 82.4 Hz, *Ph*), 117.6 (m, aromatic C (BAR^F)), 113.5 (d, *J*_{C-P} = 6.7 Hz, *Ph*), 56.5 (s, *OMe*). ¹¹B NMR (128.3 MHz, DCM, 18.6 °C): δ -8.2 (s, BAR^F). ¹⁹F NMR (376.2 MHz, DCM, 18.4 °C): δ -63.3 (s, CF₃ (BAR^F)).

6.7.4.2 – Synthesis of [Ph₂P(*o*-NMe₂-C₆H₄)I][BAR^F] [35b]BAR^F:

Pale yellow crystals, 69.1 % yield. *Anal. Calc.* for C₅₂H₃₂BF₂₄INP: C, 48.21; H, 2.49; N, 1.08. Found: C, 48.15; H, 2.40; N, 1.15. ¹H NMR (400 MHz, DCM, 17.0 °C): δ 7.96-7.89 (m, 1H, *Ph*), 7.78-7.73 (br, 2H, *Ph*), 7.72 (br, 8H, ArH (BAR^F)), 7.69-7.63 (m, 6H, *Ph*), 7.62-7.55 (m, 5H, *Ph*), 7.54 (br, 4H, ArH (BAR^F)), 2.12 (s, 6H, NMe₂). ³¹P NMR (161.8 MHz, DCM, 17.6 °C): δ 6.1 (s). ¹³C{¹H} NMR (100.5 MHz, DCM, 16.8 °C): δ 161.2 (q, *J*_{C-B} = 49.8 Hz, aromatic C (BAR^F)), 159.4 (d, *J*_{C-P} = 5.8 Hz, *Ph*), 139.4 (d, *J*_{C-P} = 2.4 Hz, *Ph*), 136.7 (d, *J*_{C-P} = 12.5 Hz, *Ph*), 135.7 (d, *J*_{C-P} = 3.4 Hz, *Ph*), 134.9 (br, aromatic C (BAR^F)), 133.0 (d, *J*_{C-P} = 12.0 Hz, *Ph*), 130.4 (d, *J*_{C-P} = 14.89 Hz, *Ph*), 129.0 (qq, *J*_{C-F} = 31.6 Hz, *J*_{C-B} = 2.9 Hz, C-CF₃ (BAR^F)), 127.3 (d, *J*_{C-P} = 8.2 Hz, *Ph*), 124.7 (q, *J*_{C-F} = 272.2, 272.7 Hz, CF₃ (BAR^F)), 122.1 (d, *J*_{C-P} = 82.9 Hz, *Ph*), 118.6 (d, *J*_{C-P} = 88.2 Hz, *Ph*), 117.6 (m, aromatic C (BAR^F)), 45.6 (s, NMe₂). ¹¹B NMR (128.3 MHz, DCM, 17.2 °C): δ -8.2 (s, BAR^F). ¹⁹F NMR (376.2 MHz, DCM, 17.4 °C): δ -63.3 (s, CF₃ (BAR^F)).

6.7.4.3 – Synthesis of [PhP(*o*-OMe-C₆H₄)₂I][BAR^F] [35d]BAR^F:

Colourless solid, 45.5 % yield. *Anal. Calc.* for C₅₂H₃₁BF₂₄IO₂P: C, 47.59; H, 2.38. Found: C, 47.40; H, 2.30. ¹H NMR (400 MHz, DCM, 17.2 °C): δ 7.82 (t, *J* = 7.4, 8.0 Hz, 2H, *Ph*), 7.76

(br, 1H, *Ph*), 7.71 (br, 8H, *ArH* (BAr^F)), 7.67-7.57 (m, 4H, *Ph*), 7.54 (br, 4H, *ArH* (BAr^F)), 7.15 (q, *J* = 7.3, 8.0 Hz, 4H, *Ph*), 7.01 (dd, *J* = 7.6, 17.3 Hz, 2H, *Ph*), 3.81 (s, 6H, *OMe*). ³¹P NMR (161.8 MHz, DCM, 16.7 °C): δ -10.0 (s). ¹³C{¹H} NMR (100.5 MHz, DCM, 17.5 °C): δ 162.1 (d, *J*_{C-P} = 2.9 Hz, *Ph*), 161.9 (q, *J*_{C-B} = 49.8 Hz, aromatic C (BAr^F)), 139.2 (d, *J*_{C-P} = 1.9 Hz, *Ph*), 135.7 (d, *J*_{C-P} = 3.4 Hz, *Ph*), 135.1 (d, *J*_{C-P} = 10.1 Hz, *Ph*), 134.9 (br, aromatic C (BAr^F)), 133.2 (d, *J*_{C-P} = 12.0 Hz, *Ph*), 130.2 (d, *J*_{C-P} = 14.9 Hz, *Ph*), 129.0 (qq, *J*_{C-F} = 31.6 Hz, *J*_{C-B} = 2.9 Hz, C-CF₃ (BAr^F)), 124.7 (q, *J*_{C-F} = 272.2, 272.7 Hz, CF₃ (BAr^F)), 122.2 (d, *J*_{C-P} = 14.4 Hz, *Ph*), 120.1 (d, *J*_{C-P} = 85.8 Hz, *Ph*), 117.6 (m, aromatic C (BAr^F)), 113.3 (d, *J*_{C-P} = 6.7 Hz, *Ph*), 105.8 (d, *J*_{C-P} = 85.8 Hz, *Ph*), 56.3 (s, *OMe*). ¹¹B NMR (128.3 MHz, DCM, 17.3 °C): δ -8.2 (s, BAr^F). ¹⁹F NMR (376.2 MHz, DCM, 17.3 °C): δ -63.3 (s, CF₃ (BAr^F)).

6.7.4.4 – Synthesis of [PhP(*o*-NMe₂-C₆H₄)₂I][BAr^F] [35e]BAr^F:

Pale yellow solid, 48.6 % yield. *Anal.* Calc. for C₅₅H₃₇BF₂₄IN₂P: C, 48.45; H, 2.79; N, 2.09. Found: C, 48.39; H, 2.72; N, 2.12. ¹H NMR (400 MHz, DCM, 17.1 °C): δ 7.96 (dd, *J* = 8.0, 16.4 Hz, 2H, *Ph*), 7.86 (t, *J* = 7.7 Hz, 2H, *Ph*), 7.71 (br, 8H, *ArH* (BAr^F)), 7.67-7.57 (m, 5H, *Ph*), 7.54 (br, 4H, *ArH* (BAr^F)), 7.50 (t, *J* = 7.7, 7.9 Hz, 4H, *Ph*), 2.07 (s, 12H, NMe₂). ³¹P NMR (161.8 MHz, DCM, 17.0 °C): δ -3.0 (s). ¹³C{¹H} NMR (100.5 MHz, DCM, 18.5 °C): δ 161.9 (q, *J*_{C-B} = 49.8 Hz, aromatic C (BAr^F)), 158.6 (d, *J*_{C-P} = 5.3 Hz, *Ph*), 138.0 (d, *J*_{C-P} = 2.4 Hz, *Ph*), 134.9 (br, aromatic C (BAr^F)), 131.4 (d, *J*_{C-P} = 11.5 Hz, *Ph*), 129.8 (d, *J*_{C-P} = 14.4 Hz, *Ph*), 129.0 (qq, *J*_{C-F} = 31.6 Hz, *J*_{C-B} = 2.9 Hz, C-CF₃ (BAr^F)), 126.6 (d, *J*_{C-P} = 8.6 Hz, *Ph*), 126.3 (d, *J*_{C-P} = 85.3 Hz, *Ph*), 124.7 (q, *J*_{C-F} = 272.2, 272.7 Hz, CF₃ (BAr^F)), 117.6 (m, aromatic C (BAr^F)), 45.75 (s, NMe₂). ¹¹B NMR (128.3 MHz, DCM, 18.1 °C): δ -8.2 (s, BAr^F). ¹⁹F NMR (376.2 MHz, DCM, 17.7 °C): δ -63.3 (s, CF₃ (BAr^F)).

6.7.4.5 – Synthesis of [PPh₃I][BAr^F] [35g]BAr^F:

Colourless blocks, 75.1 % yield. *Anal.* Calc. for C₅₀H₂₇BF₂₄IP: C, 47.95; H, 2.17. Found: C, 48.03; H, 2.03. ¹H NMR (400 MHz, DCM, 16.9 °C): δ 7.83 (t, *J* = 7.3, 7.8 Hz, 3H, *Ph* (PPh₃I)), 7.75-7.66 (m, 14H, *Ph*, *ArH* (PPh₃I, BAr^F)), 7.59 (dd, *J* = 8.0, 15.8 Hz, 6H, *Ph* (PPh₃I)), 7.54 (s, 4H, *ArH* (BAr^F)). ³¹P NMR (161.8 MHz, DCM, 17.1 °C): δ 14.1 (s). ¹³C{¹H} NMR (100.5 MHz, DCM, 18.1 °C): δ 161.9 (q, *J*_{C-B} = 49.8 Hz, aromatic C (BAr^F)), 137.0 (d, *J*_{C-P} = 3.8 Hz, *Ph*), 134.9 (bs, aromatic C (BAr^F)), 134.0 (d, *J*_{C-P} = 12.5 Hz, *Ph*), 130.9 (d, *J*_{C-P} = 14.9 Hz, *Ph*), 123.0 (qq, *J*_{C-F} = 31.6 Hz, *J*_{C-B} = 2.9 Hz, C-CF₃ (BAr^F)), 124.7 (q, *J*_{C-F} = 272.2, 272.7 Hz, CF₃ (BAr^F)), 119.7 (d, *J*_{C-P} = 79.1 Hz, *Ph*), 117.6 (m, aromatic C (BAr^F)). ¹¹B NMR (128.3 MHz, DCM, 17.0 °C): δ -8.2 (s, BAr^F). ¹⁹F NMR (376.2 MHz, DCM, 17.7 °C): δ -63.3 (s, CF₃ (BAr^F)).

6.7.4.6 – Synthesis of [Ph₂P(*o*-OMe-C₆H₄)I][I₃] [35a]I₃:

Dark red solid, 53.5 % yield. *Anal. Calc.* for C₁₉H₁₇I₄OP: C, 28.53; H, 2.14. Found: C, 28.61; H, 2.00. ¹H NMR (400 MHz, DCM, 18.1 °C): δ 7.88 (t, *J* = 7.3, 7.6 Hz, 1H, *Ph*), 7.84-7.77 (m, 2H, *Ph*), 7.73-7.65 (m, 5H, *Ph*), 7.62 (t, *J* = 7.6, 8.0 Hz, 3H, *Ph*), 7.26-7.15 (m, 2H, *Ph*), 6.98 (dd, *J* = 7.8, 16.3 Hz, 1H, *Ph*), 3.87 (s, 3H, *OMe*). ³¹P NMR (161.8 MHz, DCM, 18.4 °C): δ -2.4 (s). ¹³C{¹H} NMR (100.5 MHz, DCM, 18.6 °C): δ 162.2 (d, *J*_{C-P} = 2.4 Hz, *Ph*), 139.4 (d, *J*_{C-P} = 2.4 Hz, *Ph*), 135.7 (d, *J*_{C-P} = 3.4 Hz, *Ph*), 135.5 (d, *J*_{C-P} = 9.6 Hz, *Ph*), 133.7 (d, *J*_{C-P} = 11.5 Hz, *Ph*), 130.4 (d, *J*_{C-P} = 14.4 Hz, *Ph*), 122.4 (d, *J*_{C-P} = 13.9 Hz, *Ph*), 120.7 (d, *J*_{C-P} = 78.6 Hz, *Ph*), 113.5 (d, *J*_{C-P} = 6.7 Hz, *Ph*), 106.7 (d, *J*_{C-P} = 79.1 Hz, *Ph*), 56.9 (s, *OMe*).

6.7.4.7 – Synthesis of [PhP(*o*-OMe-C₆H₄)₂I][I₃] [35d]I₃:

Orange solid, 66.1 % yield. *Anal. Calc.* for C₂₀H₁₉I₄O₂P: C, 28.94; H, 2.31. Found: C, 28.85; H, 2.25. ¹H NMR (400 MHz, DCM, 17.2 °C): δ 7.85 (t, *J* = 7.1, 7.3 Hz, 2H, *Ph*), 7.77 (t, *J* = 7.1 Hz, 1H, *Ph*), 7.70-7.59 (m, 4H, *Ph*), 7.20 (q, *J* = 7.6, 8.2 Hz, 4H, *Ph*), 7.06 (dd, *J* = 7.8, 16.9 Hz, 2H, *Ph*), 3.85 (s, 6H, *OMe*). ³¹P NMR (161.8 MHz, DCM, 17.3 °C): δ -13.0 (s). ¹³C{¹H} NMR (100.5 MHz, DCM, 17.2 °C): δ 162.0 (d, *J*_{C-P} = 2.4 Hz, *Ph*), 138.8 (d, *J*_{C-P} = 2.4 Hz, *Ph*), 135.3 (d, *J*_{C-P} = 3.4 Hz, *Ph*), 135.2 (d, *J*_{C-P} = 9.6 Hz, *Ph*), 133.4 (d, *J*_{C-P} = 12.0 Hz, *Ph*), 130.1 (d, *J*_{C-P} = 14.4 Hz, *Ph*), 122.2 (d, *J*_{C-P} = 14.4 Hz, *Ph*), 120.7 (d, *J*_{C-P} = 82.4 Hz, *Ph*), 113.4 (d, *J*_{C-P} = 7.2 Hz, *Ph*), 106.5 (d, *J*_{C-P} = 82.9 Hz, *Ph*), 56.7 (s, *OMe*).

6.7.4.8 – Synthesis of [PhP(*o*-NMe₂-C₆H₄)₂I][I₃] [35e]I₃:

Red solid, 71.5 % yield. *Anal. Calc.* for C₂₂H₂₅I₄N₂P: C, 30.87; H, 2.94; N, 3.27. Found: C, 30.69; H, 2.85; N, 3.26. ¹H NMR (400 MHz, DCM, 17.0 °C): δ 8.0 (dd, *J* = 7.8, 16.5 Hz, 2H, *Ph*), 7.90 (t, *J* = 7.3, 7.8 Hz, 2H, *Ph*), 7.75-7.63 (m, 5H, *Ph*), 7.59 (dd, *J* = 7.8, 15.1 Hz, 2H, *Ph*), 7.55 (t, *J* = 7.3, 7.8 Hz, 2H, *Ph*), 2.12 (s, 12H, *NMe*₂). ³¹P NMR (161.8 MHz, DCM, 17.8 °C): δ -5.3 (s). ¹³C{¹H} NMR (100.5 MHz, DCM, 17.6 °C): δ 158.6 (d, *J*_{C-P} = 5.8 Hz, *Ph*), 137.6 (d, *J*_{C-P} = 2.4 Hz, *Ph*), 135.6 (br, *Ph*), 134.6 (d, *J*_{C-P} = 3.8 Hz, *Ph*), 131.5 (d, *J*_{C-P} = 11.5 Hz, *Ph*), 129.8 (d, *J*_{C-P} = 14.4 Hz, *Ph*), 128.5 (d, *J*_{C-P} = 14.9 Hz, *Ph*), 126.5 (d, *J*_{C-P} = 8.6 Hz, *Ph*), 126.4 (d, *J*_{C-P} = 82.9 Hz, *Ph*), 120.0 (d, *J*_{C-P} = 92.0 Hz, *Ph*), 45.9 (s, *NMe*₂).

6.7.4.9 – Synthesis of [PPh₃I][I₃] [35g]I₃:

PPh₃ (0.100 g, 0.381 mmol) was dissolved in Et₂O (10 cm³) and iodine (0.194g, 0.762 mmol) was added dropwise as a solution in Et₂O (10 cm³), forming a bright yellow precipitate which darkened as addition continued. After stirring overnight, the supernatant was removed *via* filtration and the solids were washed with Et₂O (2 x 5

cm³) then dried *in vacuo* yielding the product as a free flowing dark red powder. Yield: 0.262 g (0.340 mmol, 89.4 % yield). *Anal.* Calc. for C₁₈H₁₅PI₄: C, 28.08; H, 1.96. Found: C, 28.16; H, 1.87. **¹H NMR** (400 MHz, DCM, 18.6 °C): δ 7.84 (td, *J* = 2.5, 7.1, 7.8 Hz, 3H, *Ph*), 7.72 (sex, *J* = 3.0, 3.7, 4.4, 4.6 Hz, 6H, *Ph*), 7.64 (dd, *J* = 7.6, 15.3 Hz, 6H, *Ph*). **³¹P NMR** (161.8 MHz, DCM, 18.1 °C): δ 6.0 (s). **¹³C{¹H} NMR** (100.5 MHz, DCM, 18.5 °C): δ 136.1 (d, *J*_{C-P} = 2.9 Hz, *Ph*), 133.9 (d, *J*_{C-P} = 11.5 Hz, *Ph*), 130.7 (d, *J*_{C-P} = 14.4 Hz, *Ph*), 120.6 (d, *J*_{C-P} = 74.8 Hz, *Ph*).

6.8 – References

- 1 J. M. Farrell, J. A. Hatnean and D. W. Stephan, *J. Am. Chem. Soc.*, 2012, **134**, 15728–15731.
- 2 E. R. Clark and M. J. Ingleson, *Organometallics*, 2013, **32**, 6712–6717.
- 3 P. Eisenberger, B. P. Bestvater, E. C. Keske and C. M. Crudden, *Angew. Chem. Int. Ed.*, 2015, **54**, 2467–2471.
- 4 T. Vom Stein, M. Pérez, R. Dobrovetsky, D. Winkelhaus, C. B. Caputo and D. W. Stephan, *Angew. Chem. Int. Ed.*, 2015, **54**, 10178–10182.
- 5 R. Arias Ugarte, D. Devarajan, R. M. Mushinski and T. W. Hudnall, *Dalton Trans.*, 2016, **45**, 11150–11161.
- 6 M. Hirai, J. Cho and F. P. Gabbai, *Chem. Eur. J.*, 2016, **22**, 6537–6541.
- 7 G. Talavera, J. Peña and M. Alcarazo, *J. Am. Chem. Soc.*, 2015, **137**, 8704–8707.
- 8 E. R. Clark, A. M. Borys and K. Pearce, *Dalton Trans.*, 2016, **45**, 16125–16129.
- 9 G. S. Ananthnag, N. Edukondalu, J. T. Mague and M. S. Balakrishna, *Polyhedron*, 2013, **62**, 203–207.
- 10 E. Shirakawa, Y. Yamamoto, Y. Nakao, S. Oda, T. Tsuchimoto and T. Hiyama, *Angew. Chem. Int. Ed.*, 2004, **43**, 3448–3451.
- 11 V. C. Chuit, R. J. P. Corriu, P. Monforte, C. Reye, J. Declercq and A. Dubourg, *Angew. Chem. Int. Ed.*, 1993, **105**, 1529–1531.
- 12 F. Weller, D. Nuszhar, K. Dehnicke, F. Gingl and J. Strähle, *ZAAC - J. Inorg. Gen. Chem.*, 1991, **602**, 7–16.
- 13 S. M. Godfrey, C. A. Mcauli, R. G. Pritchard, J. M. She and G. M. Thompson, *J. Chem. Soc., Dalt. Trans.*, 1997, **2**, 4823–4827.
- 14 S. M. Godfrey, C. A. Mcauli, R. G. Pritchard and J. M. Sheffield, *Dalton Trans.*, 1998, 1919–1923.
- 15 M. A. H. A. Al-Juboori, P. N. Gates and A. S. Muir, *J. Chem. Soc., Chem. Commun.*, 1991, 1270–1271.
- 16 N. Bricklebank, S. M. Godfrey, A. G. Mackie, C. A. Mcauiiffe and R. G. Pritchard, *J. Chem. Soc., Chem. Commun.*, 1992, 355–356.
- 17 F. Ruthe, W. Mont and P. G. Jones, *Chem. Commun.*, 1997, **185**, 1947–1948.
- 18 S. M. Godfrey, C. A. Mcauli, I. Mushtaq, R. G. Pritchard and J. M. Sheffield, *Dalton Trans.*, 1998, 3815–3818.
- 19 C. G. Hrib, F. Ruthe, E. Seppälä, M. Bätcher, C. Druckenbrodt, C. Wismach, P. G. Jones, W. W. Du Mont, V. Lippolis, F. A. Devillanova and M. Bühl, *Eur. J. Inorg. Chem.*, 2006, 88–100.

- 20 B. W. Walther, M. Batchler, S. Pohl, W. Saak, J. Laugier and P. Rey, *Angew. Chem. Int. Ed.*, 1987, **26**, 912–913.
- 21 S. M. Godfrey, D. G. Kelly, C. A. McAuliffe, A. G. Mackie, R. G. Pritchard and S. M. Watson, *J. Chem. Soc., Chem. Commun.*, 1991, **2**, 1163–1164.
- 22 N. Bricklebank, S. M. Godfrey, H. P. Lane, C. A. McAuliffe, R. G. Pritchard and J.-M. Moreno, *J. Chem. Soc., Dalton Trans.*, 1995, 2421–2424.
- 23 F. Ruthe, P. G. Jones, W.-W. du Mont, P. Deplano and M. L. Mercuri, *Z. Anorg. Allg. Chem.*, 2000, **625**, 1105–1111.
- 24 W. Mont and F. Ruthe, *Coord. Chem. Rev.*, 1999, **189**, 101–133.
- 25 N. A. Barnes, S. M. Godfrey, R. Z. Khan, A. Pierce and R. G. Pritchard, *Polyhedron*, 2012, **35**, 31–46.
- 26 F. Teixedor, R. Nunez, C. Vinas, R. Sillanpaa and R. Kivevka, *Angew. Chem. Int. Ed.*, 2000, **39**, 4290–4292.
- 27 N. a Barnes, S. M. Godfrey, R. T. a Halton, I. Mushtaq and R. G. Pritchard, *Dalton Trans.*, 2008, 1346–54.
- 28 C. A. McAuliffe, B. Beagley, G. A. Gott, A. G. Mackie, P. P. MacRory and R. G. Pritchard, *Angew. Chem. Int. Ed.*, 1987, **26**, 264–265.
- 29 A. F. Wells, *Structural Inorganic Chemistry*, Clarendon Press, Oxford, 5th Editio., 1984.
- 30 N. A. Barnes, K. R. Flower, S. M. Godfrey, P. A. Hurst, R. Z. Khan and R. G. Pritchard, *CrystEngComm*, 2010, **12**, 4240–4251.
- 31 N. A. Barnes, S. M. Godfrey, R. T. A. Halton, I. Mushtaq and R. G. Pritchard, *Dalton Trans.*, 2006, 4795–4804.
- 32 F. N. Jones, M. F. Zinn and C. R. Hauser, *J. Org. Chem.*, 1963, **28**, 663–665.
- 33 M. Stratakis, *J. Org. Chem.*, 1997, **62**, 3024–3025.
- 34 D. W. Slocum, T. K. Reinscheld, C. B. White, M. D. Timmons, P. A. Shelton, M. G. Slocum, R. D. Sandlin, E. G. Holland, D. Kusmic, J. A. Jennings, K. C. Tekin, Q. Nguyen, S. J. Bush, J. M. Keller and P. E. Whitley, *Organometallics*, 2013, **32**, 1674–1686.
- 35 R. W. Seidel and R. Goddard, *Acta Cryst.*, 2015, **C71**, 664–666.
- 36 I. Dance and M. Scudder, *J. Chem. Soc., Chem. Commun.*, 1995, 1039–1040.
- 37 J. A. S. Howell, M. G. Palin, P. C. Yates, P. McArdle, D. Cunningham, Z. Goldschmidt, H. E. Gottlieb and D. Hezroni-Langerman, *J. Chem. Soc., Perkin Trans. 2*, 1992, 1769.
- 38 P. Deplano, S. M. Godfrey, F. Isaia, C. A. McAuliffe, M. L. Mercuri and E. F. Trogu,

- Chem. Ber.*, 1997, **130**, 299–305.
- 39 J. Trotter, *Acta Cryst.*, 1960, **13**, 86–95.
- 40 C. C. Wilson, N. Shankland and A. J. Florence, *J. Chem. Soc., Faraday Trans.*, 1996, **92**, 5051–5057.
- 41 F. A. Cotton and P. A. Kibala, *J. Am. Chem. Soc.*, 1987, **109**, 3308–3312.
- 42 F. B. Alhanash, N. A. Barnes, S. M. Godfrey, P. A. Hurst, A. Hutchinson, R. Z. Khan and R. G. Pritchard, *Dalton Trans.*, 2012, **41**, 7708.
- 43 P. J. Hay and W. R. Wadt, *J. Chem. Phys.*, 1985, **82**, 299–310.
- 44 W. R. Wadt and P. J. Hay, *J. Chem. Phys.*, 1985, **82**, 284–298.
- 45 F. Weigend and R. Ahlrichs, *Phys. Chem. Chem. Phys.*, 2005, **7**, 3297.
- 46 A. Poater, B. Cosenza, A. Correa, S. Giudice, F. Ragone, V. Scarano and L. Cavallo, *Eur. J. Inorg. Chem.*, 2009, 1759–1766.
- 47 A. Poater, F. Ragone, S. Giudice, C. Costabile, R. Dorta, S. P. Nolan and L. Cavallo, *Organometallics*, 2008, **27**, 2679–2681.
- 48 D. C. Mudalige, E. S. F. Ma, S. J. Rettig, B. O. Patrick and B. R. James, *Can. J. Chem.*, 2014, **92**, 716–723.
- 49 P. Suomalainen, S. Jääskeläinen, M. Haukka, R. H. Laitinen, J. Pursiainen and T. A. Pakkanen, *Eur. J. Inorg. Chem.*, 2000, **2000**, 2607–2613.

Supplementary Chapter 1

Crystal Structures of *N*-Arylamidines

"Hasta la vista, baby!"

Terminator 2: Judgement Day (1991)

S1.1 – A Very Brief Introduction to Amidines

Amidines are the dinitrogen analogues of carboxylic acids and esters. The synthesis of amidines was first described by Pinner in 1877¹ - the reaction of nitriles with dry hydrogen chloride in anhydrous alcohol yields the intermediate imidic ester, which on treatment with ammonia affords the desired amidine (Scheme S1.1.1). This reaction which bears his name, and variations thereof, are still widely employed to this day. Many alternative methods have also been developed and amidines have found widespread use as ligands, as structural units in drug design, and as synthons for the synthesis of heterocyclic compounds. Further information on their synthesis, applications and subsequent reactivity can be found in reviews and books.^{2,3,4,5}

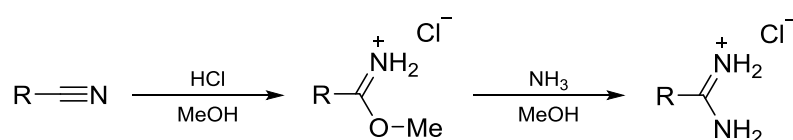
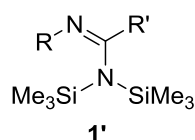
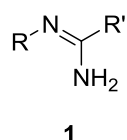


Figure S1.1.1: Synthesis of amidines *via* the Pinner reaction.

S1.2 – Monosubstituted *N*-Arylamidines

This thesis has explored the synthesis of sulfur-nitrogen and phosphorus-nitrogen heterocycles from monosubstituted *N*-arylamidines **1**. The reaction of *N*-arylamidines with SOCl₂ afforded fused-ring 1,2,4-benzothiadiazine 1-chlorides, which are reduced under mild conditions to give the corresponding neutral radical. Conversely, the reaction of *N*-arylamidines with halophosphines gave a diverse library of compounds, and was found to be highly sensitive to the substituents on the aryl-ring, the choice of halophosphine and the reaction conditions employed.

The majority of the *N*-arylamidines prepared in this thesis have been previously reported in the literature, and synthesised *via* a number of different routes. Of these twenty crystalline amidines (Figure S1.2.1) however, only three (**1b**,⁶ **1m**⁷ and **1t**⁸) have been structurally characterised by SCXRD. This chapter will therefore present and compare the remaining crystal structures.



	R	R'	Yield %		R	R'	Yield %
1a	Ph	Ph	89.7	1k	Ph	4-OMe-C ₆ H ₄	77.0
1b	2-Me-C ₆ H ₄	Ph	70.8	1l	2,3-Me ₂ -C ₆ H ₃	4-OMe-C ₆ H ₄	73.7
1c	2,3-Me ₂ -C ₆ H ₃	Ph	86.8	1m	4-Me-C ₆ H ₄	Ph	70.8
1d	2,5-Me ₂ -C ₆ H ₃	Ph	78.7	1n	2,4-Me ₂ -C ₆ H ₃	Ph	72.2
1e	3,5-Me ₂ -C ₆ H ₃	Ph	77.8	1o	2-Biphenyl	Ph	67.5
1f	3-OMe-C ₆ H ₄	Ph	64.5	1p	Ph	^t Bu	41.0
1g	Ph	2-Me-C ₆ H ₄	62.8	1r	3-NMe ₂ -C ₆ H ₄	Ph	83.3
1h	2,3-Me ₂ -C ₆ H ₃	2-Me-C ₆ H ₄	66.1	1t	2,6- ⁱ Pr ₂ -C ₆ H ₃	Ph	76.0
1i	Ph	<i>p</i> -Pyridyl	87.9	1u	4-Cl-C ₆ H ₄	Ph	85.1
1j	2,3-Me ₂ -C ₆ H ₃	<i>p</i> -Pyridyl	84.5	1a'	Ph	Ph	55.2

Figure S1.2.1: Structurally characterised *N*-arylamidines.

S1.3 – Structural Studies of Monosubstituted *N*-Arylamidines

Crystals suitable for single-crystal X-ray diffraction studies were grown by slow diffusion of hexane into a saturated solution of product in dichloromethane. SCXRD data was also collected for compound **1b**, **1m** and **1t** to permit direct and precise comparisons of unit cell parameters and bond metrics across the *N*-arylamidines, since these were originally collected at higher temperatures. A summary of space groups and unit cell parameters is presented in Table S1.3.1.

	Space Group	Cell Lengths / Å			Cell Angles / °			Cell Volume / Å ³	Z	Z'
		a	b	c	α	β	γ			
1a	<i>P</i> $\bar{1}$	5.4339(2)	8.3854(4)	11.8797(6)	73.514(4)	82.856(4)	87.377(4)	514.99(4)	2	1
1b	<i>P</i> $\bar{1}$	10.2688(3)	10.5908(4)	11.3233(4)	96.798(3)	103.414(3)	95.890(3)	1178.61(7)	4	2
1c	<i>Pccn</i>	24.3256(3)	10.1501(1)	9.9674(1)	90	90	90	2461.02(5)	8	1
1d	<i>P</i> ₂ ₁ / <i>c</i>	10.0868(2)	14.2443(2)	9.9091(2)	90	118.647(3)	90	1249.45(5)	4	1
1e	<i>P</i> ₂ ₁ 2 ₁ 2 ₁	9.5344(1)	10.6770(1)	12.4805(1)	90	90	90	1270.50(2)	4	1
1f	<i>P</i> ₂ ₁ 2 ₁ 2 ₁	9.4623(6)	10.6120(5)	11.9934(5)	90	90	90	1204.30(1)	4	1
1g	<i>P</i> ₂ ₁ / <i>c</i>	12.4627(3)	8.3753(1)	11.9105(2)	90	113.892(2)	90	1136.67(4)	4	1
1h	<i>P</i> ₂ ₁ / <i>c</i>	7.5114(1)	23.1222(2)	7.6891(1)	90	99.936(1)	90	1315.41(3)	4	1
1i	<i>P</i> ₂ ₁ / <i>c</i>	12.1511(1)	15.8057(1)	10.6230(1)	90	94.309(1)	90	2034.45(3)	8	2
1j	<i>P</i> $\bar{1}$	11.3101(4)	14.8285(5)	15.5662(5)	89.538(3)	89.587(3)	70.936(3)	2467.34(2)	8	4
1k	<i>P</i> ₂ ₁ / <i>c</i>	6.7241(2)	18.5287(4)	10.0457(2)	90	104.416(2)	90	1212.17(5)	4	1
1l	<i>C</i> ₂ / <i>c</i>	14.0729(2)	14.0982(2)	27.9338(4)	90	94.718(1)	90	5523.36(1)	16	2
1m	<i>P</i> $\bar{1}$	9.8107(3)	10.0969(3)	12.1839(4)	84.082(3)	81.768(3)	80.108(3)	1172.89(7)	4	2
1n	<i>P</i> $\bar{1}$	9.9907(3)	11.4856(5)	12.9769(5)	71.156(4)	69.266(3)	71.367(3)	1282.11(9)	4	2
1o	<i>P</i> $\bar{1}$	5.3943(2)	11.6235(4)	12.5219(4)	111.639(3)	96.098(2)	95.440(2)	718.01(5)	2	1
1p	<i>F</i> <i>dd</i> 2	21.8833(2)	18.8771(2)	10.0811(1)	90	90	90	4164.43(7)	16	1
1r	<i>P</i> <i>c</i>	9.2938(2)	11.0641(1)	12.6836(2)	90	93.393(1)	90	1301.94(4)	4	2
1t	<i>P</i> ₂ ₁ / <i>c</i>	11.2586(2)	14.6602(2)	10.1408(1)	90	92.558(1)	90	1672.10(4)	4	1
1u	<i>P</i> $\bar{1}$	5.4326(1)	8.2909(2)	13.3920(5)	73.704(3)	84.285(2)	86.871(2)	575.86(3)	2	1
1a'	<i>P</i> <i>na</i> 2 ₁	14.7232(7)	21.2711(1)	6.2506(4)	90	90	90	1957.55(2)	4	1

Table S1.3.1: Space group and unit cell parameters.

All nitrogen-bound hydrogen atoms were located in the difference map and refined freely unless otherwise stated. In all cases, both hydrogen atoms were located on a single nitrogen (tautomer **A**) and not as the tautomeric form **B** (Figure S1.3.1).²

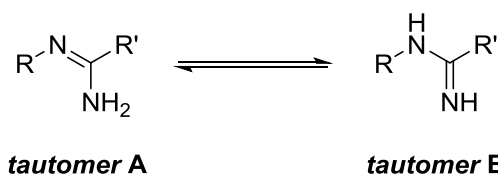


Figure S1.3.1: Tautomerism in amidines.

This is further supported by the C1=N2 and C1-N1 bond lengths (Figure S1.3.2) which are in good agreement with literature values for carbon-nitrogen single and double bonds respectively.⁹ All amidines herein adopt hydrogen bonded networks in the solid-state between H1A and N2 of a neighbouring molecule; H1B was found to not be involved in hydrogen bonding, likely due to steric hindrance. In the case of the 4-pyridyl substituted amidines, **1i-j**, the hydrogen bonding was observed between H1A and the pyridyl nitrogen, N3. A summary of hydrogen bond distances and angles is shown in Table S1.3.2.

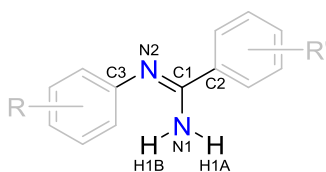


Figure S1.3.2: Structural labelling scheme.

	Torsion Angles / °		Deviation	Hydrogen Bond			Hydrogen Bond
	C3-N2-C1-N1	C3-N2-C1-C2	From Coplanarity / °	N1-H1A	H1A...N2	N1...N2	Angle / °
1a	3.2(2)	178.6(1)	88.8	0.89(2)	2.38(2)	3.093(2)	137.4(2)
1b	5.1(1)	175.2(9)	76.1	0.89(2)	2.12(2)	2.966(1)	159.6(1)
	0.7(1)	180.0(8)	77.0	0.89(2)	2.13(2)	3.001(1)	165.7(1)
1c	3.9(1)	179.3(8)	73.6	0.91(2)	2.16(2)	3.052(1)	166.2(1)
1d	4.9(2)	176.3(9)	74.8	0.89(2)	2.03(2)	2.894(1)	163.5(1)
1e	10.7(2)	171.6(1)	74.2	0.90(2)	2.19(2)	3.055(2)	161.8(2)
1f	3.1(2)	179.2(1)	65.3	0.87(2)	2.14(2)	2.998(2)	170.9(2)
1g	173.2(2)	8.7(3)	61.1	0.91(3)	2.16(3)	3.074(2)	175.7(2)
1h	0.2(2)	176.7(8)	9.1	0.87(1)	2.09(1)	2.961(1)	177.8(1)
1i	2.3(2)	176.4(8)	46.6	0.90(1)	2.12(1)*	2.987(1)*	163.2(1)*
	3.0(2)	174.8(9)	70.1	0.89(2)	2.15(2)*	3.002(1)*	161.1(1)*
1j	1.1(2)	179.6(1)	57.3	0.89(2)	2.11(2)*	2.981(1)*	166.5(2)*
	3.1(2)	179.5(1)	90.0	0.88(2)	2.20(2)*	3.050(1)*	163.1(2)*
	1.0(2)	176.9(1)	66.5	0.89(2)	2.14(2)*	2.995(2)*	160.5(2)*
	2.5(2)	173.7(1)	80.3	0.89(2)	2.17(2)*	3.032(2)*	162.8(2)*
1k	0.2(1)	177.6(8)	79.6	0.90(2)	2.02(2)	2.904(1)	166.6(1)
1l	5.3(2)	177.5(9)	76.0	0.87(1)	2.22(1)	3.076(1)	165.4(1)
	3.7(2)	179.7(9)	73.9	0.88(2)	2.20(2)	3.068(1)	167.3(1)
1m	0.4(1)	178.3(8)	56.2	0.90(2)	2.11(2)	3.005(1)	170.1(1)
	3.5(2)	177.1(9)	45.1	0.89(2)	2.18(2)	3.015(1)	157.5(1)
1n	1.1(2)	178.5(1)	60.1	0.90(2)	2.12(2)	3.009(2)	169.7(2)
	0.1(2)	179.5(1)	41.9	0.90(2)	2.15(2)	3.032(2)	166.3(2)
1o	7.4(2)	173.5(9)	85.4	0.92(2)	2.28(2)	3.067(1)	143.9(1)
1p	5.5(2)	173.6(1)	†	0.94(2)	2.46(2)	3.016(2)	117.8(2)
1r	4.4(6)	179.6(3)	73.7	0.90(6)	2.13(6)	2.951(5)	150.3(5)
	2.4(6)	178.7(4)	81.6	0.83(5)	2.19(5)	2.921(5)	146.9(5)
1t	4.1(1)	178.8(8)	43.0	0.89(2)	2.08(2)	2.921(1)	155.9(1)
1u	2.3(2)	177.5(1)	86.5	0.86(2)	2.39(2)	3.086(1)	138.4(1)
1a'	166.3(2)	11.2(4)	63.4	†	†	†	†

* N3 (pyridyl) hydrogen-bond acceptor. † Not applicable.

Table S1.3.2: Summary of key structural parameters.

Significant variation in the hydrogen bond parameters are observed across the monosubstituted *N*-arylamidines, with the H1A...N2 distance spanning a range of 2.02(2) Å to 2.46(2) Å. These would be considered as moderately weak hydrogen bonds following the notation of Jeffery,¹⁰ and is typical for N-H...N species. Amidines bearing electron withdrawing groups such as **1a**, **1o** and **1u** were found to have the longest hydrogen bond lengths, whilst those with electron-donating groups were considerably shorter. The strength of the hydrogen bond is strongly correlated with the N-H...N bond angle, with linear geometries favouring stronger interactions.¹⁰

The torsion angles for C3-N2-C1-N2 and C3-N2-C1-C2 are both close to 0° and 180° respectively such that they adopt the idealised geometry shown in Figure S1.3.3. In the case of **1g** and **1a'** however, these values are inversed such that the two aryl rings are held in much closer proximity. There is considerable deviation in the coplanarity of the two aryl rings; a deviation angle approaching 90° is observed for the majority of the amidines whilst a near coplanar conformation is only adopted for **1h**. Steric influences

and external packings forces are believed to be the primary factors responsible for these changes.

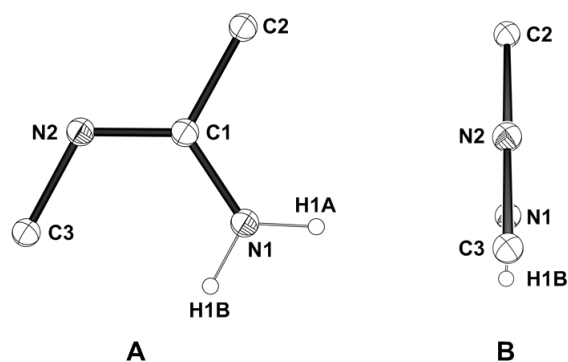


Figure S1.3.3: Idealised geometry with 0° C3-N2-C1-N2 and 180° C3-N2-C1-C2 torsion angles: (A) Side-view; (B) View along the N2-C1 bond.

S1.3.1 - Crystal Structure of **1a**

Compound **1a** crystallises as colourless plates in the triclinic space group $P\bar{1}$ with a single molecule in the asymmetric unit (Figure S1.3.1.1). The geometry adopted is typical of many of the *N*-arylamidines; the torsion angles for C3-N2-C1-N2 and C3-N2-C1-C2 are $3.2(2)^\circ$ and $178.6(1)^\circ$ respectively, whilst the deviation from coplanarity of the two phenyl rings is 88.8° .

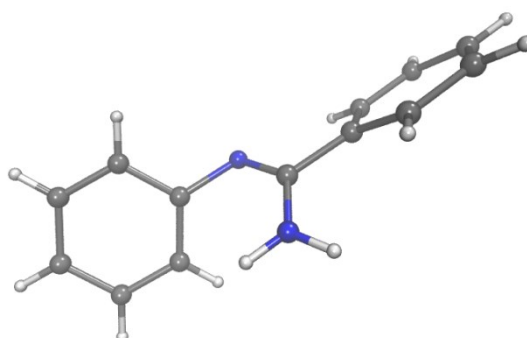


Figure S1.3.1.1: Asymmetric unit of **1a**.

Molecules of **1a** are associated through long hydrogen bonds ($2.38(2)$ Å) between H1A and N2 of neighbouring molecule, forming chains that propagate along the crystallographic *a* axis (Figure S1.3.1.2). These chains weakly interact with adjacent and parallel off-set chains through two weak edge-to-face (EF) embraces¹¹ between the phenyl rings.

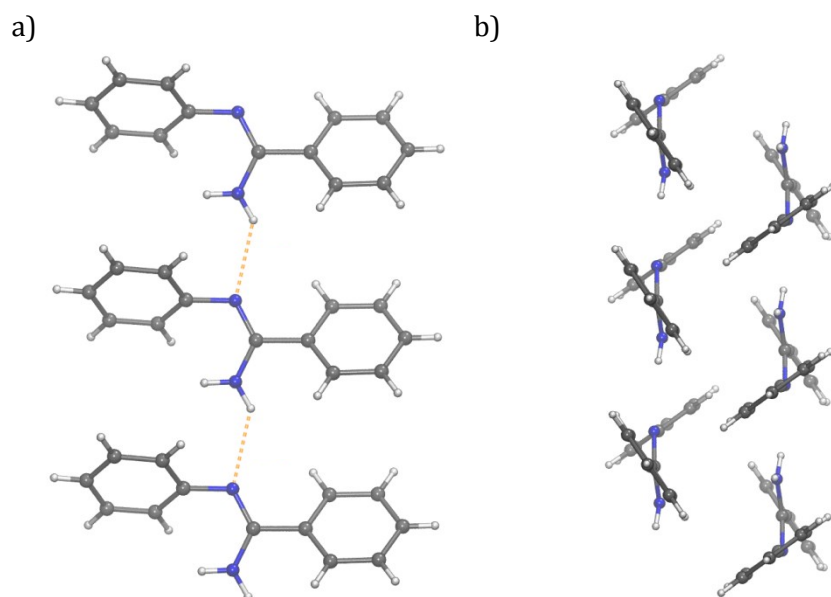


Figure S1.3.1.2: a) Hydrogen bonding chains of **1a** looking down the crystallographic *b* axis. b) Crystal packing of **1a** looking down the crystallographic *c* axis.

S1.3.2 – Crystal Structure of **1b**

Compound **1b** crystallises as colourless blocks in the triclinic space group $P\bar{1}$ with two molecules in the asymmetric unit (Figure S1.3.2.1). The two molecules differ slightly in the C3-N2-C1-N2 and C3-N2-C1-C2 torsion angles ($5.1(1)^\circ$ and $175.2(9)^\circ$ vs. $0.7(1)^\circ$ and $180.0(8)^\circ$) whilst the deviations from coplanarity of the *o*-tolyl and phenyl rings are similar at 76.1° and 77.0° . The two molecules are orientated in a head-to-tail fashion to minimise the steric hindrance resulting from the additional methyl group.

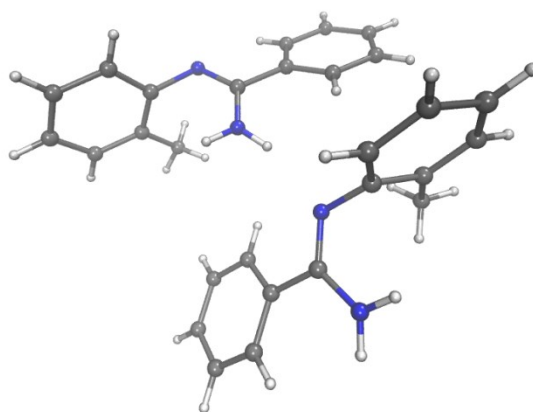


Figure S1.3.2.1: Asymmetric unit of **1b**.

Molecules of **1b** are associated through short hydrogen bonds with alternating distances of $2.12(2)$ Å and $2.13(2)$ Å between H1A and N2 of the neighbouring

molecule, resulting in infinite chains that propagate along the crystallographic *a* axis with offset chains related through an inversion centre (Figure S1.3.2.2).

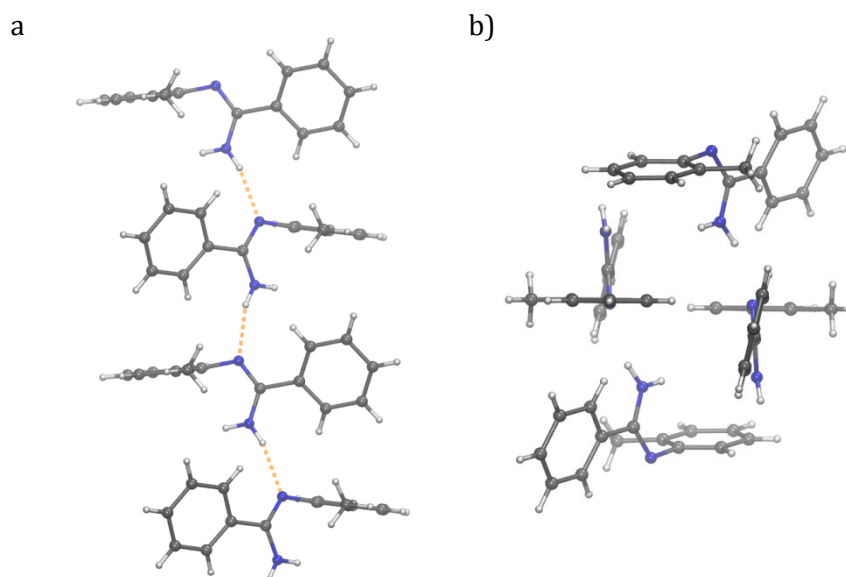


Figure S1.3.2.2: a) Hydrogen bonding chains of **1b** looking down the crystallographic *b* axis. b) Crystal packing of **1b** looking down the crystallographic *c* axis.

S1.3.3 - Crystal Structure of **1c**

Compound **1c** crystallises as colourless blocks in the orthorhombic space group *Pccn* with a single molecule in the asymmetric unit (Figure S1.3.3.1). The pendant aryl ring deviates from coplanarity of the 2,3-xylyl ring by 73.6° , slightly less than the deviation observed for **1a** and **1b**, but the C3-N2-C1-N2 and C3-N2-C1-C2 torsion angles are close to ideal at $3.9(1)^\circ$ and $179.3(8)^\circ$.

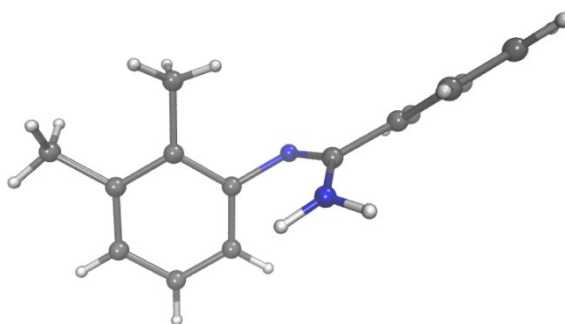


Figure S1.3.3.1: Asymmetric unit of **1c**.

Molecules of **1c** are associated through hydrogen bonds between H1A and N2 ($2.16(2)$ Å) of a neighbouring molecule, leading to infinite chains of alternating head-to-tail molecules along the crystallographic *b* axis (Figure S1.3.3.2). These chains further interact with offset parallel chains through a single weak EF embrace.

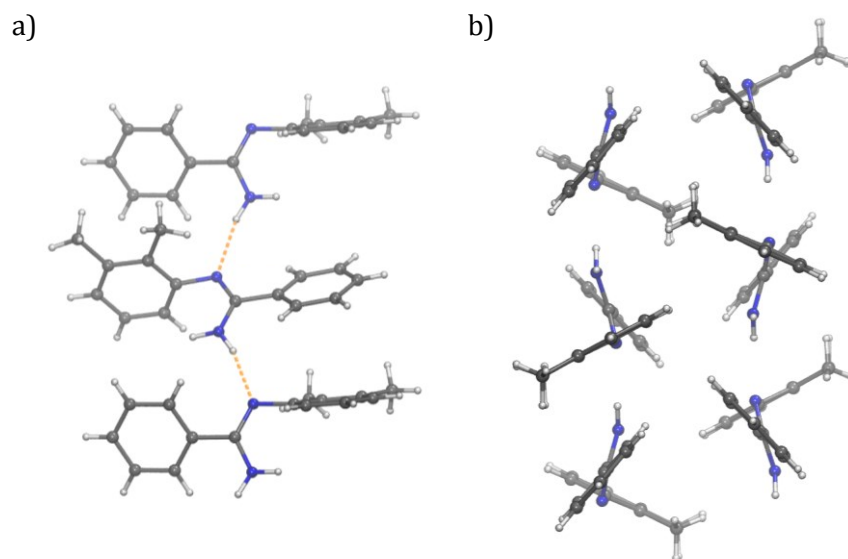


Figure S1.3.3.2: a) Hydrogen bonding chains of **1c** looking down the crystallographic *c* axis. b) Crystal packing of **1c** looking down the crystallographic *a* axis.

S1.3.4 – Crystal Structure of **1d**

Compound **1d** crystallises as colourless blocks in the monoclinic space group $P2_1/c$ with a single molecule in the asymmetric unit (Figure S1.3.4.1). The structural parameters are again similar to many of the *N*-arylamidines; the C3-N2-C1-N2 and C3-N2-C1-C2 torsion angles are $4.9(2)^\circ$ and $176.3(9)^\circ$ respectively, and the deviation from coplanarity between the 2,5-xylyl ring and pendant phenyl rings is 74.8° .

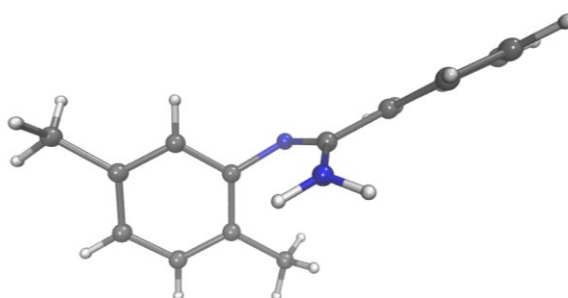


Figure S1.3.4.1: Asymmetric unit of **1d**.

Molecules of **1d** form infinite chains along the crystallographic *c* axis through a strong hydrogen bond network between H1A and N2 ($2.03(2) \text{ \AA}$) of a twisted neighbouring molecule (Figure S1.3.4.2). An inversion related offset chain runs parallel to the chain without any significant additional intermolecular interactions.

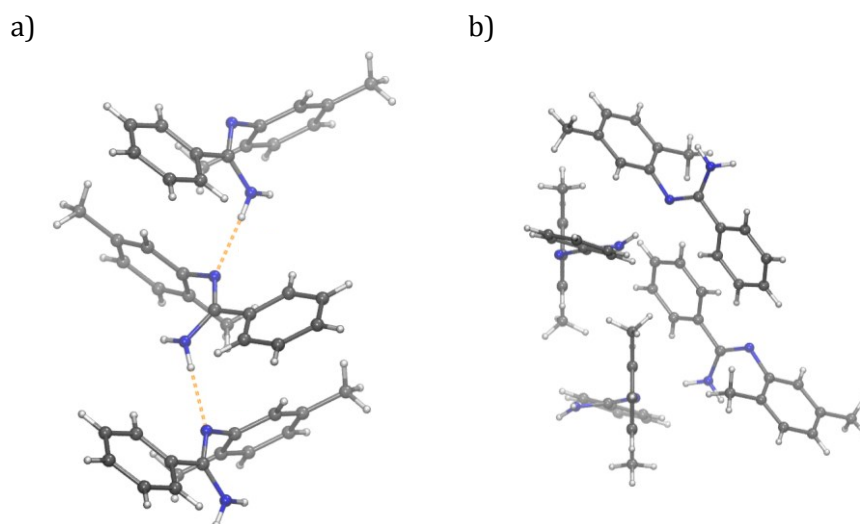


Figure S1.3.4.2: a) Hydrogen bonding chains of **1d** looking down the crystallographic *a* axis. b) Crystal packing of **1d** looking perpendicular to the crystallographic *bc* plane.

7.3.5 – Crystal Structure of **1e**

Compound **1e** crystallises as colourless irregular crystals in the orthorhombic space group $P2_12_12_1$ with a single molecule in the asymmetric unit (Figure S1.3.5.1). The C3-N2-C1-N2 and C3-N2-C1-C2 torsion angles deviate considerably from the idealised geometry at $10.7(2)^\circ$ and $171.6(1)^\circ$, whilst the difference in angles of the planes of the 3,5-xylyl and phenyl ring is typical within the other amidines at 74.2° . These deviations may arise to minimise the steric influence of the methyl groups with the NH_2 fragment, or due to other external packing effects.

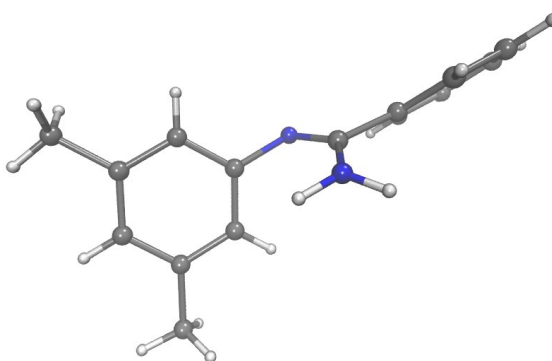


Figure S1.3.5.1: Asymmetric unit of **1e**.

Hydrogen bonded chains propagate along the crystallographic *a* axis with alternating head-to-tail molecules associated through $\text{H1A}\cdots\text{N2}$ contacts $2.19(2)$ Å (Figure S1.3.5.2). The difference in hydrogen bond length between **1e** and its isomer **1d** illustrates the impact of external packing forces on the intermolecular interactions in the solid-state.

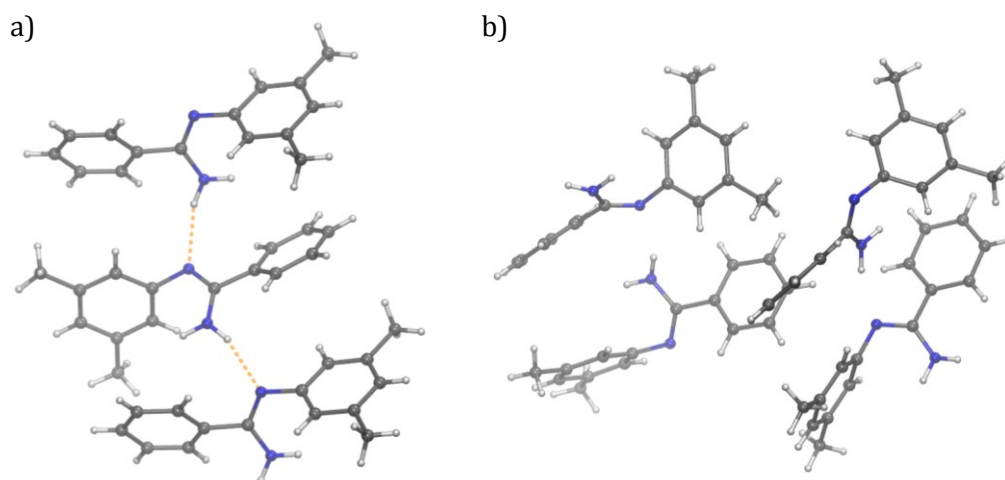


Figure S1.3.5.2: a) Hydrogen bonding chains of **1e** looking down the crystallographic *b* axis. b) Crystal packing of **1e** looking down the crystallographic *c* axis.

S1.3.6 – Crystal Structure of **1f**

Compound **1f** crystallises as colourless blocks in the orthorhombic space group $P2_12_12_1$ with a single molecule in the asymmetric unit (Figure S1.3.6.1) and is isostructural to **1e**. The C3-N2-C1-N2 and C3-N2-C1-C2 torsion angles are close to the idealised geometry at $3.1(2)^\circ$ and $179.2(1)^\circ$ respectively. The deviation from coplanarity is 65.3° and the methoxy group is coplanar with its associated aryl ring.

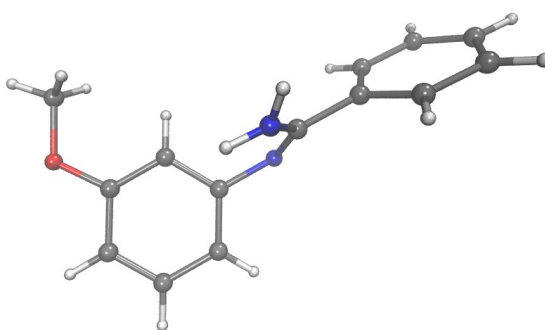


Figure S1.3.6.1: Asymmetric unit of **1f**.

Molecules of **1f** are associated through moderate H1A \cdots N2 hydrogen bonds ($2.14(2)$ Å) between neighbouring head-to-tail molecules, forming infinite chains along the crystallographic *a* axis (Figure S1.3.6.2). Offset parallel chains are weakly associated through a single EF embrace.

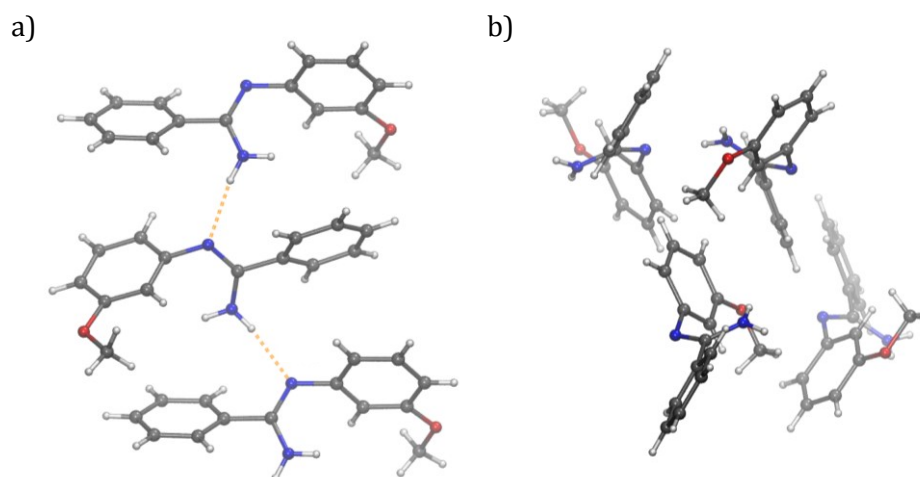


Figure S1.3.6.2: a) Hydrogen bonding chains of **1f** looking down the crystallographic *b* axis. b) Crystal packing of **1f** looking down the crystallographic *c* axis.

S1.3.7 – Crystal Structure of **1g**

Compound **1g** crystallises as colourless planks in the monoclinic space group $P2_1/c$ with a single molecule in the asymmetric unit (Figure S1.3.7.1). The C3-N2-C1-N2 and C3-N2-C1-C2 torsion angles are $173.2(2)^\circ$ and $8.7(3)^\circ$, resulting in a ‘folded’ conformation. This differs considerably from the other structurally characterised amidines discussed herein and from the idealised geometry with C3-N2-C1-N2 and C3-N2-C1-C2 torsion angles close to 0° and 180° respectively. The deviation from coplanarity of the *o*-tolyl and pendant phenyl rings is $61.1(1)^\circ$, which is smaller than many of the other substituted amidines.

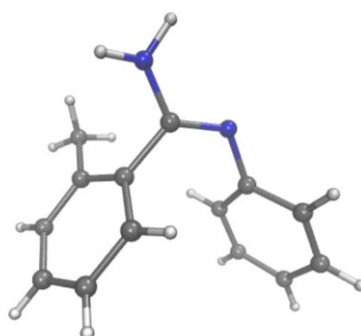


Figure S1.3.7.1: Asymmetric unit of **1g**.

Molecules of **1g** form infinite hydrogen bonded chains that propagate along the crystallographic *b* axis, associated through moderate H1A \cdots N2 contacts ($2.16(3)$ Å) between neighbouring molecules along the screw axes (Figure S1.3.7.2). Neighbouring molecules are further associated through H1B \cdots arene interactions¹² (H1B \cdots C_{aryl} range = $2.671(2)$ - $2.78(3)$ Å), and may explain why amidine **1g** favours the ‘folded’ conformation in the solid-state.

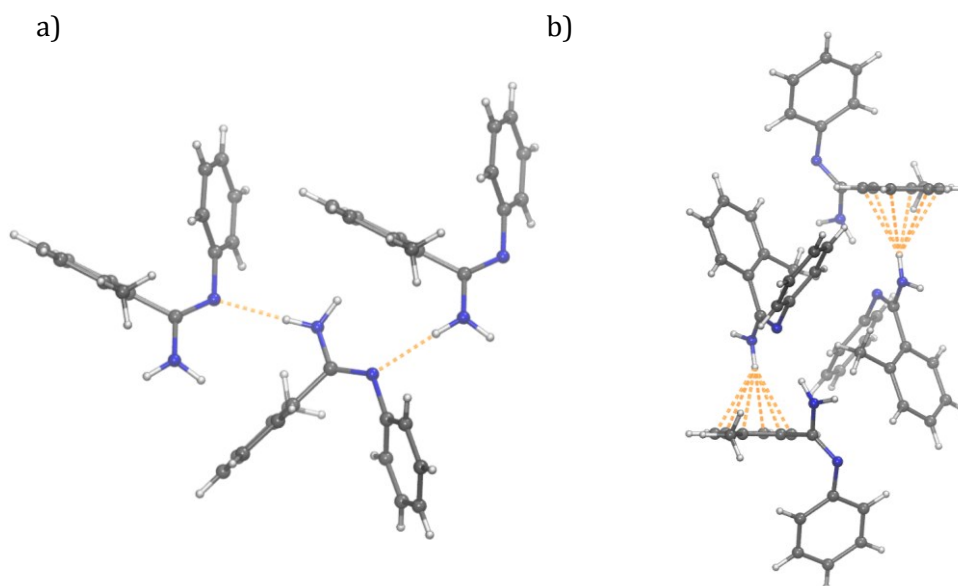


Figure S1.3.7.2: a) Hydrogen bonding chains of **1g** looking down the crystallographic *c* axis. b) Crystal packing of **1g** looking perpendicular to the crystallographic *ab* plane, highlighting the H1B...arene interactions.

S1.3.8 - Crystal Structure of **1h**

Compound **1h** crystallises as colourless blocks in the monoclinic space group $P2_1/c$ with a single molecule in the asymmetric unit (Figure S1.3.8.1). The C3-N2-C1-N2 and C3-N2-C1-C2 torsion angles are close to the idealised geometry at $0.2(2)^\circ$ and $176.7(8)^\circ$ respectively, but the two arenes are almost coplanar with only a slight deviation of 9.1° , unlike many of the other structurally characterised amidines.

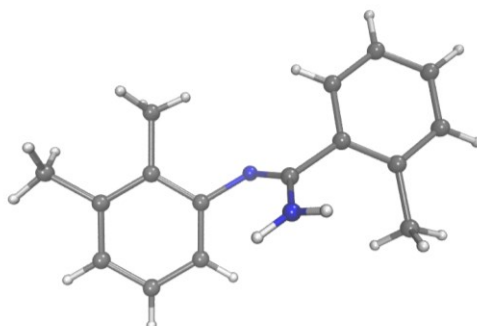


Figure S1.3.8.1: Asymmetric unit of **1h**.

Molecules of **1h** arrange in head-to-tail chains associated through moderately strong N1-H1A...N2 hydrogen bonds ($2.09(1) \text{ \AA}$); these chains propagate diagonally through the crystallographic *ac* axes. (Figure S1.3.8.2). Molecules are further associated through a single offset face-to-face (OFF) embrace¹¹ between the *o*-tolyl and 2,3-xylyl rings.

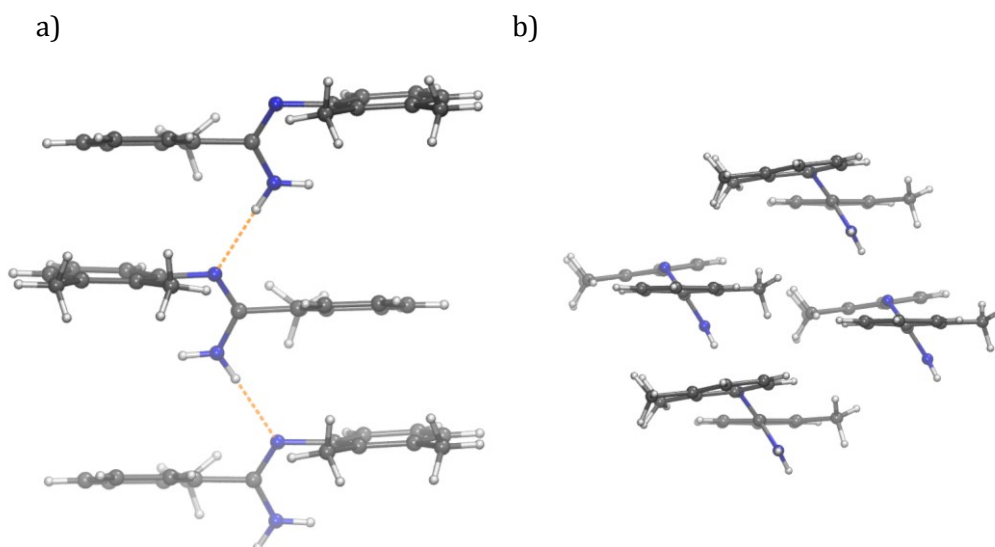


Figure S1.3.8.2: a) Hydrogen bonding chains of **1h** looking down the crystallographic *a* axis. b) Crystal packing of **1g** looking down the crystallographic *a* axis.

S1.3.9 – Crystal Structure of **1i**

Compound **1i** crystallises as colourless irregular crystals in the monoclinic space group $P2_1/c$ with two molecules in the asymmetric unit (Figure S1.3.9.1). The C3-N2-C1-N2 and C3-N2-C1-C2 torsion angles are similar for both molecules at $2.0(2)^\circ/176.4(8)^\circ$, and $3.2(2)^\circ/174.8(9)^\circ$ respectively, whilst the deviation from coplanarity of the phenyl and pyridyl rings differ markedly at 46.6° and 70.1° .

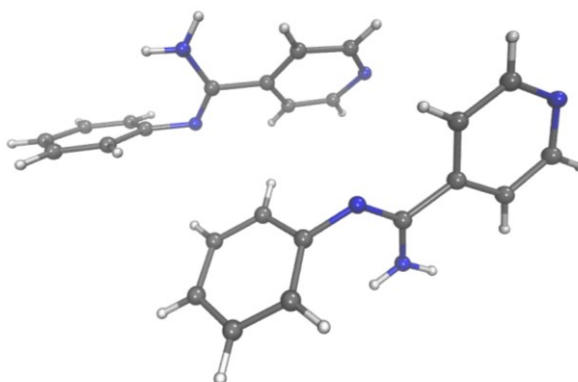


Figure S1.3.9.1: Asymmetric unit of **1i**.

Molecules of **1i** are associated through hydrogen bonds between H1A and the pyridyl nitrogen N3 ($2.12(1) \text{ \AA}$ and $2.15(2) \text{ \AA}$), resulting in square tetrameric rings that slice perpendicular to the crystallographic *ac* plane (Figure S1.3.9.2). Offset tetramers further interact through several EF embraces (Figure S1.3.9.3).

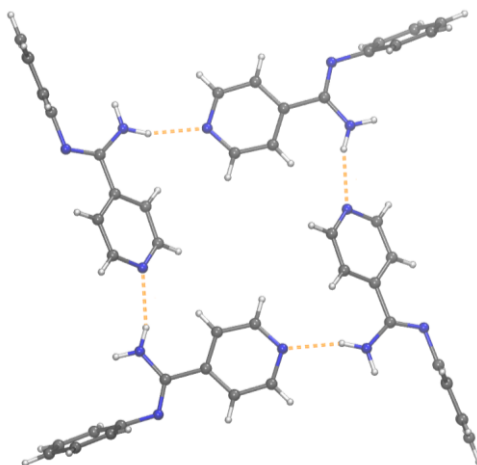


Figure S1.3.9.2: Hydrogen bonded tetramers of **1i** looking diagonally through the crystallographic *ac* axis.

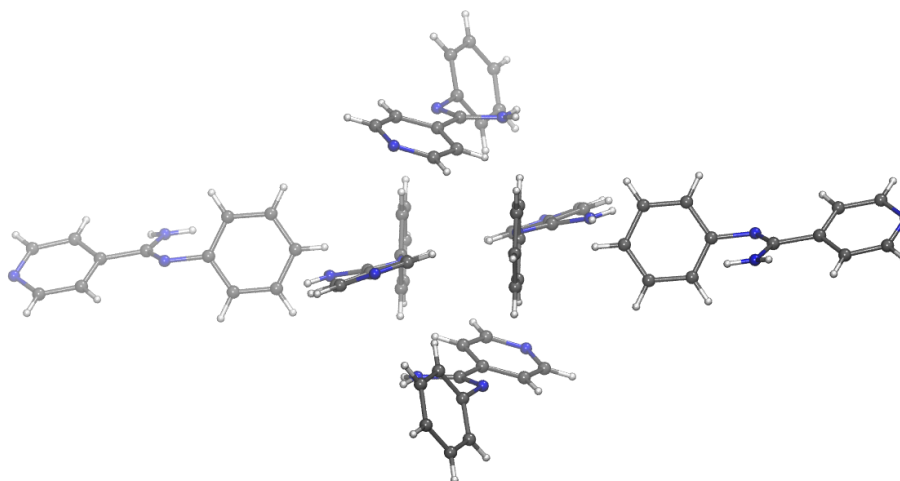


Figure S1.3.9.3: Crystal packing of **1i** looking down the crystallographic *b* axis.

S1.3.10 – Crystal Structure of **1j**

Compound **1j** crystallises as colourless plates in the triclinic space group $P\bar{1}$ with four molecules in the asymmetric unit (Figure S1.3.10.1). The C3-N2-C1-N2 and C3-N2-C1-C2 torsion angles for the four molecules are close to the idealised geometry and range from 1.0(1)-3.1(1)° and 173.7(1)-179.6(1)°. In contrast, the deviations from coplanarity of the 2,3-xylyl and 4-pyridyl rings vary considerably from 57.3° to 90.0°.

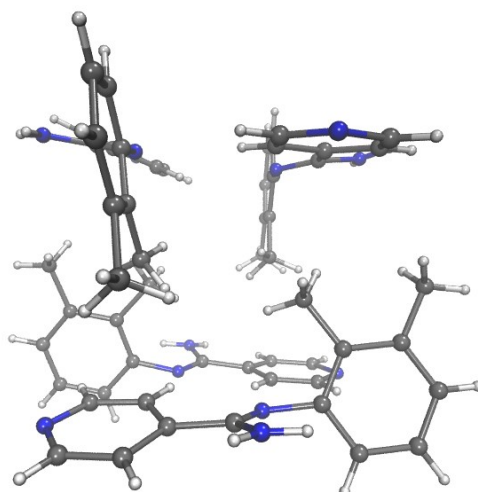


Figure S1.3.10.1: Asymmetric unit of **1j**.

Molecules of **1j** exhibit hydrogen-bonding interactions with two neighbouring molecules through N1 and N3; the H1A...N3 contacts range from 2.11(2) Å to 2.20(2) Å. This results in tetrameric rings that propagate through the crystallographic *c* axis, with each molecule representing the corner of a square (Figure S1.3.10.2).

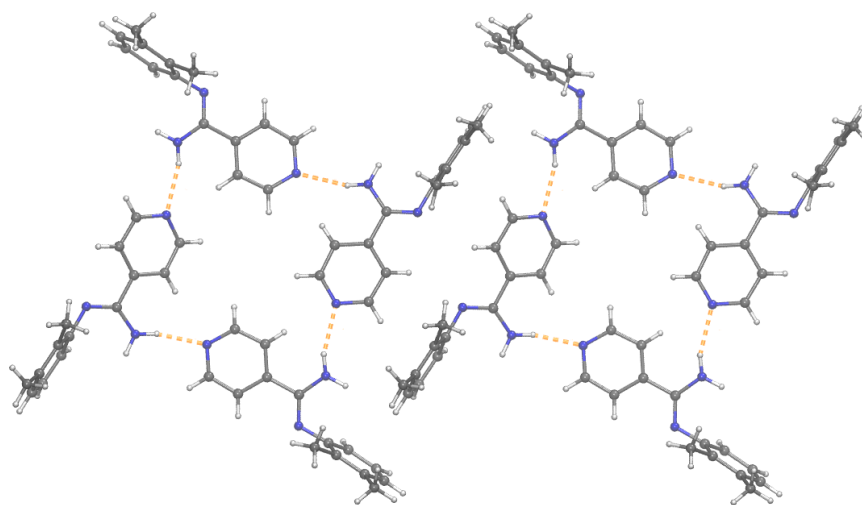


Figure S1.3.10.2: Hydrogen bonded tetramers of **1j** looking perpendicular to the crystallographic *abc* plane.

S1.3.11 – Crystal Structure of **1k**

Compound **1k** crystallises as colourless blocks in the monoclinic space group $P2_1/c$ with a single molecule in the asymmetric unit (Figure S1.3.11.1). The C3-N2-C1-N2 and C3-N2-C1-C2 torsion angles are close to the idealised geometry at $0.2(1)^\circ$ and $177.6(8)^\circ$ respectively. The deviation from coplanarity is 79.6° and the methoxy group is coplanar with the associated aryl ring.

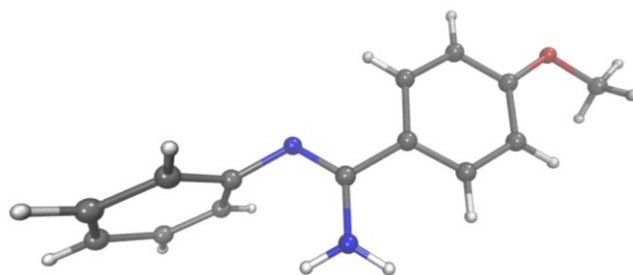


Figure S1.3.11.1: Asymmetric unit of **1k**.

Molecules of **1k** are associated through strong hydrogen bonds between H1A and N2 of a neighbouring molecule (2.02(2) Å), resulting in infinite chains that propagate along the crystallographic *c* axis (Figure S1.3.11.2). Adjacent molecules are twisted by 75.1° with respect to the pendant aryl rings, whilst the phenyl rings are almost coplanar with a minor deviation of 7.5°.

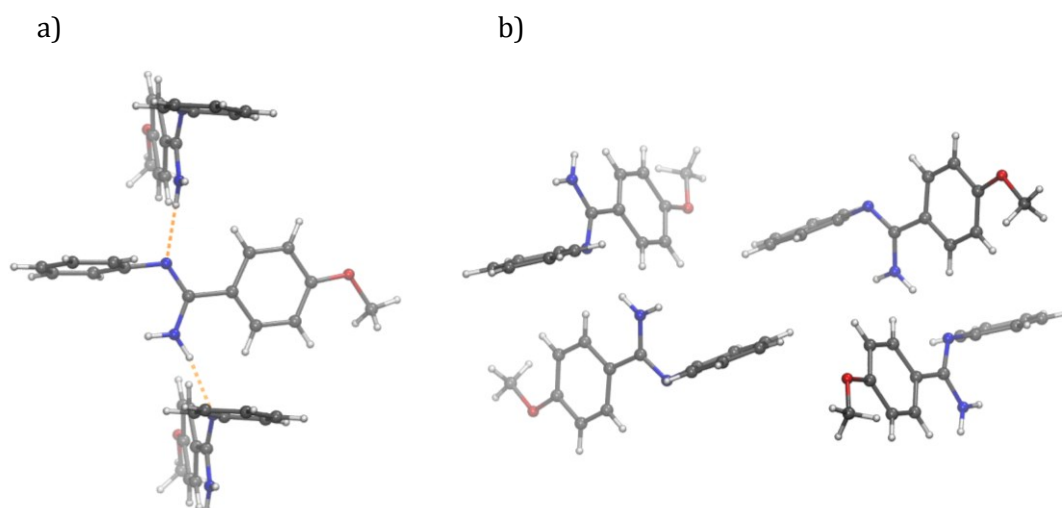


Figure S1.3.11.2: a) Hydrogen bonding chains of **1k** looking diagonally through the crystallographic *ab* axis. b) Crystal packing of **1k** looking down the crystallographic *a* axis.

S1.3.12 – Crystal Structure of **1l**

Compound **1l** crystallises as colourless blocks in the monoclinic space group *C2/c* with two molecules in the asymmetric unit (Figure S1.3.12.1). The C3-N2-C1-N2 and C3-N2-C1-C2 torsion angles are similar for both molecules at 5.3(2)°/177.5(9)° and 3.7(2)°/179.7(9)° respectively, as are the deviations from coplanarity for the two aryl rings at 76.0° and 73.9°. The methoxy group is coplanar with its associated aryl ring for both molecules.

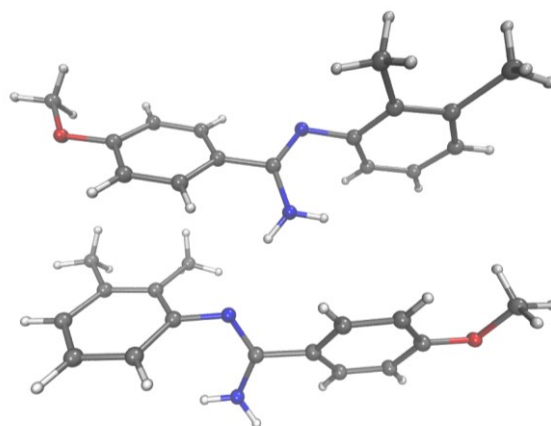


Figure S1.3.12.1: Asymmetric unit of **11**.

Molecules of **11** form infinite hydrogen bonded chains that propagate diagonally through the crystallographic *ab* axes with alternating head-to-tail molecules (Figure S1.3.12.2). The H1A...N2 distance (2.22(1) Å and 2.20(2) Å) is considerably longer than **1k** (2.02(2) Å) despite the introduction of additional electron donating groups. This is likely to arise due to the increased steric hindrance of the 2,3-xylyl ring compared to a phenyl ring, which prevents close contact of adjacent molecules. Neighbouring hydrogen bonding chains run perpendicular to the crystallographic *ab* plane.

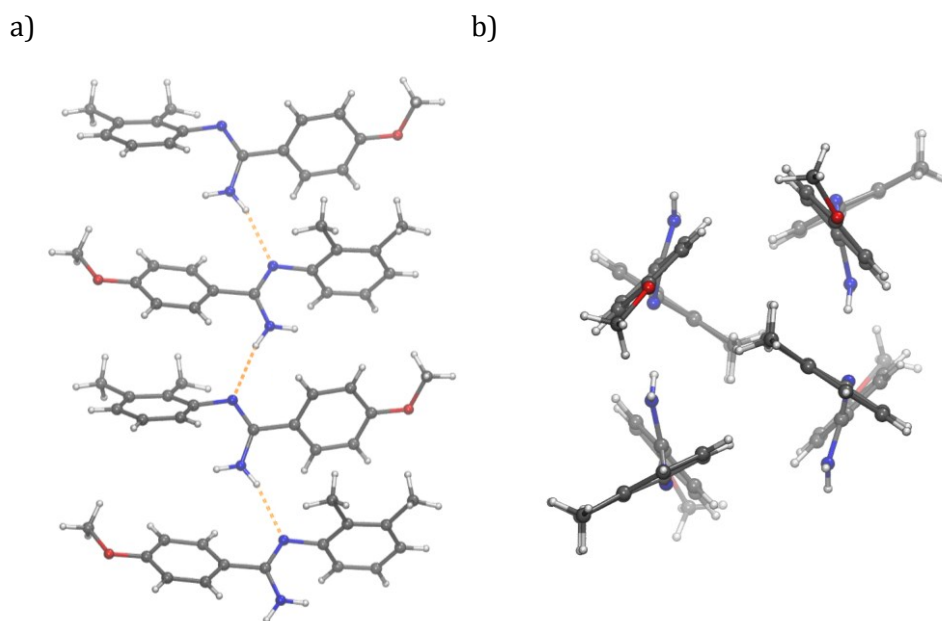


Figure S1.3.12.2: a) Hydrogen bonding chains of **11** looking perpendicular to the crystallographic *ab* plane. b) Crystal packing of **11** looking down the crystallographic *c* axis.

S1.3.13 – Crystal Structure of **1m**

Compound **1m** crystallises as colourless irregular crystals in the triclinic space group $P\bar{1}$ with two molecules in the asymmetric unit (Figure S1.3.13.1). The C3-N2-C1-N2 and C3-N2-C1-C2 torsion angles are close to the idealised geometry at $0.4(1)^\circ/178.3(8)^\circ$ and $3.5(2)^\circ/177.1(9)^\circ$ respectively, whilst the deviations from coplanarity of the two aryl rings are 56.2° and 45.1° , which is considerably less than the majority of *N*-arylamidines with values approaching 90° .

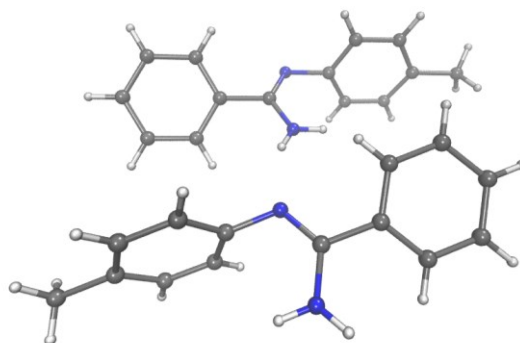


Figure S1.3.13.1: Asymmetric unit of **1m**.

Molecules of **1m** are associated through moderate hydrogen bonds between H1A and N2 ($2.11(2)$ Å and $2.18(2)$ Å) of adjacent molecules (Figure S1.13.3.2). This leads to infinite chains of alternating head-to-tail molecules that propagate along the crystallographic *b* axis, with neighbouring offset chains related through an inversion centre. a)

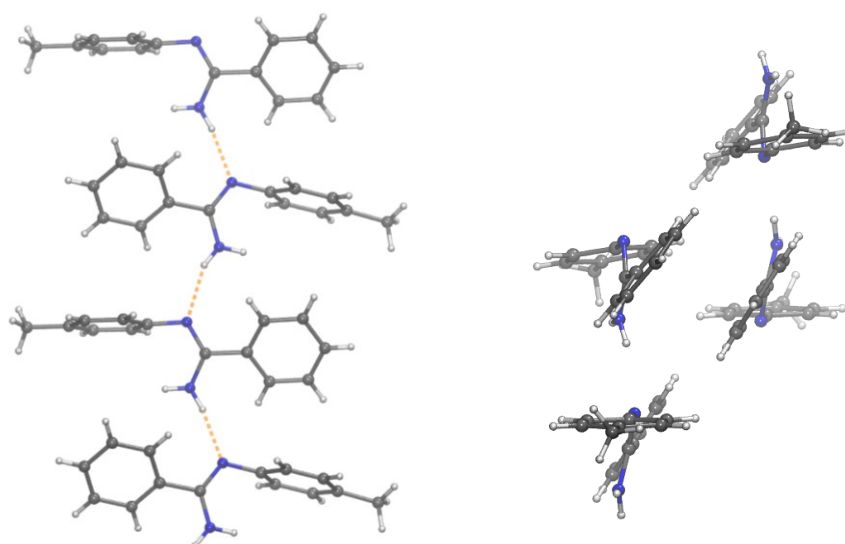


Figure S1.3.13.2: a) Hydrogen bonding chains of **1m** looking down the crystallographic *a* axis. b) Crystal packing of **1m** looking diagonally through the crystallographic *ac* axes.

S1.3.14 – Crystal Structure of **1n**

Compound **1n** crystallises as colourless rods in the triclinic space group $P\bar{1}$ with two molecules in the asymmetric unit (Figure S1.3.14.1). The C3-N2-C1-N2 and C3-N2-C1-C2 torsion angles are similar for both molecules and again close to the idealised geometry at $1.1(2)^\circ/178.5(1)^\circ$ and $0.1(2)^\circ/179.5(1)^\circ$ respectively. The deviations from coplanarity, like **1m**, are also low at 60.1° and 41.9° .

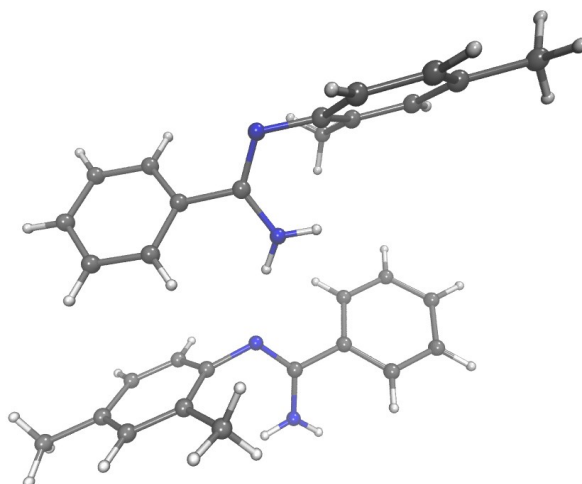


Figure S1.3.14.1: Asymmetric unit of **1n**.

Molecules of **1n** are associated through moderate H1A...N2 hydrogen bonds ($2.12(2)$ Å and $2.15(2)$ Å) resulting in infinite chains of alternating head-to-tail molecules that propagate along the crystallographic a axis (Figure S1.3.14.2).

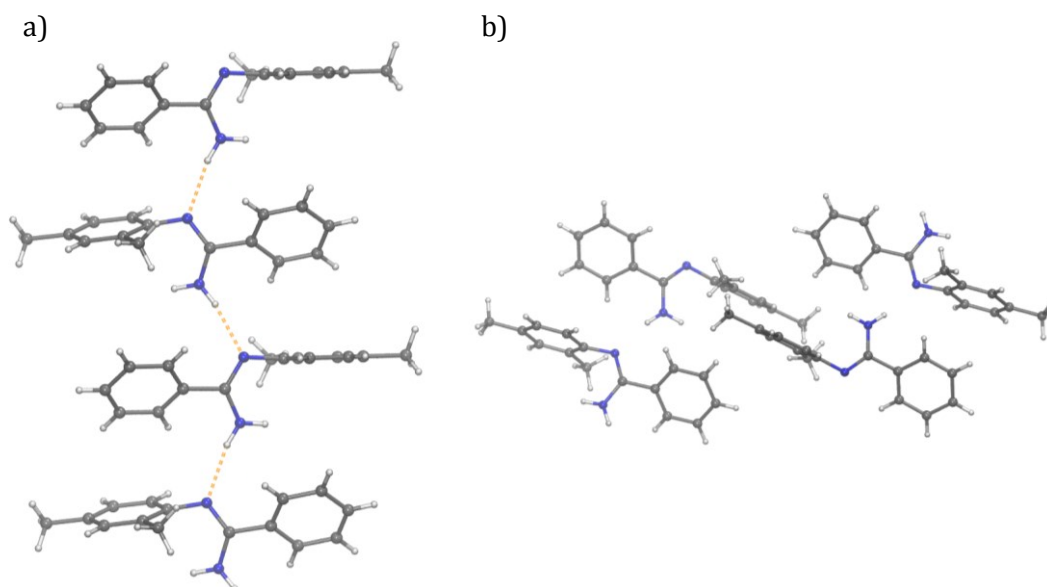


Figure S1.3.14.2: a) Hydrogen bonding chains of **1n** looking down the crystallographic b axis. b) Crystal packing of **1n** looking diagonally through the crystallographic bc axes.

S1.3.15 – Crystal Structure of **1o**

Compound **1o** crystallises as colourless rods in the triclinic space group $P\bar{1}$ with a single molecule in the asymmetric unit (Figure S1.3.15.1). Departure from the idealised C3-N2-C1-N2 and C3-N2-C1-C2 torsion angles ($7.4(2)^\circ$ and $173.5(9)^\circ$) is observed due to the increased steric hindrance of the 2-biphenyl moiety. The deviation from coplanarity for the *N*-phenyl and pendant phenyl ring is 85.4° , whilst the deviation between the two rings of the 2-biphenyl moiety is 46.5° .

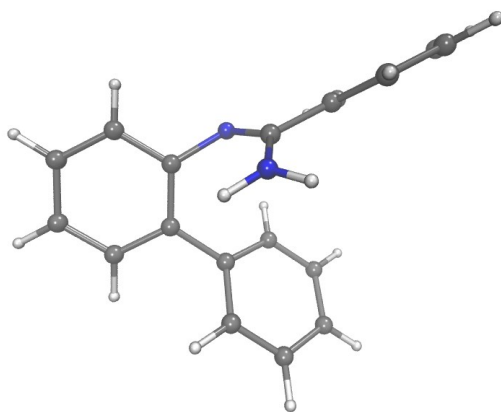


Figure S1.3.15.1: Asymmetric unit of **1o**.

Molecules of **1o** are associated through weak H1A...N2 hydrogen bonds ($2.28(2)$ Å) resulting in infinite chains that propagate along the crystallographic *a* axis (Figure S1.3.15.2). Inversion-related offset chains are further associated through two weak EF embraces.

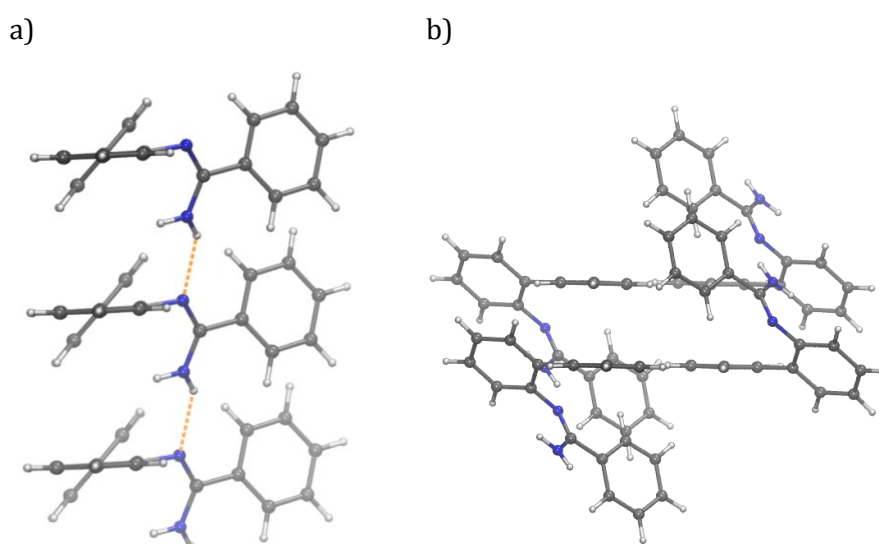


Figure S1.3.15.2: a) Hydrogen bonding chains of **1o** looking perpendicular to the crystallographic *ab* plane. b) Crystal packing of **1o** looking perpendicular to the crystallographic *abc* plane.

S1.3.16 – Crystal Structure of **1p**

Compound **1p** crystallises as colourless rods in the orthorhombic space group *Fdd2* with a single molecule in the asymmetric unit (Figure S1.3.16.1). The C3-N2-C1-N2 and C3-N2-C1-C2 torsion angles are $5.5(2)^\circ$ and $173.6(1)^\circ$, similar to the other amidines bearing a pendant aryl group. The deviation from coplanarity of the phenyl ring with respect to the C1-C2- C_{trans} fragment is 84.9° and the N2-C1-C2- C_{trans} torsion angle is $175.6(1)^\circ$.

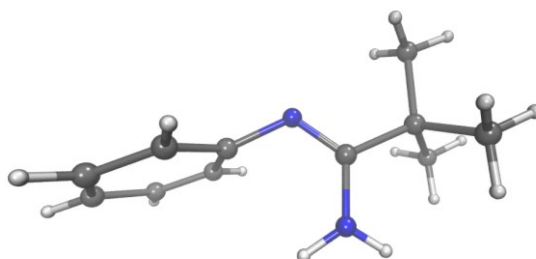


Figure S1.3.16.1: Asymmetric unit of **1p**.

Molecules of **1p** are associated through long and weak hydrogen bonds ($2.46(2)$ Å) between H1A and N2 of an adjacent molecule resulting in infinite chains that propagate along the crystallographic *c* axis with alternating head-to-tail molecules (Figure S1.3.16.2).

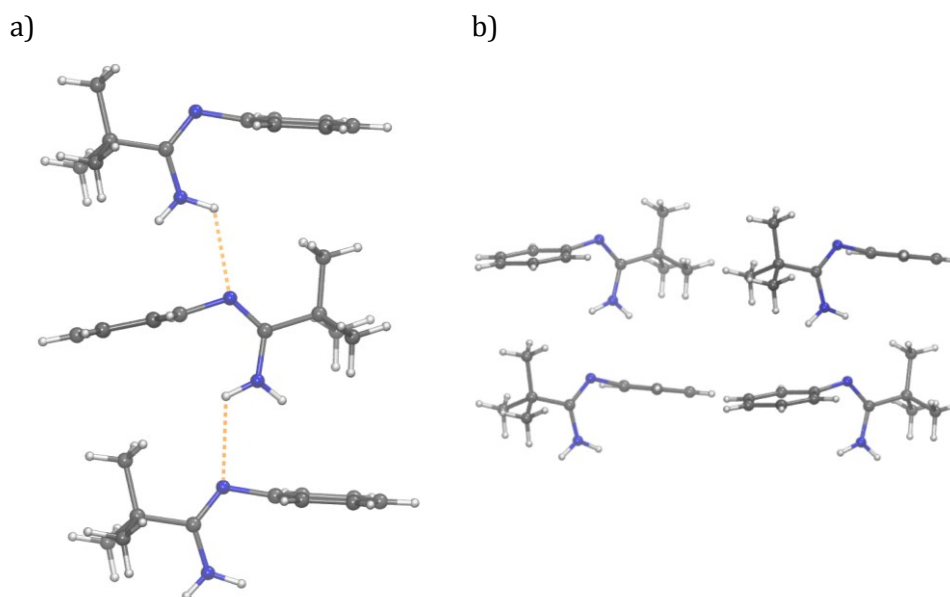


Figure S1.3.16.2: a) Hydrogen bonding chains of **1p** looking perpendicular to the crystallographic *ab* plane. b) Crystal packing of **1p** looking perpendicular to the crystallographic *ab* plane.

S1.3.17 – Crystal Structure of **1r**

Compound **1r** crystallises as colourless needles in the monoclinic space group Pc with two molecules in the asymmetric unit (Figure S1.3.17.1). The C3-N2-C1-N2 and C3-N2-C1-C2 torsion angles are similar for both molecules and close to the idealised geometry at $4.4(6)^\circ/179.6(3)^\circ$ and $2.4(6)^\circ/178.7(4)^\circ$ respectively. The deviations from coplanarity are 73.7° and 81.6° , and the NMe₂ moiety is coplanar with its associated aryl ring such that the nitrogen lone pairs are conjugated into the ring system.

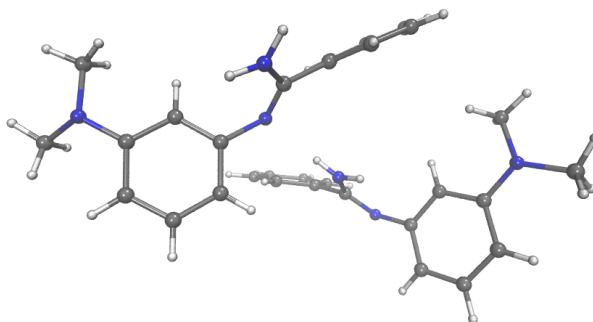


Figure S1.3.17.1: Asymmetric unit of **1r**.

Molecules of **1r** form infinite hydrogen bonded chains that propagate along the crystallographic a axis; the H1A...N2 distances are moderate at $2.13(6)$ Å and $2.19(5)$ Å, and adjacent molecules are twisted by 48.0° to minimise steric clashes (Figure S1.3.17.2).

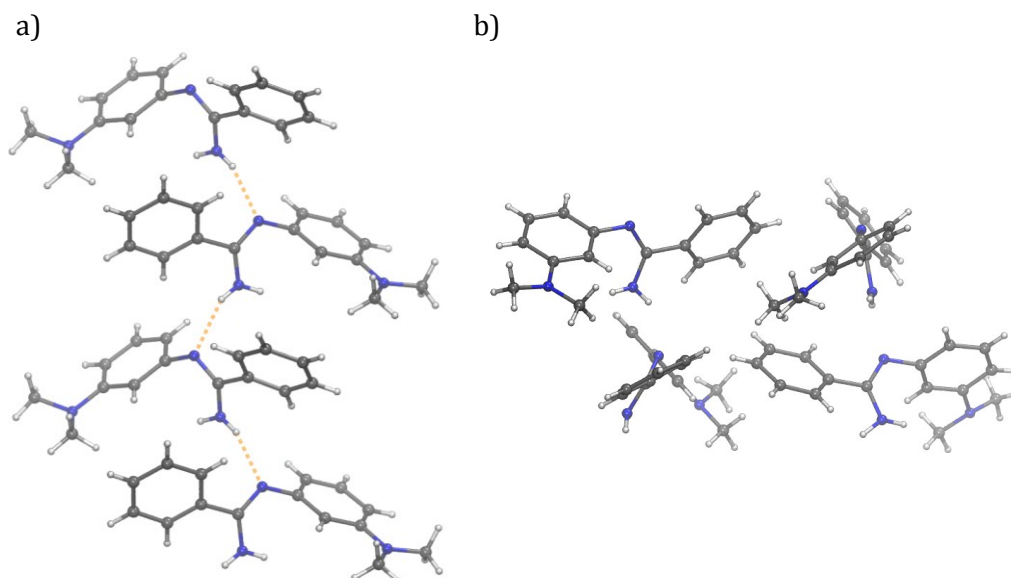


Figure S1.3.17.2: a) Hydrogen bonding chains of **1r** looking down the crystallographic b axis. b) Crystal packing of **1r** looking diagonally through the crystallographic bc axes.

S1.3.18 – Crystal Structure of **1t**

Compound **1t** crystallises as colourless hexagonal prisms in the monoclinic space group $P2_1/c$ with a single molecule in the asymmetric unit (Figure S1.3.18.1). The C3-N2-C1-N2 and C3-N2-C1-C2 torsion angles are comparable to many of the other *N*-arylamidines at $4.1(1)^\circ$ and $178.8(8)^\circ$, whilst the deviation from coplanarity of the two aryl rings is considerably smaller at 43.0° .

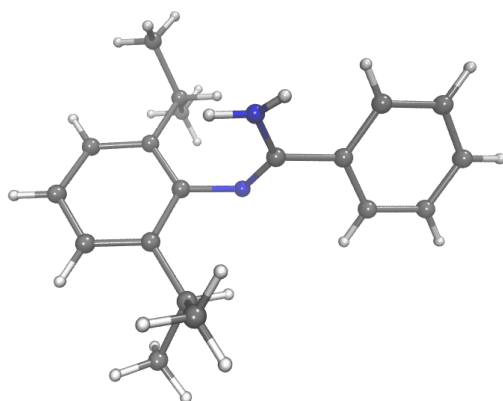


Figure S1.3.18.1: Asymmetric unit of **1t**.

Molecules of **1r** are associated through comparatively short hydrogen bonds ($2.08(2)$ Å) between H1A and N2 of a neighbouring molecule. This results in infinite chains that propagate along the crystallographic *c* axis; adjacent molecules are related by a *c* glide plane, and twisted by 60.9° (Figure S1.3.18.2).

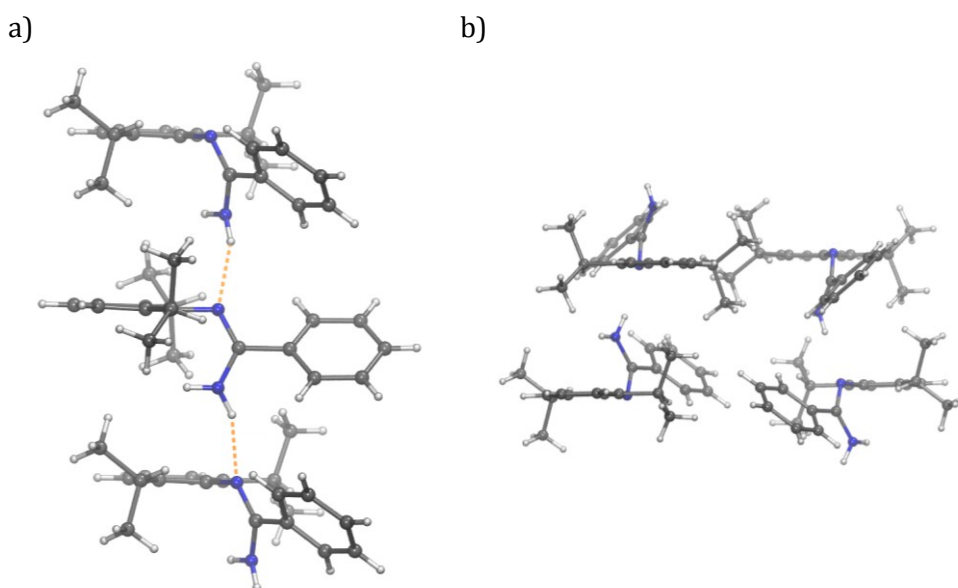


Figure S1.3.18.2: a) Hydrogen bonding chains of **1t** looking perpendicular to the crystallographic *ab* plane. b) Crystal packing of **1t** looking down the crystallographic *a* axes.

S1.3.19 – Crystal Structure of **1u**

Compound **1u** crystallises as colourless hexagonal plates in the triclinic space group $P\bar{1}$ with a single molecule in the asymmetric unit (Figure S1.3.19.1). The C3-N2-C1-N2 and C3-N2-C1-C2 torsion angles are again close to the idealised geometry at $2.3(2)^\circ$ and $177.5(1)^\circ$ respectively, and the deviation from coplanarity of the two aryl rings is 86.5° .

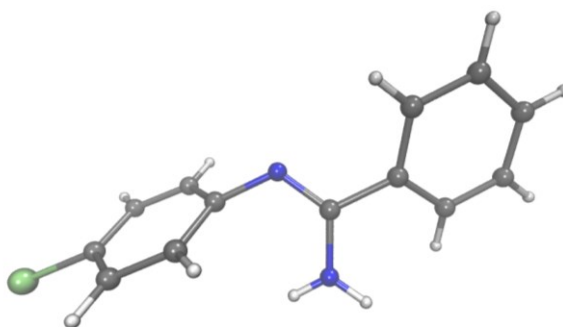


Figure S1.3.19.1: Asymmetric unit of **1u**.

Molecules of **1u** form infinite hydrogen bonded chains that propagate along the crystallographic *a* axis *via* long and weak H1A...N2 contacts ($2.39(2)$ Å) between adjacent molecules (Figure S1.3.19.2). Offset parallel chains are further associated through two weak EF embraces between the *p*-Cl-phenyl and pendant phenyl rings.

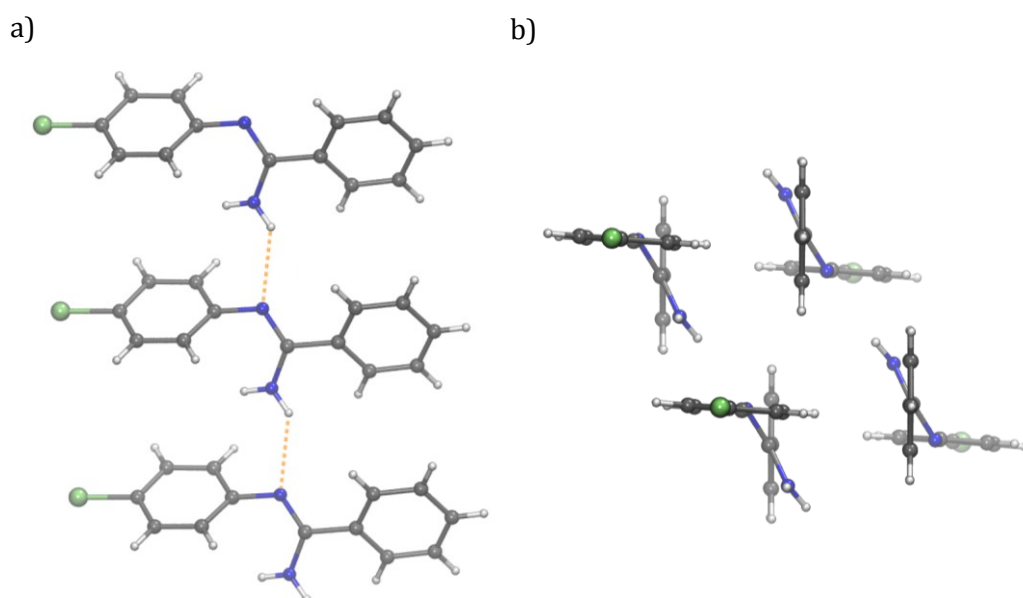


Figure S1.3.19.2: a) Hydrogen bonding chains of **1u** looking down the crystallographic *b* axis. b) Crystal packing of **1u** looking down the crystallographic *c* axes.

S1.3.20 – Crystal Structure of **1a'**

Compound **1a'** crystallises as colourless needles in the orthorhombic space group $Pna2_1$ with a single molecule in the asymmetric unit (Figure S1.3.20.1). The C3-N2-C1-N2 and C3-N2-C1-C2 torsion angles are contrary to the idealised geometry, at $166.3(2)^\circ$ and $11.2(4)^\circ$, resulting in a 'folded' conformation with the two phenyl rings in close proximity. The deviation from coplanarity is 63.1° .

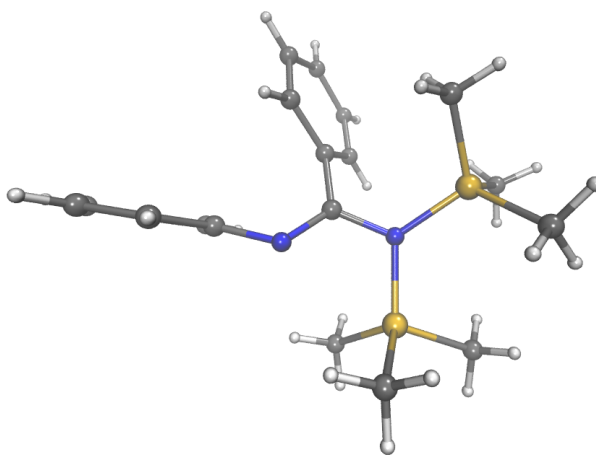


Figure S1.3.20.1: Asymmetric unit of **1a'**.

Molecules of **1a'** exhibit no significant intermolecular interactions with neighbouring molecules in the solid-state; all contacts are outside the sum of the van der Waals radii (Figure S1.3.20.1).

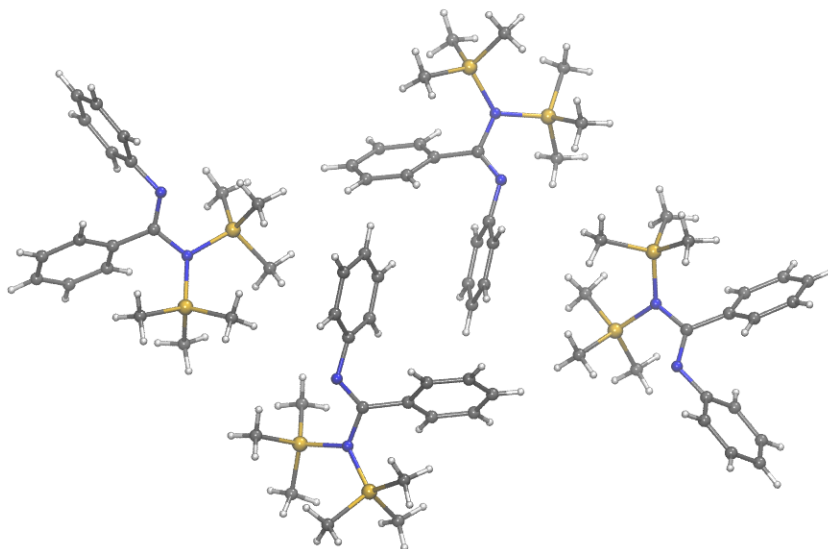


Figure S1.3.20.2: Crystal packing of **1a'** looking down the crystallographic *c* axes.

S1.4 – *N,N'*- and *N,N*-Substituted Amidines

The reactions of *N,N'* and *N,N*-substituted amidines **11-13a** (Figure S1.4.1) with PhPCl₂ was also investigated and is discussed in section 4.3.2. Symmetric *N,N'*-substituted amidines such as **12a** have been used extensively as monoanionic ligands to transition metals^{4,5} whilst asymmetric *N,N'*- and *N,N*-substituted amidines have found limited use in this field.

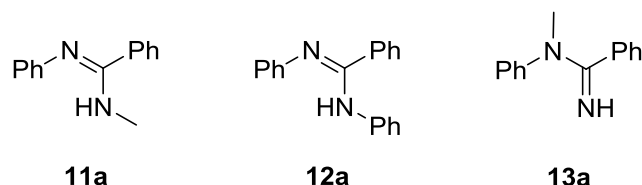


Figure S1.4.1: *N,N'* and *N,N*-substituted amidines prepared in this thesis.

S1.4.1 – Structural Studies

Crystals suitable for single-crystal X-ray diffraction studies were grown by slow diffusion of hexane into a saturated solution of product in dichloromethane. SCXRD data was also collected for compound **12a**¹³ to permit direct and precise unit comparisons of unit cell parameters and bond metrics across the *N,N'* and *N,N*-substituted amidines at the same temperature. A summary of space groups and unit cell parameters is presented in Table S1.4.1.1.

	Space Group	Cell Lengths / Å			Cell Angles / °			Cell Volume / Å ³	Z	Z'
		a	b	c	α	β	γ			
11a	<i>P</i> $\bar{1}$	8.7163(3)	11.5669(3)	11.7044(4)	101.996(2)	95.478(3)	93.621(2)	1144.82(6)	4	2
12a	<i>P</i> 2 ₁ / <i>c</i>	9.4039(1)	10.1563(1)	30.8417(5)	90	92.438(1)	90	2951.44(6)	8	2
13a	<i>P</i> na2 ₁	7.1598(6)	25.7024(2)	6.2044(4)	90	90	90	1141.76(1)	4	1

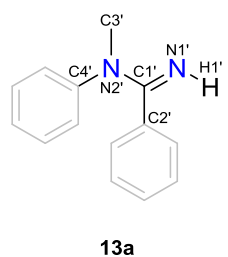
Table S1.4.1.1: Space group and unit cell parameters.

A summary of selected torsion angles and deviations from coplanarity for the *N,N'* and *N,N*-substituted amidines are shown in Tables S1.4.1.2 and S1.4.1.3, along with the corresponding structural labelling scheme.

	Torsion Angles / °				Deviation From Coplanarity / °
	C4-N2-C2-N1	C4-N2-C2-C3	C1-N2-C2-C3	C1-N1-C2-N2	
11a	176.2(1)	6.8(2)	175.9(1)	1.5(2)	62.4
12a	175.3(1)	7.1(2)	178.8(1)	0.9(2)	59.9
	172.5(1)	10.2(2)	174.4(8)	7.9(8)	71.5
	173.1(9)	9.9(1)	178.8(1)	3.8(2)	61.9

11a: R = Me
12a: R = Ph

Table S1.4.1.2: Torsion angles and deviations from planarity for *N,N'*-substituted amidines **11a** and **12a**.



	Torsion Angles / °				Deviation From Coplanarity / °
	C4'-N2'-C1'-N1'	C4'-N2'-C1'-C2'	C3'-N2'-C1'-C2'	C3'-N2'-C1'-N1'	
13a	150.8(1)	36.0(2)	170.5(1)	2.7(2)	73.1

Table S1.4.1.3: Torsion angles and deviations from coplanarity for *N,N*-substituted amidine **13a**.

S1.4.2 – Crystal Structure of **11a**

Compound **11a** crystallises as colourless rods in the triclinic space group $P\bar{1}$ with two molecules in the asymmetric unit (Figure S1.4.2.1). The C4-N2-C2-N1 and C1-N2-C2-C3 torsion angles are close to 180° whilst the C4-N2-C2-C3 and C1-N1-C2-N2 torsion angles are close to 0° for both molecules. This ‘folded’ conformation is similar to that observed for *N*-arylamidines **1g** and **1a'**, and results in the two phenyl rings being held in close proximity to each other; the deviation from coplanarity for the two rings is 62.4° and 59.9° for the two crystallographically inequivalent molecules.

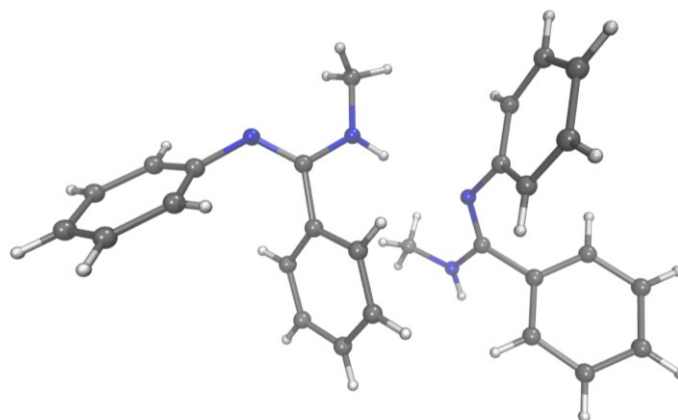


Figure S1.4.2.1: Asymmetric Unit of **11a**.

Molecules of **11a** form infinite hydrogen bonded chains that propagate along the crystallographic *a* axis via alternating short and long H1⋯N2 contacts (2.09(2) Å and 2.30(2) Å) between symmetry inequivalent molecules (Figure S1.4.2.2).

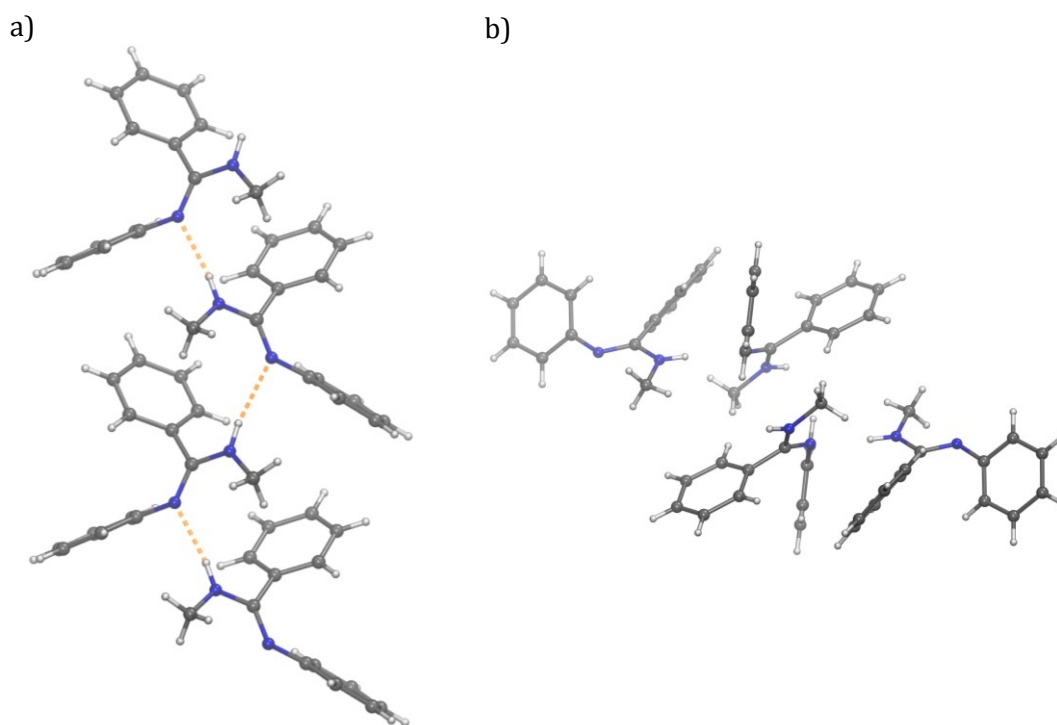


Figure S1.4.2.2: a) Hydrogen bonding chains of **11a** looking down the crystallographic *b* axis. b) Crystal packing of **11a** looking perpendicular to the crystallographic *ac* plane.

S1.4.3 - Crystal Structure of **12a**

Compound **12a** crystallises as colourless blocks in the monoclinic space group $P2_1/c$ with two molecules in the asymmetric unit (Figure S1.4.3.1).

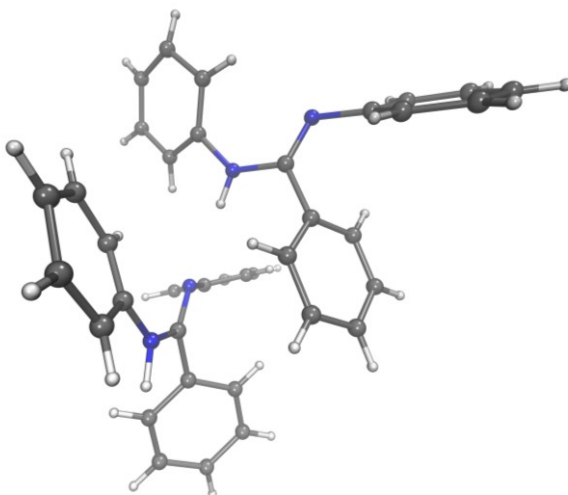


Figure S1.4.3.1: Asymmetric unit of **12a**. Disordered phenyl rings shown in a single site for clarity.

The phenyl rings at N1 are heavily disordered across two discrete atomic sites in both molecules (Figure S1.4.3.2). In molecule 1, the N1 phenyl ring can adopt two positions which differ slightly in their C1-N2-C2-C3 and C1-N1-C2-N2 torsion angles ($174.8(8)^\circ$

and $7.9(8)^\circ$ vs. $167.8(8)^\circ$ and $14.6(8)^\circ$ respectively). In contrast, the N1 phenyl ring in molecule 2 can adopt two positions which have the same C1-N2-C2-C3 and C1-N1-C2-N2 torsion angles but are twisted about the N1-C1 bond by 26.3° . Further structural parameters are given for the primary atomic positions.

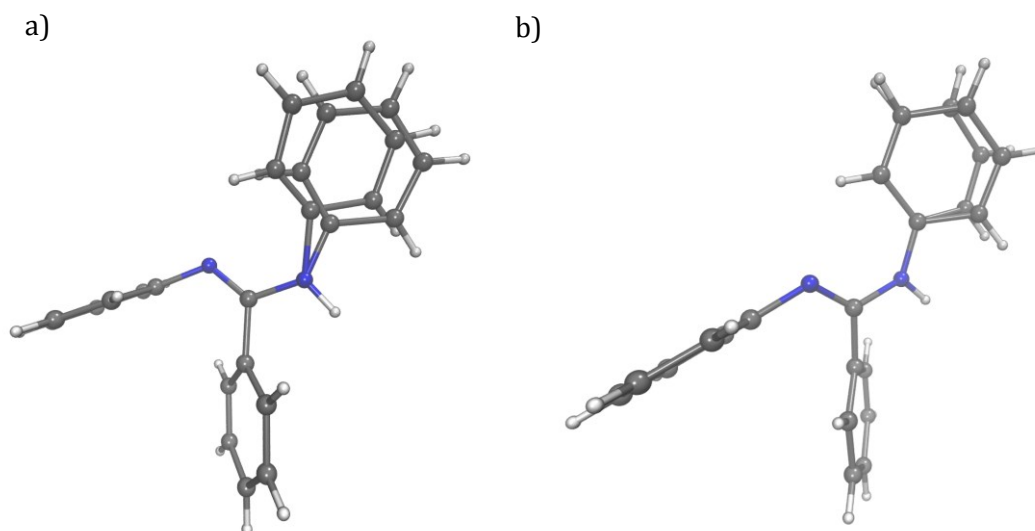


Figure S1.4.3.2: Disordered N1-phenyl rings: a) Molecule 1; b) Molecule 2. Symmetry inequivalent molecules show independently for clarity.

The C4-N2-C2-N1 and C1-N2-C2-C3 torsion angles deviate more compared to **11a** from the idealised 180° value; the same is observed for the C4-N2-C2-C3 and C1-N1-C2-N2 torsion angles. A 'folded' conformation is again observed with deviations from coplanarity for the N2- and C2-bound phenyl rings of 71.5° and 61.9° for the two molecules.

Molecules of **12a** form infinite hydrogen bonded chains that propagate along the crystallographic *a* axis *via* alternating and long H1...N2 contacts ($2.38(1)$ Å and $2.44(2)$ Å) between adjacent symmetry inequivalent molecules (Figure S1.4.3.3).

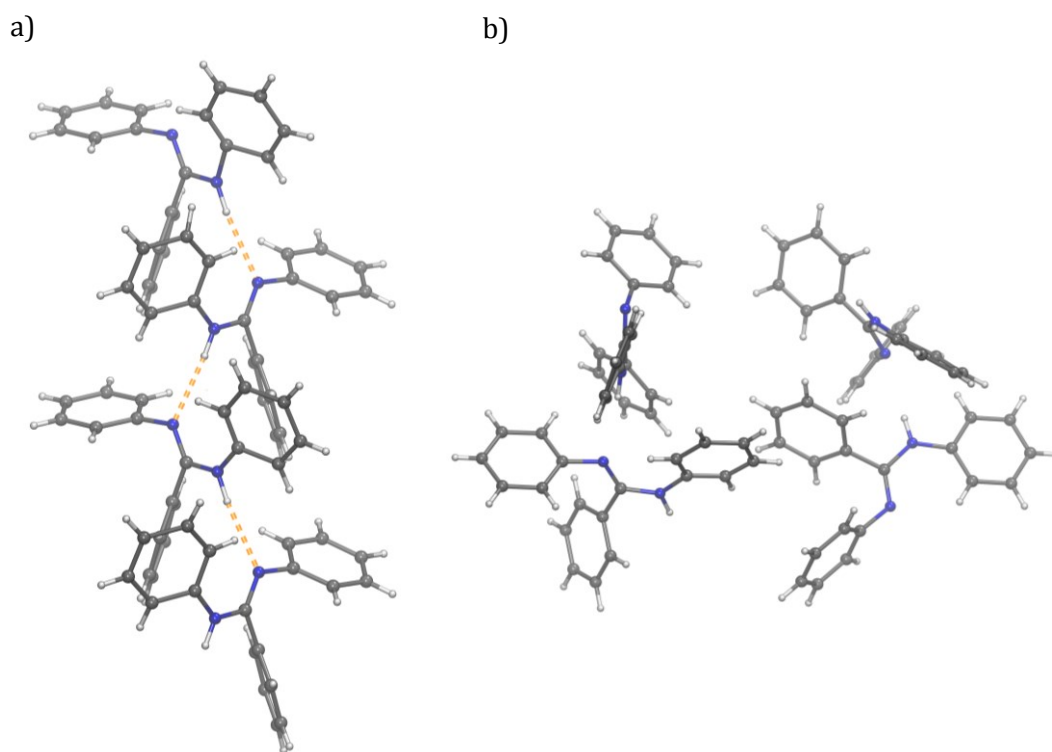


Figure S1.4.3.3: a) Hydrogen bonding chains of **12a** looking down the crystallographic *b* axis. b) Crystal packing of **12a** looking down the crystallographic *b* axis. Disordered phenyl rings shown in a single site for clarity.

S1.4.4 - Crystal Structure of **13a**

Compound **13a** crystallises as colourless irregular crystals in the orthorhombic space group $Pna2_1$ with a single molecule in the asymmetric unit (Figure S1.4.4.1). The C4-N2-C1-N1 and C4-N2-C1-C2 torsion angles deviate considerably from the idealised values of 180° and 0° respectively (see Table S1.4, whilst the C3-N2-C1-C2 and C3-N2-C1-N1 torsion angles are much closer to idealised values. Compound **13a** adopts a 'folded' conformation with the deviation from coplanarity of the two phenyl rings approaching orthogonality at 90° .

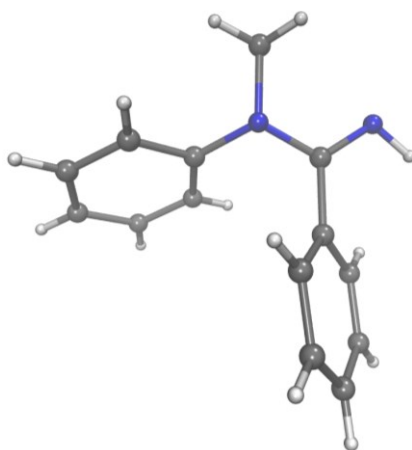


Figure S1.4.4.1: Asymmetric unit of **13a**.

Unlike the other *protio-N*-arylamidines, no hydrogen bonding is observed for compound **13a**; the addition of the *N*-methyl-group precludes N2 from acting as a hydrogen-bond acceptor. Adjacent molecules are associated through a single EF embrace (Figure S1.4.4.2).

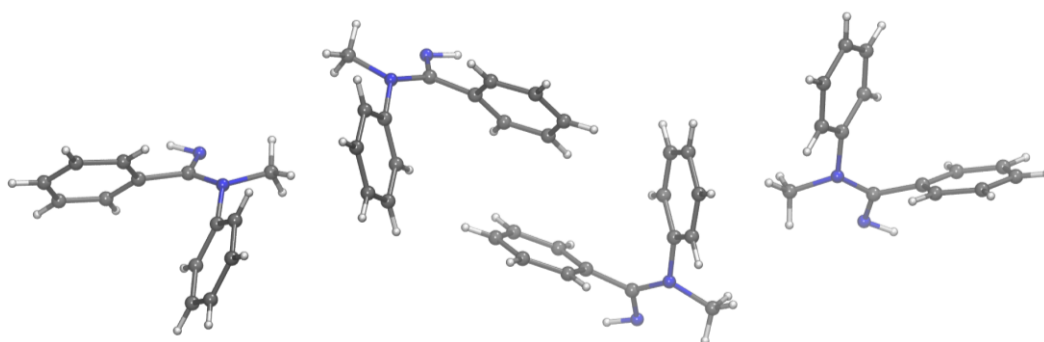


Figure S1.4.4.2: Crystal packing of **13a** looking along the crystallographic *c* axis.

S1.5 – Conclusions

The variation in conformations and bond metrics observed for the crystallographically characterised monosubstituted *N*-arylamidines highlights how minor alterations to the molecular structure can have major consequences to the solid-state structure. The *N*-arylamidines typically adopt infinite hydrogen bonded chains in the solid-state whilst tetrameric hydrogen bonded ring structures were observed for the 4-pyridyl analogues **1i** and **1j** which possess an additional hydrogen bond accepting site. The addition of electron withdrawing or donating groups was shown to influence the strength of the hydrogen bonding between adjacent molecules, with electron poor systems exhibiting the longest H1A...N2 contacts.

No apparent correlation was found in the structural parameters within the structurally characterised amidines. This was highlighted in the differences that were observed between positional isomers or symmetry inequivalent molecules within the asymmetric unit. For the *N*-arylamidines, the C3-N2-C1-N1 and C3-N2-C1-C2 torsion angles were typically close to the idealised values of 0° and 180°, with inverse values observed for **1g** and **1a'**. The deviation from coplanarity of the two aryl-rings (excluding **1p**) showed considerable variation, ranging from 41.9° to 90.0°. This suggests that there is significant freedom of rotation about the C3-N2 and C1-C2 bonds, whilst the amidine core remains fairly rigid. A single example in which the two aryl rings were close to coplanar (9.1°) was observed for **1h**, suggesting that external packing forces, including offset face-to-face (OFF) and edge-to-face (EF) embraces, may also have a significant impact on the solid-state conformation.

For the *N,N'*-substituted amidines, the torsion angles and degree of coplanarity deviated more from the idealised values for the bulkier *N*1-phenyl derivative **12a**. The amidine core of the *N,N*-disubstituted amidine **13a** was found to be severely twisted compared to the other structurally characterised amidines, with torsion angles deviating significantly from the idealised geometry. The addition of the *N*2-methyl group precludes the formation of hydrogen bonding networks.

S1.6 - References

- 1 A. Pinner and F. Klein, *Ber.*, 1877, **10**, 1889–97.
- 2 R. L. Shriner and F. W. Neumann, *Chem. Rev.*, 1944, **35**, 351–425.
- 3 P. J. Dunn, in *Comprehensive Organic Functional Group Transformations II*, Elsevier, 2005, pp. 656–692.
- 4 M. P. Coles, *J. Chem. Soc., Dalt. Trans.*, 2006, **60**, 985985–10011001.
- 5 J. Barker and M. Kilner, *Coord. Chem. Rev.*, 1994, **133**, 219–300.
- 6 L. Z. Zhang and H. B. Tong, *Acta Cryst. Sect. E*, 2008, **64**, 1031–1033.
- 7 C. P. A. T. Lawson, A. M. Z. Slawin and N. J. Westwood, *Chem. Commun.*, 2011, **47**, 1057–1059.
- 8 J. Wang, F. Xu, T. Cai and Q. Shen, *Org. Lett.*, 2008, **10**, 445–448.
- 9 A. G. Orpen, L. Brammer, F. H. Allen, O. Kennard, D. G. Watson and R. Taylor, *J. Chem. Soc., Dalt. Trans.*, 1987, S1–S83.
- 10 G. A. Jeffrey, *An Introduction to Hydrogen Bonding*, Oxford University Press, 1997.
- 11 I. Dance, *Mol. Cryst. Liq. Cryst.*, 2005, **440**, 265–293.
- 12 G. R. Desiraju and T. Steiner, *The Weak Hydrogen Bond in Structural Chemistry and Biology*, Oxford University Press, 1999.
- 13 N. W. Alcock, J. Barker and M. Kilner, *Acta Cryst. Sect. C*, 1988, **44**, 712–715.

Appendix 1
General Experimental

A1.1 – Starting Materials

Unless otherwise stated, all starting materials were used as supplied from Acros Organics, Alfa Aesar, Avocado, Fisher Scientific, Fluorochem, Lancaster Synthesis, Matrix Scientific, or Sigma Aldrich. *N*-bromo-succinimide was recrystallised from H₂O and dried in a vacuum desiccator overnight prior to use. Ph₃P was recrystallised from DCM and hexane. Ph₂PCl and PhPCl₂ were vacuum distilled prior to use and stored under argon. ¹Pr₂NPCl₂ was prepared *via* standard literature procedures¹ and purified by distillation. Pyridine and Et₃N were vacuum distilled over CaH₂ and stored under argon over activated molecular sieves.² DABCO and ferrocene were purified by vacuum sublimation. TMSOTf was purified by repeated vacuum distillations. K₂CO₃ was dried under vacuum at 100 °C for 12 hours prior to use. NaBAR^{Cl} was prepared *via* standard literature procedures.³ NaBAR^{Cl} and NaBAR^F were washed with DCM and dried *in vacuo* at 80 °C for 12 hours prior to use.

A1.2 – Drying of Solvents

All solvents were distilled over an appropriate desiccant² and stored under an atmosphere of argon. DCM, MeCN, DMF, PhCl and *o*-DCB were distilled over CaH₂ and stored over activated molecular sieves. THF was distilled over potassium and stored over activated molecular sieves. Hexane and Et₂O were distilled over sodium/benzophenone and stored over potassium mirrors. Benzene and toluene were distilled over sodium and stored over activated molecular sieves. Acetone was distilled over CaSO₄ and stored over activated molecular sieves.

A1.3 – Air and Moisture Sensitive Techniques

All manipulations were carried out under an atmosphere of argon using standard Schlenk-line techniques unless otherwise stated.⁴ Air and moisture sensitive liquid reagents and solvents were stored under argon in J. Young's ampoules. Air and moisture sensitive solids were stored and manipulated in a MBraun glovebox under an atmosphere of argon. All glassware used in the manipulation of air and moisture sensitive materials was pre-dried at 100 °C for at least 12 hours and flame-dried under vacuum prior to use.

A1.4 – NMR Spectroscopy

NMR spectra were recorded on either a JEOL ECS 400 MHz NMR spectrometer, a Bruker AV II 400 MHz spectrometer, or a Bruker Avance NEO 400 MHz spectrometer. NMR spectra were recorded in *protio*-solvents with an inset *d*₆-capillary, and referenced to residual solvent peaks in ppm.

A1.5 – Single-Crystal X-Ray Diffraction

Diffraction data were recorded on a Rigaku Oxford Diffraction Supernova Dual Diffractometer with Mo K α ($\lambda = 0.71073 \text{ \AA}$) or Cu K α ($\lambda = 1.54184 \text{ \AA}$) radiation at 100 K. Single crystals were mounted on nylon cryloops or MiTeGen microloops. Unit cell determination, data, reduction and absorption corrected were performed using CrysAlisPro 38.41. Using the Olex2 GUI,⁵ the structures were solved with the SHELXT structure solution program *via* intrinsic phasing⁶ and refined with the SHELXL refinement package using least squares minimisation.⁷ Non-hydrogen atoms were refined anisotropically, and hydrogen atoms were included using a riding model unless otherwise stated. Crystal structures images were generated using the VMD molecular graphics viewer.⁸ Crystallographic data tables for all compounds are supplied in Appendix 2.

A1.6 – Cyclic Voltammetry

Electrochemical studies were performed with a Biologic multichannel potentiostat and carried out in a three-electrode electrochemical cell consisting of a glassy carbon working electrode, a platinum wire counter-electrode, and a silver wire *pseudo*-reference electrode. The glassy carbon working electrode was polished prior to use with a 3 μm and 1 μm diamond suspension, followed by a 0.05 μm alumina suspension. All cyclic voltammetry studies were performed under an atmosphere of argon with 2 mM concentration of analyte unless otherwise stated, and a 50 mM concentration of [$n\text{Bu}_4\text{N}$][PF₆] supporting electrolyte in 10 cm³ of anhydrous DCM. All experiments were performed at 100 mV s⁻¹ unless otherwise stated. Ferrocene was added during the final measurements as an internal reference.⁹ Cyclic voltammograms were corrected *in situ* for uncompensated Ohmic loss using positive feedback at the 85% level relative to the measured solution resistance prior to the experiment. Data were processed with the EC Lab software and plotted with Matlab.

A1.7 – EPR Spectroscopy

EPR spectra were recorded on a continuous wave X-band ADANI CMS 8400 EPR spectrometer at ambient temperature in toluene. EPR spectral simulation and analysis were performed using the EasySpin computational package.¹⁰

A1.8 – SQUID Magnetometry

Magnetic studies were performed using a Quantum Design MPMS 5 magnetometer and recorded between 2-300 K in either a 1000 Oe or 10000 Oe applied magnetic field. Samples were finely ground and placed in gelatin capsules enclosed inside a pierced

straw with a uniform diamagnetic background. Diamagnetic corrections were applied according to literature procedures.¹¹

A1.9 – Elemental Analysis

Elemental analysis was performed by Stephen Boyer at London Metropolitan University.

A1.10 – References

- 1 S. Stadlbauer, R. Frank, L. Maulana, P. Lönnecke, B. Kirchner and E. Hey-Hawkins, *Inorg. Chem.*, 2009, **48**, 6072–6082.
- 2 W. L. F. Armarego and C. L. L. Chai, *Purification of Laboratory Chemicals*, Elsevier, 6th edn., 2009.
- 3 R. Anulewicz-Ostrowska, T. Kliś, D. Krajewski, B. Lewandowski and J. Serwatowski, *Tetrahedron Lett.*, 2003, **44**, 7329–7331.
- 4 D. F. Schriver and M. A. Drezdon, *The Manipulation of Air Sensitive Compounds*, Wiley, New York, 2nd edn., 1986.
- 5 O. V. Dolomanov, L. J. Bourhis, R. J. Gildea, J. A. K. Howard and H. Puschmann, *J. Appl. Crystallogr.*, 2009, **42**, 339–341.
- 6 G. M. Sheldrick, *Acta Crystallogr. Sect. A Found. Crystallogr.*, 2015, **71**, 3–8.
- 7 G. M. Sheldrick, *Acta Crystallogr. Sect. C Struct. Chem.*, 2015, **71**, 3–8.
- 8 W. Humphrey, A. Dalke and K. Schulten, *J. Mol. Graph.*, 1996, **14**, 33–38.
- 9 G. Gritzner and J. Kuta, *Int. Union Pure Appl. Chem.*, 1984, **1**, 462–466.
- 10 S. Stoll and A. Schweiger, *J. Magn. Reson.*, 2006, **178**, 42–55.
- 11 G. A. Bain and J. F. Berry, *J. Chem. Educ.*, 2008, **85**, 532.

Appendix 2

Computational Details

A2.1 -1,2,4-Benzothiadiazinyl Radicals

A2.1.1 - Electronic and EPR Studies

Calculations were performed using the Gaussian 16 suite of programs.¹ Structures were optimised in the gas-phase, from single-crystal X-ray diffraction data where available, at the DFT² UB3LYP/6-31g level of theory.³ All structures were confirmed as minima by frequency analysis and the absence of imaginary frequencies. Single-point calculations for the EPR parameters were performed at the UB3LYP/cc-pVDZ level of theory⁴ from the UB3LYP/6-31g optimised geometry. Orbital visualisations were made using the VMD molecular graphics viewer.⁵ Exemplar input files are given in section A2.1.1.1 and full Cartesian coordinates are provided in section A2.4.

A2.1.1.1 - Example Input Files

```
%chk=3a_Opt.chk
# opt ub3lyp/6-31g nosymm

3a_Opt - Initial geometry optimisation

0 2
S          1.44160731      7.23848075      8.51977556
Cl         6.70979405      8.26398912      7.17651304
Cl         6.16536031     11.41379741      7.54890333
Cl         3.22610587     12.42633569      8.42211098
N          4.33811093      6.58115710      7.68483377
N          2.08587062      5.71897321      8.00957583
C          4.04980467      7.89867758      7.85410286
C          3.42882875      5.60171975      7.75808138
C          2.77694783      8.41231480      8.21703961
C          3.88236893      4.21969127      7.49158131
C          2.53195504      9.77636134      8.40278008
H          1.55828551     10.13272189      8.71542991
C          5.08876093      8.86422254      7.64898117
C          5.21120449      3.98865575      7.08715342
H          5.87989262      4.83317218      6.97851841
C          4.85199356     10.21963402      7.81232162
C          3.00186895      3.13061981      7.64007242
H          1.98312756      3.31224393      7.95827220
C          3.56378335     10.67173131      8.19344137
C          5.64910435      2.68804889      6.83614396
H          6.67458630      2.51660294      6.52620939
C          3.44702520      1.83247910      7.38569310
H          2.76467350      0.99761978      7.50520472
C          4.76952293      1.60705121      6.98324687
H          5.11324410      0.59633713      6.78769355

%chk=3a_Opt.chk
# ub3lyp/cc-pvdz geom=check nosymm prop=epr

3a_EPR - EPR parameters
```

0 2

A2.1.2 – Magnetic Exchange Interactions

Single-point exchange energies were performed on the Gaussian 16 suite of programs¹ and calculated at the UB3LYP/6-311g(d,p) level of theory⁶ with a simple dinuclear nearest-neighbour exchange model from pairwise combinations of radicals.^{7,8} Atomic coordinates were taken from crystallographic data. The individual pairwise exchange energies, J , were estimated in terms of the difference between the total energies of the triplet (TS) and broken symmetry single (BSS) states and the respective expectation values of the two states according to the expression:

$$J = - \frac{(E_{TS} - E_{BSS})}{\langle S^2 \rangle_{TS} - \langle S^2 \rangle_{BSS}} \quad (1)$$

A2.1.2.1 – Method and Example Input Files

The atomic coordinates of a pairwise combination of radicals is first input into Gaussian 16 and a single-point calculation is performed:

```
%chk=3a_pil_triplet_spc.chk  
# ub3lyp/6-311g(d,p) scf=tight
```

```
3a_pil_triplet_spc
```

0 3

C1	8.21670000	3.11910000	5.10980000
S	9.57380000	8.29920000	4.50700000
C1	11.16690000	2.30170000	4.54680000
C1	13.31430000	4.51490000	3.90950000
N	7.72390000	5.94930000	5.04030000
N	7.97560000	8.36320000	4.78190000
C	7.32120000	7.19490000	5.02970000
C	9.03380000	5.65970000	4.77660000
C	10.03340000	6.62550000	4.49310000
C	5.87040000	7.38650000	5.30310000
C	9.42810000	4.32110000	4.77070000
C	5.28740000	8.61470000	5.31730000
C	3.94550000	8.85610000	5.55300000
C	10.75820000	3.95050000	4.50950000
C	3.13070000	7.77090000	5.75490000
C	3.60760000	6.50290000	5.73970000
C	5.00790000	6.32980000	5.52240000
C	11.35820000	6.29900000	4.22510000
C	11.68130000	4.97940000	4.23450000
H	12.46490000	7.00710000	4.05630000
H	5.37500000	5.53300000	5.48660000
H	3.12330000	5.73930000	5.87130000
H	2.24950000	7.91060000	5.96820000
H	5.75160000	9.37170000	5.24820000
H	3.61700000	9.67980000	5.62430000
C1	8.58320000	3.11910000	1.42110000
S	7.22610000	8.29920000	2.02390000
C1	5.63300000	2.30170000	1.98410000

C1	3.48560000	4.51490000	2.62140000
N	9.07600000	5.94930000	1.49060000
N	8.82430000	8.36320000	1.74900000
C	9.47870000	7.19490000	1.50120000
C	7.76610000	5.65970000	1.75430000
C	6.76650000	6.62550000	2.03780000
C	10.92950000	7.38650000	1.22780000
C	7.37180000	4.32110000	1.76020000
C	11.51250000	8.61470000	1.21360000
C	12.85440000	8.85610000	0.97790000
C	6.04170000	3.95050000	2.02140000
C	13.66920000	7.77090000	0.77600000
C	13.19230000	6.50290000	0.79120000
C	11.79200000	6.32980000	1.00850000
C	5.44170000	6.29900000	2.30580000
C	5.11860000	4.97940000	2.29640000
H	4.33500000	7.00710000	2.47460000
H	11.42490000	5.53300000	1.04430000
H	13.67660000	5.73930000	0.65960000
H	14.55040000	7.91060000	0.56270000
H	11.04830000	9.37170000	1.28270000
H	13.18290000	9.67980000	0.90660000

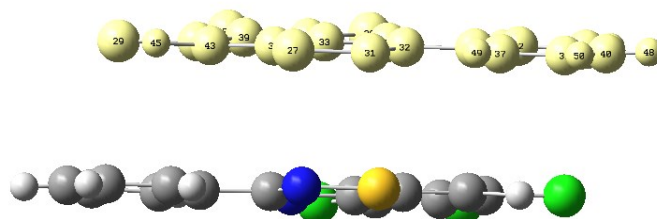
The stability of the triplet state wave-function is then confirmed to be stable in the provided geometry:

```
%chk=3a_pil_triplet_spc.chk
# ub3lyp/6-311g(d,p) guess=read geom=check stable=opt
```

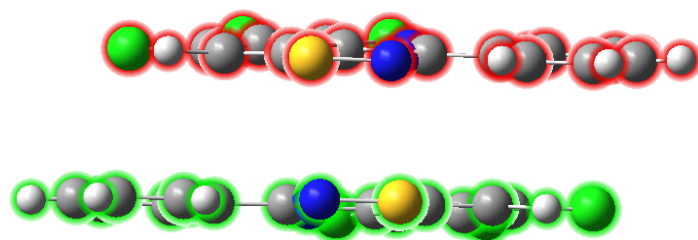
```
3a_pil_triplet_guess
```

```
0 3
```

A broken symmetry singlet fragment guess job is set up by first selecting one of the two radicals:



In the atom group editor, the selected atoms are added to fragment 2, and each fragment is given opposing spin states (α and β) for their unpaired electrons.



GI:ML:V1 - Atom Group Editor

Atom Group Class: Gaussian Fragment Exclusive Class Actions ... Group Actions ...

Group ID	Highlight	Display			Atom Tags	Atom Count	Charge	Electrons	Spin Mult.	Unpaired Spins
Gaussian Fragment (1)	<input checked="" type="checkbox"/>	Show	+	-	26-50	25	0	165	Doublet	Alpha
Gaussian Fragment (2)	<input checked="" type="checkbox"/>	Show	+	-	1-25	25	0	165	Doublet	Beta
Gaussian Fragment (3)	<input type="checkbox"/>	Show	+	-		0	0	0	Singlet	Alpha

Persistent Visuals

Ok Help

A guess calculation is performed on one of the two fragments to obtain the initial broken symmetry single wave-function:

```
%chk=3a_pil_BSS_guess.chk
# ub3lyp/6-311g(d,p) guess=(only,fragment=2) geom=connectivity
```

```
3a_pil_BSS_guess
```

```
0 1 0 2 0 -2
Cl (Fragment=2)      8.21670000      3.11910000      5.10980000
S (Fragment=2)      9.57380000      8.29920000      4.50700000
Cl (Fragment=2)     11.16690000      2.30170000      4.54680000
Cl (Fragment=2)     13.31430000      4.51490000      3.90950000
N (Fragment=2)      7.72390000      5.94930000      5.04030000
N (Fragment=2)      7.97560000      8.36320000      4.78190000
C (Fragment=2)      7.32120000      7.19490000      5.02970000
C (Fragment=2)      9.03380000      5.65970000      4.77660000
C (Fragment=2)     10.03340000      6.62550000      4.49310000
C (Fragment=2)      5.87040000      7.38650000      5.30310000
C (Fragment=2)      9.42810000      4.32110000      4.77070000
C (Fragment=2)      5.28740000      8.61470000      5.31730000
C (Fragment=2)      3.94550000      8.85610000      5.55300000
C (Fragment=2)     10.75820000      3.95050000      4.50950000
C (Fragment=2)      3.13070000      7.77090000      5.75490000
C (Fragment=2)      3.60760000      6.50290000      5.73970000
C (Fragment=2)      5.00790000      6.32980000      5.52240000
C (Fragment=2)     11.35820000      6.29900000      4.22510000
C (Fragment=2)     11.68130000      4.97940000      4.23450000
H (Fragment=2)     12.46490000      7.00710000      4.05630000
H (Fragment=2)      5.37500000      5.53300000      5.48660000
H (Fragment=2)      3.12330000      5.73930000      5.87130000
H (Fragment=2)      2.24950000      7.91060000      5.96820000
H (Fragment=2)      5.75160000      9.37170000      5.24820000
H (Fragment=2)      3.61700000      9.67980000      5.62430000
Cl (Fragment=1)      8.58320000      3.11910000      1.42110000
S (Fragment=1)      7.22610000      8.29920000      2.02390000
Cl (Fragment=1)      5.63300000      2.30170000      1.98410000
Cl (Fragment=1)      3.48560000      4.51490000      2.62140000
```

N(Fragment=1)	9.07600000	5.94930000	1.49060000
N(Fragment=1)	8.82430000	8.36320000	1.74900000
C(Fragment=1)	9.47870000	7.19490000	1.50120000
C(Fragment=1)	7.76610000	5.65970000	1.75430000
C(Fragment=1)	6.76650000	6.62550000	2.03780000
C(Fragment=1)	10.92950000	7.38650000	1.22780000
C(Fragment=1)	7.37180000	4.32110000	1.76020000
C(Fragment=1)	11.51250000	8.61470000	1.21360000
C(Fragment=1)	12.85440000	8.85610000	0.97790000
C(Fragment=1)	6.04170000	3.95050000	2.02140000
C(Fragment=1)	13.66920000	7.77090000	0.77600000
C(Fragment=1)	13.19230000	6.50290000	0.79120000
C(Fragment=1)	11.79200000	6.32980000	1.00850000
C(Fragment=1)	5.44170000	6.29900000	2.30580000
C(Fragment=1)	5.11860000	4.97940000	2.29640000
H(Fragment=1)	4.33500000	7.00710000	2.47460000
H(Fragment=1)	11.42490000	5.53300000	1.04430000
H(Fragment=1)	13.67660000	5.73930000	0.65960000
H(Fragment=1)	14.55040000	7.91060000	0.56270000
H(Fragment=1)	11.04830000	9.37170000	1.28270000
H(Fragment=1)	13.18290000	9.67980000	0.90660000

A stability calculation is then performed on the resulting wave-function to confirm that it is stable:

```
%chk=3a_pil_BSS_guess.chk
#  ub3lyp/6-311g(d,p)  scf=nosymm  guess=read  geom=check
stable=opt

3a_pil_BSS_guess_stab

0 1 0 2 0 -2
```

The exchange energy is then calculated using equation 1 from the total energies of the triplet and broken symmetry singlet states and their respective expectation values, and converted to cm^{-1} .

A2.2 - Phosphorus-Nitrogen Heterocycles

A2.2.1 - Geometry Optimisations

Calculations were performed using the Gaussian 16 suite of programs.¹ Structures were optimised from single crystal X-ray diffraction data, where available, using the M06-2X hybrid functional⁹ using the 6-311g(d,p) basis set.⁶ PCM (dichloromethane) solvation was used in all cases, and all structures were confirmed as minima by frequency analysis and the absence of imaginary frequencies. NBO calculations were performed using NBO 3.1.¹⁰ Mayer bond indices^{11,12} were calculated using Multiwfn 3.3.9.¹³ Orbital visualisations were made using the VMD molecular graphics viewer.⁵ Full Cartesian coordinates for the optimised geometries are provided in section A2.4, along with optimised energies. A typical input file is provided in section A2.2.1.1.

A2.2.1.1 - Example Input Files

```
%chk=10a-Opt.chk  
#p          opt          freq          m062x/6-311g(d,p)          nosymm  
scrf=(solvent=dichloromethane) pop=nboread
```

10a - frequency calc with PCM solvation and NBO analysis.

```
0 1  
P          2.43120000      8.90480000      5.02600000  
P          5.37230000      8.85180000      4.18810000  
N          2.70090000      7.23000000      4.72350000  
N          5.06720000      7.36970000      4.91560000  
N          4.71570000     11.34280000      3.08300000  
N          3.77520000      9.60240000      4.19230000  
C          1.82120000      6.59180000      3.79060000  
C          3.98970000      6.67910000      4.96610000  
C          4.06990000      5.26130000      5.40280000  
C          0.43870000      6.80880000      3.87160000  
H          0.08590000      7.33220000      4.55430000  
C          4.80450000     12.31570000      2.05880000  
C          3.31430000     10.35060000      7.18530000  
H          3.30910000     11.05300000      6.57580000  
C          3.00710000      8.02240000      7.68560000  
H          2.79460000      7.15780000      7.41690000  
C          3.32090000      8.27400000      9.01140000  
H          3.32850000      7.57680000      9.62630000  
C          5.31610000      4.64340000      5.43030000  
H          6.07030000      5.11390000      5.15750000  
C          7.30660000     10.58670000      5.10360000  
H          7.30180000     10.88690000      4.22350000  
C          4.38090000     12.08240000      0.74720000  
H          3.91030000     11.30720000      0.54250000  
C          2.94540000      4.54510000      5.81960000  
H          2.10810000      4.94970000      5.82010000  
C          6.39710000      9.60560000      5.50720000  
C          3.64060000     10.69640000      3.33070000  
C          3.62450000     10.59800000      8.51190000  
H          3.83270000     11.46160000      8.78750000  
C          2.27980000     10.96800000      2.77120000  
C          1.59090000      9.95920000      2.10760000  
H          1.95560000      9.10540000      2.05040000  
C          3.00890000      9.05860000      6.75170000  
C          8.21510000     11.11560000      6.00770000  
H          8.82700000     11.75770000      5.72810000  
C          5.48670000     13.49890000      2.34810000  
H          5.76590000     13.67270000      3.21810000  
C          0.49570000     12.50190000      2.28500000  
H          0.12590000     13.35310000      2.35010000  
C          6.41980000      9.16970000      6.83100000  
H          5.83120000      8.50520000      7.10860000  
C          7.31240000      9.71960000      7.73540000  
H          7.30830000      9.43750000      8.62170000  
C          -0.39870000      6.23580000      2.92560000  
H          -1.31380000      6.39690000      2.96440000  
C          5.44140000      3.33500000      5.86000000
```

H	6.28090000	2.93530000	5.88730000
C	3.08290000	3.22550000	6.23310000
H	2.33170000	2.74760000	6.50150000
C	2.32970000	5.78080000	2.77990000
H	3.24720000	5.63930000	2.71920000
C	0.11100000	5.42570000	1.92340000
H	-0.45760000	5.04630000	1.29320000
C	0.35600000	10.23060000	1.52930000
H	-0.10380000	9.55680000	1.08210000
C	-0.19350000	11.49730000	1.61600000
H	-1.01960000	11.67610000	1.22860000
C	1.48120000	5.18420000	1.86600000
H	1.82640000	4.62080000	1.21160000
C	5.74820000	14.41180000	1.34460000
H	6.19940000	15.20010000	1.54650000
C	4.32090000	2.61660000	6.25030000
H	4.40380000	1.73100000	6.52170000
C	1.73500000	12.24230000	2.85650000
H	2.19740000	12.91930000	3.29500000
C	5.34700000	14.16820000	0.04260000
H	5.53740000	14.78210000	-0.62990000
C	8.21450000	10.69230000	7.31970000
H	8.81750000	11.05750000	7.92640000
C	3.62420000	9.56320000	9.42510000
H	3.82780000	9.72970000	10.31720000
C	4.66010000	13.00360000	-0.24840000
H	4.38360000	12.83740000	-1.12060000

\$NBO BNDIDX \$END

Orbital populations were calculated using the pop=orbital keyword from the optimised geometry checkpoint file:

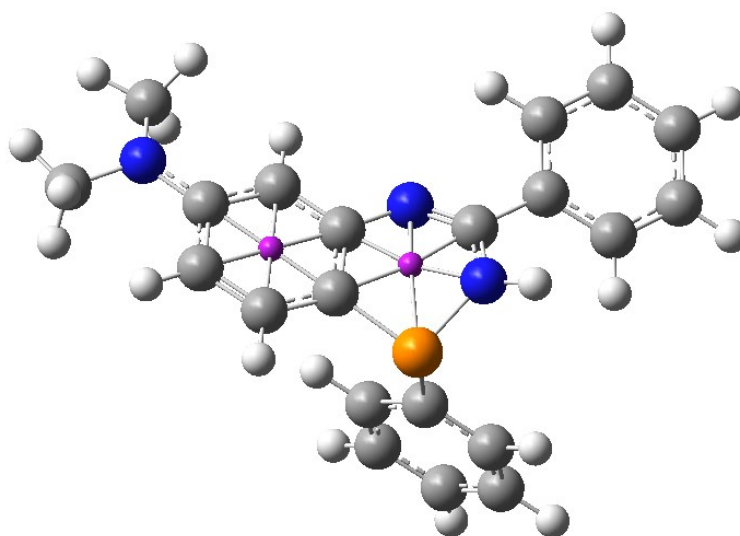
```
%chk=10aOpt.chk
#p m062x/6-311g(d,p) nosymm pop=orbital geom=check
```

10a-Pop - Orbital Population

0 1

A2.2.2 - NICS Calculations

Nucleus independent chemical shift calculations¹⁴ were performed at the M06-2X/6-311g(d,p) level of theory^{6,9} by placing a dummy atom at the geometric centre of the ring structure in question using a previously optimised geometry. An example input file is given in section A2.2.2.1.



A2.2.2.1 – Example Input Files

```
%chk=19rOptNICS.chk
#p m062x/6-311g(d,p) nosymm nmr
```

```
19r_Opt NICS Calculation
```

```
0 1
P          2.94281008      2.56485730      9.97507518
N          3.42822727      1.70674155     11.40294954
H          3.70070678      0.73784980     11.32637532
N          3.16439263      3.46341691     12.95867033
N         -0.44098167      6.61888574     12.84889785
C          4.46300476      3.59415884      9.70343617
C          1.88245300      3.73975983     10.84497907
C          5.60781095      2.93373611      9.24389065
H          5.57908594      1.86188349      9.06795620
C          6.78485250      3.63424005      9.01047999
H          7.66662124      3.11008050      8.66117903
C          2.15246009      4.05743154     12.19040069
C          3.69114828      2.34576641     12.59129913
C          0.32334042      5.68682135     12.18978161
C          4.51237954      4.97375016      9.90522113
H          3.63377048      5.50077575     10.26117549
C          0.83210224      4.39386886     10.20029767
H          0.61616344      4.15649885      9.16306745
C          1.38170105      5.02461385     12.83800516
H          1.63412000      5.23787315     13.86710182
C          5.68878317      5.67846522      9.65899438
H          5.71726444      6.74958749      9.82126452
C          0.06727360      5.35381958     10.83832335
H         -0.72365199      5.84429281     10.28941953
C          4.64669509      1.67099904     13.51236732
C          6.82544436      5.01154379      9.21611356
H          7.74017862      5.56141978      9.02926689
C         -0.02166169      7.07864928     14.16039260
H         -0.00233821      6.25223433     14.87509156
```

H	-0.73587316	7.81478457	14.52185183
H	0.97472804	7.53768001	14.13934918
C	-1.38070191	7.42857493	12.09463654
H	-0.88611476	8.02107437	11.31471347
H	-1.88742664	8.10770238	12.77628981
H	-2.14159346	6.80385568	11.62047738
C	6.43349532	0.43655601	15.26430418
H	7.12557481	-0.04401398	15.94537572
C	6.57592528	0.26571928	13.89166888
H	7.38509429	-0.33815468	13.49942090
C	5.68436613	0.87833225	13.01700440
H	5.82020005	0.76564822	11.94716024
C	4.51638347	1.84938665	14.89165772
H	3.71267715	2.47342202	15.26100523
C	5.40274657	1.23133885	15.76246291
H	5.29057274	1.36628489	16.83148747
Bq	2.876915225	2.97966226	11.66056232
Bq	1.106555067	4.70938584	11.51696459

A2.3 – Donor-Functionalised Diiodophosphoranes

A2.3.1 – Geometry Optimisations

Calculations were performed using the Gaussian 09 suite of programs.¹⁵ Structures were optimised from single-crystal X-ray diffraction data, where available, using the M06-2X hybrid functional⁹ with the def2TZVP43 split valence, triple- ζ basis set¹⁶ to describe the iodine atoms and the 6-311g(d,p) basis set⁶ for all other atoms. PCM (dichloromethane) solvation was used in all cases, and all structures were conformed as minima by frequency analysis and the absence of imaginary frequencies. NBO calculations were performed using NBO 3.1.¹⁰ Mayer bond indices^{11,12} were calculated using Multiwfn 3.3.9.¹³ Orbital visualisations were made using the VMD molecular graphics viewer.⁵ Full Cartesian coordinates for the optimised geometries are provided in section A2.4, along with optimised energies and selected bond lengths and Mayer Bond Indices. A typical input file is provided in section A2.3.1.1.

A2.3.1.1 – Example Input Files

```
%chk=34a_Opt.chk
#p opt freq gen scrf=(solvent=dichloromethane) nosymm m062x
pop=nboread pseudo=read
```

```
34a_Opt
```

0 1			
I	1.04152309	3.38584262	2.61070028
I	-0.25037821	0.36625167	2.12488543
P	2.03112774	5.67328166	3.01457760
O	-0.21976091	6.40915380	1.41672230
C	2.09358455	6.63921403	1.50189421
C	0.62960853	7.83758587	4.08868355
H	0.79741619	8.34346873	3.14525772

C	0.88720611	6.88434666	0.81911908
C	3.30292323	7.09575938	0.97610884
H	4.22917258	6.90108972	1.50328335
C	0.90677725	7.58830893	-0.38269361
H	-0.00975383	7.78667425	-0.92088901
C	4.55878724	4.50850876	3.07584048
H	4.18625715	3.82219901	2.32361161
C	3.72336652	5.48727052	3.62083004
C	1.09208630	6.53742838	4.28848485
C	-0.04574449	8.48544747	5.11739966
H	-0.40746842	9.49505775	4.96806850
C	-0.25672775	7.83915678	6.33074196
H	-0.78493649	8.34808168	7.12794695
C	3.31770714	7.79977229	-0.22065375
H	4.25495561	8.15732545	-0.62612741
C	0.88019504	5.88432660	5.50554846
H	1.24011928	4.87169969	5.65462811
C	4.20487464	6.36592542	4.59480095
H	3.55797403	7.12392298	5.02025991
C	6.35566001	5.28586776	4.47964650
H	7.38101533	5.20320316	4.81886997
C	5.87499588	4.41280469	3.50724128
H	6.52230290	3.65234597	3.08907720
C	5.52368426	6.25991560	5.02072649
H	5.89756127	6.93765667	5.77791170
C	0.20679914	6.54052269	6.52609985
H	0.04118400	6.03789791	7.47062663
C	-1.46975785	6.54757630	0.74822603
H	-1.43820669	6.05718399	-0.22703110
H	-1.72787428	7.60252464	0.63183079
H	-2.19940418	6.05648965	1.38552058
C	2.12215089	8.03724598	-0.88981393
H	2.12810329	8.58408452	-1.82495303

C H P O 0
6-311g(d,p)

I 0
def2TZVP

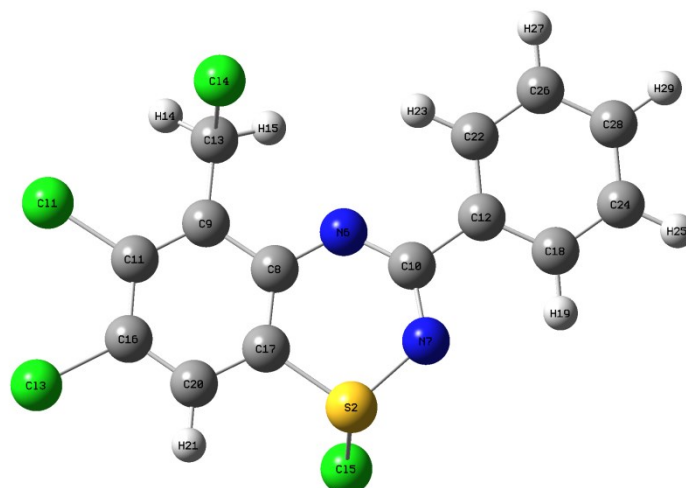
I 0
def2TZVP

\$NBO BNDIDX \$END

A2.4 – Cartesian Coordinates for Optimised Geometries

Full Cartesian coordinates and total energies for all optimised geometries are given below:

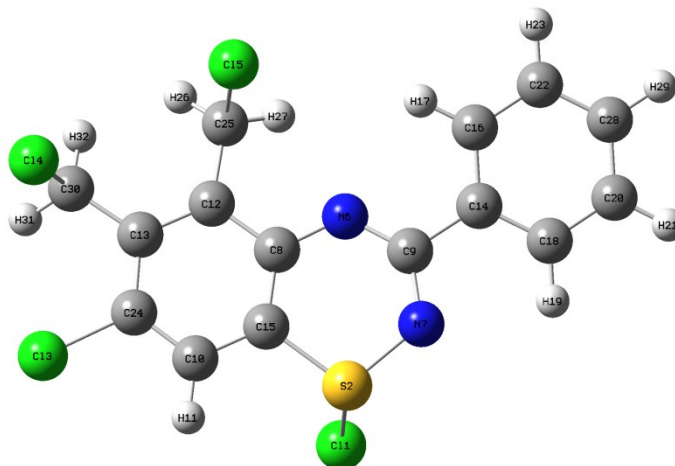
2b



Center Number	Atomic Number	Atomic Type	Coordinates (Angstroms)		
			X	Y	Z
1	17	0	7.317996	6.799277	7.292015
2	16	0	6.738006	0.908202	4.916811
3	17	0	9.046558	4.360726	8.503876
4	17	0	6.319687	6.892489	3.529507
5	17	0	5.271316	-0.041658	6.769585
6	7	0	5.264526	3.439336	3.951648
7	7	0	5.777360	1.105287	3.491726
8	6	0	6.131554	3.610985	4.989637
9	6	0	6.246488	4.934705	5.547097
10	6	0	5.134336	2.294461	3.268691
11	6	0	7.135852	5.144246	6.595202
12	6	0	4.233269	2.283770	2.096011
13	6	0	5.406740	6.019556	4.969179
14	1	0	5.191294	6.817365	5.672163
15	1	0	4.512015	5.617962	4.506204
16	6	0	7.907134	4.087977	7.135196
17	6	0	6.927209	2.582035	5.553326
18	6	0	3.861084	1.068923	1.488216
19	1	0	4.237225	0.137740	1.892684
20	6	0	7.799333	2.808122	6.623160
21	1	0	8.376360	2.000055	7.055994
22	6	0	3.744695	3.497549	1.576106
23	1	0	4.047296	4.428593	2.038309
24	6	0	3.007974	1.072195	0.383522
25	1	0	2.719693	0.132392	-0.075262
26	6	0	2.894268	3.493427	0.470114
27	1	0	2.525305	4.432863	0.072245
28	6	0	2.522362	2.282086	-0.128246
29	1	0	1.859664	2.281732	-0.987716

Total energy E(UB3LYP) = -2886.44928161 Hartrees

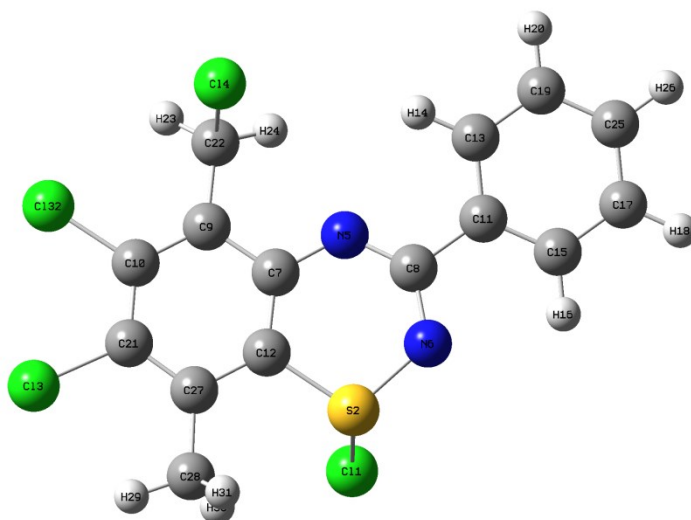
2c



Center Number	Atomic Number	Atomic Type	Coordinates (Angstroms)		
			X	Y	Z
1	17	0	5.069510	1.884385	3.627555
2	16	0	2.980081	3.320418	3.923627
3	17	0	4.578637	6.439213	-0.288167
4	17	0	3.993752	9.737949	1.286108
5	17	0	3.674616	9.282836	5.243824
6	7	0	3.913668	5.719641	5.616809
7	7	0	2.724870	3.596869	5.611955
8	6	0	4.050203	5.854892	4.265851
9	6	0	3.285649	4.695545	6.208193
10	6	0	3.819463	5.058785	1.943947
11	1	0	3.536403	4.287404	1.238464
12	6	0	4.642346	7.073407	3.772743
13	6	0	4.790342	7.275900	2.392368
14	6	0	3.114313	4.739821	7.676769
15	6	0	3.647986	4.880591	3.320195
16	6	0	3.355379	5.938374	8.374974
17	1	0	3.652443	6.820333	7.821610
18	6	0	2.705260	3.593918	8.386048
19	1	0	2.522557	2.673946	7.845157
20	6	0	2.549139	3.648010	9.772054
21	1	0	2.240821	2.759588	10.312929
22	6	0	3.194627	5.985906	9.760103
23	1	0	3.377090	6.914390	10.290852
24	6	0	4.374605	6.242574	1.504816
25	6	0	5.081542	8.067329	4.795949
26	1	0	5.897419	8.708382	4.478181
27	1	0	5.306821	7.576460	5.736788
28	6	0	2.793055	4.841826	10.462587
29	1	0	2.669862	4.881368	11.540173
30	6	0	5.368493	8.538282	1.833925
31	1	0	5.946722	8.365057	0.930664
32	1	0	5.949032	9.107504	2.551149

Total energy E(UB3LYP) = -2925.75973149 Hartrees

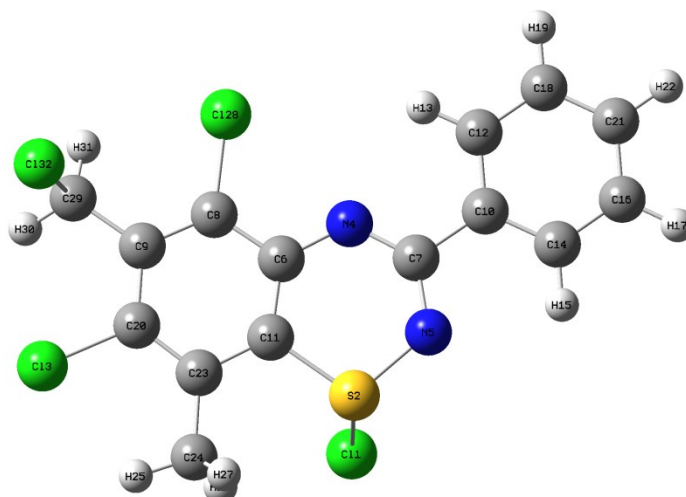
2d



Center Number	Atomic Number	Atomic Type	Coordinates (Angstroms)		
			X	Y	Z
1	17	0	5.114392	1.885218	3.656962
2	16	0	3.003736	3.325893	3.930355
3	17	0	4.573405	6.582082	-0.267685
4	17	0	3.601751	9.310635	5.201712
5	7	0	3.912534	5.722758	5.624374
6	7	0	2.752905	3.589924	5.618298
7	6	0	4.045437	5.861449	4.274344
8	6	0	3.299792	4.691635	6.218023
9	6	0	4.619588	7.091107	3.798861
10	6	0	4.746121	7.266920	2.428314
11	6	0	3.134234	4.731008	7.687015
12	6	0	3.656486	4.891050	3.316198
13	6	0	3.376034	5.927619	8.388121
14	1	0	3.670360	6.811466	7.836461
15	6	0	2.730644	3.581798	8.394010
16	1	0	2.548229	2.663070	7.850921
17	6	0	2.579857	3.631021	9.780768
18	1	0	2.275734	2.740184	10.319986
19	6	0	3.220784	5.970263	9.774047
20	1	0	3.404299	6.897109	10.307196
21	6	0	4.353820	6.270354	1.500714
22	6	0	5.042079	8.111362	4.795536
23	1	0	5.834591	8.760182	4.438177
24	1	0	5.275485	7.654048	5.750621
25	6	0	2.824130	4.823095	10.474248
26	1	0	2.705472	4.858725	11.552447
27	6	0	3.810206	5.057228	1.920647
28	6	0	3.412248	3.945013	0.981042
29	1	0	3.539749	4.231426	-0.060542
30	1	0	4.025121	3.054948	1.170443
31	1	0	2.361922	3.665224	1.126785
32	17	0	5.433075	8.819312	1.807177

Total energy E(UB3LYP) = -2925.75928790 Hartrees

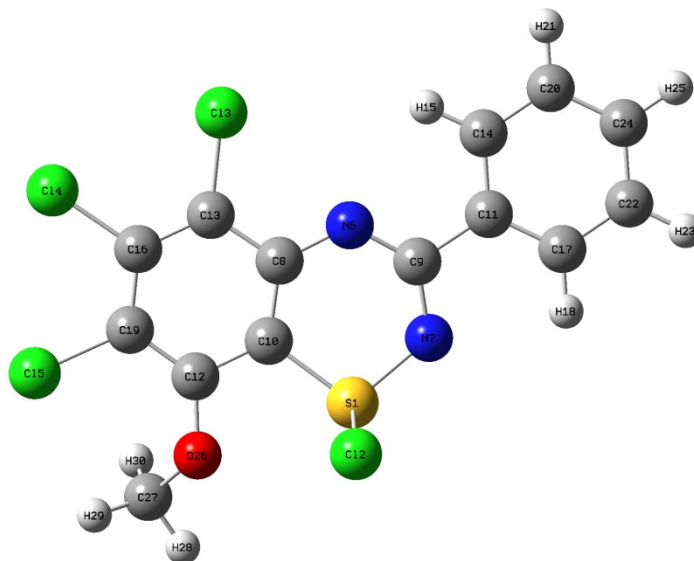
2e



Center Number	Atomic Number	Atomic Type	Coordinates (Angstroms)		
			X	Y	Z
1	17	0	5.117940	1.858223	3.670225
2	16	0	3.006183	3.305436	3.936486
3	17	0	4.619052	6.537357	-0.262588
4	7	0	3.882221	5.713190	5.632863
5	7	0	2.750009	3.566328	5.620911
6	6	0	4.029659	5.847490	4.287465
7	6	0	3.289521	4.670860	6.224801
8	6	0	4.579895	7.061717	3.776606
9	6	0	4.766971	7.280612	2.417564
10	6	0	3.140582	4.703302	7.695719
11	6	0	3.667590	4.870845	3.322145
12	6	0	3.532047	5.851467	8.410332
13	1	0	3.937668	6.694558	7.865414
14	6	0	2.613243	3.598127	8.390979
15	1	0	2.320345	2.714599	7.837986
16	6	0	2.479795	3.645095	9.779580
17	1	0	2.075904	2.789009	10.309620
18	6	0	3.396800	5.890405	9.798439
19	1	0	3.700980	6.777883	10.343405
20	6	0	4.381268	6.241351	1.518750
21	6	0	2.869998	4.789358	10.486805
22	1	0	2.766286	4.822475	11.566680
23	6	0	3.841389	5.026693	1.928042
24	6	0	3.462044	3.905290	0.991359
25	1	0	3.613960	4.181055	-0.049886
26	1	0	4.066484	3.014734	1.202579
27	1	0	2.407176	3.631056	1.113949
28	17	0	5.028235	8.333700	4.975916
29	6	0	5.348729	8.561858	1.913412
30	1	0	5.886152	8.441131	0.978892
31	1	0	5.958702	9.060984	2.658359
32	17	0	3.969639	9.816457	1.509648

Total Energy E(UB3LYP) = -2925.75684163 Hartrees

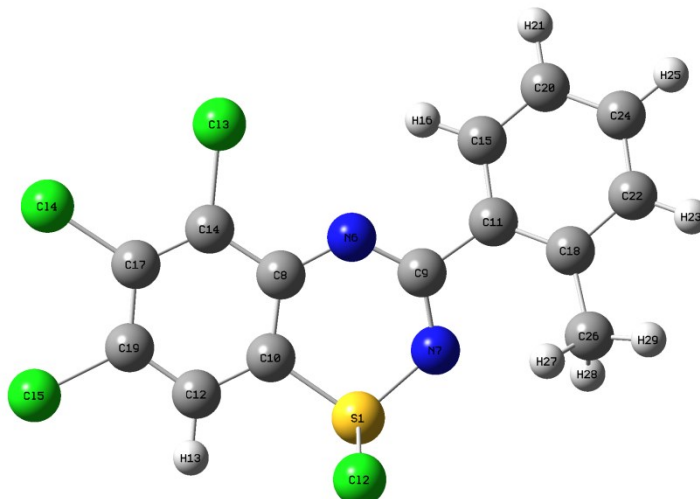
2f



Center Number	Atomic Number	Atomic Type	Coordinates (Angstroms)		
			X	Y	Z
1	16	0	1.446734	7.223536	8.427569
2	17	0	1.465630	7.186049	10.957944
3	17	0	6.769622	8.229599	7.276682
4	17	0	6.182444	11.376091	7.545914
5	17	0	3.272801	12.414003	8.335738
6	7	0	4.379787	6.542431	7.725085
7	7	0	2.108941	5.698753	7.947318
8	6	0	4.083509	7.863978	7.848103
9	6	0	3.457471	5.571616	7.752520
10	6	0	2.791643	8.375237	8.121295
11	6	0	3.913299	4.186512	7.501053
12	6	0	2.505739	9.750741	8.235887
13	6	0	5.122861	8.827736	7.661058
14	6	0	5.255735	3.947183	7.150776
15	1	0	5.933863	4.787659	7.073279
16	6	0	4.857962	10.181730	7.774266
17	6	0	3.020143	3.103433	7.610131
18	1	0	1.991182	3.292385	7.888820
19	6	0	3.554141	10.652038	8.076093
20	6	0	5.694537	2.644128	6.913382
21	1	0	6.730760	2.466325	6.645295
22	6	0	3.465904	1.802856	7.369180
23	1	0	2.773445	0.972417	7.458387
24	6	0	4.802126	1.569052	7.020290
25	1	0	5.146460	0.556415	6.835598
26	8	0	1.204031	10.036140	8.572814
27	6	0	0.416524	11.098525	7.916630
28	1	0	-0.610462	10.738796	7.964369
29	1	0	0.518976	12.034013	8.463710
30	1	0	0.730264	11.225571	6.877343

Total Energy E(UB3LYP) = -2961.60478588 Hartrees

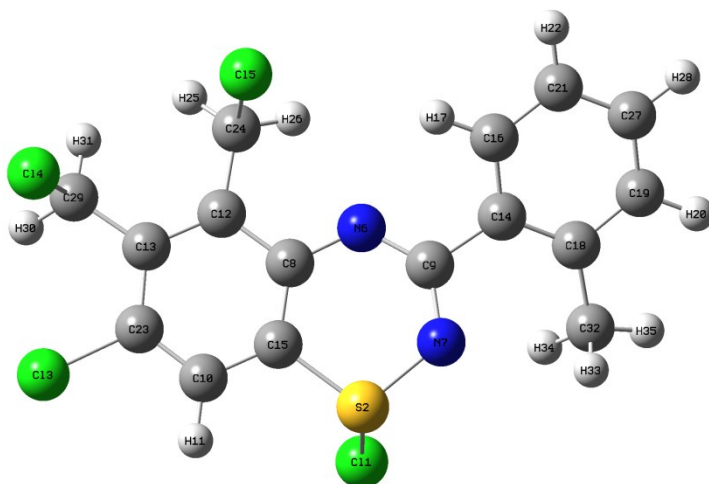
2g



Center Number	Atomic Number	Atomic Type	Coordinates (Angstroms)		
			X	Y	Z
1	16	0	1.344517	7.426041	8.045327
2	17	0	0.854436	7.381120	10.552427
3	17	0	6.816270	8.119685	7.674848
4	17	0	6.417535	11.286889	8.085817
5	17	0	3.444104	12.472938	8.504754
6	7	0	4.293500	6.590298	7.730159
7	7	0	1.975317	5.873522	7.592812
8	6	0	4.062346	7.918265	7.886768
9	6	0	3.327759	5.666026	7.606319
10	6	0	2.780237	8.509185	8.047930
11	6	0	3.758677	4.266447	7.377646
12	6	0	2.595241	9.881160	8.250386
13	1	0	1.606985	10.295029	8.407936
14	6	0	5.180708	8.816756	7.896425
15	6	0	5.041296	4.084960	6.815416
16	1	0	5.631208	4.965157	6.593355
17	6	0	5.005957	10.178639	8.076038
18	6	0	2.966100	3.132038	7.709110
19	6	0	3.702358	10.707378	8.257402
20	6	0	5.543268	2.813977	6.553479
21	1	0	6.527812	2.698953	6.113207
22	6	0	3.505487	1.861216	7.440452
23	1	0	2.916392	0.987081	7.699561
24	6	0	4.766643	1.692805	6.865869
25	1	0	5.142543	0.693381	6.670882
26	6	0	1.602051	3.197691	8.362143
27	1	0	1.576860	3.897841	9.202502
28	1	0	0.833294	3.533423	7.659620
29	1	0	1.320992	2.207271	8.733362

Total energy E(UB3LYP) = -2886.43218800 Hartrees

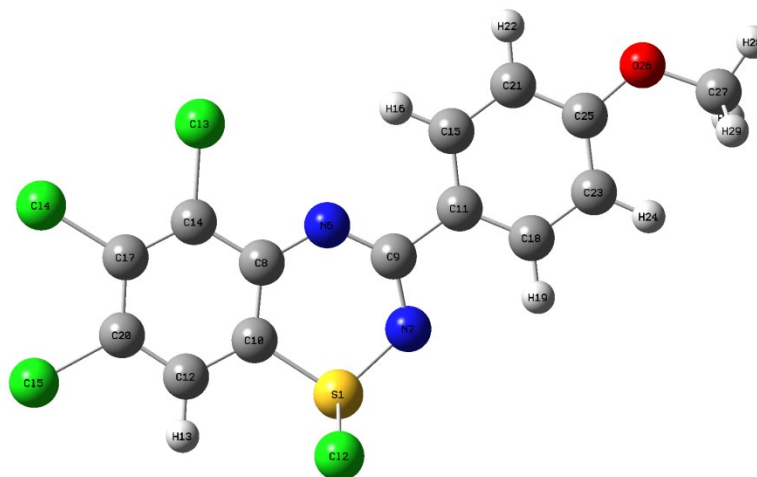
2h



Center Number	Atomic Number	Atomic Type	Coordinates (Angstroms)		
			X	Y	Z
1	17	0	4.556548	1.811706	3.475745
2	16	0	2.639022	3.480072	3.786505
3	17	0	4.599391	6.567510	-0.293639
4	17	0	4.319813	9.851085	1.412854
5	17	0	3.873386	9.249849	5.346044
6	7	0	3.840621	5.678658	5.574162
7	7	0	2.414766	3.711331	5.494349
8	6	0	3.978562	5.861785	4.230702
9	6	0	3.113032	4.698947	6.131851
10	6	0	3.684679	5.185740	1.877993
11	1	0	3.330247	4.475736	1.141082
12	6	0	4.683237	7.040203	3.788334
13	6	0	4.863760	7.279160	2.418495
14	6	0	2.971471	4.715322	7.607166
15	6	0	3.484053	4.971568	3.245991
16	6	0	3.000221	5.979717	8.233247
17	1	0	3.116621	6.860776	7.613414
18	6	0	2.826871	3.538439	8.391047
19	6	0	2.710486	3.694912	9.783468
20	1	0	2.614396	2.804131	10.396452
21	6	0	2.870358	6.103153	9.613962
22	1	0	2.882532	7.084902	10.074832
23	6	0	4.358958	6.323896	1.489131
24	6	0	5.192504	7.952778	4.853876
25	1	0	6.054733	8.545604	4.567083
26	1	0	5.370825	7.408136	5.775258
27	6	0	2.723136	4.950937	10.394020
28	1	0	2.623881	5.028272	11.472150
29	6	0	5.566414	8.499626	1.912300
30	1	0	6.129002	8.306730	1.003287
31	1	0	6.197480	8.978417	2.652586
32	6	0	2.825834	2.134377	7.825318
33	1	0	1.876600	1.900353	7.333652
34	1	0	3.607179	1.986880	7.073631
35	1	0	2.984553	1.408731	8.629049

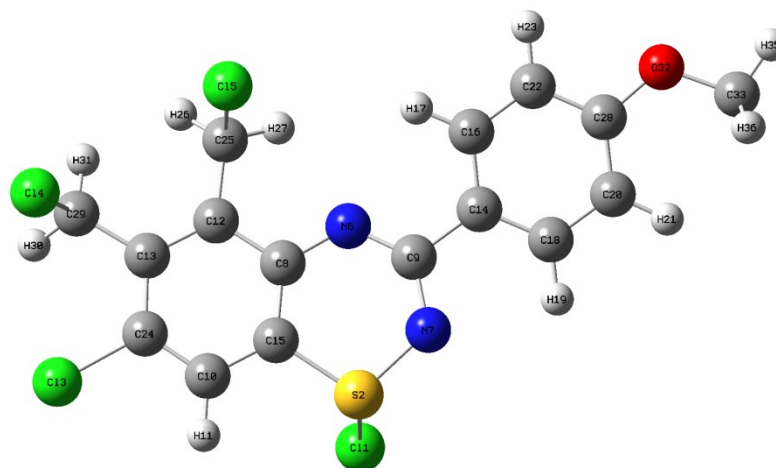
Total energy E(UB3LYP) = -2965.06307593 Hartrees

2k



Center Number	Atomic Number	Atomic Type	Coordinates (Angstroms)		
			X	Y	Z
1	16	0	1.433747	7.249040	8.360912
2	17	0	1.267296	7.136511	10.905424
3	17	0	6.755540	8.380470	7.354115
4	17	0	6.185928	11.487205	7.972145
5	17	0	3.208361	12.423493	8.802606
6	7	0	4.370066	6.661124	7.616884
7	7	0	2.103836	5.780247	7.755509
8	6	0	4.069576	7.959070	7.881167
9	6	0	3.461218	5.677309	7.565878
10	6	0	2.780404	8.442273	8.229243
11	6	0	3.927211	4.326800	7.218193
12	6	0	2.523575	9.785054	8.521997
13	1	0	1.535986	10.113441	8.821481
14	6	0	5.113123	8.939179	7.805308
15	6	0	5.277893	4.116269	6.860648
16	1	0	5.953041	4.962451	6.848442
17	6	0	4.865432	10.275444	8.074478
18	6	0	3.049145	3.227583	7.237830
19	1	0	2.014847	3.382612	7.518168
20	6	0	3.560842	10.694414	8.436945
21	6	0	5.730354	2.847193	6.534097
22	1	0	6.762407	2.667199	6.258506
23	6	0	3.496847	1.948338	6.910231
24	1	0	2.801658	1.118893	6.937964
25	6	0	4.841764	1.756228	6.556509
26	8	0	5.390865	0.535572	6.215400
27	6	0	4.547534	-0.650667	6.216757
28	1	0	5.206036	-1.465239	5.919585
29	1	0	4.142700	-0.845088	7.216043
30	1	0	3.728113	-0.552649	5.496098

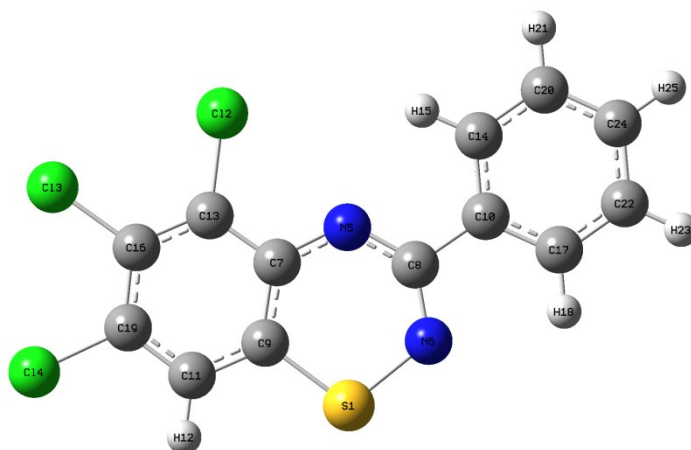
Total energy E(UB3LYP) = -2961.61586995 Hartrees



Center Number	Atomic Number	Atomic Type	Coordinates (Angstroms)		
			X	Y	Z
1	17	0	4.974897	1.870553	3.748893
2	16	0	2.913754	3.376450	3.900513
3	17	0	4.834940	6.322388	-0.301758
4	17	0	4.250859	9.684155	1.141104
5	17	0	3.686384	9.353336	5.087153
6	7	0	3.821349	5.798154	5.575628
7	7	0	2.572545	3.708147	5.559756
8	6	0	4.033263	5.890753	4.231685
9	6	0	3.134265	4.807014	6.161626
10	6	0	3.913872	5.030500	1.923372
11	1	0	3.651339	4.244668	1.225964
12	6	0	4.683074	7.079454	3.736798
13	6	0	4.915063	7.235489	2.361854
14	6	0	2.890103	4.891560	7.610010
15	6	0	3.659984	4.898952	3.291945
16	6	0	3.153007	6.091971	8.306762
17	1	0	3.521675	6.948905	7.757650
18	6	0	2.388705	3.787774	8.324185
19	1	0	2.187239	2.864664	7.795346
20	6	0	2.160982	3.866843	9.697673
21	1	0	1.783139	2.999718	10.224245
22	6	0	2.926305	6.179711	9.671824
23	1	0	3.116442	7.094488	10.219924
24	6	0	4.524003	6.186109	1.482293
25	6	0	5.087862	8.093812	4.753451
26	1	0	5.934297	8.708055	4.464165
27	1	0	5.248289	7.626770	5.719352
28	6	0	2.430880	5.066266	10.375112
29	6	0	5.558382	8.464833	1.801218
30	1	0	6.180925	8.249367	0.937440
31	1	0	6.113306	9.040400	2.533462
32	8	0	2.242353	5.255357	11.730418
33	6	0	1.724973	4.160100	12.537305
34	1	0	2.402814	3.299653	12.514903
35	1	0	1.666214	4.558352	13.548938
36	1	0	0.728219	3.857239	12.197994

Total energy E(UB3LYP) = -3040.24578786 Hartrees

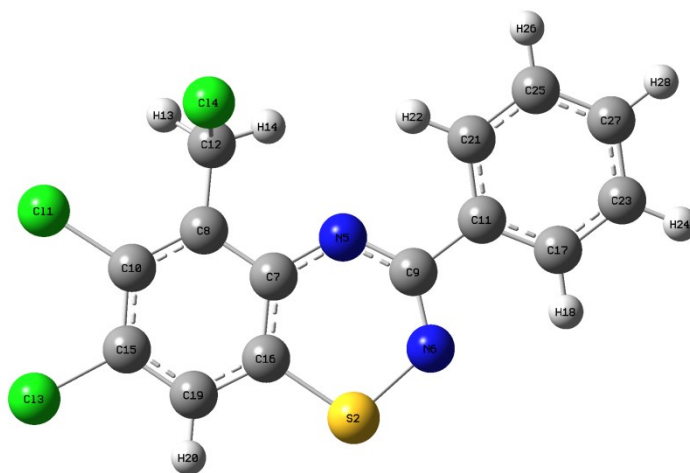
3a



Center Number	Atomic Number	Atomic Type	Coordinates (Angstroms)		
			X	Y	Z
1	16	0	1.377408	7.275125	8.482359
2	17	0	6.676776	8.230900	7.118504
3	17	0	6.210369	11.385620	7.556857
4	17	0	3.285176	12.438391	8.464905
5	7	0	4.282453	6.583468	7.615383
6	7	0	2.080180	5.671990	8.131903
7	6	0	4.014959	7.908023	7.818922
8	6	0	3.379281	5.589979	7.766559
9	6	0	2.756463	8.431951	8.216548
10	6	0	3.863097	4.209427	7.498315
11	6	0	2.546103	9.795595	8.408367
12	1	0	1.578135	10.175477	8.711954
13	6	0	5.069162	8.852071	7.621642
14	6	0	5.199101	4.000734	7.110204
15	1	0	5.854871	4.856595	7.013496
16	6	0	4.868346	10.215391	7.810882
17	6	0	2.999909	3.105159	7.627877
18	1	0	1.972220	3.269794	7.926834
19	6	0	3.599036	10.679630	8.205646
20	6	0	5.661480	2.707626	6.856413
21	1	0	6.693590	2.555770	6.557523
22	6	0	3.468470	1.815243	7.372691
23	1	0	2.796241	0.969507	7.474955
24	6	0	4.799573	1.611628	6.986385
25	1	0	5.161428	0.607544	6.788555

Total energy E(UB3LYP) = -2386.96710162 Hartrees

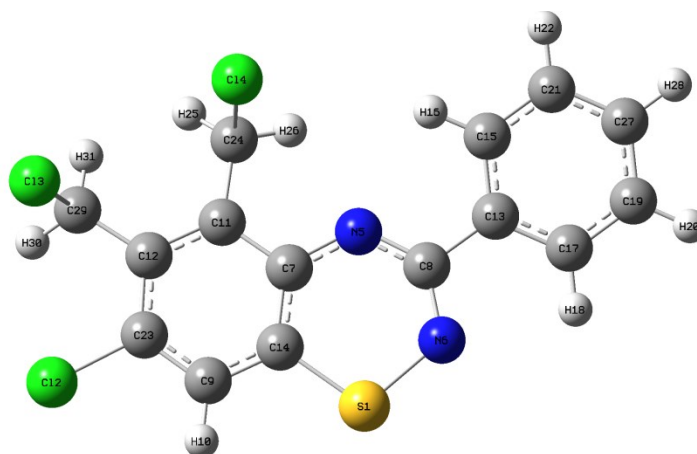
3b



Center Number	Atomic Number	Atomic Type	Coordinates (Angstroms)		
			X	Y	Z
1	17	0	7.247433	6.817043	7.309422
2	16	0	6.839585	0.889498	4.895722
3	17	0	8.988317	4.392485	8.559115
4	17	0	6.377162	6.905935	3.530429
5	7	0	5.327195	3.423619	3.913511
6	7	0	5.708827	1.047608	3.523262
7	6	0	6.172495	3.601662	4.977186
8	6	0	6.256496	4.925727	5.530998
9	6	0	5.154970	2.251925	3.261310
10	6	0	7.114039	5.154148	6.608532
11	6	0	4.233140	2.265428	2.093781
12	6	0	5.424412	6.002348	4.928107
13	1	0	5.170529	6.792625	5.627001
14	1	0	4.556129	5.591370	4.425351
15	6	0	7.880498	4.113944	7.160954
16	6	0	6.956548	2.576212	5.564139
17	6	0	3.847582	1.063881	1.469734
18	1	0	4.228717	0.124943	1.851437
19	6	0	7.805219	2.826787	6.640173
20	1	0	8.404489	2.036705	7.076739
21	6	0	3.744386	3.487380	1.597351
22	1	0	4.056012	4.409665	2.070325
23	6	0	2.982779	1.087706	0.374264
24	1	0	2.687832	0.156053	-0.097522
25	6	0	2.882390	3.505312	0.498699
26	1	0	2.515533	4.453692	0.119872
27	6	0	2.496843	2.307123	-0.114770
28	1	0	1.825736	2.323240	-0.967702

Total energy E(UB3LYP) = -2426.28581316 Hartrees

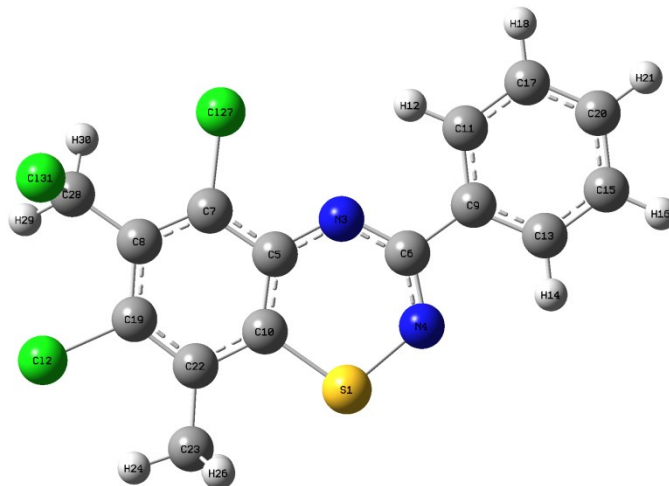
3c



Center Number	Atomic Number	Atomic Type	Coordinates (Angstroms)		
			X	Y	Z
1	16	0	2.884716	3.319212	3.868381
2	17	0	4.651132	6.444569	-0.291774
3	17	0	4.062383	9.771314	1.280322
4	17	0	3.613427	9.298375	5.205034
5	7	0	3.836220	5.719280	5.598607
6	7	0	2.777373	3.523829	5.639254
7	6	0	4.003607	5.853341	4.243197
8	6	0	3.254430	4.657683	6.198911
9	6	0	3.824021	5.069769	1.925822
10	1	0	3.533718	4.316381	1.203581
11	6	0	4.608683	7.068785	3.772034
12	6	0	4.801937	7.280231	2.391303
13	6	0	3.109807	4.721855	7.678404
14	6	0	3.626872	4.874189	3.291121
15	6	0	3.364131	5.926644	8.358312
16	1	0	3.654050	6.800803	7.789575
17	6	0	2.709821	3.587972	8.410438
18	1	0	2.509948	2.663200	7.883677
19	6	0	2.575898	3.659371	9.798114
20	1	0	2.271373	2.778773	10.354355
21	6	0	3.224529	5.993219	9.746347
22	1	0	3.416699	6.929209	10.260699
23	6	0	4.404990	6.254887	1.501238
24	6	0	5.021004	8.062744	4.805653
25	1	0	5.852077	8.696696	4.513325
26	1	0	5.207379	7.574258	5.755892
27	6	0	2.833012	4.860802	10.470927
28	1	0	2.726347	4.914434	11.549776
29	6	0	5.404020	8.539047	1.855836
30	1	0	5.998901	8.367552	0.963199
31	1	0	5.974693	9.098104	2.589098

Total energy E(UB3LYP) = -2465.59604853 Hartrees

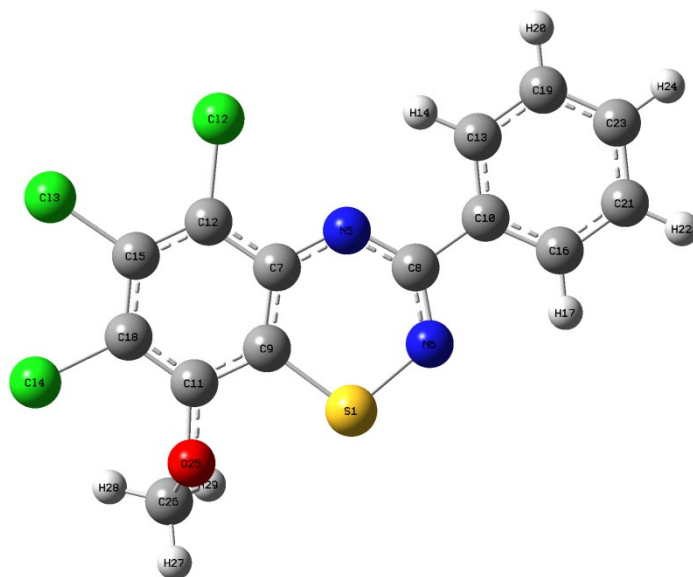
3e



Center Number	Atomic Number	Atomic Type	Coordinates (Angstroms)		
			X	Y	Z
1	16	0	2.920541	3.293032	3.885030
2	17	0	4.705361	6.529517	-0.259643
3	7	0	3.777686	5.719224	5.618465
4	7	0	2.823428	3.480270	5.656313
5	6	0	3.965105	5.847553	4.268929
6	6	0	3.255530	4.629468	6.219639
7	6	0	4.524577	7.059658	3.776207
8	6	0	4.761941	7.285607	2.419436
9	6	0	3.131622	4.683813	7.700946
10	6	0	3.645124	4.862167	3.300558
11	6	0	3.541944	5.836817	8.394449
12	1	0	3.943191	6.669834	7.831375
13	6	0	2.606989	3.593886	8.420468
14	1	0	2.291782	2.708344	7.882696
15	6	0	2.496305	3.659303	9.810500
16	1	0	2.090639	2.814380	10.357526
17	6	0	3.428319	5.895960	9.785178
18	1	0	3.746645	6.789660	10.312130
19	6	0	4.411055	6.246682	1.519941
20	6	0	2.906081	4.809344	10.497548
21	1	0	2.818622	4.857870	11.578432
22	6	0	3.854186	5.028441	1.919458
23	6	0	3.476554	3.917644	0.968691
24	1	0	3.695693	4.174832	-0.065654
25	1	0	4.020756	2.996144	1.210616
26	1	0	2.404883	3.693495	1.040201
27	17	0	4.928599	8.342279	4.985341
28	6	0	5.356534	8.566709	1.937231
29	1	0	5.919385	8.450725	1.017165
30	1	0	5.943722	9.065678	2.700426
31	17	0	3.995736	9.836099	1.492646

Total energy E(UB3LYP) = -2465.59278462 Hartrees

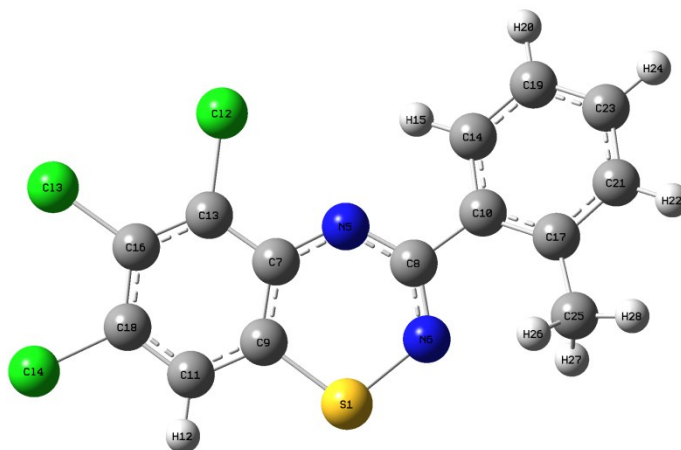
3f



Center Number	Atomic Number	Atomic Type	Coordinates (Angstroms)		
			X	Y	Z
1	16	0	1.403019	7.311891	8.477996
2	17	0	6.750398	8.236210	7.239622
3	17	0	6.273991	11.386937	7.679885
4	17	0	3.353815	12.451619	8.527337
5	7	0	4.332615	6.591805	7.664455
6	7	0	2.103567	5.712262	8.110807
7	6	0	4.066842	7.918739	7.858631
8	6	0	3.408889	5.611659	7.776050
9	6	0	2.797951	8.443514	8.206527
10	6	0	3.877229	4.227747	7.497522
11	6	0	2.570579	9.811105	8.375806
12	6	0	5.127822	8.858880	7.692059
13	6	0	5.217017	4.002994	7.132087
14	1	0	5.888097	4.849520	7.061271
15	6	0	4.916630	10.220522	7.877124
16	6	0	2.994449	3.135829	7.594730
17	1	0	1.964415	3.313615	7.877688
18	6	0	3.638237	10.699519	8.224811
19	6	0	5.663665	2.706329	6.868328
20	1	0	6.698926	2.542002	6.587350
21	6	0	3.447177	1.842232	7.329566
22	1	0	2.759907	1.005975	7.407274
23	6	0	4.782055	1.622636	6.965668
24	1	0	5.131741	0.615715	6.760329
25	8	0	1.300713	10.207296	8.777464
26	6	0	0.428855	10.849239	7.769315
27	1	0	-0.515205	11.009358	8.286985
28	1	0	0.851106	11.802730	7.446991
29	1	0	0.285949	10.181033	6.914923

Total energy E(UB3LYP) = -2501.44354252 Hartrees

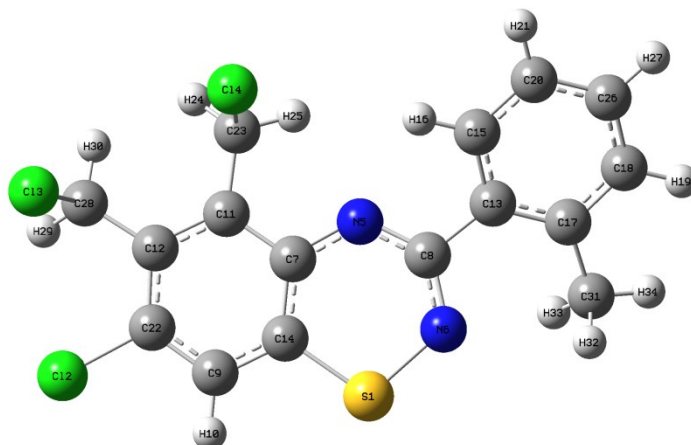
3g



Center Number	Atomic Number	Atomic Type	Coordinates (Angstroms)		
			X	Y	Z
1	16	0	1.302255	7.477658	8.124250
2	17	0	6.781885	8.099536	7.502890
3	17	0	6.466700	11.269948	7.962356
4	17	0	3.522544	12.500137	8.516446
5	7	0	4.245148	6.608597	7.657101
6	7	0	1.945374	5.830608	7.825415
7	6	0	4.035834	7.941973	7.847928
8	6	0	3.272132	5.661313	7.660365
9	6	0	2.771666	8.544447	8.089549
10	6	0	3.734874	4.261662	7.424756
11	6	0	2.627245	9.915378	8.290050
12	1	0	1.654316	10.354595	8.474059
13	6	0	5.166013	8.818351	7.811800
14	6	0	5.037208	4.109383	6.901213
15	1	0	5.618755	5.003033	6.717755
16	6	0	5.030518	10.187799	8.009974
17	6	0	2.953974	3.103574	7.698964
18	6	0	3.752815	10.729478	8.250677
19	6	0	5.571272	2.852651	6.629518
20	1	0	6.572683	2.767058	6.221077
21	6	0	3.524759	1.847788	7.421409
22	1	0	2.938638	0.959199	7.635138
23	6	0	4.808109	1.710730	6.890320
24	1	0	5.208171	0.722149	6.687720
25	6	0	1.559586	3.120243	8.287219
26	1	0	1.500843	3.736301	9.189753
27	1	0	0.829181	3.539550	7.588996
28	1	0	1.252967	2.100921	8.542843

Total energy E(UB3LYP) = -2426.26898651 Hartrees

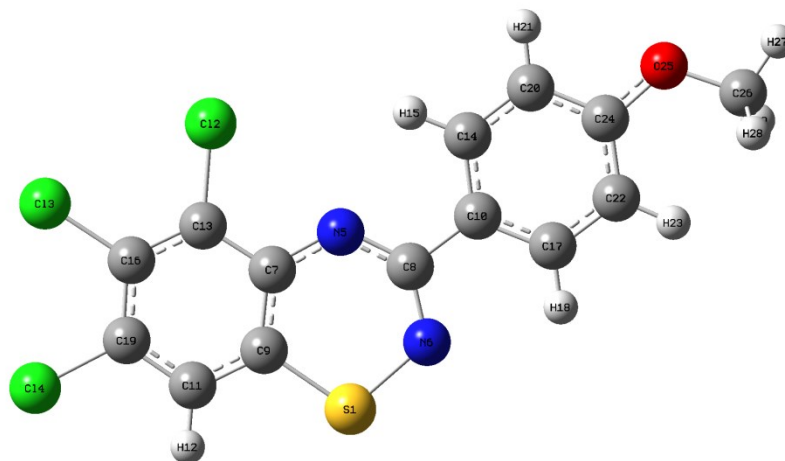
3h



Center Number	Atomic Number	Atomic Type	Coordinates (Angstroms)		
			X	Y	Z
1	16	0	2.541636	3.491537	3.716797
2	17	0	4.643213	6.596914	-0.302828
3	17	0	4.396085	9.897680	1.437784
4	17	0	3.840512	9.256270	5.333837
5	7	0	3.772438	5.676047	5.549308
6	7	0	2.461711	3.622679	5.506451
7	6	0	3.935537	5.861735	4.201318
8	6	0	3.083738	4.653490	6.112590
9	6	0	3.673880	5.213294	1.850682
10	1	0	3.306240	4.530216	1.094596
11	6	0	4.655905	7.034493	3.785043
12	6	0	4.872949	7.288710	2.415631
13	6	0	2.969098	4.690764	7.599312
14	6	0	3.455984	4.974230	3.206116
15	6	0	2.992919	5.964907	8.203430
16	1	0	3.095127	6.835384	7.566968
17	6	0	2.843665	3.530764	8.409685
18	6	0	2.744721	3.711166	9.800950
19	1	0	2.662010	2.830389	10.430601
20	6	0	2.879574	6.113892	9.584126
21	1	0	2.888644	7.105302	10.024432
22	6	0	4.375479	6.350466	1.480362
23	6	0	5.150809	7.937802	4.864502
24	1	0	6.026303	8.521747	4.599659
25	1	0	5.297793	7.389700	5.789111
26	6	0	2.754592	4.977536	10.389322
27	1	0	2.669585	5.074309	11.467183
28	6	0	5.601923	8.502493	1.937305
29	1	0	6.171019	8.314512	1.031356
30	1	0	6.232817	8.959626	2.691646
31	6	0	2.835749	2.115198	7.873596
32	1	0	1.894699	1.882493	7.366364
33	1	0	3.629011	1.948020	7.138078
34	1	0	2.973268	1.403979	8.694354

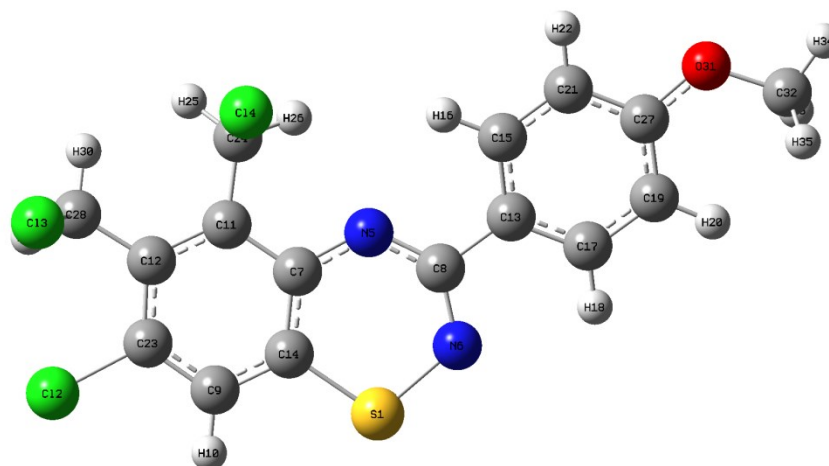
Total energy E(UB3LYP) = -2504.89884282 Hartrees

3k



Center Number	Atomic Number	Atomic Type	Coordinates (Angstroms)		
			X	Y	Z
1	16	0	1.370122	7.298982	8.341416
2	17	0	6.727186	8.336599	7.304629
3	17	0	6.242303	11.449390	7.966973
4	17	0	3.278080	12.440631	8.818341
5	7	0	4.311272	6.665038	7.558817
6	7	0	2.084550	5.725254	7.899441
7	6	0	4.035315	7.970108	7.853082
8	6	0	3.402657	5.665142	7.588499
9	6	0	2.760294	8.467353	8.231808
10	6	0	3.894860	4.313922	7.236639
11	6	0	2.541692	9.812696	8.520188
12	1	0	1.560664	10.171316	8.807379
13	6	0	5.097708	8.923112	7.779897
14	6	0	5.250398	4.122269	6.894146
15	1	0	5.914324	4.977144	6.894920
16	6	0	4.888942	10.268119	8.065965
17	6	0	3.032432	3.204200	7.235769
18	1	0	1.991122	3.345173	7.497768
19	6	0	3.603021	10.705616	8.436646
20	6	0	5.723623	2.859983	6.562198
21	1	0	6.761343	2.696824	6.297075
22	6	0	3.499989	1.931966	6.903299
23	1	0	2.813135	1.094928	6.910830
24	6	0	4.850721	1.758721	6.565113
25	8	0	5.419802	0.543940	6.219692
26	6	0	4.586187	-0.646572	6.197131
27	1	0	5.253728	-1.454460	5.900911
28	1	0	4.167375	-0.855695	7.188124
29	1	0	3.775212	-0.548426	5.466457

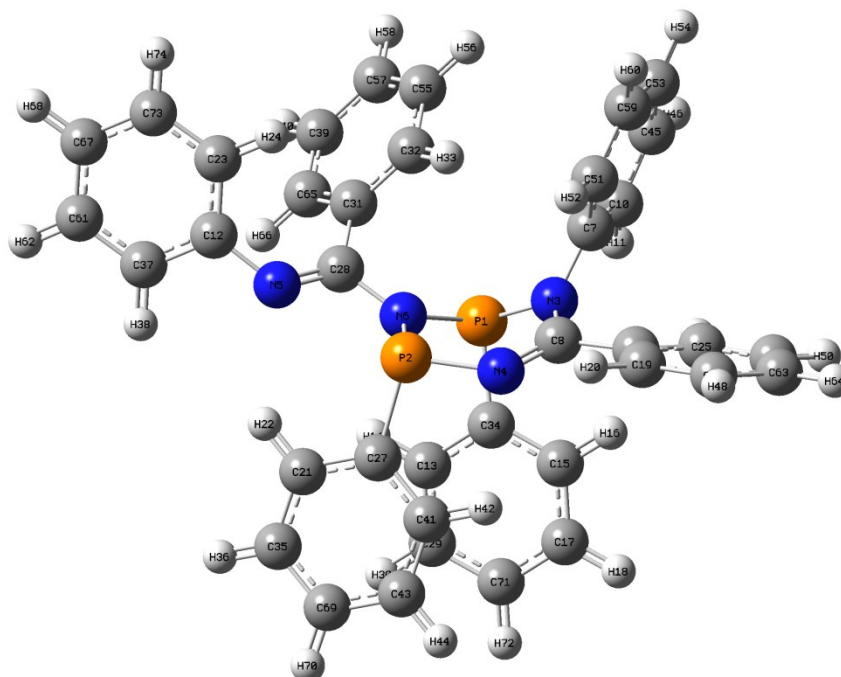
Total energy E(UB3LYP) = -2501.45226718 Hartrees



Center Number	Atomic Number	Atomic Type	Coordinates (Angstroms)		
			X	Y	Z
1	16	0	2.833199	3.368964	3.827814
2	17	0	4.911921	6.340564	-0.300994
3	17	0	4.316766	9.720496	1.146933
4	17	0	3.631529	9.365722	5.050739
5	7	0	3.744510	5.789184	5.550402
6	7	0	2.629286	3.619794	5.582458
7	6	0	3.990499	5.884624	4.204133
8	6	0	3.103119	4.758068	6.144072
9	6	0	3.924323	5.045220	1.899536
10	1	0	3.657107	4.279699	1.181098
11	6	0	4.650746	7.073212	3.737386
12	6	0	4.927805	7.243477	2.365182
13	6	0	2.878383	4.861442	7.604679
14	6	0	3.644905	4.890498	3.255734
15	6	0	3.155344	6.065965	8.285134
16	1	0	3.522293	6.914571	7.722686
17	6	0	2.378708	3.771365	8.338035
18	1	0	2.159298	2.845282	7.821309
19	6	0	2.166081	3.867274	9.714020
20	1	0	1.784733	3.009343	10.253451
21	6	0	2.943635	6.171764	9.653296
22	1	0	3.145129	7.092804	10.186961
23	6	0	4.557774	6.204537	1.479501
24	6	0	5.027377	8.084746	4.767173
25	1	0	5.890275	8.690237	4.508584
26	1	0	5.144620	7.617899	5.739052
27	6	0	2.450410	5.071724	10.375056
28	6	0	5.590878	8.473098	1.834219
29	1	0	6.233049	8.263813	0.983364
30	1	0	6.130334	9.039161	2.585494
31	8	0	2.277219	5.277301	11.733855
32	6	0	1.755505	4.194937	12.551935
33	1	0	2.423756	3.326413	12.532942
34	1	0	1.706914	4.600738	13.561378
35	1	0	0.753386	3.897483	12.222711

Total energy E(UB3LYP) = -2580.08115172 Hartrees

10a

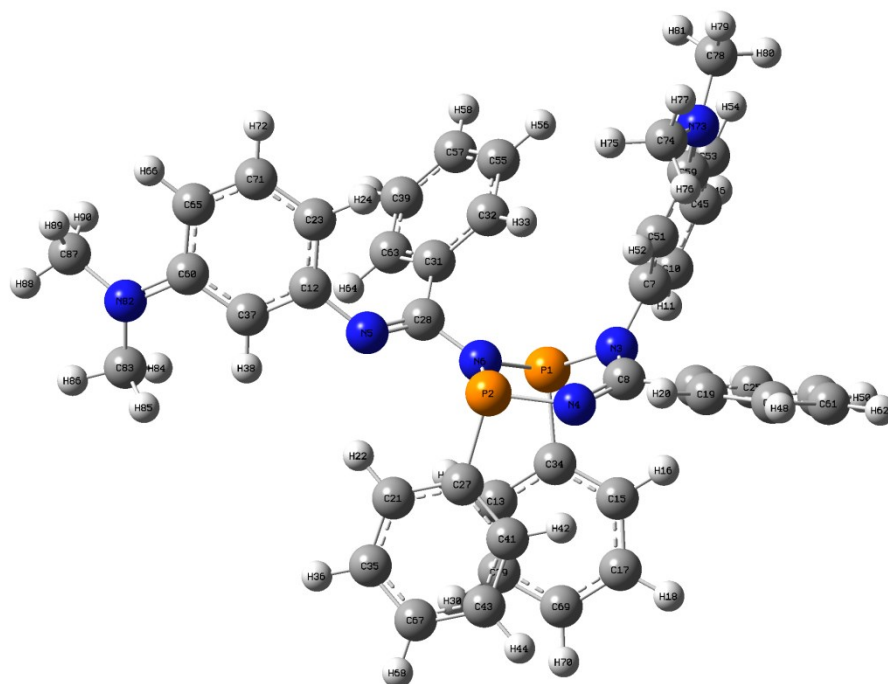


Center Number	Atomic Number	Atomic Type	Coordinates (Angstroms)		
			X	Y	Z
1	15	0	2.621030	9.059812	5.086442
2	15	0	5.562769	8.856809	4.273461
3	7	0	2.796312	7.359753	4.758920
4	7	0	5.167605	7.333644	4.901503
5	7	0	4.898422	11.350753	2.932466
6	7	0	3.990119	9.669526	4.195546
7	6	0	1.843280	6.770450	3.872048
8	6	0	4.046167	6.729353	4.944414
9	6	0	4.012643	5.279599	5.298442
10	6	0	0.478824	6.939585	4.106771
11	1	0	0.150664	7.478607	4.988147
12	6	0	4.906334	12.252836	1.850344
13	6	0	3.734157	10.400783	7.234111
14	1	0	3.784457	11.234868	6.540853
15	6	0	3.240330	8.085715	7.688513
16	1	0	2.885216	7.113981	7.364194
17	6	0	3.657078	8.260916	9.005810
18	1	0	3.625521	7.423933	9.693300
19	6	0	5.146040	4.499140	5.063323
20	1	0	6.012255	4.960881	4.605639
21	6	0	6.716175	10.933094	5.723892
22	1	0	6.467769	11.519449	4.845083
23	6	0	4.577316	11.859487	0.549219
24	1	0	4.268989	10.836200	0.367092
25	6	0	2.887766	4.697064	5.887763
26	1	0	2.001789	5.293153	6.073182
27	6	0	6.369507	9.579093	5.765189
28	6	0	3.855137	10.676817	3.237221
29	6	0	4.149820	10.573254	8.546649
30	1	0	4.513386	11.540228	8.873520
31	6	0	2.499633	10.860960	2.632480

32	6	0	1.853127	9.780032	2.031390
33	1	0	2.329684	8.804862	2.014321
34	6	0	3.292800	9.150170	6.790625
35	6	0	7.349008	11.524602	6.811549
36	1	0	7.604231	12.577652	6.778761
37	6	0	5.336447	13.562702	2.077914
38	1	0	5.612040	13.853866	3.085216
39	6	0	0.636477	12.283087	2.074976
40	1	0	0.160666	13.255906	2.097655
41	6	0	6.689321	8.819931	6.891702
42	1	0	6.412166	7.773232	6.928235
43	6	0	7.332337	9.414658	7.972449
44	1	0	7.566127	8.822211	8.849731
45	6	0	-0.447774	6.417309	3.212524
46	1	0	-1.505533	6.557740	3.399977
47	6	0	5.154529	3.154437	5.409671
48	1	0	6.035474	2.554381	5.215876
49	6	0	2.902179	3.353395	6.242086
50	1	0	2.028813	2.910810	6.705414
51	6	0	2.271512	6.064533	2.747197
52	1	0	3.333035	5.946469	2.557723
53	6	0	-0.024232	5.707745	2.092243
54	1	0	-0.749358	5.296254	1.400908
55	6	0	0.605338	9.954819	1.445150
56	1	0	0.110897	9.112942	0.974870
57	6	0	-0.005796	11.205455	1.471519
58	1	0	-0.982390	11.340490	1.021896
59	6	0	1.337162	5.528530	1.867907
60	1	0	1.677776	4.979885	0.997988
61	6	0	5.394643	14.473903	1.030383
62	1	0	5.717521	15.490424	1.223015
63	6	0	4.032930	2.578944	6.001015
64	1	0	4.039503	1.529703	6.271606
65	6	0	1.892024	12.114332	2.647795
66	1	0	2.403034	12.951816	3.109412
67	6	0	5.050202	14.084580	-0.261209
68	1	0	5.103289	14.793938	-1.078005
69	6	0	7.658557	10.766522	7.937721
70	1	0	8.152567	11.228841	8.784489
71	6	0	4.113243	9.501479	9.435461
72	1	0	4.443201	9.634107	10.459078
73	6	0	4.649061	12.772399	-0.495997
74	1	0	4.390352	12.455268	-1.499573

Total energy E(RM062X) = -2367.57640426 Hartrees

10r



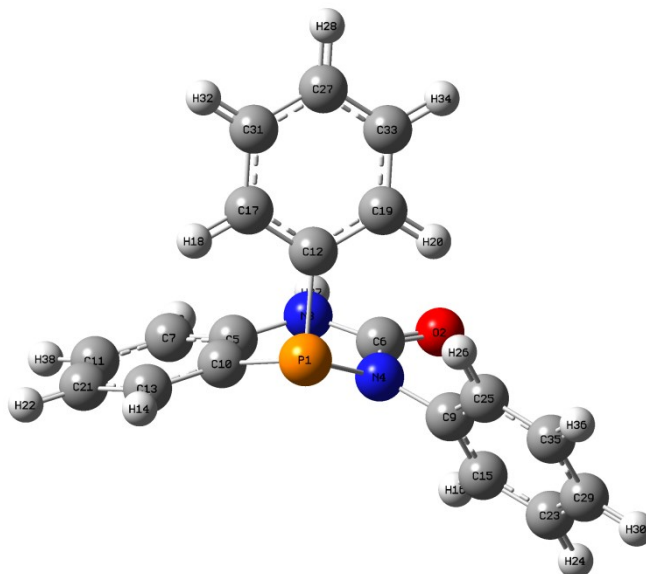
Center Number	Atomic Number	Atomic Type	Coordinates (Angstroms)		
			X	Y	Z
1	15	0	2.643634	9.079340	5.142274
2	15	0	5.561939	8.850373	4.266123
3	7	0	2.779421	7.384827	4.770410
4	7	0	5.152522	7.314739	4.853628
5	7	0	4.892832	11.424142	3.032205
6	7	0	4.006731	9.689918	4.241897
7	6	0	1.778565	6.826367	3.912928
8	6	0	4.020611	6.729791	4.906627
9	6	0	3.973312	5.271079	5.224768
10	6	0	0.431088	7.013386	4.211080
11	1	0	0.136439	7.532927	5.114077
12	6	0	4.888074	12.353598	1.969701
13	6	0	3.818421	10.353470	7.297240
14	1	0	3.856815	11.203770	6.623063
15	6	0	3.319035	8.031352	7.704703
16	1	0	2.948509	7.070446	7.366000
17	6	0	3.771460	8.169914	9.014766
18	1	0	3.752343	7.315715	9.681266
19	6	0	5.084144	4.477573	4.932561
20	1	0	5.942722	4.935996	4.457561
21	6	0	6.806421	10.850830	5.743588
22	1	0	6.555790	11.466411	4.885662
23	6	0	4.629834	11.964048	0.653634
24	1	0	4.387093	10.932406	0.431247
25	6	0	2.858745	4.693827	5.838348
26	1	0	1.988834	5.300354	6.062126
27	6	0	6.418245	9.507579	5.759948
28	6	0	3.861916	10.721370	3.306438
29	6	0	4.267316	10.490599	8.602957
30	1	0	4.644330	11.446926	8.945361

31	6	0	2.511071	10.874562	2.683003
32	6	0	1.906363	9.770032	2.081734
33	1	0	2.414782	8.811390	2.076331
34	6	0	3.357197	9.117598	6.832480
35	6	0	7.485524	11.394532	6.828144
36	1	0	7.773792	12.439347	6.813925
37	6	0	5.224795	13.673889	2.262615
38	1	0	5.428144	13.919662	3.295782
39	6	0	0.605971	12.228326	2.100064
40	1	0	0.097052	13.184498	2.111918
41	6	0	6.743711	8.710306	6.858023
42	1	0	6.437391	7.671381	6.875429
43	6	0	7.433607	9.256813	7.935487
44	1	0	7.671523	8.634363	8.790502
45	6	0	-0.513741	6.523986	3.316571
46	1	0	-1.567284	6.674626	3.521838
47	6	0	5.080525	3.124693	5.247210
48	1	0	5.943683	2.514163	5.010968
49	6	0	2.861930	3.342388	6.162048
50	1	0	1.997076	2.903700	6.644653
51	6	0	2.172146	6.147946	2.763509
52	1	0	3.229828	6.056924	2.555614
53	6	0	-0.146372	5.836822	2.169394
54	1	0	-0.917798	5.472580	1.506279
55	6	0	0.657258	9.895911	1.486657
56	1	0	0.194610	9.031578	1.024225
57	6	0	0.003714	11.125264	1.500270
58	1	0	-0.974401	11.224453	1.045001
59	6	0	1.216526	5.608932	1.878979
60	6	0	5.286500	14.651937	1.252249
61	6	0	3.970169	2.554662	5.864580
62	1	0	3.967928	1.499742	6.111486
63	6	0	1.861165	12.107217	2.685410
64	1	0	2.338135	12.964484	3.146724
65	6	0	4.994282	14.250966	-0.068745
66	1	0	5.016391	14.965364	-0.879037
67	6	0	7.801535	10.598329	7.925971
68	1	0	8.333435	11.022284	8.769766
69	6	0	4.247099	9.395896	9.464437
70	1	0	4.603735	9.499789	10.482428
71	6	0	4.685840	12.926541	-0.346305
72	1	0	4.477956	12.642288	-1.371829
73	7	0	1.603756	4.894260	0.768481
74	6	0	3.007687	4.869312	0.401158
75	1	0	3.399297	5.870215	0.175430
76	1	0	3.609321	4.437863	1.204834
77	1	0	3.131425	4.241792	-0.478461
78	6	0	0.619409	4.605416	-0.259175
79	1	0	1.102631	4.059911	-1.066489
80	1	0	-0.181844	3.975719	0.134281
81	1	0	0.170224	5.517689	-0.672538
82	7	0	5.635850	15.957236	1.544555
83	6	0	5.660836	16.375032	2.934238
84	1	0	4.688846	16.243953	3.429113
85	1	0	6.408909	15.810969	3.495568
86	1	0	5.936917	17.426232	2.982148
87	6	0	5.405824	16.979033	0.538927
88	1	0	5.713157	17.942868	0.939054
89	1	0	6.004002	16.786572	-0.354268

90 1 0 4.351071 17.043032 0.239756

Total energy E(RM062X) = -2635.46376722 Hartrees

17a

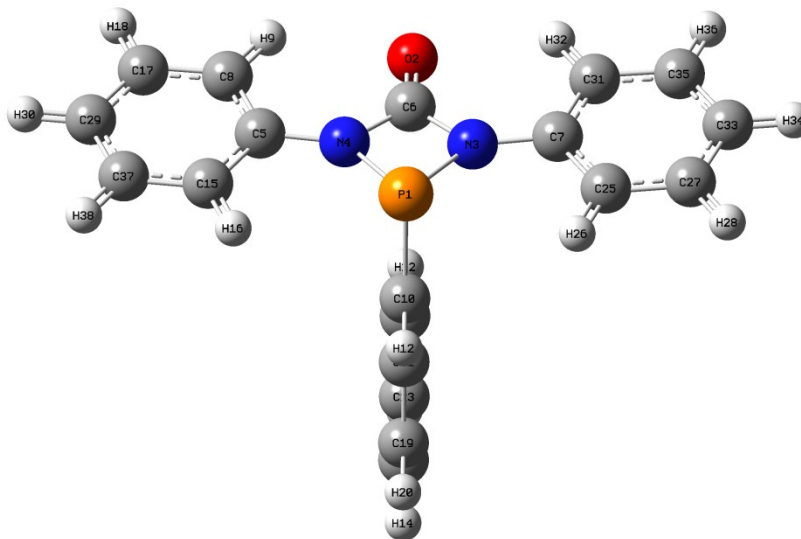


Center Number	Atomic Number	Atomic Type	Coordinates (Angstroms)		
			X	Y	Z
1	15	0	14.327384	5.036075	6.255111
2	8	0	13.448385	1.628091	7.865936
3	7	0	12.229375	2.903927	6.459085
4	7	0	14.175037	3.769387	7.450628
5	6	0	11.713107	4.129439	6.027433
6	6	0	13.301106	2.693889	7.304050
7	6	0	10.360821	4.241512	5.700487
8	1	0	9.711696	3.378158	5.793874
9	6	0	15.159977	3.686696	8.488189
10	6	0	12.553544	5.241123	5.911412
11	6	0	9.857494	5.459619	5.264383
12	6	0	14.789164	4.034471	4.770033
13	6	0	12.025361	6.465602	5.504928
14	1	0	12.678372	7.329388	5.439505
15	6	0	14.766237	3.445559	9.804092
16	1	0	13.717387	3.295030	10.026451
17	6	0	14.598981	4.595517	3.504102
18	1	0	14.123575	5.566991	3.405842
19	6	0	15.399160	2.783930	4.878024
20	1	0	15.552415	2.328458	5.851385
21	6	0	10.681439	6.578604	5.169428
22	1	0	10.279334	7.528074	4.840136
23	6	0	15.718783	3.396566	10.811818
24	1	0	15.406651	3.207074	11.831729
25	6	0	16.506250	3.881407	8.191288
26	1	0	16.816752	4.057812	7.166795
27	6	0	15.605704	2.661144	2.476717
28	1	0	15.919153	2.127205	1.587789
29	6	0	17.066019	3.601784	10.520203
30	1	0	17.805004	3.569870	11.311288

25	1	0	15.481273	3.068503	11.812177
26	6	0	16.528345	3.883246	8.185653
27	1	0	16.824815	4.100298	7.164929
28	6	0	15.623840	2.709032	2.485672
29	1	0	15.940465	2.185454	1.591652
30	6	0	17.119486	3.535290	10.497860
31	1	0	17.867743	3.489451	11.279515
32	6	0	14.997558	3.949211	2.384366
33	1	0	14.824174	4.392780	1.411048
34	6	0	15.837552	2.144631	3.737964
35	1	0	16.318819	1.177579	3.823678
36	6	0	17.489024	3.831883	9.192254
37	1	0	18.527820	4.016326	8.946905
38	6	0	7.621303	4.403665	5.138466
39	1	0	7.971800	3.556120	4.542654
40	1	0	6.622837	4.663883	4.796444
41	1	0	7.557158	4.086174	6.185852
42	6	0	7.916461	6.847913	4.658802
43	1	0	7.994000	7.544339	5.501377
44	1	0	6.864879	6.717006	4.416337
45	1	0	8.408977	7.298796	3.792813
46	1	0	11.624398	2.107915	6.425494

Total energy E(RM062X) = -1392.97929247 Hartrees

18a

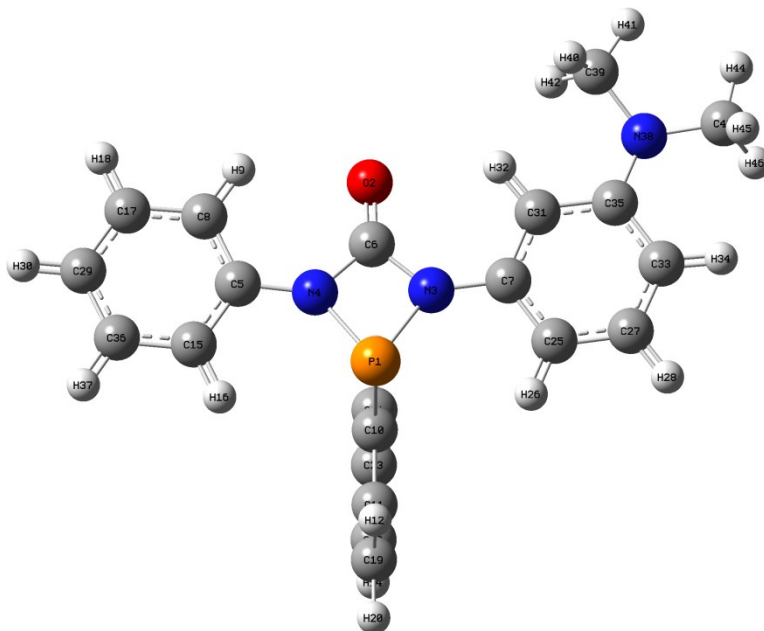


Center Number	Atomic Number	Atomic Type	Coordinates (Angstroms)		
			X	Y	Z
1	15	0	2.569487	11.330882	4.741672
2	8	0	0.438281	9.544006	6.930008
3	7	0	2.517745	9.995897	5.892618
4	7	0	0.955890	11.319652	5.452165
5	6	0	-0.186660	12.103059	5.264551
6	6	0	1.175370	10.177715	6.220946
7	6	0	3.431083	9.000453	6.253199
8	6	0	-1.422369	11.727904	5.801595
9	1	0	-1.502001	10.812513	6.370901
10	6	0	3.403089	12.638459	5.708462

11	6	0	4.317035	13.447235	5.032483
12	1	0	4.505007	13.286045	3.975623
13	6	0	4.741714	14.662223	7.065235
14	1	0	5.261680	15.450025	7.597050
15	6	0	-0.075871	13.286803	4.529567
16	1	0	0.885567	13.584155	4.123056
17	6	0	-2.529347	12.541854	5.594485
18	1	0	-3.483888	12.246434	6.013708
19	6	0	4.988078	14.460818	5.713024
20	1	0	5.698025	15.088125	5.188348
21	6	0	3.158572	12.845220	7.069488
22	1	0	2.447108	12.217436	7.596363
23	6	0	3.827001	13.855355	7.744192
24	1	0	3.639433	14.018464	8.798417
25	6	0	4.765551	9.142257	5.862627
26	1	0	5.074268	10.016686	5.298591
27	6	0	5.694721	8.168105	6.202862
28	1	0	6.725632	8.286787	5.891801
29	6	0	-2.427449	13.718159	4.857711
30	1	0	-3.297546	14.343036	4.700621
31	6	0	3.035644	7.883056	6.995341
32	1	0	2.002955	7.780194	7.297669
33	6	0	5.309688	7.053544	6.941559
34	1	0	6.036774	6.297264	7.209155
35	6	0	3.981027	6.922610	7.334320
36	1	0	3.669261	6.059139	7.909974
37	6	0	-1.194711	14.083570	4.325910
38	1	0	-1.097443	14.997360	3.752206

Total energy E(RM062X) = -1259.01258097 Hartrees

18r

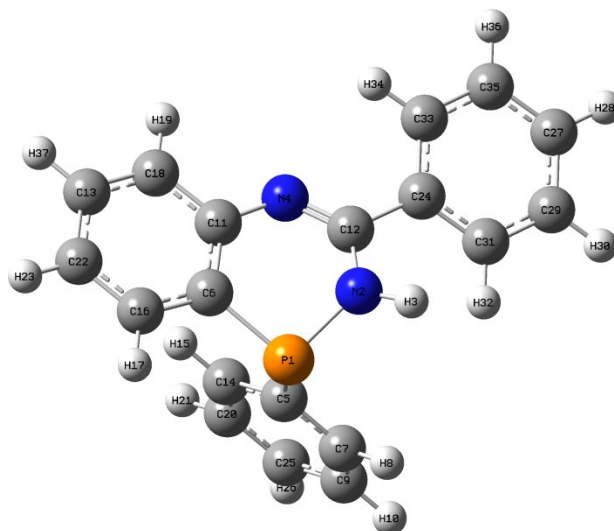


Center Number	Atomic Number	Atomic Type	Coordinates (Angstroms)		
			X	Y	Z
1	15	0	2.706747	11.314424	4.771462
2	8	0	0.614053	9.441986	6.924533

3	7	0	2.693715	9.991790	5.933797
4	7	0	1.076387	11.226579	5.439482
5	6	0	-0.109283	11.919101	5.179624
6	6	0	1.337281	10.105373	6.227112
7	6	0	3.671688	9.087913	6.367854
8	6	0	-1.337285	11.477762	5.683497
9	1	0	-1.376572	10.580174	6.284435
10	6	0	3.444846	12.672953	5.746920
11	6	0	4.279841	13.564255	5.072950
12	1	0	4.468231	13.433257	4.011972
13	6	0	4.628448	14.781795	7.118698
14	1	0	5.088313	15.602322	7.656386
15	6	0	-0.050965	13.081569	4.405536
16	1	0	0.903776	13.430661	4.025236
17	6	0	-2.488277	12.204354	5.403797
18	1	0	-3.436488	11.857665	5.797430
19	6	0	4.872017	14.621402	5.760532
20	1	0	5.519844	15.313495	5.236891
21	6	0	3.203278	12.838396	7.114045
22	1	0	2.556147	12.144056	7.640364
23	6	0	3.794676	13.890508	7.796371
24	1	0	3.610169	14.020748	8.855722
25	6	0	4.999663	9.323496	6.005180
26	1	0	5.267821	10.191937	5.414233
27	6	0	5.965185	8.417136	6.423093
28	1	0	6.999247	8.577195	6.140452
29	6	0	-2.437939	13.358429	4.627675
30	1	0	-3.341811	13.914947	4.414291
31	6	0	3.318302	7.984410	7.141630
32	1	0	2.277950	7.841248	7.386756
33	6	0	5.643619	7.311762	7.195747
34	1	0	6.428966	6.633135	7.494979
35	6	0	4.306060	7.083782	7.586272
36	6	0	-1.212484	13.790581	4.129843
37	1	0	-1.154931	14.688431	3.526330
38	7	0	3.968560	6.011647	8.382357
39	6	0	2.566252	5.692148	8.578242
40	1	0	2.054663	5.460823	7.634881
41	1	0	2.489681	4.829360	9.236055
42	1	0	2.042047	6.522825	9.056462
43	6	0	4.949856	4.965493	8.606523
44	1	0	4.507015	4.195422	9.234140
45	1	0	5.286647	4.502631	7.670042
46	1	0	5.825484	5.357315	9.129476

Total energy E(RM062X) = -1392.95662557 Hartrees

19a

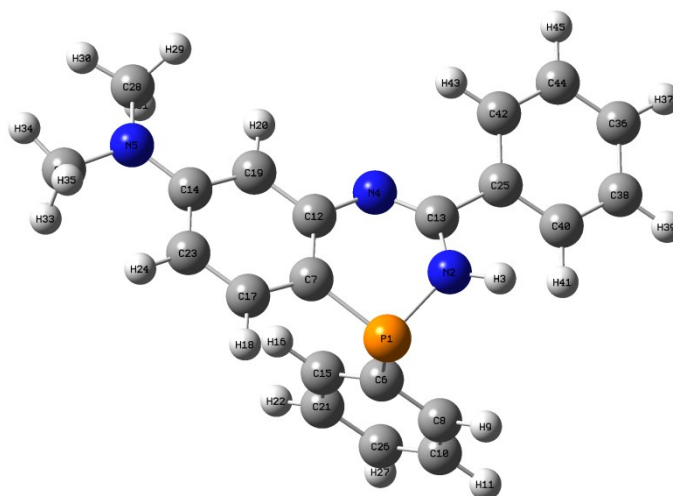


Center Number	Atomic Number	Atomic Type	Coordinates (Angstroms)		
			X	Y	Z
1	15	0	2.959156	2.564956	9.983035
2	7	0	3.433355	1.713119	11.416808
3	1	0	3.692431	0.740585	11.341965
4	7	0	3.152612	3.480573	12.975605
5	6	0	4.468809	3.601249	9.699907
6	6	0	1.890874	3.757960	10.845705
7	6	0	5.578432	2.952111	9.146922
8	1	0	5.518735	1.895602	8.901110
9	6	0	6.758725	3.645308	8.908030
10	1	0	7.612717	3.130066	8.484611
11	6	0	2.144666	4.063170	12.197749
12	6	0	3.695962	2.349647	12.609988
13	6	0	0.315713	5.656301	12.142067
14	6	0	4.555350	4.963890	9.989108
15	1	0	3.704505	5.485976	10.412503
16	6	0	0.845414	4.390216	10.169430
17	1	0	0.655581	4.138732	9.130968
18	6	0	1.341463	5.025852	12.826872
19	1	0	1.548286	5.258051	13.864839
20	6	0	5.734326	5.661571	9.737143
21	1	0	5.791622	6.719114	9.966344
22	6	0	0.061200	5.341967	10.807046
23	1	0	-0.738855	5.836880	10.270717
24	6	0	4.651380	1.673629	13.533803
25	6	0	6.836654	5.004608	9.202001
26	1	0	7.753433	5.549399	9.010519
27	6	0	6.433532	0.437598	15.290252
28	1	0	7.123570	-0.043391	15.973091
29	6	0	6.571512	0.255903	13.918958
30	1	0	7.375190	-0.356947	13.529312
31	6	0	5.682485	0.869550	13.041636
32	1	0	5.815712	0.748459	11.972437
33	6	0	4.525730	1.862295	14.912228
34	1	0	3.727368	2.494321	15.279334
35	6	0	5.410068	1.243665	15.785235
36	1	0	5.301677	1.386985	16.853553

37 1 0 -0.291189 6.397239 12.648908

Total energy E(RM062X) = -1183.78541393 Hartrees

19r

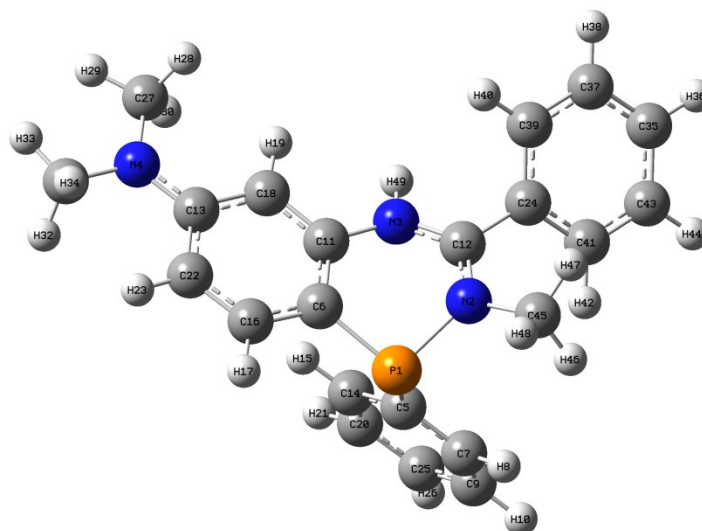


Center Number	Atomic Number	Atomic Type	Coordinates (Angstroms)		
			X	Y	Z
1	15	0	2.942810	2.564857	9.975074
2	7	0	3.428227	1.706741	11.402949
3	1	0	3.700707	0.737850	11.326374
4	7	0	3.164392	3.463417	12.958669
5	7	0	-0.440982	6.618885	12.848897
6	6	0	4.463004	3.594159	9.703435
7	6	0	1.882453	3.739760	10.844978
8	6	0	5.607811	2.933736	9.243890
9	1	0	5.579086	1.861883	9.067956
10	6	0	6.784852	3.634240	9.010479
11	1	0	7.666621	3.110080	8.661178
12	6	0	2.152460	4.057431	12.190400
13	6	0	3.691148	2.345766	12.591298
14	6	0	0.323340	5.686821	12.189781
15	6	0	4.512379	4.973750	9.905220
16	1	0	3.633770	5.500775	10.261175
17	6	0	0.832102	4.393869	10.200297
18	1	0	0.616163	4.156499	9.163067
19	6	0	1.381701	5.024613	12.838004
20	1	0	1.634120	5.237873	13.867101
21	6	0	5.688783	5.678465	9.658994
22	1	0	5.717264	6.749587	9.821264
23	6	0	0.067274	5.353819	10.838323
24	1	0	-0.723652	5.844292	10.289419
25	6	0	4.646695	1.670999	13.512366
26	6	0	6.825444	5.011543	9.216113
27	1	0	7.740178	5.561419	9.029266
28	6	0	-0.021662	7.078649	14.160392
29	1	0	-0.002338	6.252234	14.875090
30	1	0	-0.735873	7.814784	14.521851
31	1	0	0.974728	7.537679	14.139348
32	6	0	-1.380702	7.428574	12.094636

33	1	0	-0.886115	8.021074	11.314713
34	1	0	-1.887427	8.107702	12.776289
35	1	0	-2.141593	6.803855	11.620477
36	6	0	6.433495	0.436556	15.264303
37	1	0	7.125574	-0.044014	15.945375
38	6	0	6.575925	0.265719	13.891668
39	1	0	7.385094	-0.338155	13.499420
40	6	0	5.684366	0.878332	13.017003
41	1	0	5.820200	0.765648	11.947159
42	6	0	4.516383	1.849387	14.891657
43	1	0	3.712677	2.473422	15.261004
44	6	0	5.402746	1.231339	15.762462
45	1	0	5.290572	1.366285	16.831486

 Total energy E(RM062X) = -1317.73063746 Hartrees

19r - X⁺

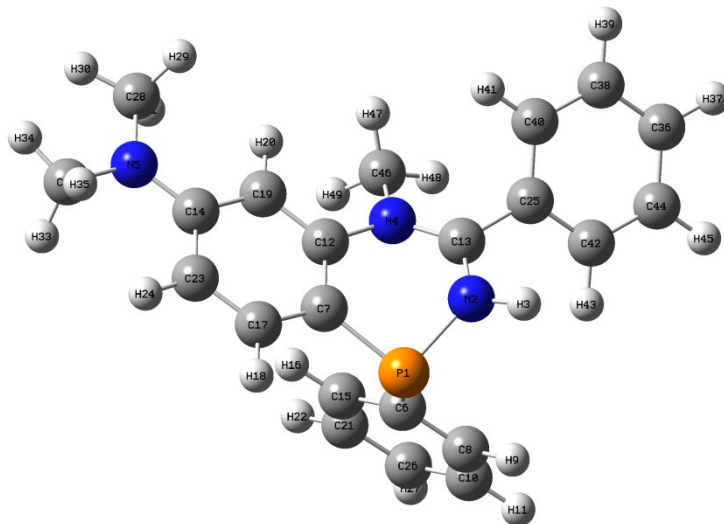


Center Number	Atomic Number	Atomic Type	Coordinates (Angstroms)		
			X	Y	Z
1	15	0	3.219342	2.857512	9.746500
2	7	0	3.710102	1.798110	11.117337
3	7	0	3.220394	3.387068	12.725176
4	7	0	-0.593593	6.322891	12.810057
5	6	0	4.695009	3.960292	9.783842
6	6	0	2.004826	3.813561	10.670116
7	6	0	5.882533	3.432538	9.262650
8	1	0	5.896531	2.425733	8.855725
9	6	0	7.044585	4.193386	9.251761
10	1	0	7.960496	3.775358	8.852310
11	6	0	2.168849	4.036748	12.037704
12	6	0	3.832848	2.263134	12.348527
13	6	0	0.241796	5.502488	12.121542
14	6	0	4.678419	5.271937	10.260601
15	1	0	3.761265	5.702435	10.646921
16	6	0	0.913313	4.425756	10.045477
17	1	0	0.748726	4.261907	8.986083
18	6	0	1.318910	4.853336	12.765781
19	1	0	1.479185	4.964333	13.829628

20	6	0	5.840914	6.037660	10.232393
21	1	0	5.821212	7.056201	10.600698
22	6	0	0.054465	5.254074	10.736998
23	1	0	-0.765796	5.715487	10.207033
24	6	0	4.659963	1.586232	13.370021
25	6	0	7.023092	5.498860	9.736752
26	1	0	7.925626	6.097658	9.719080
27	6	0	-0.383191	6.551181	14.229381
28	1	0	-0.493143	5.626937	14.806396
29	1	0	-1.119809	7.265867	14.585833
30	1	0	0.611873	6.964545	14.419114
31	6	0	-1.728743	6.935117	12.138168
32	1	0	-1.403408	7.587978	11.322973
33	1	0	-2.280339	7.535624	12.856160
34	1	0	-2.405993	6.178777	11.730036
35	6	0	6.254290	0.399090	15.299529
36	1	0	6.877651	-0.066193	16.053069
37	6	0	4.933364	0.719349	15.596429
38	1	0	4.525573	0.498964	16.574608
39	6	0	4.132576	1.323707	14.635366
40	1	0	3.099377	1.565856	14.856600
41	6	0	5.983826	1.259313	13.066820
42	1	0	6.387823	1.485788	12.086300
43	6	0	6.780919	0.673495	14.039182
44	1	0	7.812250	0.432321	13.815733
45	6	0	4.081621	0.415329	10.765539
46	1	0	5.061428	0.387682	10.286930
47	1	0	4.089674	-0.209946	11.654317
48	1	0	3.334168	0.042474	10.067306
49	1	0	3.444654	3.725077	13.653082

Total energy E(RM062X) = -1357.47208216 Hartrees

19r - Y⁺

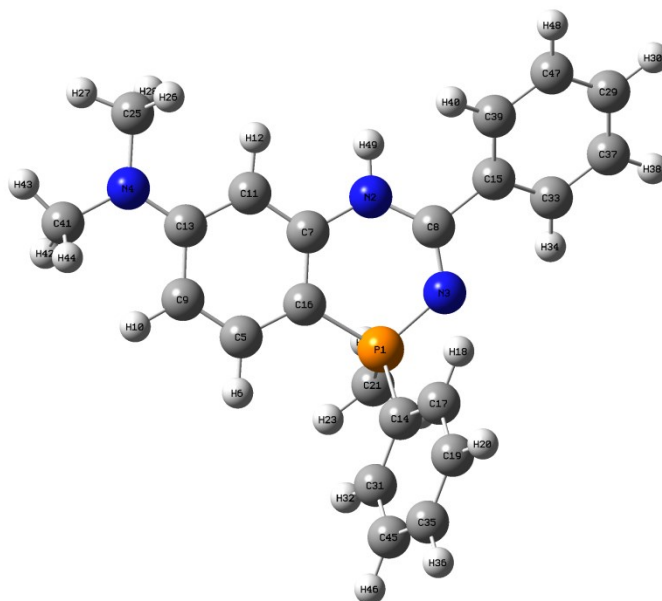


Center Number	Atomic Number	Atomic Type	Coordinates (Angstroms)		
			X	Y	Z
1	15	0	3.334376	2.920641	9.797204
2	7	0	3.725930	1.911573	11.206401
3	1	0	4.010075	0.949843	11.062429

4	7	0	3.290871	3.530523	12.800497
5	7	0	-0.705810	6.247696	12.716636
6	6	0	4.797546	4.041078	9.909879
7	6	0	2.081426	3.864507	10.682443
8	6	0	6.031037	3.509514	9.516723
9	1	0	6.094752	2.482257	9.169204
10	6	0	7.180260	4.288363	9.567977
11	1	0	8.132065	3.866673	9.268625
12	6	0	2.209349	4.109654	12.053836
13	6	0	3.854505	2.376914	12.442444
14	6	0	0.193273	5.472079	12.054966
15	6	0	4.725058	5.372180	10.322723
16	1	0	3.773650	5.804928	10.612068
17	6	0	0.981941	4.415634	10.019603
18	1	0	0.860605	4.228955	8.958165
19	6	0	1.288199	4.891465	12.735977
20	1	0	1.389832	5.035690	13.799698
21	6	0	5.876595	6.154652	10.359203
22	1	0	5.813093	7.187627	10.679377
23	6	0	0.059461	5.207471	10.670524
24	1	0	-0.765107	5.622169	10.109512
25	6	0	4.637799	1.574109	13.403064
26	6	0	7.102839	5.613621	9.989579
27	1	0	7.996799	6.224512	10.022112
28	6	0	-0.545081	6.504109	14.137551
29	1	0	-0.615423	5.582127	14.724452
30	1	0	-1.331569	7.177767	14.466257
31	1	0	0.418411	6.978542	14.347035
32	6	0	-1.856461	6.786905	12.009741
33	1	0	-1.549254	7.457194	11.201500
34	1	0	-2.465698	7.353006	12.708894
35	1	0	-2.472766	5.988664	11.585101
36	6	0	6.104344	-0.007068	15.142734
37	1	0	6.676998	-0.624099	15.824107
38	6	0	4.839634	0.444379	15.515409
39	1	0	4.426334	0.171594	16.477962
40	6	0	4.105509	1.243497	14.652031
41	1	0	3.117901	1.590077	14.932601
42	6	0	5.898003	1.110126	13.020929
43	1	0	6.305559	1.383932	12.054080
44	6	0	6.634732	0.327598	13.901191
45	1	0	7.619448	-0.020610	13.617079
46	6	0	3.730344	4.236528	14.019179
47	1	0	3.054458	4.050314	14.853052
48	1	0	4.730760	3.908064	14.280942
49	1	0	3.749593	5.300616	13.791453

Total energy E(RM062X) = -1357.47074047 Hartrees

22r.H⁺

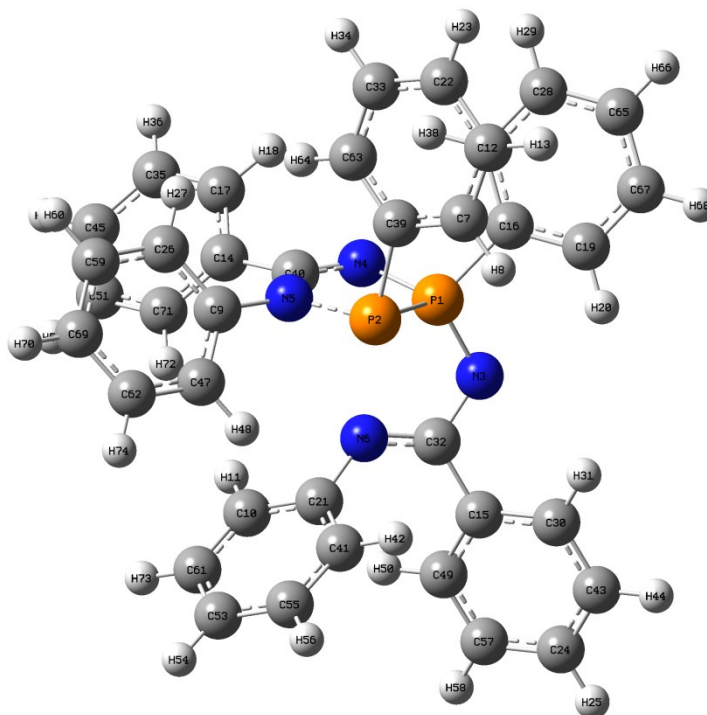


Center Number	Atomic Number	Atomic Type	Coordinates (Angstroms)		
			X	Y	Z
1	15	0	2.102424	5.434590	3.319296
2	7	0	4.899460	4.653967	3.950039
3	7	0	3.371778	6.427316	3.660074
4	7	0	4.466037	-0.015026	2.914841
5	6	0	2.026389	2.709620	2.658423
6	1	0	0.999359	2.855173	2.338780
7	6	0	4.099856	3.589013	3.509838
8	6	0	4.551749	5.962348	3.951441
9	6	0	2.573689	1.452934	2.577467
10	1	0	1.969163	0.640947	2.201735
11	6	0	4.671184	2.327035	3.434751
12	1	0	5.707234	2.211612	3.721741
13	6	0	3.919927	1.223107	2.979236
14	6	0	1.319159	5.997251	1.802724
15	6	0	5.622879	6.922298	4.321422
16	6	0	2.764227	3.802867	3.137414
17	6	0	2.113131	6.600187	0.824538
18	1	0	3.167907	6.769025	1.009406
19	6	0	1.537209	6.997606	-0.374735
20	1	0	2.146770	7.473316	-1.132584
21	6	0	0.897495	5.518225	4.654045
22	1	0	1.411323	5.260383	5.580393
23	1	0	0.089238	4.805419	4.485187
24	1	0	0.496867	6.530584	4.716620
25	6	0	5.847869	-0.221854	3.317200
26	1	0	6.535356	0.356291	2.692040
27	1	0	6.093130	-1.274733	3.211934
28	1	0	6.001230	0.063303	4.362137
29	6	0	7.576882	8.772092	5.029543
30	1	0	8.337734	9.491327	5.307009
31	6	0	-0.044091	5.789807	1.582370
32	1	0	-0.669035	5.331017	2.339405
33	6	0	5.259134	8.124161	4.931557
34	1	0	4.212198	8.320754	5.123781

35	6	0	0.179057	6.787608	-0.598782
36	1	0	-0.266839	7.098688	-1.535567
37	6	0	6.236017	9.041347	5.291824
38	1	0	5.952258	9.967068	5.776579
39	6	0	6.967825	6.656834	4.051134
40	1	0	7.265073	5.752795	3.531589
41	6	0	3.683254	-1.136647	2.416910
42	1	0	2.795771	-1.304971	3.033168
43	1	0	4.295715	-2.033290	2.449400
44	1	0	3.366664	-0.973837	1.382692
45	6	0	-0.609948	6.185431	0.375777
46	1	0	-1.666739	6.027970	0.201227
47	6	0	7.940577	7.583944	4.403966
48	1	0	8.980575	7.381147	4.181613
49	1	0	5.823978	4.419051	4.284000

Total energy E(RM062X) = -1357.48748194 Hartrees

24a



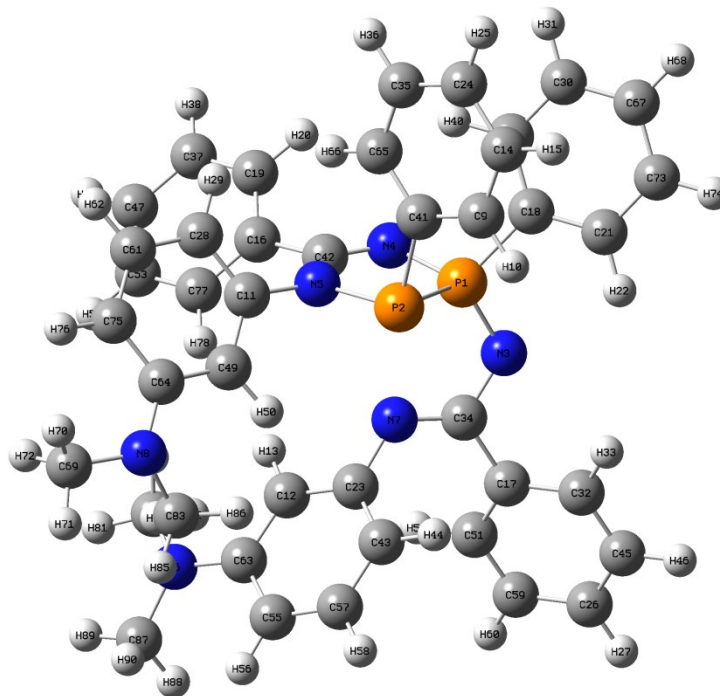
Center Number	Atomic Number	Atomic Type	Coordinates (Angstroms)		
			X	Y	Z
1	15	0	4.119442	2.084693	5.492138
2	15	0	2.944122	3.866839	4.810328
3	7	0	5.112815	1.488639	4.369579
4	7	0	4.773483	2.822710	6.848123
5	7	0	3.812529	4.799700	6.031646
6	7	0	5.791382	3.674126	4.047854
7	6	0	0.470391	2.675222	5.081683
8	1	0	0.635069	2.400579	4.043639
9	6	0	3.623506	6.224614	6.040577
10	6	0	7.090664	5.692532	3.813436
11	1	0	7.526720	5.485435	4.784383
12	6	0	-0.675699	2.236318	5.732885

13	1	0	-1.395566	1.624832	5.202116
14	6	0	5.439448	4.863253	7.899257
15	6	0	6.544124	1.915210	2.474942
16	6	0	3.059697	0.742893	6.035264
17	6	0	5.475083	4.377613	9.205932
18	1	0	4.905257	3.490918	9.456370
19	6	0	2.715420	-0.263595	5.130797
20	1	0	3.170089	-0.277664	4.147469
21	6	0	6.202761	4.756008	3.267870
22	6	0	-0.901750	2.590651	7.060528
23	1	0	-1.798960	2.255211	7.566631
24	6	0	7.915443	0.916883	0.257211
25	1	0	8.447417	0.531107	-0.604349
26	6	0	3.167257	6.874447	7.185332
27	1	0	2.968265	6.308921	8.087527
28	6	0	1.582030	-0.209924	7.679637
29	1	0	1.142486	-0.191440	8.669472
30	6	0	5.989877	0.891205	1.705927
31	1	0	5.025759	0.487007	1.989326
32	6	0	5.801076	2.432138	3.668540
33	6	0	0.025010	3.379559	7.732788
34	1	0	-0.147763	3.661163	8.764811
35	6	0	6.235784	5.029901	10.168813
36	1	0	6.249089	4.658802	11.186257
37	6	0	2.497047	0.768639	7.312017
38	1	0	2.777258	1.548508	8.010078
39	6	0	1.418864	3.446816	5.760859
40	6	0	4.643766	4.114580	6.886282
41	6	0	5.637595	5.017520	2.011741
42	1	0	4.938313	4.302386	1.591999
43	6	0	6.666681	0.402919	0.593889
44	1	0	6.223640	-0.383642	-0.005310
45	6	0	6.986172	6.149446	9.822515
46	1	0	7.585190	6.653356	10.571402
47	6	0	3.890777	6.950594	4.880625
48	1	0	4.254062	6.436602	3.997251
49	6	0	7.798968	2.424978	2.134527
50	1	0	8.243536	3.206820	2.738343
51	6	0	6.973311	6.617577	8.511533
52	1	0	7.567177	7.480385	8.235977
53	6	0	6.834053	7.113542	1.877557
54	1	0	7.072849	8.025075	1.343569
55	6	0	5.951621	6.186647	1.327888
56	1	0	5.499320	6.376719	0.361166
57	6	0	8.483711	1.922408	1.034721
58	1	0	9.461835	2.315310	0.784526
59	6	0	3.005830	8.254980	7.175323
60	1	0	2.661834	8.757579	8.070912
61	6	0	7.405948	6.855318	3.121689
62	6	0	3.714823	8.329533	4.876113
63	6	0	1.185389	3.800093	7.089469
64	1	0	1.914562	4.387438	7.633769
65	6	0	1.231679	-1.210156	6.776852
66	1	0	0.515470	-1.970358	7.065217
67	6	0	1.801912	-1.241138	5.507165
68	1	0	1.534964	-2.025956	4.810101
69	6	0	3.277442	8.985609	6.022762
70	1	0	3.146721	10.060742	6.018019
71	6	0	6.194901	5.984321	7.550751

72	1	0	6.178725	6.357177	6.533432
73	1	0	8.097111	7.566936	3.558834
74	1	0	3.930975	8.889912	3.974555

Total energy E(RM062X) = -2367.56110040 Hartrees

24r



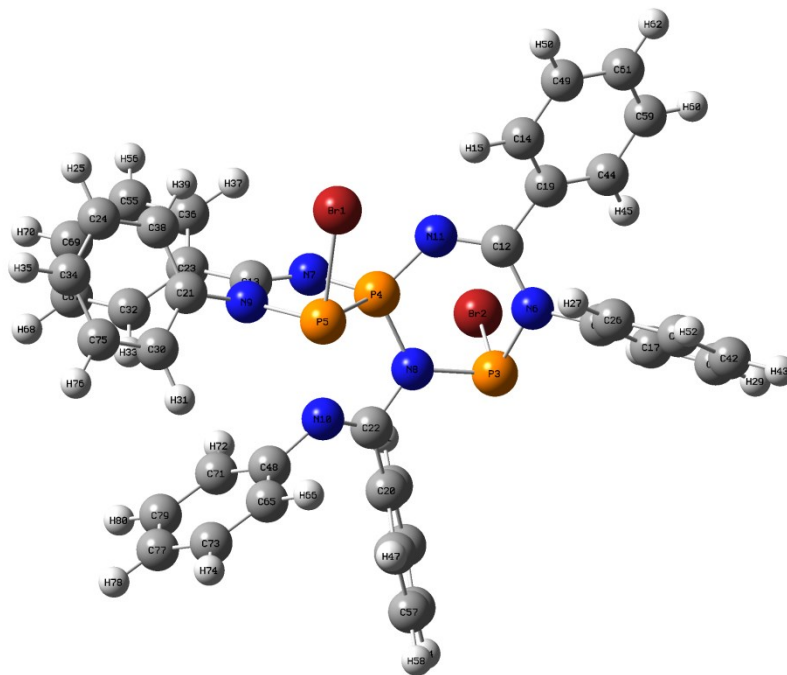
Center Number	Atomic Number	Atomic Type	Coordinates (Angstroms)		
			X	Y	Z
1	15	0	4.061416	2.161728	5.456888
2	15	0	2.841603	3.949909	4.871947
3	7	0	5.031515	1.596799	4.303331
4	7	0	4.766544	2.865278	6.805014
5	7	0	3.742531	4.849645	6.094662
6	7	0	8.402000	7.743725	3.448756
7	7	0	5.663330	3.795400	3.911714
8	7	0	3.834036	9.203340	3.952380
9	6	0	0.368943	2.763686	5.162657
10	1	0	0.486886	2.566915	4.100909
11	6	0	3.513777	6.268881	6.180023
12	6	0	7.048710	5.737056	3.635784
13	1	0	7.338414	5.586321	4.667166
14	6	0	-0.755209	2.287934	5.826962
15	1	0	-1.503580	1.724102	5.283005
16	6	0	5.439372	4.886480	7.893440
17	6	0	6.513600	1.977945	2.451602
18	6	0	3.034138	0.792691	5.998491
19	6	0	5.551831	4.356816	9.178091
20	1	0	5.015973	3.448031	9.424165
21	6	0	2.655072	-0.181731	5.072823
22	1	0	3.057163	-0.149960	4.067221
23	6	0	6.162152	4.810020	3.082809

24	6	0	-0.923366	2.546723	7.184708
25	1	0	-1.803703	2.183950	7.701519
26	6	0	7.989839	0.890227	0.345009
27	1	0	8.562213	0.470681	-0.473868
28	6	0	2.995331	6.830892	7.342267
29	1	0	2.792965	6.222333	8.213331
30	6	0	1.661206	-0.250906	7.678396
31	1	0	1.276490	-0.280313	8.690568
32	6	0	5.979601	0.951279	1.672789
33	1	0	4.989101	0.578713	1.904169
34	6	0	5.712859	2.537242	3.591217
35	6	0	0.039790	3.275664	7.873996
36	1	0	-0.087044	3.481330	8.930368
37	6	0	6.344796	4.993561	10.125472
38	1	0	6.417668	4.587353	11.126867
39	6	0	2.541088	0.756941	7.303022
40	1	0	2.848831	1.511288	8.017384
41	6	0	1.352751	3.476162	5.855694
42	6	0	4.616070	4.153723	6.890756
43	6	0	5.739614	4.957176	1.755707
44	1	0	5.033400	4.251425	1.335176
45	6	0	6.708327	0.419506	0.614382
46	1	0	6.279597	-0.367652	0.005510
47	6	0	7.050861	6.142888	9.783986
48	1	0	7.675032	6.634588	10.520319
49	6	0	3.813406	7.042467	5.066528
50	1	0	4.245140	6.544211	4.208122
51	6	0	7.801169	2.444693	2.178845
52	1	0	8.226418	3.233971	2.787441
53	6	0	6.959866	6.657411	8.493515
54	1	0	7.516805	7.546189	8.222126
55	6	0	7.187162	6.890421	1.519679
56	1	0	7.577996	7.674033	0.886440
57	6	0	6.273609	5.987422	0.992049
58	1	0	5.974535	6.092538	-0.045175
59	6	0	8.537740	1.897191	1.135529
60	1	0	9.539996	2.258150	0.937790
61	6	0	2.788048	8.204273	7.362883
62	1	0	2.401483	8.671669	8.260795
63	6	0	7.571201	6.797173	2.873931
64	6	0	3.577131	8.431690	5.072157
65	6	0	1.177664	3.731197	7.215470
66	1	0	1.937456	4.267295	7.770104
67	6	0	1.275550	-1.218398	6.754854
68	1	0	0.586569	-2.001134	7.049206
69	6	0	3.759482	10.647532	4.090773
70	1	0	2.763336	10.951621	4.415178
71	1	0	3.942494	11.099433	3.117697
72	1	0	4.495716	11.042519	4.805185
73	6	0	1.775956	-1.187528	5.455911
74	1	0	1.481774	-1.946739	4.741630
75	6	0	3.065528	8.997144	6.258812
76	1	0	2.890679	10.060847	6.328731
77	6	0	6.149303	6.038731	7.550035
78	1	0	6.068765	6.447278	6.549395
79	6	0	8.969964	7.466167	4.755277
80	1	0	8.181372	7.363378	5.504612
81	1	0	9.599992	8.302043	5.052125
82	1	0	9.573091	6.548491	4.766290

83	6	0	4.838124	8.724889	3.010616
84	1	0	5.838494	8.685282	3.462350
85	1	0	4.864420	9.398017	2.154414
86	1	0	4.593556	7.731818	2.633490
87	6	0	9.127559	8.651016	2.577865
88	1	0	9.775919	8.122531	1.866524
89	1	0	9.743358	9.308619	3.187827
90	1	0	8.435339	9.277664	2.010588

Total energy E(RM062X) = -2635.45192718 Hartrees

25a.Br



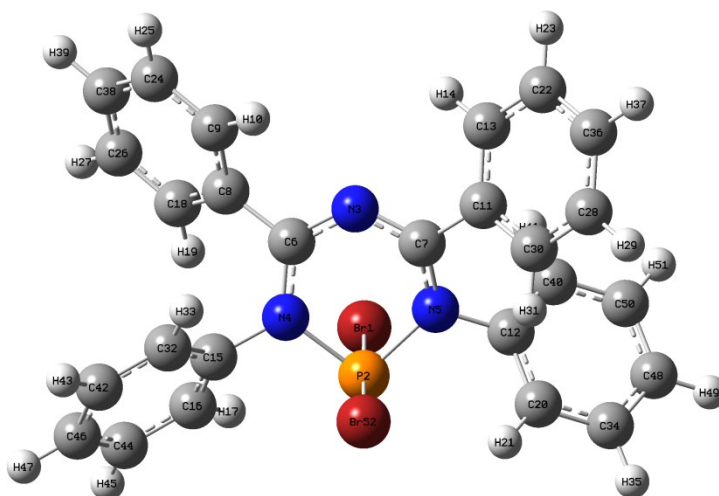
Center Number	Atomic Number	Atomic Type	Coordinates (Angstroms)		
			X	Y	Z
1	35	0	12.056950	14.753654	5.634350
2	35	0	5.645432	14.016724	7.973267
3	15	0	6.163451	15.536486	6.367236
4	15	0	8.792554	14.091283	5.972650
5	15	0	10.177241	14.368085	4.246366
6	7	0	7.348360	16.454899	7.258498
7	7	0	8.856376	12.460488	6.075025
8	7	0	7.257342	14.582902	5.410716
9	7	0	10.324738	12.614841	4.249866
10	7	0	8.021604	13.895336	3.403152
11	7	0	9.062255	14.834773	7.375602
12	6	0	8.497368	15.927125	7.804382
13	6	0	9.615360	11.887338	5.174938
14	6	0	10.511300	16.600130	9.056781
15	1	0	11.095712	16.148056	8.264029
16	6	0	7.030187	17.861598	7.391580
17	6	0	5.793669	18.248826	7.896592
18	1	0	5.080505	17.504591	8.235211
19	6	0	9.117585	16.595719	8.965140
20	6	0	5.588451	14.248504	3.607453

21	6	0	11.424356	12.060578	3.495291
22	6	0	6.990340	14.232101	4.072658
23	6	0	9.675558	10.407923	5.157628
24	6	0	13.540613	10.935147	3.441283
25	1	0	14.369046	10.470032	3.960515
26	6	0	7.965130	18.804217	6.977911
27	1	0	8.917948	18.480434	6.575691
28	6	0	5.495162	19.603101	7.994435
29	1	0	4.535220	19.910293	8.389523
30	6	0	11.409083	12.141445	2.107201
31	1	0	10.565142	12.593568	1.598148
32	6	0	9.678367	9.689067	3.958814
33	1	0	9.664201	10.206481	3.007405
34	6	0	13.532866	11.000751	2.050611
35	1	0	14.355638	10.581039	1.485259
36	6	0	9.660666	9.735765	6.381167
37	1	0	9.638562	10.307374	7.300433
38	6	0	12.490268	11.476137	4.171553
39	1	0	12.486003	11.442940	5.254708
40	6	0	4.624412	13.540279	4.329492
41	1	0	4.907184	12.974805	5.210723
42	6	0	6.430529	20.555518	7.603398
43	1	0	6.197823	21.609349	7.690190
44	6	0	8.338303	17.147652	9.986193
45	1	0	7.257544	17.112999	9.929619
46	6	0	5.243774	14.942922	2.447166
47	1	0	5.999157	15.489123	1.895502
48	6	0	7.992208	13.335121	2.102036
49	6	0	11.124826	17.190823	10.152525
50	1	0	12.205197	17.213282	10.218410
51	6	0	7.664374	20.154874	7.098996
52	1	0	8.392808	20.893539	6.789300
53	6	0	2.957581	14.239081	2.739374
54	1	0	1.929087	14.238274	2.400160
55	6	0	9.686005	8.347891	6.405277
56	1	0	9.694189	7.826817	7.354265
57	6	0	3.921973	14.943237	2.022805
58	1	0	3.644546	15.491916	1.131816
59	6	0	8.959159	17.710611	11.090971
60	1	0	8.359515	18.123190	11.892272
61	6	0	10.349932	17.744465	11.167949
62	1	0	10.830118	18.198158	12.026434
63	6	0	3.308212	13.533216	3.886355
64	1	0	2.559707	12.975709	4.434701
65	6	0	8.459979	14.081572	1.022478
66	1	0	8.752120	15.114751	1.171206
67	6	0	9.675220	8.301713	3.992097
68	1	0	9.663060	7.743793	3.064332
69	6	0	9.691602	7.631101	5.212418
70	1	0	9.703017	6.548150	5.232621
71	6	0	7.628019	11.999360	1.943574
72	1	0	7.276920	11.435020	2.800999
73	6	0	8.551275	13.482767	-0.229453
74	1	0	8.909008	14.060555	-1.072643
75	6	0	12.472263	11.608754	1.386458
76	1	0	12.463461	11.661946	0.304938
77	6	0	8.195224	12.147257	-0.397347
78	1	0	8.277198	11.683050	-1.372038
79	6	0	7.731729	11.409652	0.688603

80 1 0 7.452034 10.370854 0.562458

Total energy E(RM062X) = -8004.76011819 Hartrees

26a

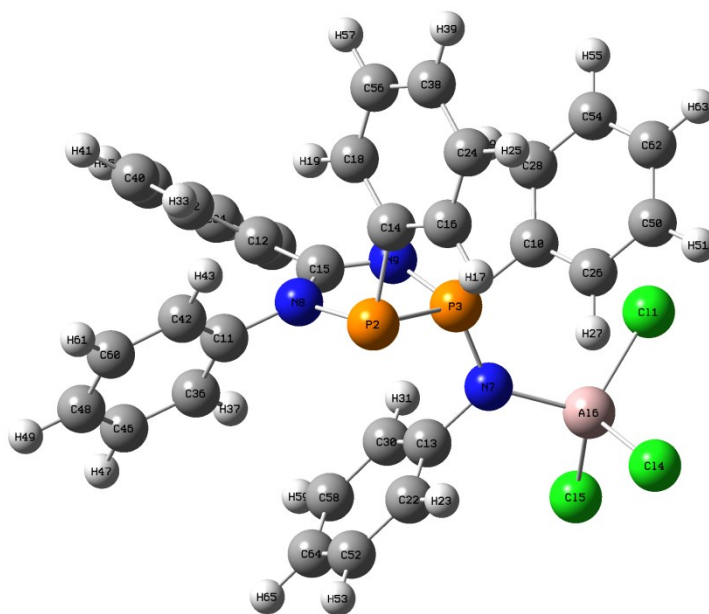


Center Number	Atomic Number	Atomic Type	Coordinates (Angstroms)		
			X	Y	Z
1	35	0	2.472162	6.549264	9.985362
2	15	0	2.890691	6.537822	7.411750
3	7	0	3.045525	3.454911	7.469835
4	7	0	1.656299	5.316273	7.198883
5	7	0	4.239621	5.455143	7.673218
6	6	0	1.850670	4.018186	7.493439
7	6	0	4.177606	4.134199	7.425436
8	6	0	0.711528	3.146059	7.830945
9	6	0	0.723541	1.816144	7.404635
10	1	0	1.543980	1.462173	6.793403
11	6	0	5.400011	3.370336	7.118332
12	6	0	5.439002	6.103844	8.144623
13	6	0	5.522816	2.062340	7.592285
14	1	0	4.741461	1.648759	8.217190
15	6	0	0.397845	5.824874	6.709786
16	6	0	-0.188695	6.927915	7.319734
17	1	0	0.260099	7.368812	8.202998
18	6	0	-0.327543	3.623418	8.636342
19	1	0	-0.312004	4.645881	8.994287
20	6	0	5.917197	7.235851	7.494614
21	1	0	5.430933	7.597856	6.595437
22	6	0	6.649879	1.319213	7.269400
23	1	0	6.758246	0.311570	7.650291
24	6	0	-0.321921	0.973788	7.756772
25	1	0	-0.326127	-0.052710	7.412589
26	6	0	-1.354281	2.767303	9.004745
27	1	0	-2.151102	3.127767	9.642805
28	6	0	7.496540	3.162724	5.956276
29	1	0	8.253903	3.579487	5.304583
30	6	0	6.386576	3.921920	6.294679
31	1	0	6.266872	4.923584	5.899560
32	6	0	-0.173407	5.225564	5.591421

33	1	0	0.323687	4.388282	5.116231
34	6	0	7.052216	7.868701	7.992814
35	1	0	7.434450	8.748240	7.490406
36	6	0	7.634497	1.868087	6.452554
37	1	0	8.509891	1.283762	6.196175
38	6	0	-1.358438	1.448221	8.555928
39	1	0	-2.169732	0.787093	8.835546
40	6	0	6.061421	5.604925	9.284714
41	1	0	5.646017	4.741322	9.790281
42	6	0	-1.369637	5.724385	5.096884
43	1	0	-1.822738	5.261716	4.229198
44	6	0	-1.380274	7.428136	6.803104
45	1	0	-1.846286	8.284182	7.274384
46	6	0	-1.973607	6.825603	5.700321
47	1	0	-2.903516	7.215500	5.305601
48	6	0	7.697235	7.367813	9.117179
49	1	0	8.583319	7.860758	9.497260
50	6	0	7.201273	6.235919	9.760830
51	1	0	7.693953	5.851970	10.645201
52	35	0	3.311249	6.485515	4.841232

Total energy E(RM062X) = -6656.63823450 Hartrees

27a.AICl3

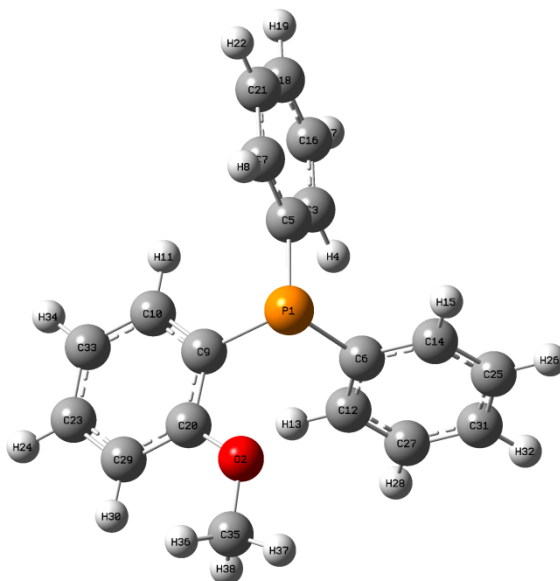


Center Number	Atomic Number	Atomic Type	Coordinates (Angstroms)		
			X	Y	Z
1	17	0	6.939607	2.719913	12.122783
2	15	0	11.306731	3.303786	7.983718
3	15	0	9.608121	3.582307	9.419993
4	17	0	9.606455	0.426442	12.453273
5	17	0	9.649849	3.422464	14.228140
6	13	0	9.057148	2.507157	12.380876
7	7	0	10.007292	3.351830	10.988307
8	7	0	11.379061	5.061706	7.930806
9	7	0	9.331441	5.188377	9.069127
10	6	0	8.209406	2.579989	8.962064

11	6	0	12.667827	5.649564	7.676692
12	6	0	10.264947	7.247302	8.271869
13	6	0	11.235291	4.029220	11.357430
14	6	0	10.202311	2.963214	6.550918
15	6	0	10.312654	5.775648	8.450059
16	6	0	9.953254	1.615770	6.275032
17	1	0	10.432721	0.838762	6.862588
18	6	0	9.595754	3.952309	5.776577
19	1	0	9.787832	5.001188	5.971217
20	6	0	9.689821	8.017137	9.284452
21	1	0	9.316772	7.525542	10.173943
22	6	0	12.453646	3.358011	11.279822
23	1	0	12.472216	2.330064	10.935753
24	6	0	9.077916	1.263444	5.254614
25	1	0	8.880157	0.217674	5.053522
26	6	0	8.259277	1.202598	9.190697
27	1	0	9.116126	0.751100	9.679087
28	6	0	7.128129	3.163372	8.302773
29	1	0	7.113756	4.231945	8.125137
30	6	0	11.188428	5.347403	11.812524
31	1	0	10.228099	5.844884	11.882905
32	6	0	10.724386	7.860208	7.103026
33	1	0	11.156424	7.268086	6.305787
34	6	0	9.602912	9.395651	9.142457
35	1	0	9.170062	9.992360	9.935562
36	6	0	13.303058	6.387822	8.669078
37	1	0	12.816799	6.526188	9.628055
38	6	0	8.466439	2.252577	4.489983
39	1	0	7.787100	1.978078	3.692246
40	6	0	10.613468	9.236072	6.957019
41	1	0	10.958427	9.708370	6.045832
42	6	0	13.282260	5.424997	6.448736
43	1	0	12.769675	4.844802	5.688497
44	6	0	10.063870	10.005268	7.979358
45	1	0	9.990146	11.080079	7.866170
46	6	0	14.555971	6.932826	8.415138
47	1	0	15.051970	7.512372	9.184187
48	6	0	15.175960	6.722529	7.186634
49	1	0	16.154811	7.144091	6.994557
50	6	0	7.196491	0.409065	8.783240
51	1	0	7.221508	-0.657868	8.965324
52	6	0	13.624702	4.006935	11.663651
53	1	0	14.570289	3.482116	11.605734
54	6	0	6.072430	2.357032	7.894970
55	1	0	5.223058	2.799517	7.389890
56	6	0	8.733753	3.593895	4.745624
57	1	0	8.265790	4.365612	4.146669
58	6	0	12.358894	5.984670	12.207045
59	1	0	12.316895	7.002617	12.575636
60	6	0	14.541411	5.963136	6.207912
61	1	0	15.022655	5.792898	5.252879
62	6	0	6.105589	0.986993	8.138568
63	1	0	5.277665	0.364691	7.821188
64	6	0	13.578695	5.315935	12.131062
65	1	0	14.490294	5.814157	12.437888

Total energy E(RM062X) = -3666.41433835 Hartrees

33a

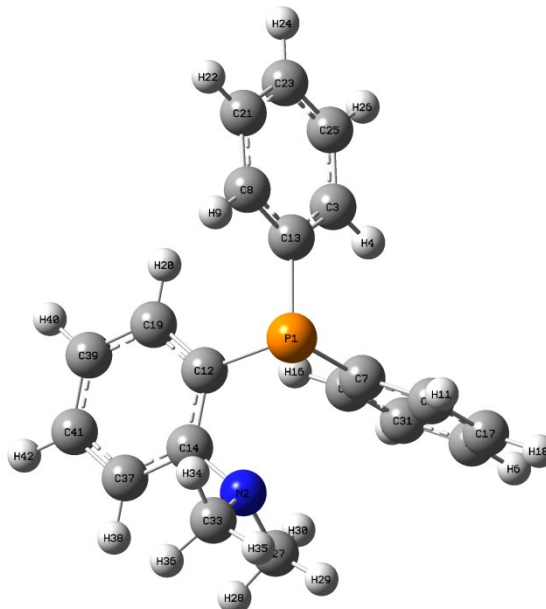


Center Number	Atomic Number	Atomic Type	Coordinates (Angstroms)		
			X	Y	Z
1	15	0	12.150100	-1.765000	14.338600
2	8	0	10.099100	-3.746800	14.209600
3	6	0	14.466000	-0.589500	15.259100
4	1	0	14.210300	-0.896600	16.100400
5	6	0	13.675500	-0.851000	14.149400
6	6	0	11.765200	-1.912300	16.079300
7	6	0	14.070100	-0.399600	12.892200
8	1	0	13.542400	-0.575300	12.146700
9	6	0	12.303000	-3.379700	13.582100
10	6	0	13.515500	-3.759400	12.982300
11	1	0	14.237300	-3.172900	12.967000
12	6	0	11.951400	-3.117900	16.725200
13	1	0	12.233300	-3.866300	16.249900
14	6	0	11.361100	-0.774900	16.784600
15	1	0	11.239600	0.038700	16.351500
16	6	0	15.642100	0.134500	15.107700
17	1	0	16.170700	0.321300	15.849300
18	6	0	16.027200	0.577400	13.856200
19	1	0	16.818300	1.060200	13.762300
20	6	0	11.195200	-4.231700	13.601300
21	6	0	15.253600	0.312300	12.754200
22	1	0	15.521100	0.609500	11.914800
23	6	0	12.557700	-5.855100	12.449500
24	1	0	12.655300	-6.700800	12.077700
25	6	0	11.145800	-0.891200	18.147200
26	1	0	10.878900	-0.146300	18.634000
27	6	0	11.712300	-3.203300	18.091600
28	1	0	11.819600	-4.014300	18.532400
29	6	0	11.319700	-5.509100	13.024400
30	1	0	10.605700	-6.105800	13.020600
31	6	0	11.320000	-2.090700	18.789200
32	1	0	11.171300	-2.149600	19.705300
33	6	0	13.624500	-4.999600	12.418800
34	1	0	14.420000	-5.261500	12.014500
35	6	0	8.965000	-4.618600	14.392800

36	1	0	8.567300	-4.809500	13.540000
37	1	0	8.319300	-4.188700	14.958200
38	1	0	9.253300	-5.437500	14.801000

Total energy E(RM062X)= -1150.67868467 Hartrees

33b

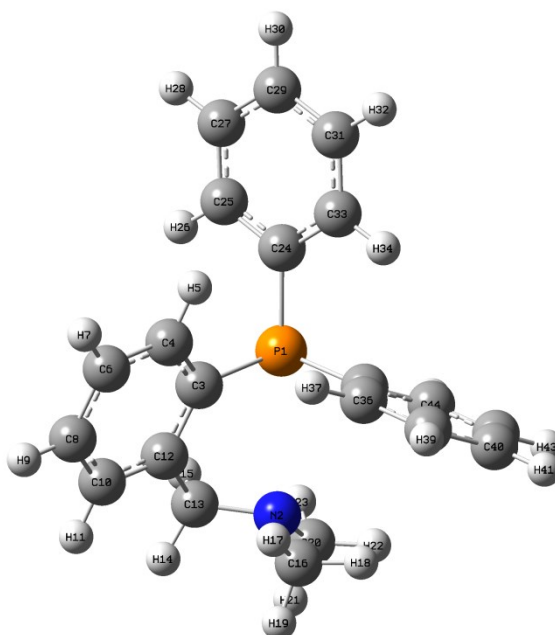


Center Number	Atomic Number	Atomic Type	Coordinates (Angstroms)		
			X	Y	Z
1	15	0	-0.993027	4.441615	4.083804
2	7	0	0.888099	2.261506	3.867163
3	6	0	-3.573367	5.521379	3.371243
4	1	0	-3.377605	5.235391	2.344620
5	6	0	-0.800932	3.964110	-0.529589
6	1	0	-0.733363	3.856292	-1.605806
7	6	0	-0.968637	4.232341	2.251019
8	6	0	-2.907751	5.651722	5.678598
9	1	0	-2.175605	5.469215	6.459969
10	6	0	-0.095650	5.032471	1.512628
11	1	0	0.530659	5.755440	2.024624
12	6	0	-1.388024	2.706816	4.587293
13	6	0	-2.630913	5.251253	4.365404
14	6	0	-0.348854	1.781484	4.417059
15	6	0	-1.758433	3.293639	1.580251
16	1	0	-2.434495	2.657758	2.143385
17	6	0	-0.011673	4.900427	0.128839
18	1	0	0.674061	5.524003	-0.432661
19	6	0	-2.602245	2.276510	5.124410
20	1	0	-3.416781	2.979725	5.254811
21	6	0	-4.107064	6.277449	5.996326
22	1	0	-4.307329	6.572384	7.019776
23	6	0	-5.041652	6.537679	4.997059
24	1	0	-5.973187	7.035262	5.239167
25	6	0	-4.768780	6.164010	3.686166
26	1	0	-5.488629	6.369492	2.902290
27	6	0	1.276872	1.588432	2.633225
28	1	0	1.559828	0.535564	2.786802

29	1	0	2.132774	2.112368	2.201438
30	1	0	0.451459	1.633076	1.920603
31	6	0	-1.677321	3.162098	0.198169
32	1	0	-2.293764	2.430330	-0.310874
33	6	0	1.964814	2.267203	4.851941
34	1	0	1.650132	2.830319	5.732354
35	1	0	2.838943	2.758917	4.420030
36	1	0	2.256285	1.253410	5.167792
37	6	0	-0.533440	0.449169	4.779420
38	1	0	0.276065	-0.260641	4.644439
39	6	0	-2.780417	0.943782	5.486508
40	1	0	-3.729411	0.620553	5.898006
41	6	0	-1.747631	0.028924	5.313581
42	1	0	-1.886309	-1.008877	5.592620

Total energy E(RM062X)= -1170.10491447 Hartrees

33c

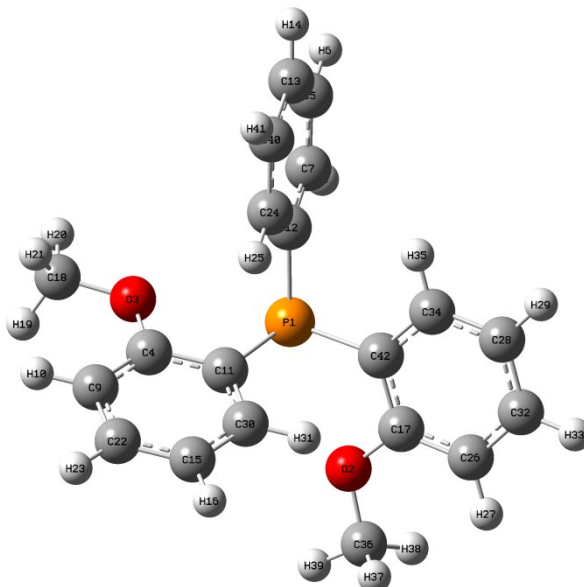


Center Number	Atomic Number	Atomic Type	Coordinates (Angstroms)		
			X	Y	Z
1	15	0	4.862035	9.592297	3.329554
2	7	0	7.148426	11.165806	2.567957
3	6	0	4.185215	11.195420	2.675815
4	6	0	2.876010	11.316396	2.202733
5	1	0	2.226593	10.448156	2.191311
6	6	0	2.384523	12.536224	1.744703
7	1	0	1.367315	12.603017	1.377180
8	6	0	3.201266	13.659060	1.758394
9	1	0	2.829199	14.612263	1.401468
10	6	0	4.506472	13.552075	2.228449
11	1	0	5.150988	14.425041	2.234523
12	6	0	5.008321	12.338383	2.691838
13	6	0	6.428696	12.255505	3.204397
14	1	0	6.932030	13.227800	3.066687
15	1	0	6.406198	12.049003	4.280332

16	6	0	7.387287	11.398375	1.155294
17	1	0	6.444324	11.619626	0.650996
18	1	0	7.802906	10.491265	0.707726
19	1	0	8.084709	12.235721	0.982062
20	6	0	8.369521	10.822244	3.269587
21	1	0	9.104038	11.645327	3.268681
22	1	0	8.827673	9.953406	2.790646
23	1	0	8.137141	10.562494	4.305152
24	6	0	3.282396	8.655055	3.576511
25	6	0	2.499400	9.014926	4.681427
26	1	0	2.817067	9.835541	5.318402
27	6	0	1.318615	8.343043	4.969029
28	1	0	0.722041	8.641393	5.823379
29	6	0	0.908253	7.279620	4.166946
30	1	0	-0.008661	6.748735	4.393718
31	6	0	1.685783	6.900574	3.079655
32	1	0	1.376919	6.070844	2.454249
33	6	0	2.863823	7.584930	2.783645
34	1	0	3.454676	7.280019	1.927930
35	6	0	5.514797	8.797621	1.797875
36	6	0	5.001151	9.042440	0.523359
37	1	0	4.164235	9.721555	0.398826
38	6	0	5.562863	8.430782	-0.593887
39	1	0	5.156846	8.631743	-1.578689
40	6	0	6.644041	7.566510	-0.448905
41	1	0	7.083093	7.093609	-1.319452
42	6	0	7.160193	7.313552	0.818840
43	1	0	8.001940	6.641421	0.938859
44	6	0	6.599096	7.928366	1.934201
45	1	0	7.014847	7.742618	2.919600

Total energy E(RM062X) = -1209.41175349 Hartrees

33d

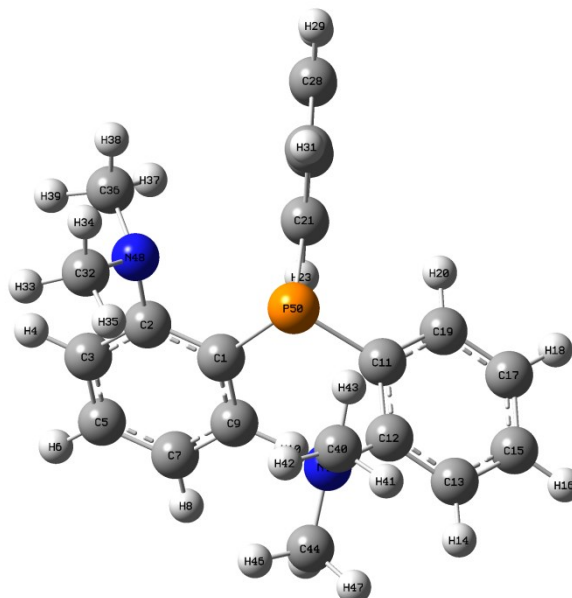


Center Number	Atomic Number	Atomic Type	Coordinates (Angstroms)		
			X	Y	Z
1	15	0	-2.273369	1.503995	5.964225

2	8	0	-4.053816	1.229113	8.181669
3	8	0	-2.723814	3.531984	4.018844
4	6	0	-2.691779	4.146557	5.228178
5	6	0	0.887921	0.318577	3.642515
6	1	0	1.092094	-0.517116	2.983519
7	6	0	-0.345853	0.414127	4.280848
8	1	0	-1.100060	-0.348204	4.113341
9	6	0	-2.873750	5.516132	5.406557
10	1	0	-3.062162	6.165711	4.562618
11	6	0	-2.443035	3.305108	6.328573
12	6	0	-0.624289	1.483161	5.134558
13	6	0	1.851700	1.300846	3.843558
14	1	0	2.810107	1.232337	3.342465
15	6	0	-2.571807	5.240516	7.786465
16	1	0	-2.520838	5.661086	8.783086
17	6	0	-2.853900	0.732035	8.574651
18	6	0	-2.934217	4.329916	2.866280
19	1	0	-3.906148	4.829329	2.906632
20	1	0	-2.911067	3.647069	2.020966
21	1	0	-2.141641	5.075161	2.756758
22	6	0	-2.816109	6.054613	6.690678
23	1	0	-2.961916	7.120175	6.823588
24	6	0	0.351598	2.463413	5.333277
25	1	0	0.148664	3.298634	5.995438
26	6	0	-2.618767	0.167666	9.826067
27	1	0	-3.410978	0.088974	10.558133
28	6	0	-0.314755	-0.216206	9.212151
29	1	0	0.674095	-0.584891	9.454658
30	6	0	-2.384527	3.871587	7.597362
31	1	0	-2.180715	3.238745	8.453758
32	6	0	-1.344916	-0.306245	10.135748
33	1	0	-1.169273	-0.747613	11.109790
34	6	0	-0.557418	0.357929	7.964349
35	1	0	0.250054	0.428512	7.244880
36	6	0	-5.124901	1.210283	9.110413
37	1	0	-4.874136	1.786656	10.005222
38	1	0	-5.383311	0.185876	9.391805
39	1	0	-5.968161	1.672642	8.603971
40	6	0	1.580649	2.374205	4.688781
41	1	0	2.329492	3.141675	4.847469
42	6	0	-1.818246	0.841029	7.626155

Total energy E(RM062X)= -1265.19251002 Hartrees

33e

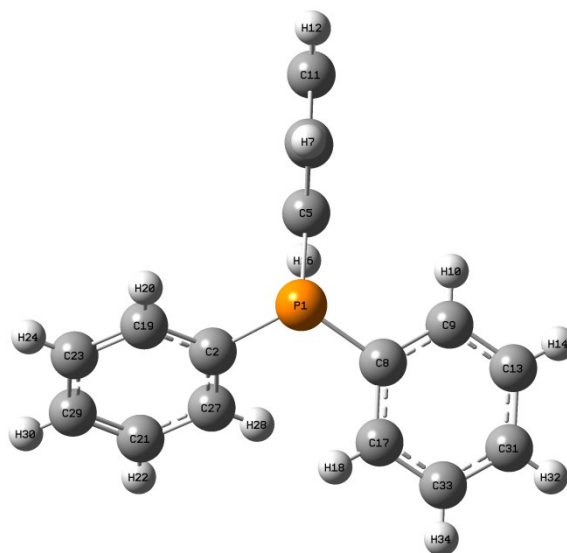


Center Number	Atomic Number	Atomic Type	Coordinates (Angstroms)		
			X	Y	Z
1	6	0	-12.798183	-19.612287	-19.457893
2	6	0	-12.876916	-18.545693	-20.361991
3	6	0	-13.478201	-18.725539	-21.607556
4	1	0	-13.532860	-17.891517	-22.299767
5	6	0	-14.003637	-19.962843	-21.961578
6	1	0	-14.467392	-20.098211	-22.931749
7	6	0	-13.927083	-21.025709	-21.066622
8	1	0	-14.327997	-21.995336	-21.338265
9	6	0	-13.326324	-20.850836	-19.823456
10	1	0	-13.256114	-21.690885	-19.141840
11	6	0	-11.898458	-20.902405	-17.065764
12	6	0	-13.112244	-21.430766	-16.583889
13	6	0	-13.134457	-22.689557	-15.985833
14	1	0	-14.073546	-23.102054	-15.635081
15	6	0	-11.958254	-23.417296	-15.825998
16	1	0	-11.988930	-24.394530	-15.358560
17	6	0	-10.751442	-22.881810	-16.254279
18	1	0	-9.829462	-23.435665	-16.123338
19	6	0	-10.725780	-21.632887	-16.871835
20	1	0	-9.779825	-21.235750	-17.219891
21	6	0	-10.238592	-19.057319	-18.498018
22	6	0	-9.723160	-19.896560	-19.490792
23	1	0	-10.331021	-20.710558	-19.873390
24	6	0	-8.444462	-19.692854	-19.996103
25	1	0	-8.056654	-20.350685	-20.765259
26	6	0	-7.665775	-18.640250	-19.519118
27	1	0	-6.671736	-18.476475	-19.918655
28	6	0	-8.168458	-17.800333	-18.531504
29	1	0	-7.568068	-16.977941	-18.160317
30	6	0	-9.449469	-18.009936	-18.024462
31	1	0	-9.846990	-17.342100	-17.267238
32	6	0	-13.351116	-16.274067	-19.736279
33	1	0	-13.874297	-15.985555	-20.661575
34	1	0	-12.888827	-15.381597	-19.309000
35	1	0	-14.085055	-16.658716	-19.025663

36	6	0	-11.263826	-16.805958	-20.842971
37	1	0	-10.508759	-17.586118	-20.958750
38	1	0	-10.789642	-15.935492	-20.383191
39	1	0	-11.630660	-16.512269	-21.838788
40	6	0	-14.500100	-19.730326	-15.612297
41	1	0	-14.772788	-20.275052	-14.695083
42	1	0	-15.304956	-19.034215	-15.858005
43	1	0	-13.592157	-19.156864	-15.425495
44	6	0	-15.507277	-21.384864	-17.039194
45	1	0	-15.319462	-22.087570	-17.852386
46	1	0	-16.276180	-20.680278	-17.363052
47	1	0	-15.901826	-21.939926	-16.174377
48	7	0	-12.322492	-17.282643	-19.961425
49	7	0	-14.293216	-20.639591	-16.739286
50	15	0	-11.962873	-19.224413	-17.851843

Total energy E(RM062X)= 1304.04612753 Hartrees

33g

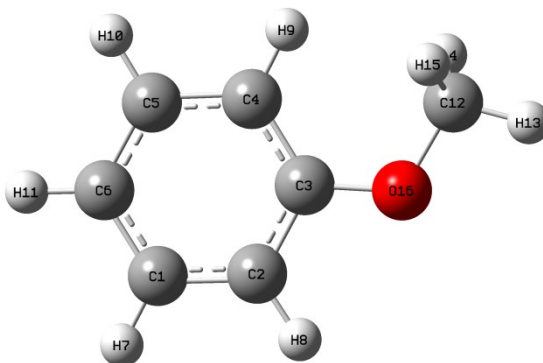


Center Number	Atomic Number	Atomic Type	Coordinates (Angstroms)		
			X	Y	Z
1	15	0	4.883200	24.319300	6.014000
2	6	0	4.297300	23.874000	7.658400
3	6	0	1.192300	25.534500	3.595400
4	1	0	0.436400	25.767800	3.108000
5	6	0	3.461500	24.849200	5.039700
6	6	0	3.338500	26.137400	4.506200
7	1	0	4.012100	26.766400	4.627200
8	6	0	5.650700	22.902600	5.215700
9	6	0	5.477400	22.743000	3.845500
10	1	0	4.983200	23.361300	3.358000
11	6	0	2.194100	26.452700	3.792200
12	1	0	2.100700	27.305900	3.437400
13	6	0	6.051400	21.643500	3.209100
14	1	0	5.956800	21.532500	2.290100
15	6	0	2.440000	23.910700	4.858300
16	1	0	2.521100	23.059100	5.228400
17	6	0	6.395600	21.993500	5.954100
18	1	0	6.519700	22.117900	6.866800

19	6	0	3.981400	24.910800	8.540400
20	1	0	4.135100	25.794600	8.293000
21	6	0	3.558600	22.274700	9.287800
22	1	0	3.422100	21.394800	9.550500
23	6	0	3.444200	24.623900	9.776100
24	1	0	3.211900	25.316400	10.353900
25	6	0	1.306700	24.245100	4.127100
26	1	0	0.631800	23.617700	3.992600
27	6	0	4.077300	22.546400	8.018600
28	1	0	4.270300	21.853900	7.427300
29	6	0	3.248800	23.303900	10.157100
30	1	0	2.908300	23.108800	11.000200
31	6	0	6.763100	20.713000	3.950200
32	1	0	7.115900	19.960000	3.531300
33	6	0	6.952400	20.897400	5.313200
34	1	0	7.453900	20.281400	5.798000

Total energy E(RM062X)= -1036.164163 Hartrees

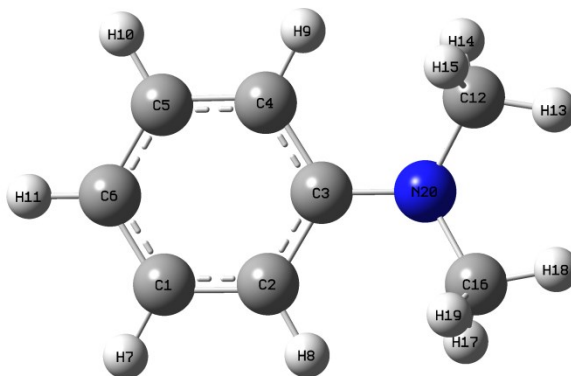
Anisole



Center Number	Atomic Number	Atomic Type	Coordinates (Angstroms)		
			X	Y	Z
1	6	0	-1.304669	0.064114	-0.103172
2	6	0	0.067646	0.095086	0.081428
3	6	0	0.725078	1.317216	0.256963
4	6	0	-0.004988	2.505599	0.245400
5	6	0	-1.386780	2.457124	0.058260
6	6	0	-2.044057	1.247637	-0.115972
7	1	0	-1.801550	-0.889498	-0.238320
8	1	0	0.658671	-0.812765	0.093706
9	1	0	0.480808	3.462600	0.379013
10	1	0	-1.947266	3.384676	0.050530
11	1	0	-3.116769	1.222510	-0.260484
12	6	0	2.777517	2.458248	0.613972
13	1	0	3.822174	2.181944	0.733007
14	1	0	2.670575	3.112979	-0.255737
15	1	0	2.434996	2.982754	1.510682
16	8	0	2.069624	1.244267	0.430497

Total energy E(RM062X)= -346.71090548 Hartrees

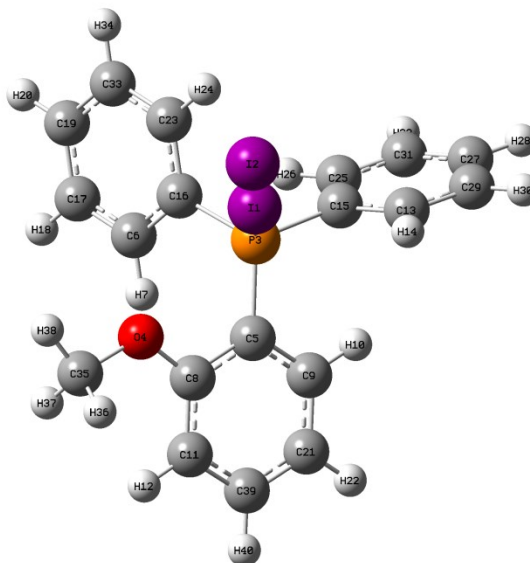
DMA



Center Number	Atomic Number	Atomic Type	Coordinates (Angstroms)		
			X	Y	Z
1	6	0	-1.315828	0.054771	-0.011471
2	6	0	0.062945	0.062187	0.153588
3	6	0	0.776751	1.276366	0.221608
4	6	0	0.032938	2.472069	0.143898
5	6	0	-1.345542	2.443853	-0.021105
6	6	0	-2.037939	1.240171	-0.103956
7	1	0	-1.830255	-0.898434	-0.062907
8	1	0	0.583294	-0.882318	0.229460
9	1	0	0.529433	3.429955	0.212495
10	1	0	-1.883334	3.383653	-0.079633
11	1	0	-3.113051	1.226478	-0.230451
12	6	0	2.800713	2.544381	0.704137
13	1	0	3.872319	2.376179	0.788054
14	1	0	2.645000	3.295881	-0.073092
15	1	0	2.433619	2.952321	1.655679
16	6	0	2.830376	0.061633	0.715142
17	1	0	2.692632	-0.700136	-0.055502
18	1	0	3.897693	0.255820	0.797723
19	1	0	2.472493	-0.346515	1.670095
20	7	0	2.153819	1.293591	0.350775

Total energy E(RM062X)= -366.14170390 Hartrees

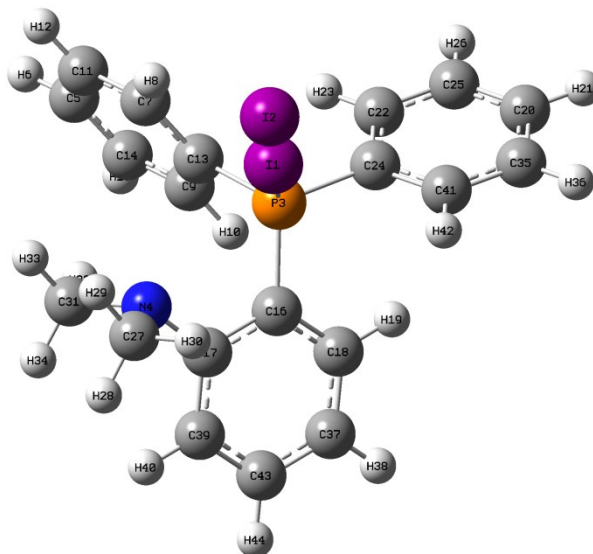
34a



Center Number	Atomic Number	Atomic Type	Coordinates (Angstroms)		
			X	Y	Z
1	53	0	1.061263	3.390237	2.622900
2	53	0	-0.177193	0.503370	2.173621
3	15	0	2.025932	5.644768	3.012977
4	8	0	-0.223891	6.380241	1.410729
5	6	0	2.088372	6.627599	1.504203
6	6	0	0.669843	7.840387	4.093155
7	1	0	0.867008	8.350617	3.157390
8	6	0	0.882256	6.868692	0.820239
9	6	0	3.294089	7.102101	0.987668
10	1	0	4.220725	6.911718	1.516003
11	6	0	0.898772	7.584075	-0.374887
12	1	0	-0.017879	7.779438	-0.913968
13	6	0	4.557075	4.492317	3.083364
14	1	0	4.178693	3.796738	2.342604
15	6	0	3.724630	5.478352	3.618772
16	6	0	1.089398	6.524598	4.285014
17	6	0	-0.003190	8.497065	5.118086
18	1	0	-0.332096	9.518703	4.974333
19	6	0	-0.253077	7.844440	6.320739
20	1	0	-0.778383	8.360378	7.115397
21	6	0	3.306541	7.817083	-0.203394
22	1	0	4.241836	8.187062	-0.602319
23	6	0	0.835877	5.864312	5.489734
24	1	0	1.159462	4.838550	5.631908
25	6	0	4.209108	6.369025	4.580026
26	1	0	3.562555	7.130631	5.000282
27	6	0	6.360224	5.288047	4.468864
28	1	0	7.387125	5.210247	4.804656
29	6	0	5.875572	4.402287	3.510139
30	1	0	6.521455	3.636547	3.099342
31	6	0	5.529851	6.268318	5.001783
32	1	0	5.907101	6.954916	5.749373
33	6	0	0.166556	6.529957	6.507518
34	1	0	-0.030610	6.021502	7.442864
35	6	0	-1.473780	6.526228	0.744193
36	1	0	-1.442699	6.048028	-0.237143
37	1	0	-1.732436	7.582467	0.640721
38	1	0	-2.203638	6.027398	1.375164
39	6	0	2.111521	8.049335	-0.874443
40	1	0	2.115137	8.604646	-1.804598

Total energy E(RM062X) = -1745.99050605 Hartrees

34b

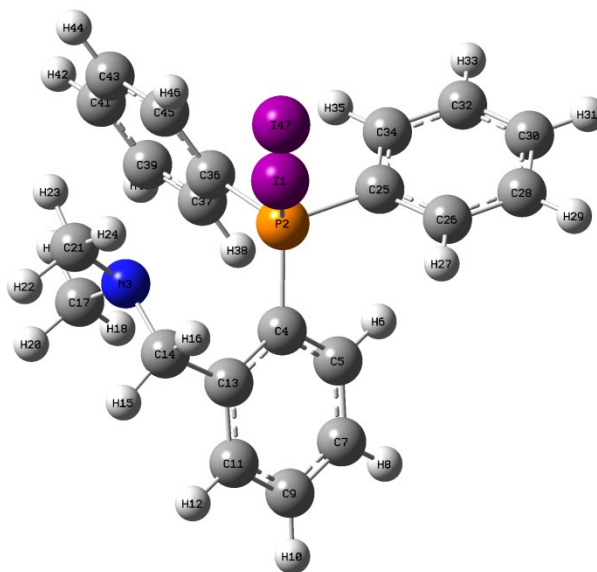


Center Number	Atomic Number	Atomic Type	Coordinates (Angstroms)		
			X	Y	Z
1	53	0	7.721586	6.226784	2.663642
2	53	0	9.552004	8.399984	1.303514
3	15	0	6.287892	4.531337	3.779955
4	7	0	4.350141	5.546788	1.893559
5	6	0	5.494974	0.750374	1.309018
6	1	0	5.286422	-0.139243	0.727194
7	6	0	6.704337	2.817116	1.597803
8	1	0	7.430489	3.536785	1.238503
9	6	0	5.072329	2.115968	3.247215
10	1	0	4.530450	2.294625	4.170277
11	6	0	6.435549	1.669864	0.857749
12	1	0	6.960008	1.499464	-0.074168
13	6	0	6.019467	3.037982	2.790095
14	6	0	4.817072	0.970099	2.505702
15	1	0	4.084492	0.254762	2.858454
16	6	0	4.641593	5.124295	4.261418
17	6	0	3.808501	5.551153	3.219163
18	6	0	4.183122	5.102173	5.579858
19	1	0	4.824818	4.759344	6.382233
20	6	0	8.467224	3.405891	7.665339
21	1	0	8.984305	3.153712	8.583096
22	6	0	7.482653	2.725363	5.571577
23	1	0	7.242253	1.942387	4.862912
24	6	0	7.141333	4.052116	5.308322
25	6	0	8.146302	2.408174	6.753377
26	1	0	8.412918	1.378206	6.955925
27	6	0	4.400889	6.888976	1.310371
28	1	0	3.401264	7.275319	1.065082
29	1	0	4.995362	6.852244	0.395334
30	1	0	4.883563	7.574660	2.007386
31	6	0	3.672722	4.606526	0.998947
32	1	0	3.648392	3.613910	1.450870
33	1	0	4.238020	4.548239	0.066534
34	1	0	2.644261	4.917801	0.765979
35	6	0	8.134303	4.732314	7.397974

36	1	0	8.391021	5.512726	8.103297
37	6	0	2.885744	5.516361	5.857238
38	1	0	2.524433	5.499850	6.877711
39	6	0	2.511475	5.960744	3.513170
40	1	0	1.860847	6.291619	2.711306
41	6	0	7.479794	5.059306	6.219358
42	1	0	7.234509	6.095276	6.008090
43	6	0	2.054146	5.944224	4.826882
44	1	0	1.042839	6.264117	5.047350

Total energy E(RM062X) = -1765.41784395 Hartrees

34c

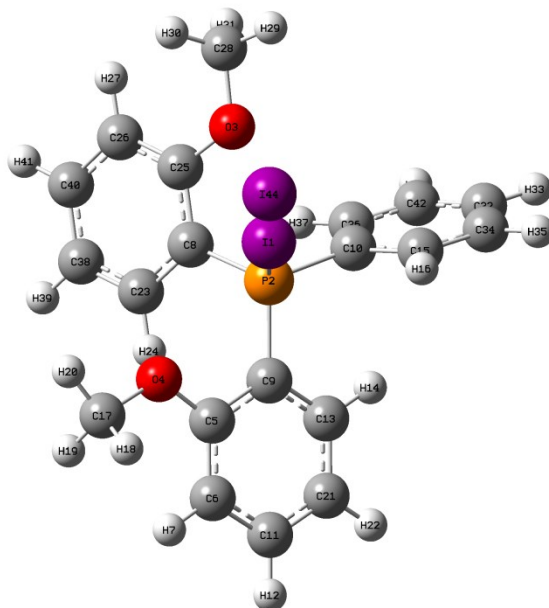


Center Number	Atomic Number	Atomic Type	Coordinates (Angstroms)		
			X	Y	Z
1	53	0	5.934125	9.404592	5.356210
2	15	0	4.725267	9.585552	3.185534
3	7	0	7.143227	11.139790	2.552504
4	6	0	4.194949	11.270373	2.710497
5	6	0	2.872491	11.425033	2.277022
6	1	0	2.209510	10.570674	2.226716
7	6	0	2.389011	12.672815	1.903262
8	1	0	1.365930	12.771126	1.563140
9	6	0	3.222909	13.779691	1.970552
10	1	0	2.856248	14.758443	1.686119
11	6	0	4.540312	13.628460	2.388158
12	1	0	5.196542	14.490974	2.417751
13	6	0	5.051232	12.387886	2.759417
14	6	0	6.501159	12.287664	3.173911
15	1	0	7.011287	13.231235	2.921979
16	1	0	6.564497	12.167694	4.260128
17	6	0	7.248787	11.305808	1.106531
18	1	0	6.262423	11.468031	0.667825
19	1	0	7.670838	10.397529	0.669714
20	1	0	7.893074	12.159688	0.844499
21	6	0	8.463242	10.893457	3.120062
22	1	0	9.161653	11.715355	2.897728
23	1	0	8.869315	9.970886	2.698156

24	1	0	8.392878	10.778564	4.202290
25	6	0	3.187906	8.658995	3.500921
26	6	0	2.337186	9.107412	4.518412
27	1	0	2.576810	10.008763	5.073536
28	6	0	1.182639	8.400227	4.816202
29	1	0	0.525157	8.751366	5.601669
30	6	0	0.875345	7.237224	4.110950
31	1	0	-0.024618	6.683449	4.349257
32	6	0	1.723736	6.785535	3.109043
33	1	0	1.489641	5.879845	2.563399
34	6	0	2.883493	7.492947	2.800053
35	1	0	3.541958	7.130386	2.020571
36	6	0	5.534672	8.754282	1.791298
37	6	0	5.000023	8.924802	0.513215
38	1	0	4.126990	9.550551	0.357504
39	6	0	5.601635	8.295229	-0.570994
40	1	0	5.190507	8.429097	-1.564022
41	6	0	6.728983	7.502997	-0.378846
42	1	0	7.199470	7.017942	-1.225503
43	6	0	7.255146	7.332626	0.898914
44	1	0	8.132925	6.716263	1.049086
45	6	0	6.659733	7.957225	1.989104
46	1	0	7.077617	7.835451	2.981910
47	53	0	7.401256	9.129604	8.128523

Total energy E(RM062X) = -1804.72433471 Hartrees

34d

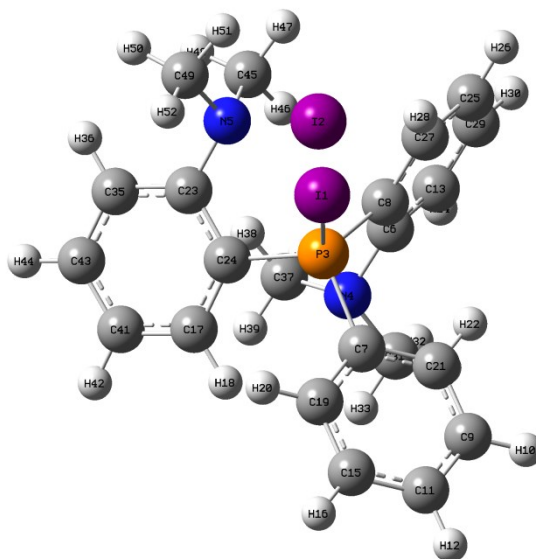


Center Number	Atomic Number	Atomic Type	Coordinates (Angstroms)		
			X	Y	Z
1	53	0	4.978642	4.733650	8.338412
2	15	0	3.810074	6.914167	8.115167
3	8	0	6.195893	7.787571	9.419355
4	8	0	1.891539	5.401053	9.631158
5	6	0	1.287324	5.841198	8.511904
6	6	0	-0.033800	5.569968	8.162959
7	1	0	-0.655571	4.950100	8.794238

8	6	0	3.878269	7.906809	9.618094
9	6	0	2.079481	6.647365	7.672338
10	6	0	4.550270	7.869761	6.765085
11	6	0	-0.554414	6.105991	6.989076
12	1	0	-1.582924	5.888877	6.726610
13	6	0	1.538036	7.175944	6.500574
14	1	0	2.149679	7.794774	5.854946
15	6	0	4.950281	7.215201	5.598846
16	1	0	4.872122	6.136478	5.519564
17	6	0	1.189068	4.498212	10.478316
18	1	0	0.904710	3.598923	9.927922
19	1	0	0.303309	4.977119	10.901850
20	1	0	1.883382	4.240137	11.272841
21	6	0	0.218186	6.908719	6.158370
22	1	0	-0.198679	7.321318	5.249182
23	6	0	2.725119	8.345324	10.266456
24	1	0	1.751161	8.097523	9.861773
25	6	0	5.145874	8.234858	10.132506
26	6	0	5.241604	8.991709	11.298919
27	1	0	6.206952	9.250572	11.711092
28	6	0	7.509850	8.046884	9.900835
29	1	0	8.181899	7.575344	9.189578
30	1	0	7.650503	7.606795	10.890379
31	1	0	7.701283	9.121791	9.935392
32	6	0	5.562293	9.338294	4.638588
33	1	0	5.959407	9.911184	3.809412
34	6	0	5.453134	7.954587	4.535641
35	1	0	5.763650	7.448053	3.630377
36	6	0	4.657852	9.257191	6.871426
37	1	0	4.348172	9.765098	7.777864
38	6	0	2.823403	9.103848	11.425557
39	1	0	1.927356	9.445414	11.926628
40	6	0	4.079250	9.416332	11.933813
41	1	0	4.162424	10.003663	12.840425
42	6	0	5.167240	9.987425	5.804031
43	1	0	5.255307	11.063840	5.884993
44	53	0	6.462604	1.920059	8.605835

Total energy E(RM062X) = -1860.50627712 Hartrees

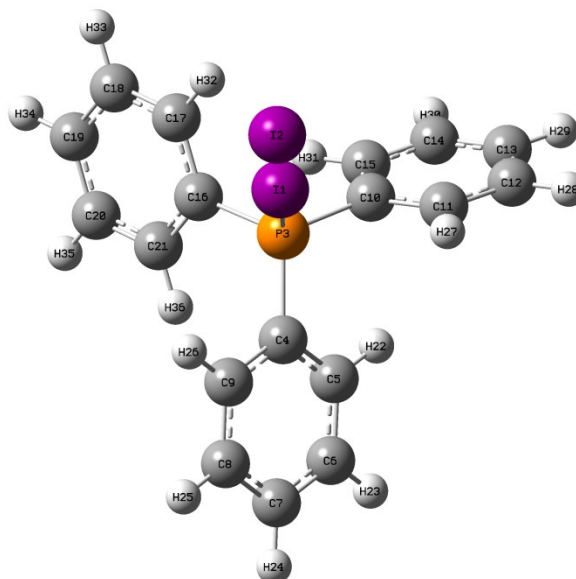
34e



Center Number	Atomic Number	Atomic Type	Coordinates (Angstroms)		
			X	Y	Z
1	53	0	5.471389	29.133660	6.956364
2	53	0	7.383260	28.378502	9.467028
3	15	0	3.983345	29.735234	5.083385
4	7	0	2.579412	30.054800	2.484456
5	7	0	6.357918	31.240791	4.347925
6	6	0	3.670430	29.126967	2.402499
7	6	0	2.349297	29.189373	5.637960
8	6	0	4.424219	28.860376	3.555703
9	6	0	0.567421	27.568939	5.583475
10	1	0	0.120463	26.684140	5.147475
11	6	0	-0.053519	28.217357	6.644831
12	1	0	-0.990979	27.840536	7.035465
13	6	0	4.018275	28.488590	1.212964
14	1	0	3.444587	28.688907	0.314824
15	6	0	0.535971	29.341209	7.218278
16	1	0	0.063008	29.837310	8.056581
17	6	0	2.829812	32.299409	4.862989
18	1	0	1.873038	31.841896	5.082096
19	6	0	1.741799	29.822976	6.726821
20	1	0	2.209221	30.681491	7.197070
21	6	0	1.771942	28.049111	5.080728
22	1	0	2.263856	27.528711	4.267231
23	6	0	5.216563	32.099163	4.450037
24	6	0	3.989362	31.524261	4.799259
25	6	0	5.833142	27.348696	2.320851
26	1	0	6.670062	26.662710	2.289586
27	6	0	5.502355	27.977307	3.514017
28	1	0	6.085707	27.784626	4.406014
29	6	0	5.090942	27.605424	1.172290
30	1	0	5.349641	27.117325	0.240382
31	6	0	1.305812	29.490597	2.031651
32	1	0	1.273893	29.338604	0.943476
33	1	0	0.505442	30.180995	2.305091
34	1	0	1.120436	28.536957	2.523744
35	6	0	5.273518	33.467752	4.190407
36	1	0	6.220174	33.919870	3.916076
37	6	0	2.862390	31.300296	1.764157
38	1	0	3.793268	31.742193	2.122327
39	1	0	2.052835	32.006685	1.957641
40	1	0	2.938780	31.140841	0.679010
41	6	0	2.903964	33.661189	4.605702
42	1	0	2.006597	34.265456	4.652845
43	6	0	4.124558	34.244326	4.273524
44	1	0	4.177713	35.306855	4.069207
45	6	0	6.820902	31.079924	2.967830
46	1	0	6.002306	30.736982	2.332671
47	1	0	7.605727	30.320772	2.951646
48	1	0	7.226626	32.014062	2.553353
49	6	0	7.457776	31.648215	5.224286
50	1	0	7.956186	32.562837	4.873707
51	1	0	8.193070	30.841793	5.257914
52	1	0	7.082204	31.813719	6.233969

Total energy E(RM062X) = -1899.36160981 Hartrees

34g

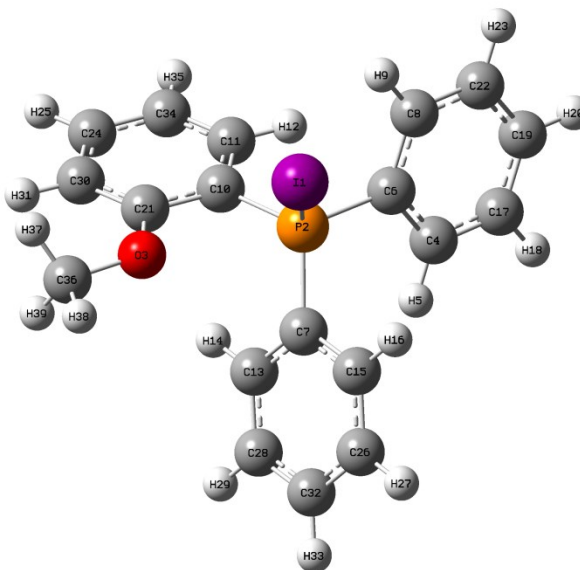


Center Number	Atomic Number	Atomic Type	Coordinates (Angstroms)		
			X	Y	Z
1	53	0	6.831006	5.419004	3.173585
2	53	0	9.702202	6.323791	2.288064
3	15	0	4.550257	4.706713	3.865210
4	6	0	3.752623	3.751338	2.552771
5	6	0	2.426650	4.003682	2.196928
6	6	0	1.820581	3.218861	1.221764
7	6	0	2.531640	2.192319	0.610250
8	6	0	3.855217	1.943982	0.966865
9	6	0	4.471830	2.723282	1.935399
10	6	0	3.510300	6.142210	4.224737
11	6	0	3.484294	7.203933	3.315601
12	6	0	2.642221	8.282486	3.547706
13	6	0	1.836061	8.306278	4.683905
14	6	0	1.869395	7.252482	5.589945
15	6	0	2.705298	6.164024	5.365081
16	6	0	4.608112	3.677862	5.352138
17	6	0	5.410236	4.079518	6.424266
18	6	0	5.402395	3.338984	7.598595
19	6	0	4.605640	2.201084	7.700518
20	6	0	3.815328	1.799170	6.629428
21	6	0	3.811584	2.535595	5.449490
22	1	0	1.870236	4.802393	2.673495
23	1	0	0.792516	3.412508	0.942160
24	1	0	2.055913	1.584847	-0.149994
25	1	0	4.408553	1.146938	0.486173
26	1	0	5.504582	2.534158	2.208520
27	1	0	4.116444	7.188153	2.434103
28	1	0	2.618617	9.106120	2.845333
29	1	0	1.182969	9.151570	4.863627
30	1	0	1.244837	7.273224	6.474334
31	1	0	2.727107	5.342407	6.071249
32	1	0	6.034980	4.962840	6.344362
33	1	0	6.021207	3.647349	8.431889
34	1	0	4.604879	1.624291	8.617393
35	1	0	3.199395	0.911984	6.707676

36 1 0 3.193391 2.222321 4.616233

Total energy E(RM062X) = -1631.47406409 Hartrees

35a+

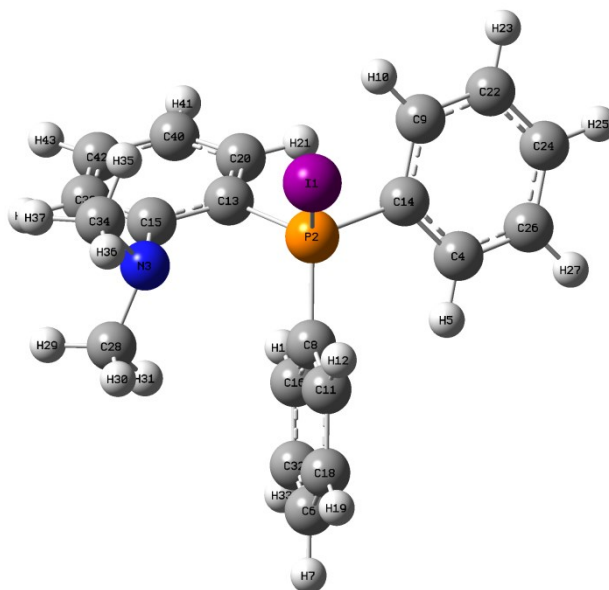


Center Number	Atomic Number	Atomic Type	Coordinates (Angstroms)		
			X	Y	Z
1	53	0	10.357613	-0.526286	13.258957
2	15	0	12.116649	-1.738491	14.348993
3	8	0	10.114503	-3.785451	14.224186
4	6	0	14.514954	-0.692342	15.225166
5	1	0	14.256995	-1.109129	16.191461
6	6	0	13.639268	-0.798652	14.141932
7	6	0	11.734848	-1.875589	16.101546
8	6	0	13.969700	-0.257085	12.896023
9	1	0	13.286598	-0.336146	12.057473
10	6	0	12.312598	-3.349958	13.594999
11	6	0	13.522017	-3.721441	13.002296
12	1	0	14.355978	-3.030417	12.988727
13	6	0	11.890895	-3.102906	16.746567
14	1	0	12.186451	-3.985918	16.191993
15	6	0	11.359262	-0.731176	16.809109
16	1	0	11.237383	0.219614	16.301748
17	6	0	15.729897	-0.038475	15.052957
18	1	0	16.411366	0.050622	15.889296
19	6	0	16.064046	0.498703	13.815549
20	1	0	17.011286	1.008126	13.687751
21	6	0	11.224253	-4.243936	13.623841
22	6	0	15.186534	0.390047	12.738759
23	1	0	15.447932	0.812925	11.777151
24	6	0	12.576298	-5.862353	12.472601
25	1	0	12.676033	-6.848416	12.035157
26	6	0	11.138400	-0.822284	18.175730
27	1	0	10.845753	0.059266	18.731738
28	6	0	11.665132	-3.180015	18.115850
29	1	0	11.781901	-4.128677	18.624106
30	6	0	11.365363	-5.509044	13.058136
31	1	0	10.545600	-6.213582	13.071210

32	6	0	11.289729	-2.044746	18.826166
33	1	0	11.111883	-2.111294	19.892451
34	6	0	13.653622	-4.982663	12.440440
35	1	0	14.589238	-5.276456	11.984196
36	6	0	8.984295	-4.649284	14.330154
37	1	0	8.624790	-4.933049	13.339300
38	1	0	8.223586	-4.073791	14.849042
39	1	0	9.238590	-5.538858	14.909884

Total energy E(RM062X) = -1448.16017141 Hartrees

35b+

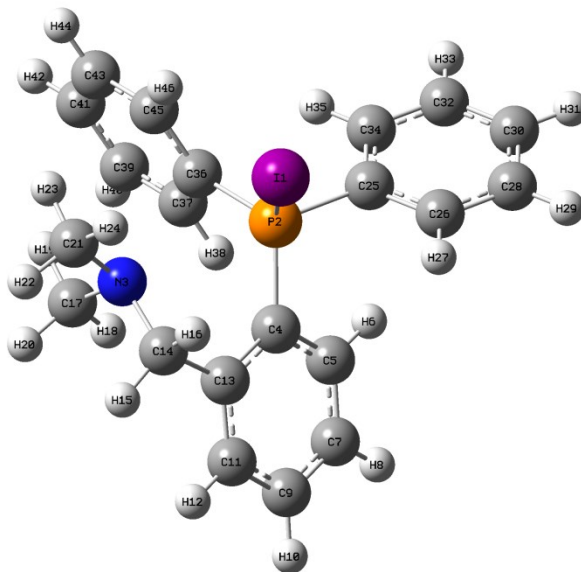


Center Number	Atomic Number	Atomic Type	Coordinates (Angstroms)		
			X	Y	Z
1	53	0	0.546279	5.525988	5.054919
2	15	0	-1.219087	4.304904	3.997744
3	7	0	0.860642	2.281833	3.866544
4	6	0	-3.554255	5.656261	3.312216
5	1	0	-3.296788	5.453286	2.279969
6	6	0	-0.740540	3.974031	-0.535107
7	1	0	-0.642574	3.879832	-1.609674
8	6	0	-0.977685	4.207742	2.214230
9	6	0	-3.053767	5.516799	5.684684
10	1	0	-2.401375	5.204106	6.493180
11	6	0	-0.050473	4.995067	1.537236
12	1	0	0.581965	5.692083	2.072931
13	6	0	-1.400738	2.638107	4.660612
14	6	0	-2.725587	5.235689	4.353064
15	6	0	-0.322785	1.760612	4.478160
16	6	0	-1.792717	3.302844	1.525166
17	1	0	-2.508295	2.681168	2.053656
18	6	0	0.066733	4.869806	0.157758
19	1	0	0.792386	5.472606	-0.373168
20	6	0	-2.593876	2.212239	5.249243
21	1	0	-3.427316	2.892711	5.370575
22	6	0	-4.222899	6.205443	5.968348
23	1	0	-4.480368	6.423466	6.997104

24	6	0	-5.057037	6.620760	4.931549
25	1	0	-5.966884	7.162911	5.158022
26	6	0	-4.722756	6.350413	3.610721
27	1	0	-5.366897	6.680321	2.805620
28	6	0	1.165874	1.651543	2.578555
29	1	0	1.485706	0.606581	2.692173
30	1	0	1.972485	2.212133	2.102256
31	1	0	0.290481	1.684236	1.929978
32	6	0	-1.672109	3.195515	0.145915
33	1	0	-2.299649	2.497059	-0.392908
34	6	0	2.019837	2.226039	4.762026
35	1	0	1.763304	2.659224	5.728997
36	1	0	2.827649	2.812537	4.320195
37	1	0	2.375427	1.198452	4.917966
38	6	0	-0.454412	0.443335	4.904362
39	1	0	0.370067	-0.247969	4.772436
40	6	0	-2.704976	0.892621	5.667796
41	1	0	-3.625356	0.550756	6.123470
42	6	0	-1.638602	0.015239	5.496604
43	1	0	-1.730537	-1.012820	5.825192

Total energy E(RM062X) = -1467.58674420 Hartrees

35c+

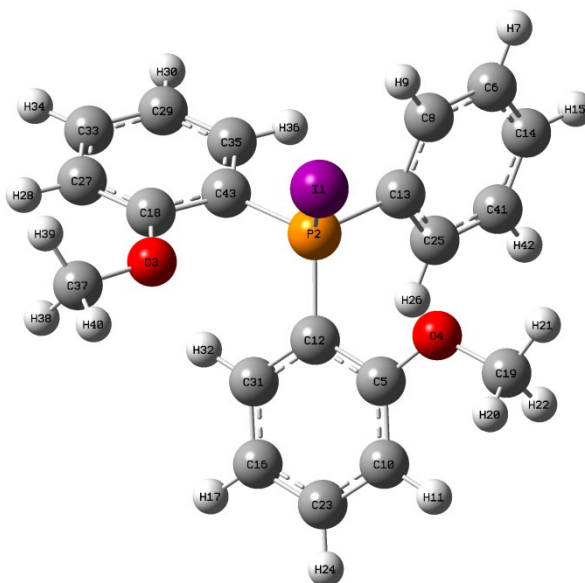


Center Number	Atomic Number	Atomic Type	Coordinates (Angstroms)		
			X	Y	Z
1	53	0	5.853805	9.421713	5.234953
2	15	0	4.689311	9.584007	3.144625
3	7	0	7.126873	11.127567	2.535659
4	6	0	4.188823	11.284603	2.737512
5	6	0	2.853880	11.447720	2.341149
6	1	0	2.183803	10.599554	2.292485
7	6	0	2.369948	12.702519	1.995924
8	1	0	1.339835	12.809837	1.681924
9	6	0	3.211538	13.803344	2.059499
10	1	0	2.842794	14.787713	1.798627
11	6	0	4.538506	13.641723	2.441880
12	1	0	5.198524	14.501060	2.467244

13	6	0	5.055392	12.395702	2.780873
14	6	0	6.513338	12.288404	3.160240
15	1	0	7.023360	13.224502	2.885296
16	1	0	6.601070	12.183872	4.246451
17	6	0	7.224617	11.294880	1.087421
18	1	0	6.238611	11.478367	0.656356
19	1	0	7.626474	10.380043	0.645923
20	1	0	7.882844	12.136572	0.824897
21	6	0	8.449228	10.856792	3.088939
22	1	0	9.158880	11.666064	2.860577
23	1	0	8.834243	9.927762	2.661730
24	1	0	8.388373	10.744123	4.171740
25	6	0	3.171722	8.647378	3.481428
26	6	0	2.313064	9.093950	4.493400
27	1	0	2.542499	9.994894	5.053071
28	6	0	1.160201	8.380701	4.777080
29	1	0	0.493506	8.726136	5.556913
30	6	0	0.864126	7.220222	4.061874
31	1	0	-0.036560	6.663321	4.289300
32	6	0	1.720431	6.774828	3.064283
33	1	0	1.492297	5.872195	2.511765
34	6	0	2.881429	7.485059	2.768186
35	1	0	3.547111	7.128182	1.992421
36	6	0	5.556029	8.745716	1.800167
37	6	0	5.046543	8.930337	0.513034
38	1	0	4.191659	9.574153	0.334495
39	6	0	5.657917	8.287832	-0.557694
40	1	0	5.268334	8.429976	-1.557800
41	6	0	6.766735	7.476373	-0.343333
42	1	0	7.245053	6.983327	-1.180676
43	6	0	7.266082	7.296916	0.943952
44	1	0	8.129629	6.665452	1.110963
45	6	0	6.661438	7.928883	2.023763
46	1	0	7.059099	7.794961	3.022593

Total energy E(RM062X) = -1506.89273656 Hartrees

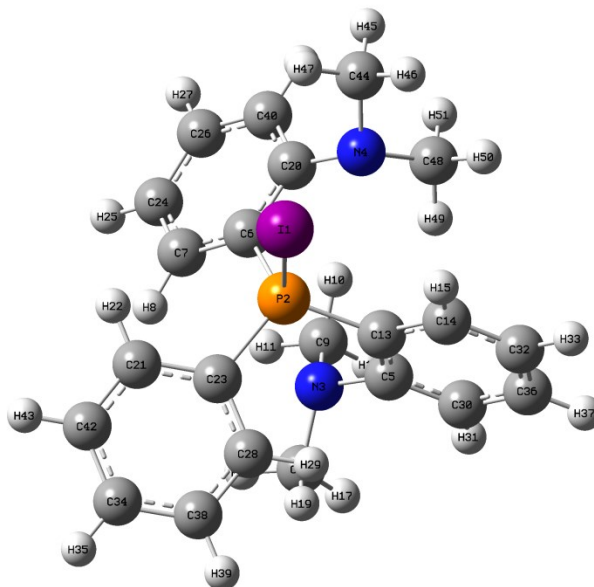
35d+



Center Number	Atomic Number	Atomic Type	Coordinates (Angstroms)		
			X	Y	Z
1	53	0	-3.836387	0.523731	4.967835
2	15	0	-2.056808	1.656235	6.117937
3	8	0	-3.982191	1.335650	8.243649
4	8	0	-2.621070	3.558013	4.058775
5	6	0	-2.683205	4.187533	5.243189
6	6	0	0.935566	0.244017	3.739121
7	1	0	1.163004	-0.660435	3.189390
8	6	0	-0.269563	0.348292	4.421564
9	1	0	-0.975753	-0.473514	4.400946
10	6	0	-2.943914	5.546199	5.411004
11	1	0	-3.130164	6.181027	4.556078
12	6	0	-2.447309	3.384656	6.375259
13	6	0	-0.557232	1.519352	5.123851
14	6	0	1.842254	1.299837	3.758396
15	1	0	2.778913	1.215152	3.221136
16	6	0	-2.718856	5.296087	7.814140
17	1	0	-2.727024	5.731698	8.804113
18	6	0	-2.834274	0.743263	8.613629
19	6	0	-2.813946	4.317136	2.867365
20	1	0	-3.810969	4.761705	2.852849
21	1	0	-2.713437	3.608781	2.050343
22	1	0	-2.051439	5.094067	2.782147
23	6	0	-2.961376	6.083725	6.692507
24	1	0	-3.164135	7.141089	6.812578
25	6	0	0.349057	2.581429	5.149126
26	1	0	0.123560	3.489473	5.696450
27	6	0	-2.628492	0.088520	9.825497
28	1	0	-3.422072	0.018814	10.556240
29	6	0	-0.345732	-0.412779	9.173917
30	1	0	0.613118	-0.861800	9.395219
31	6	0	-2.463505	3.942638	7.654915
32	1	0	-2.263633	3.322929	8.520280
33	6	0	-1.388351	-0.482087	10.091575
34	1	0	-1.239934	-0.989410	11.037100
35	6	0	-0.542182	0.239720	7.965273
36	1	0	0.264122	0.300326	7.244313
37	6	0	-5.084975	1.320386	9.147231
38	1	0	-4.828526	1.844001	10.070632
39	1	0	-5.388004	0.294564	9.365682
40	1	0	-5.888727	1.842742	8.636764
41	6	0	1.550522	2.464491	4.460973
42	1	0	2.255219	3.286210	4.473473
43	6	0	-1.779757	0.822645	7.682558

Total energy E(RM062X) = -1562.67678917 Hartrees

35e+

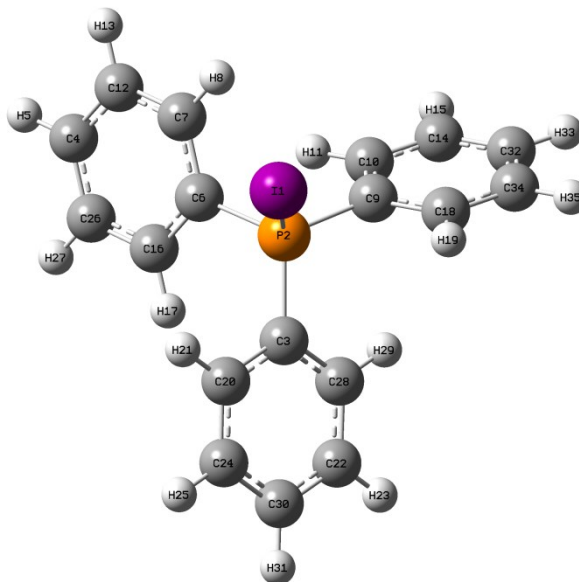


Center Number	Atomic Number	Atomic Type	Coordinates (Angstroms)		
			X	Y	Z
1	53	0	8.504766	6.318692	7.195341
2	15	0	7.305496	4.638657	8.439109
3	7	0	6.452628	2.557916	10.203364
4	7	0	8.794550	2.969786	6.569192
5	6	0	7.855322	2.807890	10.367122
6	6	0	6.531693	3.483962	7.287106
7	6	0	5.152673	3.261966	7.285290
8	1	0	4.504835	3.789955	7.973454
9	6	0	6.196331	1.245578	9.596662
10	1	0	6.733484	1.151232	8.652057
11	1	0	5.127232	1.159463	9.394566
12	1	0	6.497083	0.423035	10.259255
13	6	0	8.437526	3.809033	9.579235
14	6	0	9.799686	4.090089	9.657700
15	1	0	10.243652	4.853686	9.031406
16	6	0	5.690331	2.689186	11.449693
17	1	0	5.890933	1.866196	12.148669
18	1	0	4.626657	2.684345	11.204666
19	1	0	5.926921	3.631292	11.940515
20	6	0	7.385624	2.743081	6.461257
21	6	0	5.036838	6.233241	8.660587
22	1	0	4.895820	6.073935	7.597388
23	6	0	6.098133	5.629065	9.342172
24	6	0	4.619706	2.320265	6.417337
25	1	0	3.551860	2.143094	6.410081
26	6	0	5.456992	1.597313	5.570725
27	1	0	5.036714	0.861100	4.896389
28	6	0	6.315606	5.897819	10.693785
29	1	0	7.167028	5.471584	11.211921
30	6	0	8.662490	2.094281	11.249842
31	1	0	8.224971	1.316637	11.865458
32	6	0	10.589319	3.368598	10.542648
33	1	0	11.648759	3.580067	10.609830
34	6	0	4.359562	7.304191	10.710019

35	1	0	3.677459	7.953135	11.245339
36	6	0	10.021163	2.374622	11.335190
37	1	0	10.641856	1.811652	12.021503
38	6	0	5.438155	6.732964	11.375374
39	1	0	5.603833	6.938625	12.425427
40	6	0	6.830954	1.801157	5.596244
41	1	0	7.480963	1.220141	4.951783
42	6	0	4.163279	7.059766	9.353062
43	1	0	3.335529	7.521663	8.829991
44	6	0	9.404954	3.353416	5.293385
45	1	0	9.456354	2.515434	4.585271
46	1	0	10.419862	3.706881	5.485548
47	1	0	8.834433	4.163796	4.839887
48	6	0	9.501271	1.828562	7.159847
49	1	0	9.060578	1.568025	8.123552
50	1	0	10.541785	2.114231	7.326404
51	1	0	9.477781	0.944613	6.507983

Total energy E(RM062X) = -1601.53278983 Hartrees

35g⁺



Center Number	Atomic Number	Atomic Type	Coordinates (Angstroms)		
			X	Y	Z
1	53	0	6.681025	5.359043	3.214344
2	15	0	4.486750	4.681435	3.883592
3	6	0	3.737871	3.742835	2.546017
4	6	0	2.427420	4.033337	2.161495
5	6	0	1.825126	3.258462	1.176525
6	6	0	2.523726	2.210301	0.589327
7	6	0	3.831018	1.924334	0.979776
8	6	0	4.446410	2.689320	1.958361
9	6	0	3.504777	6.146687	4.232959
10	6	0	3.472226	7.195845	3.308975
11	6	0	2.642059	8.280604	3.546309
12	6	0	1.853565	8.317871	4.695419
13	6	0	1.890480	7.272441	5.610192
14	6	0	2.716576	6.176948	5.385412

15	6	0	4.607787	3.665226	5.361994
16	6	0	5.358271	4.116780	6.452429
17	6	0	5.361915	3.374669	7.623840
18	6	0	4.626849	2.192993	7.704063
19	6	0	3.887379	1.746736	6.615419
20	6	0	3.872222	2.480672	5.434169
21	1	0	1.881193	4.848689	2.620546
22	1	0	0.810458	3.478635	0.870376
23	1	0	2.050449	1.612221	-0.179670
24	1	0	4.371546	1.108148	0.517646
25	1	0	5.465229	2.469656	2.259127
26	1	0	4.087179	7.167039	2.416092
27	1	0	2.611459	9.098003	2.837345
28	1	0	1.209097	9.169159	4.877237
29	1	0	1.277798	7.304287	6.502071
30	1	0	2.741372	5.361249	6.097946
31	1	0	5.931734	5.035312	6.389692
32	1	0	5.939565	3.715714	8.473451
33	1	0	4.634122	1.617198	8.621377
34	1	0	3.319907	0.827137	6.679472
35	1	0	3.291026	2.135231	4.587561

Total energy E(RM062X) = -1333.64242089 Hartrees

A2.5 – References

- 1 M. J. Frisch, G. W. Trucks, H. B. Schlegel, G. E. Scuseria, M. A. Robb, G. A. Cheeseman, J. R. Scalmani, G.; Barone, V. Petersson, X. Nakatsuji, H.; Li, M. Caricato, A. V. Marenich, J. Bloino, B. G. Janesko, R. Gomperts, B. Mennucci, H. P. Hratchian, J. V. Ortiz, A. F. Izmaylov, J. L. Sonnenberg, D. Williams-Young, F. Ding, F.; Lipparini, F. Egidi, J. Goings, B. Peng, A. Petrone, T. Henderson, D. Ranasinghe, V. G. Zakrzewski, J. Gao, N. Rega, G. Zheng, W. Liang, M. Hada, M. Ehara, K. Toyota, R. Fukuda, J. Hasegawa, M. Ishida, T. Nakajima, Y. Honda, O. Kitao, H. Nakai, T. Vreven, K. Throssell, J. Montgomery, J. A., J. E. Peralta, F. Ogliaro, M. J. Bearpark, J. J. Heyd, E. N. Brothers, K. N. Kudin, V. N. Staroverov, T. A. Keith, R. Kobayashi, J. Normand, K. Raghavachari, A. P. Rendell, J. C. Burant, S. S. Iyengar, J. Tomasi, M. Cossi, J. M. Millam, M. Klene, C. Adamo, R. Cammi, J. W. Ochterski, R. L. Martin, K. Morokuma, O. Farkas, J. B. Foresman and D. J. Fox, Gaussian 16, Revision B.01 2016.
- 2 R. G. Parr and W. Yang, *Density-functional theory of atoms and molecules*, Oxford University Press, 1989.
- 3 R. Ditchfield, W. J. Hehre and J. A. Pople, *J. Chem. Phys.*, 1971, **54**, 724–728.
- 4 T. H. Dunning, *J. Chem. Phys.*, 1989, **90**, 1007–1023.
- 5 W. Humphrey, A. Dalke and K. Schulten, *J. Mol. Graph.*, 1996, **14**, 33–38.
- 6 A. D. McLean and G. S. Chandler, *J. Chem. Phys.*, 1980, **72**, 5639–5648.
- 7 L. Noodleman, *J. Chem. Phys.*, 1981, **74**, 5737–5743.
- 8 L. Noodleman and E. R. Davidson, *Chem. Phys.*, 1986, **109**, 131–143.
- 9 Y. Zhao and D. G. Truhlar, *Theor. Chem. Acc.*, 2008, **120**, 215–241.
- 10 E. D. Glendening, A. E. Reed, J. E. Carpenter and F. Weinhold, .
- 11 A. J. Bridgeman, G. Cavigliasso, L. R. Ireland and J. Rothery, *J. Chem. Soc., Dalt. Trans.*, 2001, 2095–2108.
- 12 O. V. Sizova, L. V. Skripnikov and A. Y. Sokolov, *J. Mol. Struct. THEOCHEM*, 2008, **870**, 1–9.
- 13 T. Lu and F. Chen, *J. Comput. Chem.*, 2012, **33**, 580–592.
- 14 Z. Chen, C. S. Wannere, C. Corminboeuf, R. Puchta and P. V. R. Schleyer, *Chem. Rev.*, 2005, **105**, 3842–3888.
- 15 M. J. Frisch, G. W. Trucks, H. B. Schlegel, G. E. Scuseria, M. A. Robb, J. R. Cheeseman, G. Scalmani, V. Barone, G. A. Petersson, H. Nakatsuji, X. Li, M. Caricato, A. Marenich, J. Bloino, B. G. Janesko, R. Gomperts, B. Mennucci, H. P. Hratchian and J. V. Ort, Gaussian 09, Revision E.01.2016.
- 16 F. Weigend and R. Ahlrichs, *Phys. Chem. Chem. Phys.*, 2005, **7**, 3297–3305.

Appendix 3

Crystallographic Data Tables

Compound	1a	1b	1c
Empirical formula	C ₁₃ H ₁₂ N ₂	C ₁₄ H ₁₄ N ₂	C ₁₅ H ₁₆ N ₂
Formula weight	196.25	210.27	224.3
Temperature/K	100.0(4)	100.0(4)	100.0(6)
Crystal system	triclinic	triclinic	orthorhombic
Space group	P-1	P-1	Pccn
a/Å	5.4339(2)	10.2688(3)	24.3256(3)
b/Å	8.3854(4)	10.5908(4)	10.15010(10)
c/Å	11.8797(6)	11.3233(4)	9.96740(10)
α/°	73.513(4)	96.798(3)	90
β/°	82.856(4)	103.414(3)	90
γ/°	87.377(4)	95.890(3)	90
Volume/Å ³	514.99(4)	1178.61(7)	2461.02(5)
Z	2	4	8
ρ _{calc} /cm ³	1.266	1.185	1.211
μ/mm ⁻¹	0.591	0.548	0.554
F(000)	208	448	960
Crystal size/mm ³	0.271 × 0.163 × 0.036	0.349 × 0.185 × 0.121	0.197 × 0.178 × 0.073
Radiation	CuKα (λ = 1.54184)	CuKα (λ = 1.54184)	CuKα (λ = 1.54184)
2θ range for data collection/°	7.814 to 144.216	8.116 to 137.816	7.268 to 146.974
Index ranges	-6 ≤ h ≤ 6, -9 ≤ k ≤ 10, -14 ≤ l ≤ 14	-8 ≤ h ≤ 12, -12 ≤ k ≤ 12, -13 ≤ l ≤ 13	-29 ≤ h ≤ 30, -12 ≤ k ≤ 10, -12 ≤ l ≤ 12
Reflections collected	8360	18270	37702
Independent reflections	2034 [R _{int} = 0.0281, R _{sigma} = 0.0218]	4382 [R _{int} = 0.0265, R _{sigma} = 0.0198]	2488 [R _{int} = 0.0397, R _{sigma} = 0.0115]
Data/restraints/parameters	2034/0/144	4382/0/307	2488/0/164
Goodness-of-fit on F ²	1.076	1.049	1.057
Final R indexes [I > 2σ (I)]	R ₁ = 0.0435, wR ₂ = 0.1154	R ₁ = 0.0364, wR ₂ = 0.0930	R ₁ = 0.0367, wR ₂ = 0.0965
Final R indexes [all data]	R ₁ = 0.0467, wR ₂ = 0.1186	R ₁ = 0.0379, wR ₂ = 0.0948	R ₁ = 0.0381, wR ₂ = 0.0982
Largest diff. peak/hole / e Å ⁻³	0.50/-0.19	0.13/-0.25	0.23/-0.26
Flack Parameter			

Compound	1d	1e	1f
Empirical formula	C ₁₅ H ₁₆ N ₂	C ₁₅ H ₁₆ N ₂	C ₁₄ H ₁₄ N ₂ O
Formula weight	224.3	224.3	226.27
Temperature/K	100.0(4)	100.0(5)	100.0(4)
Crystal system	monoclinic	orthorhombic	orthorhombic
Space group	P2 ₁ /c	P2 ₁ 2 ₁ 2 ₁	P2 ₁ 2 ₁ 2 ₁
a/Å	10.0868(2)	9.53440(10)	9.46225(6)
b/Å	14.2443(2)	10.67700(10)	10.61204(5)
c/Å	9.9091(2)	12.48050(10)	11.99338(5)
α/°	90	90	90
β/°	118.647(3)	90	90
γ/°	90	90	90
Volume/Å ³	1249.45(5)	1270.50(2)	1204.302(10)
Z	4	4	4
ρ _{calc} /cm ³	1.192	1.173	1.248
μ/mm ⁻¹	0.546	0.537	0.637
F(000)	480	480	480
Crystal size/mm ³	0.314 × 0.1 × 0.05	0.356 × 0.280 × 0.180	0.369 × 0.245 × 0.132
Radiation	CuKα (λ = 1.54184)	CuKα (λ = 1.54184)	CuKα (λ = 1.54184)
2θ range for data collection/°	9.992 to 135.786	10.906 to 144.194	11.132 to 138.564
Index ranges	-12 ≤ h ≤ 12, -14 ≤ k ≤ 17, -11 ≤ l ≤ 8	-11 ≤ h ≤ 11, -13 ≤ k ≤ 13, -15 ≤ l ≤ 15	-10 ≤ h ≤ 11, -12 ≤ k ≤ 12, -14 ≤ l ≤ 14
Reflections collected	13641	29924	35929
Independent reflections	2263 [R _{int} = 0.0342, R _{sigma} = 0.0180]	2511 [R _{int} = 0.0271, R _{sigma} = 0.0099]	2267 [R _{int} = 0.0309, R _{sigma} = 0.0100]
Data/restraints/parameters	2263/0/186	2511/0/164	2267/0/163
Goodness-of-fit on F ²	1.041	1.072	1.123
Final R indexes [I >= 2σ (I)]	R ₁ = 0.0336, wR ₂ = 0.0900	R ₁ = 0.0267, wR ₂ = 0.0674	R ₁ = 0.0278, wR ₂ = 0.0711
Final R indexes [all data]	R ₁ = 0.0351, wR ₂ = 0.0919	R ₁ = 0.0269, wR ₂ = 0.0676	R ₁ = 0.0278, wR ₂ = 0.0712
Largest diff. peak/hole / e Å ⁻³	0.15/-0.18	0.15/-0.16	0.15/-0.24
Flack Parameter		-0.07(8)	-0.02(4)

Compound	1g	1h	1i
Empirical formula	C ₁₄ H ₁₄ N ₂	C ₁₆ H ₁₈ N ₂	C ₁₂ H ₁₁ N ₃
Formula weight	210.27	238.32	197.24
Temperature/K	100.0(5)	100.0(5)	100.0(3)
Crystal system	monoclinic	monoclinic	monoclinic
Space group	P2 ₁ /c	P2 ₁ /n	P2 ₁ /c
a/Å	12.4627(3)	7.51140(10)	12.15110(10)
b/Å	8.37530(10)	23.1222(2)	15.80570(10)
c/Å	11.9105(2)	7.68910(10)	10.62300(10)
α/°	90	90	90
β/°	113.892(2)	99.9360(10)	94.3090(10)
γ/°	90	90	90
Volume/Å ³	1136.67(4)	1315.41(3)	2034.45(3)
Z	4	4	8
ρ _{calc} /cm ³	1.229	1.203	1.288
μ/mm ⁻¹	0.568	0.546	0.631
F(000)	448	512	832
Crystal size/mm ³	0.278 × 0.076 × 0.030	0.345 × 0.23 × 0.154	0.279 × 0.218 × 0.161
Radiation	CuKα (λ = 1.54184)	CuKα (λ = 1.54184)	CuKα (λ = 1.54184)
2θ range for data collection/°	7.758 to 136.476	7.646 to 140.148	7.296 to 137.542
Index ranges	-15 ≤ h ≤ 15, -9 ≤ k ≤ 10, -14 ≤ l ≤ 11	-9 ≤ h ≤ 9, -28 ≤ k ≤ 27, -6 ≤ l ≤ 9	-14 ≤ h ≤ 14, -19 ≤ k ≤ 19, -12 ≤ l ≤ 11
Reflections collected	16942	20606	30873
Independent reflections	2076 [R _{int} = 0.0347, R _{sigma} = 0.0156]	2496 [R _{int} = 0.0227, R _{sigma} = 0.0105]	3757 [R _{int} = 0.0267, R _{sigma} = 0.0141]
Data/restraints/parameters	2076/0/154	2496/0/185	3757/0/287
Goodness-of-fit on F ²	1.076	1.056	1.064
Final R indexes [I ≥ 2σ (I)]	R ₁ = 0.0518, wR ₂ = 0.1348	R ₁ = 0.0365, wR ₂ = 0.1020	R ₁ = 0.0347, wR ₂ = 0.0859
Final R indexes [all data]	R ₁ = 0.0534, wR ₂ = 0.1362	R ₁ = 0.0371, wR ₂ = 0.1025	R ₁ = 0.0356, wR ₂ = 0.0867
Largest diff. peak/hole / e Å ⁻³	0.55/-0.29	0.20/-0.19	0.17/-0.29
Flack Parameter			

Compound	1j	1k	1l
Empirical formula	C ₅₆ H ₆₀ N ₁₂	C ₁₄ H ₁₄ N ₂ O	C ₃₂ H ₃₆ N ₄ O ₂
Formula weight	901.16	226.27	508.65
Temperature/K	100.0(4)	100.0(5)	100.0(4)
Crystal system	triclinic	monoclinic	monoclinic
Space group	P-1	P2 ₁ /c	C2/c
a/Å	11.3101(4)	6.7241(2)	14.0729(2)
b/Å	14.8285(5)	18.5287(4)	14.0982(2)
c/Å	15.5662(5)	10.0457(2)	27.9338(4)
α/°	89.538(3)	90	90
β/°	89.587(3)	104.416(2)	94.7180(10)
γ/°	70.936(3)	90	90
Volume/Å ³	2467.35(15)	1212.17(5)	5523.36(14)
Z	2	4	16
ρ _{calc} /cm ³	1.213	1.24	1.223
μ/mm ⁻¹	0.58	0.633	0.608
F(000)	960	480	2176
Crystal size/mm ³	0.255 × 0.181 × 0.055	0.186 × 0.099 × 0.053	0.431 × 0.294 × 0.16
Radiation	CuKα (λ = 1.54184)	CuKα (λ = 1.54184)	CuKα (λ = 1.54184)
2θ range for data collection/°	8.272 to 137.556	9.546 to 141.55	8.894 to 144.256
Index ranges	-13 ≤ h ≤ 13, -17 ≤ k ≤ 17, -18 ≤ l ≤ 16	-6 ≤ h ≤ 8, -22 ≤ k ≤ 22, -12 ≤ l ≤ 11	-17 ≤ h ≤ 16, -16 ≤ k ≤ 17, -34 ≤ l ≤ 34
Reflections collected	28668	13704	34123
Independent reflections	9132 [R _{int} = 0.0298, R _{sigma} = 0.0316]	2326 [R _{int} = 0.0320, R _{sigma} = 0.0170]	5456 [R _{int} = 0.0257, R _{sigma} = 0.0146]
Data/restraints/parameters	9132/0/653	2326/0/163	5456/0/365
Goodness-of-fit on F ²	1.05	1.044	1.03
Final R indexes [I >= 2σ (I)]	R ₁ = 0.0402, wR ₂ = 0.1039	R ₁ = 0.0337, wR ₂ = 0.0888	R ₁ = 0.0361, wR ₂ = 0.0943
Final R indexes [all data]	R ₁ = 0.0438, wR ₂ = 0.1072	R ₁ = 0.0357, wR ₂ = 0.0905	R ₁ = 0.0373, wR ₂ = 0.0955
Largest diff. peak/hole / e Å ⁻³	0.24/-0.27	0.17/-0.24	0.23/-0.19
Flack Parameter			

Compound	1m	1n	1o
Empirical formula	C ₂₈ H ₂₈ N ₄	C ₁₅ H ₁₆ N ₂	C ₁₉ H ₁₆ N ₂
Formula weight	420.54	224.3	272.34
Temperature/K	100.0(4)	100.0(3)	100.00(10)
Crystal system	triclinic	triclinic	triclinic
Space group	P-1	P-1	P-1
a/Å	9.8107(3)	9.9907(3)	5.3943(2)
b/Å	10.0969(3)	11.4856(5)	11.6235(4)
c/Å	12.1839(4)	12.9769(5)	12.5219(4)
α/°	84.082(3)	71.156(4)	111.639(3)
β/°	81.768(3)	69.266(3)	96.098(2)
γ/°	80.108(3)	71.367(3)	95.440(2)
Volume/Å ³	1172.89(6)	1282.11(9)	718.01(5)
Z	2	4	2
ρ _{calc} /cm ³	1.191	1.162	1.26
μ/mm ⁻¹	0.55	0.532	0.575
F(000)	448	480	288
Crystal size/mm ³	0.299 × 0.178 × 0.105	0.408 × 0.191 × 0.103	0.786 × 0.185 × 0.057
Radiation	CuKα (λ = 1.54184)	CuKα (λ = 1.54184)	CuKα (λ = 1.54184)
2θ range for data collection/°	7.356 to 140.096	7.498 to 140.926	7.686 to 147.01
Index ranges	-11 ≤ h ≤ 11, -12 ≤ k ≤ 12, -14 ≤ l ≤ 14	-12 ≤ h ≤ 12, -13 ≤ k ≤ 14, -10 ≤ l ≤ 15	-6 ≤ h ≤ 6, -14 ≤ k ≤ 14, -15 ≤ l ≤ 15
Reflections collected	13788	15235	11549
Independent reflections	4454 [R _{int} = 0.0255, R _{sigma} = 0.0261]	4895 [R _{int} = 0.0245, R _{sigma} = 0.0241]	2902 [R _{int} = 0.0345, R _{sigma} = 0.0229]
Data/restraints/parameters	4454/0/329	4895/0/327	2902/0/254
Goodness-of-fit on F ²	1.032	1.043	1.036
Final R indexes [I > 2σ (I)]	R ₁ = 0.0372, wR ₂ = 0.0985	R ₁ = 0.0401, wR ₂ = 0.1052	R ₁ = 0.0413, wR ₂ = 0.1118
Final R indexes [all data]	R ₁ = 0.0398, wR ₂ = 0.1011	R ₁ = 0.0421, wR ₂ = 0.1073	R ₁ = 0.0430, wR ₂ = 0.1144
Largest diff. peak/hole / e Å ⁻³	0.23/-0.26	0.25/-0.26	0.19/-0.28
Flack Parameter			

Compound	1p	1r	1t
Empirical formula	C ₁₁ H ₁₆ N ₂	C ₃₀ H ₃₄ N ₆	C ₁₉ H ₂₄ N ₂
Formula weight	176.26	478.63	280.4
Temperature/K	100.0(5)	100.0(6)	100.0(4)
Crystal system	orthorhombic	monoclinic	monoclinic
Space group	Fdd2	Pc	P2 ₁ /c
a/Å	21.8833(2)	9.2938(2)	11.2586(2)
b/Å	18.8771(2)	11.06410(10)	14.6602(2)
c/Å	10.08110(10)	12.6836(2)	10.14080(10)
α/°	90	90	90
β/°	90	93.3930(10)	92.5580(10)
γ/°	90	90	90
Volume/Å ³	4164.43(7)	1301.94(4)	1672.11(4)
Z	16	2	4
ρ _{calc} /cm ³	1.125	1.221	1.114
μ/mm ⁻¹	0.517	0.577	0.495
F(000)	1536	512	608
Crystal size/mm ³	0.326 × 0.113 × 0.057	0.314 × 0.091 × 0.051	0.22 × 0.134 × 0.077
Radiation	Cu Kα (λ = 1.54184)	CuKα (λ = 1.54184)	CuKα (λ = 1.54184)
2θ range for data collection/°	10.738 to 151.896	7.99 to 144.194	7.86 to 144.25
Index ranges	-27 ≤ h ≤ 27, -23 ≤ k ≤ 23, -12 ≤ l ≤ 12	-11 ≤ h ≤ 11, -13 ≤ k ≤ 13, -15 ≤ l ≤ 15	-13 ≤ h ≤ 13, -16 ≤ k ≤ 18, -12 ≤ l ≤ 12
Reflections collected	25379	48861	26315
Independent reflections	2176 [R _{int} = 0.0409, R _{sigma} = 0.0150]	4967 [R _{int} = 0.0533, R _{sigma} = 0.0200]	3290 [R _{int} = 0.0487, R _{sigma} = 0.0234]
Data/restraints/parameters	2176/1/129	4967/2/344	3290/0/202
Goodness-of-fit on F ²	1.062	1.103	1.022
Final R indexes [I >= 2σ (I)]	R ₁ = 0.0264, wR ₂ = 0.0718	R ₁ = 0.0519, wR ₂ = 0.1594	R ₁ = 0.0383, wR ₂ = 0.0984
Final R indexes [all data]	R ₁ = 0.0266, wR ₂ = 0.0721	R ₁ = 0.0521, wR ₂ = 0.1596	R ₁ = 0.0397, wR ₂ = 0.1000
Largest diff. peak/hole / e Å ⁻³	0.14/-0.15	0.34/-0.27	0.27/-0.20
Flack parameter	0.07(12)	0.25(15)	

Compound	1u	1'a	2a
Empirical formula	C ₁₃ H ₁₁ ClN ₂	C ₁₉ H ₂₈ N ₂ Si ₂	C ₁₃ H _{5.85} Cl _{4.12} N ₂ S
Formula weight	230.69	340.61	368.33
Temperature/K	100.0(4)	293(2)	99.9(5)
Crystal system	triclinic	orthorhombic	monoclinic
Space group	P-1	Pna2 ₁	P2 ₁ /n
a/Å	5.43260(10)	14.72318(7)	8.23610(10)
b/Å	8.2909(2)	21.27110(10)	13.77720(10)
c/Å	13.3920(5)	6.25058(4)	12.41470(10)
α/°	73.704(3)	90	90
β/°	84.285(2)	90	97.4330(10)
γ/°	86.871(2)	90	90
Volume/Å ³	575.86(3)	1957.546(17)	1396.86(2)
Z	2	4	4
ρ _{calc} /cm ³	1.33	1.156	1.751
μ/mm ⁻¹	2.696	1.637	9.229
F(000)	240	736	736
Crystal size/mm ³	0.391 × 0.314 × 0.040	0.512 × 0.087 × 0.073	0.276 × 0.22 × 0.051
Radiation	CuKα (λ = 1.54184)	CuKα (λ = 1.54184)	CuKα (λ = 1.54184)
2θ range for data collection/°	6.904 to 144.248	7.302 to 139.728	9.634 to 136.156
Index ranges	-6 ≤ h ≤ 6, -10 ≤ k ≤ 10, -15 ≤ l ≤ 16	-17 ≤ h ≤ 17, -25 ≤ k ≤ 25, -7 ≤ l ≤ 7	-9 ≤ h ≤ 9, -16 ≤ k ≤ 16, -14 ≤ l ≤ 14
Reflections collected	9330	71873	21051
Independent reflections	2274 [R _{int} = 0.0293, R _{sigma} = 0.0197]	3637 [R _{int} = 0.0555, R _{sigma} = 0.0151]	2548 [R _{int} = 0.0334, R _{sigma} = 0.0150]
Data/restraints/parameters	2274/0/153	3637/1/214	2548/0/192
Goodness-of-fit on F ²	1.066	1.078	1.084
Final R indexes [I ≥ 2σ (I)]	R ₁ = 0.0299, wR ₂ = 0.0817	R ₁ = 0.0439, wR ₂ = 0.1113	R ₁ = 0.0288, wR ₂ = 0.0730
Final R indexes [all data]	R ₁ = 0.0308, wR ₂ = 0.0827	R ₁ = 0.0440, wR ₂ = 0.1114	R ₁ = 0.0289, wR ₂ = 0.0730
Largest diff. peak/hole / e Å ⁻³	0.32/-0.24	0.17/-0.19	0.72/-0.66
Flack parameter		0.05(3)	
	2b	2c	2d

Compound			
Empirical formula	C ₁₄ H ₈ Cl ₄ N ₂ S	C ₁₅ H _{9.97} Cl _{4.03} N ₂ S	C ₁₅ H ₁₀ Cl ₄ N ₂ S
Formula weight	378.08	393.31	392.11
Temperature/K	150.00(10)	100.0(5)	100.0(5)
Crystal system	triclinic	triclinic	monoclinic
Space group	P-1	P-1	P2 ₁ /c
a/Å	8.9856(5)	7.3043(3)	7.38990(10)
b/Å	9.2182(3)	9.0923(3)	10.5325(2)
c/Å	9.3740(6)	12.6109(5)	20.5855(4)
α/°	103.868(4)	80.349(3)	90
β/°	94.530(5)	86.679(3)	96.598(2)
γ/°	95.061(4)	72.338(3)	90
Volume/Å ³	746.84(7)	786.73(5)	1591.64(5)
Z	2	2	4
ρ _{calc} /cm ³	1.681	1.66	1.636
μ/mm ⁻¹	8.456	8.097	7.949
F(000)	380	397	792
Crystal size/mm ³	0.239 × 0.125 × 0.119	0.267 × 0.168 × 0.053	0.377 × 0.042 × 0.038
Radiation	CuKα (λ = 1.54184)	CuKα (λ = 1.54184)	CuKα (λ = 1.54184)
2θ range for data collection/°	9.772 to 130.764	7.11 to 137.166	8.648 to 146.978
Index ranges	-10 ≤ h ≤ 9, -10 ≤ k ≤ 10, -11 ≤ l ≤ 10	-8 ≤ h ≤ 8, -10 ≤ k ≤ 10, -15 ≤ l ≤ 15	-9 ≤ h ≤ 6, -13 ≤ k ≤ 13, -25 ≤ l ≤ 25
Reflections collected	7792	15042	19045
Independent reflections	2562 [R _{int} = 0.0194, R _{sigma} = 0.0186]	2891 [R _{int} = 0.0370, R _{sigma} = 0.0213]	3201 [R _{int} = 0.0386, R _{sigma} = 0.0244]
Data/restraints/parameters	2562/0/190	2891/0/212	3201/0/200
Goodness-of-fit on F ²	1.066	1.028	1.057
Final R indexes [I >= 2σ (I)]	R ₁ = 0.0267, wR ₂ = 0.0724	R ₁ = 0.0360, wR ₂ = 0.0943	R ₁ = 0.0456, wR ₂ = 0.1183
Final R indexes [all data]	R ₁ = 0.0275, wR ₂ = 0.0730	R ₁ = 0.0368, wR ₂ = 0.0950	R ₁ = 0.0475, wR ₂ = 0.1198
Largest diff. peak/hole / e Å ⁻³	0.38/-0.34	1.29/-0.49	1.26/-0.51
Flack parameter			

Compound	2f	2g	2h
Empirical formula	C ₁₄ H ₈ Cl ₄ N ₂ OS	C ₂₈ H ₁₆ Cl ₈ N ₄ S ₂	C ₁₆ H ₁₂ Cl ₄ N ₂ S
Formula weight	394.08	756.17	406.14
Temperature/K	100.00(10)	100.0(6)	100.00(10)
Crystal system	triclinic	monoclinic	orthorhombic
Space group	P-1	P2 ₁	Pbca
a/Å	7.10603(16)	9.0246(3)	14.2979(4)
b/Å	7.22142(17)	13.7857(5)	14.0607(3)
c/Å	15.6955(4)	12.0756(4)	16.3174(4)
α/°	83.2406(19)	90	90
β/°	78.4301(19)	98.513(3)	90
γ/°	71.106(2)	90	90
Volume/Å ³	745.33(3)	1485.78(9)	3280.41(15)
Z	2	2	8
ρ _{calc} /cm ³	1.756	1.69	1.645
μ/mm ⁻¹	8.544	8.491	7.736
F(000)	396	760	1648
Crystal size/mm ³	0.367 × 0.197 × 0.115	0.216 × 0.077 × 0.048	0.424 × 0.235 × 0.177
Radiation	CuKα (λ = 1.54184)	CuKα (λ = 1.54184)	CuKα (λ = 1.54184)
2θ range for data collection/°	5.756 to 142.51	7.402 to 142.134	10.356 to 142.54
Index ranges	-8 ≤ h ≤ 8, -8 ≤ k ≤ 8, -19 ≤ l ≤ 19	-11 ≤ h ≤ 11, -15 ≤ k ≤ 16, -14 ≤ l ≤ 14	-17 ≤ h ≤ 17, -13 ≤ k ≤ 17, -20 ≤ l ≤ 20
Reflections collected	14538	54843	63211
Independent reflections	2893 [R _{int} = 0.0297, R _{sigma} = 0.0191]	5617 [R _{int} = 0.0805, R _{sigma} = 0.0293]	3183 [R _{int} = 0.0724, R _{sigma} = 0.0183]
Data/restraints/parameters	2893/0/230	5617/1/381	3183/0/237
Goodness-of-fit on F ²	1.055	1.093	1.108
Final R indexes [I >= 2σ (I)]	R ₁ = 0.0269, wR ₂ = 0.0769	R ₁ = 0.0766, wR ₂ = 0.2049	R ₁ = 0.0399, wR ₂ = 0.0977
Final R indexes [all data]	R ₁ = 0.0277, wR ₂ = 0.0778	R ₁ = 0.0769, wR ₂ = 0.2058	R ₁ = 0.0400, wR ₂ = 0.0977
Largest diff. peak/hole / e Å ⁻³	0.36/-0.33	1.10/-0.69	1.00/-0.47
Flack parameter		0.06(3)	

Compound	2j.H[HCl₂]	2k	2l
Empirical formula	C ₁₄ H ₁₁ Cl ₆ N ₃ S	C ₁₄ H ₈ Cl ₄ N ₂ OS	C ₁₆ H ₁₂ Cl ₄ N ₂ OS
Formula weight	466.02	394.08	422.14
Temperature/K	100.0(5)	100.0(5)	99.9(6)
Crystal system	triclinic	triclinic	triclinic
Space group	P-1	P-1	P-1
a/Å	8.1354(2)	7.0073(5)	7.4264(7)
b/Å	9.2414(2)	9.6628(6)	11.9574(11)
c/Å	12.9459(6)	12.0172(7)	11.9660(9)
α/°	90.608(3)	95.257(5)	115.075(9)
β/°	101.838(3)	106.738(6)	91.228(8)
γ/°	105.699(2)	101.231(6)	95.201(8)
Volume/Å ³	914.81(5)	754.78(9)	956.37(16)
Z	2	2	2
ρ _{calc} /cm ³	1.692	1.734	1.466
μ/mm ⁻¹	9.662	8.438	6.697
F(000)	468	396	428
Crystal size/mm ³	0.393 × 0.097 × 0.043	0.222 × 0.040 × 0.035	0.415 × 0.042 × 0.028
Radiation	CuKα (λ = 1.54184)	CuKα (λ = 1.54184)	CuKα (λ = 1.54184)
2θ range for data collection/°	6.994 to 139.01	7.78 to 144.244	8.176 to 134.15
Index ranges	-9 ≤ h ≤ 8, -11 ≤ k ≤ 11, -15 ≤ l ≤ 15	-8 ≤ h ≤ 7, -11 ≤ k ≤ 10, -14 ≤ l ≤ 14	-6 ≤ h ≤ 8, -14 ≤ k ≤ 13, -14 ≤ l ≤ 14
Reflections collected	17679	11718	6147
Independent reflections	3432 [R _{int} = 0.0586, R _{sigma} = 0.0322]	2964 [R _{int} = 0.0508, R _{sigma} = 0.0319]	3403 [R _{int} = 0.0440, R _{sigma} = 0.0492]
Data/restraints/parameters	3432/0/221	2964/0/200	3403/0/218
Goodness-of-fit on F ²	1.209	1.028	1.056
Final R indexes [I >= 2σ (I)]	R ₁ = 0.1019, wR ₂ = 0.2915	R ₁ = 0.0387, wR ₂ = 0.1048	R ₁ = 0.0546, wR ₂ = 0.1486
Final R indexes [all data]	R ₁ = 0.1028, wR ₂ = 0.2917	R ₁ = 0.0408, wR ₂ = 0.1073	R ₁ = 0.0611, wR ₂ = 0.1565
Largest diff. peak/hole / e Å ⁻³	1.33/-0.97	0.64/-0.39	0.81/-0.84
Flack parameter			

Compound	2s	2t	3a
Empirical formula	C ₁₆ H _{10.42} Cl _{5.58} N ₂ OS	C ₁₅ H _{9.88} Cl _{4.12} N ₂ S	C _{13.5} H ₇ Cl ₄ N ₂ S
Formula weight	476.64	396.33	371.07
Temperature/K	100.00(13)	100.0(6)	100.0(7)
Crystal system	monoclinic	monoclinic	orthorhombic
Space group	P2 ₁ /n	P2 ₁ /n	Pbcn
a/Å	6.5698(7)	7.8074(3)	16.7712(3)
b/Å	16.562(2)	15.8724(4)	13.1359(2)
c/Å	16.941(3)	13.5003(4)	13.0495(2)
α/°	90	90	90
β/°	93.510(12)	105.795(3)	90
γ/°	90	90	90
Volume/Å ³	1839.8(5)	1609.82(9)	2874.87(8)
Z	4	4	8
ρ _{calc} /cm ³	1.721	1.635	1.715
μ/mm ⁻¹	9.11	8.049	8.764
F(000)	957	800	1488
Crystal size/mm ³	0.056 × 0.028 × 0.018	0.315 × 0.066 × 0.03	0.257 × 0.084 × 0.08
Radiation	CuKα (λ = 1.54184)	CuKα (λ = 1.54184)	CuKα (λ = 1.54184)
2θ range for data collection/°	7.472 to 136.154	8.796 to 135.814	8.55 to 142.028
Index ranges	-4 ≤ h ≤ 7, -19 ≤ k ≤ 19, -20 ≤ l ≤ 19	-9 ≤ h ≤ 9, -19 ≤ k ≤ 19, -16 ≤ l ≤ 16	-20 ≤ h ≤ 20, -16 ≤ k ≤ 16, -16 ≤ l ≤ 12
Reflections collected	6606	22798	72177
Independent reflections	3350 [R _{int} = 0.0626, R _{sigma} = 0.0882]	2931 [R _{int} = 0.0463, R _{sigma} = 0.0202]	2779 [R _{int} = 0.0861, R _{sigma} = 0.0305]
Data/restraints/parameters	3350/0/241	2931/0/210	2779/0/186
Goodness-of-fit on F ²	1.145	1.318	1.237
Final R indexes [I >= 2σ (I)]	R ₁ = 0.1055, wR ₂ = 0.2644	R ₁ = 0.0744, wR ₂ = 0.1732	R ₁ = 0.0615, wR ₂ = 0.1453
Final R indexes [all data]	R ₁ = 0.1319, wR ₂ = 0.2818	R ₁ = 0.0748, wR ₂ = 0.1733	R ₁ = 0.0638, wR ₂ = 0.1454
Largest diff. peak/hole / e Å ⁻³	0.77/-0.96	1.16/-0.73	1.15/-0.68
Flack parameter			

Compound	3c	3e	[4a]GaCl₄
Empirical formula	C ₁₅ H ₁₀ Cl ₃ N ₂ S	C ₃₀ H ₂₀ Cl ₆ N ₄ S ₂	C ₁₃ H ₆ Cl ₇ GaN ₂ S
Formula weight	356.66	713.32	540.13
Temperature/K	149.99(10)	100.00(10)	100.0(4)
Crystal system	monoclinic	triclinic	monoclinic
Space group	P2 ₁ /n	P-1	P2 ₁ /c
a/Å	11.5111(15)	9.9369(4)	9.5753(4)
b/Å	7.7055(8)	12.2664(4)	9.8718(4)
c/Å	16.9368(18)	13.3652(5)	20.0990(7)
α/°	90	91.036(3)	90
β/°	104.127(12)	107.068(4)	94.444(3)
γ/°	90	109.355(3)	90
Volume/Å ³	1456.8(3)	1457.25(10)	1894.16(13)
Z	4	2	4
ρ _{calc} /cm ³	1.626	1.626	1.894
μ/mm ⁻¹	6.972	6.97	12.113
F(000)	724	724	1056
Crystal size/mm ³	0.132 × 0.041 × 0.028	0.273 × 0.17 × 0.048	0.209 × 0.197 × 0.061
Radiation	CuKα (λ = 1.54184)	CuKα (λ = 1.54184)	CuKα (λ = 1.54184)
2θ range for data collection/°	8.42 to 131.946	6.976 to 142.122	8.826 to 142.102
Index ranges	-13 ≤ h ≤ 13, -9 ≤ k ≤ 8, -20 ≤ l ≤ 14	-12 ≤ h ≤ 12, -14 ≤ k ≤ 15, -16 ≤ l ≤ 16	-11 ≤ h ≤ 11, -12 ≤ k ≤ 12, -24 ≤ l ≤ 23
Reflections collected	7614	29597	36088
Independent reflections	2532 [R _{int} = 0.0574, R _{sigma} = 0.0513]	5631 [R _{int} = 0.0638, R _{sigma} = 0.0358]	3657 [R _{int} = 0.1269, R _{sigma} = 0.0384]
Data/restraints/parameters	2532/0/190	5631/0/381	3657/0/217
Goodness-of-fit on F ²	1.053	1.08	1.135
Final R indexes [I >= 2σ (I)]	R ₁ = 0.0388, wR ₂ = 0.1031	R ₁ = 0.0679, wR ₂ = 0.1871	R ₁ = 0.0617, wR ₂ = 0.1632
Final R indexes [all data]	R ₁ = 0.0454, wR ₂ = 0.1076	R ₁ = 0.0708, wR ₂ = 0.1907	R ₁ = 0.0617, wR ₂ = 0.1632
Largest diff. peak/hole / e Å ⁻³	0.38/-0.58	2.23/-0.49	0.92/-0.94
Flack parameter			

Compound	6m	6n	[7n]OTf
Empirical formula	C ₂₀ H ₁₆ N ₂ S	C ₂₁ H ₁₈ N ₂ S	C ₂₃ H ₂₁ F ₃ N ₂ O ₃ S ₂
Formula weight	316.41	330.43	494.54
Temperature/K	100.00(10)	100.00(10)	100.0(5)
Crystal system	monoclinic	monoclinic	triclinic
Space group	P2 ₁ /n	P2 ₁ /n	P-1
a/Å	12.6700(8)	10.4506(4)	8.2719(3)
b/Å	9.6039(6)	10.9276(3)	10.7320(5)
c/Å	12.9384(8)	14.7334(5)	12.5047(5)
α/°	90	90	97.115(4)
β/°	90.555(5)	99.672(3)	91.616(3)
γ/°	90	90	95.184(4)
Volume/Å ³	1574.29(17)	1658.64(10)	1096.17(8)
Z	4	4	2
ρ _{calc} /cm ³	1.335	1.323	1.498
μ/mm ⁻¹	1.81	1.74	2.695
F(000)	664	696	512
Crystal size/mm ³	0.394 × 0.241 × 0.135	0.286 × 0.156 × 0.112	0.301 × 0.251 × 0.085
Radiation	CuKα (λ = 1.54184)	CuKα (λ = 1.54184)	CuKα (λ = 1.54184)
2θ range for data collection/°	9.724 to 137.554	9.656 to 143.368	7.13 to 141.73
Index ranges	-15 ≤ h ≤ 15, -9 ≤ k ≤ 11, -15 ≤ l ≤ 15	-12 ≤ h ≤ 12, -13 ≤ k ≤ 13, -18 ≤ l ≤ 17	-9 ≤ h ≤ 10, -13 ≤ k ≤ 13, -15 ≤ l ≤ 15
Reflections collected	11768	31825	24880
Independent reflections	2913 [R _{int} = 0.0437, R _{sigma} = 0.0263]	3247 [R _{int} = 0.0734, R _{sigma} = 0.0242]	4217 [R _{int} = 0.0466, R _{sigma} = 0.0168]
Data/restraints/parameters	2913/0/209	3247/0/219	4217/0/302
Goodness-of-fit on F ²	1.086	1.05	1.05
Final R indexes [I >= 2σ (I)]	R ₁ = 0.0405, wR ₂ = 0.1091	R ₁ = 0.0431, wR ₂ = 0.1125	R ₁ = 0.0320, wR ₂ = 0.0849
Final R indexes [all data]	R ₁ = 0.0426, wR ₂ = 0.1099	R ₁ = 0.0432, wR ₂ = 0.1126	R ₁ = 0.0321, wR ₂ = 0.0850
Largest diff. peak/hole / e Å ⁻³	0.27/-0.40	0.44/-0.36	0.45/-0.40
Flack parameter			

Compound	8a	10a	10s
Empirical formula	C ₁₃ H ₁₂ Cl ₂ N ₂ OP	C ₃₈ H ₃₀ N ₄ P ₂	C ₃₄ H ₃₈ N ₄ P ₂
Formula weight	314.12	604.6	564.62
Temperature/K	150.00(10)	100.0(5)	100.0(6)
Crystal system	monoclinic	triclinic	monoclinic
Space group	P2 ₁ /c	P-1	P2 ₁ /n
a/Å	7.36505(7)	8.4411(7)	10.45250(10)
b/Å	18.01340(16)	10.7922(7)	9.46390(10)
c/Å	10.53806(11)	17.6347(11)	30.2669(4)
α/°	90	77.262(6)	90
β/°	95.7027(9)	81.816(6)	94.9550(10)
γ/°	90	85.402(6)	90
Volume/Å ³	1391.16(2)	1549.01(19)	2982.86(6)
Z	4	2	4
ρ _{calc} /cm ³	1.5	1.296	1.257
μ/mm ⁻¹	5.229	1.535	1.547
F(000)	644	632	1200
Crystal size/mm ³	0.3 × 0.08 × 0.06	0.072 × 0.061 × 0.023	0.225 × 0.158 × 0.094
Radiation	CuKα (λ = 1.54184)	CuKα (λ = 1.54184)	CuKα (λ = 1.54184)
2θ range for data collection/°	9.76 to 147.402	8.41 to 127.09	8.742 to 143.786
Index ranges	-9 ≤ h ≤ 9, -22 ≤ k ≤ 22, -13 ≤ l ≤ 12	-7 ≤ h ≤ 9, -12 ≤ k ≤ 12, -20 ≤ l ≤ 20	-12 ≤ h ≤ 12, -9 ≤ k ≤ 11, -37 ≤ l ≤ 37
Reflections collected	21295	9601	58446
Independent reflections	2786 [R _{int} = 0.0276, R _{sigma} = 0.0120]	5092 [R _{int} = 0.0537, R _{sigma} = 0.0521]	5860 [R _{int} = 0.0405, R _{sigma} = 0.0149]
Data/restraints/parameters	2786/0/172	5092/0/397	5860/0/367
Goodness-of-fit on F ²	1.05	1.066	1.074
Final R indexes [I > 2σ (I)]	R ₁ = 0.0345, wR ₂ = 0.0894	R ₁ = 0.0473, wR ₂ = 0.1331	R ₁ = 0.0317, wR ₂ = 0.0836
Final R indexes [all data]	R ₁ = 0.0356, wR ₂ = 0.0903	R ₁ = 0.0536, wR ₂ = 0.1400	R ₁ = 0.0322, wR ₂ = 0.0840
Largest diff. peak/hole / e Å ⁻³	0.46/-0.78	0.48/-0.43	0.33/-0.28
Flack parameter			

Compound	10u	11a	12a
Empirical formula	C ₃₉ H ₃₀ Cl ₄ N ₄ P ₂	C ₁₄ H ₁₄ N ₂	C ₃₈ H ₃₂ N ₄
Formula weight	758.41	210.27	544.67
Temperature/K	100.0(5)	100.0(6)	100.0(4)
Crystal system	triclinic	triclinic	monoclinic
Space group	P-1	P-1	P2 ₁ /c
a/Å	9.0948(9)	8.7163(3)	9.43090(10)
b/Å	10.8689(9)	11.5669(3)	10.15630(10)
c/Å	18.3916(9)	11.7044(4)	30.8417(5)
α/°	93.444(5)	101.996(2)	90
β/°	92.634(6)	95.478(3)	92.4380(10)
γ/°	98.721(7)	93.621(2)	90
Volume/Å ³	1791.0(2)	1144.82(6)	2951.44(6)
Z	2	4	4
ρ _{calc} /cm ³	1.406	1.22	1.226
μ/mm ⁻¹	4.125	0.564	0.56
F(000)	780	448	1152
Crystal size/mm ³	0.124 × 0.103 × 0.055	0.342 × 0.053 × 0.049	0.259 × 0.184 × 0.085
Radiation	CuKα (λ = 1.54184)	CuKα (λ = 1.54184)	CuKα (λ = 1.54184)
2θ range for data collection/°	8.25 to 133.198	7.77 to 137.522	9.168 to 136.496
Index ranges	-10 ≤ h ≤ 8, -12 ≤ k ≤ 12, -16 ≤ l ≤ 21	-10 ≤ h ≤ 10, -8 ≤ k ≤ 13, -14 ≤ l ≤ 12	-11 ≤ h ≤ 11, -11 ≤ k ≤ 12, -37 ≤ l ≤ 37
Reflections collected	11270	7818	42872
Independent reflections	6319 [R _{int} = 0.0774, R _{sigma} = 0.0641]	4237 [R _{int} = 0.0248, R _{sigma} = 0.0361]	5417 [R _{int} = 0.0290, R _{sigma} = 0.0124]
Data/restraints/parameters	6319/0/442	4237/0/299	5417/0/477
Goodness-of-fit on F ²	1.026	1.029	1.05
Final R indexes [I >= 2σ (I)]	R ₁ = 0.0844, wR ₂ = 0.2220	R ₁ = 0.0374, wR ₂ = 0.0955	R ₁ = 0.0363, wR ₂ = 0.0894
Final R indexes [all data]	R ₁ = 0.0889, wR ₂ = 0.2288	R ₁ = 0.0436, wR ₂ = 0.1008	R ₁ = 0.0381, wR ₂ = 0.0909
Largest diff. peak/hole / e Å ⁻³	0.78/-1.03	0.22/-0.29	0.26/-0.20
Flack parameter			

Compound	13a	17r	18a
Empirical formula	C ₁₄ H ₁₄ N ₂	C ₄₂ H ₄₀ N ₆ O ₂ P ₂	C ₁₉ H ₁₅ N ₂ OP
Formula weight	210.27	722.74	318.3
Temperature/K	99.9(4)	100.0(5)	100.0(5)
Crystal system	orthorhombic	triclinic	monoclinic
Space group	Pna2 ₁	P-1	P2 ₁ /c
a/Å	7.15983(6)	10.94660(10)	9.7440(5)
b/Å	25.70244(15)	11.6579(2)	15.8752(6)
c/Å	6.20436(4)	14.9699(2)	10.8405(5)
α/°	90	78.9240(10)	90
β/°	90	83.2090(10)	111.228(6)
γ/°	90	78.1640(10)	90
Volume/Å ³	1141.758(14)	1828.74(4)	1563.11(14)
Z	4	2	4
ρ _{calc} /cm ³	1.223	1.313	1.353
μ/mm ⁻¹	0.565	1.444	1.599
F(000)	448	760	664
Crystal size/mm ³	0.361 × 0.130 × 0.107	0.219 × 0.199 × 0.153	0.115 × 0.104 × 0.037
Radiation	CuKα (λ = 1.54184)	CuKα (λ = 1.54184)	CuKα (λ = 1.54184)
2θ range for data collection/°	6.878 to 138.634	7.866 to 140.152	9.738 to 138.25
Index ranges	-8 ≤ h ≤ 7, -31 ≤ k ≤ 31, -7 ≤ l ≤ 7	-12 ≤ h ≤ 13, -14 ≤ k ≤ 14, -18 ≤ l ≤ 18	-11 ≤ h ≤ 10, -19 ≤ k ≤ 19, -13 ≤ l ≤ 13
Reflections collected	40502	27767	32385
Independent reflections	2150 [R _{int} = 0.0423, R _{sigma} = 0.0118]	6955 [R _{int} = 0.0240, R _{sigma} = 0.0181]	2920 [R _{int} = 0.0868, R _{sigma} = 0.0254]
Data/restraints/parameters	2150/1/150	6955/0/481	2920/0/208
Goodness-of-fit on F ²	1.068	1.025	1.043
Final R indexes [I > 2σ (I)]	R ₁ = 0.0261, wR ₂ = 0.0675	R ₁ = 0.0299, wR ₂ = 0.0775	R ₁ = 0.0401, wR ₂ = 0.0977
Final R indexes [all data]	R ₁ = 0.0263, wR ₂ = 0.0677	R ₁ = 0.0310, wR ₂ = 0.0784	R ₁ = 0.0417, wR ₂ = 0.0990
Largest diff. peak/hole / e Å ⁻³	0.09/-0.14	0.39/-0.30	0.34/-0.38
Flack parameter	0.04(13)		

Compound	18r*	19r.HCl	19r
Empirical formula	C ₂₁ H ₂₉ N ₄ OP	C ₄₄ H ₄₆ Cl ₆ N ₆ P ₂	C ₂₁ H ₂₀ N ₃ P
Formula weight	384.45	933.51	345.36
Temperature/K	100.1(4)	100.0(6)	100.0(6)
Crystal system	monoclinic	monoclinic	monoclinic
Space group	P2 ₁ /c	P2 ₁	P2 ₁ /n
a/Å	18.6695(3)	10.6475(6)	9.9776(2)
b/Å	7.47220(10)	21.3060(7)	5.31450(10)
c/Å	14.6885(3)	11.2027(5)	32.2901(8)
α/°	90	90	90
β/°	94.948(2)	115.235(6)	92.492(2)
γ/°	90	90	90
Volume/Å ³	2041.44(6)	2298.9(2)	1710.59(6)
Z	4	2	4
ρ _{calc} /cm ³	1.251	1.349	1.341
μ/mm ⁻¹	1.329	4.369	1.473
F(000)	824	968	728
Crystal size/mm ³	0.17 × 0.083 × 0.075	0.135 × 0.038 × 0.033	0.24 × 0.153 × 0.034
Radiation	CuKα (λ = 1.54184)	CuKα (λ = 1.54184)	CuKα (λ = 1.54184)
2θ range for data collection/°	9.51 to 139.36	8.3 to 131.652	9.172 to 141.608
Index ranges	-22 ≤ h ≤ 21, -9 ≤ k ≤ 8, -17 ≤ l ≤ 17	-11 ≤ h ≤ 12, -25 ≤ k ≤ 25, -13 ≤ l ≤ 13	-12 ≤ h ≤ 10, -6 ≤ k ≤ 4, -37 ≤ l ≤ 39
Reflections collected	22426	38035	18495
Independent reflections	3832 [R _{int} = 0.0283, R _{sigma} = 0.0172]	7987 [R _{int} = 0.0591, R _{sigma} = 0.0412]	3301 [R _{int} = 0.0337, R _{sigma} = 0.0214]
Data/restraints/parameters	3832/0/250	7987/1/535	3301/61/244
Goodness-of-fit on F ²	1.038	1.021	1.174
Final R indexes [I >= 2σ (I)]	R ₁ = 0.0308, wR ₂ = 0.0804	R ₁ = 0.0580, wR ₂ = 0.1487	R ₁ = 0.0482, wR ₂ = 0.1028
Final R indexes [all data]	R ₁ = 0.0318, wR ₂ = 0.0813	R ₁ = 0.0631, wR ₂ = 0.1524	R ₁ = 0.0494, wR ₂ = 0.1033
Largest diff. peak/hole / e Å ⁻³	0.27/-0.29	1.04/-0.48	0.35/-0.34
Flack parameter		0.504(8)	

Compound	20r	22r.HI	23r.HCl
Empirical formula	C ₂₁ H ₁₆ Cl ₃ N ₃ P	C ₂₂ H ₂₃ IN ₃ P	C ₃₃ H ₃₀ ClN ₃ P ₂
Formula weight	447.69	487.3	565.99
Temperature/K	100.0(5)	100.0(6)	100
Crystal system	monoclinic	triclinic	100.0(2)
Space group	P2 ₁ /n	P-1	P2 ₁ /n
a/Å	10.91660(10)	10.42550(10)	14.24910(10)
b/Å	10.53500(10)	11.0267(2)	11.10540(10)
c/Å	17.4257(2)	12.5024(2)	18.20100(10)
α/°	90	93.0190(10)	90
β/°	95.8620(10)	111.6160(10)	106.2620(10)
γ/°	90	111.4290(10)	90
Volume/Å ³	1993.59(4)	1214.35(3)	2764.93(4)
Z	4	2	4
ρ _{calc} /cm ³	1.492	1.333	1.36
μ/mm ⁻¹	5.02	11.05	2.532
F(000)	916	488	1184
Crystal size/mm ³	0.186 × 0.163 × 0.094	0.3 × 0.223 × 0.15	0.242 × 0.109 × 0.058
Radiation	CuKα (λ = 1.54184)	CuKα (λ = 1.54184)	CuKα (λ = 1.54184)
2θ range for data collection/°	9.158 to 137.888	7.79 to 134.106	7.004 to 136.494
Index ranges	-10 ≤ h ≤ 13, -12 ≤ k ≤ 12, -21 ≤ l ≤ 21	-11 ≤ h ≤ 12, -13 ≤ k ≤ 13, -14 ≤ l ≤ 14	-17 ≤ h ≤ 17, -11 ≤ k ≤ 13, -21 ≤ l ≤ 21
Reflections collected	29454	40946	52498
Independent reflections	3705 [R _{int} = 0.0333, R _{sigma} = 0.0147]	4333 [R _{int} = 0.0462, R _{sigma} = 0.0168]	5069 [R _{int} = 0.0403, R _{sigma} = 0.0153]
Data/restraints/parameters	3705/0/265	4333/0/251	5069/0/354
Goodness-of-fit on F ²	4.046	1.082	1.038
Final R indexes [I >= 2σ (I)]	R ₁ = 0.1137, wR ₂ = 0.4065	R ₁ = 0.0234, wR ₂ = 0.0619	R ₁ = 0.0298, wR ₂ = 0.0773
Final R indexes [all data]	R ₁ = 0.1145, wR ₂ = 0.4087	R ₁ = 0.0234, wR ₂ = 0.0619	R ₁ = 0.0304, wR ₂ = 0.0777
Largest diff. peak/hole / e Å ⁻³	1.64/-2.28	0.49/-0.85	0.44/-0.31
Flack parameter			

Compound	24r	25a.Br	26a
Empirical formula	C ₄₂ H ₄₀ N ₆ P ₂	C ₄₀ H ₃₂ Br ₃ Cl ₂ N ₆ P ₃	C ₂₅ H ₂₀ Br ₂ N ₃ P
Formula weight	690.74	1000.25	553.23
Temperature/K	100.0(4)	100.0(5)	100.0(6)
Crystal system	triclinic	monoclinic	monoclinic
Space group	P-1	P2 ₁ /n	P2 ₁ /n
a/Å	9.5430(15)	12.54552(5)	11.6715(4)
b/Å	11.929(2)	24.25088(10)	17.1446(4)
c/Å	19.357(6)	13.42377(6)	12.5316(4)
α/°	73.14(2)	90	90
β/°	80.968(18)	92.0778(4)	110.292(4)
γ/°	68.526(15)	90	90
Volume/Å ³	1959.3(8)	4081.36(3)	2351.98(14)
Z	2	4	4
ρ _{calc} /cm ³	1.171	1.628	1.562
μ/mm ⁻¹	1.286	6.29	5.146
F(000)	728	1992	1104
Crystal size/mm ³		0.309 × 0.242 × 0.195	0.218 × 0.085 × 0.025
Radiation	CuKα (λ = 1.54184)	CuKα (λ = 1.54184)	CuKα (λ = 1.54184)
2θ range for data collection/°	18.2 to 101.43	7.29 to 148.994	8.928 to 140.142
Index ranges	-6 ≤ h ≤ 9, -5 ≤ k ≤ 10, -15 ≤ l ≤ 19	-13 ≤ h ≤ 15, -30 ≤ k ≤ 30, -16 ≤ l ≤ 16	-14 ≤ h ≤ 14, -20 ≤ k ≤ 16, -15 ≤ l ≤ 15
Reflections collected	3357	83677	25839
Independent reflections	2741 [R _{int} = 0.0551, R _{sigma} = 0.1180]	8363 [R _{int} = 0.0364, R _{sigma} = 0.0143]	4456 [R _{int} = 0.0361, R _{sigma} = 0.0208]
Data/restraints/parameters	2741/0/205	8363/0/487	4456/0/289
Goodness-of-fit on F ²	2.723	1.079	1.059
Final R indexes [I >= 2σ (I)]	R ₁ = 0.3012, wR ₂ = 0.6396	R ₁ = 0.0327, wR ₂ = 0.0875	R ₁ = 0.0508, wR ₂ = 0.1339
Final R indexes [all data]	R ₁ = 0.3628, wR ₂ = 0.6829	R ₁ = 0.0329, wR ₂ = 0.0877	R ₁ = 0.0538, wR ₂ = 0.1376
Largest diff. peak/hole / e Å ⁻³	6.14/-1.53	1.82/-1.27	3.99/-0.45
Flack parameter			

Compound	27a .AlCl ₃	[28a] OTf	31a
Empirical formula	C ₆₈ H ₅₅ Al ₂ Cl ₇ N ₆ P ₄	C ₄₀ H ₃₃ F ₃ N ₄ O ₃ P ₂ S	C ₂₆ H ₂₀ N ₄ O ₃ P ₂
Formula weight	1382.17	768.7	498.4
Temperature/K	100.0(6)	293(2)	100.0(6)
Crystal system	triclinic	monoclinic	triclinic
Space group	P-1	P2 ₁	P-1
a/Å	9.89820(10)	10.5256(5)	9.1548(3)
b/Å	16.5658(2)	16.5100(8)	11.5749(3)
c/Å	21.3668(2)	10.7619(6)	12.5889(4)
α/°	87.6080(10)	90	66.135(3)
β/°	85.1460(10)	95.571(4)	69.936(3)
γ/°	72.9720(10)	90	81.966(2)
Volume/Å ³	3337.42(6)	1861.34(16)	1145.90(7)
Z	2	2	2
ρ _{calc} /cm ³	1.375	1.372	1.444
μ/mm ⁻¹	4.244	2.089	2.045
F(000)	1420	796	516
Crystal size/mm ³	0.182 × 0.136 × 0.063	0.123 × 0.051 × 0.033	0.184 × 0.121 × 0.035
Radiation	CuKα (λ = 1.54184)	CuKα (λ = 1.54184)	CuKα (λ = 1.54184)
2θ range for data collection/°	6.898 to 137.2	8.254 to 129.288	8.096 to 137.476
Index ranges	-11 ≤ h ≤ 11, -19 ≤ k ≤ 19, -25 ≤ l ≤ 24	-12 ≤ h ≤ 12, -18 ≤ k ≤ 19, -12 ≤ l ≤ 12	-11 ≤ h ≤ 9, -13 ≤ k ≤ 13, -15 ≤ l ≤ 15
Reflections collected	64781	30639	17689
Independent reflections	12285 [R _{int} = 0.0353, R _{sigma} = 0.0211]	6150 [R _{int} = 0.0648, R _{sigma} = 0.0470]	4231 [R _{int} = 0.0375, R _{sigma} = 0.0243]
Data/restraints/parameters	12285/0/784	6150/1/479	4231/0/316
Goodness-of-fit on F ²	1.015	1.074	1.043
Final R indexes [I >= 2σ (I)]	R ₁ = 0.0270, wR ₂ = 0.0696	R ₁ = 0.0485, wR ₂ = 0.0975	R ₁ = 0.0304, wR ₂ = 0.0815
Final R indexes [all data]	R ₁ = 0.0284, wR ₂ = 0.0707	R ₁ = 0.0553, wR ₂ = 0.1004	R ₁ = 0.0317, wR ₂ = 0.0828
Largest diff. peak/hole / e Å ⁻³	0.45/-0.54	0.23/-0.26	0.31/-0.32
Flack parameter		-0.008(16)	
	34a	34b	34c

Compound	C ₁₉ H ₁₇ I ₂ OP	C ₂₀ H ₂₀ I ₂ NP	C ₂₁ H ₂₂ I ₂ NP
Empirical formula	C ₁₉ H ₁₇ I ₂ OP	C ₂₀ H ₂₀ I ₂ NP	C ₂₁ H ₂₂ I ₂ NP
Formula weight	546.09	559.14	573.16
Temperature/K	100.01(10)	100.00(10)	100.00(10)
Crystal system	triclinic	triclinic	monoclinic
Space group	P-1	P-1	P2 ₁ /c
a/Å	8.7185(3)	9.2731(3)	9.0359(3)
b/Å	9.8085(3)	10.0341(3)	25.5171(7)
c/Å	11.5663(3)	11.6573(3)	9.4963(3)
α/°	94.431(2)	67.852(3)	90
β/°	95.603(2)	88.456(2)	106.832(3)
γ/°	104.837(2)	84.209(2)	90
Volume/Å ³	946.17(5)	999.43(5)	2095.75(11)
Z	2	2	4
ρ _{calc} /cm ³	1.917	1.858	1.817
μ/mm ⁻¹	3.41	3.228	3.081
F(000)	520	536	1104
Crystal size/mm ³	0.162 × 0.09 × 0.078	0.15 × 0.113 × 0.083	0.076 × 0.044 × 0.035
Radiation	MoKα (λ = 0.71073)	MoKα (λ = 0.71073)	MoKα (λ = 0.71073)
2θ range for data collection/°	5.298 to 52.732	4.596 to 52.742	4.974 to 52.744
Index ranges	-10 ≤ h ≤ 10, -12 ≤ k ≤ 12, -14 ≤ l ≤ 14	-11 ≤ h ≤ 11, -12 ≤ k ≤ 12, -14 ≤ l ≤ 14	-11 ≤ h ≤ 11, -31 ≤ k ≤ 31, -11 ≤ l ≤ 11
Reflections collected	14803	15557	33543
Independent reflections	3870 [R _{int} = 0.0383, R _{sigma} = 0.0328]	4094 [R _{int} = 0.0202, R _{sigma} = 0.0181]	4281 [R _{int} = 0.0402, R _{sigma} = 0.0237]
Data/restraints/parameters	3870/0/209	4094/0/219	4281/0/228
Goodness-of-fit on F ²	1.05	1.075	1.037
Final R indexes [I >= 2σ (I)]	R ₁ = 0.0210, wR ₂ = 0.0407	R ₁ = 0.0153, wR ₂ = 0.0336	R ₁ = 0.0233, wR ₂ = 0.0414
Final R indexes [all data]	R ₁ = 0.0249, wR ₂ = 0.0424	R ₁ = 0.0165, wR ₂ = 0.0341	R ₁ = 0.0319, wR ₂ = 0.0437
Largest diff. peak/hole / e Å ⁻³	0.58/-0.5	0.42/-0.36	0.57/-0.38
Flack parameter			

Compound	34d	34e	34g
Empirical formula	C ₂₀ H ₁₉ I ₂ O ₂ P	C ₂₂ H ₂₅ I ₂ N ₂ P	C ₁₈ H ₁₅ I ₂ P
Formula weight	576.12	602.21	516.07
Temperature/K	100.00(10)	100.01(10)	100.00(10)
Crystal system	triclinic	monoclinic	orthorhombic
Space group	P-1	P2 ₁ /c	P2 ₁ 2 ₁ 2 ₁
a/Å	8.76192(19)	8.94007(14)	10.33101(9)
b/Å	10.48116(19)	42.9758(6)	12.83882(12)
c/Å	11.4220(3)	12.85504(19)	13.61886(13)
α/°	90.3592(17)	90	90
β/°	94.2694(18)	108.5752(17)	90
γ/°	95.4542(16)	90	90
Volume/Å ³	1041.20(4)	4681.70(13)	1806.38(3)
Z	2	8	4
ρ _{calc} /cm ³	1.838	1.709	1.898
μ/mm ⁻¹	3.09	2.764	3.555
F(000)	552	2336	976
Crystal size/mm ³	0.319 × 0.195 × 0.08	0.082 × 0.057 × 0.032	0.785 × 0.23 × 0.142
Radiation	MoKα (λ = 0.71073)	MoKα (λ = 0.71073)	MoKα (λ = 0.71073)
2θ range for data collection/°	4.684 to 52.732	4.388 to 52.744	4.36 to 58.158
Index ranges	-10 ≤ h ≤ 10, -13 ≤ k ≤ 13, -14 ≤ l ≤ 14	-11 ≤ h ≤ 11, -53 ≤ k ≤ 53, -16 ≤ l ≤ 16	-14 ≤ h ≤ 13, -17 ≤ k ≤ 17, -18 ≤ l ≤ 18
Reflections collected	42519	74293	84204
Independent reflections	4254 [R _{int} = 0.0376, R _{sigma} = 0.0163]	9569 [R _{int} = 0.0489, R _{sigma} = 0.0293]	4839 [R _{int} = 0.0700, R _{sigma} = 0.0203]
Data/restraints/parameters	4254/0/228	9569/0/495	4839/0/190
Goodness-of-fit on F ²	1.071	1.029	1.123
Final R indexes [I >= 2σ (I)]	R ₁ = 0.0172, wR ₂ = 0.0397	R ₁ = 0.0246, wR ₂ = 0.0495	R ₁ = 0.0162, wR ₂ = 0.0368
Final R indexes [all data]	R ₁ = 0.0180, wR ₂ = 0.0401	R ₁ = 0.0323, wR ₂ = 0.0523	R ₁ = 0.0163, wR ₂ = 0.0369
Largest diff. peak/hole / e Å ⁻³	1.28/-0.78	0.82/-0.71	0.36/-0.65
Flack parameter			-0.027(7)

Compound	[35a]BAR^F	[35b]BAR^F	[35d]BAR^F
Empirical formula	C _{57.5} H ₄₄ BClF ₂₄ IOP	C ₅₃ H ₃₄ BCl ₂ F ₂₄ INP	C ₁₀₅ H ₆₄ B ₂ Cl ₂ F ₄₈ I ₂ O ₄ P ₂
Formula weight	1411.05	1380.39	2709.82
Temperature/K	100.00(10)	100.01(10)	100.00(10)
Crystal system	triclinic	triclinic	monoclinic
Space group	P-1	P-1	P2 ₁
a/Å	12.3441(3)	12.50066(15)	12.46086(15)
b/Å	13.0277(2)	13.24451(17)	34.0625(3)
c/Å	19.3179(3)	17.59462(19)	13.54015(16)
α/°	86.9054(14)	90.5505(10)	90
β/°	82.8373(15)	92.5441(9)	110.6112(13)
γ/°	71.4746(17)	109.5891(12)	90
Volume/Å ³	2922.31(9)	2740.82(6)	5379.22(11)
Z	2	2	2
ρ _{calc} /cm ³	1.604	1.673	1.673
μ/mm ⁻¹	6.031	6.851	0.799
F(000)	1406	1364	2676
Crystal size/mm ³	0.727 × 0.134 × 0.098	0.251 × 0.13 × 0.043	0.288 × 0.093 × 0.068
Radiation	CuKα (λ = 1.54184)	CuKα (λ = 1.54184)	MoKα (λ = 0.71073)
2θ range for data collection/°	4.61 to 136.5	5.03 to 134.16	4.006 to 52.742
Index ranges	-14 ≤ h ≤ 14, -15 ≤ k ≤ 15, -23 ≤ l ≤ 23	-14 ≤ h ≤ 14, -15 ≤ k ≤ 14, -21 ≤ l ≤ 21	-15 ≤ h ≤ 15, -42 ≤ k ≤ 42, -16 ≤ l ≤ 16
Reflections collected	77608	96039	114233
Independent reflections	10690 [R _{int} = 0.0690, R _{sigma} = 0.0274]	9767 [R _{int} = 0.0362, R _{sigma} = 0.0144]	21933 [R _{int} = 0.0351, R _{sigma} = 0.0243]
Data/restraints/parameters	10690/127/814	9767/102/780	21933/230/1574
Goodness-of-fit on F ²	1.072	1.019	1.037
Final R indexes [I >= 2σ (I)]	R ₁ = 0.0548, wR ₂ = 0.1393	R ₁ = 0.0313, wR ₂ = 0.0826	R ₁ = 0.0354, wR ₂ = 0.0887
Final R indexes [all data]	R ₁ = 0.0551, wR ₂ = 0.1395	R ₁ = 0.0315, wR ₂ = 0.0827	R ₁ = 0.0363, wR ₂ = 0.0894
Largest diff. peak/hole / e Å ⁻³	1.22/-1.67	0.94/-0.93	1.23/-0.74
Flack parameter			0.296(11)

Compound	[35g]BAr^F	[35d]I₃	[35e]I₃
Empirical formula	C _{50.5} H ₂₈ BClF ₂₄ IP	C ₂₁ H ₂₁ Cl ₂ I ₄ O ₂ P	C ₂₂ H ₂₅ I ₄ N ₂ P
Formula weight	1294.86	914.85	856.01
Temperature/K	100.00(10)	100.00(10)	100.00(10)
Crystal system	triclinic	monoclinic	monoclinic
Space group	P-1	P2 ₁ /n	P2 ₁ /n
a/Å	12.47595(15)	14.5165(2)	11.9475(3)
b/Å	13.15500(16)	17.6860(3)	16.4754(4)
c/Å	17.7202(2)	22.1653(4)	13.5533(3)
α/°	90.8265(10)	90	90
β/°	110.2111(11)	103.2846(17)	98.650(2)
γ/°	109.0350(11)	90	90
Volume/Å ³	2553.33(5)	5538.43(16)	2637.49(11)
Z	2	8	4
ρ _{calc} /cm ³	1.684	2.194	2.156
μ/mm ⁻¹	6.847	4.746	4.774
F(000)	1274	3392	1592
Crystal size/mm ³	0.349 × 0.258 × 0.088	0.262 × 0.18 × 0.064	0.109 × 0.063 × 0.016
Radiation	CuKα (λ = 1.54184)	MoKα (λ = 0.71073)	MoKα (λ = 0.71073)
2θ range for data collection/°	5.37 to 143.81	4.424 to 52.738	4.908 to 51.226
Index ranges	-13 ≤ h ≤ 15, -16 ≤ k ≤ 16, -21 ≤ l ≤ 21	-18 ≤ h ≤ 18, -22 ≤ k ≤ 22, -27 ≤ l ≤ 27	-12 ≤ h ≤ 14, -20 ≤ k ≤ 20, -16 ≤ l ≤ 16
Reflections collected	50646	109911	19253
Independent reflections	10020 [R _{int} = 0.0432, R _{sigma} = 0.0226]	11327 [R _{int} = 0.0355, R _{sigma} = 0.0141]	4975 [R _{int} = 0.0319, R _{sigma} = 0.0272]
Data/restraints/parameters	10020/108/752	11327/0/545	4975/0/266
Goodness-of-fit on F ²	1.018	1.045	1.033
Final R indexes [I >= 2σ (I)]	R ₁ = 0.0385, wR ₂ = 0.0950	R ₁ = 0.0300, wR ₂ = 0.0810	R ₁ = 0.0211, wR ₂ = 0.0412
Final R indexes [all data]	R ₁ = 0.0387, wR ₂ = 0.0951	R ₁ = 0.0335, wR ₂ = 0.0836	R ₁ = 0.0270, wR ₂ = 0.0429
Largest diff. peak/hole / e Å ⁻³	1.13/-2.00	1.80/-2.04	0.69/-0.98
Flack parameter			

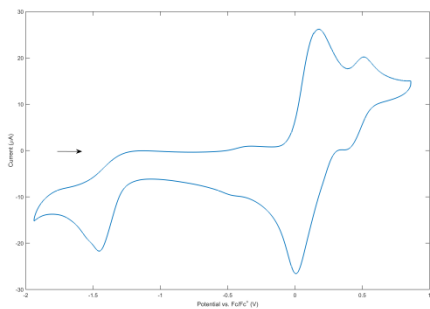
Compound	[35g]I₃	[36]I₃
Empirical formula	C ₁₈ H ₁₅ I ₄ P	C ₂₀ H ₁₉ I ₃ NP
Formula weight	769.87	685.03
Temperature/K	100.03(12)	100.00(10)
Crystal system	orthorhombic	orthorhombic
Space group	Pnma	P2 ₁ 2 ₁ 2 ₁
a/Å	12.2921(3)	18.3990(2)
b/Å	38.2596(10)	12.17869(14)
c/Å	9.0269(2)	9.99371(12)
α/°	90	90
β/°	90	90
γ/°	90	90
Volume/Å ³	4245.29(17)	2239.35(4)
Z	8	4
ρ _{calc} /cm ³	2.409	2.032
μ/mm ⁻¹	5.967	4.253
F(000)	2800	1280
Crystal size/mm ³	0.333 × 0.059 × 0.037	0.625 × 0.156 × 0.062
Radiation	MoKα (λ = 0.71073)	MoKα (λ = 0.71073)
2θ range for data collection/°	4.258 to 50.7	4.01 to 52.728
Index ranges	-14 ≤ h ≤ 14, -46 ≤ k ≤ 44, -10 ≤ l ≤ 10	-22 ≤ h ≤ 22, -15 ≤ k ≤ 15, -12 ≤ l ≤ 12
Reflections collected	39284	98437
Independent reflections	3951 [R _{int} = 0.0533, R _{sigma} = 0.0241]	4588 [R _{int} = 0.0488, R _{sigma} = 0.0119]
Data/restraints/parameters	3951/0/214	4588/0/227
Goodness-of-fit on F ²	1.311	1.125
Final R indexes [I >= 2σ (I)]	R ₁ = 0.0395, wR ₂ = 0.0734	R ₁ = 0.0253, wR ₂ = 0.0703
Final R indexes [all data]	R ₁ = 0.0416, wR ₂ = 0.0739	R ₁ = 0.0256, wR ₂ = 0.0706
Largest diff. peak/hole / e Å ⁻³	1.01/-1.09	1.21/-0.57
Flack parameter		-0.004(9)

Appendix 4

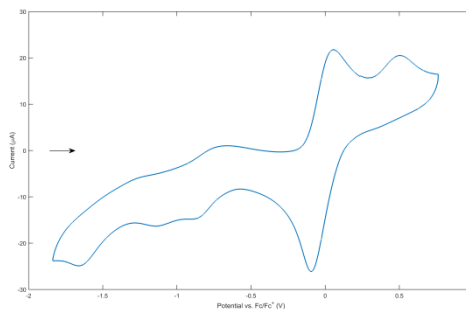
Miscellaneous Supplementary Data

A4.1 – Cyclic Voltammograms

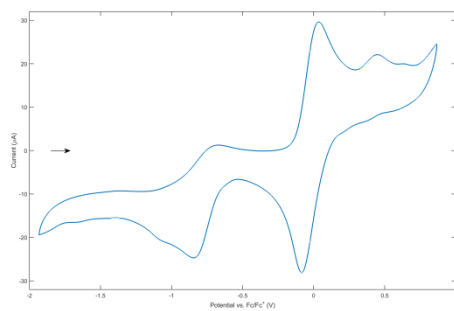
2a



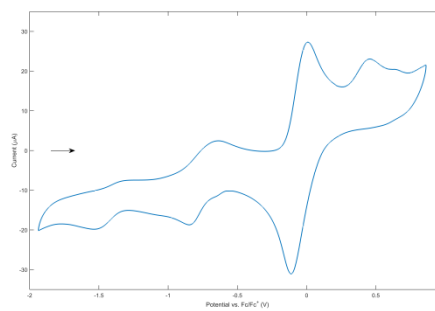
2b



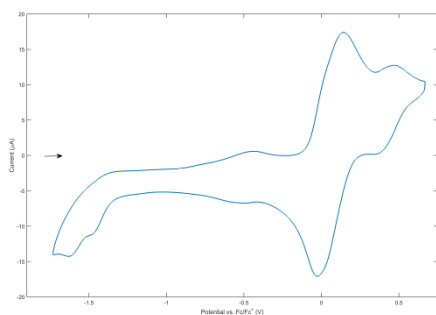
2c



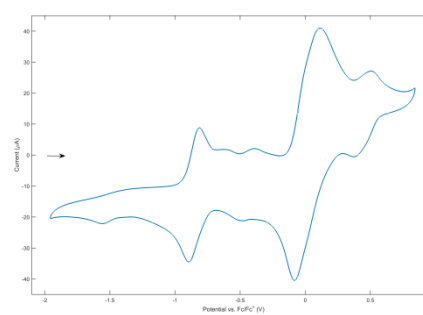
2d



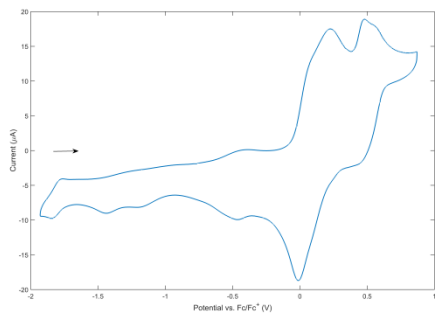
2e



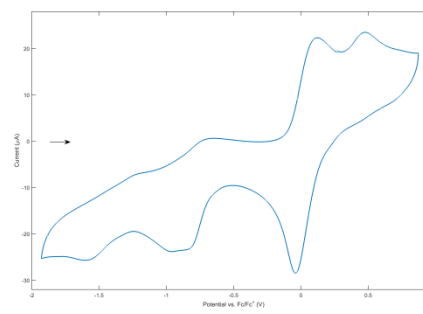
2f



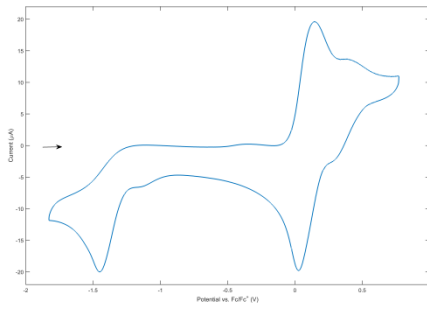
2g



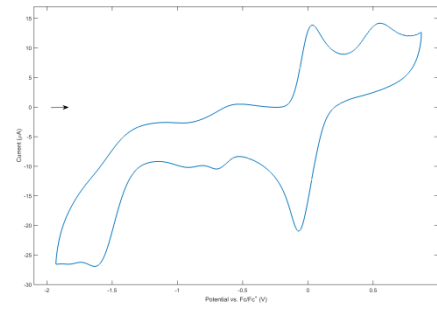
2h



2k

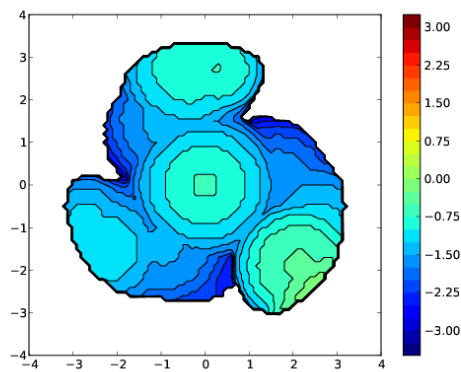


2l

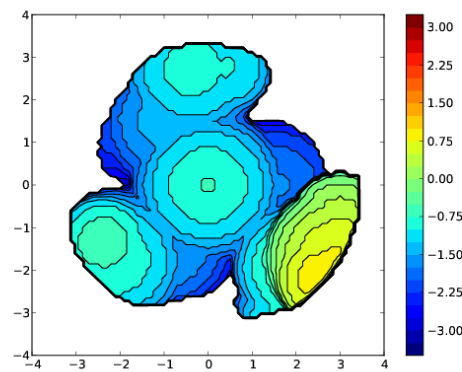


A4.2 - Buried Volume Maps

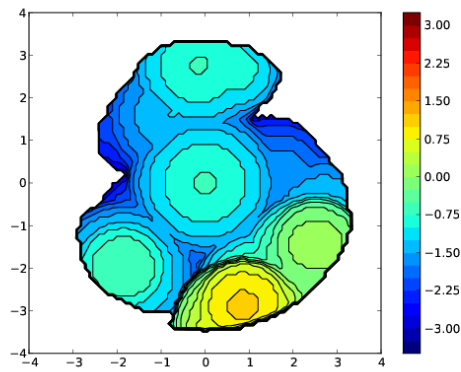
34a



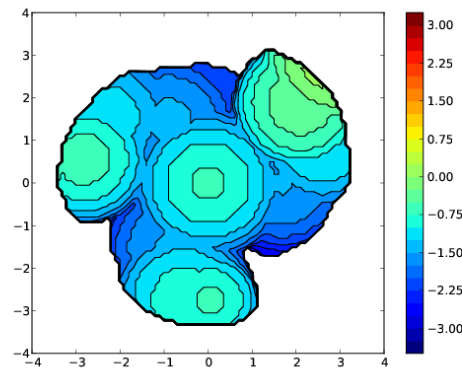
34b



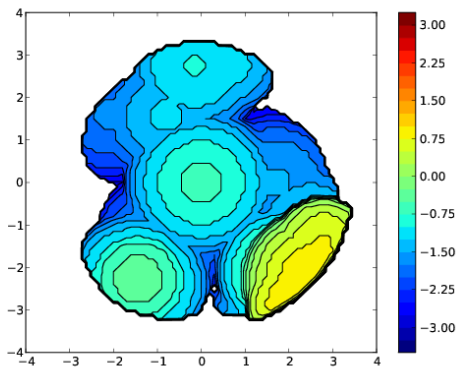
34c



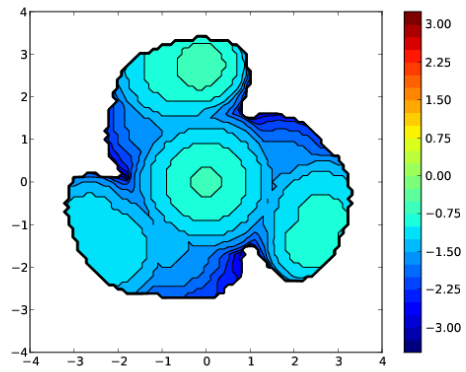
34d



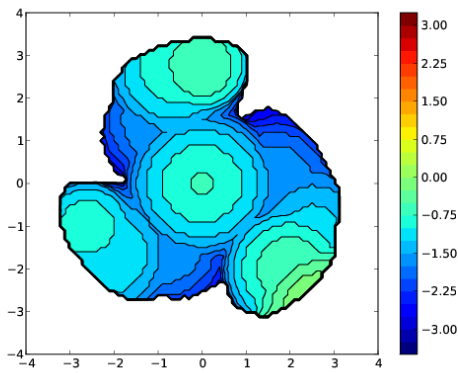
34e



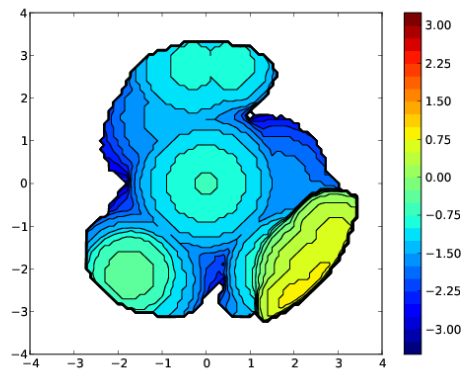
34g



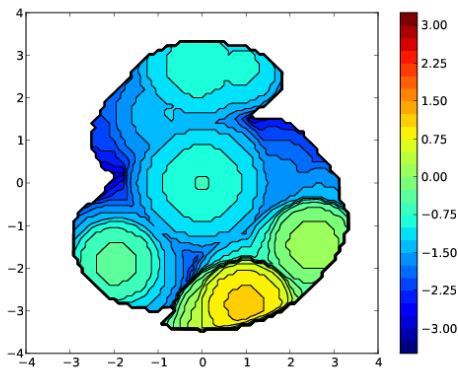
34a^c



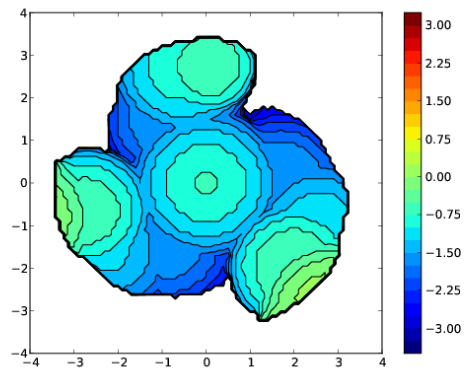
34b^c



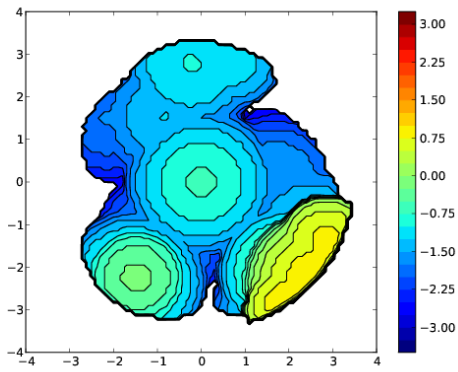
34c^c



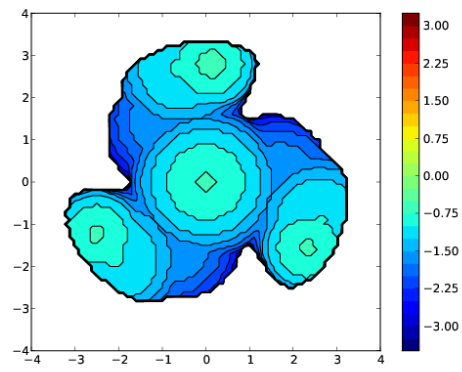
34d^c



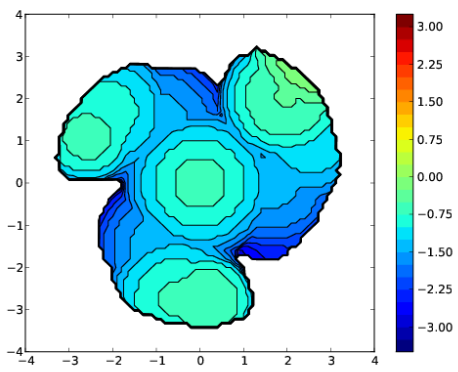
34e^c



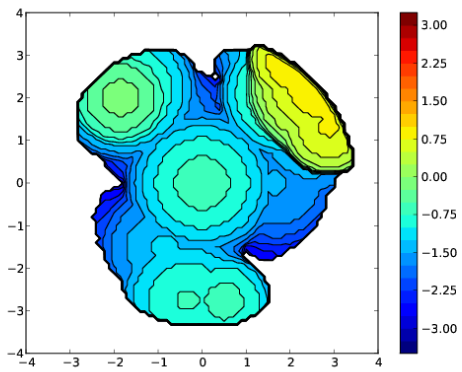
34g^c



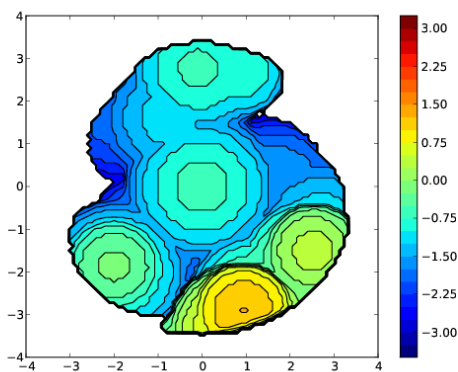
35a^c



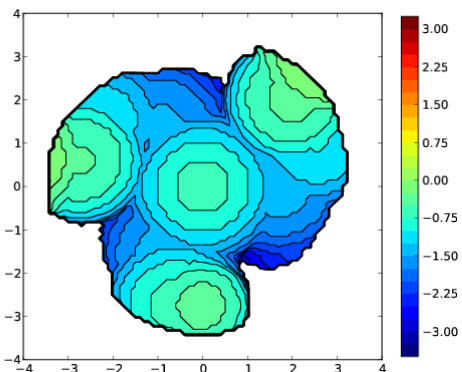
35b^c



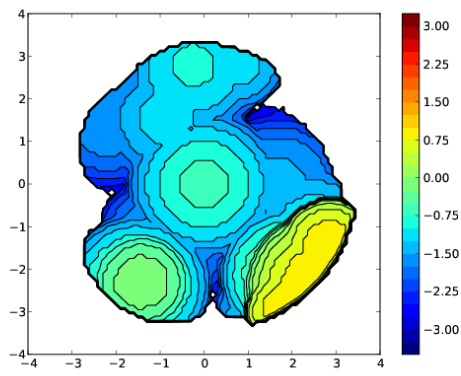
35c^c



35d^c



35e^c



35g^c

